EXPLORING THE MEDICINAL POTENTIAL OF SELECTED MEDICINAL PLANTS OF ETHIOPIA: AN INTEGRATED STUDY OF PHYTOCHEMICAL ANALYSIS, BIOLOGICAL ACTIVITIES, AND COMPUTATIONAL INSIGHTS

Hadush Gebrehiwot Gebrecherkos

A Dissertation Submitted to

The Department of Applied Chemistry

School of Applied Natural Sciences

Presented in Fulfillment of the Requirement for the Degree of Doctor of Philosophy in Applied Chemistry (Natural Products Chemistry)

Office of Graduate Studies

Adama Science and Technology University

September, 2024

Adama, Ethiopia

EXPLORING THE MEDICINAL POTENTIAL OF SELECTED MEDICINAL PLANTS OF ETHIOPIA: AN INTEGRATED STUDY OF PHYTOCHEMICAL ANALYSIS, BIOLOGICAL ACTIVITIES, AND COMPUTATIONAL INSIGHTS

Hadush Gebrehiwot Gebrecherkos

Supervisors

Major Supervisor: Aman Dekebo (PhD, Professor)

Co-supervisor: Milkyas Endale (PhD, Professor)

A Dissertation Submitted to

The Department of Applied Chemistry

School of Applied Natural Sciences

Presented in Fulfillment of the Requirement for the Degree of Doctor of Philosophy in Applied Chemistry (Natural Products Chemistry)

Office of Graduate Studies

Adama Science and Technology University

September, 2024

Adama, Ethiopia

DECLARATION

I hereby declare that this dissertation entitled "**Exploring the medicinal potential of selected medicinal plants of Ethiopia: an integrated study of phytochemical analysis, biological activities, and computational insights**" is my original work. That is, it has not been submitted to the award of any academic degree, diploma, or certificate in any other university. All sources of materials used for this dissertation have been duly acknowledged through appropriate citations.

Hadush Gebrehiwot		10/07/2024
Name of student	**Signature**	**Date**

RECOMMENDATION OF SUPERVISORS

We, the supervisors of this dissertation, hereby certify that we have read and revised the dissertation entitled "**Exploring the medicinal potential of selected medicinal plants of Ethiopia: an integrated study of phytochemical analysis, biological activities, and computational insights**" prepared under our guidance by **Hadush Gebrehiwot** submitted in partial fulfillment of the requirements for the degree of Doctor of Philosophy in Applied Chemistry (Natural Products Chemistry). Therefore, we recommend the submission of the final dissertation to the Department.

Aman Dekebo (PhD, Professor)		12/07/2024
Major Supervisor	**Signature**	**Date**
Milkyas Endale (PhD, Professor)		
Co-supervisor	**Signature**	**Date**

APPROVAL OF SUPERVISORS

We hereby certify that the recommendations and suggestions given by the board of examiners are appropriately incorporated into the final version of the dissertation entitled "**Exploring the medicinal potential of selected medicinal plants of Ethiopia: an integrated study of phytochemical analysis, biological activities, and computational insights**" by **Hadush Gebrehiwot**.

Aman Dekebo (PhD, Professor)		12/07/2024
Major Supervisor	**Signature**	**Date**
Milkyas Endale (PhD, Professor)		
Co-supervisor	**Signature**	**Date**

APPROVAL OF BOARD OF EXAMINERS

We, the undersigned, members of the board of examiners of the dissertation open defense by **Hadush Gebrehiwot** have read and evaluated the dissertation entitled "**Exploring the medicinal potential of selected medicinal plants of Ethiopia: an integrated study of phytochemical analysis, biological activities, and computational insights**" and examined the candidate during the open defense. This is therefore, to certify that the dissertation is accepted for partial fulfillment of the requirement of the degree of Doctor of Philosophy in Applied Chemistry (Natural Products Chemistry).

Hizkeal Tsade (PhD, Assis. Prof.)		
Chairperson	**Signature**	**Date**
Yadessa Melaku (PhD, Professor)		
Internal Examiner 1	**Signature**	**Date**
Worku Dinku (PhD, Assis. Prof.)		16/07/2024
Internal Examiner 2	**Signature**	**Date**
Tegene Tesfaye (PhD, Assoc. Prof.)		16/07/2024
External Examiner 1	**Signature**	**Date**
Mesfin Getachew (PhD, Assoc. Prof.)		19/07/2024
External Examiner 2	**Signature**	**Date**

Finally, approval and acceptance of the dissertation is contingent upon submission of its final copy to the Office of Postgraduate Studies (OPGS) through the candidate's Department Graduate Council (DGC) and School Graduate Committee (SGC).

Department Head	**Signature**	**Date**
School Dean	**Signature**	**Date**
Office of Postgraduate Studies, Dean	**Signature**	**Date**

ACKNOWLEDGMENTS

First and for most, I am delighted to express my heartfelt gratitude to my supervisors; Aman Dekebo (Ph.D., Professor, ASTU, Adama, Ethiopia) and Milkyas Endale (Ph.D., Professor, Armauer Hansen Research Institute, Addis Ababa, Ethiopia) for their generous help, guidance, consultation, encouragement, and limitless comments throughout the course of my study. Their assiduity, approach, and mentoring sympathy are more than advisory. I am also grateful for the technical and material supports I got from Yadessa Melaku (Ph.D., Professor, ASTU, Adama, Ethiopia). His generosity and assisting culture are vastly saluted. My next indebtedness goes to Mo Hunsen (Ph.D., Professor, Department of Chemistry, Kenyon College, Gambier, USA) for his technical supports, comments, and characterizations of most of the NMR samples. His kindness, supporting approach, and reactivity are duly acknowledged.

I am also pleased to express my thankfulness to Daniel Rentsch (Ph.D., Laboratory for Functional Polymers, Dubendorf, Switzerland), Tariku Nefo, and Jyh-Chien Chen (Ph.D., Professor, Department of Material Science and Engineering, National Taiwan University of Science and Technology, Taipei, Taiwan) for their collaborations in running NMR samples.

I would like to extend my appreciation to Mr. Kebede Shenkute (ASTU, Ethiopia) for his support in GC-MS analysis, Ms. Emebet Getaneh (ASTU, Ethiopia) for her assistance of antioxidant activity tests, Mr. Urgessa Ensermu (ASTU, Ethiopia) for the antibacterial activity tests, and Mr. Habdolo Esatu (Wachemo University, Ethiopia) for his material supports during the laboratory works.

The collaborations from Vladimir V. Zarubaev (Ph.D., Professor, Department of Virology, St. Petersburg Pasteur Institute, Petersburg, Russia) for antiviral activity, Walailak University, Nakhon Si Thammarat, Thailand, for anti-acanthamoeba activity tests, and the Ethiopian Public Health Institute for providing the bacterial strains are also highly acknowledged.

I also acknowledge Adama Science and Technology University (ASTU) for hosting and granting the scholarship, and Wachemo University for endowing the opportunity for the PhD study. Last but not least, I am very honored to express my love and respectfulness to my family for their endless prayers, support, and encouragement from the start up to the end of my entire careers.

DEDICATION

This dissertation work is dedicated to my family, principally to my father; Gebrehiwot Gebrecherkos. Dad, your dreams come true!

TABLE OF CONTENTS

CONTENT **PAGE**

TABLE OF CONTENTS (continued)

TABLE OF CONTENTS (continued)

TABLE OF CONTENTS (continued)

LIST OF TABLES

TABLE **PAGE**

LIST OF TABLES (continued)

LIST OF TABLES (continued)

LIST OF FIGURES

FIGURE **PAGE**

LIST OF FIGURES (continued)

LIST OF SCHEMES

SCHEME **PAGE**

LIST OF APPENDICES

APPENDIX **PAGE**

LIST OF APPENDICES (continued)

LIST OF ACRONYMS

AASTU	Addis Ababa Science and Technology University
ABTS	2,2'-azinobis-(3-ethylbenzothiazoline-6-sulfonic acid)
ADMET	Absorption, Distribution, Metabolism, Excretion, and Toxicity
ASTU	Adama Science and Technology University
ATCC	American Type Culture Collections
COSY	Correlation Spectroscopy
DEPT	Distortionless Enhancement by Polarization Transfer
DMSO	dimethyl sulfoxide
DPPH	2,2-diphenyl-1- picrylhydrazyl
FRAP	Ferric Reducing Antioxidant Power
FTIR	Fourier Transform Infrared Spectroscopy
GC-MS	Gas Chromatography-Mass Spectroscopy
GC-NMR	Gas Chromatography- Nuclear Magnetic Resonance
HMBC	Heteronuclear Multiple Bond Correlation
HPLC	High-Performance Liquid Chromatography
HRMS	High Resolution Mass Spectrometry
HSQC	Heteronuclear Single Quantum Coherence
IC_{50}	Half Maximal Inhibitory Concentration
IR	Infrared spectroscopy
LC-MS	Liquid Chromatography-Mass Spectrometry
LC-NMR	Liquid Chromatography-Nuclear Magnetic Resonance
LD_{50}	Median Lethal Dose
MCF-7	Michigan Cancer Foundation
MDCK	Madin-Darby Canine Kidney cells
MHA	Muller Hinton Agar
MIC	Minimum Inhibitory Concentration
MS	Mass Spectroscopy
MTT	(3-(4, 5-dimethyl thiazol-2yl)-2, 5-diphenyl tetrazolium bromide)
NMR	Nuclear Magnetic Resonance spectroscopy
PDB	Protein Data Bank

LIST OF ACRONYMS (continued)

PK	Pyruvate Kinase
PTLC	Preparative Thin Layer Chromatography
R_f	Retention factor
RMSD	Root Mean Square Deviation
SD	Standard Deviation
SEM	Standard Error of the Mean
TCM	Traditional Chinese Medicine
TLC	Thin Layer Chromatography
TM	Traditional Medicine
UV-VIS	Ultraviolet-Visible spectroscopy
WHO	World Health Organization

ABSTRACT

*Medicinal plants including herbs and spices are among the most popular sources of bioactive compounds that possess tremendous biological effects. Plant secondary metabolites such as flavonoids, quinones, alkaloids, tannins, saponins, and terpenoids have been reported as remarkable classes of natural products used in drug development. This research aimed to study the medicinal properties of extracts and compounds isolated from roots of selected medicinal plants of the Ethiopian flora, namely Cyphostemma adenocaule, Delonix regia, Senna siamea, and Ziziphus spina-christi along with their Computational Chemistry profiles. Documented protocols were used to screen the selected plants for their chemical composition, biological activities, and in silico molecular docking, drug-likeness, and ADMET profiles of the isolated compounds. A maceration technique was utilized to prepare the extracts of each plant material. The compounds were isolated using silica gel column chromatography and the structural information of the isolated compounds were established using IR and NMR spectroscopic techniques. Essential oils were extracted from the leaves and roots of the plants using Clevenger's apparatus and their compositions were analyzed using GC-MS. The antibacterial activities of the extracts and isolated compounds were screened using paper disc diffusion assay against four bacterial strains, including two Gram-negative (Escherichia coli and Pseudomonas aeruginosa) and two Gram-positive (Staphylococcus aureus and Streptococcus pyogenes) bacteria. In addition, the antioxidant activities were tested via the 2, 2-diphenyl-1-picrylhydrazyl (DPPH) radical-scavenging assay. The anti-acanthamoeba and antiviral properties of the extracts were studied using the dilution method in a 96-well polystyrene microtiter plate and micro tetrazolium (MTT) assays, respectively. In silico molecular docking screening, pharmacokinetics, and toxicity protocols of the isolated compounds were performed to offer the potential applications of the compounds in developing novel medications. An AutoDock Vina software in combination with the BIOVIA Discovery Studio Visualizer 2021, SwissADME, and ProTox-II prediction web tools were applied to generate the molecular docking, pharmacokinetics, and toxicity profiles, respectively. Notably, the chromatographic separation of the plant extracts afforded twenty four known compounds including, ten compounds namely; β-sitosterol (**19**), parthenocissin A (**23**), ε-viniferin (**25**), 3-hydroxy isoagatholactone (**28**), tricuspidatol A (**29**), myricetin (**66**), hexadec-1-ene (**82**), palmitic acid (**83**), β-sitosteryl palmitate (**84**), and diethyl phthalate (**85**) from Cyphostemma adenocaule, seven compounds namely; quercetin-3-O-rutinoside (**37**), stigmasterol (**40**), quercetin (**42**), diethyl phthalate (**85**), a mixture of β-sitosterol (**19**) and stigmasterol (**40**), β-sitosteryl-3β-glucopyranoside-6'-O-palmitate (**86**), and apigenin (**87**) from Delonix regia, seven compounds namely; lupeol (**39**), chrysophanol (**53**), betulinic acid (**63**), a mixture of β-sitosterol (**19**) and stigmasterol (**40**), glyceryl-1-hexacosanoate (**88**), and 4-(2'-hydroxymethyl-4'-hydroxyphenyl)-chrysophanol (**89**) from Senna siamea, and five compounds namely; stigmasterol (**40**), β-sitosteryl-3β-glucopyranoside-6'-O-palmitate (**86**), trimethyl trilinolein (**90**), stearic acid (**91**), and 13-hydroxyoctadeca-9, 11-dienoic acid (**92**) from Ziziphus spina-christi. The GC-MS analysis revealed perillyl alcohol (**93,** 13.08%) and nootkatone (**106**, 30.12% in leaves and 26.52% in roots) as the major components in the essential oils of Cyphostemma adenocaule and Ziziphus spina-christi, respectively. Heneicosane (**102**) was identified as the principal compound in the essential oils of Delonix regia (49.26%) and Senna siamea (53.17%). The antibacterial activity tests of the extracts and isolated compounds showed potential effects against the bacterial strains of the study. At the lowest concentrations (extracts; 6.25 mg/mL and compounds; 0.25 mg/mL), the highest inhibitory activities were observed by the Senna siamea extract (SSE, 12.00*

*± 0.41 mm) and chrysophanol (**53**, 11.17 ± 0.24 mm), respectively, against E. coli compared to ciprofloxacin (23.33 ± 0.47 mm). The 2, 2-diphenyl-1-picrylhydrazyl (DPPH) radical scavenging activity assay showed auspicious IC_{50} values for parthenocissin A (**23**, 0.98 µg/mL), **ε**-viniferin (**25**, 0.32 µg/mL), tricuspidatol A (**29**, 0.67 µg/mL), and quercetin-3-O-rutinoside (**37**, 0.81 µg/mL) compared to ascorbic acid standard (0.08 µg/mL) showcasing their potent antioxidant effects. The micro tetrazolium (MTT) assay of the CH_2Cl_2: CH_3OH (1:1) extract of Senna siamea (SI: 13.32) and methanol extract of Z. spina-christi (SI: 28.03) showed significant selectivity index (SI) values signifying their cytotoxicity against influenza types A and B viruses. The molecular docking computations showed the highest binding affinity for ε-viniferin (-9.9 kcal/mol) against topoisomerase IIα, and the drug-likeness predictions showed that only quercetin-3-O-rutinoside (**37**), β-sitosteryl palmitate (**84**), and β-sitosteryl-3β-glucopyranoside-6'-O-palmitate (**86**) failed to fulfill Lipinski's rule, though the others do with zero/one violations. All the screened compounds showed no hepatotoxicity and cytotoxicity in accordance with the prediction results of ciprofloxacin. Thus, the findings of this study support the ethno medicinal uses of the plants and further works are needed to transform the traditional uses of the plants into modern and scientific usage.*

Keywords: Biological activities, *Cyphostemma adenocaule*, *Delonix regia*, Molecular docking, Pharmacokinetics, Phytochemical analysis, *Senna siamea*, *Ziziphus spina-christi*.

CHAPTER ONE

1. INTRODUCTION

1.1. Background

Plant-derived products from various parts (roots, leaves, flowers, barks, and rhizomes), have been part of natural product medicines since time immemorial. Knowledge of the phytochemistry of plants is essential to get valuable information for the isolation of natural products and the synthesis of complex chemical compounds (Mojab *et al.*, 2003, Nna *et al.*, 2017, Parekh *et al.*, 2017). The continuing menace to global biodiversity through the devastation of land-dwelling and marine ecosystems claims urgency to enlarge the consideration of these resources as a means of novel bioactive pharmacophores and chemo-types. This would ultimately serve the aim of pharmaceutical industries to explore lead compounds for efficient drugs against a variety of ailments (Khan *et al.*, 2020). Nowadays, plant-derived medicines are highly desirable due to their safety and fewer side effects than synthetic alternatives, offering profound health benefits (Maitera *et al.*, 2011). The current developments in science and technology have made it easy the isolation and characterization of bioactive compounds from plants that are used in traditional therapeutic practices (Balunas and Kinghorn, 2005).

Plants have formed the origin of sophisticated traditional medicinal systems that have been in existence for many years and continue to offer humankind new medications. Ancient humans acquired the knowledge and skill of plant utilization for medicinal values through several years of experiences, vigilant observations, and trial and error experiments. After achieving primary needs such as food and shelter, humans have sought an appropriate remedy among plants for treating various ailments (WHO, 2019). More than 10% of all vascular plants exhibit medicinal properties and between 350,000 and half a million species of them are estimated to be in use (Salmerón-Manzano *et al.*, 2020). Since early times, plants have been frequently used in various medications and their therapeutic applications are still ongoing (Pimm *et al.*, 2014). In the beginning, trial and error applications were used to treat diseases or simply to feel healthier, and in this manner, to identify useful plants with useful effects. Eventually, the utilization of these plants has progressively advanced over the generations, and this has become common in various contexts as traditional medicine (Kunle *et al.*, 2012).

Traditional medicines (TMs) make use of plants with a considerable content of natural products and are of great significance. These forms of medicine include Ayurveda, traditional Chinese medicine (TCM), Kampo, Unani, and traditional Korean medicine (TKM). They use natural products and have been experienced all over the globe for thousands of years, and have blossomed into orderly-controlled systems of remedy. In their different forms, they may have some problems, but they continue to be an important repository knowledge of mankind (Dong, 2013). By definition, traditional medicine is considered as "the total sum of the skills, practices, and knowledge, based on the beliefs, theories, and experiences native to various cultures, whether explainable or not, used in the maintenance of health. They are applied in the diagnosis, prevention, treatment or improvement of mental and physical illnesses" (WHO, 2019). All civilizations have established this form of therapy, based on the accessibility of the medicinal plants in their habitat. Nowadays, many authors agree that this transferred narration and knowledge is the basis of medicine and pharmacy. In addition, hundreds of vascular plants are cultivated today worldwide to get expedient substances in medicine and pharmaceutical sciences. The medicinal properties of many plants gave rise to therapeutic drugs extracted from plants with these advantages. Until the 18^{th} century, the pharmaceutical properties of many plants, their method of treatment, and their effect on the human organism were recognized, but the active component was unknown. Conversely, the active compounds of many plants exhibiting considerable therapeutic applications have been known since the advancements of modern analytical and spectroscopic instruments (Faridi *et al.*, 2010).

China has been the icon of traditional medicinal practices since prehistoric times, and TCM was the principal form of health care in the country. TCM is based on five millenniums of medical experience and practice and is rich in records from "clinical experiments" which assure its efficacy and effectiveness (Chan *et al.*, 2012). It has established techniques concerning the correct dosage, methods of processing and preparing materials, and the proper time to gather the different medicinal parts of plants. Notably, there is advancing convergence between the TCM and modern medicine. With the growth of modern technology, it has become possible to identify the pharmacology of many Chinese herbs along with their mechanisms of action, and the practice has become understandable in terms of modern medications. With advances in therapeutic principles, theoretical background, understanding of the life sciences, associated technologies, and a clearer

understanding of the active components, TCM has become an input of modern medicine (Chan *et al.*, 2012, Zhang *et al.*, 2012).

At the beginning of the 19th century, "the era of modern drugs" began. In 1805, the first therapeutic compound called morphine (**1**) was isolated and found by a German pharmacist, Friedrich Sertürner, from the *opium* plant (Joo, 2014). Consequently, numerous natural products possessing therapeutic properties have been isolated from plants. The antimalarial drug quinine (**2**) which has been isolated from *Cinchona succirubra* is also one of the most significant plant medicines approved in 2004 (Dias *et al.*, 2012). Pilocarpine (**3**) is an L-histidine-derived alkaloid isolated from *Pilocarpus jaborandi* (Rutaceae) and has been used in the treatment of glaucoma for over a century. Salicin (**4**, an anti-inflammatory agent), digitoxin (**5**, used against congestive heart failure), penicillin (**6**, antibacterial drug), and podophyllotoxin (**7**, antiviral) are also among the substantial drugs of plant origin isolated from *Salix alba* L. (willow tree), *Digitalis purpurea* L. (foxglove), the fungus *Penicillium notatum*, and *podophyllum* species, respectively (Dias *et al.*, 2012) (Figure 1). Many of them follow their traditional applications and some of them do not.

Later, the advancement of synthetic methods led to a substantial reduction in the significance of natural products, and there were apprehensions that the use of some plant-based natural products for pharmaceutical purposes might be reduced. However, natural products still play an important role in the development of novel drugs, and these substances have been in constant use. Currently, some types of medications, such as antihypertensive, anticancer, and antimigraine treatments, have greatly benefited from natural products (Joo, 2014). The development of novel drugs depending on modern technology seems to be getting something of a limit. In finding novel drugs, the pharmaceutical industry has tended to adopt combinatorial chemistry-based drug development and high-throughput synthesis since the 1980s. However, the extensive efforts made in this way have not formed the drug productivity expectedly. Some huge pharmaceutical industries are facing great challenges in creating new products. Accordingly, over the past decades, increasing attention has been given to natural compounds in the search for new drugs together with new technology, such as high-throughput choices (Ngo *et al.*, 2013).

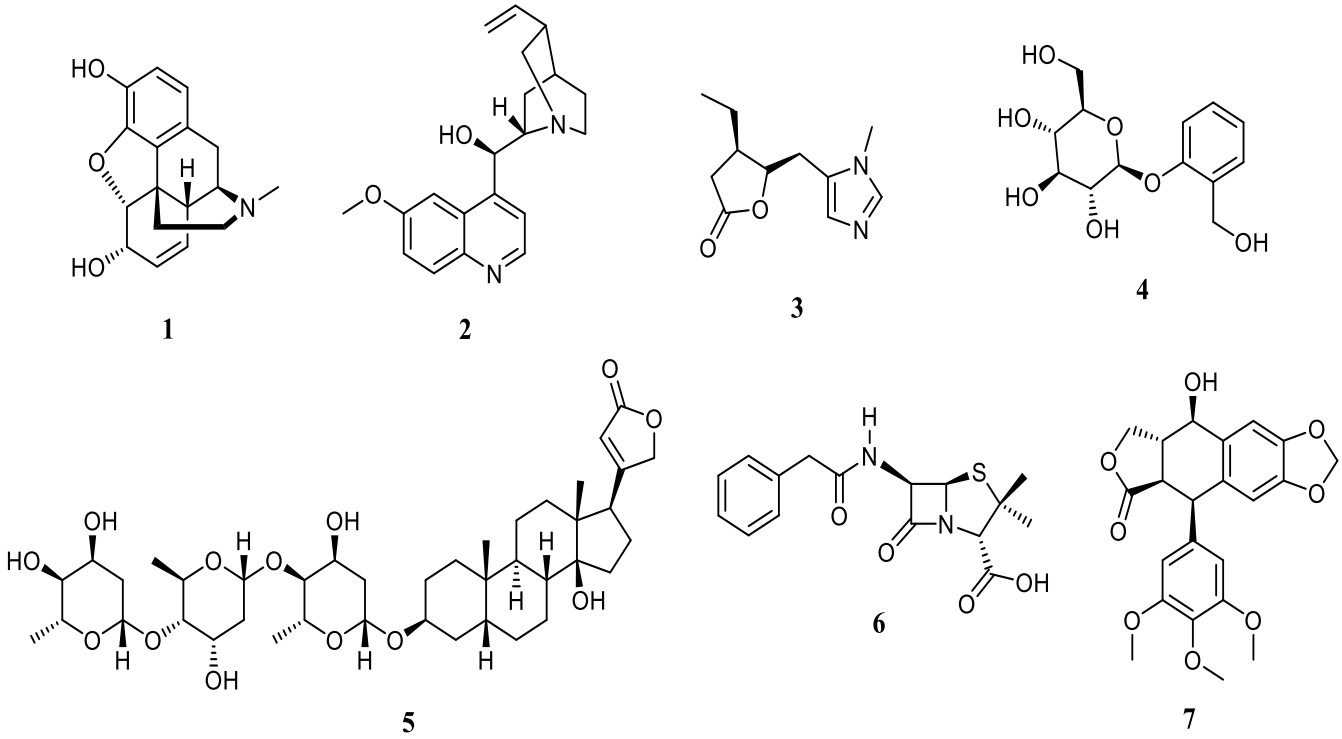

Figure 1: Chemical structures of compounds **1**-**7** isolated from plants with known clinical uses.

The emergence of isolation and structure elucidation techniques such as HPLC, NMR, HRMS, and other hyphenated techniques including GC-MS, LC-MS, LC-NMR, MS-MS, and GC-NMR made it possible to isolate the active compounds of medicinal plants. Since then, these active components have been developed synthetically in the laboratory to produce the drugs later on a large scale (Atanasov *et al.,* 2015). Today's medications intended for pharmaceutical industries largely depend on the bioactive compounds of medicinal plants and are used as lead compounds in many drug-development technologies (Arceusz *et al.*, 2010). Yet, today, the developing world failed to have access to modern synthesized medicines, and thus, many parts of the world continue to use medicines of traditional origin due to their low cost, and few side effects (Salmerón-Manzano and Manzano-Agugliaro, 2020). The possible trend to return to traditional medicine may have two major problems. The first is the utilization of medicines of plant origin without thinking of their possible risky aspects for health. Though many plants are safe like the aromatic plants used in rosemary, infusions: mint, chamomile, and thyme; others may have hazardous compounds. For instance, Bitter Melon (*Momordica charantia* L.) which is used to treat fever in cases of malaria, its green seeds are very toxic as it can induce a patient's coma (hypoglycemic coma) by forming a

sharp drop in blood sugar. Secondly, it can cause a proliferation of products giving rise to false perspectives, as they are not amply researched (Masondo and Makunga, 2019).

Medicinal plants, spices, and herbs have gotten much attention as the most essential sources of bioactive compounds. The most important of these classes of compounds include alkaloids, polyphenols, terpenoids, tannins, vitamins, and saponins. These natural compounds could be isolated from plant raw materials using water or organic solvents. Many reports have shown that these compounds extracted from plants have a broad spectrum of biological activities including antimicrobial, antioxidant, anticancer, anti-diabetic, antimalarial, anti-inflammatory, and antiviral properties (Gonçalves *et al.*, 2013).

In Ethiopia, plants have been used as a source of medicine from time immemorial to treat different ailments, due to its long history, and traditional medicine has become an integral part of culture. These traditional medicinal practices and remedies are recorded in oral tradition and in early medico-religious manuscripts and traditional pharmacopeias, which, according to the estimates of some historians, date back to the 15^{th} century (Jima and Megersa, 2018). The flora of Ethiopia is estimated to have about 6,500-7,000 species of higher plants, of which 12% are endemic (Alemu, 2017). Literature surveys revealed that more than 80% of the human population and 90% of the livestock of Ethiopia rely on traditional medicinal practices which are commonly used to treat various human and livestock diseases (Jima and Megersa, 2018). Traditional healers known by different names in different parts of the country are the primary players in the curative aspect of traditional medicine (Jima and Megersa, 2018).

In this research, four medicinal plants namely, *Cyphostemma adenocaule*, *Delonix regia*, *Senna siamea,* and *Ziziphus spina-christi* have been selected to prove their traditional medicinal applications using *in vitro* and *in silico* studies. The plants were selected based on their ethno-botanical aspects and the potential compounds they have to treat various human and livestock health problems. The study emphasized on the phytochemistry and biological activities of secondary metabolites from the selected medicinal plants along with computational profiles to validate their medicinal relevance.

1.2. Statement of the Problem

The lack of treatments for infectious diseases in the developing world is a tragic problem and one of the most serious challenges that the world needs to face in the 21st century. Virtually, most of the infectious diseases causing deaths occur in low and middle-income countries (Miranda *et al.*, 2008). Despite progress is showed in the basic knowledge of many virulent diseases, most of these have remained to cause notable morbidity and mortality. In the past few decades, many of the commonly used drugs and antibiotics have become less effective against certain ailments, not only because many of them formed toxic reactions, but also due to the emergence of drug-resistant pathogenic microorganisms. In addition, the need to replace synthetic antibiotics with natural and safe ones for the development of natural bioactive antibiotics has nurtured researchers on the screening of medicinal plants. Furthermore, most of the anticancer medications are not selective and damage both normal and tumor cells, thereby causing an increased risk of other cancers and systematic toxicity (Kaur *et al.*, 2022). Thus, there is a need the search for safer alternatives to treat infectious diseases that are accessible, affordable, have fewer side effects, and minimum toxicity.

Despite the fact that the selected plants are traditionally used for the treatment of various ailments in different parts of Ethiopia, there were no detailed previous studies on the chemical and biological activities of most of the selected medicinal plants. Reports on the whole parts of *Cyphostemma adenocaule*, and the roots of *Delonix regia*, *Senna siamea*, and *Ziziphus spina-christi* are limited which might be due to the lack of investigating materials, and inaccessibility of the plants. In addition, the isolation and characterization of location-based phytochemicals is significant to justify the qualitative and quantitative variability of bioactive compounds. Furthermore, many phytochemical studies of the selected plants emphasized only on the isolation and characterization of bioactive compounds and investigation of their biological activities *in vitro*. In this point of view, supporting this way of study with additional *in silico* computations such as pharmacokinetics, drug-likeness properties, and molecular docking studies of the isolated compounds offers the validity of research investigations. Reports on the antioxidant, anti-acanthamoeba, cytotoxicity, and antiviral activities of the extracts of the selected medicinal plants are also limited. Moreover, the uses of the plants by traditional healers for antibacterial and the aforementioned activities are not supported scientifically which leads to possible shortcomings.

This was the core problem this study addressed. Thus, inspired by their broad spectrum of traditional uses we set out to undertake the isolation and characterization of compounds from the selected plants and validate their medicinal applications with *in vitro* and *in silico* studies.

1.3. Justification of the Study

Nowadays, attention to herbal medicine is emerging a renaissance with the apparent development of new principles of "return to nature" among therapeutic companies and other stakeholders. A rational, positive, and non-prejudicial method in systematically evaluating the potential of ethnomedicinal plants against various acute and chronic ailments is a more truthful response to global health problems. This was the driving force behind the multidisciplinary screening approaches of this study. The selected medicinal plants have a historical ethno-medicinal application in folk medicine for the treatment of a wide range of ailments with the major classes of secondary metabolites reported from them. Some of the reported compounds from the plant species are pharmaceutically valuable. There are also reports on the medicinal effects of these plants which were originally not described in the manuscripts of traditional systems thus making them new chemical entities. Although few reports signifying the medicinal applications of the bioactive compounds have been documented so far, detailed knowledge of their phytochemistry, biological activities, and *in silico* computational study of most of the plants and their mode of action is still lacking. In the present study, some claims of the selected medicinal plants which are related to their medicinal profiles along with the compound isolates are addressed.

1.4. Objectives of the Study

1.4.1. General objective

The main objective of this study was to investigate the phytochemical constituents, and biological activities of the extracts and isolated phytochemicals of *Cyphostemma adenocaule, Delonix regia, Senna siamea, and Ziziphus spina-christi* along with *in silico* pharmacokinetics, drug-likeness, and molecular docking insights of the isolated compounds.

1.4.2. Specific objectives

The specific objectives that the present research entirely assessed and addressed were the following.

i. To collect and authenticate the plant materials;
ii. To extract crude extracts from the roots of *Cyphostemma adenocaule, Delonix regia, Senna siamea, and Ziziphus spina-christi* using maceration technique at room temperature;
iii. To isolate compounds from the extracts via silica gel column chromatography;
iv. To elucidate the structure of the isolated compounds using spectroscopic techniques (IR, and NMR);
v. To extract essential oils from the leaves and roots part of the plant materials *via* hydro distillation;
vi. To analyze the chemical constituents of the essential oils using GC-MS;
vii. To evaluate the *in vitro* antibacterial activities of the crude extracts, compound isolates, and essential oils against four human pathogens including two Gram-negative (*Escherichia coli* and *Pseudomonas aeruginosa)* and two Gram-positive *(Staphylococcus aureus* and *Streptococcus pyogenes)* bacteria using paper disk diffusion assay;
viii. To assess the antioxidant activities of the crude extracts, isolated compounds, and essential oils using DPPH radical-scavenging assay;
ix. To investigate the anti-acanthamoeba activities of the crude extracts by the dilution method in a 96-well polystyrene microtiter plate;
x. To evaluate the cytotoxicity properties of the crude extracts against MDCK cells using the micro-tetrazolium (MTT) test;
xi. To investigate the cytoprotection properties of the extracts against influenza types A and B viruses /Puerto Rico/8/34 (H1N1) using MTT assay;
xii. To inspect the *in silico* molecular docking profile of the isolated compounds against four bacterial (DNA gyrase B of *E. coli*, pyruvate kinase of *S. aureus*, *P. aeruginosa* PqsA, and 10782 streptopain of *S. pyogenes*), and two human (myeloperoxidase and topoisomerase II α) protein targets using molecular docking softwares;
xiii. To predict the drug-likeness ADME, and toxicity profiles of the isolated compounds using SwissADME, and Pro Tox II web tools, respectively;

1.5. Significance of the Study

In Ethiopia, the phytochemical studies and pharmaceutical industries are at their infant stage and have yet to mature. That is, much of the efforts so far have focused on nurturing the feedstock

market, i.e., the inputs needed for pharmaceuticals. Of the companies registered for large-scale commercial development of pharmaceuticals, very few are in operation. Most of the firms in operation are still very young and detailed records of costs of production and inputs use couldn't be found. Thus, the data obtained from this research can be used in the documentation of the bioactive compounds along with their medicinal values. Likewise, the findings of this study might convey an important record of transforming the traditional relevance of the studied plants into modern and scientific usage. Furthermore, this research may be used in introducing alternative sources of drugs from the extracts of the various parts of the plants that have been studied in this work. This provides a significant impute in bridging the gap between modern and traditional medicine.

CHAPTER TWO

2. LITERATURE REVIEW

Plants have existed on earth for many years and have grown resourceful chemical factories to persist endogenous and exogenous stresses. They are composed of chemical substances known as natural products or secondary metabolites to accommodate ecological changes without disturbing their cellular, physiological, and developmental processes (Adedeji and Babalola, 2020). To date, plenty of natural products are documented in the field of Natural Products Chemistry which are primarily involved in the defense mechanism in plants against biotic and abiotic stresses. These phytochemicals are also essential signals in mediating plant communications with symbiotic microorganisms and attracting pollinators. Plant natural products are stored at cellular, tissue, and organ levels through diverse biosynthetic pathways (Yang *et al.*, 2018). This chapter introduces the history of medicinal plants and their natural products in drug discovery, and entirely narrates the ethnobotanical uses, phytochemistry, and some reported biological and pharmacological activities of the studied medicinal plants which support their traditional applications.

2.1. Traditional Medicinal Plants and Modern Medicine

Considerable number of drugs in today's market are natural products and their derivatives. Latest literature surveys showed that 39.1% of all Food and Drug Administration (FDA) registered medicines are of natural product origin, and nearly half (48.6%) of cancer drugs approved today are natural products or derived from them (Boy *et al.*, 2018). The existence of more than 0.2 million metabolites of natural origin presenting numerous biological activities proves the prominence of natural products in novel drug discovery (Boy *et al.*, 2018). Natural products exhibit a broad array of diversity with multi-dimensional structures. Meanwhile, the use of natural products as therapeutic function modifiers has also got great attention. Afterwards, they were effectively used in the development of novel drugs and possessed a far-reaching effect on chemical biology (Hong, 2011). Over the past decades, the large structural variety of natural products has been recognized from a physical chemistry point of view. Their efficiency is related to the diversity of their organized three-dimensional structures, which offer many benefits in terms of the selectivity and efficiency of molecular targets. The discovery of artemisinin and its analogs have been one of the successful examples of drug development from natural products that are currently

in wide use against malaria. This reveals how natural product-based researches have made a momentous contribution to the development of modern drugs (Muschietti *et al.*, 2013).

Since time immemorial, infectious diseases become major health problems worldwide. Antimicrobial resistance and lack of effective medicines are among the major reasons that exacerbate the emergence of new pathogens which cause morbidity and mortality, and thus serious public health problems. Nowadays, pharmacological studies focus on nurturing novel medications to tackle infectious diseases though further investigations are yet to be achieved. Due to their low cost, availability, and few side effects, drugs of plant origin are in special need to minimize the threats of infectious diseases (Assob *et al.*, 2011). The armamentarium of the current antiviral drugs includes about 40 compounds that have been formally approved for clinical applications. Most of the drugs date from the last 5 years, and 50% of them are used against human immunodeficiency virus (HIV) infections. The remaining antiviral drugs that are presently in use are mainly used for the treatment of herpes simplex virus (HSV), hepatitis B virus (HBV), cytomegalovirus (CMV), varicella-zoster virus (VZV), influenza virus, hepatitis C virus (HCV), and respiratory syncytial virus (RSV) infections (De Clercq, 2004).

Due to their significance in defending cancer and the diversity of potential compounds offered by them, plants constitute significant roles in cancer medications which are directly or indirectly obtained from this flora, or medications inspired by facts related to natural products (Fridlender *et al.*, 2015). For example, the terpene paclitaxel from *Taxus baccata* and Vinca alkaloids from *Catharanthus roseus* are among the effective anticancer medications originally derived from plants (Cragg and Newman, 2013). In the time between 1981 and 2002, the use of natural products in the discovery of novel drugs particularly in the search for new chemical structures revealed conspicuous achievement. In that time of two decades, drugs developed from natural products have been substantial. That is specifically accurate in the case of antihypertensives, where approximately 64% of newly discovered medicines have been derived from natural product principles (Ngo *et al.*, 2013). Considering their unique chemical varieties and mechanisms of action, plant natural products remain to play a fundamental role in various drug discovery and research programs. Eventually, those plant-derived active principles have undergone meaningful and interesting advances in their ability to interrelate with numerous biological targets, and some

of them have become important medicines in different healthcare systems (Zhu *et al.*, 2012). For instance, among the 69 novel drugs approved between 2005-2007 globally, 13 were derived from natural products, which underlines the significance of such products in drug development and research (Ngo *et al.*, 2013).

Notably, many plant-derived drugs in clinical medicine today originated from traditional medicine (TM, Table 1). In addition, it has been revealed that the various efficient drugs obtained from plants were developed following their relevance in TM (Parasuraman *et al.*, 2014). Artemisinin (**8**), tetrahydropalmatine (**9**), tetramethyl-pyrazine (**10**), puerarin (**11**), costunolide (**12**), and gastrodin (**13**) were among the drugs isolated from herbal medicines which follow the traditional uses (Jiang *et al.*, 2015, Qian *et al.*, 2014, Wei *et al.*, 2012, Yuan *et al.*, 2016, Zhao *et al.*, 2012, Zhong *et al.*, 2014). Two decades ago, a detailed study of scientific reports regarding the pharmacopeias of developing and developed nations, and the associated world was performed as part of the WHO's TM program. That study intended to investigate whether TM had inspired modern drug developments or whether there was any relationship between the present utilization of various compounds and their uses in TM. The study focused on different compounds used as drugs from plant origin in many countries, and it verified that TM had played an important role in the discovery of novel drugs. The study focused on 122 compounds, 80% of which originated from 94 plant species, and were found to be related to therapeutic effects in folk medicine (Parasuraman *et al.*, 2014).

Table 1: Drugs isolated from the Chinese herbal medicines which follow the traditional uses.

Plant origin	Drug name	Chemical structure	Effects	References
Artemisia annua	Artemisinin (**8**)	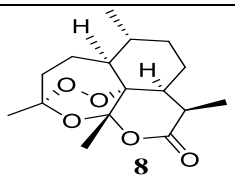 **8**	Anti-malarial	(Zhao *et al.*, 2012)
Corydalis yanhusuo	Tetrahydropalmatine (**9**)	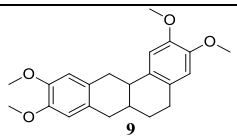 **9**	Analgesic	(Jiang *et al.*, 2015)
Ligusticum chuanxiong	Tetramethyl-pyrazine (**10**)	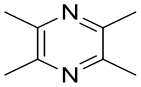 **10**	Myocardial ischemia-reperfusion injury	(Qian *et al.*, 2014)
Pueraria lobata	Puerarin (**11**)	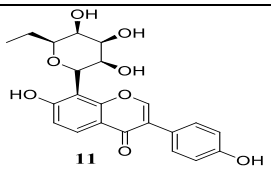 **11**	Diabetes	(Zhong *et al.*, 2014)
Saussurea lappa	Costunolide (**12**)	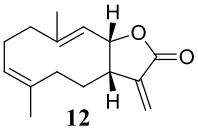 **12**	Anti-gastric ulcer	(Wei *et al.*, 2012)
Gastrodia dlata	Gastrodin (**13**)	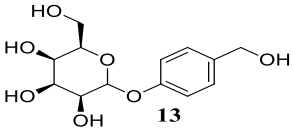 **13**	Anti-convulsion, analgesic	(Yuan *et al.*, 2016)

2.2. Botanical Description and Distribution, Ethnomedicinal Uses, Phytochemistry and Biological Activities of the Studied Plants

Human beings always depend on plants for their basic needs and have naturally learned the various applications of plants. In nomadic roaming, this state of knowledge was swapped with neighboring people, friends, and tribes, and was gradually extended. Therefore, the knowledge of plants has been broadened worldwide, and the actual plants themselves have spread throughout as well. The study of plants and their applications is one of the most basic human concerns and has been experienced by all cultures of mankind since immemorial, though it wasn't considered an 'ethnobotany'. The theory of ethnobotany was coined by J. W. Harshberger (US botanist) in 1895. It was coined with two terms i.e., "ethno", and "botany" which means “study of people”, and “study of plants”, respectively. Thus, it is the study of the relationship between people, and plants. The relationship between human cultures and plants is not limited to the application of plants for basic

needs but also includes their unlimited uses for health care, ornamentation, and religious ceremonies (Pandey and Tripathi, 2017). The emphasis of ethnobotany is on how plants are used, perceived, and managed in human cultures, and includes plants employed for food, divination, medicine, dyeing, cosmetics, textiles, currency, building, tools, rituals, clothing, music, and social life. Plants play an important part in every aspect of our daily lives and life is impossible without them (Pandey and Tripathi, 2017).

In the following review of literatures, the botanical description, and ethnomedicinal uses of the studied plants (*Cyphostemma adenocaule, Delonix regia, Senna siamea, and Ziziphus spina-christi*) along with their phytochemical constituents and pharmaco-biological activities are conferred.

2.2.1. Botanical description and distribution

The botanical description of plants provides evidence about the plant's classification, habits, habitat, structure, properties, and biochemical processes. This enables to study the botanical and ecological properties of plant species prior to further steps. In this sub-topic, the botanical descriptions and distributions of the studied medicinal plants are addressed to recognize their location and ecological properties.

2.2.1.1. *Cyphostemma adenocaule* (Steud. ex A. Rich.)

The genus *Cyphostemma* (Vitaceae), includes approximately 259 taxonomically recognized species of prostrate, erect, or climbing perennial shrubs, or herbs with or without tendrils, distributed in the tropics and subtropics of the world (De Sousa *et al.*, 2011). *C. adenocaule* (Figure 2A) is one of the most popular species of the genus *Cyphostemma* which is grown in many parts of Africa, i.e. Ethiopia, Angola, Nigeria, Eritrea, Ghana, Uganda, Congo, Senegal, Malawi, and Mozambique (Bello *et al.*, 2019, Ochwang'i *et al.*, 2014). In Ethiopia, the plant has different vernacular names, in which it is called Hareg-Temen (Tigrinya), Aserkuh-Aserkush (Amharic), and Hida-Bofa (Afan Oromo) (Abebe *et al.*, 2021). The plant is widespread in the bush land, grassland, and savanna regions of tropical Africa and grows with or without scattered trees in granitic rocks, rainy and gallery forests, sandy river-banks, secondary forests, and abandoned cultivations as well (Bello *et al.*, 2019). *C. adenocaule* is a herbaceous climber with an annual

stem thrown up from a large fleshy perennial rootstock with a branched tendril and slightly fleshy 5-foliolate leaves. Flowers are red, and yellow green, and is an extremely variable species, varying from non-glandular to densely glandular, and glabrous to densely pubescent (Ochwang'i *et al.*, 2014).

Figure 2: Pictures of the studied plants. A; *C. adenocaule*, B; *D. regia*, C; *S. siamea*, D; *Z. spina-christi*. (Picture by Hadush G., October, 2021-July, 2022, Adama, Ethiopia).

2.2.1.2. *Delonx regia* (Boj. Ex. Hook)

D. regia (Figure 2B) belongs to the Fabaceae and Caesalpinioideae family and subfamily, respectively. Up to date, eleven species have been discovered in the genus *Delonix*, nine species occur as endemic to Madagascar, one is found in Northeast Africa, and the remaining one species is located from India to East and Northeast Africa (Rivers *et al.*, 2011). In Ethiopia, the plant is called Ye-Dire Dawa Zaf (Amharic) (Fenetahun and Eshetu, 2017). It is a higher tree, approximately 10-15 m high, and possesses many branches with an umbrella-shaped crown. It has light green, feathery leaves with 10-25 pairs of pinnae, each possessing 12-40 pairs of small leaflets. The twigs have 15-30 cm long corymbs, each having slightly sweet-smelling orange to red flowers, appearing between May and June (Sharma and Arora, 2015). The plant is native to Madagascar and has been broadly planted for the last fifteen decades as a garden and avenue tree in both moist and dry areas of tropical India. It is widely distributed in countries like Egypt, Sudan, Kenya, Uganda, Nigeria, Ethiopia, Tanzania, Brazil, Burkina Faso, Eritrea, India, Singapore, Cyprus, Jamaica, Sri Lanka, Mexico, South Africa, and the United States of America. It grows slowly and sparsely in locations with both high and scanty annual rainfall (Orwa *et al.*, 2013).

2.2.1.3. *Senna siamea* (Lam.) H. S. Irwin and Barneby

S. siamea (synonyms *Cassia siamea*, Figure 2C) is an angiosperm plant native to Southeast Asia (Malaysia, Burma, Japan, Ceylon, Thailand, India, and Sri Lanka) and distributed in wide areas of Africa (Ethiopia, Cote d'Ivoire, Kenya, Eritrea, Nigeria, Ghana, Malaysia, South Africa, Sierra Leone, Uganda, Tanzania, Zambia, and Togo), in Oceania (Fiji and Australia), and Latin America (Chile, St Lucia, Cuba, Trinidad and Tobago, Antigua and Barbuda, and St Vincent and Grenadines) (Kamagaté *et al.*, 2014, Thongsaard *et al.*, 2001). It was initially categorized in the Caesalpiniacae family, then in Leguminoseae, and now in the Fabaceae family (Veerachari and Bopaiah, 2011). *S. siamea* is about 10-12 m tall, sometimes growing up to 20 m. The young bark looks smooth and grey and later exhibits longitudinal properties. The leaves are about 15-30 cm long with 6-14 branches of leaflets, and the flowers are yellow and about 60 cm long with pyramid-shaped panicles. It has flat fruits 5-30 cm long which are confined between the seeds. The seeds are greenish-brown, bean-shaped, and 8-15 mm long (Haba *et al.*, 2000, Kamagaté *et al.*, 2014). The plant has various vernacular names. It is called Yeferenj digita (Amharic) in Ethiopia, Oyieko, and Ndek obino in Kenya (Owuor and Kisangau, 2006), Bikini raskata in Nigeria, Casse du siam

in France, Flamboyan amarillo in Spain (Otimenyin *et al.*, 2010), Angkanh in Cambodia, Kassod, Minjri, Ponavari, Kilek in India (Prasad *et al.*, 2010), Johar, Bujuk in Indonesia, Criminal in Nepal, Robles in the Philippines, Yellow cassia, Shower Thailand, Kassod tree, Thai pod copper, Khilek-yai in Thailand, and Humbo in Vietnam (Prasad *et al.*, 2010).

2.2.1.4. *Ziziphus spina-christi* (L.) Desf.

The genus *Ziziphus* in the Rhamnaceae family comprises about 100 species of evergreen trees and shrubs widely found all over the tropical and subtropical parts of the world. *Z. spina-christi* (Figure 2D), locally known as Gaba (Amharic and Tigrinya) and Qurqura (Afan Oromo) is among the well-known species of the genus which is about 5-10 m tall with a trunk diameter of 45 cm. The color of the bark changes from white-brown to pale gray, and the leaves are curly and simple with 1-9 cm length, and 1-3.5 cm width. The flowers are found at the top of the leaves with a small greenish-white color. The fruits are reddish-brown with a diameter ranging up to 1.5 cm and contain a solid seed around them with a sweet-tasting pulp, and thrive from October to April (Singh *et al.*, 2012). The tree is native to vast areas of Africa (Kenya, Chad, Eritrea, Djibouti, Ethiopia, Tunisia, Mali, Libyan Arab Jamahiriya, Nigeria, Senegal, Mauritania, Algeria, Somalia, and Zimbabwe) and exotic to India, Comoros, Egypt, Israel, Iran, Madagascar, Iraq, Netherlands, Jordan, Syrian Arab Republic, Morocco, Zanzibar, Saudi Arabia, and United Arab Emirates. It is very resistant to heat, drought hardy, and able to grow in desert regions with even 100 mm annual rainfall. It prefers rivers, edges of ponds, and groundwater-containing areas. The plant is frost-tender and can survive for up to 8-10 months of dry season (Rojas-Sandoval, 2019).

2.2.2. Ethnomedicinal uses

2.2.2.1. *Cyphostemma adenocaule*

Plants in the genus *Cyphostemma* have long been used in human remedies to cure various diseases, including inflammation, tumors, rabies, malaria, snake bite, toothache, kwashiorkor, and marasmus in children (Bitew *et al.*, 2019, Teklay *et al.*, 2013). Reports also revealed that the herb is used in traditional pharmacopeia against many infections, such as bloody diarrhea, syphilis, and urinary tract infections (Chouna *et al.*, 2016). *C. adenocaule* was reported as one of the most important medicinal herbs to treat blackleg in Oromia, Ethiopia. The roots of *C. adenocaule* are powdered and boiled with the pounded roots of *Verbascum sinaiticum*, *Rumex abyssinicus*, and

Rumex nepalensis and given orally to the animal to treat blackleg (Kefalew *et al.*, 2015). Traditional healers in Amhara, around Gondar City, Ethiopia use the boiled roots of the plant, mix it with milk, and the filtrate is orally administered before food to treat rabies (Birhanu *et al.*, 2015). In Tigray, Northern Ethiopia, the fresh roots of *C. adenocaule* are crushed, and boiled with water, and the filtrate is drunk orally to treat snake bites (Yirga *et al.*, 2011). In Tanzania, traditional medicines have been prepared from the leaves of *C. adenocaule* to treat pneumonia, cough, and sore throat. In addition, the aerial parts are macerated in water and used for skin medications. In East Africa, Gabon, and Ghana, a paste prepared from the roots is used against abscesses and inflammation (Udegbunam *et al.*, 2013). In Kenya, *C. adenocaule* is applied against colorectal, skin, and breast cancers in which the root bark is boiled, leaves are milled and half a glass of the medicine is drunk orally as an infusion once per day until complete recovery. (Ochwang'i *et al.*, 2014). The traditional applications of *C. adenocaule* in some African cultures are summarized in Table 2.

Table 2: Ethnomedicinal uses and classes of compounds isolated from *C. adenocaule* in some African cultures.

Parts	Country	Mode of preparation	Ethnomedicinal uses	Classes of isolated compounds	References
Roots	Tanzania	Decoction of the roots;	Treatment of appendicitis, hernia, and uvulitis against excessive bleeding;	Tannins and saponins	(Bello *et al.*, 2019)
Leaves	Uganda	Leaves are boiled and the infusion is mixed with local brew and drunk;	Against hookworms and tapeworms	Saponins, tannins, and terpenoids	(Namukobe *et al.*, 2011)
Leaves and roots	Ethiopia	Pounded leaves are boiled and the filtrate is drunk;	Congenital abnormality and rabies;	Terpenoids, tannins, and saponins	(Seble *et al.*, 2015)
Whole plant	Uganda	Infusion is drunk and smeared on the infected area;	Warts, measles, and genital management of hernia;	Tannins	(Kibuuka and Anywar, 2015)
Leaves and roots	Kenya	Decoction of the roots and the leaves are heated and put on the chest as a poultice;	Treatment of swollen abdomen, purgative, and treat pneumonia;	Saponins and tannins	(Bello *et al.*, 2019)
Leaves and roots	DR Congo	Roots are macerated and applied;	To treat tapeworms, headache, and malaria;	Tannins	(Bello *et al.*, 2019)
Fresh roots	Somalia	Roots are boiled and drunk;	Against sterility and dysmenorrhea;	Saponins, terpenoids, and tannins	(Bello *et al.*, 2019)

2.2.2.2. *Delonix regia*

In countries such as Zambia, India, Cameroon, and Bangladesh, many literatures focus on the traditional applications of the plant (Sharma and Arora, 2015). For instance, the flowers of the plant are used as an acid-base indicator, and as a natural color (El-Sayed *et al.*, 2011). Villagers use these flowers to prepare homemade water extracts and in tropical countries, several parts of the tree including the flowers and leaves are used to prepare traditional medicines (Yarnell and Abascal, 2004). Although some researchers have explored its biological activities, there is scanty experimental proof for its traditional usage. Traditional healers in Southwestern Bangladesh use

the flowers of *D. regia* to treat chronic fever (Halim *et al.*, 2007). A decoction of about 250 g of the flowers is prepared with 1.5 L of water and 2 mL of the mixture is continuously taken in the morning and evening for some days. In the Nigerian traditional medicine, the flowers are used against bacterial infections (Ode *et al.*, 2011).

In Tamil Nadu, India, the leaves of *D. regia* have been used to cure arthritis, inflammation, constipation, and hemiplegia. The seeds are applied against pyorrhea; the leaves are roasted, crushed, and wrapped in a cloth and inhaled after the scorpion bite. Infusion of the flowers is used against malarial fever, asthma, and bronchitis (Rekha, 2013). The leaves and fruits are applied against helminthiasis in some regions of Bangladesh, and investigations revealed the use of the two parts in piles and boils (Mohammed Rahmatullah *et al.*, 2010). The bark is used to treat fever in Zambia (Fowler, 2006). Furthermore, the leaves are used as purgatives and possess sparmogenic, and antirheumatic properties. The aqueous and ethanol extracts from the bark show febrifuge and antiperiodic potential and are also used against roundworms (Khare, 2008). The traditional application of *D. regia* extends to the people of Patan, North Gujarat, India. The tree is also included in the list of traditional plants utilized by the people of Cameroon against peptic ulcer. The aqueous extracts of the flowers also play a significant role in the traditional beverages of many African countries (Kamagaté *et al.*, 2014).

2.2.2.3. *Senna siamea*

For many years, *S. siamea* has been used by tropical residents for its numerous medicinal applications (Singh *et al.*, 2013). It is known for its common applications in agriculture and cattle rearing. The flowers, leaves, seeds, stems, and roots of *S. siamea* have been utilized for the treatment of various ailments including malaria, a tropical endemic disease with high mortality (Kamagaté *et al.*, 2014). The most used parts are the leaves which possess ample traditional applications in Asian and African cultures. In Burkina Faso, a decoction from the fresh and dried leaves of *S. siamea* is drunk with lemon juice to cure malaria and liver infections (Nadembega *et al.*, 2011). Similarly, in Togo and Sierra Leone, a decoction of the leaves is administered orally to treat malaria (Koudouvo *et al.*, 2011). In Nigeria, the dried leaves are mixed with pawpaw, lime, and lemon leaves, boiled for an hour, and drunk as tea form to treat malaria (Ogunkunle and Ladejobi, 2006). In Uganda, the leaves are washed, chewed, and the liquid is swallowed against

abdominal problems (Kamatenesi *et al.*, 2011). In India, decoction of the leaves is mixed with honey and drunk three times a day (150 mL) to treat fever and anemia (Sati *et al.*, 2010).

In Thailand, the leaves are dried and sprayed to be commonly taken in tablet form as vegetable, and used as a laxative and sleeping pill (Ngamrojanavanich *et al.*, 2006). Besides, it has been reported that the decoction of the leaves of *S. siamea* is drunk to cure hypertension, toothache, and constipation (Mbatchi *et al.*, 2006). In Benin, a decoction of the roots is applied to treat hypertension, fever, insomnia, and constipation (Allabi *et al.*, 2011). In Kenya, the decoction, and infusion of the mixture of the roots of *S. siamea* and *Z. chalybeum* are used against snake bites (Owuor and Kisangau, 2006). In Sub-Saharan Africa, traditional healers employ the root decoction against diabetes mellitus (Odason and Kolawole, 2007). In addition, the roots are ground and mixed with water and the extract is orally administered to cure sore throat (Kamatenesi *et al.*, 2011). In Côte d'Ivoire, 0.5 L of the decoction of leaves is taken orally twice a day for healing oral and stomach inflammations (Koné and Atindehou, 2008). Small doses of the decoction of the roots are drunk to treat malaria and angina (Swier, 2012). The seeds are applied against intestinal worms and snake bites. The decoction of the mixture of *S. siamea* and *F. thonnigii* fruits is drunk to treat typhoid fever and convulsions in children (Sati *et al.*, 2010). In Sri Lanka, young fruits and flowers are daily consumed to prevent curries and provide laxative and sleeping-aid properties (Kamagaté *et al.*, 2014).

2.2.2.4. *Ziziphus spina-christi*

In Central and Western Sudan, and other Saharan and sub-Saharan countries, fruits of *Z. spina-christi* are used for culinary purposes. Women and children harvest the fruits and sold on local markets which offers an extra source of income for them. Likewise, in Oman, fruits are collected from the wild, planted in local areas, and some years later the fruits given are sold in local markets. The fruits are eaten either freshly or in dried form and their sweet pulp is dried and powdered to yield fine flour (Ads *et al.*, 2017). In addition, various traditional practices of *Z. spina-christi* have been reported worldwide against various health problems (Madani *et al.*, 2021). In Iran, Malawi, and Sudan, traditional practitioners use the leaves, flowers, and roots to treat abdominal pain (Delfan *et al.*, 2015). The plant is also well-known as a source of energy and nourishment. In Bahrain, the leaf extract is used to treat wounds, dandruff, and hair loss (Alalwan *et al.*, 2019), and

in Palestine, they are applied against skin infections (Abou Auda, 2011). People in Turkey use the contents of the fruit's fiber as a remedy for constipation (Tetik *et al.*, 2013). In Nigeria, the roots are used to treat cough. Traditional healers in Sudan use the fruits to cure malaria, diarrhea, antispasmodics, rheumatism, and scorpion stings. Decoction of the leaves and fruits is prepared in water for 30 min, and orally administered three times a day to prevent cancer and increasing cholesterol risks (Abdulrahman *et al.*, 2022). Some ethnomedicinal uses of the studied plants in Ethiopian traditional medicine are depicted in Table 3.

Table 3: Summary of the ethnomedicinal profile of the studied plants in Ethiopia.

Scientific name	Common name	Family	Vernacular name	Parts used	Ethnomedicinal uses in Ethiopia	References
C. adenocaule	Not specified	Vitaceae	Aserkuh Aserkush (Am), Hareg Temen (Tg), and Hida Bofa (AO)	Whole parts	Treats snake bite, malaria, rabies, helminthic infection, and anthrax;	(Abebe *et al.*, 2021)
D. regia	Flame tree, phoenix flower, royal poinciana, and flamboyant	Fabaceae	Ye-Dire Dawa Zaf (Am)	Whole parts	Treats malaria, diabetes, acute bleeding, inflammation, fever, wound, and diarrhea;	(Fenetahun and Eshetu, 2017)
S. siamea	Kassod tree	Fabaceae	Yeferenj Digita (Am)	Whole parts	Used as purgative, against nose bleeding, treat fever, cure intestinal worms, and difficulties of breathing;	(Abdo, 2017)
Z. spina-christi	Christ's thorn jujube	Rhamnaceae	Gaba (Am, Tg) and Qurqura (AO)	Leaves and roots	Used against wounds, dandruff, dysentery, tuberculosis, bronchitis, and cough;	(Ads *et al.*, 2017)

Am; Amharic, AO; Affan Oromo, Tg; Tigrinya.

2.2.3. Phytochemistry

The knowledge of phytochemistry is crucial in drug discovery and repurposing of the existing ones, standardization, and characterization of drugs derived from herbal plants. It is also vital in the evaluation of the toxicity of plants, understanding of the biosynthetic pathways, and screening of intra and interspecific chemical distinctions of plant metabolomics (Egbuna *et al.*, 2018). In this section, the phytochemical makeup of the studied plant species along with the parts and solvents employed to extract the specific compounds are evidently addressed.

2.2.3.1. *Cyphostemma adenocaule*

Although the reports on the phytochemistry of the genus are limited, stilbenes, alkaloids, flavonoids, terpenoids, coumarins, saponins, and tannins have been reported from the different parts and extracts of the herb (Al-Mahweety, 2016, Chouna *et al.*, 2016). Chouna and co-workers (2016) isolated ceanothane-type triterpenoids from the methanol extract of the bark and stem of *C. adenocaule*. Cyphostemmic acid A (**14**), cyphostemmic acid B (**15**), cyphostemmic acid C (**16**), cyphostemmic acid D (**17**), and zizyberanal acid (**18**) were among the reported compounds in the study (Chouna *et al.*, 2016). Another report on the roots of *C. adenocaule* revealed the isolation of *β*-sitosterol (**19**) (Fikadu and Mulugeta, 2022). In the study by Ducrot and co-workers (1998), two oligostilbenes namely cyphostemmins A (**20**) and B (**21**), and other six known stilbene derivatives namely *trans*-resveratrol (**22**), parthenocissin A (**23**), gnetin E (**24**) *ε*-viniferin (**25**), pallidol (**26**), and gnetin C (**27**) were reported from the methanol extract of the roots of *C. crotalarioides* which is a related species of *C. adenocaule* (Ducrot *et al*., 1998). In a recent report from the roots of *C. cyphopetalum* (related species of the present plant), *β*-sitosterol (**19**), *trans*-resveratrol (**22**), *ε*-viniferin (**25**), 3-hydroxy isoagatholactone (**28**), tricuspidatol A (**29**), gnetin H (**30**), parthenostilbenin B (**31**), and *ε*-viniferin diol (**32**) were identified from the roots extract of the plant (Degfie *et al.*, 2022) (Figure 3).

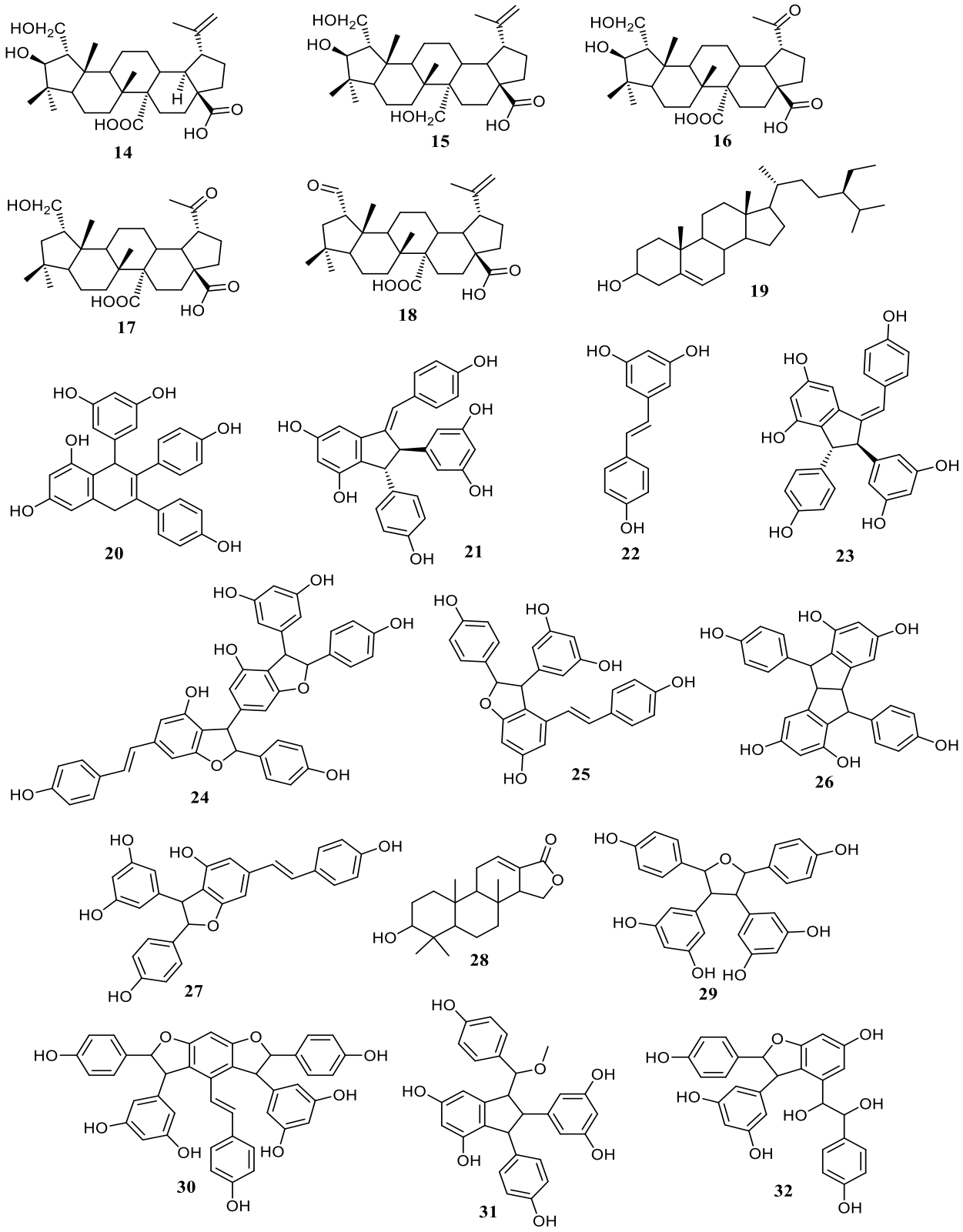

Figure 3: Chemical structures of compounds **14-32** reported from the various parts of *C. adenocaule*.

2.2.3.2. *Delonix regia*

The broad pharmacological activities of *D. regia* are related to the presence of useful phytochemicals in various parts of the plant. The phytochemical investigations of the plant showed that it contains flavonoids, steroids, tannins, saponins, terpenoids, glycosides, alkaloids, sterols, and carotenes (Sama *et al.*, 2011, Shanmukha *et al.*, 2011). A report by Azab and co-workers (2013) showed the presence of glycoside flavonoids such as kaempferol-3-*O*-rhamnoside (**33**), quercetin-3-*O*-rhamnoside (**34**), kaempferol-3-*O*-glucoside (**35**), kaempferol-3-*O*-rutinoside (**36**), quercetin-3-*O*-rutinoside (**37**), and quercetin-3-*O*-glucoside (**38**) in the leaves methanol extract of *D. regia* (Azab *et al.*, 2013). Lupeol (**39**), *β*-sitosterol (**19**), and stigmasterol (**40**) were also among the reported terpenoids and sterols, respectively, from the methanol extract of the stem bark of the plant (Jahan *et al.*, 2010). Reports from the flowers of *D. regia* revealed significant flavonoids such as cyanidin-3-*O*-glucoside (**41**), quercetin (**42**), kaempferol (**43**), and isorhamnetol (**44**) (Adje *et al.*, 2008, Adjé *et al.*, 2012, Veigas *et al.*, 2012). Furthermore, *cis*-ferulate glucopyranoside (**45**) and blumenol C-*O*-*β*-D-glucopyranoside (**46**) were reported from the ethyl acetate extract of the roots (Hosny, 2012), and ursolic acid (**47**) was isolated from the ethanol extract of the flowers of *D. regia* (El-Sayed *et al.*, 2011) (Figure 4).

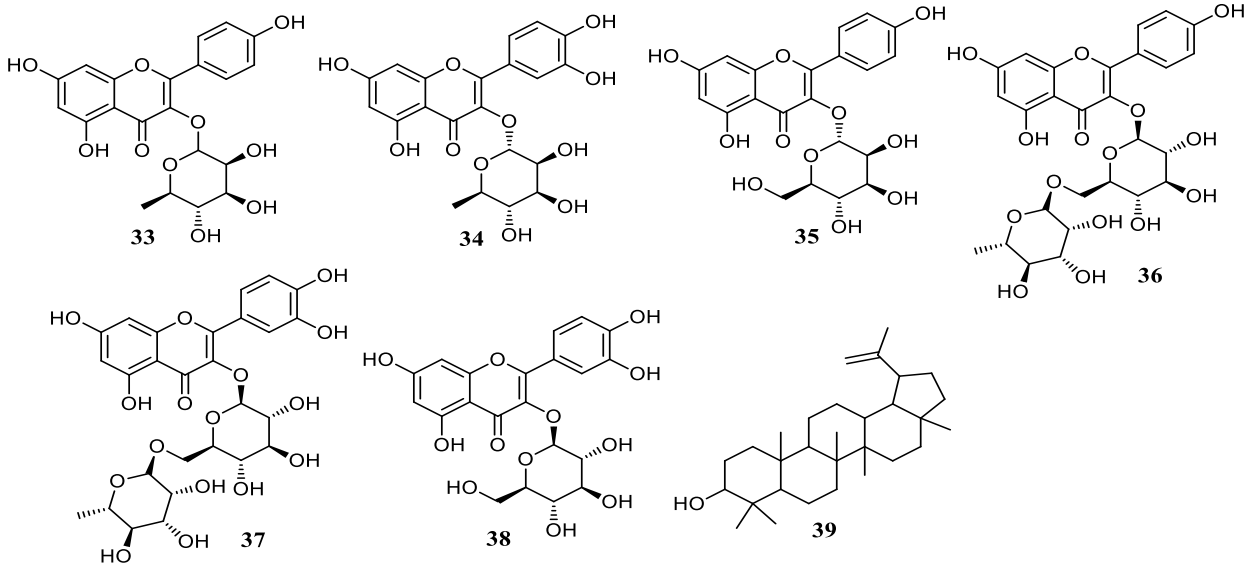

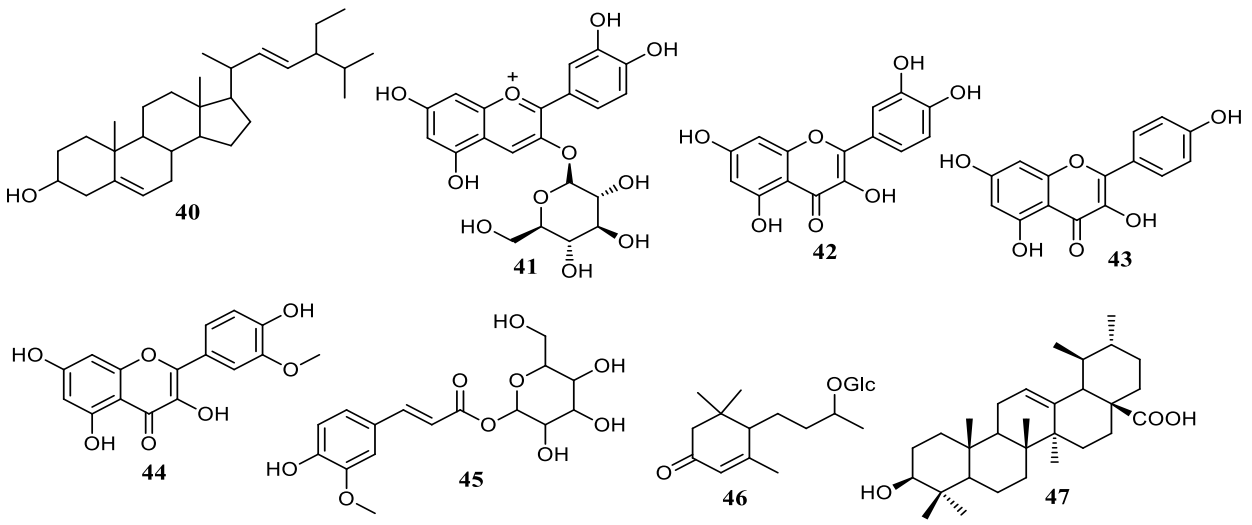

Figure 4: Chemical structures of compounds **33**-**47** reported from the various parts of *D. regia*.

2.2.3.3. *Senna siamea*

The phytochemistry of the genus (*Senna*) is diverse; thereby, the qualitative phytochemical screening of the various parts of *S. siamea* revealed the presence of polyphenols (flavonoids, anthraquinones, tannins, anthrone, bisanthraquinones, isoflavonoids, and phenolics), chromones and derivatives (chromones glycosides, chromone alkaloids, bischromone, and dihydronaphthalenone compounds), steroids, alkaloids, carotenoids, saponins, and reducing sugars (Kaur and Arora, 2010, Mohammed *et al.*, 2013, Smith, 2009, Subramanian and Venugopal, 2011, Veerachari and Bopaiah, 2011). The phytochemical studies on different parts of the plant revealed the presence of various bioactive compounds, including barakol (**48**) (Padumanonda *et al.*, 2006), anhydrobarakol (**49**), and 5-acetonyl-7-hydroxy-2-methylchromone (**50**) (Oshimi *et al.*, 2008) from the chloroform extract of the leaves of *S. siamea*. Cassiarin A (**51**) and B (**52**) (Morita *et al.*, 2007), chrysophanol (**53**), emodin (**54**), physcion (**55**), rhein (**56**), and sennosides A (**57**), B (**58**), C (**59**), D (**60**), E (**61**), and F (**62**) (Koyama *et al.*, 2002), lupeol (**39**) (Adedoyin *et al.*, 2020), and *β*-sitosterol (**19**) (Bukar *et al.*, 2009) were reported from the methanol and ethanol extracts of *S. siamea* (leaves). Betulinic acid (**63**) (Nsonde-Ntandoua *et al.*, 2010), kaempferol (**43**) (M Calderon-Montano *et al.*, 2011), chrysophanol (**53**), and emodin (**54**) (Dave and Ledwani, 2012) have also been isolated from the stem and root barks of the plant. In addition, the *n*-hexane and aqueous extracts of the seeds of the plant afforded stigmasterol (**40**) (Teangpook *et al.*, 2011), and aloe emodin (**54**) (Ahmed *et al.*, 2011b). Furthermore, a report by Kaisoon and co-workers (2011)

revealed the presence of gallic acid (**64**), *p*-coumaric acid (**65**), myricetin (**66**), and quercetin (**42**) in the methanol extract of the flowers of the plant (Kaisoon *et al.*, 2011) (Figure 5).

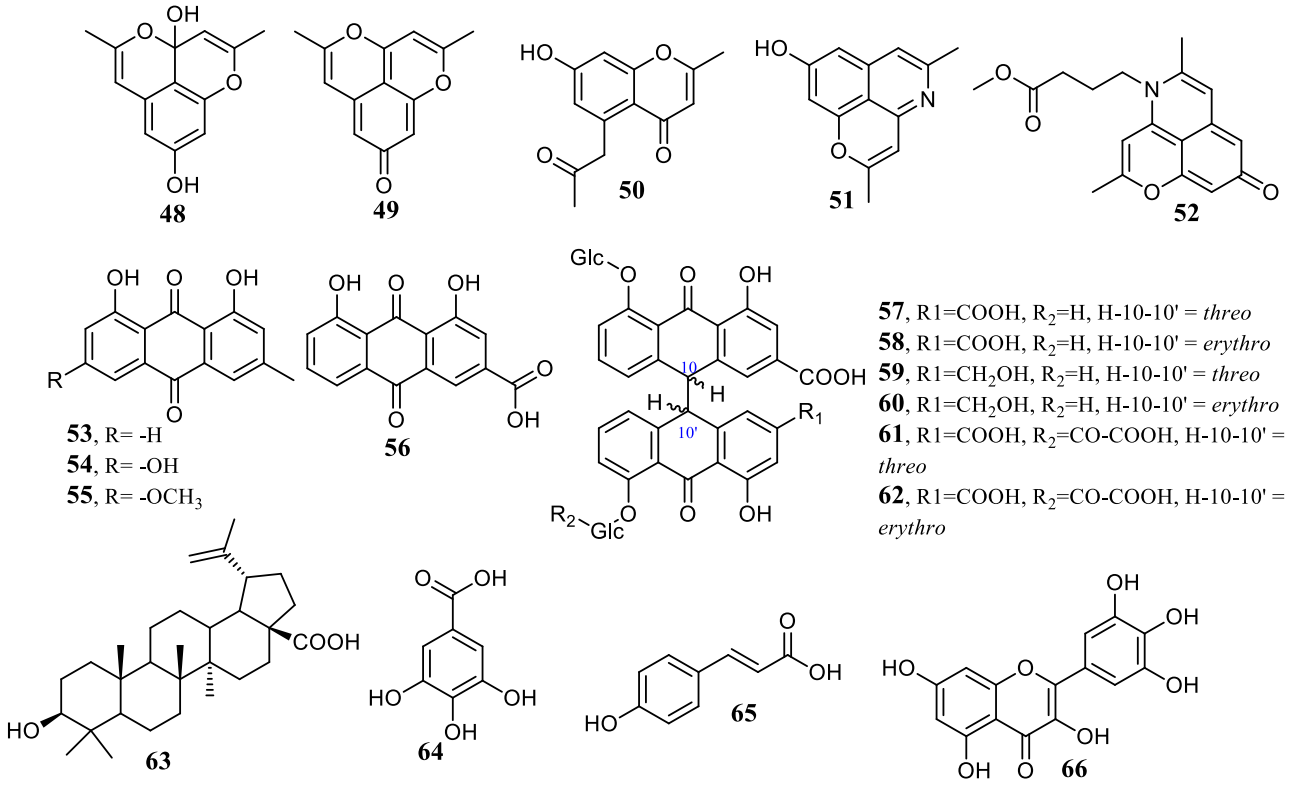

Figure 5: Chemical structures of compounds **48**-**66** reported from various parts of *S. siamea*.

2.2.3.4. *Ziziphus spina-christi*

The phytochemistry of *Z. spina-christi* is broad, consisting of various classes of secondary metabolites mainly terpenoids, flavonoids, saponins, alkaloids, and essential oils (Almeer *et al.*, 2018). Cyclopeptide alkaloids are among the commonly reported compounds of the plant. They are compounds exhibiting polyimide structures with 13-/14- or 15-member rings with neutral or basic side chains (El Maaiden *et al.*, 2020). Accordingly, spinanine B (**67**), and other related compounds were reported from the dichloromethane fraction of the stem bark extract (Abdulrahman *et al.*, 2022). In addition, a new cyclopeptide alkaloid named nummularine U (**68**) was reported from the methanol leaf extract of the tree (Sakna *et al.*, 2019). Mauritine A (**69**), and sanjonine F (**70**) were also among the reported cyclopeptide-type alkaloids from the plant (Sakna *et al.*, 2019, Tuenter *et al.*, 2017).

The quantitative phytochemical investigations of the leaves of *Z. spina-christi* showed a high content of saponins that have commercial applications in the production of shampoo and detergents (Bozicevic *et al.*, 2017). Notably, dammarane (tetracyclic triterpene) (**71**), christinin (**72**) jujuboside B1 (**73**), and lotoside III (**74**) were among the reported saponins from the plant (Abdulrahman *et al.*, 2022, Bozicevic *et al.*, 2017, Sakna *et al.*, 2019). Flavonoids including, spinosin (**75**), kaempferol-3-*O*-rhamnoside (**33**), swertisin (**76**), and myricetin-3-*O*-(6- rhamnosyl) hexoside (**77**) were also reported from various extracts of the plant (Abdulrahman *et al.*, 2022, Ads *et al.*, 2017, Bozicevic *et al.*, 2017, Sakna *et al.*, 2019). The phytoconstituent investigation of the plant is extended to the isolation of terpenoids such as ceanothic acid (**78**), zizyberanalic acid (**79**), granulosic acid (**80**), betulin (**81**), and betulinic acid (**63**) from the various extracts of *Z. spina-christi* (Ads *et al.*, 2022) (Figure 6).

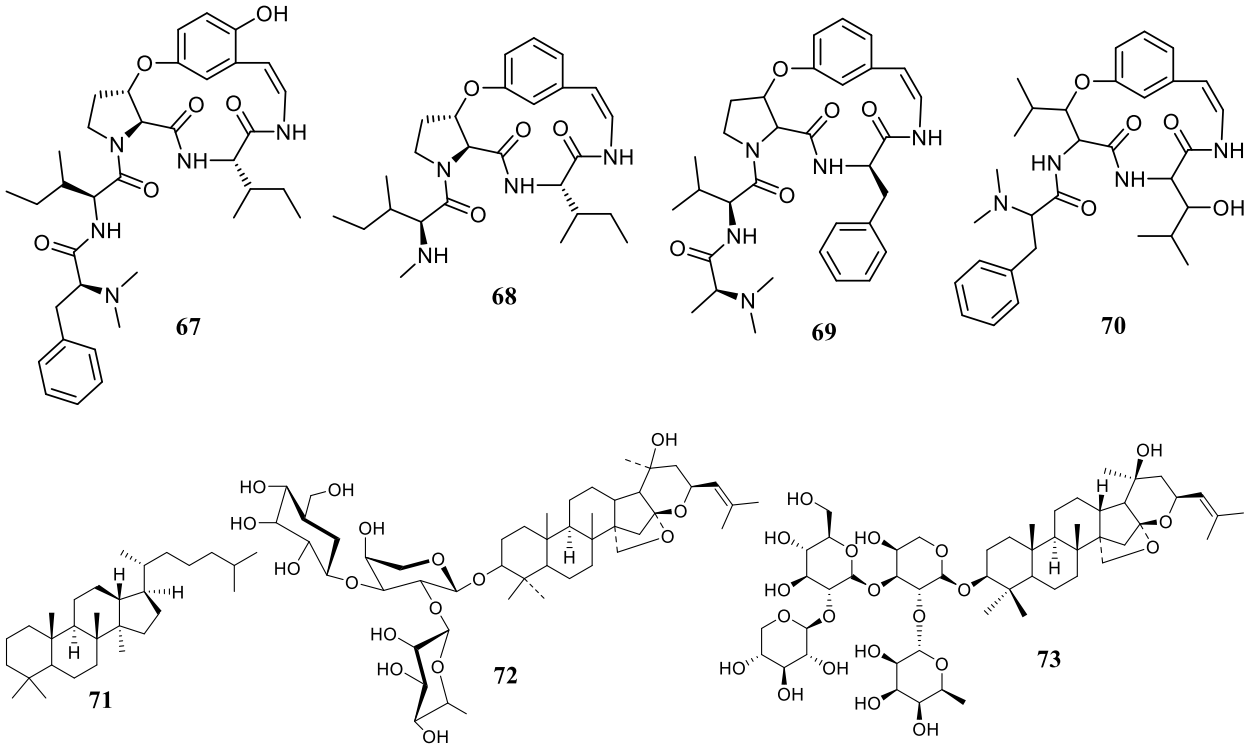

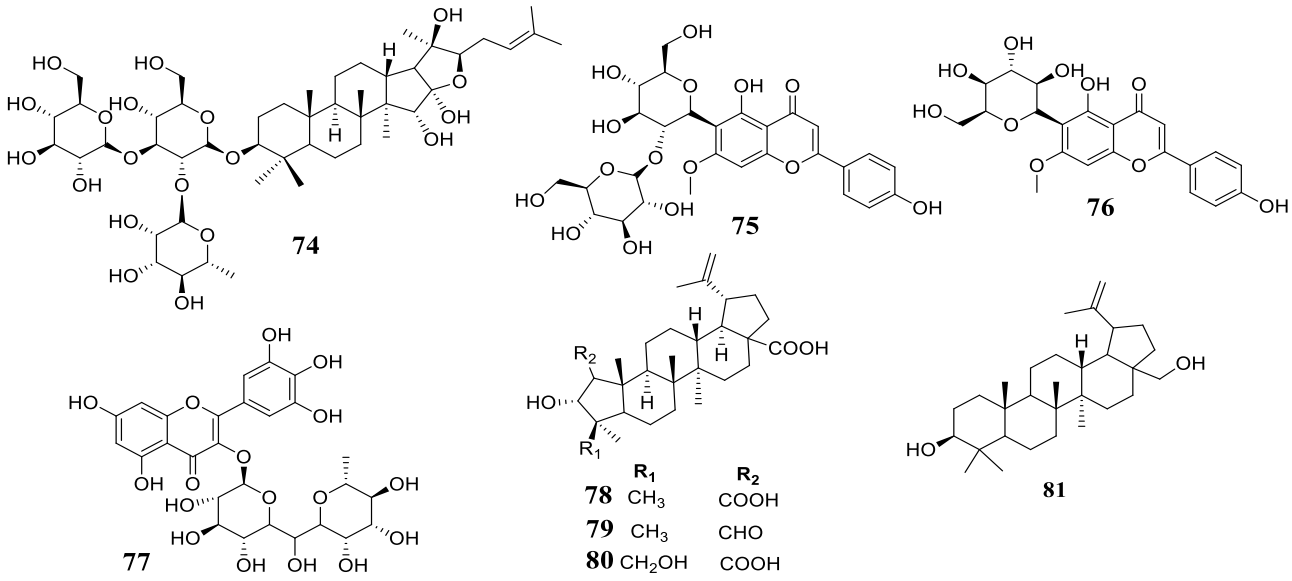

Figure 6: Chemical structures of compounds **67**-**81** reported from the various parts of *Z. spina-christi*.

2.2.4. Biological activities

In pharmacology, biological activity denotes the useful or possible effects of a drug/candidate compound on living organisms. These activities are commonly determined using bioassay techniques and the effects are generally dose-dependent which are evaluated via dose-response curves. The search for phytochemicals that exhibit biological activities is always an attractive research field for scientific teams and centers worldwide. Novel products of natural origin are keenly awaited by the pharmaceutical, health, cosmetics, and food industries. Natural products unveiling potential biological activity are mostly found in higher medicinal plants. Furthermore, fungi, endophytes, lichens algae, and animals comprise valuable sources of these compounds (Ekiert and Szopa, 2023). In this section, proved biological activities of the extracts and isolated compounds of all the investigated plants are reviewed.

2.2.4.1. *Cyphostemma adenocaule*

Although *C. adenocaule* exhibits ample traditional uses, proof of its pharmacological activities is still lacking. It is among the few plants whose medicinal applications and published reports are unsurpassed. The roots are employed to assess antimicrobial activities and inhibit the growth of *S. aureus,* and *S. agalactiae* (Fikadu and Mulugeta, 2022). The herb is also used to treat peptic ulcers.

Chouna and his group (2016) isolated two novel ceanothane-type triterpenoids along with other known terpenoids and tested them *in vitro* for their antiplasmodial effects against the *Plasmodium falciparum* strain. The results displayed poor to moderate activity for the investigated compounds except for 3*β*, 28-dihydroxy-30-norlupan-20-one that exhibited an IC_{50} value of 10.1 μg/mL against the chloroquine-sensitive strain (Chouna *et al.*, 2016). In addition, the DPPH radical scavenging activities of the ethanol extracts of both the leaves and roots of *C. adenocaule* were studied and promising activities were recorded (Feyisayo and Oluokun, 2013). According to the report, the DPPH radical scavenging activity of the extracts was dose-dependent and exhibited quite reducing power. It was noted that the root extracts showed higher scavenging potential than the leaf extract. This was in accordance with the traditional medicinal applications of the plant. Furthermore, the extracts also revealed appreciable anti-inflammatory activity (Feyisayo *et al.*, 2015) (Table 4).

In the study of antibacterial activities towards the various root extracts of the plant by Yakubu and co-workers (2021), the sensitivity assay revealed the highest activity by the chloroform extract against *E. coli* (24.00 ± 0.15 mm) and moderate activity against *S. aureus* (12.50 ± 0.18 mm) at 100 mg/mL. The sensitivity profiles were also promising compared to the activities of the ciprofloxacin standard (31.00 ± 0.75 and 29.70 ± 0.17 mm for *E. coli* and *S. aureus*, respectively) (Yakubu *et al.*, 2021). In the DPPH radical scavenging assay, the methanol extract showed the best activity with an IC_{50} value of 10.87μg/mL. Furthermore, it has been confirmed that the root extracts of *C. adenocaule* possess cytotoxicity effects against the HeLa cervical cancer cell lines. According to the report, the toxicity of three extracts namely, petroleum ether, ethyl acetate, and methanol extracts were subjected to brine shrimps, and the ethyl acetate extract showed high brine shrimp toxicity with an average LC_{50} value of 3.9 μg/mL, and 95% confidence interval (2.3-6.7). Notably, this extract also displayed a higher toxicity profile than the reference drug, cyclophosphamide (LC_{50} = 16.1 μg/mL) which is a common anticancer drug. The methanol extract also showed a toxicity with LC_{50} of 22.1 μg/mL (Matata *et al.*, 2021).

2.2.4.2. *Delonix regia*

Previous biological activity reports on various extracts of *D. regia* showed that the plant is used to treat diabetes, pneumonia, inflammation, jungle fever, blockage, joint agony, joint pain, and viral

infections (Wang *et al.*, 2016). The roots ethyl acetate fractions and leaves methanol extracts of the plant were also reported to exhibit significant anti-inflammatory properties higher than the bark extracts (Wijayasiriwardena *et al.*, 2009). The leaves ethyl alcohol extract of the plant unveiled a strong anti-inflammatory activity at doses of 400 mg/kg compared to a well-known standard drug indomethacin at doses of 10 mg/kg (Shewale *et al.*, 2012). Parul and co-workers evaluated the calming, mitigating, and pain-relieving activities of 70% ethanol extract of *D. regia* barks in carrageenan-actuated rear paw edema models applying the Randall-Sellito technique. In this case, Ibuprofen was used as the medication of choice, and it was concluded that the barks extract showed fundamentally more calming properties than the blossom extract. At long last, it was verified that both the bark and bloom showed essential pain-relieving action (Parul *et al.*, 2014).

Many efforts have been made to study the antibacterial activities of *D. regia* which suggests that working with the Gram-positive bacteria *S. aureus*, and Gram-negative bacteria *E. coli* is quite substantial. The extracts were assessed for their antibacterial performance using MIC via the broth micro-dilution method. The results showed that all the extracts displayed high sensitivity to the bacteria (Karthika and Jayshree, 2013). In addition, the methanol extract exhibited potent effects against *E. coli*, *S. aureus*, *P. aeruginosa*, and *E. faecalis* (Madu *et al.*, 2021). On the other hand, the ethanol extract of *D. regia* revealed considerable antidiarrheal effects toward castor-oil-tested loose bowels in rodents. Castor oil prompts changes in mucosal porousness and electrolyte transport enabling a hyper-secretory reaction (Vivek *et al.*, 2013). The antidiarrheal properties can be correlated to the presence of potential phytochemicals such as tannins and flavonoids in the roses which are capable of inhibiting protein precipitation, and the release of gastrointestinal motility (Sachidananda Swamy *et al.*, 2014).

Various extracts of *D. regia* are suggested to exhibit hepatoprotective properties. Previous tests avowed that the methanol extract of the aerial parts of *D. regia* in CCl_4 attained liver failure in rodents. At 100 and 50 mg/kg doses, the ethanol concentrate and its two fractions were tested for hepatoprotective activities against CCl_4-induced hepatic cell injury in rats. At the higher dose, the flavonoid-containing fraction affirmed a significant hepatoprotection. The properties can be explained by the presence of flavonoid active principles, which can scavenge harmful radicals (Ahmed *et al.*, 2011a). Yusuf and his group performed a study aimed to evaluate the potential

effect of a methanol extract obtained from the leaves and flowers of *D. regia* on liver injury induced by CCl_4 in rats. At last, the finding showed that the extract exhibits hepatoprotective efficacy against CCl_4-induced hepatotoxicity in rats (Yusuf *et al.*, 2023). Furthermore, the flower extracts of *D. regia* have been applied against cancer cells. Recent investigations have proven that the flower extracts possess anticancer activities. Extracts of the plant with silver nanoparticles (AgNps) meaningfully reduced the number of cells treated (Ali *et al.*, 2013).

2.2.4.3. *Senna siamea*

Due to the diverse phytochemicals it contains, it is no surprise that *S. siamea* possesses various pharmacological actions. The main activities include antimicrobial, anticancer or antitumor, antimalarial, antidiabetic, antioxidant, hypotensive, anti-inflammatory, diuretic, antipyretic, laxative, analgesic, anxiolytic, sedative, and antidepressant properties (Kamagaté *et al.*, 2014). Various extracts of the flowers, leaves, and stem barks, of *S. siamea* were tested for their antimalarial properties (Jun *et al.*, 2012). Most of the screened activities were tested *in vitro* on *P. falciparum* pathogens. The tests were investigated on different protozoan strains, among which are multidrug-resistant (K1), chloroquine-resistant (W2), and chloroquine-sensitive (3D7) so that active principles against malaria can be found. The finding showed that the leaves alkaloid fraction revealed higher antiplasmodial effects than the others. This alkaloid fraction, the ethanol, and chloroform extracts of the leaves of the plant exhibited activity against 3D7 with IC_{50} values of 0.24, 7.06, and 2.41 μg/mL, respectively. Cassiarin A (alkaloid) was supposed to exhibit potential antiplasmodial effects (Ekasari *et al.*, 2009).

The potential activities of the leaves and roots of *S. siamea* in the endocrinological system were screened by different methods. The hexane, ethyl acetate, and ethanol extracts of the leaves of the plant were evaluated at the doses of 300, and 150 mg/kg for antidiabetic effects in the alloxan-induced diabetes model. The blood glucose levels were assessed by glucose oxidase-peroxidase (GOD-POD) method for 12 h with 2 h intervals. The results showed that the ethyl acetate extract revealed a significant reduction at both doses compared to the others ($P<0.001$) (Luangpirom and Saenbuaphan, 2006). In addition, the ethanol extract affirms antihyperglycemic and hypoglycemic effects in non-diabetic rats after the introduction of hyperglycemia with 2 g/kg/bw (bw stands for body weight) of glucose food in the first 5 h. Undeniably, this extract taken orally at the doses of

750, and 500 mg/kg/bw significantly decreased the level of blood glucose by 47.29 and 50.32% per hour using glibenclamide (10 mg/kg/bw) as a reference drug ($P< 0.05$) (Jangiti *et al.*, 2013). Furthermore, the roots' aqueous extract administered orally at doses of 1000-3000 mg/kg caused progress in the blood glucose level and body weights within one day in alloxan-induced hyperglycaemic rats (Kumar *et al.*, 2010, Patel *et al.*, 2012).

Various works also reported the antioxidant potential of the plant. The extracts of *S. siamea* which have been screened *in vitro* showed that the plant exhibits considerable antioxidant activities determined using 2,2'-azinobis(3-ethylbenzothiazoline-6-sulfonic acid) (ABTS), *β*-carotene bleaching, and radical scavenging assays (Xu *et al.*, 2008). Kaur and the group reported the DPPH radical scavenging potential of the flowers which showed that the methanol extract (250 μg/mL) scavenged 96% of the DPPH radical. At 500 μg/mL, this extract also scavenged 32.7%, 42.7%, and 64.5% of the $H_2O_2^{\bullet}$, $O_2^{\bullet-}$, and NO radicals, respectively (Kaur *et al.*, 2006).

Notably, further studies on *S. siamea* have focused on its antibacterial effects screened against various bacterial strains with auspicious findings (Majji *et al.*, 2013). Nanasombat and Teckchuen reported that the leaves methanol extract exhibited strong antibacterial potential against *Listeria monocytogenes* and *Bacillus cereus* with MIC values of 20.8 mg/mL and 5.2 mg/mL, respectively (Nanasombat and Teckchuen, 2009). Another finding affirmed that at 400 μg/disc, the hexane extract displayed high effects on *Salmonella typhi, Corynebacterium diptheriae*, *P. aeruginosa, Shigella sonnei*, and *Shigella boydii* (Ali *et al.*, 1999). In addition, the leaves ethanol extracts (500-1000 μg/disc) revealed higher effects than ciprofloxacin (30 μg/disc) against *S. aureus*, and moderate activity against *B. subtilis* (Bukar *et al*., 2009).

2.2.4.4. *Ziziphus spina-christi*

In a hunt for natural antioxidants, the activities of the genus *Ziziphus* and other plants have been the subject of recent studies. Khaleel and co-workers studied the potential antioxidant properties of *Z. spina-christi* in animal models using FRAP, ribosomal degradation, ABTS, DPPH, and *β*-carotene-linoleic acid assays, and the antioxidant effects were screened in all the assessment methods. The finding revealed high antioxidant properties for the radical scavenging activity with IC_{50} values of 24.2, 21.4, and 54.3 μg/mL for the aqueous, methanol, and ethanol extracts,

respectively. In this case, the trapping power of the concentrates was found to be concentration-dependent (Khaleel *et al.*, 2016). In addition, extracts of the plant were tested to be efficient for various types of inflammation-related ailments. This evidenced why these species have been used by traditional practitioners to treat ulcers (Ugwah *et al.*, 2013). Khaleel and the group screened the anti-inflammatory properties of the extracts by protein denaturation method at different concentrations and significant differences were observed in the inhibition of thermally induced protein denaturation for the methanol extract compared to the ethanol extract and the standard at 50, 75, and 100 μg/mL. At the highest concentration (100 μg/mL), the methanol extract revealed better anti-inflammatory activity (95.3%) than the ethanol extract (25.2%) and diclofenac sodium standard (20.2%) (Khaleel, 2018).

The preliminary evaluation of *Z. spina-christi* extracts against various bacterial pathogens affirmed that its activities were potent. In a study by El-Kamali and Mahjoub, the stem bark methanol extract exhibited antibacterial effects against *B. subtilis*, *S. paratyphi* B, and *K. pneumoniae* with a MIC of 12.5, 6.25, and 12.5 μg/mL, respectively (El-Kamali and Mahjoub, 2009). Another report revealed that the ethanol extract showed the highest inhibition zone (18.10 ± 0.10 mm) against *S. aureus* followed by *B. subtilis* (16.10 ± 0.30 mm), and *E. faecalis* (15.40 ± 0.40 mm) (Suliman and Mohammed, 2018). Furthermore, a study conducted by Korji *et al*. (2012) reported considerable activities for the aqueous extract (40%) of *Z. spina-christi* against *E. coli* (20.00 ± 0.00 mm), and *Klebsiella* spp. (20.00 ± 0.00 mm) (Korji, 2012). Thus, it can be noted that *Z. spina-christi* extracts can be used as a valuable source of novel antibacterial compounds. Various findings also revealed that *Z. spina-christi* extracts exhibited antifungal (Ali *et al.*, 2015), antidiarrheal (Adzu *et al.*, 2003), antiparasitic (Godini *et al.*, 2009), antiviral (Alzahrani *et al.*, 2020), antimalarial (Hafiz and Mubaraki, 2016), antidiabetic (Khaleel, 2018), antiobesity (El Rabey *et al.*, 2014), antianxiety (Almeer *et al.*, 2022), and anticancer (Abu-Raghif *et al.*, 2017) properties supported with experimental evidence (Table 4).

Table 4: Summary of reported biological activities of the studied plants.

Plant name	Biological activity	Method employed	Extraction solvent	Parts studied	Results	References
C. adenocaule	Antiplasmodial	*In vitro*	Methanol	Barks and woods	Of the isolated compounds, 3β, 28-dihydroxy-30-norlupan-20-one showed good activity with IC_{50} = 10.1 μg/mL;	(Chouna *et al.*, 2016)
	Antioxidant	*In vitro* (DPPH)	Ethanol	Leaves and roots	The effects were dose-dependent, and showed low reducing power;	(Feyisayo *et al.*, 2015)
	Anti-inflammatory	*In vitro*	Ethanol	Leaves and roots	Both extracts protect membrane red blood cells against hypotonic and heat-induced lyses;	(Feyisayo *et al.*, 2015)
	Antimicrobial	*In vitro*	Methanol	Leaves and stems	The extracts displayed poor activity to inhibition;	(Hamill *et al.*, 2003)
D. regia	Antimicrobial	*In vitro*	Methanol, ethanol, and acetone	Leaves, flowers, and barks	The flowers and leaves methanol extracts (80%) showed MIC of 23 ± 1.30 and 20 ± 0.80 mg/mL, respectively against *P. stutzeri*;	(Shabir *et al.*, 2011)
	Hepatoprotective	*In vivo*	Methanol	Aerial parts	Showed a significant reduction in serum enzymes;	(Ahmed *et al.*, 2011a)
	Anticancer	*In vivo*	Methanol	Leaves	The cells treated with the extract and Dox showed IC_{50} values of 20.40 and 4.15 μg/mL, respectively;	(Azab *et al.*, 2013)
	Antidiarrheal	*In vivo*	Ethanol	Flowers	The extract displayed a dose-dependent effects;	(Shiramane *et al.*, 2011)

Table 4 (continued)						
S. siamea	Antimalarial	*In vitro*	Methanol, chloroform, and aqueous	Flowers, leaves, and barks	The methanol and chloroform extracts showed moderate effects on chloroquine-resistant (W2) with IC_{50} values of up to 10 μg/mL;	(Sanon *et al.*, 2003)
	Antioxidant	*In vitro* (DPPH)	Methanol	Flowers	The 250 μg/mL extract scavenged 96% of the DPPH radicals;	(Kaur *et al.*, 2006)
	Anti-inflammatory	*In vivo*	Ethanol and aqueous	Leaves and barks	The extracts displayed potential activity against rats;	(Ntandou *et al.*, 2010)
	Antibacterial	*In vitro*	Methanol	Leaves	The extract revealed strong activity against *L. monocytogenes*, and *B. cereus* with MIC values of 20.8 and 5.2 mg/mL, respectively;	(Nanasombat and Teckchuen, 2009)
Z. spina-christi	Anti-inflammatory	*In vivo*	Hexane, $CHCl_3$, EtOAc, and MeOH	Roots	In all cases, the extracts exhibited some dose-related effects;	(Abdulrahman *et al.*, 2022)
	Antioxidant	*In vivo*	Methanol	Fruits	The finding revealed that the extract may resist the growth of chronic colitis in rats;	(Almeer *et al.*, 2018)
	Antifungal	*In vitro*	Ethanol and methanol	Leaves	The report showed that the ethanol extract exhibited activities, and can be utilized to treat fungal infections;	(Abdulrahman *et al.*, 2022)
	Antibacterial	*In vitro*	Ethanol and aqueous	Leaves	The extracts revealed significant action against all the tested pathogens;	(Ogbiko *et al.*, 2021)

Thus, based on the above justifications and the vast applications of the selected plants in Ethiopian traditional medicine, we showed a desire to perform this research and offer our findings to the scientific world.

2.3. Antiacanthamoeba, Antiviral, and Cytotoxicity Activities

Acanthamoeba species are amoebaean protozoa found in a wide range of habitats, including air, soil, and water atmospheres. These parasites cause pneumonitis and granulomatous amoebic encephalitis (GAE), skin lesions, chronic lung, and a corneal infection known as *Acanthamoeba* keratitis (AK) (Rusciano *et al.*, 2013). In comparison to the infections triggered by other amoebae, *Acanthamoeba* species can produce cysts within the tissue. The corneal ailment is one of the alarming sight-threatening diseases which affects both healthy and immuno-compromised individuals. In addition, *Acanthamoeba* species can be used as a host for virulent bacteria, including *Legionella pneumophila*, and other infectious microorganisms (Greub and Raoult, 2004). Nowadays, the diagnosis of *Acanthamoeba* disease remains a challenge. Beyond their toxicity, the medications of the diseases are not as active as predicted due to their flexible efficacy on amoeban pathogens. Currently, medications of GAE are lacking and most cases are recognized at the post-mortem stage. Drug resistance against AK diagnosis (combination of a diamidine and a biguanide) has also been reported (Ferrari *et al.*, 2011).

Viral infectious diseases have become the main health problems worldwide causing various deadly diseases including influenza, hepatitis, HIV-AIDS, herpes, and Ebola. Nowadays, the spread and prevention of these infectious ailments is the aim of many researchers targeting to discover novel antiviral drugs. The major routes of viral entry are the oral and respiratory routes and it causes severe diseases. These viruses have become difficult to cure and prevent by drugs and vaccines. It is estimated that nearly 4 million global deaths every year are related to acute respiratory ailments including influenza, pneumonia, and bronchitis (Priya and Kumari, 2017). Influenza viruses have developed resistance to the present classes of medications, signifying their eventual virulence, and can cause more hospitalization and mortality. Although vaccination is the most favored method for influenza treatments, it is related to numerous rates of protection due to incongruities with the prevalent influenza strains and poor absorption (Holmes *et al.*, 2021). Hence, antiviral medications

that specifically target the structural and functional proteins of the influenza virus are also vital for treating and preventing influenza ailments (Hayden and Pavia, 2006). Thus, considering the aforementioned problems associated with the *Acanthamoeba* and influenza infectious, the various extracts of the selected medicinal plants of this study were tested for their efficacy against selected *Acanthamoeba* and influenza strains along with their cytotoxicity profiles.

2.4. *In Silico* Pharmacokinetics and Molecular Docking Study

In the field of drug discovery, poor ADME and high toxicity profile of compounds are the key reasons for the failure of most drug candidates during clinical trials. Hence, a significant aspect of drug development is to screen the main physiochemical and toxicity outlooks in the first steps of drug discovery. The use of computational approaches to predict ADME/Toxicity profiles is a vital stage to investigate the new chemical entities to minimize the wasting of time and cost in drug development. Thus, to advance the quality control of drugs, it is important to predict the absorption, distribution, metabolism, excretion, and toxicity (ADMET) of new compound isolates using *in silico* computational approaches (Guan *et al.*, 2019, Hosen *et al.*, 2017). Plant active principles can be identified using different methods. However, the use of *in silico* computational studies has minimized the time and cost required to bring a drug to the market. The appropriate pharmacokinetic and toxicity profile along with effectiveness are the main factors for an effective medicine in drug discovery. Accordingly, various medium and high throughput *in silico* ADMET screening technologies are currently in use (Bharath *et al.*, 2011, Moroy *et al.*, 2012).

Molecular docking is an important *in silico* approach used to predict the binding orientation of drug candidates (ligands) to their protein targets and to study the activity and affinity of compounds. Thus, docking also plays a substantial role in the field of drug development. It predicts the chosen orientation of a molecule to another molecule after binding to each other to form a stable complex. Knowledge of the chosen orientation is critical to predict the power of binding affinity between two molecules using scoring functions (Gaba *et al.*, 2010). Docking intends to attain an optimized conformation for both the ligand and protein and plays a vital role in supporting important bio-molecular events such as drug-protein, enzyme-substrate, and drug-nucleic acid interactions. Thorough knowledge of the general principles that manage the type of interactions (hydrogen bonding, van der Waals, and electrostatic) between the protein targets and ligands may

provide a basis for designing the specificity and potency of drug leads for a given medicinal target. The practical utilization of this understanding needs structural data for the target of interest and a method for appraising candidate leads (Gaba *et al.*, 2010).

In silico studies including molecular docking and pharmacokinetic profiles of the isolated compounds of the investigated plant materials are very limited. Thus, this study offered a valuable contribution to fill the gap in supporting the *in vitro* biological activities with the *in silico* computational results of the compounds.

CHAPTER THREE

3. MATERIALS AND METHODS

This chapter offered details of the materials and experimental protocols this study utilized. The various chemicals and reagents, apparatuses and instruments, and way of identification of the plant materials along with the details of the experimental methods including the extraction of the plant materials, isolation process of the extracts, extraction, and GC-MS analyses of the essential oils are addressed. In addition, the different experimental procedures employed for the bioassay tests and computational study of the isolated compounds are clearly illustrated.

3.1. Materials

3.1.1. Chemicals and reagents

The research work employed the following chemicals and reagents. *n*-hexane (99.9%, Pentokey Organy, India), petroleum ether (Indenta Chemicals, India), ethyl acetate (99.9%, Sisco Research Laboratories, India), dichloromethane, chloroform, methanol, and DMSO (99.8%, Loba Chemie, India), vanillin (Sisco Research Laboratories, India), ciprofloxacin (Wellona Pharma, India), anhydrous Na_2SO_4, ascorbic acid, Mueller Hinton Agar (Micro express, India), DPPH (98.5%, China), ethanol, distilled water, and silica gel for column chromatography (60-200 mesh, Merck, India) were purchased from the local markets, Addis Ababa, Ethiopia. All the solvents and reagents used were in analytical grade.

3.1.2. Apparatus and instruments

The apparatus and instruments which have been utilized in the study are: mortar and pestle, electric blender (Shanghai Jingke, JK-HSG-100A, China), polyethylene bag, electronic balance, beakers (different size), shaker (Gemmy Industries, VRN-200, Taiwan), filter paper (Whatman No.1 filter paper, 125 mm diameter, India)), column chromatography set up, separatory funnel, vials, oven, stove, heating mantle, TLC plate (thickness; 0.25 mm, size; 20 x 20 cm Aluminum coated with high-grade silica gel, 230–400 mesh, pore size 60 Å, Merck Grade 64271, Darmstadt, Germany), capillary tube, water bath, UV lamp (UV4AC6/2, CBIO Bioscience and Technologies, China), Clevenger's apparatus (Aarson Scientific Works, India), flasks (different size), measuring cylinder, rotary evaporator (DW-RE-3000, China), aluminum foil, glass rod, chromatographic chamber, ruler, pencil, spatula, distillation flask, petri dish, refrigerator, holder, incubator, digital

melting point (Japson-type apparatus, JA90161, India), UV-VIS spectrophotometer (Cecil CE4001, UK), GC-MS (Santa Clara, CA, USA), IR and NMR spectrometers.

3.1.3. Geographical location, collection, and identification of the plant materials

The plant materials were collected from Adama Science and Technology University (ASTU) campus and the mountains of Adama city (located at 8.54°N and 39.27°E, elevation of 1712 m, about 99 km southeast of Addis Ababa. The city is located between the base of an escarpment to the west and the great Rift Valley to the east) (File *et al.*, 2019). The plant materials were collected from two sites. The roots and leaves of *C. adenocaule* were harvested from Kechema mountains (Northwest of Adama City) in October 2021. Whereas, the roots and leaves of *D. regia, S. siamea,* and *Z. spina-christi* were collected from Adama Science and Technology University campus from October, 2021 up to July, 2022. Mr. Reta Regassa (Chief botanist, Hawassa Teachers Training College) in collaboration with Mr. Melaku Wendafrash (Chief botanist, Addis Ababa University) identified the plant materials as *C. adenocaule, D. regia*, *S. siamea*, and *Z. spinachristi* with voucher numbers of HCA003, HDR008, HSS006, and HZS007, respectively. Thereafter, the botanical specimens were deposited at the National Herbarium, Addis Ababa University, Ethiopia.

3.2. Experimental Methods

3.2.1. Experimental sites

Extraction of the plant materials, chromatographic separations, and antioxidant activity tests were done at the research laboratory of the Department of Applied Chemistry, Adama Science and Technology University (ASTU), Adama, Ethiopia. In addition, the antibacterial activity tests of the extracts were achieved at the research laboratory of the Department of Applied Biology, ASTU, Adama, Ethiopia. IR analysis was performed at the Department of Chemistry, Addis Ababa Science and Technology University (AASTU), Addis Ababa, Ethiopia. The NMR spectral data were generated in cooperation with collaborators from the Department of Chemistry, Kenyon College, Gambier, USA, laboratory for functional polymers, Empa Materials Science and Technology, Dubendorf, Switzerland, and Department of Materials Science, National Taiwan University of Science and Technology, Taipei, Taiwan. Conversely, the anti-acanthamoeba and antiviral/cytotoxicity test assays of the extracts were achieved at Walailak University, Thailand, and the Department of Virology, St. Petersburg Pasteur Institute, Russia, respectively.

3.2.2. General experimental procedures

The plant materials were powdered using a grinder (Shanghai Jingke, JK-HSG-100A, China). The powdered samples were macerated using the cold maceration technique on an orbital shaker (Gemmy Industries, VRN-200, Taiwan). For filtration, a Whatman No.1 type filter paper (125 mm diameter, India) was employed. The extracts were concentrated using a rotary evaporator (DW-RE-3000, China). Crude extracts were chromatographed on silica gel (180-200 g, 60-200 mesh) in a column (size; 725 mm) and eluted with an increasing gradient of solvents. In addition, further purifications of fractions were achieved using 30-35 g of silica gel (60-200 mesh) on small columns (500 mm). The purity of fractions was analyzed using TLC (thickness; 0.25 mm, size; 20 x 20 cm Aluminum coated with high-grade silica gel, 230–400 mesh, pore size 60 Å, Merck Grade 64271, Darmstadt, Germany) and UV lamp (UV4AC6/2, CBIO Bioscience and Technologies, China, at 254 and 365 nm). Conversely, UV inactive compounds were detected using a spraying reagent (1% vanillin in ethanol and 2 mL sulfuric acid reagent) followed by direct heating (110 °C) over a stove for 5 min. Melting points were measured using a Japson-type apparatus (JA90161, India), and antioxidant activities were determined using a UV-Vis spectrophotometer (Cecil CE4001, UK) equipped with tungsten and deuterium lamps. The IR spectral data were generated on a Perkin Elmer Bx infrared spectrometer equipped with KBr pellets. The NMR spectra were generated using 400 and 600 MHz Bruker AVANCE type NMR instruments in deuterated chloroform, deuterated methanol, and deuterated DMSO as solvents, and TMS as a reference. The chemical shift (δ) values were conveyed in ppm and referred against the resonance values of the solvents at 2.50 (δ_H) and 39.5 ppm (δ_C) for deuterated DMSO, 3.31 ppm (δ_H) and 49.1 ppm (δ_C) for deuterated methanol, and 7.28 ppm (δ_H) and 77.2 ppm (δ_C) for deuterated chloroform. Furthermore, essential oils were extracted on Clevenger type apparatus (Aarson Scientific Works, India) and the components of the essential oils were analyzed using GC-MS (Santa Clara, CA, USA). For antibacterial activity, an autoclave, incubator, micropipettes (1000 μL), Petri dishes (90 mm), and a hood equipped with laminar airflow and UV radiation were utilized.

3.2.3. Preparation of the plant materials

After collection, the plant samples were washed repeatedly first with tap water and then with sterilized distilled water, and were allowed to air dry for over a month at room temperature without

direct exposure to sunlight. Thereafter, the dried plant materials were pounded using an electric blender and the resulting powders were stored in a polyethylene bag to avoid certain environmental conditions (moisture, air, and other surrounding dust) until required for further use.

3.2.4. Extraction and isolation

Two different parts (leaves and roots) of the plant materials were used for the investigation. The extracts of each plant material were obtained by dissolving in an appropriate solvent using a maceration technique. Generally, about 450-700 g of the powdered plant materials were utilized for the extraction process and similar extraction scenarios were followed for each of them. This section highlights the experimental protocols employed for the extraction of crude extracts and isolation of compounds, further purification techniques utilized, and the schematic workflows for the overall isolation processes of the plant materials.

3.2.4.1. Extraction and isolation of compounds from *Cyphostemma adenocaule*

The pulverized roots of *C. adenocaule* (600 g) were successively extracted three times by maceration technique with 3 L of CH_2Cl_2: CH_3OH (1:1) each followed by equal volumes of methanol for 72 h each with continuous shaking over an orbital shaker at room temperature (Abubakar and Haque, 2020). The extracts were filtered over gravity with Whatman No. 1 filter paper, and the filtrates were concentrated *in vacuo* on a rotary evaporator at 40 °C (Abubakar and Haque, 2020) to generate 22.0 g and 28.0 g of CH_2Cl_2:CH_3OH (1:1) and methanol extracts, respectively. Both extracts exhibited similar TLC profiles in different solvent systems (10%-80% EtOAc in *n*-hexane) and were mixed to give 50 g of extract. The combined extract (20 g) was applied to silica gel column chromatographic separation (180 g silica gel, 60-120 mesh as stationary phase) and eluted with increasing gradient of *n*-hexane: ethyl acetate to chloroform: methanol mixtures successively. A total of 65 fractions (50 mL each) were collected, and their purities were monitored using TLC and UV lamp at 254 and 365 nm. The main fractionation process of the extract failed to generate pure compounds; thereby further purifications were performed for fractions exhibiting promising TLC profiles.

Fractions that showed similar TLC profiles were mixed for further purifications. Accordingly, fractions 1 and 2 (82.5 mg) initially isolated using *n*-hexane were chromatographed under isocratic

conditions with *n*-hexane (33.0 g silica gel) to yield hexadec-1-ene (**82**, 31.5 mg). Fractions 6-9 (43.3 mg) obtained with 20% EtOAc in *n*-hexane were combined and purified using the gradient elution of *n*-hexane up to 30% EtOAc in *n*-hexane to afford palmitic acid (**83**, 8.4 mg). Fractions 10-15 (98.5 mg) collected with 30% EtOAc in *n*-hexane were further purified under gradient conditions (34.0 g silica gel) of *n*-hexane up to 50% EtOAc in *n*-hexane to afford *β*-sitosterol (**19**, 23.8 mg) and *β*-sitosteryl palmitate (**84**, 18.6 mg). Fractions 21-23 (116.2 mg) collected with 50% EtOAc in *n*-hexane were mixed and purified using the gradient elution (33.0 g silica gel) of 20-70% EtOAc in *n*-hexane to yield 3-hydroxy isoagatholactone (**28**, 12.9 mg). The PTLC purification (mobile phase: 40% EtOAc in *n*-hexane) of fractions 24-27 (67.3 mg) which were initially isolated using 70% EtOAc in *n*-hexane yielded diethyl phthalate (**85**, 11.5 mg). Fractions 30-33 (150.4 mg), collected with 75% EtOAc in *n*-hexane were mixed and purified with PTLC (mobile phase: 40% EtOAc in *n*-hexane) to afford *ε*-viniferin (**25**, 32.0 mg). Furthermore, the PTLC purification (mobile phase: 40% EtOAc in *n*-hexane) of fraction 34 (63.0 mg) isolated using 75% EtOAc in *n*-hexane yielded myricetin (**66**, 19.2 mg). Fraction 39 (122.0 mg), isolated with 85% EtOAc in *n*-hexane was subjected to an isocratic elution (34.0 g silica gel) with 80% EtOAc in *n*-hexane to afford tricuspidatol A (**29**, 51.2 mg). Finally, the PTLC purification (mobile phase: 60% EtOAc in *n*-hexane) of fractions 40-42 (61.0 mg) collected with 90% EtOAc in *n*-hexane yielded parthenocissin A (**23**, 15.1 mg) (Scheme 1).

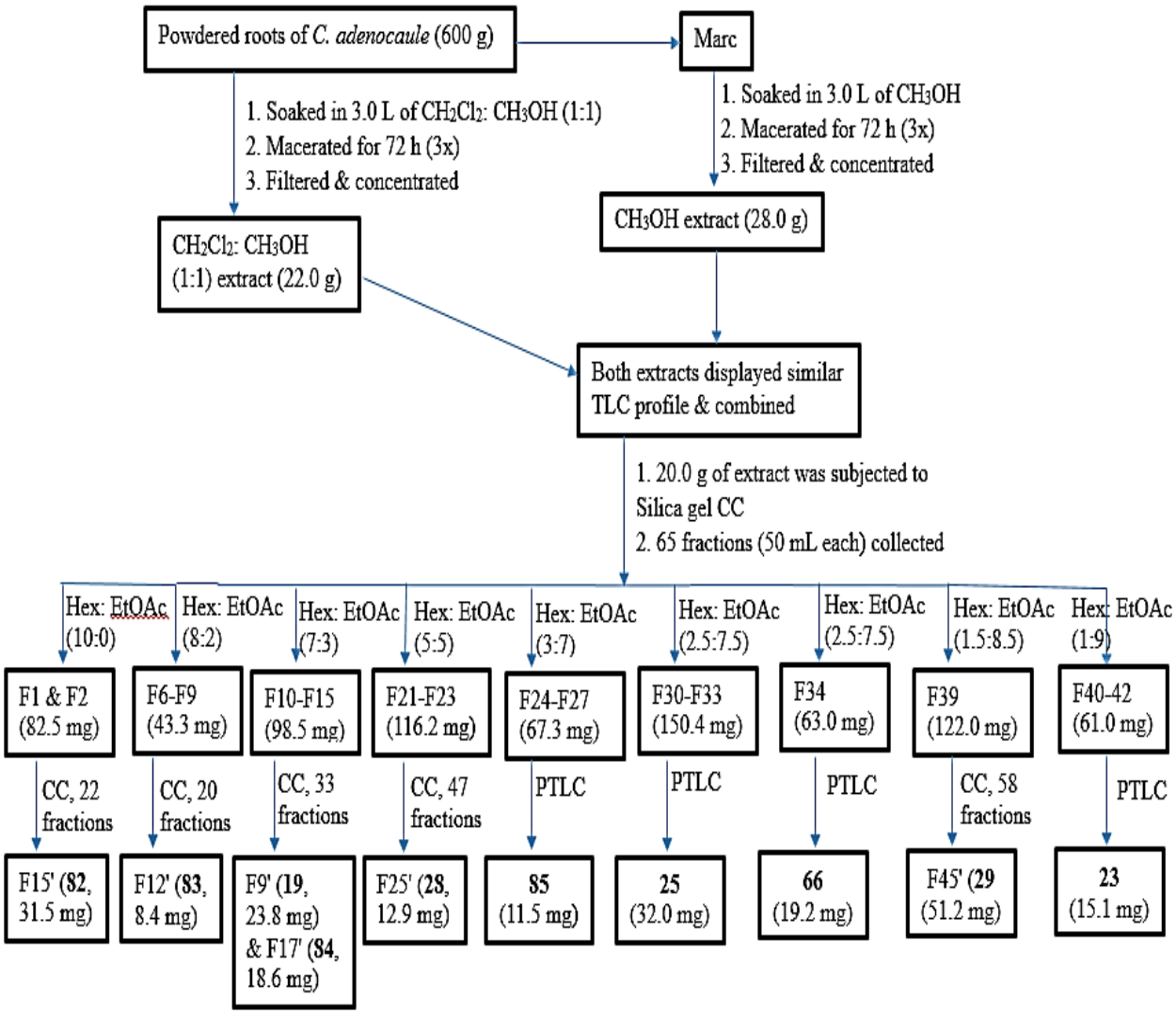

Scheme 1: Extraction, isolation, and purification scenario of the roots of *C. adenocaule*. CC; column chromatography, EtOAc; ethyl acetate, Hex; *n*-hexane, PTLC; preparative TLC.

3.2.4.2. Extraction and isolation of compounds from *Delonix regia*

The powdered roots of *D. regia* (700 g) were first defatted with 3.5 L of petroleum ether to generate 3.4 g of extract. The marc was further extracted three times with equal volumes of CH_2Cl_2: CH_3OH (1:1) and methanol for 72 h each with continuous shaking over an orbital shaker at room temperature. The successive filtration and concentration of the sample materials yielded 7.5 g and 6.5 g of extracts for CH_2Cl_2:CH_3OH (1:1) and methanol, respectively. The CH_2Cl_2:CH_3OH (1:1) and methanol extracts exhibited similar TLC profiles and were mixed. Part of the combined extract (12.0 g) was applied to an open glass column packed with silica gel (200 g silica gel, 60-200 mesh) and eluted with increasing gradient of petroleum ether: ethyl acetate to ethyl acetate: methanol

mixtures successively, to afford 65 fractions of about 100 mL each. The fractions were further purified using silica gel column chromatography and preparative TLC (PTLC) techniques and the pure fractions were sent for NMR analysis.

Fractions were combined based on the pattern (R_f and characteristic color) they showed on TLC. Hence, stigmasterol (**40**, 20.8 mg) was precipitated following the continuous washing of the combined fractions (3-5, 108.3 mg) with methanol which were initially collected with 35% EtOAc in petroleum ether (PE). Subsequently, the addition of methanol to the combined fractions of 6-7 (75.0 mg) eluted with 40% EtOAc in PE precipitated a mixture of *β*-sitosterol (**19**) and stigmasterol (**40**, 23.5 mg). In addition, fractions 12-15 (128.8 mg) eluted with 50% EtOAc in PE displayed similar TLC profiles and were mixed and purified using PTLC (mobile phase: 30% EtOAc in PE) to afford diethyl phthalate (**85**, 15.0 mg) and *β*-sitosteryl-3*β*-glucopyranoside-6'-*O*-palmitate (**86**, 17.8 mg). Further PTLC purification of fractions 20 and 21 (143.7 mg) which were isolated with 65% EtOAc in PE yielded two main yellow bands. The two bands were scratched and dissolved in methanol to afford quercetin (**42**, 23.0 mg), and apigenin (**87**, 5.5 mg). Finally, fraction 55 (43.7 mg) collected with 15% methanol in EtOAc was purified using the isocratic elution with 10% methanol in EtOAc to yield quercetin-3-*O*-rutinoside (**37**, 10.8 mg) (Scheme 2).

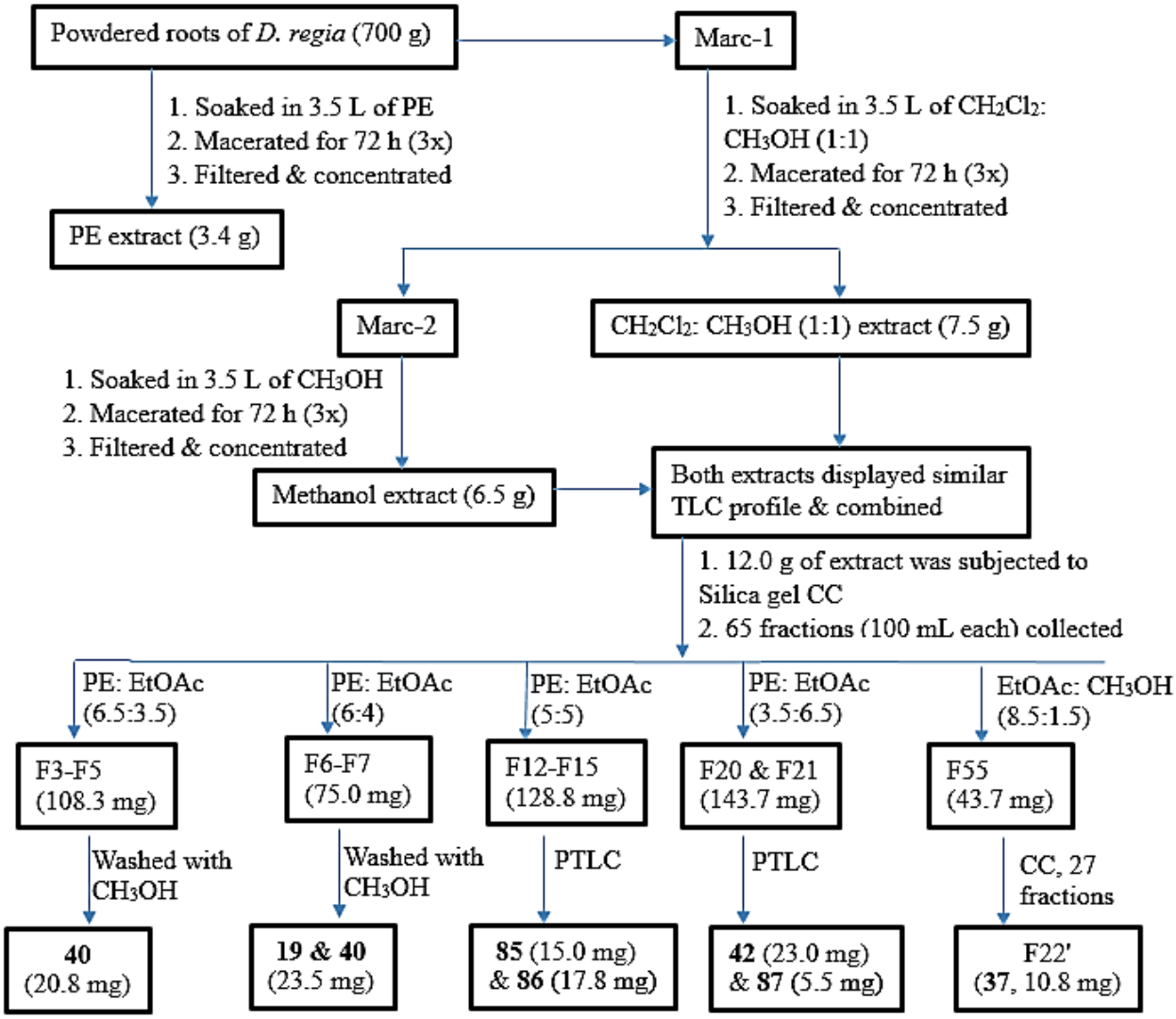

Scheme 2: Extraction, isolation, and purification scenario of the roots of *D. regia*. CC; column chromatography, EtOAc; ethyl acetate, PE; petroleum ether, PTLC; preparative TLC.

3.2.4.3. Extraction and isolation of compounds from *Senna siamea*

The dried powder of the roots of *S. siamea* (700 g) was extracted using 3.5 L of CH_2Cl_2: CH_3OH (1:1) only over an orbital shaker for 72 h three times by maceration technique. The filtered extract was evaporated to dryness on a vacuum rotary evaporator to generate 25.0 g of crude extract. The majority of the crude extract (24.0 g) was adsorbed on silica gel (25 g, 60-200 mesh) and subjected to silica gel column chromatography (200 g, 60-200 mesh). Then, the extract was eluted with an increasing gradient of EtOAc in *n*-hexane, followed by methanol in $CHCl_3$ ratio to generate a total of 75 fractions (100 mL each). The purity of each fraction was monitored using TLC, a UV lamp, and vanillin-sulfuric acid reagent. Fractions with similar TLC profiles were combined and purified,

and their structural information was established using 1D and 2D NMR spectroscopic techniques. Fractions 8-10 (75.2 mg) collected with 25% EtOAc in *n*-hexane were mixed and purified with increasing polarity of *n*-hexane up to 50% EtOAc in *n*-hexane to afford lupeol (**39**, 12.6 mg) and a mixture of *β*-sitosterol (**19**) and stigmasterol (**40**, 23.8 mg). Fractions 15, 16, and 17 (87.5 mg) obtained with 40%, 45%, and 50% EtOAc in *n*-hexane, respectively, were combined and purified with a gradient elution of 20%-70% EtOAc in *n*-hexane to yield chrysophanol (**53**, 10.3 mg) and betulinic acid (**63**, 13.8 mg). Furthermore, fractions 18 (42.5 mg) and 20 (40.7 mg) isolated with 50% EtOAc in *n*-hexane were purified with preparative TLC using 25% EtOAc in *n*-hexane as a mobile phase to afford glyceryl-1-hexacosanoate (**88**, 9.5 mg), and 4-(2'-hydroxymethyl-4'-hydroxyphenyl)-chrysophanol (**89**, 10.2 mg), respectively (Scheme 3).

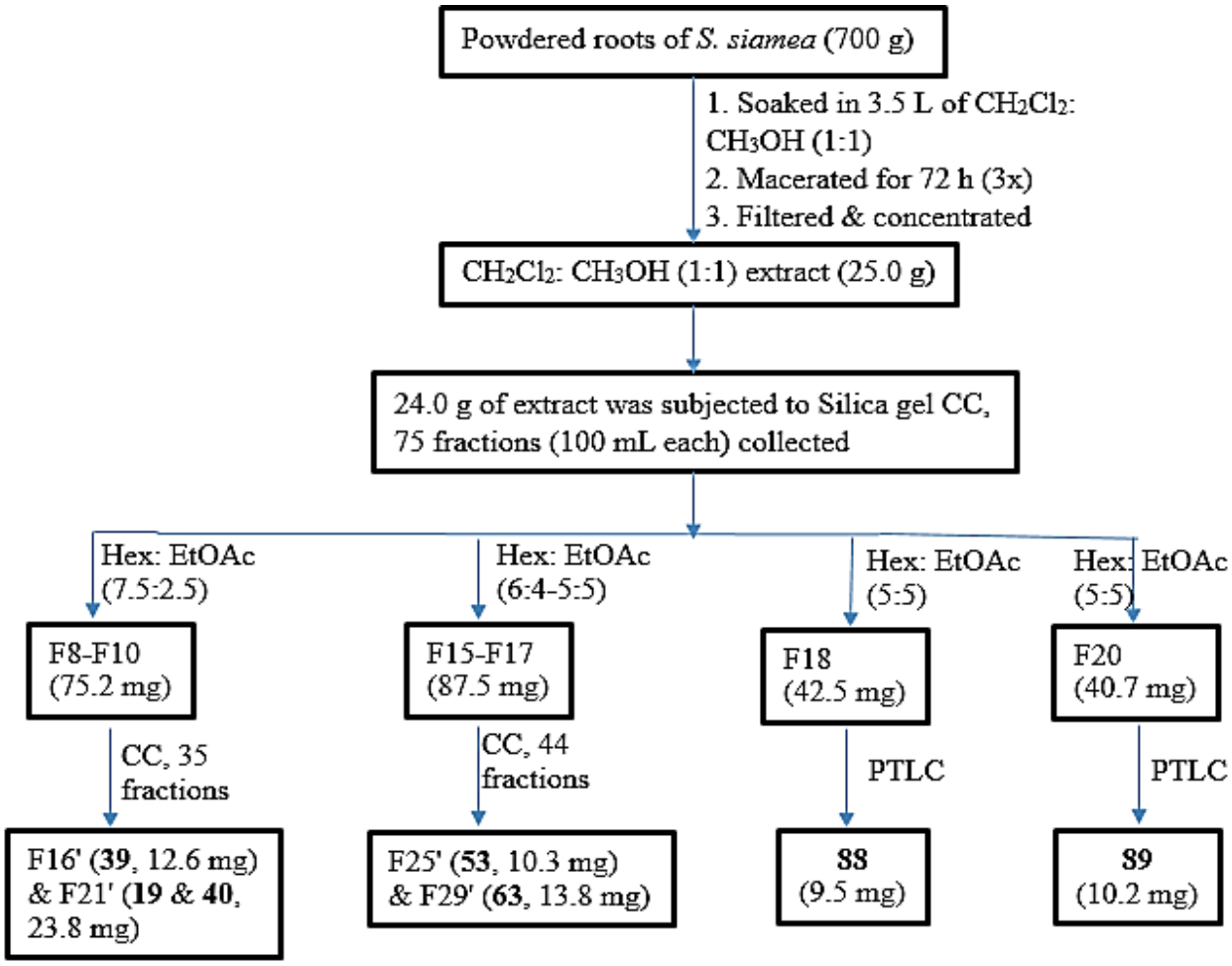

Scheme 3: Extraction, isolation, and purification scenario of the roots of *S. siamea*. CC; column chromatography, EtOAc; ethyl acetate, Hex; *n*-hexane, PTLC; preparative TLC.

3.2.4.4. Extraction and isolation of compounds from *Ziziphus spina-christi*

The air-dried powder from the roots of *Z. spina-christi* (450 g) was extracted in 2.25 L of CH_2Cl_2: CH_3OH (1:1) followed with an equal volume of methanol for 72 h three times each with continuous shaking at room temperature by maceration technique. Filtration and concentration of the extracts were achieved using the common techniques mentioned above. The combined extract (22.5 g) was adsorbed in 23 g of silica gel (60-120 mesh) and chromatographed on an open column containing 180 g of silica gel (60-120 mesh). Then, the extract was eluted with an increasing gradient of ethyl acetate in *n*-hexane followed by methanol in chloroform ratio successively, to offer 175 fractions (25 mL each). Finally, the structural information of the pure fractions was achieved using IR and NMR spectroscopic techniques.

Fractions 25-27 (125.5 mg) obtained with 20% EtOAc in *n*-hexane were combined and purified using the gradient elution of *n*-hexane up to 40% EtOAc in *n*-hexane to afford trimethyl linolein (**90,** 28.4 mg). Fractions 50-62 (321.5.0 mg) isolated using 30% EtOAc in *n*-hexane were mixed and purified with the isocratic elution of 30% EtOAc in *n*-hexane as eluent to afford stigmasterol (**40**, 36.2 mg). In addition, fractions 70-80 (116.3 mg) isolated with 30% EtOAc in *n*-hexane were subjected to gradient elution with 20% EtOAc in *n*-hexane up to 60% EtOAc in *n*-hexane to yield stearic acid (**91**, 36.0 mg mg). Conversely, 13-hydroxyoctadeca-9, 11-dienoic acid (**92**, 22.0 mg) was isolated from fractions 81-94 (143.7 mg) using the isocratic elution of 40% EtOAc in *n*-hexane mixture. Fractions 105-124 (170.5 mg) obtained using 60% EtOAc in *n*-hexane were mixed and purified with the gradient elution of 20% EtOAc in *n*-hexane up to 80% EtOAc in *n*-hexane to afford *β*-sitosteryl-3*β*-glucopyranoside-6'-*O*-palmitate (**86**, 26.4 mg) (Scheme 4).

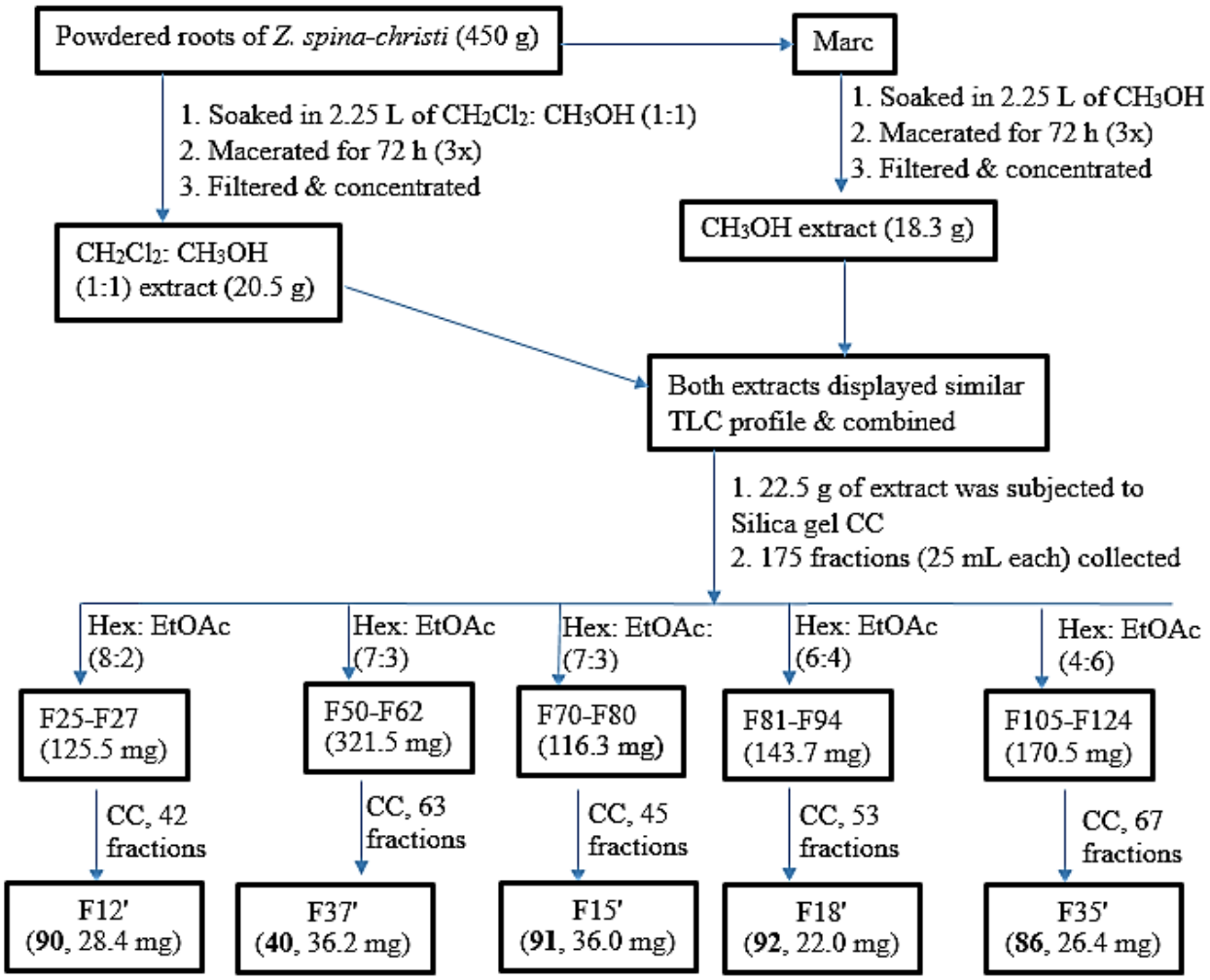

Scheme 4: Extraction, isolation, and purification scenario of the roots of *Z. spina-christi*. CC; column chromatography, EtOAc; ethyl acetate, Hex; *n*-hexane.

3.2.5. Extraction of essential oils

Essential oils (EOs) were extracted from different parts (roots and leaves) of all the plant materials via the hydrodistillation method. About 30 g of the dried powder of roots of *C. adenocaule* and *Z. spinachristi* and 40 g of the leaves of *C. adenocaule* and *Z. spinachristi*, and roots of *D. regia* and *S. siamea* were placed in the round bottom flask (1000 mL) separately. Then, 400 mL of distilled water was added and mixed thoroughly with each powdered sample. The flasks were fitted with a Clevenger-type apparatus, a glass condenser, and heated using a heating mantle. Subsequently, the mixtures were hydro-distilled at atmospheric pressure for 3 h. The oil part of each extract was separated from the aqueous layer by adding 100 mL of chloroform in a separatory funnel. A small amount of aqueous left with the organic layer was dried by adding 5 g of anhydrous Na_2SO_4 and

filtered using Whatman No 1. Finally, the extracts were concentrated *in vacuo* using a rotary evaporator and the essential oils were kept in a refrigerator at 4 °C until further analysis (Elyemni *et al.*, 2019).

3.2.6. GC-MS analysis of the essential oils

The chemical analysis of the EOs was achieved via gas chromatography-mass spectrometry (GC-MS) by adopting the previous protocol (Hema *et al.*, 2010). A GC–MS instrument from Agilent Technologies (Santa Clara, CA, USA) equipped with a 6890 N network GC system, 5975 inert mass selective detector, 7683B series auto sampler injector (10 μL in size), G1701DA GC/MS Chem Station and HP5MS column (30 m length × 0.25 mm internal diameter × 0.25 μm film thickness) coated with 5% phenyl 95% methyl poly siloxane was used for analyzing the EOs. 1-2 μL of EO solutions in chloroform were injected through an auto sampler and run for analyses. The column temperature was programmed as follows: 55–120 °C at 20 °C/min, 120–150 °C at 1.5 °C/min, 150–250 °C at 20 °C/min, 250 °C (10 min) and 3 min solvent delay. The mass spectra transfer line temperature was 280 °C. The carrier gas was helium (1 mL/min) with a split ratio equal to 100:1. The mass spectra were recorded in electron ionization mode at 70 eV with scanning from 50 to 500 amu (atomic mass unit) at 0.5 s with the mass source being set at 230 °C (Hema *et al.*, 2010).

3.2.7. Acid-catalyzed transesterification

Compounds **84** and **86** were heated at 70 °C with 10% HCl in methanol (5 mL) for 18 h followed by extraction with *n*-hexane. The *n*-hexane layers containing the fatty acid methyl esters (FAME) were dried *in vacuo* and the residues were analyzed using a GC-MS (Suleiman *et al.*, 2022).

3.2.8. *In vitro* biological activities

3.2.8.1. *In vitro* antibacterial activity

3.2.8.1.1. Bacterial strains

The bacterial strains used in this study were American-type culture collections (ATCCs). Four bacterial strains including two Gram-negative (*Escherichia coli* (ATCC-25922) and *Pseudomonas aeruginosa* (ATCC-27853)) and two Gram-positive (*Staphylococcus aureus* (ATCC-25923) and *Streptococcus pyogenes* (ATCC-19615)) bacteria were collected from the Ethiopian Public Health

Institute (EPHI). The microorganisms were handled and transported aseptically. The strains were grown and preserved in test tubes containing nutrient broths at 4 °C in a refrigerator until required for the bioassay.

3.2.8.1.2. Preparation of inoculum, culture media, and plates

The Mueller Hinton broth (MHB) and Mueller Hinton Agar (MHA) were organized as per the directions of the manufacturers. The media were cooled and sterilized at 45 °C and 20 mL of it was poured into sterilized petri dishes to form the Mueller Hinton media with uniform thickness of about 3 mm. The MHA plates were of six equal segments to confirm that the disks were not very close to 24 mm on the MHA. Each bacterial strain was cultured overnight at 37 °C in Petri dishes containing the MHA. The bacterial inoculums were prepared by the direct colony suspension method (Sengera *et al.*, 2023).

3.2.8.1.3. Paper disc diffusion assay

The mode of action of the extracts against the strains was evaluated by paper disc-diffusion assay as per the standard protocols of the Clinical and Laboratory Standards Institute (CLSI) (Balouiri *et al.*, 2016). About five colonies of each bacterial strain were transferred into a saline solution using an incubating loop and grown in Brain Heart Infusion (BHI) broth. The turbidity of the bacterial strains was attuned to about 0.5 McFarland standard solution (1.5×10^8 CFU/mL). The bacterial suspension was transferred by swapping with a sterilized cotton swap onto the Petri dishes containing the media (MHA) (solidified 20-25 mL). Whatman No.1 filter paper discs (6 mm in diameter) were then prepared using a puncher for the impregnation of the test samples and sterilized in an oven at 180 °C for 1 hr. Stock solutions of the crude extracts (50 mg/mL), EOs (10 mg/mL), and compound isolates (2 mg/mL) were prepared in 4% DMSO followed by the preparation of different concentrations by serial dilution. Accordingly, three different concentrations of the crude extracts (25, 12.5, and 6.25 mg/mL) and the isolated compounds (1, 0.5, and 0.25 mg/mL), and two different concentrations of the EOs (5 and 2.5 mg/mL) were prepared from their respective stock solutions. The mixture of CH_2Cl_2: CH_3OH (1:1) extract which can yield compounds of different polarity was utilized for the biological activities. A standard antibiotic (ciprofloxacin, 0.25 mg/mL) and DMSO were used as positive and negative controls, respectively. Part of each solution (100 μL) was impregnated onto the sterilized paper discs of

about 6 mm in diameter which were placed over the petri dishes containing the bacterial culture inoculated MHA. The Petri dishes were left for 30 min for diffusion and incubated at 37 °C for 24 h. The antibacterial activities were evaluated by measuring the zone of inhibition (mm) of the extracts using the digital zone of inhibition measuring caliper against the test organism. The entire tests were performed in triplicate and the results were recorded as mean ± standard error of the mean (SEM) using statistical analysis software (Balouiri *et al.*, 2016). After the completion of the assay, the used bacterial inoculums, petri dishes, swabs, and other disposable materials were autoclaved and discarded into trash.

3.2.8.2. *In vitro* antioxidant activity

The crude extracts, EOs, and compound isolates of each plant material were screened for their antioxidant efficacy using 2, 2-diphenyl-1-picrylhydrazyl (DPPH) radical scavenging assay *in vitro*. The free radical trapping potential of the extracts along with a reference drug (ascorbic acid) was tested against DPPH radical using the protocol described by (Khorasani Esmaeili *et al.*, 2015). Four different concentrations (500, 250, 125, and 62.5 μg/mL) of each extract, EOs, compound isolates, and ascorbic acid (AA) were prepared from the corresponding stock solutions (1 mg/mL in methanol). To each prepared concentration, freshly prepared DPPH solution (1 mL, 0.04% w/v in methanol) was added followed by incubating for 30 min at room temperature. After incubation, the absorbance of each solution was measured at 517 nm using the UV-Vis spectrophotometer in triplicate. Sample-free DPPH solution in methanol was used as a negative control. The DPPH radical scavenging potential of each sample was expressed in terms of the percent of scavenging activity (Equation 1) (Khorasani Esmaeili *et al.*, 2015).

$$\text{DPPH radical scavenging activity (\%)} = \left(1 - \frac{A}{A_{\circ}}\right) \text{x } 100 \qquad \text{Equation (1)}$$

Where; A and A_0 signify the absorbance of DPPH containing sample in methanol, and DPPH radical in methanol, respectively.

Finally, the DPPH free radical scavenging power of the extracts was compared to AA, and the IC_{50} (the concentration needed to scavenge the total DPPH radicals by 50%) values were calculated from the relationship curves of the plots of concentration versus the mean percentages of the

antioxidant activity. The trend line options were displayed and relationships that revealed the highest coefficient of determination (R^2) values were selected for the calculations.

3.2.8.3. Anti-acanthamoeba activity

3.2.8.3.1. Cultivation of *A. triangularis* and *A. castellanii* strains

A. triangularis WU19001, a strain from the recreational reservoir at Walailak University, Nakhon Si Thammarat-Thailand, and *A. castellanii* ATCC50739 (reference pathogen strains) were used in this study. The parasite was grown in peptone yeast glucose (PYG) medium (20 g proteose peptone, 2 g yeast extract, 0.98g $MgSO_4 \cdot 7H_2O$, 0.35g $Na_2HPO_4 \cdot 7H_2O$, 0.34g KH_2PO_4, 0.02 g $(NH_4)_2Fe(SO_4)_2 \cdot 6H_2O$, 18 g glucose). The trophozoites were observed after 72 h of incubation at room temperature. Trophozoites were centrifuged at 4000 rpm for 5 min and re-suspended in fresh PYG thereafter. For counting, 50 μL of cell suspension was mixed with 50 μL of trypan blue. Viability was investigated under the inverted microscope based on the principle that the dye can cross the membrane of dead cells with blue color, but not the intact membrane of viable cells with colourless appearances.

3.2.8.3.2. Screening of anti-acanthamoeba activity

The CH_2Cl_2: CH_3OH (1:1) extract of *C. adenocaule* (CAE1), and CH_2Cl_2: CH_3OH (1:1) (ZSE1) and methanol (ZSE2) extracts of *Z. spina-christi* were screened for their anti-acanthamoeba activity by the dilution method in a 96-well polystyrene microtiter plate. The stock solutions (100 mg/mL) of the extracts were diluted to 4 mg/mL with PYG medium. Then, 100 μL of each extract was transferred to each well. The aliquot of 100 μL (2×10^5 trophozoites/mL) was added to give a final concentration of 2 mg/mL, and incubated at 25 °C for 24 h. Finally, the relative percentage of parasite viability was calculated using Equation 2.

$$\text{Viability (\%)} = \frac{\text{mean of the treated parasite}}{\text{mean of the control}} \text{x } 100 \qquad \text{Equation (2)}$$

3.2.8.4. *In vitro* antiviral activity

Nowadays, i*n vitro* cytotoxicity tests are among the most essential assays to date and focus mainly on cell death or the measurement of growth impairment. The approach is used to ensure the safety

and toxicity of potential candidate drugs. In modern research, naturally occurring substances including plant extracts and their compound isolates have got keen attention for their cytotoxicity tests. In this study, the *in vitro* cytotoxicity properties of the ethyl acetate (CA1) (from preliminary extraction), CH_2Cl_2: CH_3OH (1:1) (CA2), and methanol (CAE) extracts of roots of *C. adenocaule*, CH_2Cl_2: CH_3OH (1:1) (SSE) extract of roots of *S. siamea*, and CH_2Cl_2: CH_3OH (1:1) (ZSE) and methanol (ZSE1) extracts of roots of *Z. spina-christi* were tested against influenza types A and B viruses.

3.2.8.4.1. Cytotoxicity assay

In this work, the cytotoxicity properties of the extracts were tested using a micro tetrazolium (MTT) assay using the previous protocol (Sudarikov *et al.*, 2022). Initially, a series of three-fold dilutions of each extract were prepared in a minimum essential medium (MEM) of about 3.7–300 μg/mL. Then, Madin-Darby canine kidney (MDCK) cells were incubated for 48 h at 36 °C in 5% CO_2 in the presence of dissolved specimens. A phosphate-buffered saline (PBS) was used to clean and wash the cells twice, and 0.5 μg/mL solution of 3-(4, 5-dimethylthiazolyl-2) 2, 5-diphenyltetrazolium bromide (ICN Biochemicals Inc. Aurora, Ohio) in PBS was added to the wells. The wells were inoculated for 1 h and repeatedly washed, and the formazan residue was dissolved in 0.1 mL of DMSO per well. Subsequently, the optical density of the wells was determined on a Thermo Multiskan FC plate reader at 540 nm wavelength and plotted against the concentration of extracts. The concentrations were tested in triplicate and half of the cytotoxic concentrations (CC_{50}) of the extracts were calculated from the obtained data (Sudarikov *et al.*, 2022).

3.2.8.4.2. Cytoprotection assay

0.1 mL of DMSO was used to dissolve and prepare the stock solution of the extracts, and a minimum essential medium (MEM) with 1 μg/mL of trypsin was employed to prepare the final serial solutions (300-3.7 μg/mL). The extracts were incubated with MDCK cells for 1 h at 36 °C and each extract concentration was tested in triplicate. Later, the cell culture was infected with influenza virus A/Puerto Rico/8/34 (H1N1) (multiplicity of infection, 0.01) for 48 h at 36 °C in the presence of 5% CO_2. Then after, the viability of cells was screened by MTT assay as labeled above and calculated using Equation 3. Based on the results of photometry, half of the inhibiting

concentration (IC_{50}) which is the concentration needed for the protection of 50% cells compared to the wells without extracts, was calculated for each extract. Furthermore, the selectivity indexes (SI) designating the ratio of CC_{50} to IC_{50} were calculated and a GraphPad Prism software was employed for the calculations. Finally, the specimens exhibiting SI values of ≥10 were considered active and prospective for further development (Sudarikov *et al.*, 2022).

$$\text{Cell viability (\%)} = \frac{\text{mean optical density}}{\text{control optical density}} \text{x } 100 \qquad \text{Equation (3)}$$

3.3. Computational Study

3.3.1. *In silico* molecular docking

The modes of binding of the compound isolates to protein targets of the bacterial strains and human enzymes were studied using molecular docking experiments and compared to the reference drugs. Molecular docking parameters, such as binding affinity (kcal/mol), hydrogen bonds, and residual amino acid interactions along with 2D and 3D structural depictions of the most stable conformations were provided. Accordingly, DNA gyrase B of *E. coli* (PDB ID: 6F86), pyruvate kinase (PK) of *S. aureus* (PDB ID: 3T07), *P. aeruginosa* PqsA (PDB ID: 5OE3), 10782 streptopain of *S. pyogenes* (PDB ID: 6UKD), human myeloperoxidase (PDB ID: 1DNU), and topoisomerase II α (PDB ID: 4FM9) were obtained from the Protein Data Bank (PDB) (http://www.rcsb.org) and saved in the PDB format. The bacterial protein targets were chosen based on their metabolic significance to the bacteria and the similarity of the compound isolates to the co-crystallized ligands in the protein complexes.

3.3.1.1. Protein preparation

The protein preparations were performed following the reported standard protocol (Baby *et al.*, 2016). Initially, the crystal structures of the protein targets were retrieved from the Protein Data Bank (http://www.rcsb.org) using their PDB identifications. The 3D crystal structures were imported into Biovia Discovery Studio Visualizer 2021 followed by the removal of water molecules, heteroatoms, and complexes bound to the receptor molecules. To compute a site-specific molecular docking, ligand groups were selected from the co-crystallized protein structures and defined, and the binding sites were retrieved by identifying the x, y, and z coordinates from the SBD site spheres. The active sites were recognized by studying the binding interaction of the

ligand and the receptor and the molecular dockings were computed on the active sites of the prepared proteins. Thereby, the dimensions of the SBD site sphere of each target protein were established as follows; PDB ID: 6F86 (61.680, 28.330, and 64.290), PDB ID: 5OE3 (29.262, 21.848, and 19.863), PDB ID: 3T07 (0.014, 0.147, and -0.003), PDB ID: 6UKD (-25.515, -13.743, and 13.171), PDB ID: 1DNU (36.727, 9.922, and 10.989), and PDB ID: 4FM9 (17.245, 39.350, and 25.275) Å for x, y and z dimensions, respectively. Subsequently, polar hydrogens were added for the correct ionization of the amino acid residues. Finally, the energy of the proteins was minimized using the CHARMM Force Field steepest descent algorithm with a maximum number of 1000 steps at a root mean square (RMS) gradient of 0.01. The energy minimization process was continued until the protein fulfilled a convergence gradient of 0.001 kcal mol^{-1} (Baby *et al.*, 2016).

3.3.1.2. Ligand preparation

The chemical structures of the compound isolates were drawn using the ChemOffice tool (Chem Draw 16.0) and assigned with suitable 2D orientations. By applying the ChemBio3D tool, energy minimizations were performed with the molecular modeling (MM2) algorithm until it fulfilled the RMS gradient of 0.01 kcal mol^{-1} to achieve the minimum energy conformers. Lastly, the ligand molecules with minimized energy were saved in PDB format and used as an input for the AutoDock Vina to perform molecular docking simulations (Baby *et al.*, 2016).

3.3.1.3. Protein-ligand docking strategy

The docking protocol was validated to confirm the reliability and accuracy of the molecular docking outcomes as per the methods of Warren and co-workers (Warren *et al.*, 2006). The objective was to precisely reproduce the docking interactions and binding pores of the co-crystallized ligands inside the experimentally crystallized structure of proteins. Thus, the original ligand of the co-crystalized protein was separated and prepared for the molecular docking of the ligands of interest. The ligands of interest were then docked back into the active sites of the protein using the MGL AuthoDock Tools 1.5.6 program and all the files saved in the working directory were run via Command Prompt to generate the affinity and root mean square deviation (RMSD) values. Notably, the RMSD values ranging from (0-2) Å were suitable for the molecular docking demonstrating that the protocol is feasible for other compound inhibitors (Warren *et al.*, 2006). Nine different poses (out ligands) were generated and only a single pose with the most stable

binding affinity and RMSD was chosen. Finally, the ligand interactions, hydrogen bonds, residual amino acid interactions, 2D and 3D structural orientations, and image preparations were run using the Biovia Discovery Studio Visualizer 2021 (Narramore *et al.*, 2019).

3.3.2. *In silico* drug-likeness and pharmacokinetic properties

In this study, the drug-likeness and collective absorption, distribution, metabolism, and excretion (ADME) properties of the compound isolates along with the standard drug (ciprofloxacin) were predicted using SwissADME (http://www.swissadme.ch/) and ADMETSAR (http://lmmd.ecust.edu.cn/admetsar1) online web tools (Daina *et al.*, 2017). Chemical structures of the compound isolates and the reference drug were converted to their canonical simplified molecular-input line-entry system (SMILE) and submitted to the SwissADME tool to estimate the drug-likeness and pharmacokinetic parameters (Daina *et al.*, 2017). The drug-likeness properties of compounds with auspicious *in vitro* antibacterial and antioxidant activities were predicted based on Lipinski's rule of five (Lipinski *et al.*, 2012) and Veber's rule (Veber *et al.*, 2002). Furthermore, the organ toxicity predictions of the compound isolates were generated using Pro Tox II web tools (https://tox-new.charite.de/) (Banerjee *et al.*, 2018).

3.4. Spectral and Statistical Data Analyses

The raw data obtained from the FTIR spectrometer were manipulated using Origin software. In addition, the NMR data were operated using MestReNova software (version 14.2). In GC-MS, the compounds were identified using their retention time, and mass spectral fragmentation pattern and by comparing their mass spectra with the mass spectra of compounds in the NIST 2005 library. The antibacterial and antioxidant data were tabulated on a Microsoft Excel spreadsheet and the values were conveyed as mean ± standard error of the mean (SEM). The antibacterial activities were investigated by comparing the inhibition zones of the target samples with the inhibition zones of the control drug. The one-way ANOVA with Tukey's *post hoc* test was applied for data comparisons. SPSS version 21.0 was used and the data were assumed significant for the P values < 0.05.

CHAPTER FOUR

4. RESULTS AND DISCUSSION

This section presented the diverse findings of the study, including the phytochemical analysis of the extracts, structure elucidations, Chemistry of the essential oils, and biological activities of all forms of the extracts of the plant materials. In addition, this section gives insight into the correlation of the *in vitro* biological activities of the isolated compounds to their *in silico* molecular docking, drug-likeness, ADME, and toxicity profiles. This offers a remarkable step to predict the medicinal values of the compounds and enhance to further investigations.

4.1. Extraction Yields and Physical Characteristics

The percent yield of an extractable matter is one of the parameters that should be considered during the characterization of natural product drugs. In this study, the CH_2Cl_2: CH_3OH (1:1) and methanol extracts of most of the investigated plants yielded low to moderate yields compared to previous reports. The maximum (4.67%) and minimum (0.49%) contents of extractable matter were obtained from the methanol extract of the roots of *C. adenocaule* and petroleum ether extract of the roots of *D. regia*, respectively (Table 5).

Table 5: Yield and physical characteristics of the extracts of the plant materials.

No.	Plant species	Parts studied	Extraction solvent	Plant mass (g)	Extract (g)	Yield (%)	Texture	Color
1	*C. adenocaule*	Roots	CH_2Cl_2: CH_3OH (1:1)	600	22.0	3.67	Sticky	Deep brown
			methanol	600	28.0	4.67	Sticky	Deep brown
2	*D. regia*	Roots	Petroleum ether	700	3.4	0.49	Sticky	Light brown
			CH_2Cl_2: CH_3OH (1:1)	700	7.5	1.07	Sticky	Yellow
			methanol	700	6.5	0.93	Sticky	Yellow
3	*S. siamea*	Roots	CH_2Cl_2: CH_3OH (1:1)	700	25.0	3.57	Sticky	Yellow
4	*Z. spina-christi*	Roots	CH_2Cl_2: CH_3OH (1:1)	450	10.5	2.34	Sticky	Brown
			methanol	450	12.0	2.67	Sticky	Deep brown

4.2. Phytochemical Analysis and Structure Elucidations

In this study, the isolation and spectroscopic characterization of the four plant species afforded a total of 24 compounds including the mixture of β-sitosterol (**19**) and stigmasterol (**40**). The structural information of the compound isolates was obtained from the IR and NMR spectral data and verified by comparing the data with reported spectral values in the literature. The given codes along with the physical characteristics of the isolated compounds of the plant materials are depicted in Table 6.

Table 6: Given codes and physical characteristics of the isolated compounds.

Plant species	Given code	Eluting solvent	TLC solvent	Color	Amount (mg)	Retention factor (R_f)	Melting point (°C)
C. adenocaule	**82**	*n*-hexane	H:EA (9:1)	white gel	31.5	0.95	-
	83	H:EA (8:2)	H:EA (9:1)	white crystals	10.4	0.70	61-63
	19	H:EA (7:3)	H:EA (8:2)	white needles	23.8	0.47	135-137
	84	H:EA (7:3)	H:EA (7:3)	white waxy crystals	18.6	0.65	-
	28	H:EA (5:5)	H:EA (7:3)	yellow crystals	12.4	0.66	-
	85	H:EA (3:7)	H:EA (3.5:6.5)	colorless crystals	11.5	0.72	-
	25	H:EA (2.5:7.5)	H:EA (3:7)	pale brown crystals	32.0	0.57	180-182
	66	H:EA (2.5:7.5)	H:EA (3:7)	yellow crystals	19.2	0.55	352-354
	29	H:EA (1.5:8.5)	H:EA (3:7)	grey-brown powder	51.2	0.45	165-167
	23	H:EA (1:9)	H:EA (2:8)	brown crystals	15.1	0.73	-
D. regia	**40**	PE:EA (6.5:3.5)	H:EA (8:2)	yellow-green crystals	20.8	0.55	167-168
	19 and **40** (mixture)	PE:EA (6:4)	H:EA (8:2)	white needles	23.5	0.38	-
	86	PE:EA (5:5)	H:EA (6:4)	white crystals	17.8	0.78	-
	42	PE:EA (3.5:6.5)	H:EA (5:5)	yellow powder	23.0	0.70	315-317
	87	PE:EA (3.5:6.5)	H:EA (4:6)	yellow powder	5.5	0.58	345-348
	37	EA:M (8.5:1.5)	C:M:AA (8:1.5:0.5)	yellow crystalline powder	9.5	0.20	191-193
S. siamea	**39**	H:EA (7.5:2.5)	H:EA (9:1)	white powder	12.6	0.45	212-214
	53	H:EA (6:4) - H:EA (5:5)	H:EA (7:3)	orange crystals	10.3	0.55	193-194
	63	H:EA (6:4) - H:EA (5:5)	H:EA (7:3)	white crystalline solid	13.8	0.60	296-298
	88	H:EA (5:5)	H:EA (7:3)	white solid	9.5	0.50	92-94
	89	H:EA (5:5)	H:EA (7:3)	orange powder	10.2	0.75	-
Z. *spina-christi*	**90**	H:EA (8:2)	H:EA (8:2)	pale yellow gel	28.4	0.83	-
	91	H:EA (7:3)	H:EA (8:2)	white powder	36.0	0.63	69-71
	92	H:EA (5:5)	H:EA (6:4)	yellow powder	23.0	0.49	-

AA; acetic acid, C; chloroform, EA; ethyl acetate, H; *n*-hexane, M; methanol, PE; petroleum ether.

4.2.1. Structure elucidation of compounds isolated from roots of *Cyphostemma adenocaule*

The silica gel chromatographic separations of the combined CH_2Cl_2: CH_3OH (1:1) and methanol extracts of roots of *C. adenocaule* yielded ten known compounds namely; hexadec-1-ene, (**82**) palmitic acid (**83**), *β*-sitosterol (**19**), *β*-sitosteryl palmitate (**84**), 3-hydroxy isoagatholactone (**28**), diethyl phthalate (**85**), *ε*-viniferin (**25**), myricetin (**66**), tricuspidatol A (**29**), and parthenocissin A (**23**). The structural elucidations of the compounds were supported by comparison with literature reports. The TLC profiles of the compound isolates of *C. adenocaule* are depicted in Appendix 1.

4.2.1.1. Compound 82

Compound **82** was isolated as a white gel. The ^{1}H NMR (400 MHz, $CDCl_3$) spectrum exhibited signals of olefinic protons at δ_H 5.84 (1H, *m*, H-2), 5.02 (1H, *dd*, *J* = 17.1, 1.1 Hz, H-1b), and 4.96 (1H, *dd*, *J* = 10.2, 1.1 Hz, H-1a) suggesting that the compound possesses vinylic protons. The spectrum also showed signals at δ_H 2.07 (2H, *q*, *J* = 6.7 Hz) and 0.91 (3H, *t*, *J* =7.0 Hz) assignable to the methylene protons adjacent to the unsaturation (H-3) and terminal methyl protons (H-16), respectively. The remaining signals overlapped in the range of δ_H 1.26-1.38 (24H, *brs*). The ^{13}C NMR (100 MHz, $CDCl_3$) spectrum showed seven well-resolved carbon signals assignable to sixteen carbons, including olefinic signals at δ_C 139.2 (C-2) and 114.0 (C-1), and terminal methyl signal at δ_C 14.1 (C-16). This suggested that the compound possesses an open chain structure. Furthermore, the types of carbon signals were verified using the DEPT-135 NMR spectrum. Thereby, the spectrum revealed two sp^2 methine and methylene signal at δ_C 139.2 (C-2) and 114.0 (C-1) attributed to the vinylic carbons of the compound. In addition, a set of thirteen secondary carbons and one primary carbon (δ_C 14.1, C-16) observed on the upfield region of the spectrum confirm the open-chain form of the structure (Table 7, Appendices 2A-C).

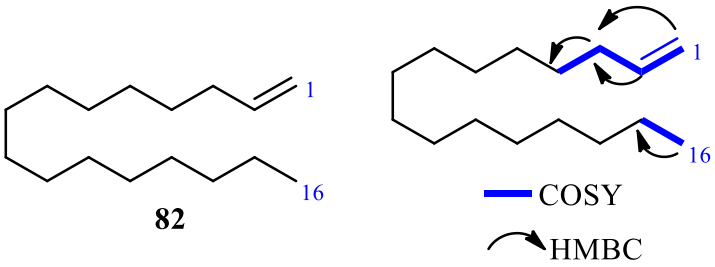

Figure 7: Chemical structure of compound **82**, and key COSY and HMBC correlations.

The proton-proton coupling, proton-carbon linkages, and connectivity of the compound were verified using 2D NMR experiments. Accordingly, the COSY spectrum exhibited key ^{3}J correlations between H-1 (δ_H 4.96, 5.02) and H-2 (δ_H 5.84), and H-2 (δ_H 5.84) and H-3 (δ_H 2.07). In addition, the HSQC spectrum revealed ^{1}J correlations between H-1 (δ_H 4.96, 5.02) and C-1 (δ_C 114.0), H-2 (δ_H 5.84) and C-2 (δ_C 139.2), H-3 (δ_H 2.07) and C-3 (δ_C 33.8), H-16 (δ_H 0.91) and C-16 (δ_C 14.1). Notably, the HMBC spectrum also showed ^{3}J correlation between H-1 (δ_H 4.96, 5.02) and C-3 (δ_C 33.8), ^{2}J correlation between H-2 (δ_H 5.84) and C-3 (δ_C 33.8), and ^{3}J correlation between H-3 (δ_H 2.07) and C-1 (δ_C 114.0) (Table 7, Appendices 2D-F). Overall, the data were in close agreement with the literature values of hexadec-1-ene (**82**) (Olonisakin, 2014) (Figure 7).

Table 7: ^{1}H (400 MHz), ^{13}C (100 MHz), COSY, and HMBC NMR ($CDCl_3$, δ in ppm, J in Hz) spectral data of compound **82**, and ^{1}H and ^{13}C NMR values of 1-hexadecene in the literature.

C. No.	**Compound 82**				**1-Hexadecene** (Olonisakin, 2014)	
	^{1}H NMR	**^{13}C NMR**	**COSY**	**HMBC**	**^{1}H NMR**	**^{13}C NMR**
1	4.96 (1H, *dd, J* = 10.2, 1.1), 5.02 (1H, *dd, J* = 17.1, 1.1)	114.0	H-2	C-3	4.82 (1H, *d, J* = 10.0), 4.88 (1H, *d, J* = 12.0)	114.4
2	5.84 (1H, *m*)	139.2	H-1, 3	C-3	5.71 (1H, *m*)	139.5
3	2.07 (2H, *q, J* = 6.7)	33.8	H-2, 4	C-1, 2, 4	1.95 (2H, *m*)	34.1
4	1.26-1.38 (2H, *brs*)	29.7	H-3		1.05-1.34 (2H, *m*)	29.7
5	1.26-1.38 (2H, *brs*)	29.7			1.05-1.34 (2H, *m*)	29.7
6	1.26-1.38 (2H, *brs*)	29.7			1.05-1.34 (2H, *m*)	29.7
7	1.26-1.38 (2H, *brs*)	29.7			1.05-1.34 (2H, *m*)	29.7
8	1.26-1.38 (2H, *brs*)	29.7			1.05-1.34 (2H, *m*)	29.7
9	1.26-1.38 (2H, *brs*)	29.7			1.05-1.34 (2H, *m*)	29.7
10	1.26-1.38 (2H, *brs*)	29.7			1.05-1.34 (2H, *m*)	29.7
11	1.26-1.38 (2H, *brs*)	29.6			1.05-1.34 (2H, *m*)	29.6
12	1.26-1.38 (2H, *brs*)	29.6			1.05-1.34 (2H, *m*)	29.6
13	1.26-1.38 (2H, *brs*)	29.3			1.05-1.34 (2H, *m*)	29.3
14	1.26-1.38 (2H, *brs*)	31.9			1.05-1.34 (2H, *m*)	32.3
15	1.26-1.38 (2H, *brs*)	22.7	H-16		1.05-1.34 (2H, *m*)	22.7
16	0.91 (3H, *t, J* = 7.0)	14.1	H-15	C-15	0.81 (3H, *t*)	14.2

brs; broad singlet.

4.2.1.2. Compound 83

Compound **83** was obtained as white crystals and its melting point was determined in the range of 61-63 °C in accordance with the reported value (63 °C) of palmitic acid (Soliman and Shattory,

2017). The ^{1}H NMR (400 MHz, $CDCl_3$) spectrum revealed the presence of aliphatic protons at δ_H 2.35 (2H, *t*, *J* = 7.5 Hz), 1.62 (2H, *m*), and 0.87 (3H, *t*, *J* = 7.1 Hz) attributed to H-2, H-3, and H-16, respectively. The remaining protons appeared as a broad singlet signal in the range δ_H 1.25-1.30 (24H, *m*) corresponding to the other sp^3 methylene protons of the compound (H-4 to H-15). In its ^{13}C NMR (100 MHz, $CDCl_3$) spectrum, the compound displayed ten signals assignable to sixteen carbons. The signals at the two edges of the spectrum δ_C 178.9 (C-1) and 14.3 (C-16) were evident to the presence of a fatty acid skeleton. The majority of the signals appeared in between δ_C 34.0 (C-2) and 22.9 (C-15) and the down-phased appearance of the signals in this range (from the DEPT-135 spectrum) verifies the fatty acid skeleton of the compound (Table 8, Appendices 3A-C).

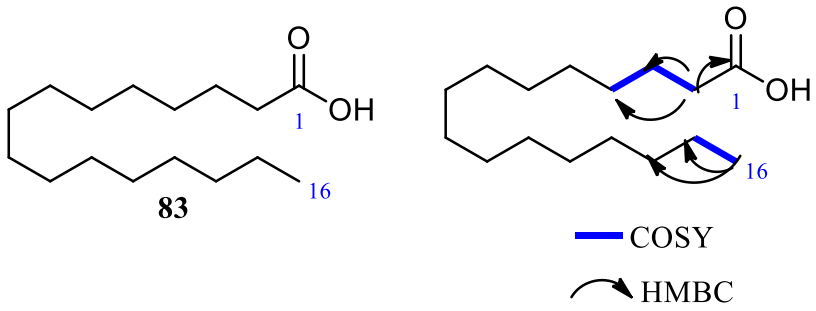

Figure 8: Chemical structure of compound **83**, and key COSY and HMBC correlations.

The structural information was verified by 2D NMR experiments. Thereby, the COSY spectrum showed ^{3}J correlations between H-2 (δ_H 2.35) and H-3 (δ_H 1.62), H-3 (δ_H 1.62) and H-4 (δ_H 1.30), and H-15 (δ_H 1.27) and H-16 (δ_H 0.87). Furthermore, the HMBC spectrum exhibited ^{2}J and ^{3}J correlations between H-2 (δ_H 2.35) and C-3, 4 (δ_C 24.9, 29.3), ^{3}J and ^{2}J correlations between H-3 (δ_H 1.62) and C-1, 4 (δ_C 178.9, 29.3), and ^{3}J and ^{2}J correlations between H-16 (δ_H 0.87) and C-14, 15 (δ_C 32.1, 22.9) (Table 8, Appendices 3D-F). The data generated matches to the reported values (Bulama *et al.*, 2014) of palmitic acid (**83**) (Figure 8). The spectral analyses were also supported by a GC-MS fragmentation pattern (EI MS), where the gas chromatogram (GC) showed a peak at 51.24 min and its mass fragmentation process revealed a molecular ion peak $[M]^+$ at *m/z*: 256.2 in agreement with the molecular formula of $C_{16}H_{32}O_2$. (Appendix 3G).

Table 8: ^{1}H (400 MHz), ^{13}C (100 MHz), COSY, and HMBC NMR ($CDCl_3$, δ in ppm, J in Hz) spectral data of compound **83**, and ^{1}H and ^{13}C NMR values of palmitic acid in the literature.

C. No.	**Compound 83**				**Palmitic acid** (Bulama *et al.*, 2014)	
	^{1}H NMR	**^{13}C NMR**	**COSY**	**HMBC**	**^{1}H NMR**	**^{13}C NMR**
1	-	178.9			-	179.2
2	2.35 (2H, *t*, *J* = 7.5)	34.0	H-3	C-1, 3, 4	2.32 (2H, *t*, *J* = 6.7)	34.0
3	1.62 (2H, *m*)	24.9	H-2, 4	C-1, 4	1.40 (2H, *m*)	25.9
4	1.30 (2H, *brs*)	29.3	H-3		1.31 (2H, *m*)	29.1
5	1.25 (2H, *brs*)	29.4			1.31 (2H, *m*)	29.1
6	1.25 (2H, *brs*)	29.9			1.31 (2H, *m*)	29.1
7	1.25 (2H, *brs*)	29.9			1.31 (2H, *m*)	29.1
8	1.25 (2H, *brs*)	29.9			1.31 (2H, *m*)	29.1
9	1.25 (2H, *brs*)	29.9			1.31 (2H, *m*)	29.1
10	1.25 (2H, *brs*)	29.9			1.31 (2H, *m*)	29.1
11	1.25 (2H, *brs*)	29.9			1.31 (2H, *m*)	29.1
12	1.27 (2H, *brs*)	29.6			1.31 (2H, *m*)	29.1
13	1.27 (2H, *brs*)	29.6			1.31 (2H, *m*)	29.1
14	1.25 (2H, *brs*)	32.1			1.31 (2H, *m*)	31.9
15	1.27 (2H, *brs*)	22.9	H-16		1.39 (2H, *m*)	22.8
16	0.87 (3H, *t*, *J* = 7.1)	14.3	H-15	C-14, 15	0.91 (3H, *t*)	14.1

brs; broad singlet.

4.2.1.3. Compound 19

Compound **19** (mp; 135-137 °C) was isolated as white needles. The melting point range was very close to the literature values of *β*-sitosterol (134-135 °C) (Ododo *et al.*, 2016). Its ^{1}H NMR (400 MHz, $CDCl_3$) spectrum revealed signals of olefinic proton at δ_H 5.34 (1H, *m*, H-6) suggesting that the compound has a single sp^2 olefinic proton. The spectrum also showed a signal of oxymethine proton at δ_H 3.51 (1H, *m*) assignable to H-3. The signals at δ_H 2.27 (1H, *m*, H-4a), 2.22 (1H, *m*, H-4b), and 1.98 (1H, *m*, H-7a) and 1.94 (1H, *m*, H-7b) suggest diastereotopic protons attributed to the methylene protons adjacent to the sp^2 unsaturated olefinic carbons. Furthermore, the spectrum exhibited six methyl signals at δ_H 1.00 (3H, *s*, H-19), 0.91 (3H, *d*, *J* = 6.6 Hz, H-21), 0.83 (3H, *t*, H-29), 0.81 (3H, *d*, *J* = 6.1 Hz, H-27), 0.80 (3H, *d*, *J* = 6.2 Hz, H-26), and 0.67 (3H, *s*, H-18). The other proton signals coincided in the range δ_H 1.87-0.90 (25H, *m*) (Table 9, Appendix 4A).

The ^{13}C NMR (100 MHz, $CDCl_3$) spectrum in agreement with the DEPT-135 spectrum of the compound exhibited twenty-nine well-resolved carbon signals, including two olefinic carbons at

δ_C 140.8 (C-5) and 121.8 (C-6) of which the earlier embodies a quaternary carbon. It also showed an oxymethine carbon at δ_C 71.9 (C-3), seven sp^3 methine signals at δ_C 56.8 (C-14), 56.1 (C-17), 50.2 (C-9), 45.9 (C-24), 36.2 (C-20), 32.0 (C-8), and 29.2 (C-25), eleven methylene signals at δ_C 42.4 (C-4), 39.8 (C-12), 37.3 (C-1), 34.0 (C-22), 32.0 (C-7), 31.7 (C-2), 28.3 (C-16), 26.1 (C-23), 24.4 (C-15), 23.1 (C-28), and 21.1 (C-11), six methyl carbons at δ_C 19.9 (C-27), 19.5 (C-19), 19.1 (C-26), 18.8 (C-21), 12.0 (C-18), and 11.9 (C-29), and two sp^3 quaternary carbons at δ_C 42.3 (C-13) and 36.6 (C-10) (Table 9, Appendices 4B and C).

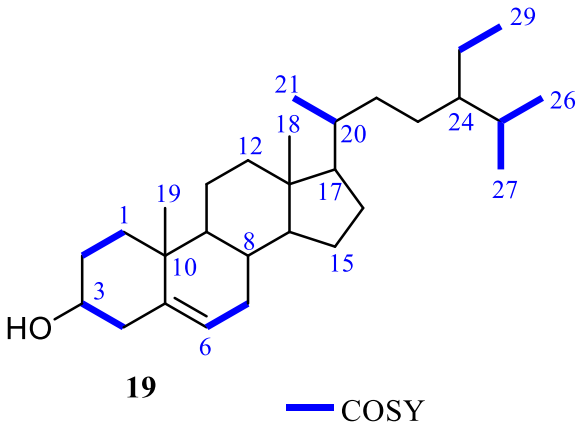

Figure 9: Chemical structure of compound **19**, and key COSY correlations.

In addition, the proton NMR assignments were verified by COSY correlations. Thereby, the spectrum showed significant ^3J correlations between H-1b (δ_H 1.07) and H-2a (δ_H 1.81), H-3 (δ_H 3.51) and H-4 (δ_H 2.27, 2.22), H-6 (δ_H 5.34) and H-7 (δ_H 1.98, 1.94), H-20 (δ_H 1.33) and H-21 (δ_H 0.91), H-25 (δ_H 1.64) and H-26, 27 (δ_H 0.80, 81), and H-28 (δ_H 1.20) and H-29 (δ_H 0.83) (Table 9, Appendix 4D). Overall, the spectral data matches the reported values of β-sitosterol (**19**) (Cayme and Ragasa, 2004) (Figure 9).

Table 9: ^{1}H (400 MHz), ^{13}C (100 MHz), DEPT-135, and COSY NMR ($CDCl_3$, δ in ppm, J in Hz) spectral data of compound **19**, and ^{1}H and ^{13}C NMR values of β-sitosterol in the literature.

C. No.	Compound 19				***β*-Sitosterol** (Cayme and Ragasa, 2004)	
	^{1}H NMR	**^{13}C NMR**	**DEPT -135**	**COSY**	**^{1}H NMR**	**^{13}C NMR**
1	1.84 (1H, *m*), 1.07 (1H, *m*)	37.3	$-CH_2-$	H-2	1.83 (1H, *m*), 1.08 (1H, *m*)	37.2
2	1.81 (1H, *m*), 1.52 (1H, *m*)	31.7	$-CH_2-$	H-1	1.82 (1H, *m*), 1.49 (1H, *m*)	32.6
3	3.51 (1H, *m*)	71.9	-CH-O	H-4	3.53 (1H, *m*)	71.8
4	2.27 (1H, *m*), 2.22 (1H, *m*)	42.4	$-CH_2-$	H-3	2.28 (1H, *m*), 2.24 (1H, *m*)	42.3
5	-	140.8	-		-	140.7
6	5.34 (1H, *m*)	121.8	=CH-	H-7	5.35 (1H, *d, J* = 4.7)	121.7
7	1.98 (1H, *m*), 1.94 (1H, *m*)	32.0	$-CH_2-$	H-6, 8	1.98 (1H, *m*), 1.56 (1H, *m*)	31.9
8	1.49 (1H, *m*)	32.0	-CH-	H-7	1.46 (1H, *m*)	31.9
9	0.95 (1H, *m*)	50.2	-CH-		0.94 (1H, *m*)	50.1
10	-	36.6	-		-	36.5
11	1.45 (1H, *m*), 1.43 (1H, *m*)	21.1	$-CH_2-$		1.48 (1H, *m*), 1.45 (1H, *m*)	21.0
12	2.00 (1H, *m*), 1.13 (1H, *m*)	39.8	$-CH_2-$		1.97 (1H, *m*), 1.15 (1H, *m*)	39.8
13	-	42.3	-		-	42.2
14	1.03 (1H, *m*)	56.8	-CH-		1.03 (1H, *m*)	56.7
15	1.55 (1H, *m*), 1.05 (1H, *m*)	24.4	$-CH_2-$		1.55 (1H, *m*), 1.05 (1H, *m*)	24.3
16	1.26 (2H, *m*)	28.3	$-CH_2-$		1.24 (2H, *m*)	28.2
17	1.10 (1H, *m*)	56.1	-CH-		1.13 (1H, *m*)	56.0
18	0.67 (3H, *s*)	12.0	$-CH_3$		0.68 (3H, *s*)	11.9
19	1.00 (3H, *s*)	19.5	$-CH_3$		1.01 (3H, *s*)	19.4
20	1.33 (1H, *m*)	36.2	-CH-	H-21	1.36 (1H, *m*)	36.1
21	0.91 (3H, *d, J* = 6.6)	18.8	$-CH_3$	H-20	0.94 (3H, *d*)	18.8
22	1.30 (2H, *m*)	34.0	$-CH_2-$		1.32 (2H, *m*)	33.9
23	1.14 (2H, *m*)	26.1	$-CH_2-$		1.15 (2H, *m*)	26.0
24	0.93 (1H, *m*)	45.9	-CH-		0.93 (1H, *m*)	45.8
25	1.64 (1H, *m*)	29.2	-CH-	H-26, 27	1.65 (1H, *m*)	29.1
26	0.80 (3H, *d, J* = 6.2)	19.1	$-CH_3$	H-25	0.82 (3H, *d, J* = 6.3)	19.0
27	0.81 (3H, *d, J* = 6.1)	19.9	$-CH_3$	H-25	0.83 (3H, *d, J* = 6.1)	19.8
28	1.20 (2H, *m*)	23.1	$-CH_2-$	H-29	1.22 (2H, *m*)	23.0
29	0.83 (3H, *t*)	11.9	$-CH_3$	H-28	0.85 (3H, *t*)	11.8

4.2.1.4. Compound 84

Compound **84** was isolated as a white waxy crystal. The ^{1}H NMR (400 MHz, $CDCl_3$) spectrum of the compound analyzed with the help of ^{1}H-^{13}C HSQC correlations revealed signals at δ_H 5.37 (1H, *d, J* = 5.4, H-6) and 4.18 (1H, *m*, H-3) attributed to characteristics of olefinic and oxygen-bearing methine protons, respectively. It also showed six methyl signals at δ_H 1.02 (3H, *s*, H-19), 0.93 (3H, *d, J* = 6.3, H-21), 0.86 (3H, *d, J* = 6.7, H-26), 0.85 (3H, *t, J* = 7.5, H-29), 0.82 (3H, *d, J*

= 6.7, H-27), and 0.70 (3H, *s*, H-18) assignable to a stigmastane type steroidal methyl protons, and additional methyl signals at δ_H 0.89 (3H, *t*, *J* = 7.0, H-16') which correspond to the terminal methyl protons of long chain fatty acids. The fatty acid (palmitate) side chain was verified by GC-MS analysis following the transesterification process of compound **84** which yielded *β*-sitosterol and methyl palmitate (*m/z*, 270) (Appendix 5E). The triplet signals at δ_H 2.37 (2H, *t*, *J* = 7.5, H-2') attributed to the methylene protons nearest to the carboxylate group of the fatty acid moiety (Table 10, Appendix 5A).

The ^{13}C NMR (100 MHz, $CDCl_3$) spectrum showed 39 signals assignable to 45 carbons, of which 29 carbons attributed to a stigmastane steroidal moiety. The spectrum revealed carbonyl (δ_C 173.9, C-1'), and olefinic signals at δ_C 140.7 (C-5) and 121.7 (C-6), of which the former two signals attributed to quaternary carbons (from DEPT-135 spectrum). The signal at δ_C 71.8 (C-3) suggests the presence of a sp^3 oxymethine carbon, and the intense signals observed at δ_C 31.9 (C-14'), 29.7 (C-10'-13'), 22.7 (C-15'), and 14.1 (C-16') correspond to carbons in the fatty acid chain. In addition, the types of carbons were confirmed by the DEPT-135 spectral data. Accordingly, the spectrum displayed one sp^2 methine, one oxymethine, seven sp^3 methine, twenty-five sp^3 methylene, and seven methyl carbons which were consistent with the ^{13}C NMR data of the compound (Table 10, Appendices 5B and C).

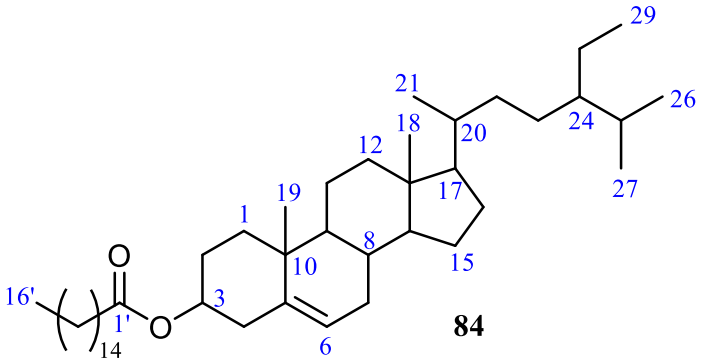

Figure 10: Chemical structure of compound **84**.

The ^{1}H-^{13}C linkages were verified by the HSQC correlations. Thus, the spectrum revealed important ^1J correlations between H-6 (δ_H 5.37) and C-6 (δ_C 121.7), H-19 (δ_H 1.02) and C-19 (δ_C 19.4), H-21 (δ_H 0.93) and C-21 (δ_C 18.8), H-26 (δ_H 0.86) and C-26 (δ_C 19.8), H-29 (δ_H 0.85) and C-29 (δ_C 12.0), H-27 (δ_H 0.82) and C-27 (δ_C 19.0), and H-18 (δ_H 0.70) and C-18 (δ_C 11.8) (Table

10, Appendix 5D). Finally, the spectral analyses were in good agreement with the reported data of *β*-sitosteryl palmitate (**84**) (Elsbaey *et al.*, 2023, Satiraphan, 2012, Yun *et al.*, 2014) (Figure 10).

Table 10: ^{1}H (400 MHz), ^{13}C (100 MHz), and DEPT-135 NMR ($CDCl_3$, δ in ppm, *J* in Hz) spectral data of compound **84**, and ^{1}H and ^{13}C NMR values of *β*-sitosteryl palmitate in the literature.

C. No.	**Compound 84**			***β*-sitosteryl palmitate** (Elsbaey *et al.*, 2023, Satiraphan, 2012, Yun *et al.*, 2014)	
	^{1}H NMR	**^{13}C NMR**	**DEPT-135**	**^{1}H NMR**	**^{13}C NMR**
			***β*-sitosteryl moiety**		
1	1.86 (1H, *m*), 1.08 (1H, *m*)	37.2	-CH_2-	1.90 (1H, *m*), 1.13 (1H, *m*)	37.3
2	1.88 (1H, *m*), 1.57 (1H, *m*)	31.6	-CH_2-	2.02 (1H, *m*), 1.58 (1H, *m*)	31.7
3	4.18 (1H, *m*)	71.8	-CH-O-	4.16 (1H, *m*)	71.8
4	2.30 (1H, *m*), 2.24 (1H, *m*)	42.3	-CH_2-	2.31 (2H, *m*)	42.3
5	-	140.7	Q	-	140.8
6	5.37 (1H, *d, J* = 5.4)	121.7	=CH-	5.35 (1H, *d, J* = 5.2)	121.7
7	1.98 (1H, *m*), 1.95 (1H, *m*)	31.9	-CH_2-	1.59 (2H, *m*)	32.0
8	1.46 (1H, *m*)	31.9	-CH-	1.49 (1H, *m*)	31.9
9	0.95 (1H, *m*)	50.1	-CH-	0.95 (1H, *m*)	50.2
10	-	36.5	Q	-	36.5
11	1.53 (1H, *m*), 1.03 (1H, *m*)	21.1	-CH_2-	1.54 (2H, *m*)	21.1
12	2.03 (1H, *m*), 1.16 (1H, *m*)	39.8	-CH_2-	2.07 (1H, *m*), 1.20 (1H, *m*)	39.8
13	-	42.3	Q	-	42.3
14	1.01 (1H, *m*)	56.8	-CH-	1.03 (1H, *m*)	56.8
15	1.64 (1H, *m*), 1.34 (1H, *m*)	24.3	-CH_2-	1.64 (1H, *m*), 1.33 (1H, *m*)	24.3
16	1.87 (1H, *m*), 1.34 (1H, *m*)	28.2	-CH_2-	1.92 (1H, *m*), 1.30 (1H, *m*)	28.3
17	1.14 (1H, *m*)	56.1	-CH-	1.16 (1H, *m*)	56.1
18	0.70 (3H, *s*)	11.8	-CH_3	0.73 (3H, *s*)	11.9
19	1.02 (3H, *s*)	19.4	-CH_3	1.06 (3H, *s*)	19.4
20	1.36 (1H, *m*)	36.1	-CH-	1.39 (1H, *m*)	36.2
21	0.93 (3H, *d, J* = 6.3)	18.8	-CH_3	0.97 (3H, *d, J* = 6.5)	18.8
22	1.35 (1H, *m*), 1.02 (1H, *m*)	33.9	-CH_2-	1.36 (1H, *m*), 0.93 (1H, *m*)	34.0
23	1.18 (2H, *m*)	26.1	-CH_2-	1.21 (2H, *m*)	26.1
24	0.95 (1H, *m*)	45.8	-CH-	0.95 (1H, *m*)	45.9
25	1.69 (1H, *m*)	29.1	-CH-	1.71 (1H, *m*)	29.2
26	0.86 (3H, *d, J* = 6.7)	19.8	-CH_3	0.88 (3H, *d, J* = 1.8)	19.8
27	0.82 (3H, *d, J* = 6.7)	19.0	-CH_3	0.86 (3H, *d*)	19.1
28	1.27 (2H, *brs*)	23.1	-CH_2-	1.27 (2H, *brs*)	23.1
29	0.85 (3H, *t, J* = 7.5)	12.0	-CH_3	0.89 (3H, *s*)	12.0
			Palmitate moiety		
1'	-	173.9	Q (-C=O)	-	175.5
2'	2.37 (2H, *t, J* = 7.5)	34.1	-CH_2-	2.34 (2H, *t, J* = 7.6)	34.1

Table 10 (continued)

3'	1.63 (2H, *m*)	24.9	-CH_2-	1.57 (2H, *m*)	24.9
4'	1.27 (2H, *brs*)	29.1	-CH_2-	1.31-1.21 (2H, *brs*)	29.2
5'	1.27 (2H, *brs*)	29.1	-CH_2-	1.31-1.21 (2H, *brs*)	29.2
6'	1.27 (2H, *brs*)	29.3	-CH_2-	1.31-1.21 (2H, *brs*)	29.3
7'	1.27 (2H, *brs*)	29.4	-CH_2-	1.31-1.21 (2H, *brs*)	29.4
8'	1.27 (2H, *brs*)	29.6	-CH_2-	1.31-1.21 (2H, *brs*)	29.5
9'	1.27 (2H, *brs*)	29.6	-CH_2-	1.31-1.21 (2H, *brs*)	29.6
10'-13'	1.27 (8H, *brs*)	29.7	-CH_2-	1.31-1.21 (2H, *brs*)	29.7
14'	1.27 (2H, *brs*)	31.9	-CH_2-		31.9
15'	1.31 (2H, *brs*)	22.7	-CH_2-		22.7
16'	0.89 (3H, *t*, *J* = 7.0)	14.1	-CH_3	0.86 (3H, *t*, *J* = 6.4)	14.1

brs; broad singlet.

4.2.1.5. Compound 28

Compound **28** was isolated as yellow crystals. Its ^{1}H NMR spectrum (400 MHz, $CDCl_3$) revealed signals of an olefinic proton at δ_H 6.85 (1H, *dd*, *J* = 3.5, 3.5 Hz, H-12) and diastereotopic oxymethylene signals at δ_H 4.36 (1H, *t*, *J* = 9.2 Hz, H-15a) and 4.03 (1H, *t*, *J* = 9.1 Hz, H-15b). The deshielded δ_H value of H-12 was evident that the proton is nearest to an electron-withdrawing group. The signals at δ_H 5.28 (1H, *brs*) and 3.42 (1H, *t*, *J* = 2.9 Hz) suggest hydroxyl (OH) and oxymethine (H-3) protons, respectively. The peaks at δ_H 2.79 (1H, *dd*, *J* = 8.7, 4.4 Hz, H-14), and 2.37 (1H, *q*, *J* = 5.6 Hz, H-11a), and 2.32 (1H, *q*, *J* = 5.7 Hz, H-11b) were assignable to the sp^3 methine and methylene protons adjacent to the oxymethylene and sp^2 methine groups, respectively. The spectrum also displayed four groups of methyl protons at δ_H 0.95 (3H, *s*), 0.92 (3H, *s*), 0.85 (3H, *s*), and 0.76 (3H, *s*) assignable to H-20, H-18, H-19, and H-17, respectively (Table 11, Appendix 6A).

In its ^{13}C NMR (100 MHz, $CDCl_3$) spectrum, compound **28** displayed signals at δ_C 170.3 (C-16), 136.4 (C-12), 127.0 (C-13), and 67.3 (C-15) associated with a spongiane diterpenoid lactone skeleton (also supported by the ^{1}H NMR spectral analysis). Due to the resonance effects of the carboxylate group, the δ_C value of C-12 (olefinic methine) was deshielded than the quaternary olefinic carbon (C-13). An additional sp^3 oxymethine signal was observed at δ_C 75.8 assignable to C-3. The spectrum also revealed four methyl signals at δ_C 28.4, 22.2, 15.2, and 14.2 corresponding to C-18, C-19, C-20, and C-17, respectively. Moreover, the carbon signals at δ_C 54.1, 51.1, 49.3,

40.7, 37.5, 37.1, 34.5, 32.8, 25.1, 24.2, and 18.0 attributed to C-5, C-9, C-14, C-7, C-4, C-10, C-8, C-1, C-2, C-11, and C-6, respectively. The types of the carbons were verified by the DEPT-135 spectrum. Thereby, the spectral information revealed one sp^2 olefinic methine signal at δ_C 136.4 (C-12), two sp^3 oxymethine and oxymethylene signals at δ_C 75.8 (C-3) and 67.3 (C-15), respectively, three sp^3 methine carbons, five sp^3 methylene and four methyl signals and were consistent with the ^{13}C NMR spectral analysis of the compound (Table 11, Appendices 6B and C).

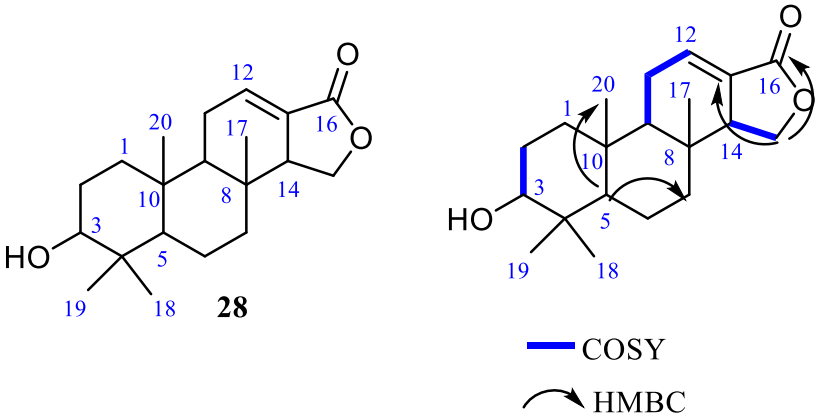

Figure 11: Chemical structure of compound **28**, and key COSY and HMBC correlations.

The spectral analyses were supported by 2D NMR correlations. Accordingly, the COSY spectrum exhibited ^3J correlations between H-2 (δ_H 2.11, 1.56) and H-3 (δ_H 3.42), H-9 (δ_H 1.43) and H-11 (δ_H 2.37), H-11 (δ_H 2.37) and H-12 (δ_H 6.85), and H-14 (δ_H 2.79) and H-15 (δ_H 4.36, 4.03). In addition, the connectivities were confirmed by HMBC correlations, thereby the spectrum showed ^3J correlations between H-5 (δ_H 1.38) and C-7, 20 (δ_C 40.7, 15.2), H-15 (δ_H 4.36, 4.03), and C-13, 16 (δ_C 127.0, 170.3) (Table 11, Appendices 6D and E). Finally, the spectral data were in close agreement with the reported values of 3-hydroxy isoagatholactone (**28**) (Degfie *et al.*, 2022) (Figure 11).

Table 11: ^{1}H (400 MHz), ^{13}C (100 MHz), DEPT-135, COSY, and HMBC NMR ($CDCl_3$, δ in ppm, J in Hz) spectral data of compound **28**, and ^{1}H and ^{13}C NMR values of 3-hydroxy isoagatholactone in the literature.

C. No.	**Compound 28**					**3-Hydroxy isoagatholactone** (Degfie *et al.*, 2022)	
	^{1}H NMR	**^{13}C NMR**	**DEPT-135**	**COSY**	**HMBC**	**^{1}H NMR**	**^{13}C NMR**
1	1.94 (1H, *m*), 1.54 (1H, *m*)	32.8	-CH_2-			1.60 (2H, *m*)	32.7
2	2.11 (1H, *m*), 1.56 (1H, *m*)	25.1	-CH_2-	H-3		1.52 (2H, *m*)	25.0
3	3.42 (1H, *t*, *J* = 2.9)	75.8	-CH-O-	H-2		3.42 (1H, *t*, *J* = 2.9)	75.7
4	-	37.5	Q			-	37.4
5	1.38 (1H, *m*)	54.1	-CH-		C-7, 20	1.36 (1H, *m*)	56.6
6	1.46 (1H, *m*), 1.35 (1H, *m*)	18.0	-CH_2-			1.39 (2H, *m*)	17.9
7	1.68 (1H, *m*), 1.66 (1H, *m*)	40.7	-CH_2-			1.45 (2H, *m*)	40.6
8	-	34.5	Q			-	34.4
9	1.43 (1H, *m*)	51.1	-CH-	H-11		1.36 (1H, *m*)	51.1
10	-	37.1	Q			-	37.0
11	2.37 (1H, *q*, *J* = 5.6), 2.32 (1H, *q*, *J* = 5.7)	24.2	-CH_2-	H-9, 12		2.31 (2H, *m*)	24.1
12	6.85 (1H, *dd*, *J* = 3.5, 3.5)	136.4	=CH-	H-11		6.85 (1H, *dd*, *J* = 3.5, 3.5)	136.4
13	-	127.0	Q			-	127.0
14	2.79 (1H, *dd*, *J* = 8.7, 4.4)	49.3	-CH-	H-15		2.79 (1H, *m*)	53.9
15	4.36 (1H, *t*, *J* = 9.2), 4.03 (1H, *t*, *J* = 9.1)	67.3	-CH_2-O-	H-14	C-13, 16	4.36 (1H, *t*, *J* = 9.1), 4.03 (1H, *t*, *J* = 9.1)	67.2
16	-	170.3	Q (-C=O)			-	170.3
17	0.76 (3H, *s*)	14.2	-CH_3			0.78 (3H, *s*)	14.1
18	0.92 (3H, *s*)	28.4	-CH_3			0.94 (3H, *s*)	28.3
19	0.85 (3H, *s*)	22.2	-CH_3			0.97 (3H, *s*)	22.1
20	0.95 (3H, *s*)	15.2	-CH_3			0.87 (3H, *s*)	15.1
OH	5.28 (1H, *brs*)	-	-			5.32 (1H, *brs*)	-

4.2.1.6. Compound 85

Compound **85** was isolated as colorless crystals. The ^{1}H NMR (400 MHz, CD_3OD) spectrum of the compound revealed signals of aromatic protons at δ_H 7.71 (2H, *dd*, *J* = 5.7, 3.3 Hz, H-3, 6) and 7.52 (2H, *dd*, *J* = 5.7, 3.3 Hz, H-4, 5) with AA'BB' spin pattern of aromatic rings. The proton signals at δ_H 4.36 (4H, *q*, *J* = 7.1 Hz, H-1', 1") and 1.36 (6H, *t*, *J* = 7.1 Hz, H2', 2") were assignable to the oxymethylene and methyl protons of the ethoxy group (Table 12, appendix 7A). Notably, the ^{13}C NMR (100 MHz, CD_3OD) spectrum of the compound revealed six well-resolved signals with significant peak intensity, suggesting that the compound possesses a molecular symmetry. Thus, the signals at δ_C 167.7 (C-7, 8), 132.3 (C-1, 2), 131.0 (C-4, 5), and 128.9 (C-3, 6) attributed to an aromatic moiety with a diester functional group. The spectrum also showed signals at δ_C 61.7 (C-1', 1") and 14.2 (C-2', 2") assignable to the oxymethylene and methyl carbons of the ethoxy substituent. In addition, the DEPT-135 spectrum displayed two sp^2 aromatic signals assignable to four carbons, one oxymethylene signal assignable to two carbons, and one methyl signal assignable to two carbons, and was in accordance with the ^{13}C NMR spectral analysis of the compound (Table 12, appendices 7B and C).

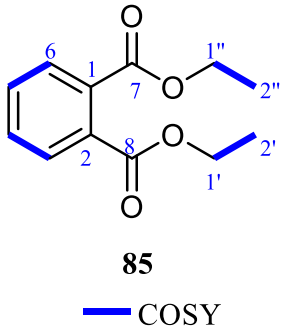

85

COSY

Figure 12: Chemical structure of compound **85**, and key COSY correlations.

The spectral analyses were also supported by 2D NMR correlations. Accordingly, the COSY spectrum exhibited correlations between H-3 (δ_H 7.71) and H-4 (δ_H 7.52), H-5 (δ_H 7.52) and H-6 (δ_H 7.71), H-1' (δ_H 4.36) and H-2' (δ_H 1.36), and H-1" (δ_H 4.36) and H-2" (δ_H 1.36) (Table 12, appendices 7D). After all, the spectral data presented matches with the literature values of diethyl phthalate (**85**) (Garg *et al.*, 2014) (Figure 12). Phthalate compounds are isolated from plant materials due to possible plasticizers of industrial origin accumulated in plants. This is due to the fact that plants can be contaminated by plasticizers leading to the accretion and isolation of phthalates in plant extracts (Bianco *et al.*, 2014).

Table 12: ^{1}H (400 MHz), ^{13}C (100 MHz), DEPT-135, and COSY NMR (CD_3OD, δ in ppm, J in Hz) spectral data of compound **85**, and ^{1}H and ^{13}C-NMR values of diethyl phthalate in the literature.

C. No.	**Compound 85**				**Diethyl phthalate** (Garg *et al.*, 2014)	
	^{1}H NMR	**^{13}C NMR**	**DEPT-135**	**COSY**	**^{1}H NMR**	**^{13}C NMR**
1	-	132.3	Q		-	132.3
2	-	132.3	Q		-	132.3
3	7.71 (1H, *dd*, *J* = 5.7, 3.3)	128.9	=CH-	H-4	7.60 (1H, *dd*, *J* = 8.5)	128.7
4	7.52 (1H, *dd*, *J* = 5.7, 3.3)	131.0	=CH-	H-3	7.50 (1H, *dd*, *J* = 8.5)	131.4
5	7.52 (1H, *dd*, *J* = 5.7, 3.3)	131.0	=CH-	H-6	7.50 (1H, *dd*, *J* = 8.5)	131.4
6	7.71 (1H, *dd*, *J* = 5.7, 3.3)	128.9	=CH-	H-5	7.60 (1H, *dd*, *J* = 8.5)	128.7
7	-	167.7	Q (-C=O)		-	167.0
8	-	167.7	Q (-C=O)		-	167.0
1'	4.36 (2H, *q*, *J* = 7.1)	61.7	$-CH_2-$	H-2'	4.27 (2H, *q*)	61.4
2'	1.36 (3H, *t*, *J* = 7.1)	14.2	$-CH_3$	H-1'	1.23 (3H, *t*)	13.8
1''	4.36 (2H, *q*, *J* = 7.1)	61.7	$-CH_2-$	H-2''	4.27 (2H, *q*)	61.4
2''	1.36 (3H, *t*, *J* = 7.1)	14.2	$-CH_3$	H-1''	1.23 (3H, *t*)	13.8

4.2.1.7. Compound 25

Compound **25** was obtained as pale brown crystals, and its melting point was determined in the range of 180-182 °C (literature mp: 185 °C (Rohaiza *et al.*, 2012)). Its ^{1}H NMR (400 MHz, CD_3OD) spectrum exhibited aromatic signals with AA'BB' spin pattern at δ_H 7.14 (2H, *d*, *J* = 8.7 Hz, H-2, 6) and 6.78 (2H, *d*, *J* = 8.7 Hz, H-3, 5) (ring A_1), AA'BB' spin pattern at δ_H 7.03 (2H, *d*, *J* = 8.8 Hz, H-2', 6') and 6.66 (2H, *d*, *J* = 8.8 Hz, H-3', 5') (ring B_1), AB spin pattern at δ_H 6.64 (1H, *s*, H-14') and 6.26 (1H, *s*, H-12') (ring B_2), and AB_2 spin pattern at δ_H 6.21 (1H, *s*, H-12) and 6.18 (2H, *s*, H-10, 14) (ring A_2). The signals appeared at δ_H 6.84 (1H, *d*, *J* = 16.7 Hz) and 6.57 (1H, *d*, *J* = 16.3 Hz) attributed to trans-oriented olefinic protons (H-7' and H-8', respectively). The spectrum also displayed signals at δ_H 5.37 (1H, *d*, *J* = 6.6, H-7) and 4.35 (1H, *d*, *J* = 6.6, H-8) corresponding to the oxymethine (H-7) and methine protons (H-8) of the substituted tetrahydro-furan skeleton (ring C) (Table 13, Appendix 8A).

The ^{13}C NMR (100 MHz, CD_3OD) spectrum revealed 22 identifiable signals assignable to 28 carbons. The signals at δ_C 162.7 (C-11') (ring B_2), 160.0 (C-11, 13) (ring A_2), 159.7 (C-13') (ring B_2), 158.5 (C-4) (ring A_1), and 158.4 (C-4') (ring B_1) attributed to the oxygen linked aromatic carbons of the structure, and other non-oxygenated quaternary carbons were appeared at δ_C 147.3 (C-9), 136.8 (C-9'), 133.8 (C-1), 131.2 (C-1'), and 120.0 (C-10'). The spectrum also showed sp^2 aromatic methine signals at δ_C 128.8 (C-2', 6'), 128.1 (C-2, 6), 116.4 (C-3, 5), 116.3 (C-3', 5'), 107.5 (C-10, 14), 104.3 (C-14'), 102.3 (C-12) and 96.9 (C-12'), and sp^2 olefinic methine signals at δ_C 130.3 (C-7') and 123.6 (C-8'). The substituted tetrahydro-furan carbons appeared at δ_C 94.8 and 58.3 were assignable to C-7 and C-8, respectively. Furthermore, the DEPT-135 spectrum indicated eight sp^2 aromatic methine signals assignable to thirteen carbons, two sp^2 olefinic methine signals, and two sp^3 oxymethine and methine carbons which were consistent with the ^{13}C NMR spectral data of the compound (Table 13, Appendices 8B and C).

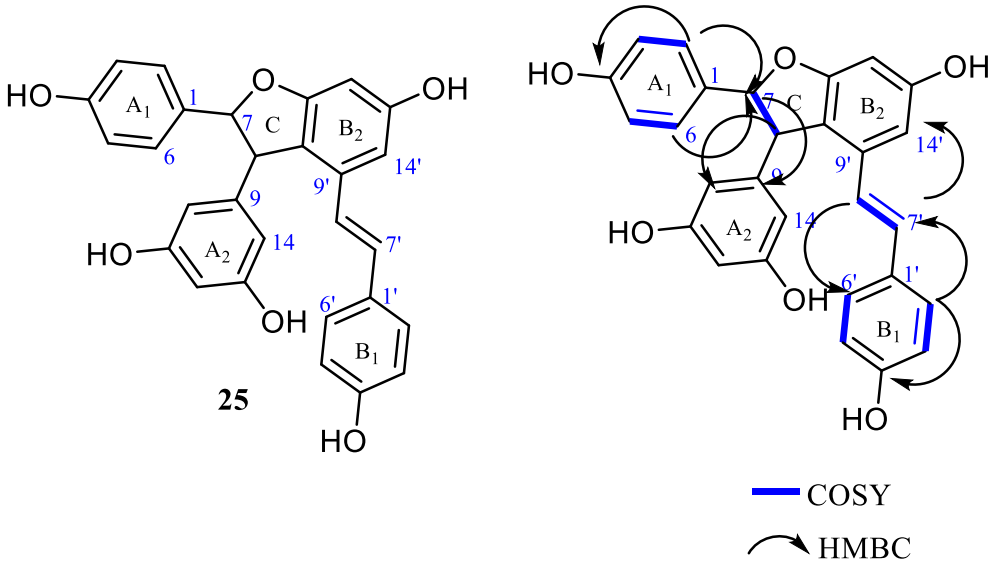

Figure 13: Chemical structure of compound **25**, and key COSY and HMBC correlations.

The connections and substitution patterns of the compound were established from the COSY and HMBC correlations. The COSY spectrum showed correlations between H-2, 6 (δ_H 7.14) and H-3, 5 (δ_H 6.78), H-7 (δ_H 5.37) and H-8 (δ_H 4.35), H-2', 6' (δ_H 7.03) and H-3', 5' (δ_H 6.66), H-7' (δ_H 6.84) and H-8' (δ_H 6.57) in agreement with rings A_1, C, B_1, and trans olefinic protons, respectively. The HMBC spectrum also revealed ^3J correlations between H-2/6 (δ_H 7.14) and C-4, 7 (δ_C 158.5, 94.8), ^2J correlations between H-3, 5 (δ_H 6.78) and C-2, 6 (δ_C 128.1), ^3J correlations between H-7 (δ_H 5.37) and C-2/6, 9 (δ_C 128.1 and 147.3, respectively), ^3J, ^2J, ^2J, ^3J, ^2J, and ^3J correlations between

H-8 (δ_H 4.35) and C-1, 7, 9, 10/14 10', 11' (δ_C 133.8, 94.8, 147.3, 107.5, 120.0 and 162.7, respectively), ^3J, ^2J and ^3J correlations between H-10/14 (δ_H 6.18) and C-8, 11/13, 12 (δ_C 58.3, 160.0 and 102.3, respectively), ^3J correlations between H-2'/6' (δ_H 7.03) and C-4', 7' (δ_C 158.4 and 130.3, respectively), and ^4J correlations between H-7' (δ_H 6.84) and C-14' (δ_C 104.3) (Table 13, Appendices 8D-F). Overall, the spectral analyses were consistent with the literature data for ***ε***-viniferin (**25**) (Degfie *et al.*, 2022, Yadav *et al.*, 2019) (Figure 13).

Table 13: ^{1}H (400 MHz), ^{13}C (100 MHz), DEPT-135, COSY, and HMBC NMR (CD_3OD, δ in ppm, J in Hz) spectral data of compound **25**, and ^{1}H and ^{13}C NMR values of ε-viniferin in the literature.

C. No.	**Compound 25**					***ε*-Viniferin** (Degfie *et al.*, 2022, Yadav *et al.*, 2019)	
	^{1}H NMR	**^{13}C NMR**	**DEPT-135**	**COSY**	**HMBC**	**^{1}H NMR**	**^{13}C NMR**
1	-	133.8	Q			-	133.8
2/6	7.14 (2H, *d*, *J* =8.7)	128.1	=CH-	H-3/5	C-4, 7	7.16 (2H, *d*, *J* = 8.6)	128.2
3/5	6.78 (2H, *d*, *J* = 8.7)	116.4	=CH-	H-2/6	C-2/6	6.79 (2H, *d*, *J* = 8.6)	116.3
4	-	158.5	Q			-	159.4
7	5.37 (1H, *d*, *J* = 6.6)	94.8	-CH-O-	H-8	C-2, 6, 9	5.39 (1H, *d*, *J* = 6.6)	94.8
8	4.35 (1H, *d*, *J* = 6.6)	58.3	-CH-	H-7	C-1, 7, 9, 10, 10', 11', 14	4.37 (1H, *d*, *J* = 6.6)	58.2
9	-	147.3	Q			-	147.3
10/14	6.18 (2H, *s*)	107.5	=CH-		C-8, 11, 12, 13	6.19 (2H, *s*)	107.6
11, 13	-	160.0	Q			-	159.9
12	6.21 (1H, *s*)	102.3	=CH-			6.18 (1H, *s*)	102.2
1'	-	131.2	Q			-	131.1
2'/6'	7.03 (2H, *d*, *J* = 8.8)	128.8	=CH-	H-3'/5'	C-4', 7'	7.06 (2H, *d*, *J* = 8.7)	128.8
3'/5'	6.66 (2H, *d*, *J* = 8.8)	116.3	=CH-	H-2'/6'		6.67 (2H, *d*, *J* = 8.8)	116.3
4'	-	158.4	Q			-	158.3
7'	6.84 (1H, *d*, *J* = 16.7)	130.3	=CH-	H-8'	C-14'	6.84 (1H, *d*, *J* = 16.4)	130.3
8'	6.57 (1H, *d*, *J* = 16.3)	123.6	=CH-	H-7'	C-2',6', 9'	6.59 (1H, *d*, *J* = 16.5)	123.6
9'	-	136.8	Q			-	136.8
10'	-	120.0	Q			-	120.0
11'	-	162.7	Q			-	162.7
12'	6.26 (1H, *s*)	96.9	=CH-			6.25 (1H, *s*)	96.8
13'	-	159.7	Q			-	159.7
14'	6.64 (1H, *s*)	104.3	=CH-			6.63 (1H, *s*)	104.3

4.2.1.8. Compound 66

Compound **66** was collected as yellow crystals, and its melting point was determined in the range of 352-354 °C (literature mp: 357 °C, (Perkin, 1902)). In its ^{1}H NMR (400 MHz, CD_3OD) spectrum, the compound exhibited signals of aromatic protons at δ_H 7.35 (2H, *s*, H-2', 6') with AA' spin pattern (ring B), 6.38 (1H, *d*, *J* = 2.0 Hz, H-8), and 6.18 (1H, *d*, *J* = 2.0 Hz, H-6) with AB spin pattern (ring A), attributed to a 3, 3', 4', 5, 5', 7-hexahydroxy flavone skeleton (Table 14, Appendix 9A). In addition, the ^{13}C NMR (100 MHz, CD_3OD) spectrum showed a signal at δ_C 177.2 (C-4) suggesting the presence of an *α, β*-unsaturated carbonyl compound. The signals at δ_C 165.5 (C-7), 162.4 (C-5), 158.1 (C-9) (ring A), 147.9 (C-2), 137.3 (C-3) (ring C), 146.7 (C-3', 5') and 136.9 (C-4') (ring B) were assignable to the oxygenated quaternary aromatic carbons. The spectrum also revealed non-oxygenated quaternary carbons at δ_C 123.0 (C-1') and 104.4 (C-10), and sp^2 aromatic methine signals at δ_C 108.5 (C-2', 6'), 99.2 (C-6) and 94.3 (C-8) associated with a hexa-substituted flavone skeleton. The types of carbon signals were confirmed by DEPT-135 spectral information. Accordingly, the spectrum displayed three sp^2 aromatic methine signals assignable to four carbons (Table 14, Appendices 9B and C).

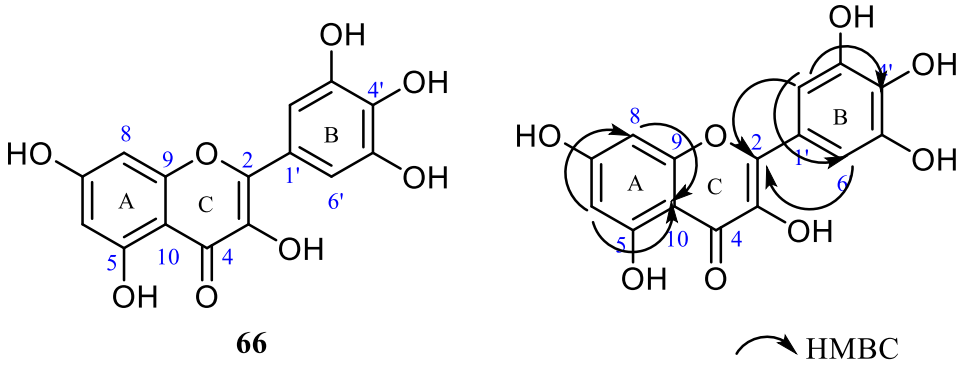

Figure 14: Chemical structure of compound **66**, and key HMBC correlations.

The ^{1}H-^{13}C linkages and connectivities of the compound were recognized from the HSQC and HMBC spectra, respectively. The HSQC spectrum exhibited ^{1}J correlations between H-6 (δ_H 6.18) and C-6 (δ_C 99.2), H-8 (δ_H 6.38) and C-8 (δ_C 94.3), and H-2'/6' (δ_H 7.35) and C-2'/6' (δ_C 108.5). The HMBC spectrum also showed ^{3}J correlations between H-6 (δ_H 6.18) and C-8, 10 (δ_C 94.3, 104.4), H-8 (δ_H 6.38) and C-6, 10 (δ_C 99.2, 104.4), ^{2}J, ^{3}J, ^{2}J, ^{3}J, and ^{3}J correlations between H-2' (δ_H 7.35) and C-1', 2, 3', 4', 6' (δ_C 123.0, 147.9, 146.7, 136.9, and 108.5, respectively), and ^{2}J, ^{3}J, ^{3}J, ^{3}J, and ^{2}J correlations between H-6' (δ_H 7.35) and C-1', 2, 2', 4', and 5' (δ_C 123.0, 147.9, 108.5, 136.9 and

146.7, respectively) (Table 14, Appendices 9D and E). The data were consistent with the reported values of myricetin (**66**) (Li *et al.*, 2022) (Figure 14).

Table 14: ^{1}H (400 MHz), ^{13}C (100 MHz), DEPT-135, and HMBC NMR (CD_3OD, δ in ppm, J in Hz) spectral data of compound **66**, and ^{1}H and ^{13}C NMR values of myricetin in the literature.

C. No.	**Compound 66**				**Myricetin** (Li *et al.*, 2022)	
	^{1}H NMR	**^{13}C NMR**	**DEPT-135**	**HMBC**	**^{1}H NMR**	**^{13}C NMR**
1	-	-	-		-	-
2	-	147.9	Q		-	148.0
3	-	137.3	Q		-	137.0
4	-	177.2	Q (–C=O)		-	177.3
5	-	162.4	Q		-	162.5
6	6.18 (1H, *d*, *J* = 2.0)	99.2	=CH-	C-8, 10	6.17 (1H, *d*, *J* = 2.1)	99.3
7	-	165.5	Q		-	165.6
8	6.38 (1H, *d*, *J* = 2.0)	94.3	=CH-	C-6, 10	6.37 (1H, *d*, *J* =2.1)	94.4
9	-	158.1	Q		-	158.2
10	-	104.4	Q		-	104.5
1'	-	123.0	Q		-	123.2
2'	7.35 (1H, *s*)	108.5	=CH-	C-1', 2, 3', 4', 6',	7.34 (1H, *s*)	108.6
3'	-	146.7	Q		-	146.8
4'	-	136.9	Q		-	137.4
5'	-	146.7	Q		-	146.8
6'	7.35 (1H, *s*)	108.5	=CH-	C-1', 2, 2' 4', 5'	7.34 (1H, *s*)	108.6

4.2.1.9. Compound 29

Compound **29** (mp: 165-167 °C) was collected as a grey-brown powder, and its melting point agreed with the literature values of tricuspidatol A (mp: 163-169 °C) (Lins *et al.*, 1991). In its ^{1}H NMR (400 MHz, CD_3OD) spectrum, seven different signals were observed. The doublet signals at δ_H 7.28 (4H, *d*, *J* = 8.6 Hz) and 6.77 (4H, *d*, *J* = 8.6 Hz) exhibiting an AA'BB' spin orientation were assignable to the aromatic protons in rings A and D (H-2, 2', 6, 6' and H-3, 3', 5, 5', respectively). The strong signal at δ_H 6.03 (4H, *s*, H-10, 10', 14, 14') and weak signals at δ_H 5.98 (2H, *s*, H-12, 12') attributed to the aromatic protons with AB_2 spin orientation in rings B and E. The spectrum also displayed signals of a 2, 3, 4, 5-substituted tetrahydro furan skeleton at δ_H 5.41 (2H, *d*, *J* = 6.5 Hz) and 3.59 (2H, *d*, *J* = 6.7 Hz) assignable to the oxymethine and methine protons in ring C (H-7, 7' and H-8, 8', respectively) (Table 15, Appendix 10A).

The ^{13}C NMR (100 MHz, CD_3OD) spectrum of the compound exhibited ten intense and well-resolved signals suggesting that the compound affords molecular symmetry. Thus, the signals at δ_C 158.7 (C-11, 11', 13, 13') (rings B and E), 157.9 (C-4, 4') (rings A and D) were assignable to the oxygen-linked aromatic carbons, while the signals at δ_C 142.1 (C-9, 9') (rings B and E) and 133.8 (C-1, 1') (rings A and D) attributed to the non-oxygenated quaternary carbons of the structure. The spectrum also displayed sp^2 aromatic methine signals at δ_C 128.8, 116.0, 108.9, and 101.8 corresponding to (C-2, 2', 6, 6'), (C-3, 3', 5, 5'), (C-10, 10', 14, 14'), and (C-12, 12'), respectively. In addition, the spectrum revealed signals at δ_C 85.9 (C-7/7') and 59.0 (C-8/8') assignable to the sp^3 oxymethine and methine carbons of the substituted tetrahydrofuran skeleton, respectively (ring C). Furthermore, the DEPT-135 spectrum showed four sp^2 aromatic methine signals, one oxymethine and another one sp^3 methine carbons, and was consistent with the ^{13}C NMR spectral analysis of the compound (Table 15, Appendices 10B and C).

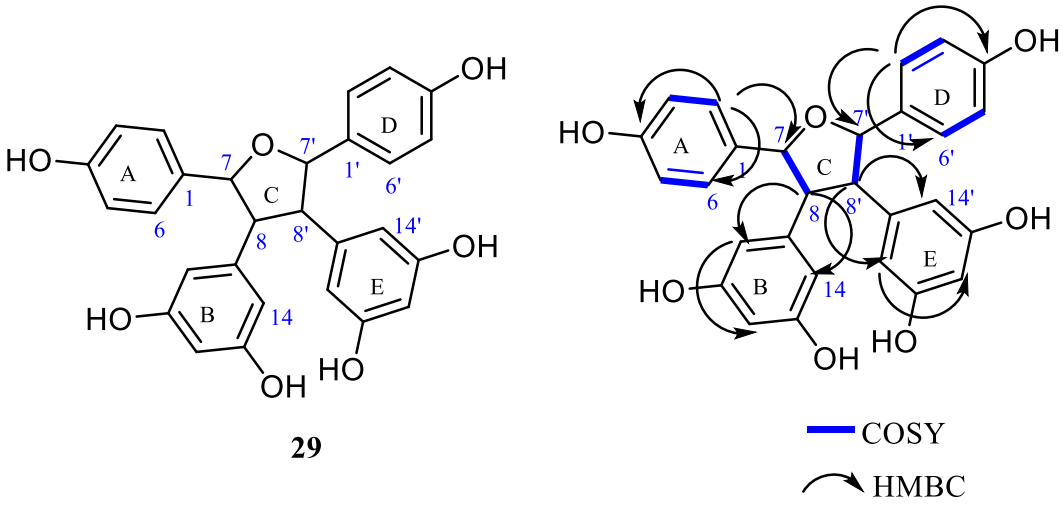

29

Figure 15: Chemical structure of compound **29**, and key COSY and HMBC correlations.

The connectivity and substitution patterns of the compound were proven by the COSY and HMBC correlations. Accordingly, the COSY spectrum revealed ^3J correlations between H-2/2'/6/6' (δ_H 7.28) and H-3/3/5/5' (δ_H 6.77), H-7/7' (δ_H 5.41) and H-8/8' (δ_H 3.59). The HMBC spectrum also revealed ^3J correlations between H-2/2' (δ_H 7.28) and C-4/4', 6/6' and 7/7' (δ_C 157.9, 128.8 and 85.9, respectively), ^3J and ^2J correlations between H-3/3', 5/5' (δ_H 6.77) and C-1/1', 4/4' (δ_C 133.8, 157.9), ^3J and ^2J correlations between H-5/5' (δ_H 6.77) and C-1/1', 4/4' (δ_C 133.8, 157.9), ^3J correlations between H-10/10' (δ_H 6.03) and C-8/8', 12/12' (δ_C 59.0, 101.8), and ^3J correlations

between H-8/8' (δ_H 3.59) and C-10/10', 14/14' (δ_C 108.9) (Table 15, Appendices 10D-F). Overall, the data presented were consistent with the reported values of tricuspidatol A (**29**) (Degfie *et al.*, 2022, Lins *et al.*, 1991) (Figure 15).

Table 15: ^{1}H (400 MHz), ^{13}C (100 MHz), DEPT-135, COSY, and HMBC NMR (CD_3OD, δ in ppm, *J* in Hz) spectral data of compound **29**, and ^{1}H and ^{13}C NMR values of tricuspidatol A in the literature.

C. No.	**Compound 29**					**Tricuspidatol A** (Degfie *et al.*, 2022, Lins *et al.*, 1991)	
	^{1}H NMR	**^{13}C NMR**	**DEPT-135**	**COSY**	**HMBC**	**^{1}H NMR**	**^{13}C NMR**
1,1'	-	133.8	Q			-	133.9
2/2'	7.28 (2H, *d*, *J* = 8.6)	128.8	=CH-	H-3 /3'	C-4, 6, 7/4', 6', 7'	7.27 (2H, *d*, *J* = 8.5)	128.8
3/3'	6.77 (2H, *d*, *J* = 8.6)	116.0	=CH-	H-2 /2'	C-1, 4, /1', 4'	6.76 (2H, *d*, *J* = 8.4)	116.1
4, 4'	-	157.9	Q			-	158.0
5/5'	6.77 (2H, *d*, *J* = 8.6)	116.0	=CH-	H-6 /6'	C-1, 4, /1', 4'	6.76 (2H, *d*, *J* = 8.4)	116.1
6/6'	7.28 (2H, *d*, *J* = 8.6)	128.8	=CH-	H-5 /5'	C-1, 4, 7/1', 4', 7'	7.27 (2H, *d*, *J* = 8.5)	128.8
7/7'	5.41 (2H, *d*, *J* = 6.5)	85.9	-CH-O-	H-8 /8'		5.40 (2H, *d*, *J* = 6.0)	85.9
8/8'	3.59 (2H, *d*, *J* = 6.7)	59.0	-CH-	H-7 /7'	C-10, 14, /10', 14'	3.58 (2H, *d*, *J* = 4.4)	59.0
9, 9'	-	142.1	Q			-	142.1
10/10'	6.03 (2H, *s*)	108.9	=CH-		C-8, 12, /8', 12'	6.02 (2H, *s*)	109.0
11, 11'	-	158.7	Q			-	158.8
12/12'	5.98 (2H, *s*)	101.8	=CH-			6.23 (2H, *s*)	101.8
13, 13'	-	158.7	Q			-	158.8
14/14'	6.03 (2H, *s*)	108.9	=CH-		C-8, 12, /8', 12'	6.02 (2H, *s*)	109.0

4.2.1.10. Compound 23

Compound **23** was obtained as brown crystals. The ^{1}H NMR (400 MHz, CD_3OD) spectrum revealed eleven different signals that were assignable. Accordingly, aromatic signals with AA'BB' spin pattern were appeared at δ_H 7.19 (2H, *d*, *J* = 8.5 Hz, H-2, 6) and 6.78 (2H, *d*, *J* = 8.5 Hz, H-3, 5) (ring A_1). The signals at δ_H 6.94 (2H, *d*, *J* = 8.5 Hz, H-2', 6') and δ_H 6.69 (2H, *d*, *J* = 8.6 Hz, H-3', 5') possessing another AA'BB' spin pattern were assignable to the protons in ring B_1. In addition, the signals at δ_H 6.45 (1H, *s*, H-14) and 6.18 (1H, *s*, H-12) with AB spin pattern correspond to the

protons in ring A_2. An AB_2 type protons were also observed at δ_H 6.14 (2H, *s*, H-10', 14') and 6.11 (1H, *s*, H-12') assignable to the aromatic protons in ring B_2. The spectrum also showed an olefinic proton at δ_H 6.25 (1H, *s*, H-7) and an sp^3 methine protons at δ_H 4.19 (1H, *d*, *J* = 2.7 Hz, H-7') and 3.68 (1H, *d*, *J* = 2.2 Hz, H-8') revealing the presence of pentacyclic ring protons (ring C) (Table 16, Appendix 11A).

In its ^{13}C (100 MHz, CD_3OD) NMR spectrum, the compound showed signals at δ_C 159.3 (C-11', 13') (ring B_2), 158.4 (C-13) (ring A_2), 157.4 (C-4) (ring A_1), 156.4 (C-4') (ring B_1), and 155.6 (C-11) (ring A2) attributed to the oxygenated aromatic carbons. The signals at δ_C 150.2 (C-8), 146.2 (C-9'), 143.4 (C-9), 138.1 (C-1'), 130.5 (C-1), and 128.3 (C-10) were assignable to the non-oxygenated quaternary aromatic and olefinic (C-8) carbons of the structure. The spectrum also showed sp^2 methine aromatic signals at δ_C 130.8 (C-2, 6), 129.1 (C-2', 6'), 116.1 (C-3, 5), 115.9 (C-3', 5'), 106.9 (C-10', 14'), 104.2 (C-12), 103.6 (C-14), 101.5 (C-12'), and a sp^2 olefinic methine signal at δ_C 125.6 (C-7). Two more signals appeared at δ_C 65.1 (C-8') and 55.6 (C-7') correspond to the sp^3 methine carbons of the pentacyclic ring (ring C). Furthermore, the DEPT-135 spectrum was used to validate the types of carbons. Thereby, the spectrum indicated eight sp^2 aromatic methine signals, one sp^2 olefinic methine, and two sp^3 methine signals and was compatible with the ^{13}C NMR spectral data of the compound (Table 16, Appendices 11B and C).

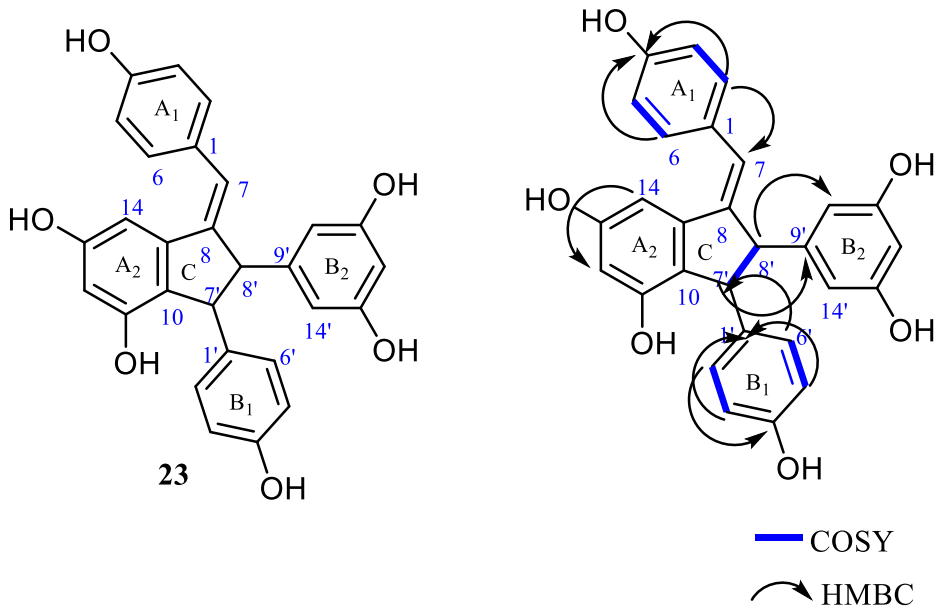

Figure 16: Chemical structure of compound **23**, and key COSY and HMBC correlations.

The proton-proton and proton-carbon connectivities of the compound were verified through bond (COSY) and HMBC correlations, respectively. Thus, the COSY spectrum exhibited ^{3}J correlations between H-2/6 (δ_H 7.19) and H-3/5 (δ_H 6.78), H-2'/6' (δ_H 6.94) and H-3'/5' (δ_H 6.69), H-7' (δ_H 4.19) and H-8' (δ_H 3.67). In addition, the HMBC spectrum showed ^{2}J, ^{3}J and ^{3}J correlations between H-2/6 (δ_H 7.19) and C-1, C-4, and C-7 (δ_C 130.5, 157.4, and 125.6, respectively), ^{3}J correlations between H-7 (δ_H 6.25) and C-2/6 (δ_C 130.8), ^{3}J correlations between H-14 (δ_H 6.45) and C-12 (δ_C 104.2), ^{3}J correlations between H-2'/6' (δ_H 6.94) and C-4', 7' (δ_C 156.4 and 55.6, respectively), ^{3}J correlations between H-3'/5' (δ_H 6.69) and C-1' (δ_C 138.1), ^{2}J and ^{3}J correlations between H-7' (δ_H 4.19) and C-1', 9' (δ_C 138.1, and 146.2, respectively), and ^{2}J and ^{3}J correlations between H-8' (δ_H 3.68) and C-9', 10'/14' (δ_C 146.2 and 106.9, respectively) (Table 16, Appendices 11D-F). Overall, the spectral data were in good coherence with the literature values of parthenocissin A (**23**) (Tanaka *et al.*, 1998) (Figure 16).

Table 16: ^{1}H (400 MHz), ^{13}C (100 MHz), DEPT-135, COSY, and HMBC NMR (CD_3OD, δ in ppm, J in Hz) spectral data of compound **23** and ^{1}H and ^{13}C NMR values of parthenocissin A in the literature.

C. No.	Compound 23					Parthenocissin A (Tanaka *et al.*, 1998)	
	^{1}H NMR	**^{13}C NMR**	**DEPT -135**	**COSY**	**HMBC**	**^{1}H NMR**	**^{13}C NMR**
1	-	130.5	Q			-	129.9
2/6	7.19 (2H, *d*, *J* = 8.5)	130.8	=CH-	H-3/5	C-1, 4, 7	7.20 (2H, *d*, *J* = 8.3)	130.6
3/5	6.78 (2H, *d*, *J* = 8.5)	116.1	=CH-	H-2/6	C-2/6	6.72 (2H, *d*, *J* = 8.3)	115.8
4	-	157.4	Q			-	157.1
7	6.25 (1H, *s*)	125.6	=CH-		C-2/6	6.31 (1H, *s*)	125.2
8	-	150.2	Q			-	149.8
9	-	143.4	Q			-	142.8
10	-	128.3	Q			-	128.0
11	-	155.6	Q			-	155.4
12	6.18 (1H, *s*)	104.2	=CH-			6.26 (1H, *d*, *J* = 1.5)	104.1
13	-	158.4	Q			-	158.4
14	6.45 (1H, *s*)	103.6	=CH-		C-12	6.52 (1H, *d*, *J* = 1.5)	103.1
1'	-	138.1	Q			-	137.4
2'/6'	6.94 (2H, *d*, *J* = 8.5)	129.1	=CH-	H-3'/5'	C-4', 7'	6.99 (2H, *d*, *J* = 8.8)	128.9
3'/5'	6.69 (2H, *d*, *J* = 8.6)	115.9	=CH-	H-2'/6'	C-1'	6.80 (2H, *d*, *J* = 8.8)	115.8
4'	-	156.4	Q			-	156.4
7'	4.19 (1H, *d*, *J* = 2.7)	55.6	-CH-	H-8'	C-1', 9'	4.26 (1H, *d*, *J* = 1.8)	54.9
8'	3.68 (1H, *d*, *J* = 2.2)	65.1	-CH-	H-7'	C-9', 10',14'	3.45 (1H, *brs*)	64.4
9'	-	146.2	Q			-	145.6
10'/14'	6.14 (2H, *s*)	106.9	=CH-			6.19 (2H, *s*)	106.9
11', 13'	-	159.3	Q			-	159.3
12'	6.11 (1H, *s*)	101.5	=CH-			6.19 (1H, *s*)	101.4

Notably, except palmitic acid (**83**) and *β*-sitosterol (**19**), all the compounds were isolated for the first time from *C. adenocaule*. The isolated compounds belong to different classes of compounds including olefines (hexadec-1-ene, **82**), fatty acids (palmitic acid, **83**), sterols (*β*-sitosterol (**19**) and *β*-sitosteryl palmitate (**84**)), diterpenes (3-hydroxy isoagatholactone, **28**), flavonoids (myricetin, **66**), and stilbenes (parthenocissin A (**23**), *ε*-viniferin (**25**), and tricuspidatol A (**29**)).

4.2.2. Structure elucidation of compounds isolated from roots of *Delonix regia*

The silica gel column chromatography of the combined CH_2Cl_2:CH_3OH (1:1) and methanol extracts of roots of *D. regia* yielded seven known compounds namely; stigmasterol (**40**), a mixture

of *β*-sitosterol (**19**) and stigmasterol (**40**), diethyl phthalate (**85**), *β*-sitosteryl-3*β*-glucopyranoside-6'-*O*-palmitate (**86**), quercetin (**42**), apigenin (**87**), and quercetin-3-*O*-rutinoside (**37**), and their structural information were supported by literature references. The TLC profiles of the compound isolates of *D. regia* are depicted in Appendix 12.

4.2.2.1. Compound 40

Compound **40** (mp: 167-168 °C) was isolated as yellow-green crystals. Its melting point matches with the reported values (165-168 °C) for stigmasterol (Amaro-Luis *et al.,* 2021). The ^{1}H NMR (400 MHz, $CDCl_3$) spectrum displayed signals at δ_H 5.35 (1H, *dd, J* = 5.0, 2.7, H-6), 5.14 (1H, *dd, J* = 15.1, 8.6, H-22), and 5.00 (1H, *dd, J* = 15.2, 8.6, H-23) signifying the presence of three olefinic protons, of which the *J* values of the latter two protons suggest their trans configuration. The spectrum also displayed multiplet peaks at δ_H 3.51 (1H, *m*, H-3) assignable to oxymethine protons and six groups of methyl protons at δ_H 1.02 (3H, *d, J* = 7.2, H-21), 0.99 (3H, *s*, H-19), 0.83 (3H, *d, J* = 6.1, H-27), 0.82 (3H, *d, J* = 6.3, H-26), 0.79 (3H, *t, J* = 6.0, H-29), and 0.68 (3H, *s*, H-18) was evident for a stigmastane tetracyclic triterpenoid. The remaining proton signals overlapped in the range between δ_H 2.30 and 0.90 (25H, *m*) (Table 17, Appendix 13A).

The ^{13}C NMR (100 MHz, $CDCl_3$) spectrum displayed 29 carbons associated with the structure of stigmastane tetracyclic triterpenoids. The signals at δ_C 140.8 (C-5), 138.4 (C-22), 129.3 (C-23), and 121.8 (C-6) were assignable to the olefinic carbons and the signal at δ_C 71.9 attributed to the oxymethine carbon of the compound (C-3). The spectrum also displayed signals at δ_C 56.9 (C-14), 56.0 (C-17), 51.3 (C-24), and 50.2 (C-9) corresponding to the sp^3 methine carbons of the structure. Furthermore, aliphatic carbon signals were observed at δ_C 42.4, 42.3, 40.6, 39.7, 37.3, 36.6, 32.0, 31.9 (x 2), 31.7, 29.8, 25.5, 24.4, 21.3, 21.2, 21.1, 19.5, 19.0, 12.3, and 12.1 assignable to C-4, C-13, C-20, C-12, C-1, C-10, C-7, (C-8, 25), C-2, C-16, C-28, C-15, C-26, C-21, C-11, C-19, C-27, C-29, and C-18, respectively. In agreement with the ^{13}C NMR spectral data, the DEPT-135 spectrum revealed three sp^2 olefinic carbons, one oxymethine, seven sp^3 methine, six methyl signals pointing up, and nine sp^3 methylene signals pointing down (Table 17, Appendices 13B and C).

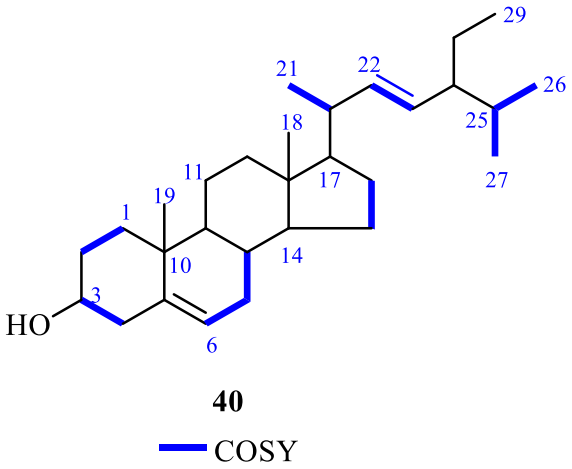

Figure 17: Chemical structure of compound **40**, and key COSY correlations.

The ^{1}H NMR assignments were verified by 2D COSY correlations. Accordingly, the spectrum revealed ^{3}J correlations between H-1b (δ_H 1.09) and H-2a (δ_H 1.82), H-3 (δ_H 3.51) and H-4a (δ_H 2.25), H-6 (δ_H 5.35) and H-7a (δ_H 1.96), H-7a (δ_H 1.96) and H-8 (δ_H 1.49), H-15 (δ_H 1.52) and H-16 (δ_H 1.81), H-20 (δ_H 2.03) and H-21 (δ_H 1.02), H-22 (δ_H 5.14) and H-23 (δ_H 5.00), and H-25 (δ_H 1.43) and H-26, 27 (δ_H 0.82, 0.83) (Table 17, Appendix 13D). Finally, the spectral analyses were in close agreement with the literature values (Cayme and Ragasa, 2004) of stigmasterol (**40**) (Figure 17).

Table 17: ^{1}H (400 MHz), ^{13}C (100 MHz), DEPT-135, and COSY NMR ($CDCl_3$, δ in ppm, J in Hz) spectral data of compound **40**, and ^{1}H and ^{13}C NMR values of stigmasterol in the literature.

C No.	**Compound 40**				**Stigmasterol** (Cayme and Ragasa, 2004)	
	^{1}H NMR	**^{13}C NMR**	**DEPT-135**	**COSY**	**^{1}H NMR**	**^{13}C NMR**
1	1.84 (1H, *m*), 1.09 (1H, *m*)	37.3	-CH_2-	H-2a	1.83 (1H, *m*), 1.08 (1H, *m*)	37.2
2	1.82 (1H, *m*), 1.50 (1H, *m*)	31.7	-CH_2-	H-1b	1.82 (1H, *m*), 1.49 (1H, *m*)	31.6
3	3.51 (1H, *m*)	71.9	-CH-O-	H-4a	3.53 (1H, *m*)	71.8
4	2.25 (1H, *m*), 2.21 (1H, *m*)	42.4	-CH_2-	H-3	2.28 (1H, *m*), 2.24 (1H, *m*)	42.3
5	-	140.8	Q		-	140.7
6	5.35 (1H, *dd, J* = 5.0, 2.7)	121.8	=CH-	H-7a	5.35 (1H, *d, J* = 4.7)	121.7
7	1.96 (1H, *m*), 1.51 (1H, *m*)	32.0	-CH_2-	H-6, 8	1.98 (1H, *m*), 1.53 (1H, *m*)	31.9
8	1.49 (1H, *m*)	31.9	-CH-	H-7a	1.46 (1H, *m*)	31.9
9	0.92 (1H, *m*)	50.2	-CH-		0.94 (1H, *m*)	50.1
10	-	36.6	Q		-	36.5
11	1.47 (1H, *m*), 1.43 (1H, *m*)	21.1	-CH_2-		1.48 (1H, *m*), 1.45 (1H, *m*)	21.0
12	1.99 (1H, *m*), 1.16 (1H, *m*)	39.7	-CH_2-		1.97 (1H, *m*), 1.15 (1H, *m*)	39.7
13	-	42.3	Q		-	42.2
14	1.06 (1H, *m*)	56.9	-CH-		1.00 (1H, *m*)	56.8
15	1.52 (1H, *m*), 1.07 (1H, *m*)	24.4	-CH_2-	H-16	1.55 (1H, *m*), 1.06 (1H, *m*)	24.4
16	1.81 (1H, *m*), 1.28 (1H, *m*)	29.8	-CH_2-	H-15	1.71 (1H, *m*), 1.27 (1H, *m*)	28.9
17	1.14 (1H, *m*)	56.0	-CH-		1.13 (1H, *m*)	55.9
18	0.68 (3H, *s*)	12.1	-CH_3		0.70 (3H, *s*)	12.0
19	0.99 (3H, *s*)	19.5	-CH_3		1.01 (3H, *s*)	19.4
20	2.03 (1H, *m*)	40.6	-CH-	H-21	2.04 (1H, *m*)	40.5
21	1.02 (3H, *d, J* = 7.2)	21.2	-CH_3	H-20	1.02 (3H, *d, J* = 6.8)	21.1
22	5.14 (1H, *dd, J* = 15.1, 8.6)	138.4	=CH-	H-23	5.15 (1H, *dd, J* = 15.1, 8.4)	138.3
23	5.00 (1H, *dd, J* = 15.2, 8.6)	129.3	=CH-	H-22	5.02 (1H, *dd, J* = 15.1, 8.4)	129.2
24	1.54 (1H, *m*)	51.3	-CH-		1.53 (1H, *m*)	51.2
25	1.43 (1H, *m*)	31.9	-CH-	H-26, 27	1.44 (1H, *m*)	31.9
26	0.82 (3H, *d, J* = 6.3)	21.3	-CH_3	H-25	0.84 (3H, *d, J* = 6.4)	21.2
27	0.83 (3H, *d, J* = 6.1)	19.0	-CH_3	H-25	0.83 (3H, *d, J* = 6.1)	18.9
28	0.90 (2H, *m*)	25.5	-CH_2-		1.15 (2H, *m*)	25.4
29	0.79 (3H, *t, J* = 6.0)	12.3	-CH_3		0.80 (3H, *t, J* = 6.0)	12.3

4.2.2.2. A mixture of compounds 19 and 40

The mixture of compounds **19** and **40** was collected as white needles. Based on the integration patterns and intensity of signals, its ^{1}H NMR (400 MHz, $CDCl_3$) spectrum revealed resonances of

a mixture of two compounds (approximately 3:1 of **19** and **40**). The spectrum displayed four sp^2 methine signals (two overlapped) at δ_H 5.35 (2H, *m*, H-6a, 6b), 5.15 (1H, *dd*, *J* = 15.1, 8.7, H-22b), and 5.02 (1H, *dd*, *J* = 15.2, 8.7, H-23b), sp^3 oxymethine signals at δ 3.53 (2H, *m*, H-3a, 3b) and ten groups of methyl protons at δ_H 1.02 (3H, *d*, *J* = 6.7, H-21b), 1.01 (6H, *s*, H-19), 0.92 (3H, *d*, *J*= 6.5, H-21a), 0.84 (3H, *t*, H-29a), 0.83 (6H, *d*, *J* = 6.1, H-27), 0.82 (3H, *d*, *J* = 6.3, H-26b), 0.81 (3H, *d*, *J* = 6.2, H-26a), 0.79 (3H, *t*, *J* = 6.0, H-29b), 0.69 (3H, *s*, H-18b), and 0.68 (3H, *s*, H-18a) which were characteristics of a mixture of phytosterols (Table 18, Appendix 14A).

The ^{13}C NMR (100 MHz, $CDCl_3$) spectrum associated with the DEPT-135 spectrum revealed resonances of fifty-eight carbon atoms including the signals overlapped in the same chemical environment with the under-cited functionalities. Six olefinic carbons at δ_C 140.7 (2x, C-5a, 5b), 138.3 (C-22b), 129.3 (C-23b), and 121.7 (2x, C-6a, 6b), two oxymethine carbons at δ_C 71.8 (2x, C-3a, 3b), fourteen methine carbons at δ_C 56.9 (C-14b), 56.8 (C-14a), 56.0 (C-17b), 55.9 (C-17a), 51.2 (C-24b), 50.2 (C-9b), 50.1 (C-9a), 45.8 (C-24a), 40.5 (C-20b), 36.1 (C-20a), 31.9 (3x, C-8a, 8b, 25b) and 29.1 (C-25a), four sp^3 quaternary carbons (from the DEPT-135 spectrum) at δ_C 42.3 (C-13b), 42.2 (C-13a) and 36.5 (2x, C-10a, 10b), twenty methylene carbons at δ_C 42.3 (2x, C-4a, 4b), 39.8 (C-12b), 39.7 (C-12a), 37.2 (2x, C-1a, 1b), 33.9 (C-22a), 31.9 (2x, C-7a, 7b), 31.6 (2x, C-2a, 2b), 29.4 (C-16b), 28.2 (C-16a), 26.0 (C-23a), 25.4 (C-28b), 24.7 (C-15a), 24.3 (C-15b), 23.0 (C-28a) and 21.1 (2x, C-11a, 11b), and twelve methyl carbons at δ_C 21.2 (C-21b), 21.1 (C-26b), 19.8 (C-19b), 19.4 (2x, C-19a, 26a), 19.0 (C-21a), 18.9 (C-27b), 18.8 (C-27a), 12.2 (C-29b), 12.0 (2x, C-18b, 29a), and 11.8 (C-18a). Many of the chemical shifts in the ^1H and ^{13}C NMR spectra of the compounds were overlapped designating resemblances in chemical structures. The only difference noted was the presence of a double bond at C-22 and C-23 in compound **40** which were converted to methylene carbons at δ_C 33.9 (C-22a) and 26.0 (C-23a) in the case of **19**, and the methine carbon at δ_C 51.2 (C-24b) in **40** were shielded to δ_C 45.8 (C-24a) in **19** (Table 18, Appendices 14B and C).

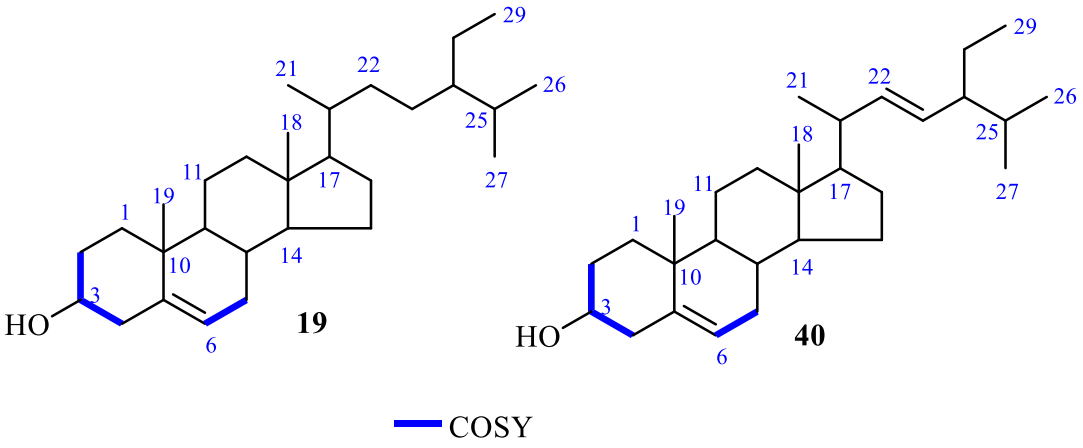

Figure 18: Chemical structures of the mixture of compounds **19** and **40**, and key COSY correlations.

The ^{1}H and ^{13}C NMR assignments of the compounds were verified by 2D NMR (COSY and HSQC) experiments. Thereby, the COSY spectrum exhibited ^{3}J correlations between H-6 (δ_H 5.35) and H-7 (δ_H 1.98), H-3 (δ_H 3.53) and H-4 (δ_H 2.28), H-3 (δ_H 3.53) and H-2 (δ_H 1.51), H-7 (δ_H 1.98) and H-8 (δ_H 1.51), and many more overlapped correlations in the up filled region. Furthermore, the HSQC spectrum exhibited ^{1}H-^{13}C linkages between H-6 (δ_H 5.35) and C-6 (δ_C 121.7), H-22b (δ_H 5.15) and C-22b (δ_C 138.3), H-23b (δ_H 5.02) and C-23b (δ_C 129.3), H-3 (δ_H 3.53) and C-3 (δ_C 71.8), H-4 (δ_H 2.28, 2.23 and C-4 (δ_C 42.3), H-12 (δ_H 2.01, 1.16) and C-12 (δ_C 39.7), H-2 (δ_H 1.82, 1.51) and C-2 (δ_C 31.6), H-1 (δ_H 1.83, 1.08) and C-1 (δ_C 37.2), H-18a (δ_H 0.68) and C-18a (δ_C 11.8), H-18b (δ_H 0.69) and C-18b (δ_C 12.0), H-21a (δ_H 0.92) and C-21a (δ_C 19.0), H-21b (δ_H 1.02) and C-21b (δ_C 21.2), H-26a (δ_H 0.81) and C-26a (δ_C 19.4), H-26b (δ_H 0.82) and C-26b (δ_C 21.1), H-27a (δ_H 0.83) and C-27a (δ_C 18.8), H-27b (δ_H 0.83) and C-27b (δ_C 18.9), H-29a (δ_H 0.84) and C-29a (δ_C 12.0), and H-29b (δ_H 0.79) and C-29b (δ_C 12.2) (Table 18, Appendices 14D and E). Overall, the spectral analyses were consistent with the reported values (Cayme and Ragasa, 2004) of a mixture of β-sitosterol (**19**) and stigmasterol (**40**) (Figure 18).

Table 18: ^{1}H (400 MHz), ^{13}C (100 MHz), and DEPT-135 NMR ($CDCl_3$, δ in ppm, J in Hz) spectral data of the mixture of compounds **19** and **40**, and ^{1}H and ^{13}C NMR values of β-sitosterol and stigmasterol in the literature.

C. No.	**Compound 19**		***β*-Sitosterol** (Cayme and Ragasa, 2004)			**Compound 40**		**Stigmasterol** (Cayme and Ragasa, 2004)	
	^{1}H NMR	**^{13}C NMR**	**^{1}H NMR**	**^{13}C NMR**	**DEPT-135**	**^{1}H NMR**	**^{13}C NMR**	**^{1}H NMR**	**^{13}C NMR**
1	1.83 (1H, *m*), 1.08 (1H, *m*)	37.2	1.83 (1H, *m*), 1.08 (1H, *m*)	37.2	$-CH_2-$	1.83 (1H, *m*), 1.08 (1H, *m*)	37.2	1.83 (1H, *m*), 1.08 (1H, *m*)	37.2
2	1.82 (1H, *m*), 1.51 (1H, *m*)	31.6	1.82 (1H, *m*), 1.49 (1H, *m*)	32.6	$-CH_2-$	1.82 (1H, *m*), 1.51 (1H, *m*)	31.6	1.82 (1H, *m*), 1.49 (1H, *m*)	31.6
3	3.53 (1H, *m*)	71.8	3.53 (1H, *m*)	71.8	-CH-O-	3.53 (1H, *m*)	71.8	3.53 (1H, *m*)	71.8
4	2.28 (1H, *m*), 2.23 (1H, *m*)	42.3	2.28 (1H, *m*), 2.24 (1H, *m*)	42.3	$-CH_2-$	2.28 (1H, *m*), 2.23 (1H, *m*)	42.3	2.28 (1H, *m*), 2.24 (1H, *m*)	42.3
5	-	140.7	-	140.7	Q	-	140.7	-	140.7
6	5.35 (1H, *m*)	121.7	5.35 (1H, *d*, J = 4.7)	121.7	=CH-	5.35 (1H, *m*)	121.7	5.35 (1H, *d*, J = 4.7)	121.7
7	1.98 (1H, *m*), 1.96 (1H, *m*)	31.9	1.98 (1H, *m*), 1.56 (1H, *m*)	31.9	$-CH_2-$	1.98 (1H, *m*), 1.96 (1H, *m*)	31.9	1.98 (1H, *m*), 1.53 (1H, *m*)	31.9
8	1.51 (1H, *m*)	31.9	1.46 (1H, *m*)	31.9	-CH-	1.51 (1H, *m*)	31.9	1.46 (1H, *m*)	31.9
9	0.93 (1H, *m*)	50.1	0.94 (1H, *m*)	50.1	-CH-	0.93 (1H, *m*)	50.2	0.94 (1H, *m*)	50.1
10	-	36.5	-	36.5	Q	-	36.5	-	36.5
11	1.50 (1H, *m*), 1.45 (1H, *m*)	21.1	1.48 (1H, *m*), 1.45 (1H, *m*)	21.0	$-CH_2-$	1.50 (1H, *m*), 1.45 (1H, *m*)	21.1	1.48 (1H, *m*), 1.45 (1H, *m*)	21.0
12	2.01 (1H, *m*), 1.16 (1H, *m*)	39.7	1.97 (1H, *m*), 1.15 (1H, *m*)	39.8	$-CH_2-$	2.01 (1H, *m*), 1.16 (1H, *m*)	39.8	1.97 (1H, *m*), 1.15 (1H, *m*)	39.7
13	-	42.2	-	42.2	Q	-	42.3	-	42.2
14	1.00 (1H, *m*)	56.8	1.03 (1H, *m*)	56.7	-CH-	1.00 (1H, *m*)	56.9	1.00 (1H, *m*)	56.8
15	1.64 (1H, *m*), 1.07 (1H, *m*)	24.7	1.55 (1H, *m*), 1.05 (1H, *m*)	24.3	$-CH_2-$	1.64 (1H, *m*), 1.07 (1H, *m*)	24.3	1.55 (1H, *m*), 1.06 (1H, *m*)	24.4
16	1.29 (2H, *m*)	28.2	1.24 (2H, *m*)	28.2	$-CH_2-$	1.81 (1H, *m*), 1.32 (1H, *m*)	29.4	1.71 (1H, *m*), 1.27 (1H, *m*)	28.9
17	1.10 (1H, *m*)	55.9	1.13 (1H, *m*)	56.0	-CH-	1.10 (1H, *m*)	56.0	1.13 (1H, *m*)	55.9
18	0.68 (3H, *s*)	11.8	0.68 (3H, *s*)	11.9	$-CH_3$	0.69 (3H, *s*)	12.0	0.70 (3H, *s*)	12.0

Table 18 (continued)									
19	1.01 (3H, *s*)	19.4	1.01 (3H, *s*)	19.4	$-CH_3$	1.01 (3H, *s*)	19.8	1.01 (3H, *s*)	19.4
20	1.35 (1H, *m*)	36.1	1.36 (1H, *m*)	36.1	-CH-	2.05 (1H, *m*)	40.5	2.04 (1H, *m*)	40.5
21	0.92 (3H, *d*, *J*= 6.5)	19.0	0.94 (3H, *d*)	18.8	$-CH_3$	1.02 (3H, *d*, *J* = 6.7)	21.2	1.02 (3H, *d*, *J* = 6.8)	21.1
22	1.33 (2H, *m*)	33.9	1.32 (2H, *m*)	33.9	$-CH_2$- (a), =CH- (b)	5.15 (1H, *dd*, *J* = 15.1, 8.7)	138.3	5.15 (1H, *dd*, *J* = 15.1, 8.4)	138.3
23	1.17 (2H, *m*)	26.0	1.15 (2H, *m*)	26.0	$-CH_2$- (a), =CH- (b)	5.02 (1H, *dd*, *J* = 15.2, 8.7)	129.3	5.02 (1H, *dd*, *J* = 15.1, 8.4)	129.2
24	0.93 (1H, *m*)	45.8	0.93 (1H, *m*)	45.8	-CH-	1.64 (1H, *m*)	51.2	1.53 (1H, *m*)	51.2
25	1.48 (1H, *m*)	29.1	1.65 (1H, *m*)	29.1	-CH-	1.45 (1H, *m*)	31.9	1.44 (1H, *m*)	31.9
26	0.81 (3H, *d*, *J* = 6.2)	19.4	0.82 (3H, *d*, *J* = 6.3)	19.0	$-CH_3$	0.82 (3H, *d*, *J* = 6.3)	21.1	0.84 (3H, *d*, *J* = 6.4)	21.2
27	0.83 (3H, *d*, *J* = 6.1)	18.8	0.83 (3H, *d*, *J* = 6.1)	19.8	$-CH_3$	0.83 (3H, *d*, *J* = 6.1)	18.9	0.83 (3H, *d*, *J* = 6.1)	18.9
28	1.01 (2H, *m*)	23.0	1.22 (2H, *m*)	23.0	$-CH_2$-	0.91 (2H, *m*)	25.4	1.15 (2H, *m*)	25.4
29	0.84 (3H, *t*)	12.0	0.85 (3H, *t*)	11.8	$-CH_3$	0.79 (3H, *t*, *J* = 6.0)	12.2	0.80 (3H, *t*, *J* = 6.0)	12.3

4.2.2.3. Compound 85

Compound **85** was also isolated from the roots of *C. adenocaule* (above). Hence, the entire structural elucidation of the compound is depicted under section 4.2.1.6, and Table 12, and its spectra are portrayed on Appendices 7A-D.

4.2.2.4. Compound 86

Compound **86** was isolated as white crystals, and its ^{1}H NMR (400 MHz, $CDCl_3$) spectrum exhibited multiplet signals at δ_H 5.34 (1H, *m*, H-6) signifying the presence of a single olefinic proton. A group of signals observed at δ_H 4.37 (1H, *dd*, *J* = 12.1, 5.2, H-6'a), 4.27 (1H, *d*, *J* = 11.5, H-1'), 4.13 (1H, *dd*, *J* = 12.1, 6.3, H-6'b), 3.65 (1H, *m*, H-3'), 3.37 (1H, *m*, H-4'), 3.44 (1H, *m*, H-5'), and 3.36 (1H, *m*, H-2') suggest the presence of a glucose moiety. The signals observed at δ_H 3.54 (1H, *m*, H-3) were assignable to an oxymethine proton evidencing the presence of a glycoside linkage. In addition, the singlet peaks appeared in the range δ_H 0.66-0.99 (18H, *m*, H-18, H-19, H-21, H-26, H-27, and H-29) confirm the presence of a steroidal skeleton that corresponds to the methyl groups of the main skeleton. The attachment of an extra fatty acid moiety was confirmed by the appearance of long-chain methylene signals in the upfield region of both the ^{1}H and ^{13}C NMR spectra. The majority of the proton signals overlaid in the region δ_H 2.40-1.00 (Table 19, Appendix 15A).

The ^{13}C NMR (100 MHz, $CDCl_3$) spectrum revealed forty-five well-resolved carbon signals assignable to fifty-one carbons attributed to a steroidal skeleton with additional glucose and fatty acid moieties. The fatty acid moiety was confirmed by the presence of an ester carbonyl at δ 174.7 (C-1'') and the identity of the fatty acid linkage was verified as palmitic acid based on the acid-catalyzed methanolysis (Scheme 5) followed by GC-MS analysis (Appendix 5E). The signals at δ_C 140.3 and 122.2 assignable to C-5 and C-6, respectively, indicated the presence of two olefinic carbons, of which the first δ_C value corresponds to an sp^2 quaternary carbon (from DEPT-135 spectrum). The spectrum also showed the resonance of six sugar carbon signals at δ_C 101.2 (C-1'), 76.1 (C-3'), 73.9 (C-5'), 73.6 (C-2'), 70.1 (C-4'), and 63.4 (C-6'), of which the signal of the anomeric carbon resonates at δ_C 101.2. Another oxymethine signal observed at δ_C 79.7 was attributed to the carbon atom forming a glycoside linkage (C-3) in the main skeleton of the structure. In addition, the carbon signals at δ_C 56.8, 56.1, 50.2, 45.8, and 36.2 correspond to the

sp^3 methine carbons of the structure and were assignable to C-14, C-17, C-9, C-24, and C-20, respectively. The spectrum also showed two sp^3 quaternary carbons at δ_C 42.4 (C-13) and 36.8 (C-10) supported by the DEPT-135 spectrum. The values of the remaining methylene and methyl signals are clearly stated in Table 19. In agreement with the ^{13}C NMR spectral data, the DEPT-135 spectrum displayed one sp^2 methine, six oxymethines, one oxymethylene, seven sp^3 methines, nineteen sp^3 methylenes assignable to twenty-five carbons, and seven methyl signals (Appendices 15B and C).

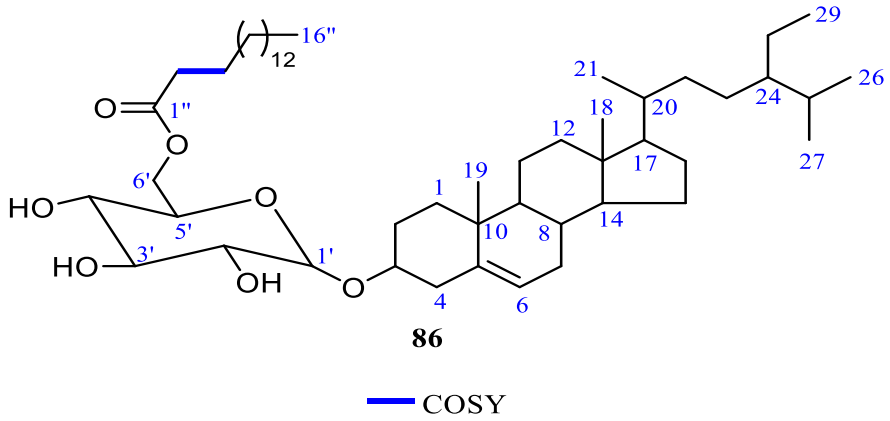

Figure 19: Chemical structure of compound **86**, and key COSY correlations.

Moreover, the ^1H-^1H COSY NMR spectrum showed correlations for two spin systems. Accordingly, ^3J correlations were observed between H-2" (δ_H 2.31) and H-3" (δ_H 1.61) (Table 19, Appendix 15D). Overall, the data generated matches with the reported values (Nguyen *et al.*, 2004) of *β*-sitosteryl-3*β*-glucopyranoside-6'-*O*-palmitate (**86**) (Figure 19).

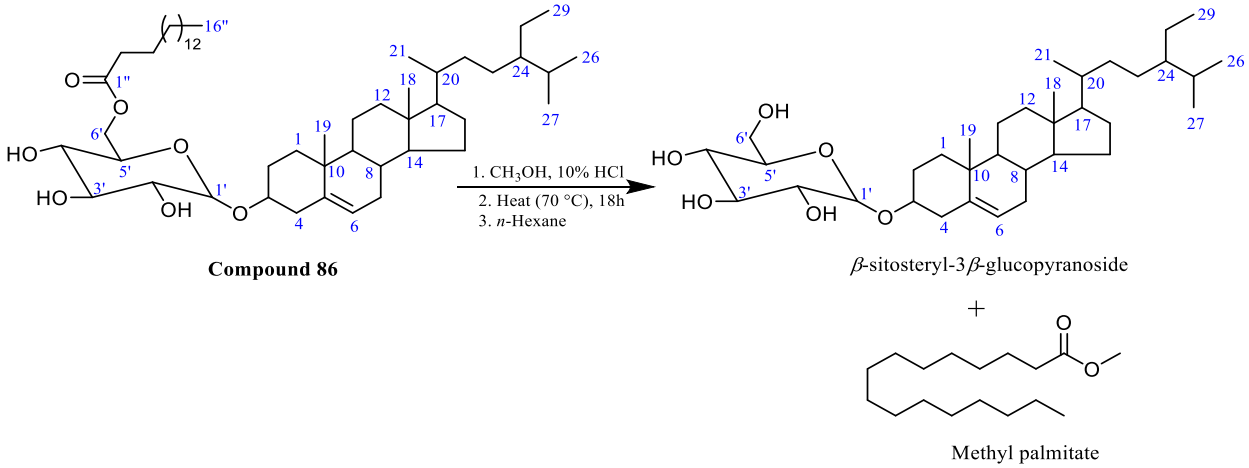

Scheme 5: Acid-catalyzed transesterification reaction of compound **86**.

Table 19: ^{1}H (400 MHz), ^{13}C (100 MHz), DEPT-135, and COSY NMR ($CDCl_3$, δ in ppm, J in Hz) spectral data of compound **86**, and ^{1}H and ^{13}C NMR values of β-sitosteryl-3β-glucopyranoside-6'-*O*-palmitate in the literature.

C. No.	**Compound 86**				***β*-sitosteryl-3*β*-glucopyranoside-6'-*O*-palmitate** (Nguyen *et al.*, 2004)	
	^{1}H NMR	**^{13}C NMR**	**DEPT-135**	**COSY**	**^{1}H NMR**	**^{13}C NMR**
1	1.82 (1H, *m*), 1.06 (1H, *m*)	37.3	$-CH_2-$		1.85 (1H, *m*), 1.06 (1H, *m*)	37.3
2	1.91 (1H, *m*), 1.59 (1H, *m*)	29.8	$-CH_2-$		1.95 (1H, *m*), 1.61 (1H, *m*)	29.7
3	3.54 (1H, *m*)	79.7	-CH-O-		3.54 (1H, *m*)	79.6
4	2.26 (1H, *m*), 2.24 (1H, *m*)	38.9	$-CH_2-$		2.36 (1H, *m*), 2.27 (1H, *m*)	38.9
5	-	140.3	Q		-	140.3
6	5.34 (1H, *m*)	122.2	=CH-		5.38 (1H, *m*)	122.1
7	1.98 (1H, *m*), 1.92 (1H, *m*)	32.0	$-CH_2-$		1.98 (2H, *m*)	31.9
8	1.50 (1H, *m*)	31.9	-CH-		1.52 (1H, *m*)	31.9
9	0.91 (1H, *m*)	50.2	-CH-		0.93 (1H, *m*)	50.1
10	-	36.8	Q		-	36.7
11	1.54 (1H, *m*), 1.01 (1H, *m*)	21.2	$-CH_2-$		1.56 (1H, *m*), 1.02 (1H, *m*)	21.0
12	2.01 (1H, *m*), 1.14 (1H, *m*)	39.8	$-CH_2-$		2.02 (1H, *m*), 1.18 (1H, *m*)	39.7
13	-	42.4	Q		-	42.3
14	1.00 (1H, *m*)	56.8	-CH-		1.01 (1H, *m*)	56.7
15	1.13 (1H, *m*), 1.08 (1H, *m*)	24.3	$-CH_2-$		1.12 (1H, *m*), 1.08 (1H, *m*)	24.3
16	1.47 (1H, *m*), 1.45 (1H, *m*)	27.3	$-CH_2-$		1.86 (1H, *m*), 1.83 (1H, *m*)	28.2
17	1.12 (1H, *m*)	56.1	-CH-		1.12 (1H, *m*)	56.1
18	0.66 (3H, *s*)	11.9	$-CH_3$		0.68 (3H, *s*)	11.8
19	0.99 (3H, *s*)	19.4	$-CH_3$		1.00 (3H, *s*)	19.3
20	1.32-1.26 (1H, *m*)	36.2	-CH-		1.36 (1H, *m*)	36.2
21	0.87 (3H, *d*, J = 6.3)	18.8	$-CH_3$		0.92 (3H, *d*, J =6.4)	18.8
22	1.32-1.26 (2H, *m*)	33.8	$-CH_2-$		1.34 (1H, *m*), 1.00 (1H, *m*)	33.9
23	1.14 (2H, *m*)	25.5	$-CH_2-$		1.18 (2H, *m*)	26.1
24	0.91 (1H, *m*)	45.8	-CH-		0.95 (1H, *m*)	45.8
25	1.57 (1H, *m*)	29.2	-CH-		1.66 (1H, *m*)	29.1
26	0.80 (3H, *d*, J = 6.7)	19.1	$-CH_3$		0.82 (3H, *d*, J = 6.8)	19.0
27	0.81 (3H, *d*, J = 6.7)	19.9	$-CH_3$		0.84 (3H, *d*, J = 6.8)	19.8
28	1.24 (2H, *brs*)	23.1	$-CH_2-$		1.26 (2H, *m*)	23.0
29	0.82 (3H, *t*, J = 7.5)	12.3	$-CH_3$		0.84 (3H, *t*, J = 7.6)	12.0
			Glucopyranoside moiety			
1'	4.27 (1H, *d*, J = 11.5)	101.2	-CH-O-		4.38 (1H, *d*, J = 7.7)	101.2
2'	3.36 (1H, *m*)	73.6	-CH-O-		3.35 (1H, *dd*, J = 8.7, 7.7)	73.4
3'	3.65 (1H, *m*)	76.1	-CH-O-		3.57 (1H, *dd*, J = 9.9, 8.7)	76.0
4'	3.37 (1H, *m*)	70.1	-CH-O-		3.38 (1H, *dd*, J = 9.9, 8.6)	70.2
5'	3.44 (1H, *m*)	73.9	-CH-O-		3.45 (1H, *m*)	73.8

Table 19 (continued)

6'	4.37 (1H, *dd*, *J* = 12.1, 5.2), 4.13 (1H, *dd*, *J* = 12.1, 6.3)	63.4	-CH_2-O-		4.42 (1H, *dd*, *J* = 12.1, 5.3), 4.29 (1H, *dd*, *J* = 12.1, 1.7)	63.4
			Palmitate moiety			
1"	-	174.7	Q (-C=O)		-	174.6
2"	2.31 (2H, *t*, *J* = 7.5)	34.3	-CH_2-	H-2"↔H-3"	2.34 (2H, *t*, *J* = 7.6)	34.2
3"	1.61 (2H, *m*)	25.0	-CH_2-	H-3"↔H-2"	1.61 (2H, *m*)	24.9
4"	1.24 (2H, *brs*)	29.4	-CH_2-		1.28 (2H, *brs*)	29.2
5"	1.24 (2H, *brs*)	29.6	-CH_2-		1.26 (2H, *brs*)	29.4
6"	1.24 (2H, *brs*)	29.7	-CH_2-		1.26 (2H, *brs*)	29.6
7"-12"	1.24 (12H, *brs*)	29.8	-CH_2-		1.26 (2H, *brs*)	29.8
13"	1.24 (2H, *brs*)	29.4	-CH_2-		1.26 (2H, *brs*)	29.4
14"	1.24 (2H, *brs*)	31.9	-CH_2-		1.26 (2H, *brs*)	31.9
15"	1.24 (2H, *brs*)	22.8	-CH_2-		1.30 (2H, *brs*)	22.7
16"	0.86 (3H, *t*, *J* = 7.0)	14.2	-CH_3		0.88 (3H, *t*, *J* = 7.1)	14.1

brs; broad singlet.

4.2.2.5. Compound 42

Compound **42** was obtained as a yellow crystalline powder. Its melting point was determined as 315-317 °C in accordance with the reported values (314-316 °C) of quercetin (El-Sayed *et al.*, 2011). The ^{1}H NMR (400 MHz, DMSO-*d*$_6$) spectrum revealed the resonance of five spin systems (excluding the hydroxyl protons) attributed to sp^2 aromatic methine protons. The ABX-type aromatic protons (ring B) of the compound were evidenced by the presence of doublet signals at δ_H 7.64 (1H, *d*, *J* = 1.5, H-2'), 7.50 (1H, *dd*, *J* = 8.5, 1.4, H-6'), and 6.85 (1H, *d*, *J* = 8.5, H-5') indicating that the three sets of signals are in different chemical environments. The spectrum further exhibited *meta*-coupled doublet protons at δ_H 6.37 (1H, *d*, *J* = 1.2, H-8), and 6.15 (1H, *d*, *J* = 1.3, H-6) showcasing the compound is un-substituted at these positions. Thus, the ^{1}H NMR evidence validates that compound **42** exhibits a pentahydroxylated flavonoid skeleton (Table 20, Appendix 16A).

In the ^{13}C NMR (100 MHz, DMSO-d_6) data, the signal at δ_C 176.3 (C-4) supported evidence for the presence of α, β-unsaturated carbonyl group. The signals at δ_C 164.4 (C-7), 161.2 (C-5), 156.6 (C-8a), 148.2 (C-4'), 147.3 (C-2), 145.5 (C-3'), and 136.2 (C-3) were assignable to the oxygen linked quaternary carbons of the compound. The spectrum also showed two quaternary carbons at δ_C 122.5 (C-1') and 103.5 (C-4a), and tertiary aromatic methine signals at δ_C 120.5 (C-6'), 116.1 (C-5'), 115.5 (C-2'), 98.7 (C-6), and 93.8 (C-8) confirming the 3, 3', 4', 5, 7-pentahydroxylated flavonoid skeleton. In addition, the types of carbons were established from the DEPT-135 spectrum confirming the presence of only five tertiary aromatic methine signals in accordance with the ^{13}C NMR spectrum of the compound (Table 20, Appendices 16B and C).

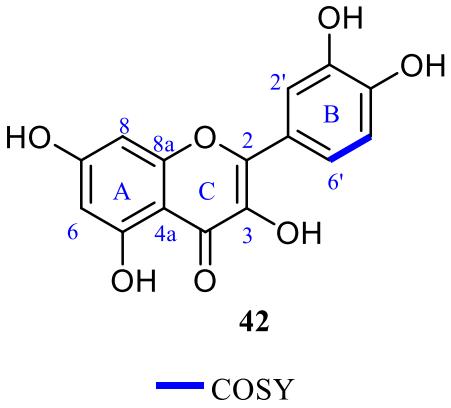

Figure 20: Chemical structure of compound **42**, and key COSY correlations.

In the COSY spectrum, correlations of only two spin systems were observed between H-5' (δ_H 6.85) and H-6' (δ_H 7.50) (Table 20, Appendix 16D). Overall, the spectral analyses matches with the reported NMR data for quercetin (**42**) (Zhang *et al.*, 2014) (Figure 20).

Table 20: ^{1}H (400 MHz*)*, ^{13}C (100 MHz*)*, DEPT-135, and COSY NMR (DMSO-d_6, δ in ppm, *J* in Hz) spectral data of compound **42**, and ^{1}H and ^{13}C NMR values of quercetin in the literature.

C. No.	**Compound 42**				**Quercetin** (Zhang *et al.*, 2014)	
	^{1}H NMR	**^{13}C NMR**	**DEPT-135**	**COSY**	**^{1}H NMR**	**^{13}C NMR**
1	-	-	-		-	-
2	-	147.3	Q		-	147.2
3	-	136.2	Q		-	136.1
4	-	176.3	Q (-C=O)		-	176.2
4a	-	103.5	Q		-	103.4
5	-	161.2	Q		-	161.1
6	6.15 (1H, *d*, *J* = 1.3)	98.7	=CH-		6.19 (1H, *d*, *J* = 2.1)	98.6
7	-	164.4	Q		-	164.3
8	6.37 (1H, *d*, *J* = 1.2)	93.8	=CH-		6.42 (1H, *d*, *J* = 2.1)	93.8
8a	-	156.6	Q		-	156.6
1'	-	122.5	Q		-	122.4
2'	7.64 (1H, *d*, *J* = 1.5)	115.5	=CH-		7.66 (1H, *d*, *J* = 2.1)	115.4
3'	-	145.5	Q		-	145.4
4'	-	148.2	Q		-	148.1
5'	6.85 (1H, *d*, *J* = 8.5)	116.1	=CH-	H-5'↔H-6'	6.88 (1H, *d*, *J* = 8.4)	116.0
6'	7.50 (1H, *dd*, *J* = 8.5, 1.4)	120.5	=CH-	H-6'↔H-5'	7.53 (1H, *dd*, *J* = 8.4, 2.1)	120.5
3-OH	9.42 (1H, *brs*)	-	-		-	-
5-OH	12.46 (1H, *brs*)	-	-		12.47 (1H, *brs*)	-
7-OH	10.71 (1H, *brs*)	-	-		10.93 (1H, *brs*)	-
3'-OH	9.34 (1H, *brs*)	-	-		9.35 (1H, *brs*)	-
4'-OH	9.60 (1H, *brs*)	-	-		9.69 (1H, *brs*)	-

brs; broad singlet.

4.2.2.6. Compound 87

Compound **87** was isolated as a yellow powder. Its melting point was determined in the range of 345-348 °C in accordance with the reported values (347-348 °C) of apigenin (Fotie *et al.*, 2004). The structure of the compound was elucidated based on the spectral data obtained from the ^{1}H NMR (400 MHz, CD_3OD) spectrum only. Accordingly, the spectrum showed four aromatic protons at δ_H 7.84 (2H, *d*, *J* = 8.8, H-2', 6'), 6.91 (2H, *d*, *J* = 8.8, H-3', 5') signifying the presence of an AA'BB' ring orientation in ring B of the skeleton. In addition, it showed two doublet signals at δ_H 6.44 (1H, *d*, *J* = 2.1, H-8), and 6.19 (1H, *d*, *J* = 2.0, H-6) suggesting the presence of *meta*-coupled protons in ring A. The spectrum also revealed a singlet signal at δ_H 6.58 (1H, *s*, H-3)

attributed to the proton in ring C of a 4', 5, 7-trisubstituted flavone (Table 21, Appendix 17). Finally, the ^{1}H NMR spectral information along with its determined melting point suggests that compound **87** is an apigenin (**87**) which was also in agreement with the published data of the compound (Fajriah *et al.*, 2016) (Figure 21).

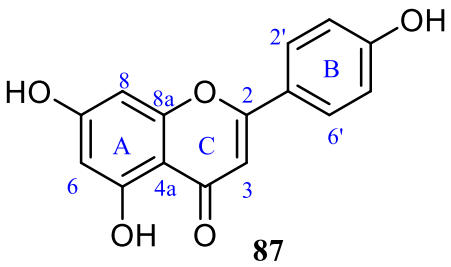

87

Figure 21: Chemical structure of compound **87**.

Table 21: ^{1}H NMR (400 MHz, CD_3OD, δ in ppm, *J* in Hz) spectral data of compound **87**, and ^{1}H and ^{13}C NMR values of apigenin in the literature.

C. No.	**Compound 87**	**Apigenin** (Fajriah *et al.*, 2016)	
	^{1}H NMR	**^{1}H NMR**	**^{13}C NMR**
2	-	-	163.7
3	6.58 (1H, *s*)	6.75 (1H, *s*)	102.8
4	-	-	181.7
4a	-	-	103.5
5	-	-	161.2
6	6.19 (1H, *d*, *J* = 2.0)	6.15 (1H, *d*, *J* = 1.9)	98.9
7		-	164.5
8	6.44 (1H, *d*, *J* = 2.1)	6.44 (1H, *d*, *J* = 1.9)	94.0
8a	-	-	157.3
1'	-	-	121.1
2', 6'	7.84 (2H, *d*, *J* = 8.8)	7.91 (2H, *d*, *J* = 9.0)	128.5
3', 5'	6.91 (2H, *d*, *J* = 8.8)	6.90 (2H, *d*, *J* = 9.0)	116.0
4'	-	-	161.4
7-OH	4.59 (1H, *brs*)	-	-

4.2.2.7. Compound 37

Compound **37** was collected as a yellow crystalline powder. Its melting point was determined in the range of 191-193 °C in good agreement with the reported values (190-192 °C) of quercetin-3-*O*-rutinoside (Bui *et al.*, 2022, El-Sayed *et al.*, 2011). The ^{1}H NMR (400 MHz, CD_3OD) spectrum exhibited five signals of aromatic protons at δ_H 7.64 (1H, *d*, *J* = 2.2, H-2'), 7.61 (1H, *dd*, *J* = 8.5, 2.1, H-6'), and 6.85 (1H, *d*, *J* = 8.4, H-5') with ABX spin orientation, and *meta* coupled protons at

δ_H 6.38 (1H, *d*, *J* = 2.1, H-8) and 6.19 (1H, *d*, *J* = 2.2, H-6). The spectrum also showed the presence of *β*-glucose and *α*-rhamnose moieties via the multiplet signals between δ_H 3.80-3.30 (10H, *m*) including two anomeric proton signals at δ_H 5.09 (1H, *d*, *J* = 7.6, H-1''), and 4.49 (1H, *brs*, H-1''') referring to *β*-glucose and *α*-rhamnose moieties, respectively. In addition, doublet signals referring to the methyl group of the *α*-rhamnose moiety appeared at δ_H 1.09 (3H, *d*, *J* = 6.2, H-6''') (Table 22, Appendix 18A).

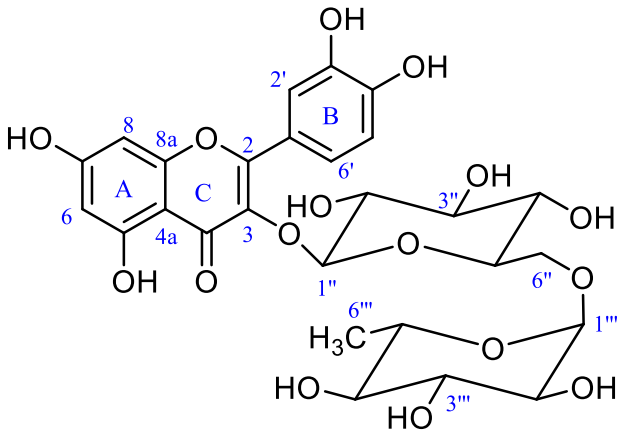

37

Figure 22: Chemical structure of compound **37**.

The ^{13}C NMR (100 MHz, CD_3OD) spectrum in agreement with the DEPT-135 spectral data revealed the resonance of 27 carbon signals including *α*, *β*-unsaturated carbonyl group at δ_C 178.0 (C-4), seven quaternary carbons linked to oxygen at δ_C 164.7 (C-7), 161.6 (C-5), 157.9 (C-8a), 157.1 (C-2), 148.4 (C-4'), 144.4 (C-3'), and 134.2 (C-3), two quaternary carbons at δ_C 121.7 (C-1') and 104.2 (C-4a), five sp^2 aromatic carbons at δ_C 122.1 (C-6'), 116.2 (C-5'), 114.6 (C-2'), 98.5 (C-6), and 93.4 (C-8), ten oxymethine signals at δ_C 103.3 (anomeric, C-1''), 101.0 (anomeric, C-1'''), 76.7 (C-3''), 75.8 (C-5''), 74.3 (C-2''), 72.5 (C-4'''), 70.8 (C-3'''), 70.7 (C-2'''), 70.0 (C-4''), and 68.3 (C-5'''), one oxymethylene signal at δ_C 67.1 (C-6''), and one methyl signal at δ_C 16.5 (C-6'''). The six quaternary signals at C-2, C-3, C-4, C-4a, C-8a, and C-1', and four oxygenated quaternary carbons at C-5, C-7, C-3', and C-4' are in accordance with a flavanol skeleton and its hydroxyl substituents in rings A and B, respectively (Table 22, Appendices 18B and C). After all, the ^1H and ^{13}C NMR spectral analyses of the compound were in close agreement with the published data of quercetin-3-*O*-rutinoside (**37**) (Bui *et al.*, 2022, Kim *et al.*, 2017) (Figure 22).

Table 22: ^{1}H (400 MHz), ^{13}C (100 MHz), and DEPT-135 NMR (CD_3OD, δ in ppm, J in Hz) spectral data of compound **37**, and ^{1}H and ^{13}C NMR values of quercetin-3-*O*-rutinoside in the literature.

C. No.	**Compound 37**			**Quercetin-3-*O*-rutinoside** (Bui *et al.*, 2022, Kim *et al.*, 2017)	
	^{1}H NMR	**^{13}C NMR**	**DEPT-135**	**^{1}H NMR**	**^{13}C NMR**
			Quercetin moiety		
2		157.1	Q		156.7
3		134.2	Q		134.1
4		178.0	Q (-C=O)		178.2
4a		104.2	Q		104.2
5		161.6	Q		161.5
6	6.19 (1H, *d*, *J* = 2.2)	98.5	=CH-	6.11 (1H, *d*, *J* = 2.2)	98.7
7		164.7	Q		164.3
8	6.38 (1H, *d*, *J* = 2.1)	93.4	=CH-	6.40 (1H, *d*, *J* = 2.0)	93.6
8a		157.9	Q		157.1
1'		121.7	Q		121.9
2'	7.64 (1H, *d*, *J* = 2.2)	114.6	=CH-	7.55 (1H, *d*, *J* = 2.1)	115.2
3'		144.4	Q		144.8
4'		148.4	Q		148.7
5'	6.85 (1H, *d*, *J* = 8.4)	116.2	=CH-	6.85 (1H, *d*, *J* = 8.4)	116.3
6'	7.61 (1H, *dd*, *J* = 8.5, 2.1)	122.1	=CH-	7.56 (1H, *dd*, *J* = 9.0, 2.1)	122.0
			Glycosyl moiety		
1"	5.09 (1H, *d*, *J* = 7.6)	103.3	-O-CH-O-	5.35 (1H, *d*, *J* = 7.8)	101.4
2"	3.80-3.30 (1H, *m*)	74.3	-CH-O-	3.83-3.35 (1H, *m*)	74.1
3"	3.80-3.30 (1H, *m*)	76.7	-CH-O-	3.83-3.35 (1H, *m*)	76.7
4"	3.80-3.30 (1H, *m*)	70.0	-CH-O-	3.83-3.35 (1H, *m*)	70.0
5"	3.80-3.30 (1H, *m*)	75.8	-CH-O-	3.83-3.35 (1H, *m*)	75.9
6"	3.80-3.30 (2H, *m*)	67.1	$-CH_2-O-$	3.83-3.35 (2H, *m*)	67.0
			Rhamnosyl moiety		
1'"	4.49 (1H, *brs*)	101.0	-O-CH-O-	4.38 (1H, *brs*)	101.0
2'"	3.80-3.30 (1H, *m*)	70.7	-CH-O-	3.83-3.35 (1H, *m*)	70.4
3'"	3.80-3.30 (1H, *m*)	70.8	-CH-O-	3.83-3.35 (1H, *m*)	70.6
4'"	3.80-3.30 (1H, *m*)	72.5	-CH-O-	3.83-3.35 (1H, *m*)	71.9
5'"	3.80-3.30 (1H, *m*)	68.3	-CH-O-	3.83-3.35 (1H, *m*)	68.2
6'"	1.09 (3H, *d*, *J* = 6.2)	16.5	$-CH_3$	1.13 (3H, *d*, *J* = 6.2)	17.7

Outstandingly, diethyl phthalate (**85**) and *β*-sitosteryl-3*β*-glucopyranoside-6'-*O*-palmitate (**86**) were reported herein for the first time from the plant. The isolated compounds belong to different classes of compounds including sterols (stigmasterol (**40**), a mixture of *β*-sitosterol (**19**) and

stigmasterol (**40**)), steryl glycosides (*β*-sitosteryl-3*β*-glucopyranoside-6'-*O*-palmitate, **86**), flavonoids (quercetin (**42**) and apigenin (**87**)), and glycosidic flavonoids (quercetin-3-*O*-rutinoside (**37**)).

4.2.3. Structure elucidation of compounds isolated from roots of *Senna siamea*

The gravity silica gel column chromatography of the CH_2Cl_2: CH_3OH (1:1) extract of roots of *S. siamea* yielded seven known compounds namely; lupeol (**39**), a mixture of *β*-sitosterol (**19**) and stigmasterol (**40**), chrysophanol (**53**), betulinic acid (**63**), glyceryl-1-hexacosanoate (**88**), and 4-(2'-hydroxymethyl-4'-hydroxyphenyl)-chrysophanol (**89**). The structural informations were also supported by literature references. The TLC profiles of the isolated compounds of *S. siamea* are depicted in Appendix 19.

4.2.3.1. Compound 39

Compound **39** was obtained as white powder with a melting point of 212-214 °C which was in good agreement with the reported values (210-213 °C) for lupeol (Adedoyin *et al.*, 2020, Musa *et al.*, 2024). The ^{1}H NMR (400 MHz, $CDCl_3$) spectrum showed a pair of doublets at δ_H 4.67 (1H, *d*, *J* = 2.5, H-29a) and 4.55 (1H, *d*, *J* = 1.2, H-29b) suggesting the presence of terminal isopropenyl group in the lupane series of triterpenoids. The doublet of doublets observed at δ_H 3.18 (1H, *dd*, *J* = 11.2, 5.0, H-3) attributed to the oxymethine proton at C-3. The multiplet signals at δ_H 2.36 (1H, *m*, H-19) were characteristic of a pentacyclic methine proton, where the isopropenyl group is attached. Signals of seven singlets displayed at δ_H 1.66 (3H, *s*), 1.01 (3H, *s*), 0.95 (3H, *s*), 0.93 (3H, *s*), 0.81 (3H, *s*), 0.77 (3H, *s*), and 0.74 (3H, *s*) belong to the methyl groups of the structure assignable to Me-30, Me-26, Me-27, Me-23, Me-25, Me-28, and Me-24, respectively. The remaining protons overlapped within the range of δ_H 1.65-1.15 (24H, *m*) (Table 23, Appendix 20A).

The ^{13}C NMR (100 MHz, $CDCl_3$) spectrum revealed thirty well-resolved signals attributed to the lupane series of a triterpenoid skeleton. Characteristics of sp^2 hybridized carbon signals were observed at δ_C 151.1 and 109.4 assignable to C-20 and C-29, respectively, of which the former belongs to an sp^2 quaternary carbon, whereas, the latter belongs to a terminal sp^2 methine carbon (from the DEPT-135 spectrum). The signal at δ_C 79.1 (C-3) indicated an oxymethine carbon, and

groups of methine signals were observed at δ_C 55.3 (C-5), 50.5 (C-9), 48.3 (C-18), 48.0 (C-19) and 38.1 (C-13). Seven methyl signals were also clearly evident at δ_C 28.0 (C-23), 19.4 (C-30), 18.0 (C-28), 16.2 (C-25), 16.0 (C-26), 15.5 (C-24), and 14.6 (C-27) in good agreement with the triterpenoid skeleton. Furthermore, the DEPT-135 spectrum exhibited an sp^2 olefinic methylene carbon at δ_C 109.4, an sp^3 oxymethine carbon at δ_C 79.1, five sp^3 methine, ten sp^3 methylene, and seven methyl carbons consistent with the ^{13}C NMR spectrum (Table 23, Appendices 20B and C).

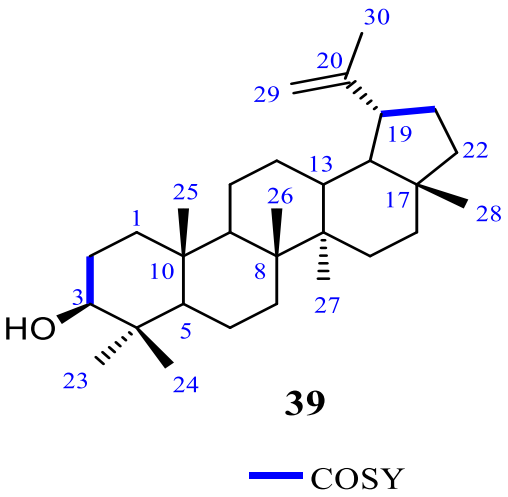

Figure 23: Chemical structure of compound **39** and key COSY correlations.

The connectivity of the protons was also supported by the COSY correlations. Accordingly, important ^3J correlations were observed between H-2 (δ_H 1.54) and H-3 (δ_H 3.18), H-19 (δ_H 2.36) and H-21 (δ_H 1.33), and H-29a (δ_H 4.67) and H-29b (δ_H 4.55) (Table 23, Appendix 20D). Based on the spectral analyses and comparison with previous reports, the compound was elucidated as lupeol (**39**) (Adedoyin *et al.*, 2020, Shwe *et al.*, 2019) (Figure 23). The compound was also previously reported from the stem barks of *S. siamea* (Ogbole *et al.*, 2014).

Table 23: ^{1}H (400 MHz*)*, ^{13}C (100 MHz*)*, DEPT-135, and COSY NMR ($CDCl_3$, δ in ppm, *J* in Hz) spectral data of compound **39**, and ^{1}H and ^{13}C NMR values of lupeol in the literature.

C. No.	**Compound 39**				**Lupeol** (Adedoyin *et al.*, 2020, Shwe *et al.*, 2019)	
	^{1}H NMR	**^{13}C NMR**	**DEPT-135**	**COSY**	**^{1}H NMR**	**^{13}C NMR**
1	1.60-1.15 (2H, *m*)	38.7	-CH_2-		0.90, 1.65 (2H, *m*)	38.7
2	1.63, 1.54 (2H, *m*)	27.5	-CH_2-	H-3	1.67, 1.52 (2H, *m*)	27.4
3	3.18 (1H, *dd*, *J* = 11.2, 5.0)	79.1	-CH-O-	H-2	3.20 (1H, *m*)	79.0
4	-	38.9	Q		-	38.9
5	1.60-1.15 (1H, *m*)	55.3	-CH-		0.67 (1H, *m*)	55.5
6	1.60-1.15 (2H, *m*)	18.4	-CH_2-		1.37, 1.52 (2H, *m*)	18.5
7	1.60-1.15 (2H, *m*)	34.3	-CH_2-		1.39 (2H, *m*)	34.2
8	-	40.9	Q		-	40.9
9	1.60-1.15 (1H, *m*)	50.5	-CH-		1.25 (1H, *m*)	50.5
10	-	37.2	Q		-	37.2
11	1.60-1.15 (2H, *m*)	21.0	-CH_2-		1.20, 1.40 (2H, *m*)	21.0
12	1.60-1.15 (2H, *m*)	25.2	-CH_2-		1.06, 1.62 (2H, *m*)	25.2
13	1.60-1.15 (1H, *m*)	38.1	-CH-		1.66 (1H, *m*)	38.1
14	-	42.9	Q		-	42.9
15	1.60-1.15 (2H, *m*)	27.4	-CH_2-		1.05, 1.60 (2H, *m*)	27.1
16	1.60-1.15 (2H, *m*)	35.6	-CH_2-		1.35, 1.45 (2H, *m*)	35.5
17	-	43.0	Q		-	43.0
18	1.60-1.15 (1H, *m*)	48.3	-CH-		1.36 (1H, *m*)	48.3
19	2.36 (1H, *m*)	48.0	-CH-	H-21	2.40 (1H, *m*)	48.0
20	-	151.1	Q		-	151.0
21	1.60-1.15 (2H, *m*)	29.9	-CH_2-	H-19	1.30, 1.91 (2H, *m*)	29.9
22	1.60-1.15 (2H, *m*)	40.0	-CH_2-		1.18, 1.37 (2H, *m*)	40.0
23	0.93 (3H, *s*)	28.0	-CH_3		0.90 (3H, *s*)	28.0
24	0.74 (3H, *s*)	15.5	-CH_3		0.76 (3H, *s*)	15.5
25	0.81 (3H, *s*)	16.2	-CH_3		0.83 (3H, *s*)	16.1
26	1.01 (3H, *s*)	16.0	-CH_3		1.03 (3H, *s*)	16.0
27	0.95 (3H, *s*)	14.6	-CH_3		0.94 (3H, *s*)	14.8
28	0.77 (3H, *s*)	18.0	-CH_3		0.79 (3H, *s*)	18.0
29	4.67 (1H, *d*, *J* = 2.5), 4.55 (1H, *d*, *J* = 1.2)	109.4	=CH_2	H-29a ↔H-29b	4.70, 4.55 (2H, *d*, *J* = 1.9)	109.0
30	1.66 (3H, *s*)	19.4	-CH_3		1.67 (3H, *s*)	19.5

4.2.3.2. A mixture of compounds 19 and 40

The mixture of compounds **19** and **40** was isolated as white needles. Based on the integration patterns and intensity of signals, its ^{1}H NMR spectrum revealed resonances of a mixture of two compounds (**19** and **40**). The mixture of compounds was also isolated from the roots of *D. regia*

and its entire structure elucidations are depicted in section 4.2.2.2 and Table 18, along with its NMR spectra portrayed on Appendices 14A-E. For mixtures of *β*-sitosterol and stigmasterol, the relative composition of the two compounds can be calculated from the integral values of the three olefinic protons in the ^{1}H NMR spectrum. Accordingly, stigmasterol was displayed in a higher composition than *β*-sitosterol (approximately 3: 2, for **40** and **19**) (Figure 18). The two compounds were eluted and developed together on column and TLC, respectively, and the difficulty to separate them was related to their similar polarity.

4.2.3.3. Compound 53

Compound **53** (mp: 193-194 °C) was isolated as orange crystals. The melting point range of the compound matches the reported values of chrysophanol (194-195 °C) in the literature (Mining *et al.*, 2014). Its ^{1}H NMR (400 MHz, $CDCl_3$) spectrum displayed two deshielded protons at δ_H 12.12 (1H, *s*) and 12.01 (1H, *s*) with peri-effect properties assignable to the hydroxyl protons at C-1 and C-8, respectively. Five aromatic signals were also observed at δ_H 7.81 (1H, *dd*, *J* = 7.5, 1.2, H-5), 7.67 (1H, *dd*, *J* = 8.2, H-6), 7.65 (1H, *d*, *J* = 1.6, H-4), 7.28 (1H, *dd*, *J* = 8.4, 1.2, H-7), and 7.09 (1H, *d*, *J* = 1.4, H-2) attributed to ABX and AB type spin patterns in rings A and C of an anthraquinone skeleton, respectively. The singlet signal observed at δ_H 2.46 (3H, *s*) revealed a characteristic of methyl substituent attached to C-3 of ring C (Table 24, Appendix 21A).

The ^{13}C NMR (100 MHz, $CDCl_3$) spectral data exhibited fifteen well-resolved carbon signals including two carbonyl signals at δ_C 192.6 and 182.1 assignable to C-9 and C-10, respectively. The chemical shift difference between the two carbonyl carbons is more than 10 ppm suggesting that C-9 is deshielded due to the peri-effect of hydroxyl groups at C-1 and C-8 (Schripsema and Dagnino, 1996). In addition, the spectrum revealed two oxygenated aromatic carbons at δ_C 162.8 (C-1) and 162.5 (C-8), five quaternary aromatic carbons (from DEPT-135 spectrum) at δ_C 149.4 (C-3), 133.7 (C-4a), 133.3 (C-10a), 115.9 (C-8a) and 113.8 (C-9a), five sp^2 aromatic methine signals at δ_C 137.0 (C-6), 124.7 (C-7), 124.5 (C-2), 121.5 (C-4), and 120.0 (C-5), and a sp^3 methyl signal at δ 22.4 (CH_3). Furthermore, the DEPT-135 spectrum revealed five aromatic methines and a single sp^3 methyl signal consistent with the ^{13}C NMR spectral analyses of the compound (Table 24, Appendices 21B and C).

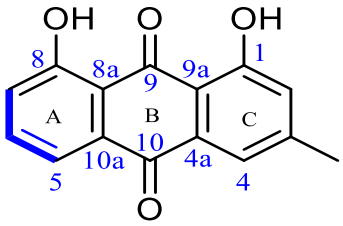

Figure 24: Chemical structure of compound **53** and key COSY correlations.

Notably, the assignments of adjacent protons were validated by COSY correlations. Accordingly, the spectrum revealed important ^{3}J correlations between H-5 (δ_H 7.81) and H-6 (δ_H 7.67), and H-6 (δ_H 7.67) and H-7 (δ_H 7.28) (Table 24, Appendix 21D). Based on the spectral analyses and comparison with related reports, the compound was elucidated as chrysophanol (**53**) (Kuwabara *et al.*, 2022, Mining *et al.*, 2014) (Figure 24). Previous reports also support the isolation of chrysophanol from the stem barks of *S. siamea* (Ledwani and Singh, 2004, Ogbole *et al.*, 2014).

Table 24: ^{1}H (400 MHz), ^{13}C (100 MHz), DEPT-135, and COSY NMR ($CDCl_3$, δ in ppm, J in Hz) spectral data of compound **53**, and ^{1}H and ^{13}C NMR values of chrysophanol in the literature.

C. No.	**Compound 53**				**Chrysophanol** (Kuwabara *et al.*, 2022, Mining *et al.*, 2014)	
	^{1}H NMR	**^{13}C NMR**	**DEPT-135**	**COSY**	**^{1}H NMR**	**^{13}C NMR**
1	-	162.8	Q		-	162.8
2	7.09 (1H, *d*, *J* = 1.4)	124.5	=CH-		7.10 (1H, *s*)	124.5
3	-	149.4	Q		-	150.2
4	7.65 (1H, *d*, *J* = 1.6)	121.5	=CH-		7.65 (1H, *s*)	121.3
4a	-	133.7	Q		-	134.1
5	7.81 (1H, *dd*, *J* = 7.5, 1.2)	120.0	=CH-	H-6	7.83 (1H, *dd*, *J* = 7.1)	119.8
6	7.67 (1H, *dd*, *J* = 8.2)	137.0	=CH-	H-5, 7	7.67 (1H, *t*, *J* = 7.6)	137.3
7	7.28 (1H, *dd*, *J* = 8.4, 1.2)	124.7	=CH-	H-6	7.31 (1H, *dd*, *J* = 8.4)	124.6
8	-	162.5	Q		-	162.6
8a	-	115.9	Q		-	116.4
9	-	192.6	Q (-C=O)		-	192.6
9a	-	113.8	Q		-	114.2
10	-	182.1	Q (-C=O)		-	181.9
10a	-	133.3	Q		-	133.7
CH_3	2.46 (3H, *s*)	22.4	-CH_3		2.47 (3H, *s*)	21.8
1-OH	12.12 (1H, *s*)	-	-		-	-
8-OH	12.01 (1H, *s*)	-	-		12.01 (1H, *s*)	-

4.2.3.4. Compound 63

Compound **63** (mp: 296-298 °C) was collected as a white crystalline solid and exhibited a very close melting point range to the reported values (295-298 °C) of betulinic acid (Aung *et al.*, 2023, Santos *et al.*, 2018). Its ^{1}H NMR (400 MHz, $CDCl_3$) spectrum revealed two proton signals corresponding to geminal sp^2 methylene protons at δ_H 4.73 (1H, *s*, H-29a) and 4.60 (1H, *s*, H-29b). The broad singlet and doublet of doublet signals observed at δ_H 12.05 (1H, *brs*, acidic OH), and 3.18 (1H, *dd*, J = 11.1, 4.9, H-3) suggest the presence of carboxylic acid and carbinol methine protons, respectively. The attachment of the β-hydroxyl group at C-3 was verified by the coupling constant (J = 11.1) of the biaxial protons (H-3α, δ_H 3.18 and H-2α, δ_H 1.60). The spectrum also showed six methyl signals at δ_H 1.67 (3H, *s*, Me-30), 0.96 (3H, *s*, Me-23), 0.95 (3H, *s*, Me-27), 0.92 (3H, *s*, Me-26), 0.81 (3H, *s*, Me-25), and 0.74 (3H, *s*, Me-24) suggesting a characteristic pattern of a lupane type skeleton (Table 25, Appendix 22A).

The ^{13}C NMR (100 MHz, $CDCl_3$) spectrum exhibited a resonance of 29 well-resolved carbon signals including vinylic carbons at δ_C 150.4 (C-20) and 109.8 (C-29), and carbinol methine signal at δ_C 79.1 (C-3) associated with the structure of lupane type triterpenoid. In agreement with the DEPT-135 spectrum, the ^{13}C NMR spectrum also revealed five sp^3 quaternary carbons at δ_C 56.3 (C-17), 42.5 (C-14), 40.7 (C-8), 38.9 (C-4), and 37.3 (C-10), five sp^3 methine signals at δ_C 55.4 (C-5), 50.6 (C-9), 49.3 (C-18), 46.9 (C-19), and 38.4 (C-13), ten sp^3 methylene signals at δ_C 38.8 (C-1), 37.1 (C-22), 34.4 (C-7), 32.2 (C-16), 30.6 (C-21), 29.8 (C-15), 27.4 (C-2), 25.5 (C-12), 20.9 (C-11), and 18.3 (C-6), and six methyl signals at δ_C 28.0 (C-23), 19.4 (C-30), 16.2 (C-26), 16.1 (C-25), 15.4 (C-24), and 14.7 (C-27) (Table 25, Appendices 22B and C). Due to the small NMR scanning time, the carbonyl signal of the acidic moiety was not displayed in the spectrum.

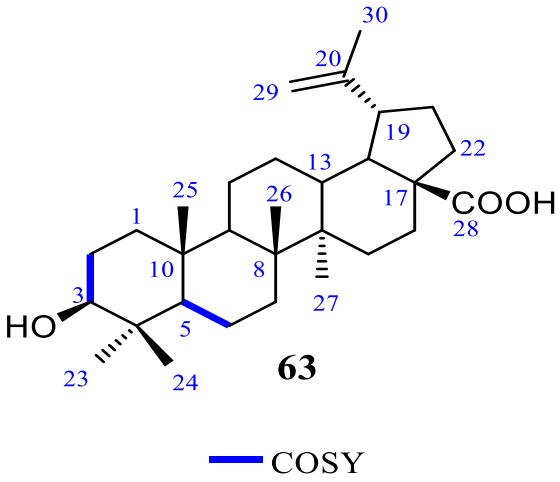

Figure 25: Chemical structure of compound **63** and key COSY correlations.

In addition, the orientations of adjacent protons were confirmed by COSY correlations. Accordingly, the spectrum showed ^{3}J correlations between H-2 (δ_H 1.60) and H-3 (δ_H 3.18), H-5 (δ_H 0.67) and H-6 (δ_H 1.50, 1.36), and ^{2}J correlations between H-29a (δ_H 4.73) and H-29b (δ_H 4.60) (Table 25, Appendix 22D). Overall, the spectral data of the compound agreed with the reported values of betulinic acid (**63**) (Aung *et al.*, 2023) (Figure 25).

Table 25: ^{1}H (400 MHz), ^{13}C (100 MHz), DEPT-135, and COSY NMR ($CDCl_3$, δ in ppm, J in Hz) spectral data of compound **63**, and ^{1}H and ^{13}C NMR values of betulinic acid in the literature.

C. No.	Compound 63				Betulinic acid (Aung *et al.*, 2023)	
	^{1}H NMR	**^{13}C NMR**	**DEPT-135**	**COSY**	**^{1}H NMR**	**^{13}C NMR**
1	1.63 (1H, *m*), 0.88 (1H, *m*)	38.8	$-CH_2-$		1.64 (1H, *m*), 0.88 (1H, m)	38.7
2	1.60 (2H, *m*)	27.4	$-CH_2-$	H-3	1.59 (2H, *m*)	27.4
3	3.18 (1H, *dd*, *J* = 11.1, 4.9)	79.1	-CH-O-	H-2	3.17 (1H, *dd*, *J* = 11.5, 4.7)	79.0
4	-	38.9	Q		-	38.9
5	0.67 (1H, *m*)	55.4	-CH-	H-6	0.66 (1H, *m*)	55.4
6	1.50 (1H, *m*), 1.36 (1H, *m*)	18.3	$-CH_2-$	H-5	1.50 (1H, *m*), 1.35 (1H, *m*)	18.3
7	1.36 (2H, *m*)	34.4	$-CH_2-$		1.35 (2H, *m*)	34.3
8	-	40.7	Q		-	40.7
9	1.24 (1H, *m*)	50.6	-CH-		1.24 (1H, *m*)	50.5
10	-	37.3	Q		-	37.1
11	1.38 (1H, *m*), 1.24 (1H, *m*)	20.9	$-CH_2-$		1.38 (1H, *m*), 1.24 (1H, *m*)	20.9
12	1.63 (1H, *m*), 1.00 (1H, *m*)	25.5	$-CH_2-$		1.64 (1H, *m*), 1.00 (1H, *m*)	25.5
13	2.18 (1H, *m*)	38.4	-CH-		2.18 (1H, *m*)	38.4
14	-	42.5	Q		-	42.5
15	1.60 (1H, *m*), 1.19 (1H, *m*)	29.8	$-CH_2-$		1.59 (1H, *m*), 1.19 (1H, *m*)	29.7
16	2.23 (1H, *m*), 1.38 (1H, *m*)	32.2	$-CH_2-$		2.24 (1H, *m*), 1.38 (1H, *m*)	32.2
17	-	56.3	Q		-	56.3
18	1.60 (1H, *m*)	49.3	-CH-		1.59 (1H, *m*)	49.3
19	2.98 (1H, *m*)	46.9	-CH-		2.98 (1H, *m*)	46.9
20	-	150.4	Q		-	150.4
21	1.95 (1H, *m*), 1.38 (1H, *m*)	30.6	$-CH_2-$		1.95 (1H, *m*), 1.38 (1H, *m*)	30.6
22	1.95 (1H, *m*), 1.42 (1H, *m*)	37.1	$-CH_2-$		1.95 (1H, *m*), 1.43 (1H, *m*)	37.0
23	0.96 (3H, *s*)	28.0	$-CH_3$		0.96 (3H, *s*)	28.0
24	0.74 (3H, *s*)	15.4	$-CH_3$		0.73 (3H, *s*)	15.3
25	0.81 (3H, *s*)	16.1	$-CH_3$		0.80 (3H, *s*)	16.0
26	0.92 (3H, *s*)	16.2	$-CH_3$		0.91 (3H, *s*)	16.1
27	0.95 (3H, *s*)	14.7	$-CH_3$		0.94 (3H, *s*)	14.7
28	-	-	-C=O		-	179.4
29	4.73 (1H, *s*), 4.60 (1H, *s*)	109.8	$=CH_2$	H-29a↔ H-29b	4.72 (1H, *s*), 4.60 (1H, *s*)	109.7
30	1.67 (3H, *s*)	19.4	$-CH_3$		1.67 (3H, *s*)	19.4
OH	12.05 (1H, *brs*)	-	-		-	-

brs; broad singlet.

4.2.3.5. Compound 88

Compound **88** (mp: 92-94 °C) was isolated as a white solid. The melting point range was very close to the reported values of glyceryl-1-hexacosanoate (91-93 °C) in the literature

(Mbouangouere *et al.*, 2007). Its ^{1}H NMR (400 MHz, $CDCl_3$) spectrum revealed signals of geminal oxymethylenes at δ_H 4.20 (1H, *dd*, *J* = 11.7, 4.6, H-1a), 4.14 (1H, *dd*, *J* = 11.6, 6.1, H-1b), 3.69 (1H, *dd*, *J* = 11.4, 4.0, H-3a), and 3.59 (1H, *dd*, *J* = 11.4, 5.8, H-3b) and an oxymethine proton at δ_H 3.92 (1H, *m*, H-2) which are characteristic of a glycerol protons. In addition, four methylene protons were observed at δ_H 2.34 (2H, *t*, *J* = 14.6, H-2') and 1.62 (2H, *m*, H-3'), and three methyl protons were displayed at δ_H 0.86 (3H, *t*, *J* = 12.8, H-26') attributed to fatty acid/ester protons nearest to the carboxylic/ate group and terminal methyl protons, respectively. The remaining protons overlapped in the region δ_H 1.31-1.23 (44H, *brs*) (Table 26, Appendix 23A). The ^{13}C NMR (100 MHz, $CDCl_3$) spectral data exhibited a carbonyl (ester) signal at δ_C 174.5 (C-1'), three sp^3 carbinol signals at δ_C 70.3 (C-2), 65.2 (C-1), and 63.4 (C-3), four methylene signals at δ_C 34.2 (C-2'), 32.0 (C-24'), 25.0 (C-3'), and 22.8 (C-25') and a terminal methyl signal at δ 14.2 (C-26'). Twenty sp^3 methylene signals observed in the range δ_C 29.8-29.2 (C-4'-C-23') suggest some long-chain fatty acid-containing glycerol (Table 26, Appendix 23B).

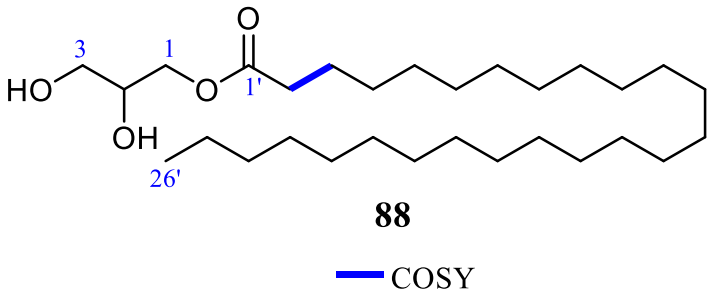

88

COSY

Figure 26: Chemical structure of compound **88** and key COSY correlations.

Moreover, the proton-proton coupling assignments of the compound were supported by COSY correlations, thereby the ^{2}J correlations between H-1a (δ_H 4.20) and H-1b (δ_H 4.14), H-3a (δ_H 3.69) and H-3b (δ_H 3.59), and ^{3}J correlations between H-2' (δ_H 2.34) and H-3' (δ_H 1.62) revealed confirmatory information of the structure (Table 26, Appendix 23C). Finally, the spectral analyses agreed with the reported values of glyceryl-1-hexacosanoate (**88**) (Chimi Fotso *et al.*, 2021, Mbouangouere *et al.*, 2007) (Figure 26).

Table 26: ^{1}H (400 MHz), ^{13}C (100 MHz), and COSY NMR ($CDCl_3$, δ in ppm, J in Hz) spectral data of compound **88**, and ^{1}H and ^{13}C NMR values of glyceryl-1-hexacosanoate in the literature.

C. No.	**Compound 88**			**Glyceryl-1-hexacosanoate** (Chimi Fotso *et al.*, 2021, Mbouangouere *et al.*, 2007)	
	^{1}H NMR	**^{13}C NMR**	**COSY**	**^{1}H NMR**	**^{13}C NMR**
1	4.20 (1H, *dd*, *J* = 11.7, 4.6), 4.14 (1H, *dd*, *J* = 11.6, 6.1)	65.2	H-1a↔H-1b	3.97 (1H, *dd*, *J* = 11.8, 6.3), 3.95 (1H, *dd*, *J* = 11.8, 4.8)	66.7
2	3.92 (1H, *m*)	70.3		3.70 (1H, *q*, *J* = 5.8)	70.9
3	3.69 (1H, *dd*, *J* = 11.4, 4.0), 3.59 (1H, *dd*, *J* = 11.4, 5.8)	63.4	H-3a↔H-3b	3.46 (1H, *dd*, *J* = 12.4, 4.2), 3.39 (1H, *dd*, *J* = 12.4, 6.1)	64.3
1'	-	174.5		-	173.7
2'	2.34 (2H, *t*, *J* = 14.6)	34.2	H-3'	2.19 (2H, *t*, *J* = 15.0)	34.4
3'	1.62 (2H, *m*)	25.0	H-2'	1.46 (2H, *q*, *J* = 14.0)	25.3
4'	1.31-1.23 (2H, *br s*)	29.2		1.11-1.03 (2H, *br s*)	29.4-32.1
5'	1.31-1.23 (2H, *br s*)	29.3		1.11-1.03 (2H, *br s*)	29.4-32.1
6'	1.31-1.23 (2H, *br s*)	29.7		1.11-1.03 (2H, *br s*)	29.4-32.1
7'-21'	1.31-1.23 (30H, *br s*)	29.8		1.11-1.03 (30H, *br s*)	29.4-32.1
22'	1.31-1.23 (2H, *br s*)	29.4		1.11-1.03 (2H, *br s*)	29.4-32.1
23'	1.31-1.23 (2H, *br s*)	29.5		1.11-1.03 (2H, *br s*)	29.4-32.1
24'	1.31-1.23 (2H, *br s*)	32.0		1.11-1.03 (2H, *br s*)	29.4-32.1
25'	1.31-1.23 (2H, *br s*)	22.8		1.11 (2H, *br s*)	22.9
26'	0.86 (3H, *t*, *J* = 12.8)	14.2		0.72 (3H, *t*, *J* = 13.0)	14.2

4.2.3.6. Compound 89

Compound **89** was collected as an orange crystalline powder. Due to its small sample size, the NMR instrument failed to generate the carbon spectra. Thus, the structure elucidation of the compound was achieved based on its ^{1}H NMR spectral information in comparison with related reports. The ^{1}H NMR (400 MHz, $CDCl_3$) spectrum showed two chelated protons at δ_H 12.13 (1H, *s*) and 12.02 (1H, *s*) assignable to the hydroxyl protons in rings A and C, respectively. Three aromatic signals observed at δ_H 7.82 (1H, *dd*, *J* = 7.5, 1.2, H-5), 7.65 (1H, *t*, *J* = 8.5, H-6), and 7.29 (1H, *dd*, *J* = 8.4, 1.1, H-7) with ABX spin pattern (ring A) and a single sp^2 aromatic signal at δ_H 7.10 (1H, *brs*, H-2) (ring C) suggested the presence of an anthraquinone skeleton. The spectrum also revealed additional aromatic signals at δ_H 7.68 (1H, *d*, *J* = 8.0, H-6'), 7.51 (1H, *s*, H-3'), and 6.98 (1H, *d*, H-5') assignable to the protons in the hydroxymethyl-4'-hydroxyphenyl moiety. Moreover, two singlet signals at δ_H 3.63 (2H, *brs*) and 2.46 (3H, *s*) indicated additional

oxymethylene, and methyl attachments in the hydroxymethyl-4'-hydroxyphenyl and anthraquinone moieties, respectively (Table 27, Appendix 24). Overall, the spectral analysis closely matches with the reported values for 4-(2'-hydroxymethyl-4'-hydroxyphenyl)-chrysophanol (**89**) (Alemayehu *et al.*, 2015) (Figure 27).

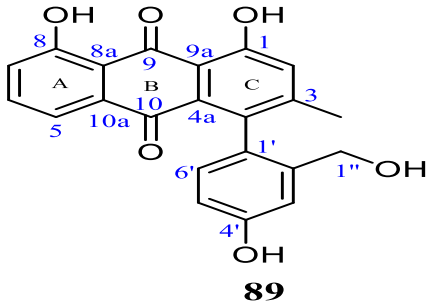

89

Figure 27: Chemical structure of compound **89**.

Table 27: ^{1}H NMR (400 MHz, $CDCl_3$, δ in ppm, *J* in Hz) spectral data of compound **89**, and ^{1}H and ^{13}C NMR values of 4-(2'-hydroxymethyl-4'-hydroxyphenyl)-chrysophanol in the literature.

C. No.	**Compound 89**	**4-(2'-hydroxymethyl-4'-hydroxyphenyl)-chrysophanol** (Alemayehu *et al.*, 2015)	
	^{1}H NMR	**^{1}H NMR**	**^{13}C NMR**
1	-	-	162.7
2	7.10 (1H, *brs*)	7.13 (1H, *s*)	124.4
3	-	-	149.4
4	-	-	121.4
4a	-	-	115.9
5	7.82 (1H, *dd*, *J* = 7.5, 1.2)	7.55 (1H, *d*, *J* = 8.4)	119.9
6	7.65 (1H, *t*, *J* = 8.5)	7.75 (1H, *t*, *J* = 8.5)	137.0
7	7.29 (1H, *dd*, *J* = 8.4, 1.1)	7.32 (1H, *d*, *J* = 8.1)	124.6
8	-	-	162.4
8a	-	-	115.9
9	-	-	192.5
9a	-	-	113.8
10	-	-	182.0
10a	-	-	133.3
CH_3	2.46 (3H, *s*)	2.45 (3H, *s*)	22.3
1-OH	12.02 (1H, *s*)	12.05 (1H, *s*)	-
8-OH	12.13 (1H, *s*)	12.25 (1H, *s*)	-
1'	-	-	133.3
2'	-	-	133.7
3'	7.51 (1H, *s*)	7.65 (1H, *d*, *J* = 1.2)	121.8
4'		-	149.4
5'	6.98 (1H, *d*)	7.45 (1H, *dd*, *J* = 8.2, 1.2)	124.3
6'	7.68 (1H, *d*, *J* = 8.0)	7.84 (1H, *d*, *J* = 8.2)	136.9
4'-OH	-	7.28 (1H, *s*)	-
1"	3.63 (2H, *s*)	3.78 (2H, *s*)	68.2
1"-OH	3.93 (1H, *s*)	-	-

All the isolated compounds were also previously reported from the plant. Of the compounds, lupeol (**39**) and betulinic acid (**63**) are triterpenoids, *β*-sitosterol (**19**) and stigmasterol (**40**) are sterols, chrysophanol (**53**) and 4-(2'-hydroxymethyl-4'-hydroxyphenyl)-chrysophanol (**89**) are anthraquinones, and glyceryl-1-hexacosanoate (**88**) is a fatty acid derivative.

4.2.4. Structure elucidation of compounds isolated from roots of *Ziziphus spina-christi*

Five compounds namely; trimethyl trilinolein (**90**), stearic acid (**91**), 13-hydroxyoctadeca-9, 11-dienoic acid (**92**), stigmasterol (**40**), and *β*-sitosteryl-3*β*-glucopyranoside-6'-*O*-palmitate (**86**) were isolated from the combined CH_2Cl_2: CH_3OH (1:1) and methanol extracts of *Z. spina-christi*, and their TLC profiles are depicted in Appendix 25. The compounds were characterized with the help of IR and NMR spectroscopic techniques and a comparison of their spectral data with literature references. Compounds **40** and **86** were previously isolated from the roots of *D. regia* and their spectral information are depicted in sections 4.2.2.1, Table 17, and Appendices 13A-D (compound **40**) and 4.2.2.4, Table 19, and Appendices 15A-E (compound **86**).

4.2.4.1. Compound 90

Compound **90** was isolated as a pale yellow gel. The FTIR spectrum revealed strong absorption bands at 2918 and 2849 cm^{-1} attributed to -C-H stretching frequencies in the aliphatic region. In addition, the strong and weak absorption bands observed at 1739 and 1162 cm^{-1} are evident to the presence of -C=O and –C-O-C stretching frequencies in esters, respectively (Appendix 26A). The ^{1}H NMR (600 MHz, $CDCl_3$) spectrum displayed signals at δ_H 5.40 (3H, *m*, H-10', 10''), 5.38 (3H, *m*, H-9', 9''), and 5.14 (3H, *t*, *J* = 7.4, H-13', 13'') suggesting the presence of three groups of olefinic protons. The Multiplet peaks observed at δ_H 5.29 (1H, *m*, H-2), and 4.32 (2H, *dd*, *J* = 12.0, 4.4, H-1b, 3b) and 4.17 (2H, *dd*, *J* = 11.8, 5.8, H-1a, 3a) attributed to oxymethine and oxymethylene protons of a glycerol backbone in triglycerides, respectively. The doublet and triplet signals at δ_H 2.79 (6H, *d*, *J* = 6.9, H-11', 11'') and 2.33 (6H, *t*, *J* = 7.6, H-2', 2'') correspond to the methylene protons between the unsaturation and adjacent to the carbonyl groups, respectively. Furthermore, the multiplet signals at δ_H 2.07 (12H, *m*) and 1.63 (6H, *m*) were assignable to (H-8', 8'', 14', 14''), and (H-3', 3''), respectively. The spectrum also exhibited signals of methyl protons at δ_H 1.70 (9H, *s*, Me-19', 19''), and 0.90 (9H, *brt*, *J* = 6.7, Me-18', 18''). The remaining protons were observed as

multiplet signals at δ_H 1.33 (6H, *m*, H-17', H-17"), and 1.28 (36H, *m*, H-4', H-4", H-5', H-5", H-6', H-6", H-7', H-7", H-15', H-15", H-16', H-16") (Table 28, Appendix 26B).

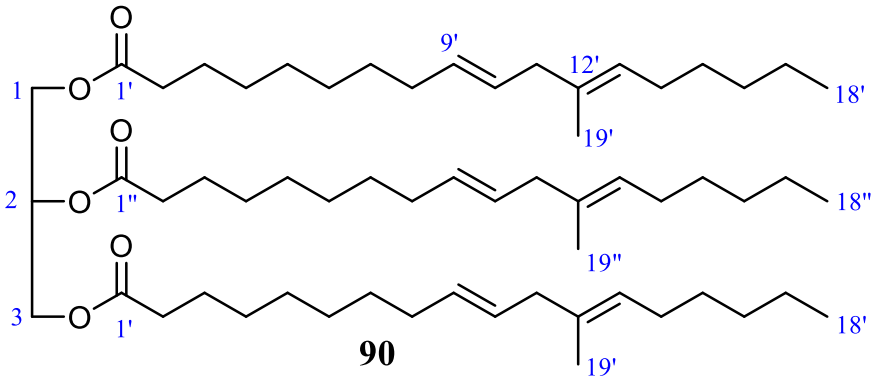

90

Figure 28: Chemical structure of compound **90**.

Notably, the ^{13}C NMR (150 MHz, $CDCl_3$) spectrum displayed carbonyl signals at δ_C 173.2 (C-1') and 172.1 (C-1"), olefinic carbons at δ_C 135.2 (C-12', 12"), 130.2 (C-9', 9"), 127.9 (C-10', 10"), and 125.0 (C-13', 13"), oxymethine and oxymethylene signals at δ_C 68.9 (C-2) and 62.1 (C-1, 3), respectively, associated to the structure of triglycerides with unsaturated fatty acid chains. The presence of methyl signals at δ_C 23.4 (C-19', C-19") and a quaternary carbon at δ_C 135.2 (from DEPT-135 spectrum) are evident that one of the olefinic moiety of the fatty acid group exhibits an additional methyl substituent. In addition, the types of carbons were verified by the DEPT-135 spectrum which revealed three olefinic signals assignable to nine carbons, one oxymethine and two oxymethylene signals, twelve sp^3 methylene signals assignable to thirty-six carbons, and two methyl signals assignable to six carbons, in accordance with the ^{13}C NMR spectrum of the compound (Table 28, Appendices 26C and D). Finally, the spectral analyses agreed with the literature values of trimethyl trilinolein (**90**) (Ramsewak *et al.*, 2001, Yakubu *et al.*, 2020) (Figure 28).

Table 28: ^{1}H (600 MHz), ^{13}C (150 MHz), and DEPT-135 NMR ($CDCl_3$, δ in ppm, J in Hz) spectral data of compound **90**, and ^{1}H and ^{13}C NMR values of trimethyl trilinolein in the literature.

C. No.	**Compound 90**			**trimethyl trilinolein** (Ramsewak *et al.*, 2001, Yakubu *et al.*, 2020)	
	^{1}H NMR	**^{13}C NMR**	**DEPT-135**	**^{1}H NMR**	**^{13}C NMR**
1a, 1b	4.17 (1H, *dd*, *J* = 11.8, 5.8), 4.32 (1H, *dd*, *J* = 12.0, 4.4)	62.1	-CH_2-O-	4.12 (1H, *dd*, *J* = 14.0, 6.0), 4.28 (1H, *dd*, *J* = 14.0, 4.2)	62.1
2	5.29 (1H, *m*)	68.9	-CH-O-	5.25 (1H, *m*)	68.9
3a, 3b	4.17 (1H, *dd*, *J* = 11.8, 5.8), 4.32 (1H, *dd*, *J* = 12.0, 4.4)	62.1	-CH_2-O-	4.12 (1H, *dd*, *J* = 14.0, 6.0), 4.28 (1H, *dd*, *J* = 14.0, 4.2)	62.1
1', 1"	-	173.2, 172.1	Q	-	173.3, 172.8
2', 2"	2.33 (6H, *t*, *J* = 7.6)	34.0, 34.2	-CH_2-	2.28 (4H, *t*, *J* = 7.6), 2.29 (2H, *t*, *J* = 7.6)	34.0, 34.2
3', 3"	1.63 (6H, *m*)	24.8, 25.6	-CH_2-	1.59 (6H, *m*)	24.8
4', 4"	1.28 (6H, *m*)	29.2, 29.1	-CH_2-	1.25 (6H, *m*)	29.1, 29.0
5', 5"	1.28 (6H, *m*)	29.4	-CH_2-	1.25 (6H, *m*)	29.2, 29.3
6', 6"	1.28 (6H, *m*)	29.3, 29.3	-CH_2-	1.25 (6H, *m*)	29.1, 29.2
7', 7"	1.28 (6H, *m*)	29.7	-CH_2-	1.25 (6H, *m*)	29.6
8', 8"	2.07 (6H, *m*)	32.2	-CH_2-	2.02 (6H, *m*)	27.2
9', 9"	5.38 (3H, *m*)	130.2	=CH-	5.33 (3H, *m*)	130.0
10', 10"	5.40 (3H, *m*)	127.9	=CH-	5.33 (3H, *m*)	128.0
11', 11"	2.79 (6H, *d*, *J* = 6.9)	39.7	-CH_2-	2.75 (4H, *m*), 2.02 (2H, *m*)	29.7
12', 12"	-	135.2	Q	5.33 (2H, *m*), 1.25 (2H, *m*)	127.9
13', 13"	5.14 (3H, *t*, *J* = 7.4)	125.0	=CH-	5.33 (2H, *m*), 1.25 (2H, *m*)	130.2
14', 14"	2.07 (6H, *m*)	27.2	-CH_2-	2.02 (4H, *m*), 1.25 (2H, *m*)	27.1
15', 15"	1.28 (6H, *m*)	29.6	-CH_2-	1.25 (6H, *m*)	29.3
16', 16"	1.28 (6H, *m*)	31.9	-CH_2-	1.25 (6H, *m*)	31.9
17', 17"	1.33 (6H, *m*)	22.7	-CH_2-	1.25 (6H, *m*)	22.7
18', 18"	0.90 (9H, *brt*, *J* = 6.7)	14.1	-CH_3	0.86 (6H, *brt*), 0.87 (3H, *brt*)	14.1
19', 19"	1.70 (9H, *s*)	23.4	-CH_3	-	-

4.2.4.2. Compound 91

Compound **91** (mp: 69-71 °C, lit. mp: 69.5 °C (Singleton *et al.*, 1950)) was obtained as a white powder. In its FTIR spectrum, a broad absorption band observed between 3500 and 2554 cm^{-1} suggested the presence of –O-H stretching in carboxylic acid. In addition, the strong absorption bands at 2918 and 2842 cm^{-1} correspond to -C-H stretching frequencies in the aliphatic region. The spectrum also showed absorption bands at 1705 and 1167 cm^{-1} attributed to the -C=O and –C-O stretching frequency of carboxylic acids, respectively (Appendix 27A). The ^{1}H NMR (600 MHz, $CDCl_3$) spectrum of the compound displayed triplet signals at δ_H 2.37 (2H, *t*, *J* = 7.6) and 0.90 (3H, *t*, *J* = 7.0) attributed to the methylene protons at C-2 and terminal methyl protons (C-18) of a fatty acid skeleton, respectively. The spectrum also exhibited multiplet peaks at δ_H 1.66 (2H, *m*) and 1.28-1.32 (26H, *m*) assignable to C-3, and C-4 up to C-17 of the fatty acid chain, respectively (Table 29, Appendix 27B).

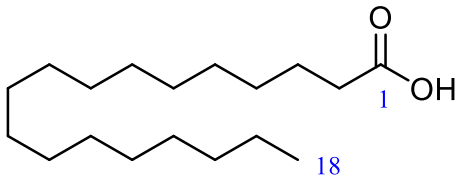

91

Figure 29: Chemical structure of compound **91**.

In its ^{13}C NMR (150 MHz, $CDCl_3$) spectrum, the compound displayed eleven signals assignable to eighteen carbons. The signals observed at δ_C 179.3 (C-1) and 14.1 (C-18) revealed the presence of carbonyl and terminal methyl carbons of a fatty acid skeleton. The spectrum also showed signals at δ_C 33.9, 31.9, 29.6, 29.4, 29.3, 29.2, 29.0, 24.6, and 22.7 assignable to C-2, C-16, (C-6 up to C-13), C-14, C-15, C-5, C-4, C-3, and C-17, respectively. Notably, the DEPT-135 spectrum revealed one methyl signal at δ_C 14.1 and sixteen methylene signals which were consistent with the ^{13}C NMR spectral analysis of the compound (Table 29, Appendices 27C and D). The data generated matches with a previous report for stearic acid (**91**) (Abdurrahman and Cai-Xiab, 2020) (Figure 29). The compound was also identified from the GC-MS analysis of the volatile oils of *Z. spina-christi*, and its structural information was supported by mass fragmentation patterns (Appendix 27E).

Table 29: ^{1}H (600 MHz), ^{13}C (150 MHz), and DEPT-135 NMR ($CDCl_3$, δ in ppm, J in Hz) spectral data of compound **91**, and ^{1}H and ^{13}C NMR values of stearic acid in the literature.

C No.	Compound 91			**Stearic acid** (Abdurrahman and Cai-Xiab, 2020)	
	^{1}H NMR	**^{13}C NMR**	**DEPT-135**	**^{1}H NMR**	**^{13}C NMR**
1	-	179.3	Q (C=O)	-	178.7
2	2.37 (2H, *t*, *J* = 7.6)	33.9	-CH_2-	2.34 (2H, *t*, *J* = 7.5)	33.8
3	1.66 (2H, *m*)	24.6	-CH_2-	1.63 (2H, *m*)	24.7
4	1.28-1.32 (2H, *m*)	29.0	-CH_2-	1.28-1.30 (2H, *m*)	29.7-30.0
5	1.28-1.32 (2H, *m*)	29.2	-CH_2-	1.28-1.30 (2H, *m*)	29.7-30.0
6	1.28-1.32 (2H, *m*)	29.6	-CH_2-	1.28-1.30 (2H, *m*)	29.7-30.0
7	1.28-1.32 (2H, *m*)	29.6	-CH_2-	1.28-1.30 (2H, *m*)	29.7-30.0
8	1.28-1.32 (2H, *m*)	29.6	-CH_2-	1.28-1.30 (2H, *m*)	29.7-30.0
9	1.28-1.32 (2H, *m*)	29.6	-CH_2-	1.28-1.30 (2H, *m*)	29.7-30.0
10	1.28-1.32 (2H, *m*)	29.6	-CH_2-	1.28-1.30 (2H, *m*)	29.7-30.0
11	1.28-1.32 (2H, *m*)	29.6	-CH_2-	1.28-1.30 (2H, *m*)	29.7-30.0
12	1.28-1.32 (2H, *m*)	29.6	-CH_2-	1.28-1.30 (2H, *m*)	29.7-30.0
13	1.28-1.32 (2H, *m*)	29.6	-CH_2-	1.28-1.30 (2H, *m*)	29.7-30.0
14	1.28-1.32 (2H, *m*)	29.4	-CH_2-	1.28-1.30 (2H, *m*)	29.7-30.0
15	1.28-1.32 (2H, *m*)	29.3	-CH_2-	1.28-1.30 (2H, *m*)	29.7-30.0
16	1.28-1.32 (2H, *m*)	31.9	-CH_2-	1.28-1.30 (2H, *m*)	31.9
17	1.28-1.32 (2H, *m*)	22.7	-CH_2-	1.28-1.30 (2H, *m*)	22.7
18	0.90 (3H, *t*, *J* = 7.0)	14.1	-CH_3	0.88 (3H, *t*, *J* = 7.0)	14.1

4.2.4.3. Compound 92

Compound **92** was isolated as a yellow powder and its ^{1}H NMR (600 MHz, $CDCl_3$) spectrum showed signals at δ_H 6.51 (1H, *dd*, *J* = 15.2, 11.1, H-11), 5.99 (1H, *t*, *J* = 11.0, H-10), 5.68 (1H, *dd*, *J* = 15.2, 6.9, H-12), and 5.48 (1H, *m*, H-9) suggesting the presence of four olefinic protons. The coupling constant (*J*) values of the protons were evident for the *cis* and *trans* geometry of (H-9 and H-10) and (H-11 and H-12), respectively. It also displayed signals of oxymethine protons at δ_H 4.18 (1H, *q*, *J* = 6.6, H-13) evident for the presence of a secondary alcohol. The triplet and multiplet peaks at δ_H 2.37 (2H, *t*, *J* = 7.5) and 2.20 (2H, *m*) were assignable to the methylene protons adjacent to the carbonyl (H-2) and olefinic protons (H-8), respectively. Furthermore, the triplet signals observed at δ_H 0.91 (3H, *t*, *J* = 7.3, H-18) attributed to the terminal methyl protons of a fatty acid chain. The remaining protons overlapped in the range of δ_H 1.50-1.62 (4H, *m*) and 1.28-1.34 (14H, *m*) (Table 30, Appendix 28A).

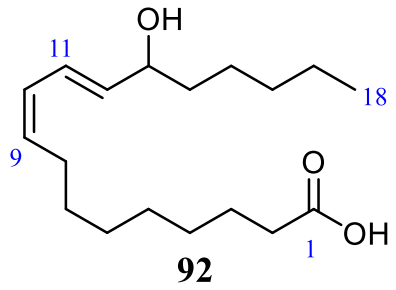

92

Figure 30: Chemical structure of compound **92**.

The ^{13}C NMR (150 MHz, $CDCl_3$) spectrum revealed the resonance of eighteen carbons associated with the structure of linoleic acid. This was confirmed by the presence of a carbonyl signal at δ_C 179.7 (C-1), olefinic signals at δ_C 135.6 (C-12), 133.1 (C-9), 127.6 (C-10), and 125.9 (C-11) and a terminal methyl signal at δ_C 14.1 (C-18). The signal at δ_C 72.9 demonstrated an oxymethine carbon assignable to C-13. The spectrum also showed a group of aliphatic signals at δ_C 37.2, 33.7, 31.9, 31.4, 29.7, 29.3, 29.1, 27.7, 25.3, 24.6, 22.7, and 14.1 assignable to C-14, C-2, C-16, C-7, C-6, C-5, C-4, C-8, C-15, C-3, C-17, and C-18, respectively. In addition, the types of carbons were identified by the DEPT-135 spectral information, thereby four sp^2 olefinic carbons, one oxymethine carbon, eleven sp^3 methylene, and one methyl signals were displayed in the spectrum which agreed with the ^{13}C NMR spectral data of the compound (Table 30, Appendices 28B and C). Based on the evidences, the spectral analyses match with the reported values for 13-hydroxyoctadeca-9, 11-dienoic acid (**92**) (d'Almeida Gameiro *et al.*, 2022) (Figure 30).

Table 30: ^{1}H (600 MHz), ^{13}C (150 MHz), and DEPT-135 NMR ($CDCl_3$, δ in ppm, J in Hz) spectral data of compound **92**, and ^{1}H and ^{13}C NMR values of 13-hydroxyoctadeca-9, 11-dienoic acid in the literature.

C No.	**Compound 92**			**13-hydroxyoctadeca-9, 11-dienoic acid** (d'Almeida Gameiro et al., 2022)	
	^{1}H NMR	**^{13}C NMR**	**DEPT-135**	**^{1}H NMR**	**^{13}C NMR**
1	-	179.7	Q (C=O)	-	179.5
2	2.37 (2H, *t*, *J* = 7.5)	33.7	$-CH_2-$	2.33 (2H, *t*, *J* =7.4)	34.1
3	1.60 (2H, *m*)	24.6	$-CH_2-$	1.62 (2H, *m*)	24.8
4	1.28-1.34 (2H, *m*)	29.1	$-CH_2-$	1.24-1.34 (2H, *m*)	29.0
5	1.28-1.34 (2H, *m*)	29.3	$-CH_2-$	1.24-1.34 (2H, *m*)	29.0
6	1.28-1.34 (2H, *m*)	29.7	$-CH_2-$	1.24-1.34 (2H, *m*)	29.0
7	1.28-1.34 (2H, *m*)	31.4	$-CH_2-$	1.34-1.42 (2H, *m*)	29.5
8	2.20 (2H, *m*)	27.7	$-CH_2-$	2.17 (2H, *q*, *J* = 9.8, 7.4, 4.1, 2.4)	27.7
9	5.48 (1H, *m*)	133.1	=CH-	5.43 (1H, *dt*, *J* = 10.8, 7.6)	132.9
10	5.99 (1H, *t*, *J* = 11.0)	127.6	=CH-	5.97 (1H, *t*, *J* = 11.0, 1.1)	128.0
11	6.51 (1H, *dd*, *J* = 15.2, 11.1)	125.9	=CH-	6.48 (1H, *m*, *J* = 15.2, 11.1, 1.2)	126.0
12	5.68 (1H, *dd*, *J* =15.2, 6.9)	135.6	=CH-	5.66 (1H, *dd*, *J* = 15.2, 6.8)	135.8
13	4.18 (1H, *q*, *J* = 6.6)	72.9	-CH-O-	4.17 (1H, *q*, *J* = 6.1)	73.1
14	1.52 (2H, *m*)	37.2	$-CH_2-$	1.53 (2H, *m*)	37.4
15	1.28-1.34 (2H, *m*)	25.3	$-CH_2-$	1.24-1.34 (2H, *m*)	25.2
16	1.28-1.34 (2H, *m*)	31.9	$-CH_2-$	1.24-1.34 (2H, *m*)	31.9
17	1.28-1.34 (2H, *m*)	22.7	$-CH_2-$	1.24-1.34 (2H, *m*)	22.7
18	0.91 (3H, *t*, *J* =7.3)	14.1	$-CH_3$	0.84-0.92 (3H, *t*, *J* =7.4)	14.2

Remarkably, three of the isolated compounds (trimethyl trilinolein (**90**), 13-hydroxyoctadeca-9, 11-dienoic acid (**92**), and *β*-sitosteryl-3*β*-glucopyranoside-6'-*O*-palmitate (**86**)) were reported herein for the first time from the plant.

4.2.5. Essential oils profile

Essential oils (EOs) are volatile mixtures of organic and natural bioactive compounds in plants and possess as many as 10-70 compounds in different concentrations (Nerio *et al.*, 2010). They are characterized by their contents of 1-3 major compounds in relative high concentrations compared to the other components of the essential oil present in minimal amounts. They are mainly comprised of terpenoids, fatty acid methyl esters, and phenyl propanes with different functional groups (Nerio *et al.*, 2010). EOs are colorless liquids naturally present in all parts of plants

including flowers, barks, roots, stems, seeds, and leaves. As a result of their good aroma and flavor, EOs have been widely used in many parts of the world as cosmetics, perfumes, medicines, and foods (Bhavaniramya *et al.*, 2019). In this section, the essential oils (EOs) profile of the four plants (*C. adenocaule, D. regia, S. siamea,* and *Z. spina-christi*) are entirely presented and compared to similar reports of the plant materials.

4.2.5.1. Essential oils profile of the leaves and roots of *C. adenocaule*

The powdered leaves (40 g) and roots (30 g) of *C. adenocaule* yielded a colorless and pleasant odor EOs of about 20 mg (0.05% w/w) and 15.04 mg (0.05% w/w), respectively. The GC-MS analysis (Appendix 29A) of the leaves EO of *C. adenocaule* showed a total of 70 components, of which 43 compounds accounting for 94.30% of the total composition were reported based on their areal records (compounds with peak area of 0.20% and above were reported). Perillyl alcohol (**93**, 13.08%), geranyl isovalerate (**94**, 10.29%), germacra-4(15), 5, 10(14)-trien-1α-ol (**95**, 9.65%), (+)-spathulenol (**96**, 7.45%), piperitenone (**97**, 7.06%), *τ*-cadinol (**98**, 5.76%), and caryophyllene oxide (**99**, 4.83%) were among the major compounds identified from the leaves EOs of the plant (Figure 31). The chemical classes of the compounds along with their composition were also determined. Sesquiterpenes and derivatives (43.45%) comprised the majority of the leaves EO of *C. adenocaule* followed by monoterpenes and derivatives (41.76%), fatty acids (3.91%), aromatics (2.18%), diterpenes (1.53%), others (1.18%) and hydrocarbons (0.29%) (Table 31).

Table 31: Essential oil composition of the leaves of *C. adenocaule*.

No.	Compound name	Molecular formula	RT	RI	Relative percentage (%)
		Monoterpenes and derivatives			
1	Sabinol isovalerate	$C_{15}H_{24}O_2$	5.11	1515	0.60
2	Borneol	$C_{10}H_{18}O$	23.99	1167	0.69
3	*α*-Terpeneol	$C_{10}H_{18}O$	25.25	1189	2.50
4	Carveol	$C_{10}H_{16}O$	26.61	1229	0.43
5	*cis*-Geraniol	$C_{10}H_{18}O$	27.10	1228	0.94
6	Lavandulol	$C_{10}H_{18}O$	28.35	1170	3.45
7	Perillal	$C_{10}H_{14}O$	29.12	1272	2.72
8	Perillyl alcohol	$C_{10}H_{16}O$	30.30	1296	13.08
9	Piperitenone	$C_{10}H_{14}O$	32.14	1340	7.06

Table 31 (continued)

10	Geranyl isovalerate	$C_{15}H_{26}O_2$	54.23	1606	10.29
	Sesquiterpenes and derivatives				
11	(-)-Aromadendrene	$C_{15}H_{24}$	35.48	1440	0.48
12	*trans*-*β*-Ionone	$C_{13}H_{20}O$	38.28	1486	0.86
13	*β*-Bisabolene	$C_{15}H_{24}$	39.20	1509	0.31
14	Epicubebol	$C_{15}H_{26}O$	39.37	1493	0.52
15	*δ*-Cadinene	$C_{15}H_{24}$	39.76	1524	0.63
16	2-Methyl-9-(prop-1-en-3-ol-2-yl)-Bicyclo[4.4.0]dec-2-ene-4-ol	$C_{15}H_{24}O_2$	40.52	1555	0.51
17	Nerolidol	$C_{15}H_{26}O$	41.37	1544	0.91
18	(+)-Spathulenol	$C_{15}H_{24}O$	41.85	1576	7.45
19	Caryophyllene oxide	$C_{15}H_{24}O$	42.04	1581	4.83
20	(+)-Ledene	$C_{15}H_{24}$	42.35	1493	0.53
21	Mintketone	$C_{15}H_{24}O$	42.44	1595	0.91
22	Cedrol	$C_{15}H_{26}O$	42.67	1598	1.03
23	Costol	$C_{15}H_{24}O$	42.97	1778	1.09
24	Aromadendrene oxide	$C_{15}H_{24}O$	44.26	1678	1.86
25	*τ*-Cadinol	$C_{15}H_{26}O$	44.40	1640	5.76
26	*β*-Acorenol	$C_{15}H_{26}O$	44.50	1649	0.67
27	Mustakone	$C_{15}H_{22}O$	45.09	1687	1.92
28	Germacra-4(15),5,10(14)-trien-1*α*-ol	$C_{15}H_{24}O$	45.30	1695	9.65
29	Dehydrosaussurea lactone	$C_{15}H_{20}O_2$	47.30	1838	0.69
30	Nootkatone	$C_{15}H_{22}O$	48.11	1808	0.87
31	Diepicedrene-1-oxide	$C_{15}H_{24}O$	48.86	1551	0.67
32	Phytone	$C_{18}H_{36}O$	48.98	1844	1.00
33	*trans*-Longipinocarveol	$C_{15}H_{24}O$	49.27	1618	0.30
	Diterpenes				
34	Phytol	$C_{20}H_{40}O$	53.76	2114	1.53
	Aromatics				
35	8,9-Dehydrothymol	$C_{10}H_{12}O$	26.45	1221	0.34
36	Cuminol	$C_{10}H_{14}O$	29.93	1289	0.26
37	Eugenol	$C_{10}H_{12}O_2$	32.88	1357	0.72
38	Dihydroactinolide	$C_{11}H_{16}O_2$	39.90	1532	0.86
	Fatty acids				
39	Palmitic acid	$C_{16}H_{32}O_2$	51.24	1968	3.91
	Hydrocarbons				

Table 31 (continued)

40	Heptacosane	$C_{27}H_{56}$	56.55	2700	0.29
		Others			
41	4-(2-Methyl-3-oxocyclohexyl)-butanal	$C_{11}H_{18}O_2$	39.60	1515	0.42
42	8α-11-Elemadiol	$C_{14}H_{24}O_2$	40.71	1745	0.28
43	3-Deoxyestradiol	$C_{18}H_{24}O$	51.80	2259	0.48
Total					**94.30**

RI; retention index**,** RT; retention time.

The GC-MS analysis (Appendix 29B) of the roots EO of *C. adenocaule* revealed a total of 75 components, of which 48 compounds which account for 97.08% of the oil composition were reported based on their areal records. Phytone (**100**, 12.64%), geranyl isovalerate (**94**, 12.15%), phytol (**101**, 10.50%), palmitic acid (**83**, 8.60%), germacra-4(15), 5, 10(14)-trien-1α-ol (**95**, 4.73%), and τ-cadinol (**98**, 4.21%) were among the major components of the roots EO of the plant (Figure 31). Among the identified compounds, sesquiterpenes and derivatives (39.87%) afford the highest composition followed by fatty acids and derivatives (19.34%), diterpenes and derivatives (16.60%), monoterpenes and derivatives (13.03%), others (4.64%), hydrocarbons (1.88%), and aromatics (1.72%) (Table 32). The chemical composition of the roots EO of *C. adenocaule* showed slight differences from those identified in the leaves of the plant. This might be due to the fact that the composition of plant EOs collected from different parts varies with the age of the plant, type of soil, and genetic differences (Azadi and Khaef, 2015). To the best of our knowledge, the chemical composition of EOs from *C. adenocaule* is reported herein for the first time.

Table 32: Essential oil composition of the roots of *C. adenocaule*.

No.	Compound name	Molecular formula	RT	RI	Relative abundance (%)
		Monoterpenes and derivatives			
1	Sabinol isovalerate	$C_{15}H_{24}O_2$	5.02	1515	0.88
2	Geranyl isovalerate	$C_{15}H_{26}O$	40.91	1606	12.15
		Sesquiterpenes and derivatives			
3	Cedrene	$C_{15}H_{24}$	22.20	1422	0.23
4	Caryophyllene	$C_{15}H_{24}$	22.34	1419	0.36
5	*cis*-Thujopsene	$C_{15}H_{24}$	22.59	1429	0.24
6	α-Bisabolene	$C_{15}H_{24}$	23.06	1504	0.20

Table 32 (continued)

7	(+)-Spathulenol	$C_{15}H_{24}O$	25.58	1576	2.11
8	Isoaromadendrene epoxide	$C_{15}H_{24}O$	25.71	1589	1.25
9	Caryophyllene oxide	$C_{15}H_{24}O$	25.83	1581	0.41
10	(-)-Globulol	$C_{15}H_{26}O$	25.87	1580	0.69
11	Cedrol	$C_{15}H_{26}O$	26.09	1598	3.07
12	β-Costol	$C_{15}H_{24}O$	26.87	1778	0.81
13	Ledene oxide	$C_{15}H_{24}O$	26.95	1631	1.16
14	τ-Cadinol	$C_{15}H_{26}O$	27.03	1640	4.21
15	Humulenol-II	$C_{15}H_{24}O$	27.26	1650	1.32
16	*trans*-Bisabolene epoxide	$C_{15}H_{24}O$	27.42	1586	0.18
17	Thujopsenal	$C_{15}H_{22}O$	27.51	1724	0.56
18	Germacra-4(15),5,10(14)-trien-1α-ol	$C_{15}H_{24}O$	27.64	1695	4.73
19	Hexahydro-farnesol	$C_{15}H_{32}O$	29.37	1571	0.67
20	Phytone	$C_{18}H_{36}O$	30.30	1844	12.64
21	Shyobunol	$C_{15}H_{26}O$	38.12	1701	3.81
22	Longiborneol	$C_{15}H_{26}O$	41.72	1592	1.22
	Diterpenes and derivatives				
23	Neophytadiene	$C_{20}H_{38}$	30.19	1837	4.02
24	Isophytol acetate	$C_{22}H_{42}O_2$	32.00	2064	0.73
25	Phytol	$C_{20}H_{40}O$	34.60	2114	10.50
26	Phytyl-acetate	$C_{22}H_{42}O_2$	35.21	2064	1.35
	Aromatics				
27	Resorcinol	$C_6H_6O_2$	12.44	1372	0.47
28	1-Isocyanato-2-methyl-Benzene	C_8H_7NO	13.67	1131	0.58
29	*o*-Toluidine	C_7H_9N	13.91	1070	0.27
30	Chavicol	$C_9H_{10}O$	18.45	1255	0.40
	Fatty acids and derivatives				
31	Lauric acid	$C_{12}H_{24}O_2$	25.09	1568	1.00
32	Ethyl-linolenate	$C_{20}H_{34}O_2$	28.72	2169	0.28
33	Myristic acid	$C_{14}H_{28}O_2$	28.81	1768	2.56
34	di-Linoleylmethylketone	$C_{19}H_{34}O$	30.92	2075	0.64
35	Methyl-palmitate	$C_{17}H_{34}O_2$	31.64	1926	1.53
36	Palmitic acid	$C_{16}H_{32}O_2$	32.23	1968	8.60
37	Oleic acid	$C_{18}H_{34}O_2$	32.35	2141	1.80
38	*cis*-13-Eicosenoic acid	$C_{20}H_{38}O_2$	32.72	2366	0.95
39	Methyl-linoleate	$C_{19}H_{34}O_2$	34.33	2097	1.09

Table 32 (continued)

40	Linoleic acid	$C_{18}H_{32}O_2$	36.17	2133	0.53
41	Octyl-palmitoleate	$C_{24}H_{46}O_2$	40.64	2559	0.36
	Hydrocarbons				
42	Heptacosane	$C_{27}H_{56}$	40.05	2700	1.88
	Others				
43	Xanthinin	$C_{17}H_{22}O_5$	29.27	2383	0.46
44	2-Methylene cholestan-3-ol	$C_{28}H_{48}O$	30.74	2317	1.22
45	7-Hexadecenal	$C_{16}H_{30}O$	31.48	1798	0.34
46	Aspidocarpine	$C_{22}H_{30}N_2O_3$	31.58	-	0.68
47	1,13-Tetradecadien-3-one	$C_{14}H_{24}O$	31.76	1571	0.82
48	2-Hexadecenal	$C_{16}H_{30}O$	32.90	1878	1.12
Total					**97.08**

RI; retention index**,** RT; retention time.

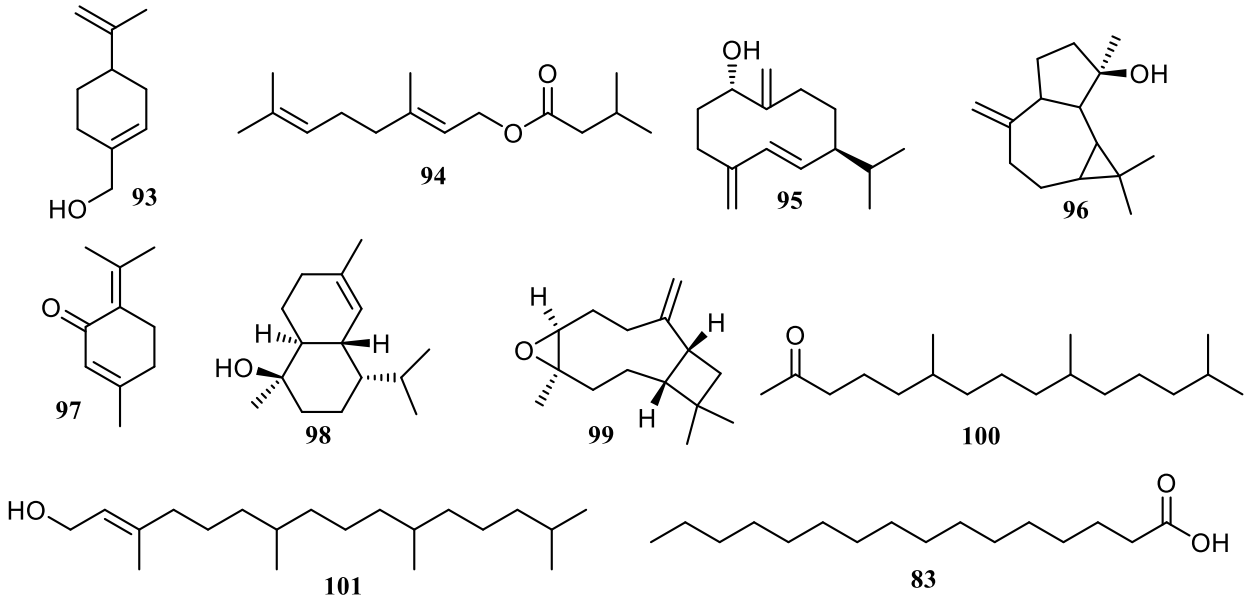

Figure 31: Chemical structures of the major compounds of *C. adenocaule* essential oils.

4.2.5.2. Essential oil profile of the roots of *D. regia*

The yield of the pounded roots (40 g) of *D. regia* obtained by hydrodistillation technique in a Clevenger's type apparatus was about 5.5 mg (0.00014% w/w) with aromatic odor and no characteristic color. The GC-MS analysis (Appendix 30) of the EOs showed 19 compounds accounting for 98.72% of the identified components. The EO is principally composed of heneicosane (**102**, 49.26%), and hentriacontane (**103**, 38.67%) followed by caryophyllene oxide

(**99**, 2.87%), and *β*-eudesmol (**104**, 1.61%) (Table 33, Figure 32). Heneicosane is used as a pheromone by the king or queen termites of *Reticulitermes flavipes* species. It is one of the vital pheromones for attracting mosquitoes of *Aedes* species and controlling disease transmission by the vectors by letting them lay their eggs around fresh water. This is based on the principle that the compound is produced in the skin of the larva (Kumar *et al.*, 2016). Notably, the chemical composition of the EO of *D. regia* shared some similar compounds, such as caryophyllene and germacrane with previously reported studies. Njoku and co-workers identified a total of 22 constituents each from the hydrodistilled (99.85%) and steam distilled (99.85%) EOs of the leaves of *D. regia*, of which thymol (40.09%) and caryophyllene (41.64%) constituted the highest composition of the hydrodistilled and steam distilled EOs, respectively (Njoku *et al.*, 2022). The majority of compounds in the report were different from the findings of this study. This is because the EOs were extracted from different parts and chemical compositions also rely on certain environmental factors, such as type of soil, climate, developmental stage, harvesting time, and growth altitude (Azadi and Khaef, 2015).

Table 33: Essential oil composition of the roots of *D. regia*.

No.	Compound name	Molecular formula	RT	RI	Relative percentage (%)
	Sesquiterpenes and derivatives				
1	Epi-*α*-elemol	$C_{15}H_{26}O$	18.65	1625	0.27
2	Spathulenol	$C_{15}H_{24}O$	19.26	1576	0.28
3	Caryophyllene oxide	$C_{15}H_{24}O$	19.40	1578	2.87
4	5,5-dimethyl-4-(3-methyl-1,3-butadienyl)-1-oxaspiro[2.5]-octane	$C_{14}H_{22}O$	19.90	-	0.31
5	2-methylene-4,8,8-trimethyl-4-vinyl bicyclo[5.2.0]-nonane	$C_{15}H_{24}$	20.32	-	0.17
6	Caryophylladienol II	$C_{15}H_{24}O$	20.39	2336	0.31
7	*τ*-Cadinol	$C_{15}H_{26}O$	20.44	1639	0.42
8	*β*-Eudesmol	$C_{15}H_{26}O$	20.67	1621	1.61
9	*τ*-Muurolol	$C_{15}H_{26}O$	20.72	1640	0.79
10	Aromadendrene epoxide	$C_{15}H_{24}O$	20.77	1622	0.66
11	1,3-di(propen-1-yl)-adamantane	$C_{16}H_{24}$	20.85	-	0.47
12	Germacra-4(15),5,10(14)-trien-1-*β*-ol	$C_{15}H_{24}O$	21.02	1684	0.65

Table 33 (continued)

13	Mustakone	$C_{15}H_{22}O$	21.19	1687	0.39
14	Boronal	$C_{14}H_{22}O$	21.43	1584	0.19
15	Longiverbenone	$C_{15}H_{22}O$	22.37	1632	0.13
	Fatty acids				
16	Palmitic acid	$C_{16}H_{32}O_2$	25.88	1964	1.11
17	Linoleic acid	$C_{18}H_{32}O_2$	28.61	2111	0.16
	Hydrocarbons				
18	Hentriacontane	$C_{31}H_{64}$	38.90	478	38.67
19	Heneicosane	$C_{21}H_{44}$	47.19	348	49.26
	Total				**98.72**

RI; retention index**,** RT; retention time.

4.2.5.3. Essential oil profile of the roots of *S. siamea*

The essential oil composition of the roots of *S. siamea* was also the subject of this study. Thereby, the hydrodistillation of the roots (40 g) of *S. siamea* yielded a yellowish EO with a sweet floral aroma of about 8.0 mg (0.0002 % w/w). The GC-MS analysis (Appendix 31) of the EO afforded a total of 19 components accounting for 98.25% of the total recovered oil, of which heneicosane (**102**, 53.17%) and eicosane (**105**, 38.34%) constitute the majority of the EO (Table 34, Figure 32). The identified compounds belong to different classes of compounds such as alcohols, sesquiterpenes, fatty acids, and hydrocarbons, and eicosane and heneicosane comprise the majority of the composition (91.51%). Previous studies also reported the chemistry of the EOs of *S. siamea*. A report by Ogunwande and co-workers identified 53 components from the leaves of the plant, of which *iso* italicene (15.4%), *β*-damascenone (11.0%), linalool (7.8%) and 1-octene-3-ol (5.8%) constituted the major composition (Ogunwande *et al.*, 2013). In this case, only caryophyllene oxide and palmitic acid were similar to the components of the present finding.

Table 34: Essential oil composition of the roots of *S. siamea*.

No.	Compound name	Molecular formula	RT	RI	Relative percentage (%)
	Alcohols				
1	1-Nonanol	$C_9H_{20}O$	10.35	1163	0.14
2	4,4,6-Trimethyl-cyclohex-2-en-1-ol	$C_9H_{16}O$	14.29	-	0.23
	Sesquiterpenes and derivatives				
3	Hedycaryol	$C_{15}H_{26}O$	18.65	1534	0.12
4	Spathulenol	$C_{15}H_{24}O$	19.27	1576	0.13
5	Caryophyllene oxide	$C_{15}H_{24}O$	19.34	1578	0.53
6	Bicyclo[7.2.0]undecan-3-ol	$C_{15}H_{24}O$	20.39	-	0.11
7	*τ*-Cadinol	$C_{15}H_{26}O$	20.44	1639	0.32
8	*β*-Eudesmol	$C_{15}H_{26}O$	20.67	1621	0.89
9	*τ*-Muurolol	$C_{15}H_{26}O$	20.71	1640	0.52
10	Alloaromadendrene oxide	$C_{15}H_{24}O$	20.77	1457	0.26
11	*β*-Turmerone	$C_{15}H_{22}O$	20.85	1680	0.22
12	Germacra-4(15),5,10(14)-trien-1-*β*-ol	$C_{15}H_{24}O$	21.02	1684	0.46
13	Longiverbenone	$C_{15}H_{22}O$	21.18	1632	0.11
	Fatty acids				
14	Palmitic acid	$C_{16}H_{32}O_2$	25.86	1964	0.81
15	Linoleic acid	$C_{18}H_{32}O_2$	28.62	2111	0.24
	Hydrocarbons				
16	Eicosane	$C_{20}H_{42}$	46.45	345	38.34
17	Heneicosane	$C_{21}H_{44}$	41.57	348	53.17
	Others				
18	N-vinyl-5-ethyl-2-oxazolidinone	$C_7H_{11}NO_2$	9.62	-	1.53
19	*γ*-Nonalactone	$C_9H_{16}O_2$	14.73	1330	0.12
	Total				**98.25**

RI; retention index**,** RT; retention time.

4.2.5.4. Essential oils profile of the leaves and roots of *Z. spina-christi*

The hydrodistillation of the leaves (40 g) and roots (30 g) EOs of *Z. spina-christi* yielded a colorless and sweet floral aroma EOs of 34.53 mg (0.12% w/w) and 17.64 mg (0.06% w/w), respectively. The GC-MS analysis (Appendix 32A) of the leaves EO of *Z. spina-christi* showed a

total of 65 components, of which 41 compounds were identified comprising 95.26% of the total oil composition. Nootkatone (**106**, 30.12%), palmitic acid (**83**, 23.53%), nuciferyl acetate (**107**, 8.47%), and germacra-4(15), 5, 10(14)-trien-1α-ol (**95**, 7.51%) were among the predominant compounds identified from the leaves of the plant (Table 35, Figure 32). The relative compositions of the classes of compounds exhibited that sesquiterpenes and derivatives (52.74%) afford the highest composition followed by fatty acids and derivatives (28.84%), others (10.15%), aromatics (2.34%), and monoterpenes and derivatives (1.19%).

Table 35: Essential oil composition of the leaves of *Z. spina-christi*.

No.	Compound name	Molecular formula	RT	RI	Relative abundance (%)
	Monoterpenes and derivatives				
1	*cis*-Piperitol	$C_{10}H_{18}O$	32.24	1195	0.58
2	Geranyl isovalerate	$C_{15}H_{26}O_2$	51.86	1606	0.61
	Sesquiterpenes and derivatives				
3	8,14-Cedranoxide	$C_{15}H_{24}O$	41.86	1545	0.39
4	*cis*-Thujopsene	$C_{15}H_{24}$	42.45	1429	0.78
5	Cedrol	$C_{15}H_{26}O$	42.66	1598	0.58
6	β-Longipinene	$C_{15}H_{24}$	43.83	1403	0.23
7	β-Guaiene	$C_{15}H_{24}$	44.04	1490	0.87
8	τ-Cadinol	$C_{15}H_{26}O$	44.40	1640	0.78
9	(+)-Ledene	$C_{15}H_{24}$	44.48	1493	0.16
10	β-Costol	$C_{15}H_{24}O$	44.66	1778	1.57
11	*trans*-Longipinocaveol	$C_{15}H_{24}O$	45.00	1618	0.89
12	Germacra-4(15),5,10(14)-trien-1α-ol	$C_{15}H_{24}O$	45.30	1695	7.51
13	Epizizanone	$C_{15}H_{22}O$	45.59	1669	0.52
14	Thujopsenal	$C_{15}H_{22}O$	46.80	1724	0.35
15	Aromadendrene oxide	$C_{15}H_{24}O$	47.21	1678	1.34
16	β-Santalol	$C_{15}H_{24}O$	47.56	1715	1.13
17	Caryophyllene oxide	$C_{15}H_{24}O$	47.87	1581	0.35
18	α-Atlantone	$C_{15}H_{22}O$	48.03	1717	0.46
19	Nootkatone	$C_{15}H_{22}O$	48.15	1808	30.12
20	Ylangenal	$C_{15}H_{22}O$	48.63	1675	1.53
21	Isolongifolene	$C_{15}H_{20}$	48.80	1544	2.54
22	Diepicedrene-1-oxide	$C_{15}H_{24}O$	50.84	1551	0.26
23	Hexahydro farnesol	$C_{15}H_{32}O$	56.55	1571	0.38

Table 35 (continued)

		Aromatics			
24	Tolune	C_7H_8	5.14	763	1.76
25	Resorcinol	$C_6H_6O_2$	16.69	1372	0.23
26	2,4-Di-*tert*-Butylphenol	$C_{14}H_{22}O$	39.36	1519	0.35
		Fatty acids and derivatives			
27	Capric acid	$C_{10}H_{20}O_2$	29.17	1373	0.42
28	10,12-Tricosadiynoic acid, methyl ester	$C_{24}H_{40}O_2$	47.29	2832	0.28
29	Methyl-palmitate	$C_{17}H_{34}O_2$	50.56	1926	1.39
30	Palmitic acid	$C_{16}H_{32}O_2$	51.33	1968	23.53
31	Isopropyl palmitate	$C_{19}H_{38}O_2$	51.59	2023	0.29
32	Methyl arachidonate	$C_{21}H_{34}O_2$	53.15	2274	0.39
33	Erucic acid	$C_{22}H_{42}O_2$	53.27	2547	0.30
34	Linoleic acid	$C_{18}H_{32}O_2$	54.15	2133	0.74
35	Stearic acid	$C_{18}H_{36}O_2$	54.51	2172	0.45
36	Oleamide	$C_{18}H_{35}NO$	57.45	2386	1.05
		Others			
37	Methyl *o*-tolylcarbamate	$C_9H_{11}NO_2$	34.81	1379	0.40
38	α-Calacorene	$C_{15}H_{20}$	40.50	1542	0.25
39	1-Methyl-3-ethyladamantane	$C_{13}H_{22}$	42.53	1263	0.25
40	Retinal	$C_{20}H_{28}O$	49.48	2466	0.78
41	Nuciferyl acetate	$C_{17}H_{24}O_2$	50.97	1837	8.47
		Total			**95.26**

RI; retention index**,** RT; retention time.

Notably, the GC-MS analysis (Appendix 32B) of the roots EO of *Z. spina-christi* showed a total of 60 components, of which 32 compounds representing 96.15% of the total oil composition were reported based on their areal records. Unidentified components were present in such low amounts that either no mass spectrum was recorded or the spectrum was too poor for interpretation. The relative abundance of the identified compounds showed that nootkatone (**106**, 26.52%), palmitic acid (**83**, 16.46%), isopropyl palmitate (**108**, 13.26%), germacra-4(15), 5, 10(14)-trien-1α-ol (**95**, 8.73%), and nuciferyl acetate (**107**, 6.28%) were found abundantly in the roots of the plant (Figure 32). Of the obtained compounds, sesquiterpenes and derivatives (60.18 %) form the highest composition followed by fatty acids and derivatives (31.76%), aromatics (1.79%), others (1.31%), monoterpenes and derivatives (0.73%) and hydrocarbons (0.38%) (Table 36). The majority of the

compounds identified from the roots EO of the plant were in good agreement with the composition of the leaves.

Table 36: Essential oil composition of the roots of *Z. spina-christi*.

No.	Compound name	Molecular formula	RT	RI	Relative abundance (%)
		Monoterpenes and derivatives			
1	*cis*-Piperitol	$C_{10}H_{18}O$	21.56	1195	0.45
2	Geranyl isovalerate	$C_{15}H_{26}O_2$	33.87	1606	0.28
		Sesquiterpenes and derivatives			
3	*α*-Panasinsen	$C_{15}H_{24}$	24.81	1527	0.22
4	*cis*-Thujopsene	$C_{15}H_{24}$	26.91	1429	0.70
5	*β*-Guaiene	$C_{15}H_{24}$	27.80	1490	0.58
6	γ-Himachalene	$C_{15}H_{24}$	27.87	1477	0.74
7	(+)-Ledene	$C_{15}H_{24}$	28.04	1493	3.23
8	*trans*-Longipinocaveol	$C_{15}H_{24}O$	28.44	1618	0.82
9	Germacra-4(15),5,10(14)-trien-1*α*-ol	$C_{15}H_{24}O$	28.65	1695	8.73
10	β-Costol	$C_{15}H_{24}O$	28.87	1778	4.10
11	*α*-Atlantone	$C_{15}H_{22}O$	29.66	1717	0.47
12	Isolongifolene	$C_{15}H_{20}$	29.82	1544	2.13
13	*β*-Santalol	$C_{15}H_{24}O$	30.30	1715	1.54
14	Nootkatone	$C_{15}H_{22}O$	30.77	1808	26.52
15	Nuciferyl acetate	$C_{17}H_{24}O_2$	31.12	1837	6.28
16	Thujopsenal	$C_{15}H_{24}O$	31.15	1724	2.19
17	4,5,9,10-Dehydro-isolongifolene	$C_{15}H_{20}$	31.26	1544	1.27
18	*β*-Curcumene	$C_{15}H_{24}$	35.10	1514	0.41
19	Hexahydro farnesol	$C_{15}H_{32}O$	39.66	1571	0.25
		Aromatics			
20	Toluene	C_7H_8	5.11	763	1.49
21	2,4-Di-tert-butyl-phenol	$C_{14}H_{22}O$	25.13	1519	0.30
		Fatty acids and derivatives			
22	Methyl-palmitate	$C_{17}H_{34}O_2$	32.64	1926	0.94
23	Palmitic acid	$C_{16}H_{32}O_2$	33.31	1968	16.46
24	Linoleic acid	$C_{18}H_{32}O_2$	35.96	2133	0.43
25	Oleamide	$C_{18}H_{35}NO$	39.18	2386	0.67
26	Isopropyl palmitate	$C_{19}H_{38}O_2$	41.92	2023	13.26

Table 36 (continued)

Hydrocarbons					
27	Tricosane	$C_{23}H_{48}$	38.28	2300	0.38
Others					
28	2-Indolinone	C_8H_7NO	14.58	1487	0.18
29	3-Quinuclidinol	$C_7H_{13}NO$	14.74	1157	0.19
30	Methyl-*o*-tolylcarbamate	$C_9H_{11}NO_2$	22.87	1379	0.34
31	1-Methyl-3-ethyladamantane	$C_{13}H_{22}$	26.83	1263	0.34
32	2-Hexadecanol	$C_{16}H_{34}O$	36.59	1571	0.26
Total					**96.15**

RI; retention index**,** RT; retention time.

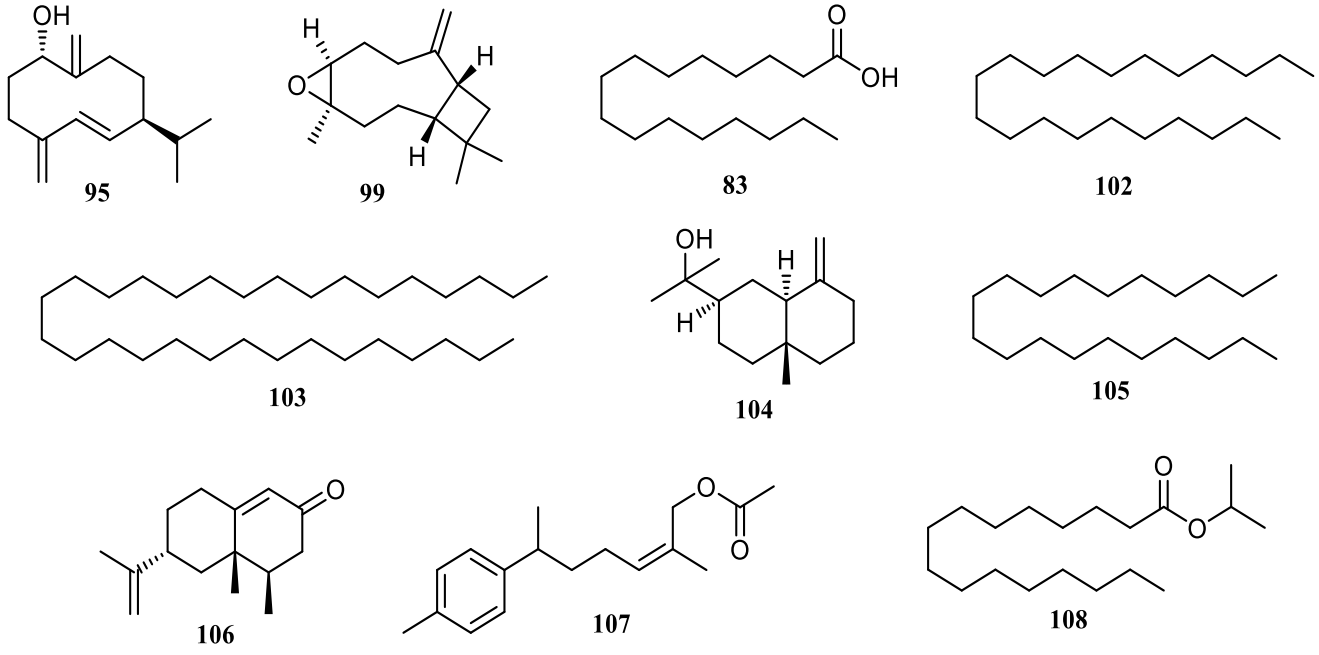

Figure 32: Chemical structures of the major compounds from *D. regia* (**99** and **102**-**104**), *S. siamea* (**102** and **105**), and *Z. spina-christi* (**83**, **95**, and **106**-**108**) essential oils.

The chemical composition of the EOs of *Z. spina-christi* along with its biological activities were the subject of previous reports (Bahmani *et al.*, 2020, Papari Moghadam Fard *et al.*, 2020, Said *et al.*, 2010). A previous study on the EOs of *Z. spina-christi* collected from Egypt identified a total of 21 compounds constituting 99.3% of the oil, of which dodecanoic acid (22.4%), oleic acid methyl ester (17.1%), and octanoic acid (10.3%) were among the major ones (Said *et al.*, 2010).

Another report by Fard and his colleagues identified the presence of 11 compounds (92.14 %) in the EOs (leaves) of the plant, of which carotol (42.20%), hexadecanoic acid (13.75%), linoleic acid (11.76%), and vetivenic acid (9.56%) were found as the most abundant components (Papari Moghadam Fard *et al.*, 2020). The reports showed some correlations with the EO composition of the present study. The presence of 13.75% hexadecanoic acid (palmitic acid) in the report was also in good agreement with the composition of the compound in the roots EO of *Z. spina-christi* in our work (16.46%). Linoleic acid was identified in the EOs (leaves; 0.74% and roots; 0.43%) of *Z. spina-christi* but with a significant difference (11.76%) compared to the findings of the previous report (Papari Moghadam Fard *et al.*, 2020). The differences in the percentage composition of the EOs are related to various environmental factors, such as geographical location, climatic conditions, genetic factors, physiological variations, and method of extraction (Azadi and Khaef, 2015).

4.3. *In Vitro* Biological Activities

In this section, the *in vitro* biological activities of the crude extracts and most of the isolated compounds of all the plants, and essential oils of two plant materials (*C. adenocaule* and *Z. spina-christi*) are addressed. Notably, the findings of various bioassay tests including antibacterial and antioxidant activities of all forms of the extracts, and antiacanthamoeba and antiviral activities along with cytotoxicity properties of the crude extracts are presented.

4.3.1. *In vitro* antibacterial activity

In this study, the extracts and compound isolates were evaluated for their antibacterial activities against four bacterial strains *in vitro*, and results showed that all the extracts and most of the compounds exhibit potential activity against all the bacterial strains. At 50 mg/mL, the *C. adenocaule* (CAE) and *S. siamea* extracts (SSE) showed the highest activity (18.00 ± 0.00 mm each) against *E. coli* followed by the *D. regia* (DRE) and *S. siamea* extracts (SSE) (17.17 ± 0.24 mm each) against *E. coli* and *S. aureus*, respectively, and CAE against *S. aureus* (17.16 ± 0.24 mm). Notably, the inhibition diameters were not far from the ciprofloxacin standard which inhibits the *E. coli* and *S. aureus* pathogens by 23.33 ± 0.47 and 22.00 ± 0.00 mm, respectively. At the lowest concentration (6.25 mg/mL), the *S. siamea* extract (SSE) also revealed more auspicious

activities than the others. Thereby, it inhibited the *E. coli*, *S. aureus*, and *S. pyogenes* strains by 12.00 ± 0.41 mm, 10.33 ± 0.47 mm, and 10.00 ± 0.00 mm, respectively (Table 37).

Our findings corroborate previous research reports wherein the leaves ethanol extract of *S. siamea* showed comparable activities against *E. coli* which were 14.00 ± 00, 10.00 ± 00, and 9.00 ± 00 mm at 50, 30, and 10 mg/mL, respectively. Whereas, against *S. aureus* it displayed 15.00 ± 00, 13.00 ± 00, and 11.00 ± 00 mm at 40, 30, and 10 mg/mL, respectively (Abdallah *et al.*, 2019). The antibacterial effects of the acetone, ethanol, and aqueous extracts of *S. siamea* have been reported previously (Vasait, 2016). According to the report, the acetone extract of *S. siamea* exhibited remarkable bactericidal activity against *E. coli* (22.00 ± 00 mm) and *S. aureus* (20.00 ± 00 mm) at 0.1 mg/mL with more efficient activity than the present finding. The ethanol and aqueous extracts were also susceptible to *E. coli* (20.00 ± 00 and 18.00 ± 00 mm, respectively), and *S. aureus* (17.50.00 ± 00 mm and 13.00 ± 00 mm, respectively), at 0.1 mg/mL (Vasait, 2016). Previous studies on the roots of *C. adenocaule* also showed that the chloroform (22.50 ± 00 mm) and methanol (15.00 ± 00 mm) root extracts of *C. adenocaule* exhibited comparable antibacterial activities against *E. coli*. Promising zones of diameters were also observed for the chloroform (15.00 ± 00 mm) and methanol (10.50 ± 00 mm) extracts against *S. aureus* at unknown concentrations (Fikadu and Mulugeta, 2022). The activity of the *C. adenocaule* extract was also compared to the antibacterial susceptibility of *C. adenocaule* extracts included in the survey of antimicrobial medicinal plants from Uganda (Hamill *et al.*, 2003). Again, better antibacterial activities were recorded from our findings compared to the report of similar bacterial strains.

Furthermore, the activities of the *D. regia* extract were in accordance with previous experimental studies. Hussain and his group demonstrated the dichloromethane, methanol, and ethanol extracts of the root barks of *D. regia* and reported comparable activities with the present finding (Hussain *et al.*, 2014). According to the report, the dichloromethane extract inhibited *E. coli*, *S. aureus*, and *P. aeruginosa* by 12.00 ± 0.00, 14.00 ± 0.00, and 15.00 ± 0.00 mm, respectively. In addition, the methanol extract showed potent activities against *E. coli* (20.00 ± 0.00 mm), *S. aureus* (21.00 ± 0.00 mm), and *P. aeruginosa* (19.50 ± 0.00 mm) with better inhibition zones (Hussain *et al.*, 2014) compared to the present study. Previous work on the methanol extracts of the roots and leaves of *Z. spina-christi* revealed attractive activities against *E. coli* (15.00 ± 0.50 mm) and *P. aeruginosa*

(12.00 ± 1.00 mm), respectively (Temerk *et al.*, 2017). In a related study by Ads and co-workers, the chloroform extract from the stem bark of *Z. spina-christi* displayed substantial antibacterial efficacy against *E. coli* (15.90 ± 0.63 mm), *S. aureus* (16.40 ± 1.20 mm), and *P. aeruginosa* (15.30 ± 1.50 mm) (Ads *et al.*, 2022) and the activities match with the results of the present work.

Of the compound isolates, tricuspidatol A (**29**) exhibited the highest activity against *S. aureus* (16.67 ± 0.47 mm) followed by quercetin (**42**, 16.50 ± 0.41 mm), chrysophanol (**53**, 16.33 ± 0.24 mm), and tricuspidatol A (**29**, 16.17 ± 0.24 mm) against *E. coli*, and chrysophanol (**53**) against *S. pyogenes* (16.00 ± 0.00 mm) at 2 mg/mL. The inhibition zones of these compounds weren't too far from the ciprofloxacin standard (23.33 ± 0.47, 22.00 ± 0.00, and 21.67 ± 0.47 mm against *E. coli, S. aureus,* and *S. pyogenes,* respectively) suggesting their potent antibacterial activity towards the bacterial strains. At the smallest concentration (0.25 mg/mL), the highest inhibition activity was observed by chrysophanol (**53**) against *E. coli* (11.17 ± 0.24 mm) followed by tricuspidatol A (**29**) and betulinic acid (**63**) against *E. coli* (9.83 ± 0.24 mm), and lupeol (**39**), chrysophanol (**53**), and betulinic acid (**63**) against *S. pyogenes* (9.83 ± 0.24 mm). The investigation results showed that most of the compound isolates were susceptible to both Gram-negative (*E. coli* and *P. aeruginosa*) and Gram-positive (*S. aureus* and *S. pyogenes*) bacteria and the activities were dose-dependent which revealed smooth relationships with concentration (Table 37).

The activities of the most potent compounds were compared and verified by previous investigations. A previous report on the antibacterial activity of tricuspidatol A (**29**) showed promising inhibitory effects against *S. aureus* (10.79 ± 0.24 mm) and *P. aeruginosa* (10.32 ± 0.29 mm) at 1 mg/mL compared to chloramphenicol standard (11.76 ± 0.77 mm) (Degfie *et al.*, 2022). Regardless of the reference drug, the results were as good as compared with the findings of the present work. In a study by Elumalai and co-workers, quercetin (**42**) exhibited auspicious inhibitory activities against *P. aeruginosa* (12.82 ± 0.32 mm), *S. aureus* (11.45 ± 0.43 mm), and *E. coli* (9.18 ± 0.37 mm) at 62.5 μg/mL with better activities than the present work (Elumalai *et al.*, 2022). Melaku and co-workers (2022) reported the antibacterial activity of chrysophanol (**53**) which is positively correlated with the present study. According to the report, the compound exhibited an inhibition diameter of 13.00 ± 0.20 mm at 1 mg/mL against *S. aureus* which was comparable to the inhibition zone of this study (13.17 ± 0.24 mm) (Melaku *et al.*, 2022). Thus, the

in vitro antibacterial activity findings support the use of *C. adenocaule*, *D. regia*, *S. siamea*, and *Z. spina-christi* along with their isolated compounds in traditional medicinal practices.

Table 37: Antibacterial activity (inhibition zone, mean ± SD in mm) of the CH_2Cl_2: CH_3OH (1:1) extracts and compound isolates against *E. coli*, *S. aureus*, *P. aeruginosa*, and *S. pyogenes* bacterial strains.

Bacterial strain	Extract/compound	Concentration (mg/mL)			
		2	1	0.5	0.25
E. coli			***C. adenocaule***		
	CAE	18.00 ± 0.00	14.50 ± 0.41	11.50 ± 0.41	9.83 ± 0.24
	19	12.67 ± 0.47	10.50 ± 0.41	9.33 ± 0.47	7.00 ± 0.00
	23	15.33 ± 0.24	12.50 ± 0.41	10.50 ± 0.41	9.67 ± 0.47
	25	14.30 ± 0.47	11.67 ± 0.47	9.83 ± 0.24	8.83 ± 0.24
	28	13.50 ± 0.87	11.33 ± 0.47	9.50 ± 0.00	7.67 ± 0.47
	29	16.17 ± 0.24	13.50 ± 0.41	11.33 ± 0.47	9.83 ± 0.24
	66	14.67 ± 0.47	12.00 ± 0.00	10.00 ± 0.00	9.00 ± 0.00
			D. regia		
	DRE	17.17 ± 0.24	13.83 ± 0.24	11.50 ± 0.41	9.50 ± 0.41
	37	15.33 ± 0.47	12.67 ± 0.47	10.67 ± 0.47	9.00 ± 0.00
	40	13.50 ± 0.00	11.25 ± 0.35	8.50 ± 0.70	NT
	42	16.50 ± 0.41	13.00 ± 0.00	11.00 ± 0.00	9.17 ± 0.24
	87	15.17 ± 0.24	12.50 ± 0.41	10.33 ± 0.47	7.00 ± 0.00
			S. siamea		
	SSE	18.00 ± 0.00	15.67 ± 0.47	13.50 ± 0.41	12.00 ± 0.41
	39	14.17 ± 0.24	12.17 ± 0.24	10.67 ± 0.47	9.50 ± 0.41
	53	16.33 ± 0.24	14.33 ± 0.24	12.50 ± 0.41	11.17 ± 0.24
	63	14.33 ± 0.47	12.33 ± 0.47	10.83 ± 0.24	9.83 ± 0.24
			Z. spina-christi		
	ZSE	15.25 ± 0.35	13.00 ± 0.00	11.00 ± 0.00	NT
	86	14.25 ± 0.35	12.00 ± 0.00	9.25 ± 0.35	NT
	Ciprofloxacin (0.25 mg/mL)		23.33 ± 0.47		
S. aureus	**CAE**	17.16 ± 0.24	13.83 ± 0.24	11.00 ± 0.00	9.50 ± 0.41
	19	11.83 ± 0.24	9.83 ± 0.24	8.16 ± 0.24	NA
	23	15.33 ± 0.47	11.67 ± 0.47	9.67 ± 0.47	8.83 ± 0.24
	25	14.00 ± 0.00	11.33 ± 0.47	9.33 ± 0.47	8.16 ± 0.24
	28	13.33 ± 0.47	10.16 ± 0.24	8.50 ± 0.41	7.33 ± 0.47
	29	16.67 ± 0.47	12.67 ± 0.47	10.00 ± 0.00	9.33 ± 0.47
	66	14.33 ± 0.47	11.50 ± 0.41	9.50 ± 0.41	8.33 ± 0.47
	DRE	16.17 ± 0.62	13.33 ± 0.47	11.83 ± 0.24	9.17 ± 0.24
	37	14.83 ± 0.24	13.00 ± 0.00	10.67 ± 0.47	7.50 ± 0.41
	40	12.50 ± 0.35	10.75 ± 0.35	9.00 ± 0.70	NT
	42	12.67 ± 0.47	11.33 ± 0.47	10.00 ± 0.41	7.67 ± 0.47
	87	14.67 ± 0.47	12.67 ± 0.47	10.50 ± 0.41	7.33 ± 0.47
	SSE	17.17 ± 0.24	14.83 ± 0.24	12.50 ± 0.41	10.33 ± 0.47
	39	14.00 ± 0.00	11.83 ± 0.24	10.50 ± 0.41	9.33 ± 0.47
	53	14.67 ± 0.47	13.17 ± 0.24	11.33 ± 0.47	9.83 ± 0.24
	63	14.33 ± 0.47	12.00 ± 0.00	11.00 ± 0.41	9.67 ± 0.47
	ZSE	14.25 ± 0.35	12.00 ± 0.00	9.75 ± 0.35	NT
	86	12.25 ± 0.35	10.50 ± 0.70	8.50 ± 0.70	NT

Table 37 (continued)

	Ciprofloxacin (0.25 mg/mL)	22.00 ± 0.00			
P. aeruginosa	**CAE**	15.67 ± 0.47	12.00 ± 0.00	10.16 ± 0.24	8.50 ± 0.00
	19	12.00 ± 0.00	9.33 ± 0.47	8.00 ± 0.00	NA
	23	13.83 ± 0.24	11.16 ± 0.24	9.50 ± 0.41	8.00 ± 0.00
	25	14.16 ± 0.24	11.50 ± 0.41	10.00 ± 0.00	8.33 ± 0.47
	28	12.50 ± 0.41	10.16 ± 0.24	8.83 ± 0.24	7.16 ± 0.24
	29	12.67 ± 0.47	10.33 ± 0.47	9.16 ± 0.24	7.33 ± 0.47
	66	13.16 ± 0.24	10.83 ± 0.24	9.33 ± 0.47	7.67 ± 0.47
	DRE	15.00 ± 0.00	12.83 ± 0.24	11.00 ± 0.00	9.33 ± 0.47
	37	14.33 ± 0.47	12.67 ± 0.47	10.83 ± 0.24	9.33 ± 0.47
	40	13.00 ± 0.00	10.50 ± 0.35	8.50 ± 0.70	NT
	42	14.00 ± 0.00	12.33 ± 0.47	10.67 ± 0.47	9.17 ± 0.24
	87	13.50 ± 0.41	11.83 ± 0.24	10.00 ± 0.00	8.00 ± 0.00
	SSE	11.67 ± 0.47	9.67 ± 0.47	8.50 ± 0.41	7.17 ± 0.24
	39	10.00 ± 0.00	8.33 ± 0.47	7.00 ± 0.00	NA
	53	10.33 ± 0.47	8.33 ± 0.47	7.00 ± 0.00	7.00 ± 0.00
	63	10.17 ± 0.24	8.33 ± 0.47	7.00 ± 0.00	NA
	ZSE	14.50 ± 0.70	11.75 ± 0.35	9.50 ± 0.70	NT
	86	13.50 ± 0.00	11.25 ± 0.35	9.25 ± 0.35	NT
	Ciprofloxacin (0.25 mg/mL)	20.00 ± 0.41			
S. pyogenes	**CAE**	16.33 ± 0.47	13.16 ± 0.24	10.83 ± 0.24	9.50 ± 0.41
	19	12.50 ± 0.41	9.67 ± 0.47	8.33 ± 0.47	7.16 ± 0.24
	23	13.83 ± 0.24	10.83 ± 0.24	9.16 ± 0.24	8.00 ± 0.81
	25	15.33 ± 0.47	11.67 ± 0.47	10.16 ± 0.24	9.00 ± 0.81
	28	12.83 ± 0.24	10.00 ± 0.00	8.67 ± 0.47	7.33 ± 0.47
	29	13.67 ± 0.47	10.67 ± 0.47	9.00 ± 0.00	7.83 ± 0.24
	66	14.50 ± 0.00	11.33 ± 0.47	9.50 ± 0.00	8.67 ± 0.47
	DRE	15.67 ± 0.47	13.17 ± 0.24	11.17 ± 0.24	9.33 ± 0.47
	37	14.00 ± 0.00	11.50 ± 0.41	9.67 ± 0.47	9.00 ± 0.00
	40	13.50 ± 0.70	9.75 ± 0.35	7.50 ± 0.70	NT
	42	13.33 ± 0.47	11.50 ± 0.41	9.33 ± 0.47	NA
	87	12.83 ± 0.24	10.67 ± 0.47	9.17 ± 0.24	NA
	SSE	16.50 ± 0.41	13.67 ± 0.47	11.83 ± 0.24	10.00 ± 0.00
	39	14.33 ± 0.47	12.33 ± 0.47	11.00 ± 0.00	9.83 ± 0.24
	53	16.00 ± 0.00	13.00 ± 0.00	11.33 ± 0.47	9.83 ± 0.24
	63	14.67 ± 0.47	12.67 ± 0.47	11.17 ± 0.24	9.83 ± 0.24
	ZSE	14.00 ± 0.00	11.50 ± 0.70	10.00 ± 0.00	NT
	86	12.75 ± 0.35	9.75 ± 0.70	7.50 ± 0.70	NT
	Ciprofloxacin (0.25 mg/mL)	21.67 ± 0.47			

CAE; *C. adenocaule* extract, DRE; *D. regia* extract, NA; No Activity, NT; not tested, SSE; *S. siamea* extract, ZSE; *Z. spina-christi* extract. For the extracts, 2; 50 mg/mL, 1; 25 mg/mL, 0.5; 12.5 mg/mL, and 0.25; 6.25 mg/mL.

In this study, the leaves and roots essential oils (EOs) of *C. adenocaule* and *Z. spina-christi* were investigated for their antibacterial effects and results showed that the roots EOs of *C. adenocaule* and leaves EOs of *Z. spina-christi* afford potential antibacterial activities against the four bacterial pathogens at all the tested concentrations. Conversely, the leaves EOs of *C. adenocaule* and roots

EOs of *Z. spina-christi* exhibited weak to moderate activities with dose-dependent relationships. The highest inhibitory activities were observed by the roots EOs of *C. adenocaule* at 10 mg/mL against *S. pyogenes* (13.67 ± 0.34 mm), *E. coli* (13.34 ± 0.22 mm), and *S. aureus* (13.34 ± 0.27 mm). Whereas, the leaves EOs of *Z. spina-christi* showed the highest inhibition zones against *S. pyogenes* (12.67 ± 0.10 mm) and *S. aureus* (12.33 ± 0.32 mm) at 10 mg/mL compared to ciprofloxacin (29.67 ± 0.48 and 28.66 ± 0.38 mm, respectively). The leaves and roots EOs of both plants showed significantly larger inhibition zones against the evaluated bacterial strains at 10 mg/mL than at lower concentrations ($P<0.05$). There was no significant statistical difference in growth inhibition of the bacterial strains with 2.5 mg/mL and 5 mg/mL of the leaves EO of *Z. spina-christi* ($P>0.05$). On the contrary, there were significant statistical differences in inhibitory diameters of the tested bacterial pathogens with 2.5 mg/mL and 5 mg/mL, and 5 mg/mL and 10 mg/mL of the roots EOs of *C. adenocaule* ($P<0.05$) (Table 38).

Table 38: Inhibition zones (mean ± SEM) of the essential oils of *C. adenocaule* and *Z. spina-christi* against *E. coli*, *S. aureus*, *P. aeruginosa*, and *S. pyogenes* bacterial strains.

Plant name & parts used	**Concentration (mg/mL)**	**Zone of inhibition (mm)**			
		E. coli	*S. aureus*	*P. aeruginosa*	*S. pyogenes*
C. adenocaule (leaves)	10	7.75 ± 0.36[a]	7.50 ± 0.41[a]	7.50 ± 0.22[a]	10.00 ± 0.31[a]
	5	7.12 ± 0.22[b]	7.00 ± 0.19[b]	7.45 ± 0.20[b]	8.00 ± 0.28[b]
	2.5	NA	NA	NA	7.00 ± 0.33[c]
C. adenocaule (roots)	10	13.34 ± 0.22[a]	13.34 ± 0.27[a]	12.67 ± 0.30[a]	13.67 ± 0.34[a]
	5	10.34 ± 0.48[b]	11.67 ± 0.18[b]	11.34 ± 0.20[b]	11.33 ± 0.27[b]
	2.5	8.34 ± 0.12[c]	9.67 ± 0.43[b]	9.67 ± 0.15[c]	10.00 ± 0.00[b]
Z. spina-christi (leaves)	10	12.00 ± 0.00[a]	12.33 ± 0.32[a]	12.00 ± 0.18[a]	12.67 ± 0.10[a]
	5	9.33 ± 0.11[b]	10.66 ± 0.29[b]	10.66 ± 0.16[a]	11.00 ± 0.21[b]
	2.5	8.00 ± 0.21[c]	9.00 ± 0.00[c]	9.00 ± 0.33[b]	9.67 ± 0.22[c]
Z. spina-christi (roots)	10	9.00 ± 0.13[a]	8.50 ± 0.25[a]	8.00 ± 0.20[a]	8.00 ± 0.25[b]
	5	8.00 ± 0.36[b]	8.10 ± 0.26[b]	7.50 ± 0.31[b]	7.00 ± 0.15[c]
	2.5	NA	NA	NA	NA
Ciprofloxacin (0.25 mg/mL)	0.25	29.66 ± 0.44[a]	28.66 ± 0.38[a]	30.34 ± 0.41[a]	29.67 ± 0.48[a]

NA; no activity, SEM; standard error of the mean. Values are displayed as mean ± SEM. Columns with the same letter didn't differ significantly ($P<0.05$) according to ANOVA analysis.

The antibacterial properties of the EOs can be related to the presence of abundant components in the EOs of the two plants identified in this study. Accordingly, the high composition of perillyl alcohol (**93**) (Sultana *et al.*, 2013), phytone (**100**) (Balogun *et al.*, 2017), and spathulenol (**96**) (Dzul-Beh *et al.*, 2020) in *C. adenocaule*, and nootkatone (**106**) (Clarkson *et al.*, 2021), palmitic acid (**83**) (Innis, 2016), and *β*-costol (Sharifi-Rad *et al.*, 2023) in *Z. spinachristi* form the attractive antibacterial activities.

Perillyl alcohol (**93**, the most abundant compound in the leaves EO of *C. adenocaule*) is a hydroxylated monoterpene that is mainly found in the EOs of sage, perilla, spearmint, lavender, peppermint, cherries, lemongrass, cranberries, ginger grass, and celery seeds. It is implicated against different stages of tumors such as gastric, lung, colon, breast, skin, and liver cancers in rodent models (Prado *et al.*, 2011). It also plays significant roles in pathophysiologic processes like oxidative stress, thymidine incorporation into DNA, and inflammation (Sultana *et al.*, 2013). Spathulenol (**96**, another abundant compound in the leaves EO of *C. adenocaule*) is a tricyclic sesquiterpene with 5, 10-cycloaromadendrane skeleton (Doorandishan *et al.*, 2021). Literature surveys revealed that spathulenol (**96**) possesses significant biological applications such as antihyperalgesic, antioxidant, anticholinesterase, antibacterial, antiproliferative, anti-inflammatory, antioedematogenic, chemotherapy of cancer, and cytotoxicity (Dzul-Beh *et al.*, 2020). Thus, the high composition of spathulenol in the leaves EO also supports the aforementioned activities of *C. adenocaule*. Phytone (**100**, Hexahydrofarnesyl acetone), one of the most abundant compounds in the roots EO of *C. adenocaule* identified in this study is a sesquiterpene that exhibits various biological activities, including anti-inflammatory, antibacterial, and anti-nociceptive activities (Balogun *et al.*, 2017). Phytol (**101**) is an acyclic hydrogenated diterpenoid alcohol that can be used as a precursor for the synthesis of vitamin E and vitamin K1. It is frequently available in the EOs of certain aromatic plants. Some insects, such as the sumac flea beetle uses the compound as a chemical deterrent against predation. Phytol (**101**) is also used for commercial applications such as the fragrance industry (shampoos, cosmetics, household cleaners, toilet soaps, and detergents (Assefa *et al.*, 2023, McGinty *et al.*, 2010).

Nootkatone (**106**, the major compound identified from the EOs of *Z. spina-christi*) is a natural product that is widely found in grapefruit and other plants and functions as an insecticide and

repellant against mosquito vectors of parvoviruses (Clarkson *et al.*, 2021). It is a sesquiterpene and is safely used in products such as cosmetics and juices to enhance the fragrance and flavor. Nootkatone (**106**) possesses the advantage of being neither genotoxic nor carcinogenic and is approved for use in and on people. It could offer consumers a favorable alternative than synthesized compounds like N,N-diethyl-*m*-toluamide (DET), since nootkatone at >98 % purity causes no skin and other health problems (Clarkson *et al.*, 2021). Palmitic acid (**83**, the second abundant compound in the EOs of *Z. spina-christi*), is a saturated fatty acid which is mainly found in palm oil, olive oil and animal products and possess antibacterial properties. It is also known as *n*-hexadecanoic acid and is the most common saturated fatty acid which can be provided in the diet or synthesized from other fatty acids, amino acids and carbohydrates (Innis, 2016). *β*-costol, was also another compound reported in the leaves EO of *Z. spina-christi* with significant composition. It belongs to the class of organic compounds called eudesmane, isoeudesmane sesquiterpenoids. The compound was reported in the EOs of various plants and exhibit antibacterial and antifungal activities (Sharifi-Rad *et al.*, 2023). Significant composition of (+)-ledene was also observed in the GC-MS analysis of the roots EO of *Z. spina-christi*. The compound is also known as leden, which belongs to the class of compounds called 5, 10-cycloaromadendrane sesquiterpenoids and was reported to possess antibacterial, antifungal, antioxidant, and anticancer activities (Donadu *et al.*, 2020).

The antibacterial activities of the EOs of *Z. spina-christi* were in good agreement with previous reports towards different bacterial pathogens (Papari Moghadam Fard *et al.*, 2020). The EOs of the plant evaluated towards six bacterial and fungal strains exhibited good activity against one bacterial strain (*Klebsiella pneumonia*) and two fungal strains (*Aapergillus niger*, *Penicillium digitatum*) (Papari Moghadam Fard *et al.*, 2020). Reports on the antibacterial activity of the EOs of *C. adenocaule* are very limited, and thus in the present work, none of the results was compared with previous findings. This is due to the fact that the habitat of the plant is limited to certain countries of the world. Thus, we suggest further works on the antibacterial and other biological activities of the plant to support its ethno medicinal values.

4.3.2. *In vitro* antioxidant activity

Oxidative stress is caused by the storage of free radicals and reactive oxidants in the body which is formed by the discrepancy between oxidation and antioxidant reaction (Pizzino *et al.*, 2017). Cells generate free radicals through various metabolic pathways, and free radicals are fundamental factors that lead to oxidative impairment of proteins, causing high reactivity (Pieczenik and Neustadt, 2007). Reactive oxygen species (ROS) are the highest free radicals in human cells which are mostly made by mitochondria. Excess amounts of ROS damage cells and tissues, impact metabolic function, and causes various health complications (Al-Gubory *et al.*, 2012). In addition, ROS has something to do with cancer, aging, arthritis, the occurrence of atherosclerosis, and neurodegenerative diseases such as Parkinson's disease and Alzheimer's (Lin *et al.*, 2021). Cells sustain ROS homeostasis through catalase (CAT) system, superoxide dismutase (SOD) system, and glutathione peroxidase (GSH-Px) system (Venza *et al.*, 2021).

Antioxidants are classes of compounds that trap and neutralize free radicals and reactive oxidants, thus reduce the damage to cells caused by free radicals. Additionally, they play a defensive role against certain ailments including cancer and inflammation caused by oxidative stress. Natural products have strong antioxidant potential with slight toxicity and side effects. As a result, antioxidant compounds of natural origin have many application prospects to treat various health problems related to oxidative stress (Bouyahya *et al.*, 2021).

In this study, the *in vitro* antioxidant activity tests showed that the extracts exhibited better scavenging potential than the compound isolates. Accordingly, the *C. adenocaule* and *D. regia* extracts displayed the highest DPPH radical scavenging activity with IC_{50} values of 0.30 and 0.40 μg/mL, respectively. The scavenging activities were also not too far from ascorbic acid (IC_{50}: 0.08 μg/mL). The *S. siamea* and *Z. spina-christi* extracts also revealed good scavenging activities with IC_{50} values of 1.24 and 1.51 μg/mL, respectively (Table 39, Appendix 33). This was in accordance with previous findings regarding the antioxidant activities of the various extracts of the plants. Yakubu and his group studied the antioxidant potentials of the *n*-hexane, chloroform, and methanol extracts of *C. adenocaule* using a DPPH radical scavenging assay whose methanol extract exhibited the highest scavenging activity with IC_{50} of 10.87 μg/mL compared to ascorbic acid (IC_{50}: 4.50 μg/mL) (Yakubu *et al.*, 2021). With respect to the IC_{50} value of the standard, the results

of the present finding were better than the previous report. In addition, the ethanol root and leaf extracts were investigated for their antioxidant susceptibility using a DPPH radical scavenging assay, and the root extract with IC_{50} of 38.42 μg/mL was found to be the most potent than the leaf extract (IC_{50}: 66.85 μg/mL). According to the report, the scavenging potential of the root extract was almost half of the ascorbic acid (IC_{50}: 17.40 μg/mL) (Feyisayo *et al.*, 2015).

Conversely, reports on the various extracts of *D. regia* revealed its potential antioxidant activity. The tests affirmed that the aqueous extract of the leaves of the plant exhibited an auspicious DPPH radical scavenging activity with an IC_{50} value of 41.40 μg/mL, and the results were not too far from ascorbic acid (IC_{50}: 20.43 μg/mL) (Remi-Esan *et al.*, 2020). The present study also suggests that the extract of *S. siamea* exhibited promising antioxidant activities which align with previous reports. In a study by Oyebade and co-workers, the antioxidant properties of the leaf extracts of *S. siamea* were tested *in vitro* and the hexane, ethyl acetate, ethanol, and aqueous extracts showed potential DPPH scavenging activities with IC_{50} values of 35.41, 32.77, 25.73, and 12.89 μg/mL, respectively. The activities were promising compared to ascorbic acid (IC_{50}: 11.12 μg/mL) (Oyebade *et al.*, 2021). Elalouri and co-workers aiming to study the phenolic composition, antioxidant and insecticidal activity of the methanol, aqueous, ethanol, and acetone extracts of the roots of *Z. spina-christi* reported the antiradical properties of the extracts with good antioxidant activities. According to the report, the extracts displayed comparable scavenging activities with IC_{50}: 0.47, 0.43, 0.41, and 0.60 μg/mL for methanol, aqueous, ethanol, and acetone extracts, respectively (Elaloui *et al.*, 2021).

Of the compounds, ***ε***-viniferin (**25**), tricuspidatol A (**29**), quercetin-3-*O*-rutinoside (**37**), parthenocissin A (**23**), myricetin (**66**), and quercetin (**42**) exhibited greater than 90% scavenging potential at 1000 μg/mL with IC_{50} values of 0.32, 0.67, 0.81, 0.98, 1.05, and 1.12 μg/mL, respectively. This was in accordance with the scavenging potential of ascorbic acid (96.4 ± 0.28, IC_{50}: 0.08 μg/mL). Whereas, the smallest scavenging activity was displayed by diethyl phthalate (**85**, IC_{50}: 21.11 μg/mL) followed by β-sitosteryl palmitate (**84,** IC_{50}: 20.28 μg/mL) and stearic acid (**91**, IC_{50}: 17.46 μg/mL) (Table 39, Appendix 33). Generally, the radical scavenging activity of the compounds can be related to their proton-donating capabilities. As a result, the aforementioned compounds which are comprised of many proton-donating sites showed strong scavenging

activities. Antioxidants have been investigated to show cell protection from free radicals causing oxidative cleavage which avoids aging and cancer. They serve as oxygen scavengers by interacting with free radicals, thereby disrupting the oxidation process (Islam *et al.*, 2023). Previous studies revealed that synthetic antioxidants loom to cause cancer diseases. Consequently, antioxidants of natural origin have become the target of modern research (Jacob and Latha, 2013). The antioxidant activities of 3-hydroxy isoagatholactone (**28**) and ***ε***-viniferin (**25**) were reported in a recently published study from the roots of *C. cyphopetalum* (Degfie *et al.*, 2022). The report affirmed the potential antioxidant effects of the compounds and their IC_{50} values were calculated as 6.05 and 0.017 μg/mL, respectively, compared to ascorbic acid (IC_{50}: 0.0012 μg/mL). In comparison with the IC_{50} values of the standard, the results were comparable with the present finding. Chrysophanol (**53**) was also the subject of previous research. Melaku and co-workers reported the DPPH radical scavenging activity of the compound with an IC_{50} value of 6.2 μg/mL compared to ascorbic acid (IC_{50}: 3.38 μg/mL) (Melaku *et al.*, 2022) accounting for smaller scavenging values than the present finding.

Table 39: DPPH radical scavenging activity (%) of the extracts and compound isolates from *C. adenocaule*, *D. regia*, *S. siamea*, and *Z. spina-christi*.

Sample code	**Concentration (μg/mL)**					
	1000	**500**	**250**	**125**	**62.5**	**IC_{50} (μg/mL)**
	C. adenocaule					
Extract	94.97 ± 0.07	91.64 ± 0.13	88.64 ± 0.16	84.35 ± 0.03	79.14 ± 0.11	0.30
19	80.98 ± 0.15	77.01 ± 0.05	73.41 ± 0.07	67.78 ± 0.11	61.79 ± 0.17	9.87
23	94.37 ± 0.10	90.86 ± 0.21	87.17 ± 0.13	81.77 ± 0.22	76.32 ± 0.21	0.98
25	91.97 ± 0.08	87.35 ± 0.26	83.47 ± 0.14	81.17 ± 0.24	77.24 ± 0.23	0.32
28	81.21 ± 0.23	78.26 ± 0.10	76.41 ± 0.07	70.18 ± 0.17	65.43 ± 0.07	3.56
29	93.07 ± 0.12	89.10 ± 0.09	86.06 ± 0.04	81.95 ± 0.05	76.00 ± 0.00	0.67
66	91.55 ± 0.13	88.04 ± 0.11	84.77 ± 0.03	77.66 ± 0.08	75.49 ± 0.05	1.05
84	76.69 ± 0.22	71.71 ± 0.17	67.14 ± 0.16	62.06 ± 0.12	57.91 ± 0.13	20.28
85	79.97 ± 0.18	75.35 ± 0.00	70.09 ± 0.00	64.28 ± 0.14	58.09 ± 0.07	21.11
	D. regia					
Extract	92.38 ± 0.00	89.47 ± 0.11	85.44 ± 0.07	81.12 ± 0.22	77.61 ± 0.29	0.40
37	91.41 ± 0.15	88.80 ± 0.00	84.25 ± 0.20	79.85 ± 0.08	75.37 ± 0.00	0.81
40	76.86 ± 0.06	73.50 ± 0.13	69.32 ± 0.23	65.74 ± 0.20	61.94 ± 0.00	6.88
42	90.52 ± 0.29	87.38 ± 0.23	82.98 ± 0.23	78.08 ± 0.25	74.25 ± 0.05	1.12
19 & **40**	77.61 ± 0.10	74.47 ± 0.20	71.26 ± 0.00	66.79 ± 0.15	62.68 ± 0.00	5.58
86	81.12 ± 0.15	78.28 ± 0.00	73.95 ± 0.00	69.02 ± 0.27	64.55 ± 0.22	5.41
87	87.16 ± 0.00	83.43 ± 0.07	79.47 ± 0.20	73.58 ± 0.15	69.92 ± 0.30	2.80

Table 39 (continued)

			S. siamea			
Extract	89.25 ± 0.00	86.34 ± 0.21	81.19 ± 0.15	76.79 ± 0.35	73.50 ± 0.00	1.24
39	80.44 ± 0.21	77.08 ± 0.18	72.46 ± 0.12	68.50 ± 0.35	65.67 ± 0.21	3.93
53	85.59 ± 0.15	82.61 ± 0.18	78.50 ± 0.35	74.40 ± 0.25	70.07 ± 0.33	1.71
63	83.73 ± 0.25	79.92 ± 0.31	76.19 ± 0.18	71.64 ± 0.27	69.02 ± 0.23	2.06
88	80.82 ± 0.28	77.68 ± 0.30	73.28 ± 0.27	69.70 ± 0.25	66.26 ± 0.12	3.06
			Z. spina-christi			
Extract	91.81 ± 0.17	87.81 ± 0.09	82.96 ± 0.12	78.73 ± 0.16	73.93 ± 0.10	1.51
90	83.29 ± 0.22	76.33 ± 0.05	73.64 ± 0.35	68.95 ± 0.18	63.88 ± 0.23	7.67
91	75.80 ± 0.06	71.88 ± 0.02	67.21 ± 0.32	63.03 ± 0.22	57.87 ± 0.08	17.46
92	77.00 ± 0.03	73.26 ± 0.05	68.86 ± 0.30	64.76 ± 0.12	60.54± 0.00	10.59
Ascorbic acid	96.4 ± 0.28	94.92 ± 0.21	91.41 ± 0.27	87.44 ± 0.41	82.78 ± 0.35	0.08

The EOs of the leaves and roots of *C. adenocaule* and *Z. spina-christi* were also subjected to *in vitro* antioxidant activities against DPPH free radicals and the results were promising. The antioxidant activity tests of the EOs of both plants along with the standard (ascorbic acid) were performed in four different concentrations (500, 250, 125, and 62.5 μg/mL) which were prepared from their stock solutions (1000 μg/mL). The results revealed that the absorbance values along with their radical scavenging activity (%) were attractive and the activities were dose-dependent which showed smooth relationships with concentrations. Both *C. adenocaule* (roots) and *Z. spina-christi* (leaves) exhibited better scavenging activity (90.52 ± 0.10 and 90.61 ± 0.25, respectively) against DPPH radical relative to ascorbic acid (96.40 ± 0.28, IC_{50}: 0.08 μg/mL) at 1000 μg/mL and their IC_{50} values were calculated as 7.41 and 4.15 μg/mL, respectively (Table 40, Appendix 34). The good IC_{50} values of the roots and leaves EOs of *C. adenocaule* and *Z. spina-christi*, respectively, can be related to the presence of antioxidant compounds with high composition including phytone (**100**), phytol (**101**), and palmitic acid (**83**) in the roots EOs of *C. adenocaule,* and palmitic acid (**83**) and germacra-4(15), 5, 10(14)-trien-1α-ol (**95**) in the leaves EOs of *Z. spina-christi*. Our findings revealed better results than Fard and co-workers who studied the scavenging potential of the EOs (leaves) of *Z. spina-christi*. According to the report, the EOs of *Z. spina-christi* collected from Iran showed antioxidant activity with an IC_{50} of 53.91 μg/mL, and the activity was related to the presence of linoleic acid (Papari Moghadam Fard *et al.*, 2020). Notably, the present finding showed better IC_{50} values and thereby better scavenging potential than the previous report. To the best of our knowledge, no study was reported in the literature on the antioxidant activity of the EOs of *C. adenocaule*.

Table 40: DPPH radical scavenging assay (%) of the essential oils of *C. adenocaule* and *Z. spina-christi*.

Conc. (μg/mL)	% of scavenging activity (mean ± SD)				
	C. adenocaule (leaves)	*C. adenocaule* (roots)	*Z. spina-christi* (leaves)	*Z. spina-christi* (roots)	Ascorbic acid
62.5	64.23 ± 0.26	67.92 ± 0.16	69.52 ± 0.13	60.40 ± 0.24	82.78 ± 0.35
125	71.66 ± 0.28	73.35 ± 0.22	75.97 ± 0.20	66.28 ± 0.10	87.44 ± 0.41
250	76.29 ± 0.15	78.78 ± 0.26	80.78 ± 0.22	73.13 ± 0.20	91.41 ± 0.27
500	82.65 ± 0.30	85.85 ± 0.14	85.27 ± 0.09	80.78 ± 0.05	94.92 ± 0.21
1000	88.52 ± 0.33	90.52 ± 0.10	90.61 ± 0.25	84.69 ± 0.10	96.40 ± 0.28
IC_{50} (μg/mL)	11.22	7.41	4.15	19.86	0.08

Values are displayed as mean ± SEM.

4.3.3. Anti-acanthamoeba activity

Acanthamoeba is a protozoa that causes a serious corneal infection and is very challenging to treat and diagnose. *Acanthamoeba keratitis* (AK) is caused by *Acanthamoeba* protozoa which leads to severe corneal infection. Its transformation from the active trophozoites feeding stage to the resilient quiescent stage cysts which are very hard to kill makes the AK difficult to treat and diagnose (Siddiqui and Khan, 2012). Chlorhexidine is widely used to cure this infection. However, treatment still requires a long duration and the infection can relapse upon ceasing the treatment (Szentmáry *et al.*, 2019). Hence, there is an interest in getting a better treatment alternative such as decreasing relapse upon ceasing the treatment by minimizing cyst formation *in situ*. In this study, the CH_2Cl_2: CH_3OH (1:1) extract of *C. adenocaule* (CAE1) and methanol extract of *Z. spina-christi* (ZSE2) which have been investigated for their anti-acanthamoeba activities displayed promising inhibitory activity (% viability < 10) at 2 mg/mL against *A. triangularis* trophozoites. Conversely, the CH_2Cl_2: CH_3OH (1:1) extract of *Z. spina-christi* (ZSE1) failed to show activities against both *A. triangularis* and *A. castellanii* trophozoites. All the tested extracts of both plants also showed weak anti-acanthamoeba activities against *A. castellanii* trophozoites (Table 41).

Table 41: Screening of anti-acanthamoeba activity of the extracts against *A. triaugularis* WU19001 and *A. castellanii* ATCC50739 trophozoites.

No.	Extract code and solvents	Viability of trophozoites (%)				
		A. triangularis WU19001		*A. castellanii* ATCC50739		Solvent
		Average	SD	Average	SD	
1	CAE1	3.70	0.57	63.16	7.06	methanol
2	ZSE1	41.94	5.00	20.93	0.00	methanol
3	ZSE2	3.70	0.57	18.42	4.08	methanol
4	1% DMSO	96.77	8.66	100.00	3.60	
5	1% MeOH	96.77	8.66	100.00	3.60	
6	1% $CHCl_3$	90.32	5.00	97.67	0.00	
7	Growth control	100.00	0.00	100.00	0.00	

CAE1; *C. adenocaule* extract (CH_2Cl_2: CH_3OH, 1:1), ZSE1; *Z. spina-christi* extract (CH_2Cl_2: CH_3OH, 1:1), and ZSE2; *Z. spina-christi* extract (methanol).

4.3.4. *In vitro* antiviral and cytotoxicity tests

Influenza A and B are viral infections that cause severe and contagious infections. Typical symptoms include fever, cough, and sore throat which lasts from 1 up to 2 weeks and jeopardizes high-risk patients like immune-compromised or elderly people by developing serious life-threatening complications (Javanian *et al.*, 2021). Nowadays, effective anti-influenza medications are eagerly desired to address the limitations of the present influenza vaccinations. To date, only two types of anti-influenza medications namely oseltamivir and zanamivir have been approved globally, though other drugs also exist in some countries. The majority of these drugs suffer from a fast emergence of resistance and limited efficiency. Hence, it is vital to progressively search for further alternatives to treat influenza infections with special emphasis on the vast range of natural products synthesized by plants and animals (Eichberg *et al.*, 2022).

In this study, the CH_2Cl_2: CH_3OH (1:1) and methanol root extracts of *C. adenocaule, S. simea,* and *Z. spina-christi* were chosen based on the ethnomedicinal information of the plants and investigated against influenza types A and B viruses. Notably, three parameters namely toxicity (median cytotoxic concentration, CC_{50}), activity (median inhibitory concentration, IC_{50}), and selectivity index (ratio of the former to the latter) were performed. For a compound/extract to be prospective, its selectivity index (SI) should be 10 or higher. Thereby, the results showed that the

CH_2Cl_2: CH_3OH (1:1) extract of *S. siamea* and methanol extract of *Z. spina-christi* exhibited potential anti-influenza types A and B activities with SI values of 13.32 and 28.03, respectively. In addition, the CH_2Cl_2: CH_3OH (1:1) extract of *C. adenocaule* showed moderate anti-influenza activity against the investigated viruses with an SI value of 4.30 (Table 42). Thus, the *in vitro* experimental results showed that the extracts of the three plants can be used for further tests against various viruses. The findings also support the traditional uses of *C. adenocaule*, *S. simea*, and *Z. spina-christi* against various viral infections.

Table 42: *In vitro* antiviral and cytotoxic activities of *C. adenocaule*, *S. simea*, and *Z. spina-christi* extracts against influenza types A and B.

Extract code	Influenza type A			Influenza type B	
	CC_{50} (μg/mL)	IC_{50} (μg/mL)	SI	IC_{50} (μg/mL)	SI
CAE	8.60	2.00	4.30	2.00	4.30
CA1	14.10	11.00	1.28	11.00	1.28
SSE	41.30	3.10	13.32	3.10	13.32
SSE1	15.30	11.00	1.39	11.00	1.39
ZSE	300.00	300.00	1.00	300.00	1.00
ZSE1	300.00	10.70	28.03	10.70	28.03

CAE; *C. adenocaule* extract (CH_2Cl_2: CH_3OH, 1:1), CA1; *C. adenocaule* extract (methanol), SSE; *S. simea* extract (CH_2Cl_2: CH_3OH, 1:1), SSE1; *S. simea* extract (methanol), ZSE; *Z. spina-christi* extract (CH_2Cl_2: CH_3OH, 1:1), ZSE1; *Z. spina-christi* extract (methanol).

4.4. Computational Study of the Isolated Compounds

Nowadays, computational approaches are routinely used to facilitate the long and costy drug development process. Computational methods can impact and speed up a given phase of drug development, from docking and molecular dynamics to identify lead compounds for ADMET optimizations (Palermo and De Vivo, 2015). This section addresses the entire computational profiles of the isolated compounds including molecular docking, drug likeness, ADME, and toxicity properties. In addition, the docking and pharmacokinetic profiles of the compounds are compared with the results of the standard drugs utilized during the *in vitro* studies.

4.4.1. Molecular docking

Molecular docking is a structure-based *in silico* approach that generates the binding affinity and mode between compounds and targets by studying their binding interactions (Sulimov *et al.*, 2019). There are various docking softwares applied for this technique. PyMOL, AutoDock Vina, Auto-Dock, FlexX, molecular operating environment (MOE), genetic optimization for ligand docking (GOLD), and internal coordinate mechanics (ICM) are among the popular docking tools in use (Chen, 2015). Nowadays, molecular docking has become an important computational tool in drug design and discovery. Its uses in side effect prediction of drugs, virtual screening, drug repurposing, and polypharmacology are phenomenal (Elokely and Doerksen, 2013). In this study, the molecular docking analyses of compound isolates with promising antibacterial and antioxidant activity profiles were performed using the MGL AuthoDock tools 1.5.6 program, and their degree of binding interactions were validated by comparing them with standard drugs.

A molecular docking study was performed to establish the binding affinity and binding interactions of the compound isolates against protein targets of four bacterial pathogens. DNA gyrase B of *E. coli* (PDB ID: 6F86), pyruvate kinase (PK) of *S. aureus* (PDB ID: 3T07), PqsA of *P. aeruginosa* (PDB ID: 5OE3), and 10782 streptopain of *S. pyogenes* (PDB ID: 6UKD) were selected to consolidate the *in vitro* experimental results. The molecular docking properties of the compounds were also studied against human myeloperoxidase (PDB ID: 1DNU) and topoisomerase II α (PDB ID: 4FM9) and their respective binding affinity, H-bond, and residual interactions were reported in both tabular and figure forms (Tables 43-48 and Figures 33-38). The protein targets were selected based on their metabolic importance to the microorganisms, the respective strains' *in vitro* antibacterial and antioxidant activities, and the similarity of the compound to the co-crystalized ligands in the protein complex.

4.4.1.1. Molecular docking study against *E. coli* DNA gyrase B

DNA gyrase B belongs to the bacterial type II A topoisomerase enzymes and regulates the topology of DNA during replication, recombination, and transcription by importing transient breaks to DNA strands and providing the necessary energy for catalytic functions (Collin *et al.*, 2011). It plays a vital role in the survival of bacterial cells and is mostly used as a drug target for *in silico* computational studies. Reports revealed that its enzymatic activities are also critical in

transcription, initiation, and elongation during DNA replication, DNA superhelicity regulation, and chromosome decatenation (Levine *et al.*, 1998). The molecular docking process against *E. coli* DNA gyrase B revealed binding affinities ranging from -7.4 kcal/mol up to -6.6 kcal/mol and all the compounds displayed smaller binding affinity than ciprofloxacin (-7.6 kcal/mol). This was in agreement with the *in vitro* experimental results of the compounds. Small values (greater negative values) of binding affinities are always related to good stability and hence improved binding interaction of compounds/ligands with protein binding sites. Of the docked compounds, tricuspidatol A (**29**) and quercetin (**42**) unveiled the highest binding affinity (-7.4 kcal/mol) against *E. coli* DNA gyrase B. The H-bond and residual amino acid interactions of the compounds along with the ciprofloxacin standard were also clearly stated. All the docked compounds showed at least one H-bond interaction with the target amino acids, of which quercetin-3-*O*-rutinoside (**37**) formed the most (four) H-bond interactions with Asn-46, Arg-76, Thr-165, and Glu-50. Notably, the compound shared two common H-bond interactions (Asn-46 and Arg-76) with ciprofloxacin (Asp-73, Asn-46, and Arg-76) (Table 43 and Figure 33).

Table 43: Binding affinity, hydrogen bonds, and residual amino acid interactions of the compound isolates and ciprofloxacin against *E. coli* DNA gyrase B.

Compound/ ligand	Binding affinity (kcal/mol)	H-bond	Residual amino acid interactions	
			Hydrophobic/Electrostatic/Halogen	Van der Waals
			C. adenocaule	
23	-7.3	Gly-77, and Arg-136	Arg-76, Glu-50, Pro-79, Ile-78, and Ile-94	Ala-47, Asp-73, Gly-164, Thr-165, Asn-46, and Gly-75
25	-7.1	Asp-73, and Arg-76	Arg-76, Glu-50, and Ile-78	Ile-94, Ala-53, Arg-136, Pro-79, Gly-77, Gly-75, Thr-165, Ala-47, and Asn-46
28	-6.9	Gly-77	__	Asn-46, Glu-50, Asp-49, Asp-73, Thr-165, Gly-75, Ile-78, Pro-79, and Ile-94
29	-7.4	Thr-165, Ile-94, and Asp-49	Glu-50, Ile-78, and Ile-94	Val-120, Val-97, Ser-121, Asn-46, Gly-77, Asp-73, Arg-76, and Ala-53
66	-7.1	Arg-76, Gly-77, and Asp-73	Glu-50, Thr-165, Gly-77, Ile-78, and Ala-47	Pro-79, Gly-75, Val-71, Val-43, Val-167, and Val-120
			D. regia	
37	-7.2	Asn-46, Arg-76, Thr-165, and Glu-50	Glu-50, Ile-78, and Pro-79	Ile-94, Val-120, Ala-53, Asp-49, Asp-73, Gly-77, Gly-164, and Gly-75
42	-7.4	Gly-77, Asp-73, and Asn-46	Glu-50, Ile-94, and Ile-78	Asp-49, Pro-79, Arg-76, Gly-164, Gly-75, Thr-165, and Ala-47
87	-7.0	Glu-50 and Gly-77	Glu-50, Thr-165, Asn-46, Ala-47, and Ile-78	Pro-79, Arg-76, Asp-73, Val-43, Val-71, and Val-167
			S. siamea	
39	-6.6	Glu-50	__	Ile-94, Arg-76, Asp-49, Asn-46, Gly-117, Val-120, Gly-119, and Ser-121
53	-7.2	Asn-46, Gly-77, and Pro-79	Pro-79, Glu-50, Ile-78, and Ile-94	Arg-76, Thr-165, Asp-73, and Ala-47
63	-7.0	Asn-46, Val-120, and Glu-50	__	Asp-49, Gly-117, Gly-119, Ile-94, Ile-78, Gly-77, Pro-79, and Arg-76
			Z. spina-christi	
40	-7.0	Gly-77, Asp-73, and Thr-165	Ile-78 and Ile-94	Asn-46, Ala-47, Gly-164, Gly-75, Glu-50, Arg-76, Pro-79, Val-93, and Val-97
Ciprofloxacin	-7.6	Asp-73, Asn-46, and Arg-76	Glu-50, Arg-76, Gly-77 Asn-46, Ile-94, and Ile-78	Pro-79, Thr-165, and Ala-47

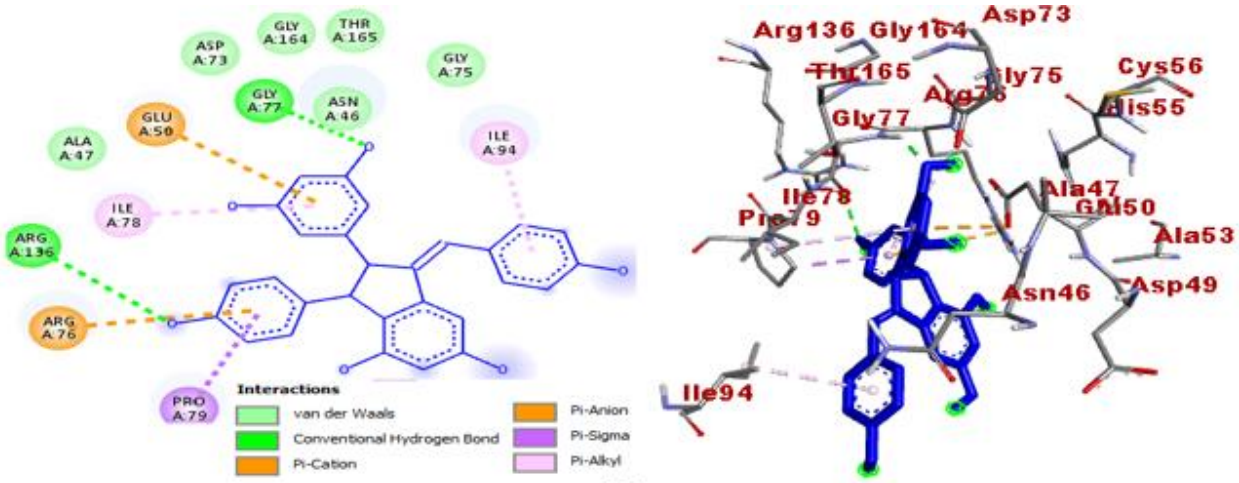
ASP A:73
GLY A:164
THR A:165
GLY A:75
GLY A:77
ASN A:46
GLU A:50
ALA A:47
ILE A:94
ILE A:78
ARG A:136
ARG A:76
PRO A:79
Interactions
van der Waals
Conventional Hydrogen Bond
Pi-Cation
Pi-Anion
Pi-Sigma
Pi-Alkyl
Arg136
Gly164
Asp73
Thr165
Gly75
Cys56
Gly77
His55
Ile78
Ala47
Pro79
Glu50
Ala53
Asn46
Asp49
Ile94

23

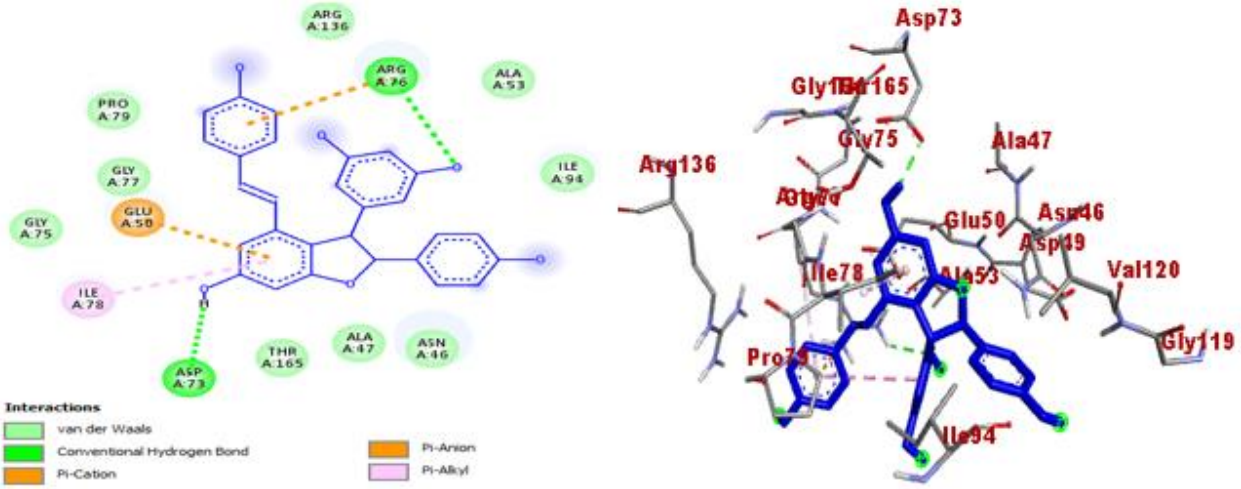
ARG A:136
ARG A:76
ALA A:53
PRO A:79
GLY A:77
ILE A:94
GLU A:50
GLY A:75
ILE A:78
THR A:165
ALA A:47
ASN A:46
ASP A:73
Interactions
van der Waals
Conventional Hydrogen Bond
Pi-Cation
Pi-Anion
Pi-Alkyl
Asp73
Gly164
Thr165
Gly75
Ala47
Arg136
Glu50
Asn46
Asp49
Ile78
Ala53
Val120
Gly119
Pro79
Ile94

25

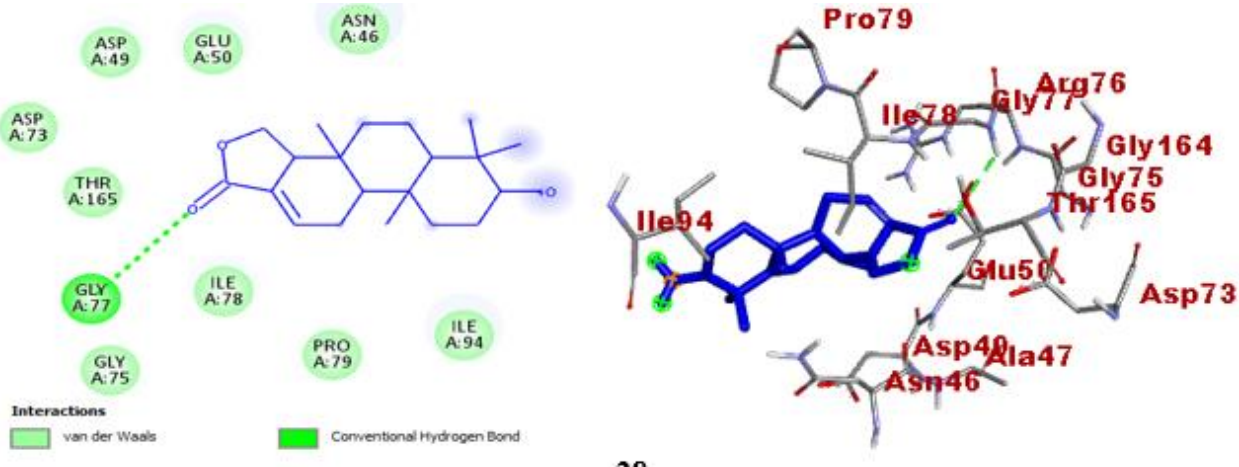
ASN A:46
ASP A:49
GLU A:50
ASP A:73
THR A:165
GLY A:77
ILE A:78
ILE A:94
PRO A:79
GLY A:75
Interactions
van der Waals
Conventional Hydrogen Bond
Pro79
Arg76
Ile78
Gly77
Gly164
Gly75
Thr165
Ile94
Glu50
Asp73
Asp49
Ala47
Asn46

28

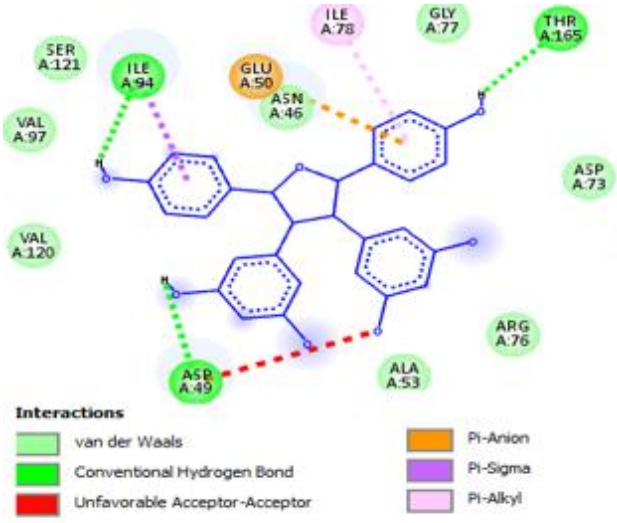
SER A:121
ILE A:94
ILE A:78
GLY A:77
THR A:165
GLU A:50
ASN A:46
VAL A:97
ASP A:73
VAL A:120
ARG A:76
ASP A:49
ALA A:53
Interactions
van der Waals
Conventional Hydrogen Bond
Unfavorable Acceptor-Acceptor
Pi-Anion
Pi-Sigma
Pi-Alkyl

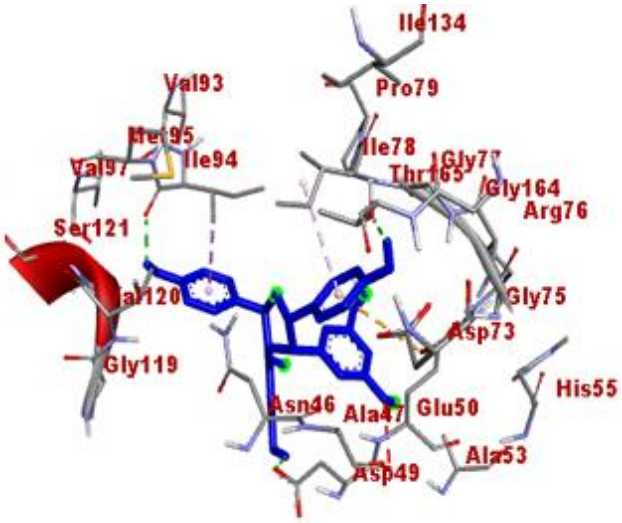
Ile134
Pro79
Val93
Ile78
Gly77
Thr165
Gly164
Arg76
Ile94
Ser121
Val120
Gly75
Asp73
Gly119
His55
Asn46
Ala47
Glu50
Ala53
Asp49

29

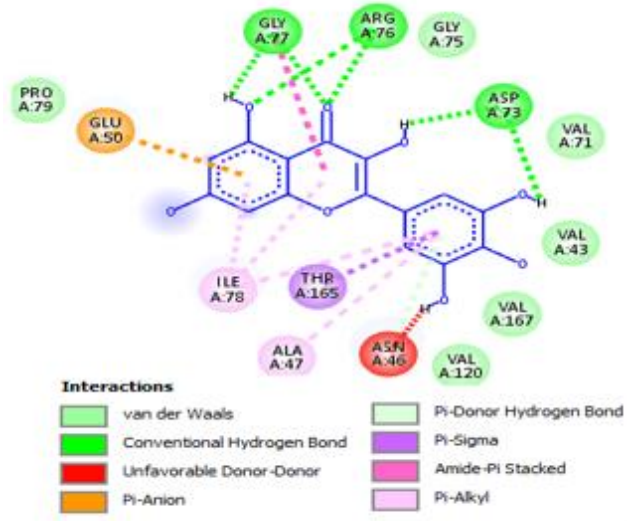
GLY A:77
ARG A:76
GLY A:75
PRO A:79
GLU A:50
ASP A:73
VAL A:71
VAL A:43
ILE A:78
THR A:165
VAL A:167
ALA A:47
ASN A:46
VAL A:120
Interactions
van der Waals
Conventional Hydrogen Bond
Unfavorable Donor-Donor
Pi-Anion
Pi-Donor Hydrogen Bond
Pi-Sigma
Amide-Pi Stacked
Pi-Alkyl

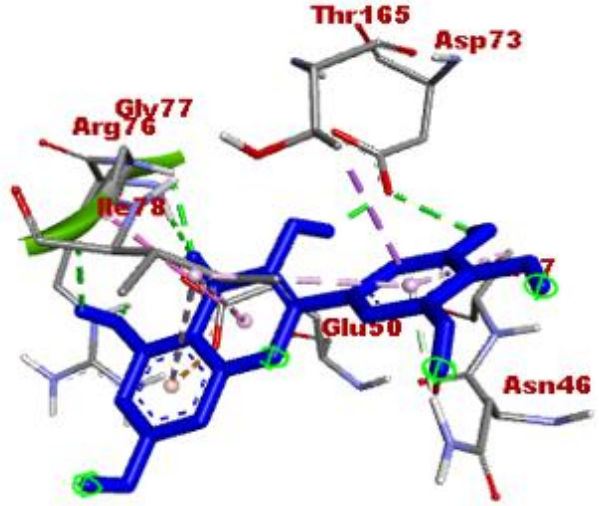
Thr165
Asp73
Gly77
Arg76
Ile78
Glu50
Asn46

66

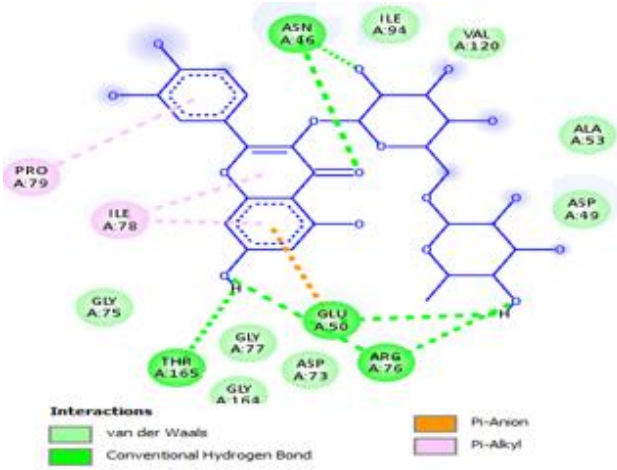
ASN A:46
ILE A:94
VAL A:120
ALA A:53
PRO A:79
ILE A:78
ASP A:49
GLY A:75
GLU A:50
GLY A:77
THR A:165
ASP A:73
ARG A:76
GLY A:164
Interactions
van der Waals
Conventional Hydrogen Bond
Pi-Anion
Pi-Alkyl

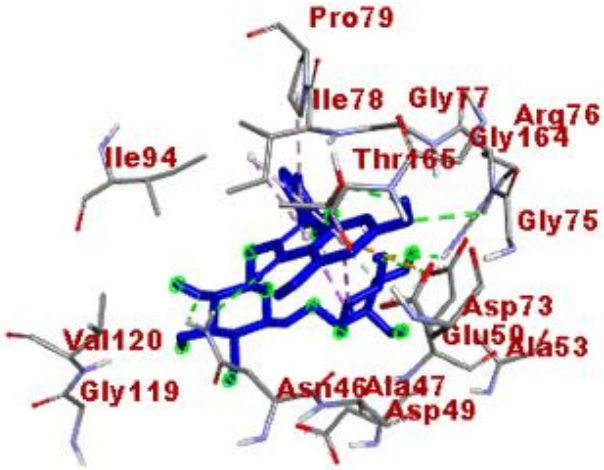
Pro79
Ile78
Gly77
Arg76
Gly164
Ile94
Thr165
Gly75
Asp73
Val120
Glu50
Ala53
Gly119
Asn46
Ala47
Asp49

37

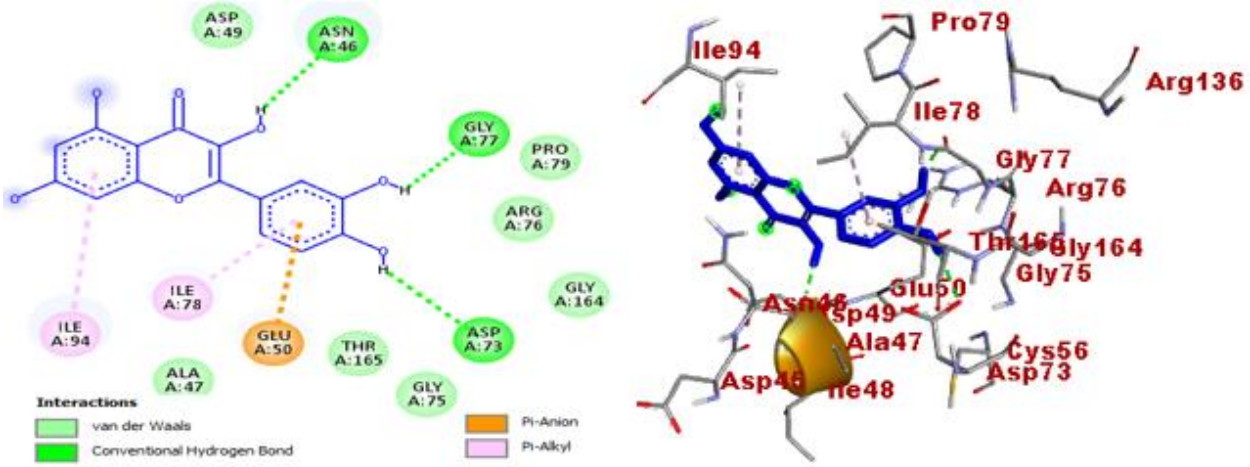
ASP A:49
ASN A:46
GLY A:77
PRO A:79
ARG A:76
ILE A:78
GLY A:164
ILE A:94
GLU A:50
THR A:165
ASP A:73
ALA A:47
GLY A:75
Interactions
van der Waals
Conventional Hydrogen Bond
Pi-Anion
Pi-Alkyl
Pro79
Ile94
Arg136
Ile78
Gly77
Arg76
Thr166
Gly164
Gly75
Glu50
Asn46
Asp49
Ala47
Cys56
Asp73
Asp48
Ile48

42

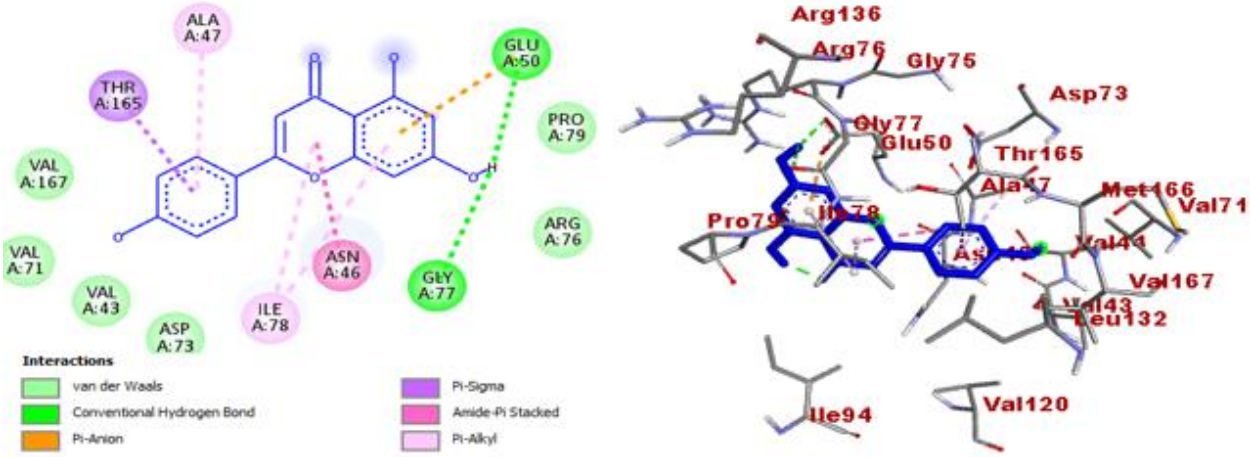
ALA A:47
GLU A:50
THR A:165
PRO A:79
VAL A:167
ARG A:76
VAL A:71
ASN A:46
GLY A:77
VAL A:43
ILE A:78
ASP A:73
Interactions
van der Waals
Conventional Hydrogen Bond
Pi-Anion
Pi-Sigma
Amide-Pi Stacked
Pi-Alkyl
Arg136
Arg76
Gly75
Asp73
Gly77
Glu50
Thr165
Ala47
Met166
Val71
Pro79
Ile78
Val44
Val167
Leu132
Ile94
Val120

87

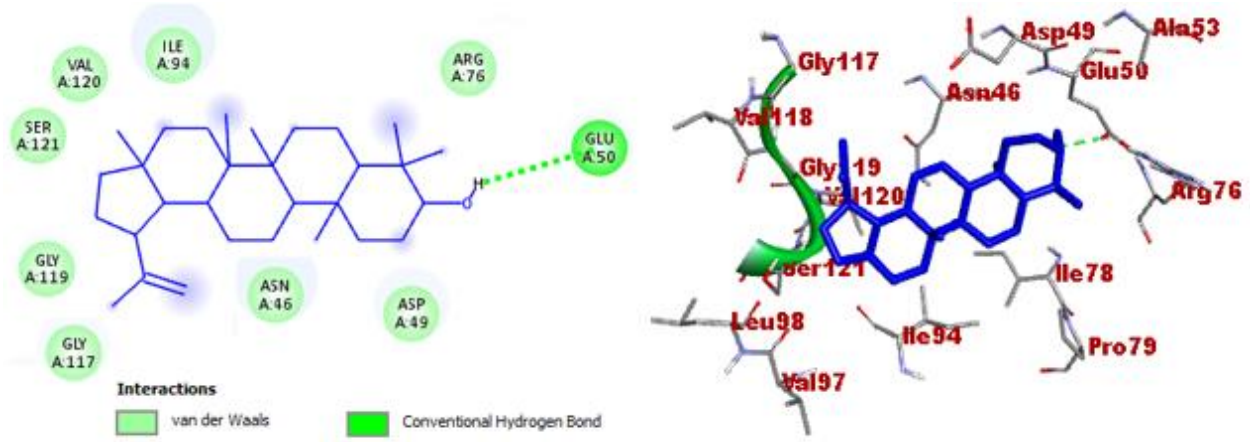
ILE A:94
VAL A:120
ARG A:76
SER A:121
GLU A:50
GLY A:119
ASN A:46
ASP A:49
GLY A:117
Interactions
van der Waals
Conventional Hydrogen Bond
Asp49
Ala53
Gly117
Glu50
Asn46
Val118
Arg76
Ile78
Leu98
Ile94
Pro79
Val97

39

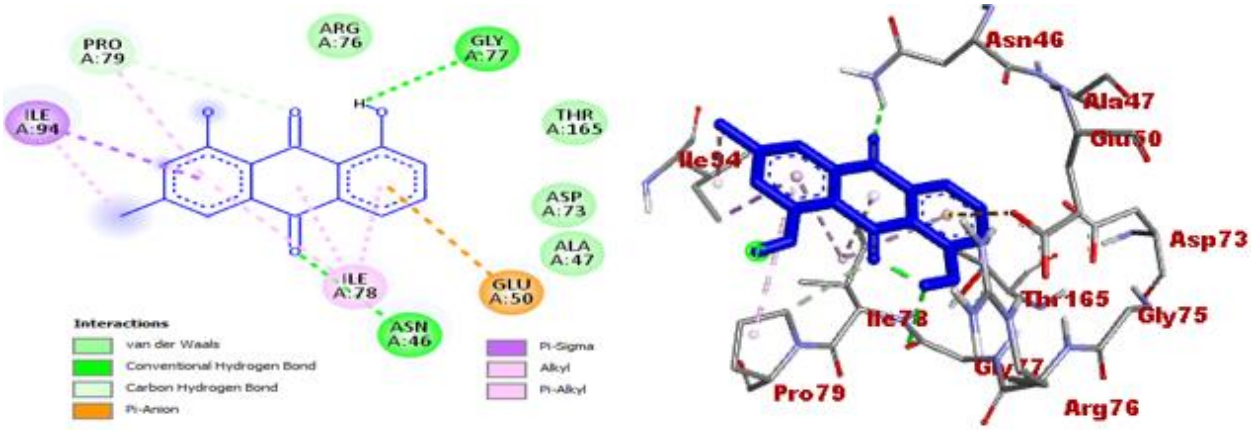
PRO A:79
ARG A:76
GLY A:77
ILE A:94
THR A:165
ASP A:73
ALA A:47
ILE A:78
GLU A:50
ASN A:46
Interactions
van der Waals
Conventional Hydrogen Bond
Carbon Hydrogen Bond
Pi-Anion
Pi-Sigma
Alkyl
Pi-Alkyl
Asn46
Ala47
Glu50
Ile94
Asp73
Thr165
Gly75
Ile78
Gly77
Pro79
Arg76

53

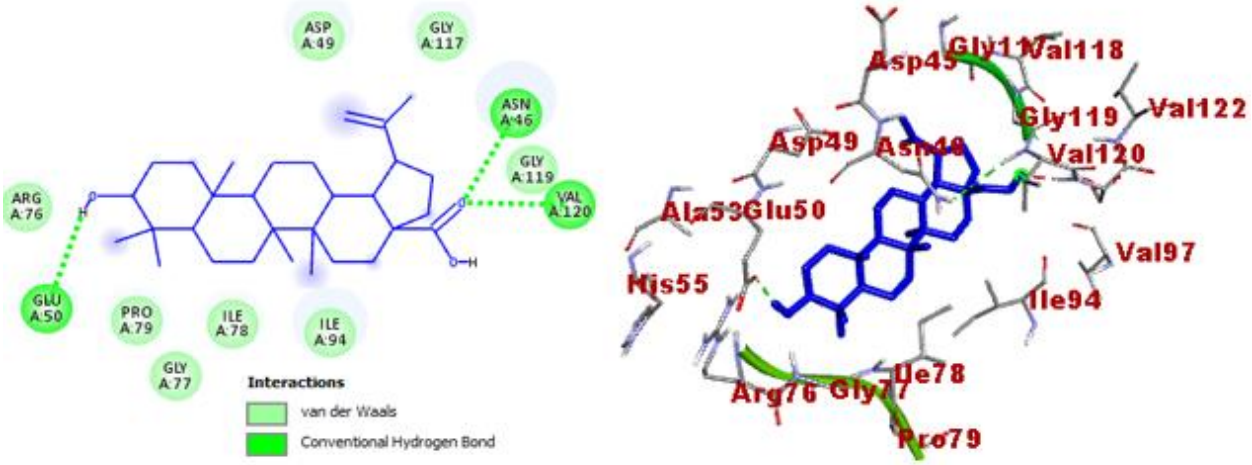
ASP A:49
GLY A:117
ASN A:46
GLY A:119
VAL A:120
ARG A:76
GLU A:50
PRO A:79
ILE A:78
ILE A:94
GLY A:77
Interactions
van der Waals
Conventional Hydrogen Bond
Asp45
Gly117
Val118
Gly119
Val122
Asp49
Asn48
Val120
Ala53
Glu50
Val97
His55
Ile94
Ile78
Arg76
Gly77
Pro79

63

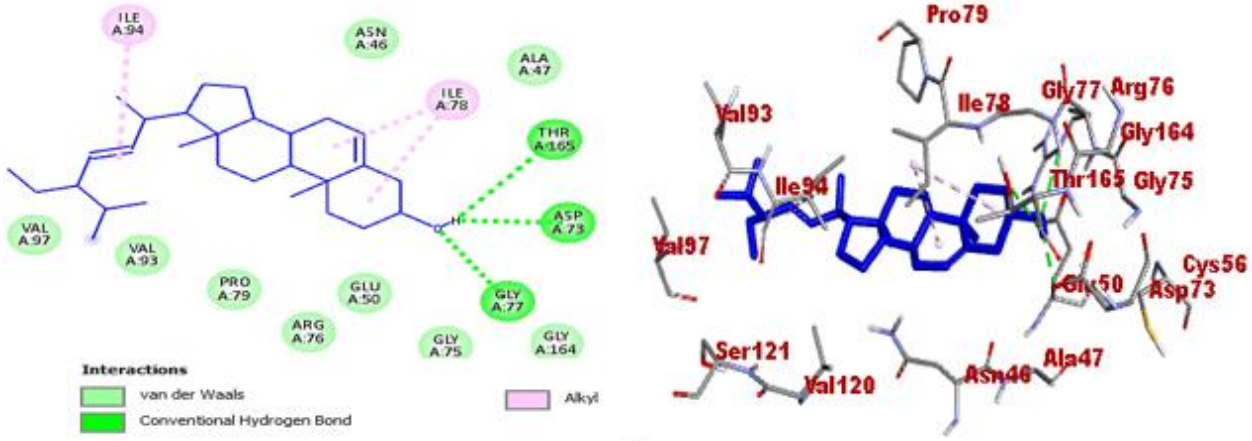
ILE A:94
ASN A:46
ALA A:47
ILE A:78
THR A:165
ASP A:73
VAL A:97
VAL A:93
PRO A:79
GLU A:50
GLY A:77
ARG A:76
GLY A:75
GLY A:164
Interactions
van der Waals
Conventional Hydrogen Bond
Alkyl
Pro79
Val93
Ile78
Gly77
Arg76
Gly164
Ile94
Thr165
Gly75
Val97
Cys56
Glu50
Asp73
Ser121
Ala47
Val120
Asn46

40

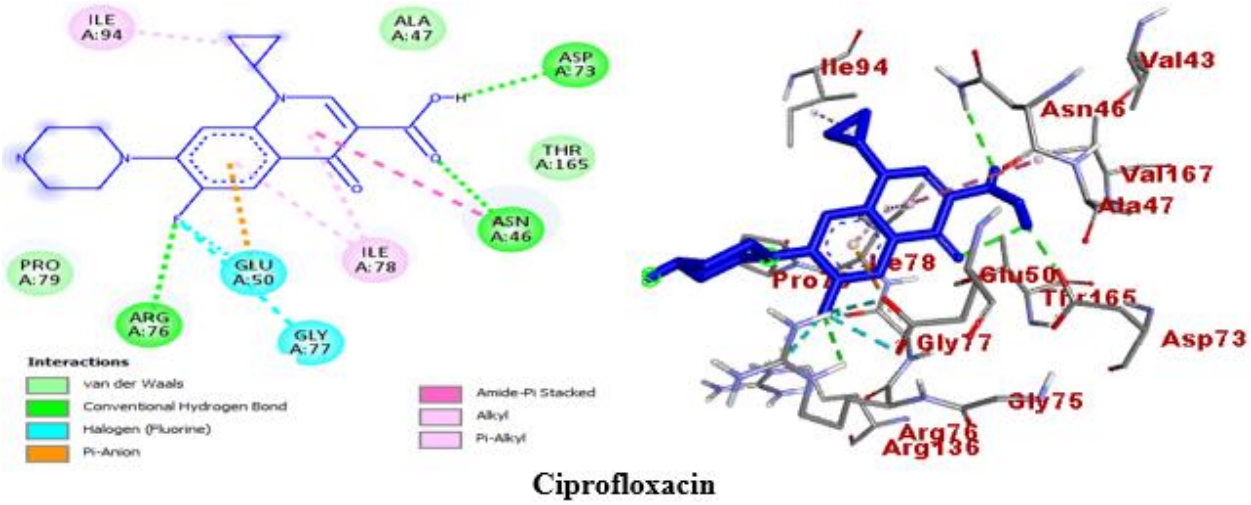

Figure 33: 2D (left) and 3D (right) binding interactions of the compound isolates and ciprofloxacin against *E. coli* DNA gyrase B.

4.4.1.2. Molecular docking study against *S. aureus* PK

Pyruvate kinase (PK), the enzyme at the last stage of glycolysis catalyzes the formation of adenosine triphosphate (ATP) and pyruvate by transferring a phosphoryl group from phosphoenolpyruvate (PEP) to adenosine diphosphate (ADP) (Valentini *et al.*, 2000). PK plays a crucial role in metabolic flux distribution and energy generation. Inhibition of PK disrupts the metabolic stability and energy production of bacteria (Zhai *et al.*, 2015). The molecular docking performances against the *S. aureus* PK showed that the investigated compounds exhibit auspicious binding affinities ranging from -8.8 up to -7.7 kcal/mol signifying their potential antibacterial effects compared to ciprofloxacin (-8.9 kcal/mol). Quercetin-3-*O*-rutinoside (**37**) revealed a stronger binding affinity (-8.8 kcal/mol). In contrast, lupeol (**39**) and stigmasterol (**40**) exhibited the least binding affinities (-7.7 kcal/mol each). Quercetin-3-*O*-rutinoside (**37**) and parthenocissin A (**23**) formed six (Lys-260, Arg-264, Arg-347, Asp-303, Asn-299, and Tyr-302) and five (Lys-260, Asp-339, Gln-338, Asn-299, and Asp-261) H-bond interactions, respectively. While, lupeol (**39**), stigmasterol (**40**), and betulinic acid (**63**) formed the least H-bond interactions with no, one (Gln-338), and one (Asp-339) H-bonds, respectively (Table 44 and Figure 34).

Table 44: Binding affinity, hydrogen bonds, and residual amino acid interactions of the compound isolates and ciprofloxacin against *S. aureus* PK.

Compound/ligand	Binding affinity (kcal/mol)	H-bond	Residual amino acid interactions	
			Hydrophobic/Electrostatic/Halogen	Van der Waals
		C. adenocaule		
23	-8.5	Lys-260, Asp-339, Gln-338, Asn-299, and Asp-261	Asp-303, Tyr-302, Lys-342, Leu-343, and Lys-260	Asn-299, Asp-303, Tyr-302, and Arg-264
25	-8.2	Lys-260, and Asn-299	Asp-303, Lys-260, and Leu-343	Asp-339, Tyr-340, Lys-342, Gln-338, Asp-346, Arg-347, Asp-261, Arg-264, Tyr-302, Asp-303, and Tyr-302
28	-8.0	Asp-303 and Asn-29	__	Arg-264, Lys-342, Tyr-302, Lys-260, and Asp-303
29	-8.7	Lys-260, Arg-264, Asn-299, and Tyr-302	Lys-260	Asp-346, Ile-263, Asp-303, Asn-299, Tyr-302, Arg-347, Leu-343, Gln-338, Asp-339, and Lys-342
66	-8.3	Thr-366, and Ala-358	Ile-361, and His-365	Thr-353, Asn-369, Ser-362, Thr-366, and Ala-358
		D. regia		
37	-8.8	Lys-260, Arg-264, Arg-347, Asp-303, Asn-299, and Tyr-302	Leu-343	Leu-343, Lys-342, Asp-339, Tyr-302, Gln-338, Asp-346, Gly-304, and Asn-267
42	-8.1	Lys-260, Tyr-302, Asn-299, and Asp-303	Tyr-302 and Lys-260	Arg-264, Asp-261, Asn-299, Tyr-302, Asp-303, and Ile-263
87	-8.3	Asn-369	Ile-361 and His-365	Asn-369, Ala-358, Thr-366, and Ser-362
		S. siamea		
39	-7.7	__	Lys-260 and Tyr-302	Arg-264, Lys-342, Asp-303, Asp-339, Gln-338, Tyr-302, and Lys-260
53	-8.1	Ser-362 and Ala-358	His-365 and Ile-361	Thr-353, Asn-369, Ile-361, Thr-366, and His-365
63	-8.0	Asp-339	Lys-342	Gln-338, Ala-337, Asp-339, Tyr-302, Lys-342, Arg-264, Leu-343, Asp-346, Asp-303, and Lys-260
		Z. spina-christi		
40	-7.7	Gln-338	Lys-260, Arg-264, and Tyr-302	Asp-261, Asn-299, Asp-303, Asp-339, and Ala-337
Ciprofloxacin	-8.9	Ser-362, Thr-366, and Asn-369	His-365, and Ile-361	Ala-358, Asn-369, Thr-348, Ile-361, and Met-467

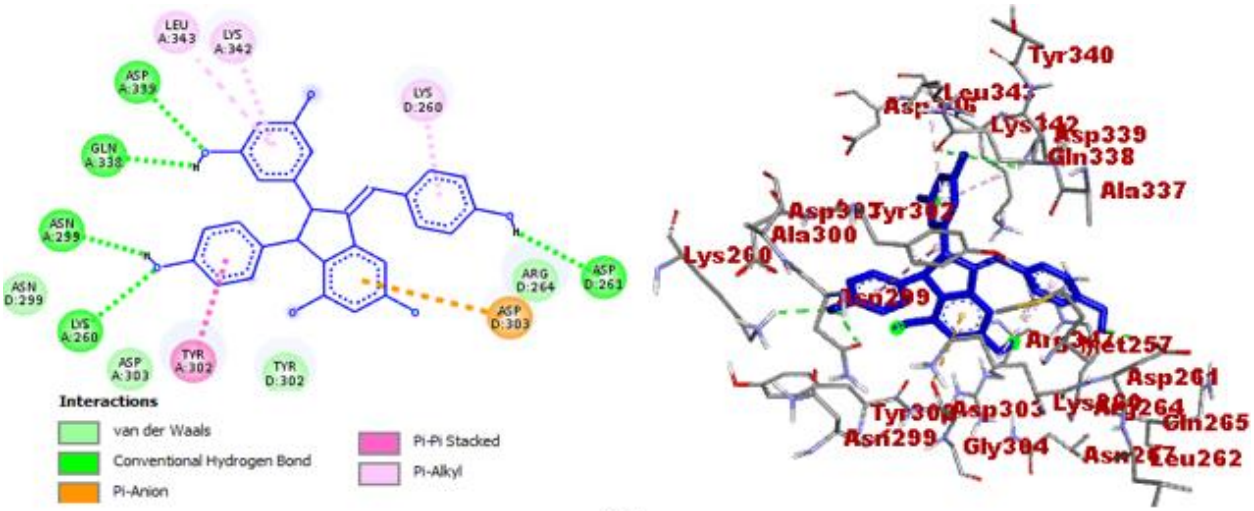
LEU A:343
LYS A:342
ASP A:339
GLN A:338
LYS D:260
ASN A:299
ASN D:299
LYS A:260
ASP A:303
TYR A:302
TYR D:302
ARG D:264
ASP D:261
ASP D:303
Interactions
van der Waals
Conventional Hydrogen Bond
Pi-Anion
Pi-Pi Stacked
Pi-Alkyl
Tyr340
Leu343
Lys342
Asp339
Gln338
Ala337
Asp303
Tyr302
Ala300
Lys260
Asn299
Arg347
Met257
Asp261
Tyr302
Asp303
Lys264
Gln265
Asn299
Gly304
Leu262

23

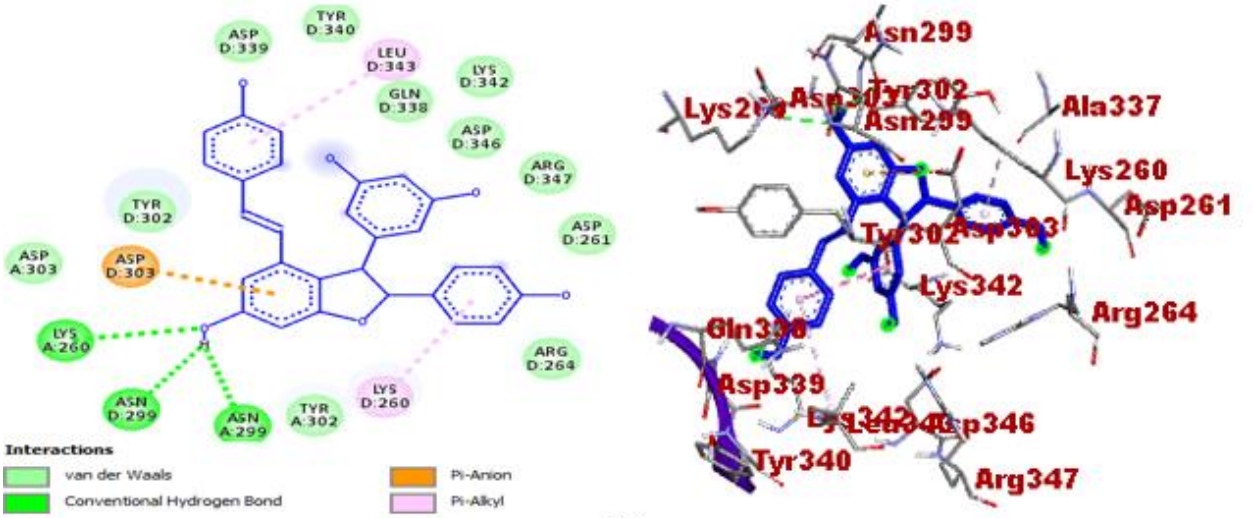
ASP D:339
TYR D:340
LEU D:343
LYS D:342
GLN D:338
ASP D:346
ARG D:347
TYR D:302
ASP D:261
ASP A:303
ASP D:303
LYS A:260
ARG D:264
ASN D:299
ASN A:299
TYR A:302
LYS D:260
Interactions
van der Waals
Conventional Hydrogen Bond
Pi-Anion
Pi-Alkyl
Asn299
Tyr302
Ala337
Asp303
Lys260
Asp261
Lys342
Arg264
Gln338
Asp339
Asp346
Tyr340
Arg347

25

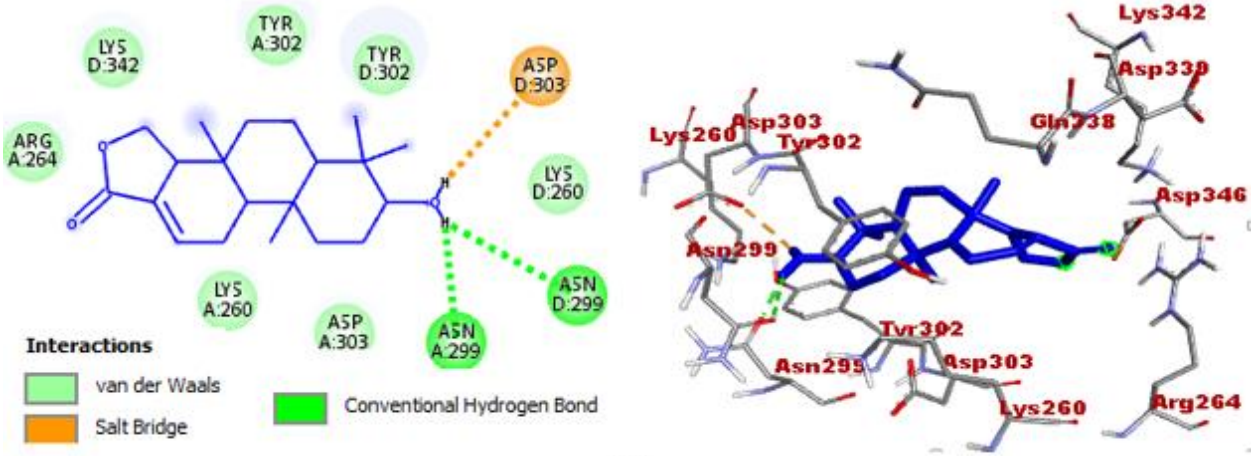
LYS D:342
TYR A:302
TYR D:302
ASP D:303
ARG A:264
LYS D:260
LYS A:260
ASN D:299
ASP A:303
ASN A:299
Interactions
van der Waals
Salt Bridge
Conventional Hydrogen Bond
Lys342
Asp339
Lys260
Asp303
Tyr302
Gln338
Asp346
Asn299
Tyr302
Asn299
Asp303
Lys260
Arg264

28

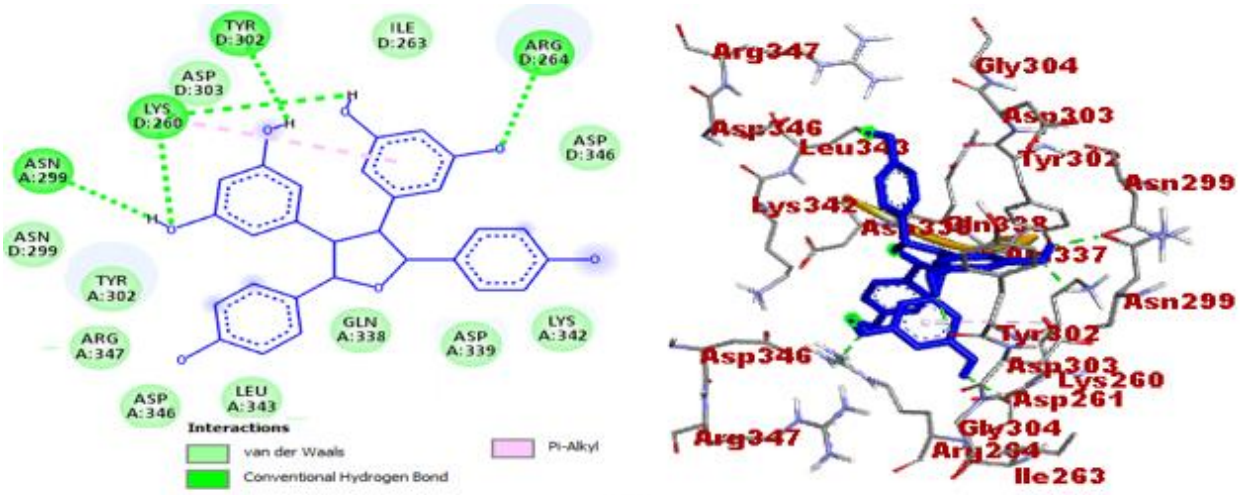
TYR D:302
ILE D:263
ARG D:264
ASP D:303
LYS D:260
ASP D:346
ASN A:299
ASN D:299
TYR A:302
ARG A:347
GLN A:338
ASP A:339
LYS A:342
ASP A:346
LEU A:343
Interactions
van der Waals
Conventional Hydrogen Bond
Pi-Alkyl
Arg347
Gly304
Asp303
Asp346
Leu343
Tyr302
Asn299
Lys342
Asp261
Lys260
Ile263

29

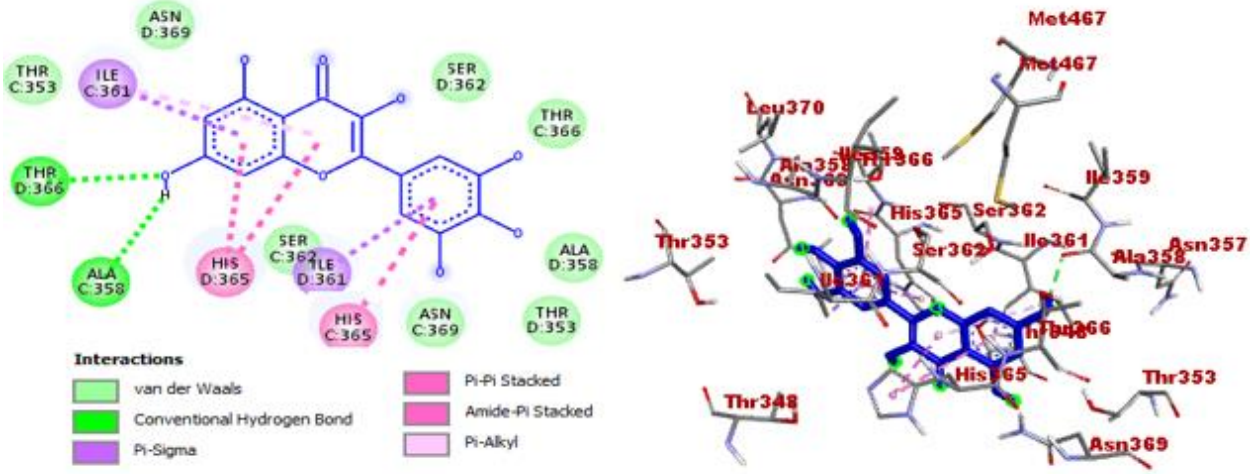
ASN D:369
THR C:353
ILE C:361
SER D:362
THR C:366
THR D:366
ALA C:358
HIS D:365
SER C:362
ILE D:361
ALA D:358
HIS C:365
ASN C:369
THR D:353
Interactions
van der Waals
Conventional Hydrogen Bond
Pi-Sigma
Pi-Pi Stacked
Amide-Pi Stacked
Pi-Alkyl
Met467
Leu370
Ile359
Thr353
Ser362
Asn357
Ala358
Thr348
Asn369

66

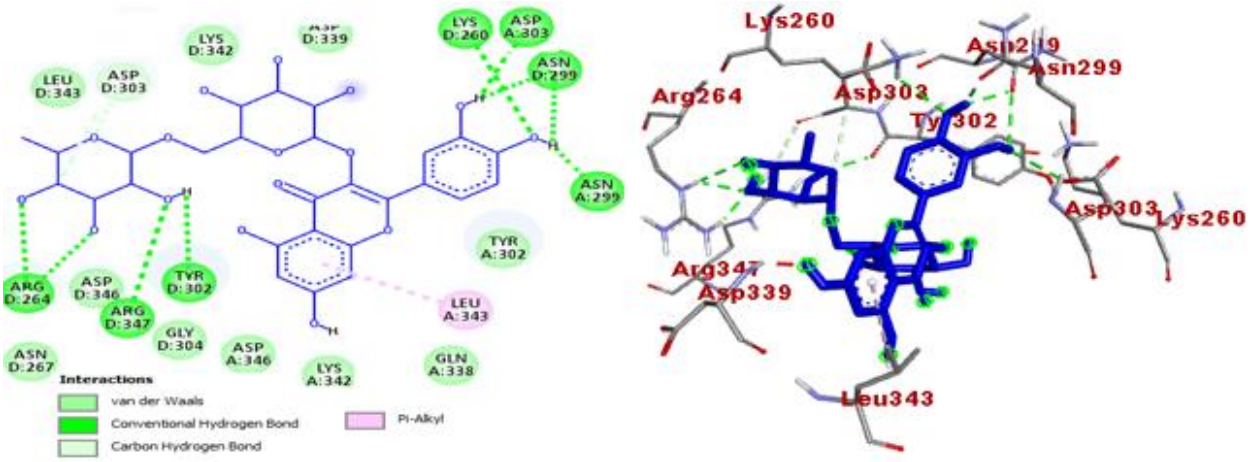
LYS D:342
ASP D:339
LYS D:260
ASP A:303
LEU D:343
ASP D:303
ASN D:299
ASN A:299
TYR A:302
ARG D:264
ASP D:346
TYR D:302
ARG D:347
GLY D:304
ASP A:346
LYS A:342
GLN A:338
LEU A:343
ASN D:267
Interactions
van der Waals
Conventional Hydrogen Bond
Carbon Hydrogen Bond
Pi-Alkyl
Lys260
Asn299
Arg264
Asp303
Tyr302
Asp303
Lys260
Arg347
Asp339
Leu343

37

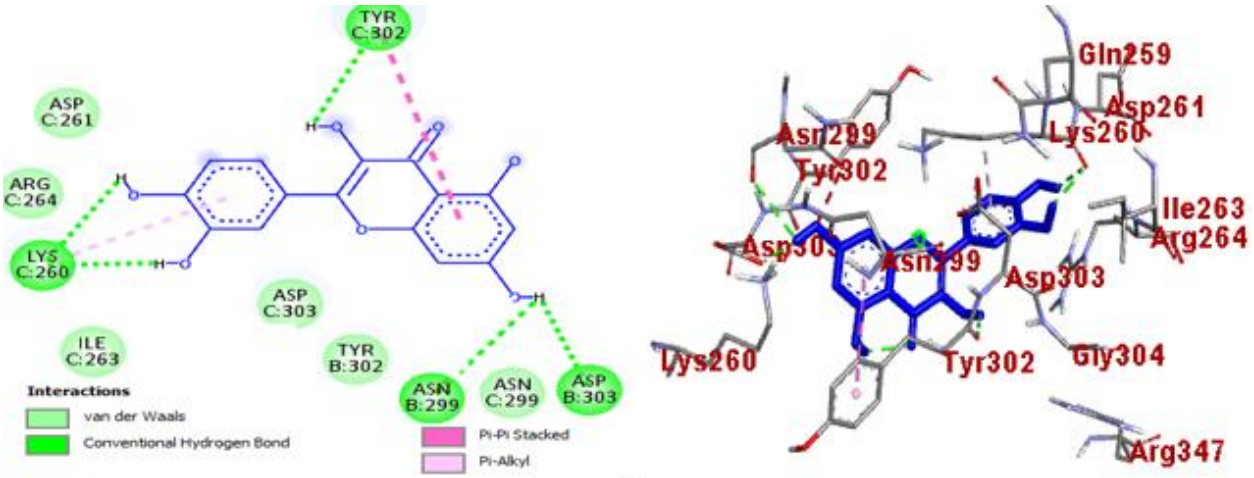
TYR C:302
ASP C:261
ARG C:264
LYS C:260
ASP C:303
ILE C:263
TYR B:302
ASN B:299
ASN C:299
ASP B:303
Interactions
van der Waals
Conventional Hydrogen Bond
Pi-Pi Stacked
Pi-Alkyl
Gln259
Asp261
Asn299
Lys260
Tyr302
Ile263
Arg264
Asp303
Gly304
Arg347

42

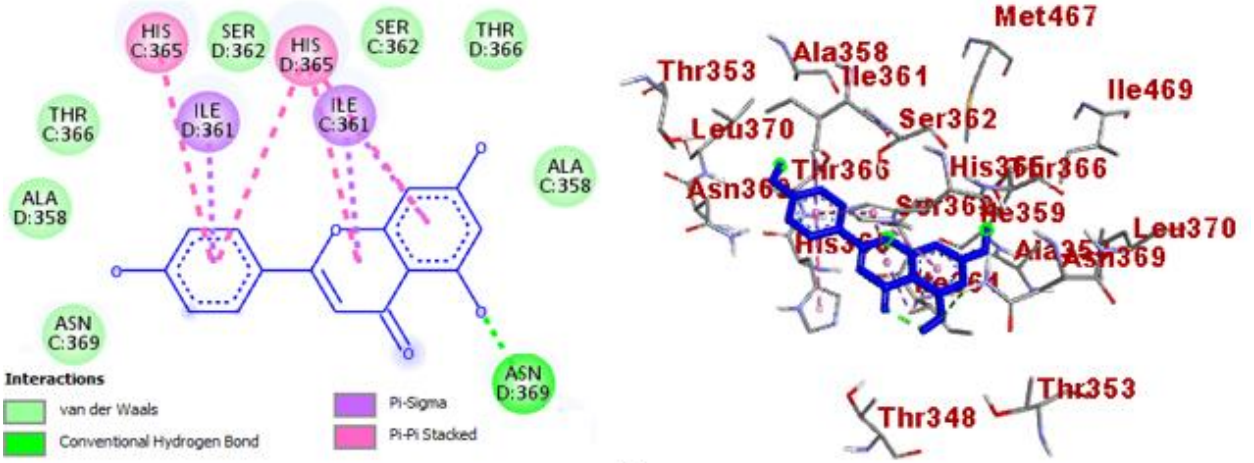
HIS C:365
SER D:362
HIS D:365
SER C:362
THR D:366
THR C:366
ILE D:361
ILE C:361
ALA C:358
ALA D:358
ASN C:369
ASN D:369
Interactions
van der Waals
Conventional Hydrogen Bond
Pi-Sigma
Pi-Pi Stacked
Met467
Ala358
Thr353
Ile361
Ile469
Leu370
Ser362
Thr366
Asn369
Ile359
Thr348

87

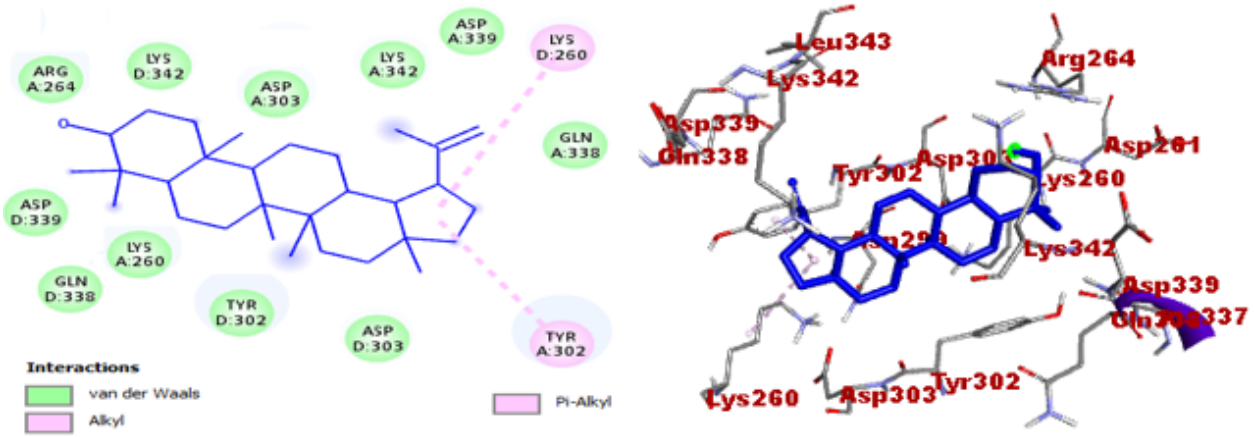
ASP A:339
LYS D:260
ARG A:264
LYS D:342
LYS A:342
ASP A:303
GLN A:338
ASP D:339
LYS A:260
GLN D:338
TYR D:302
ASP D:303
TYR A:302
Interactions
van der Waals
Alkyl
Pi-Alkyl
Leu343
Arg264
Lys342
Asp339
Gln338
Asp261
Tyr302
Lys260
Asp339
Lys260
Asp303
Tyr302

39

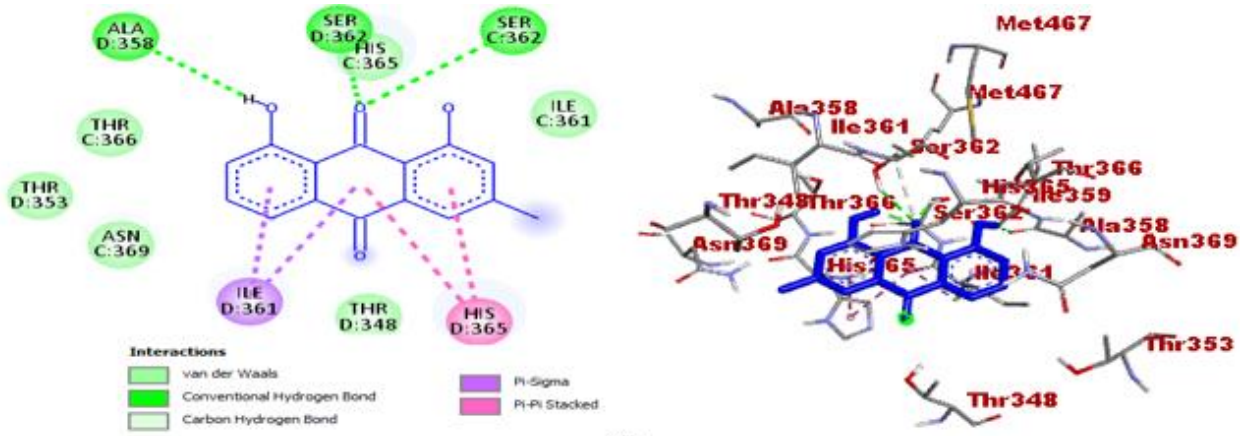
ALA D:358
SER D:362
SER C:362
HIS C:365
ILE C:361
THR C:366
THR D:353
ASN C:369
ILE D:361
THR D:348
HIS D:365
Interactions
van der Waals
Conventional Hydrogen Bond
Carbon Hydrogen Bond
Pi-Sigma
Pi-Pi Stacked
Met467
Met467
Ala358
Ile361
Ser362
Thr366
His365
Ile359
Thr348
Thr366
Ser362
Ala358
Asn369
Asn369
His365
Thr353
Thr348

53

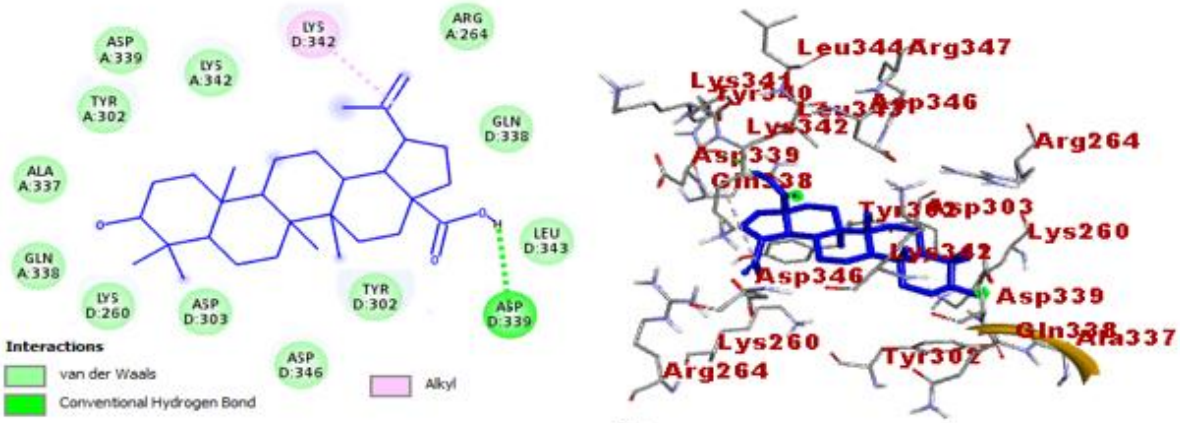
ASP A:339
LYS D:342
ARG A:264
LYS A:342
TYR A:302
GLN D:338
ALA A:337
LEU D:343
GLN A:338
LYS D:260
ASP D:303
TYR D:302
ASP D:339
ASP D:346
Interactions
van der Waals
Conventional Hydrogen Bond
Alkyl
Leu344
Arg347
Lys341
Tyr340
Asp346
Leu343
Lys342
Arg264
Asp339
Gln338
Tyr302
Asp303
Lys260
Lys342
Asp346
Asp339
Gln338
Ala337
Lys260
Tyr302
Arg264

63

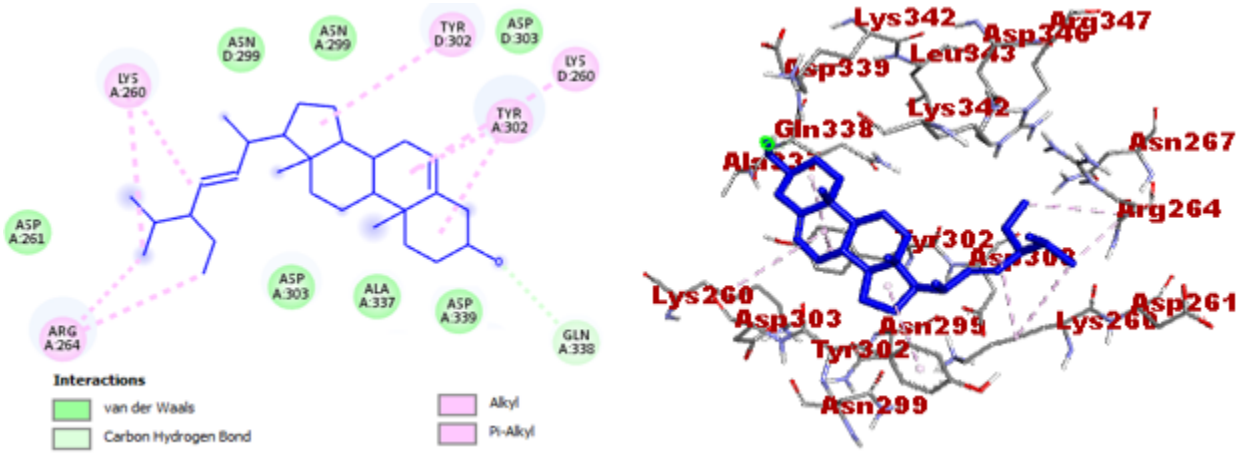
ASN D:299
ASN A:299
TYR D:302
ASP D:303
LYS D:260
LYS A:260
TYR A:302
ASP A:261
ASP A:303
ALA A:337
ASP A:339
ARG A:264
GLN A:338
Interactions
van der Waals
Carbon Hydrogen Bond
Alkyl
Pi-Alkyl
Lys342
Arg347
Asp346
Asp339
Leu343
Lys342
Gln338
Asn267
Arg264
Tyr302
Lys260
Asp303
Asn299
Tyr302
Asp261
Asn299

40

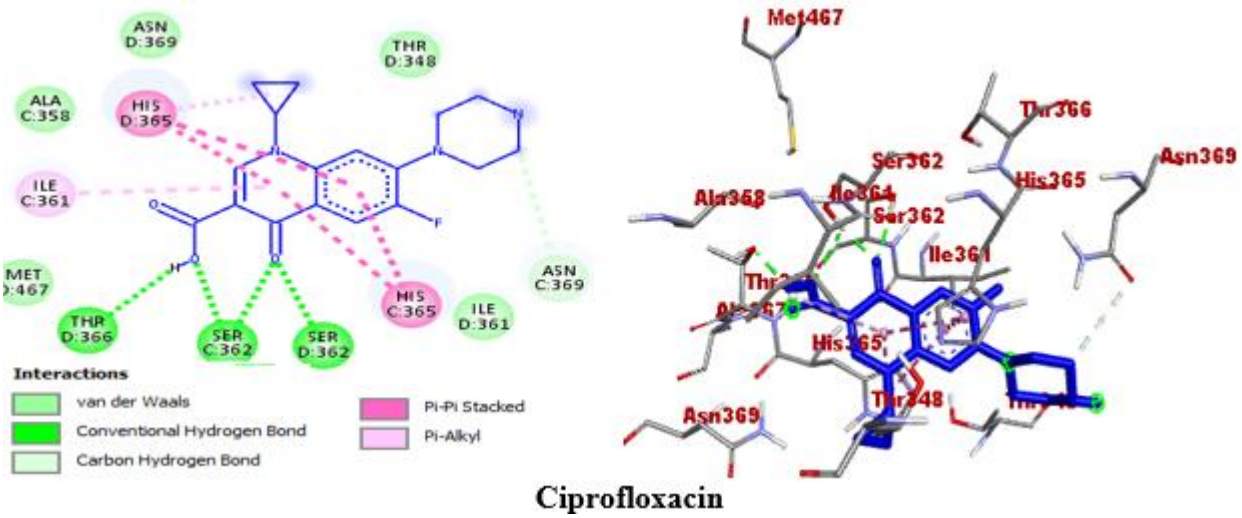

Figure 34: 2D (left) and 3D (right) binding interactions of the compound isolates and ciprofloxacin against *S. aureus* PK.

4.4.1.3. Molecular docking study against *P. aeruginosa* PqsA

P. aeruginosa is an opportunistic Gram-negative bacteria that causes a momentous threat to human health (Page and Heim, 2009). It has been categorized by the WHO as one of the keen priority bacterial pathogens and avowed an urgent call for novel antibiotics (Shrivastava *et al.*, 2018). *P. aeruginosa* is severely resistant to drugs because of inherent and advanced mechanisms, such as biofilm development, reduced cell permeability, and enzymatic drug inactivation. Furthermore, the pathogen possesses a *β*-lactamase gene inside it that makes penicillin and cephalosporins ineffective. It has been reported that about 65% of antibiotic resistance and patient mortality are caused by biofilm-forming *P. aeruginosa* (Zavascki *et al.*, 2010). To confront these challenges, some of the compound isolates of this study with promising *in vitro* activities against *P. aeruginosa* were supported by *in silico* molecular docking computations and the results were also encouraging. The docked compounds exhibited binding affinities ranging from -9.2 kcal/mol up to -7.8 kcal/mol and except for stigmasterol (**40**), all the compounds showed closer scores to the ciprofloxacin standard (-9.3 kcal/mol). *ε*-Viniferin (**25**) and quercetin-3-*O*-rutinoside (**37**) revealed the highest binding affinity (-9.2 kcal/mol each) followed by parthenocissin A (**23**, -9.0 kcal/mol) and quercetin (**42**, -8.9 kcal/mol) showcasing their potential activity against *P. aeruginosa.* The molecular docking studies also showed H-bond and residual amino acid interactions with the selected protein pockets. Accordingly, all the investigated compounds formed H-bonds with at least one amino acid, of which quercetin (**42**) showed the maximum (eight) H-bonds with Tyr-25,

Gly-27, Thr-29, Gln-34, Asp-19, Gln-28, Asn-242, and Phe-246 followed by quercetin-3-*O*-rutinoside (**37**) which formed seven H-bonds with Arg-200, Ala-245, Gln-34, Asp-19, His-24, Gly-198, and Thr-29 (Table 45 and Figure 35).

Table 45: Binding affinity, hydrogen bonds, and residual amino acid interactions of the compound isolates and ciprofloxacin against *P. aeruginosa* PqsA.

Compound/ ligand	Binding affinity (kcal/mol)	H-bond	Residual amino acid interactions	
			Hydrophobic/Electrostatic/Halogen	Van der Waals
C. adenocaule				
23	-9.0	Phe-208, Asn-84, and Lys-206	Trp-233, Lys-206, and Pro-234	Lys-86, Ile-257, Phe-209, Pro-205, and Ile-204
25	-9.2	Gly-27 and Asn-242	Ala-21, Ala-245, and His-24	Leu-228, Thr-29, Gln-28, Phe-246, Arg-247, Gln-34, Leu-30, Asp-19 ,Ser-31, and Arg-200
28	-8.5	Gln-34	__	Ala-245, Phe-246, Arg-247, Ser-31, Asp-19, Arg-200, Ala-21, Thr-20, Thr-29, and His-24
29	-8.7	Arg-200, Ser-226, and Ser-31	Ala-21, Arg-200, and Thr-29	Ala-245, Arg-247, Gln-34, Asp-19, Thr-20, Phe-246, Arg-200, His-24, Ala-21, Gly-198, and Thr-29
66	-8.8	Gly-27	Phe-246	Ser-31, Asp-19, Arg-247, His-24, Ala-245, Tyr-25, Gln-28, Leu-228, Thr-29, and Ala-21
D. regia				
37	-9.2	Arg-200, Ala-245, Gln-34, Asp-19, Thr-29, His-24, and Gly-198	Arg-200 and Ala-21	Thr-20, His-24, Phe-246, Arg-247, Leu-30, Ser-31, Asp-19, Ala-21, and Gly-198
42	-8.9	Tyr-25, Gly-27, Thr-29, Gln-34, Asp-19, Gln-28, Asn-242, and Phe-246	Phe-246, Leu-228, and Ala-245	Ser-31, Arg-200, His-24, Arg-26, Thr-29, and Leu-30
87	-8.7	Asn-61 and Asp-132	Ala-124, Arg-128, and Ala-108	Glu-107, Leu-60, Phe-134, Leu-66, Ser-63, Ser-65, Pro-129, Ala-125, Gly-127, Ala-126, and Asp-109
Z. spina-christi				
40	-7.8	Pro-326	Pro-328, Pro-326, Leu-325, and Leu-182	Gly-183, Glu-343, Pro-356, Cys-332, Glu-331, Gly-329, Tyr-330, Arg-314, Glu-191, Arg-386, Gly-390, and Arg-186
Ciprofloxacin	-9.3	Arg-200, Ala-21, Ala-245, and Thr-29	His-24 and Ala-21	Asp-19, Ser-31, Ser-226, Gly-198, Arg-200, Phe-246, Arg-247, Thr-29, and Thr-20

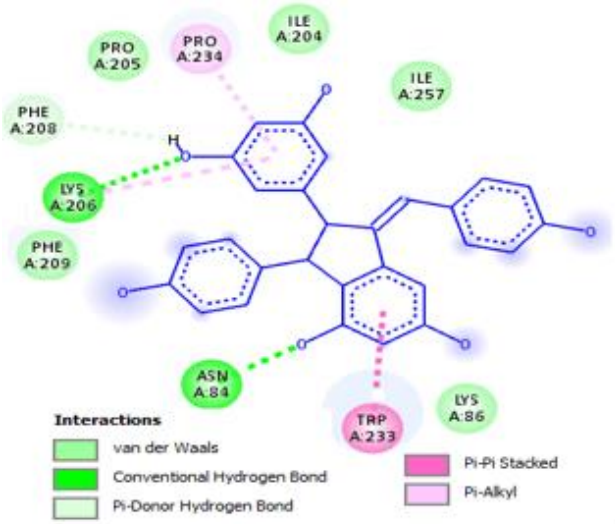
PRO A:205
PRO A:234
ILE A:204
ILE A:257
PHE A:208
LYS A:206
PHE A:209
ASN A:84
TRP A:233
LYS A:86
Interactions
van der Waals
Conventional Hydrogen Bond
Pi-Donor Hydrogen Bond
Pi-Pi Stacked
Pi-Alkyl

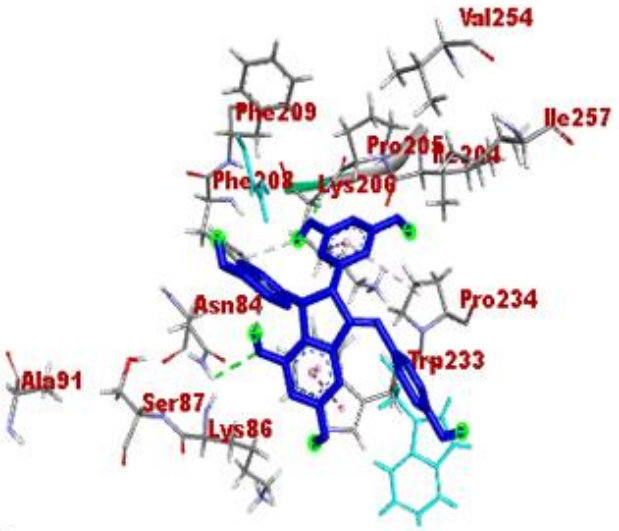
Val254
Phe209
Ile257
Pro205
Ile204
Phe208
Lys206
Asn84
Pro234
Trp233
Ala91
Ser87
Lys86

23

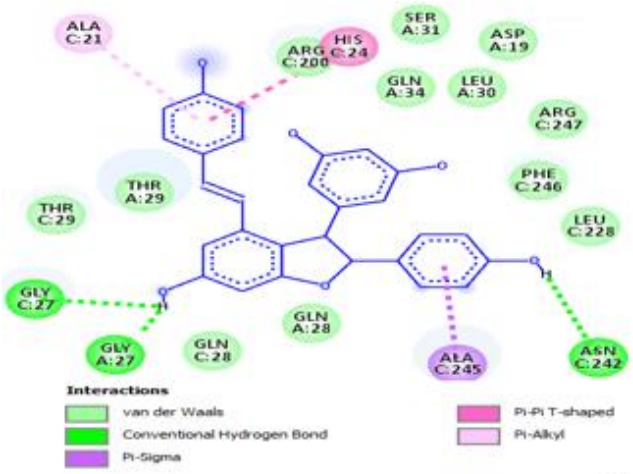
ALA C:21
HIS C:24
ARG C:200
SER A:31
ASP A:19
GLN A:34
LEU A:30
ARG C:247
THR A:29
PHE C:246
THR C:29
LEU C:228
GLY C:27
GLN A:28
GLY A:27
GLN C:28
ALA C:245
ASN C:242
Interactions
van der Waals
Conventional Hydrogen Bond
Pi-Sigma
Pi-Pi T-shaped
Pi-Alkyl

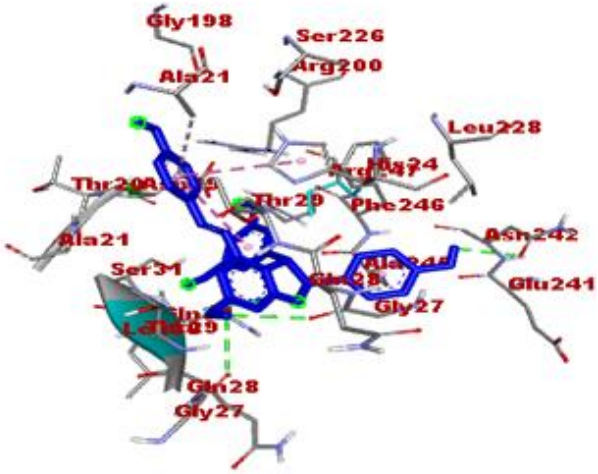
Gly198
Ser226
Arg200
Ala21
Leu228
Thr29
Phe246
Asn242
Ser31
Glu241
Gly27
Glu28

25

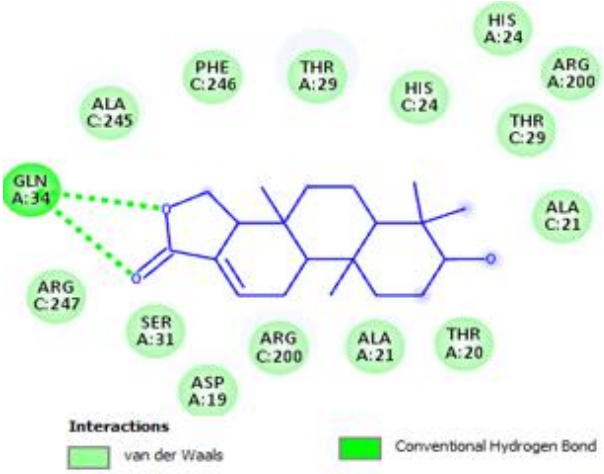
HIS A:24
PHE C:246
THR A:29
ARG A:200
HIS C:24
ALA C:245
THR C:29
GLN A:34
ALA C:21
ARG C:247
SER A:31
ARG C:200
ALA A:21
THR A:20
ASP A:19
Interactions
van der Waals
Conventional Hydrogen Bond

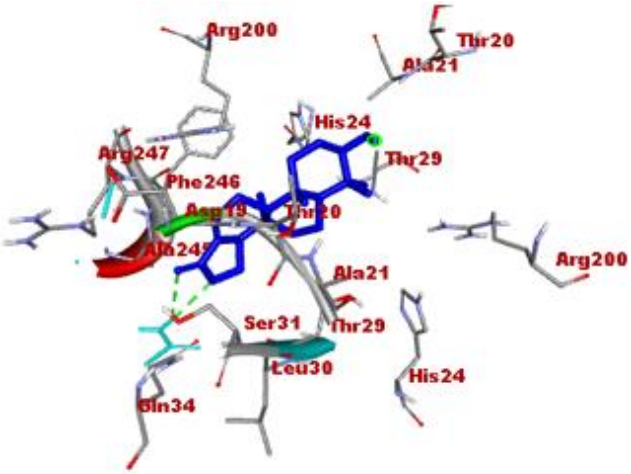
Arg200
Thr20
Ala21
His24
Arg247
Thr29
Phe246
Asp19
Ala21
Arg200
Ser31
Thr29
Leu30
His24
Gln34

28

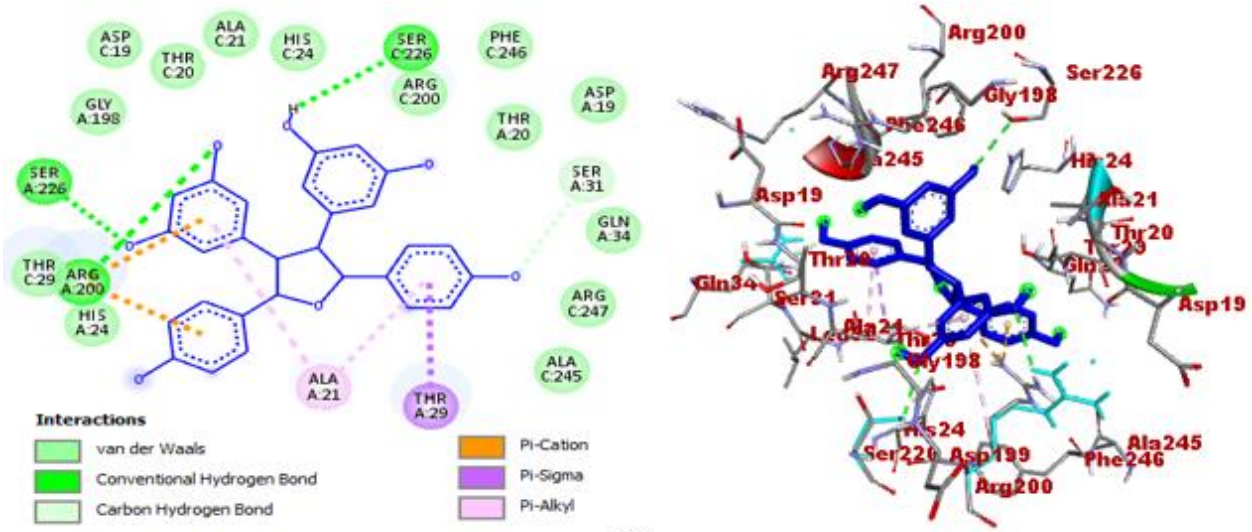
ASP C:19
ALA C:21
HIS C:24
SER C:226
PHE C:246
THR C:20
ARG C:200
GLY A:198
ASP A:19
THR A:20
SER A:226
SER A:31
GLN A:34
THR C:29
ARG A:200
ARG C:247
HIS A:24
ALA C:245
ALA C:21
THR A:29
Interactions
van der Waals
Conventional Hydrogen Bond
Carbon Hydrogen Bond
Pi-Cation
Pi-Sigma
Pi-Alkyl
Arg200
Arg247
Ser226
Gly198
Asp19
Thr20
Gln34
Ser21
Asp19
Gly198
His24
Ser226
Asp199
Ala245
Phe246
Arg200

29

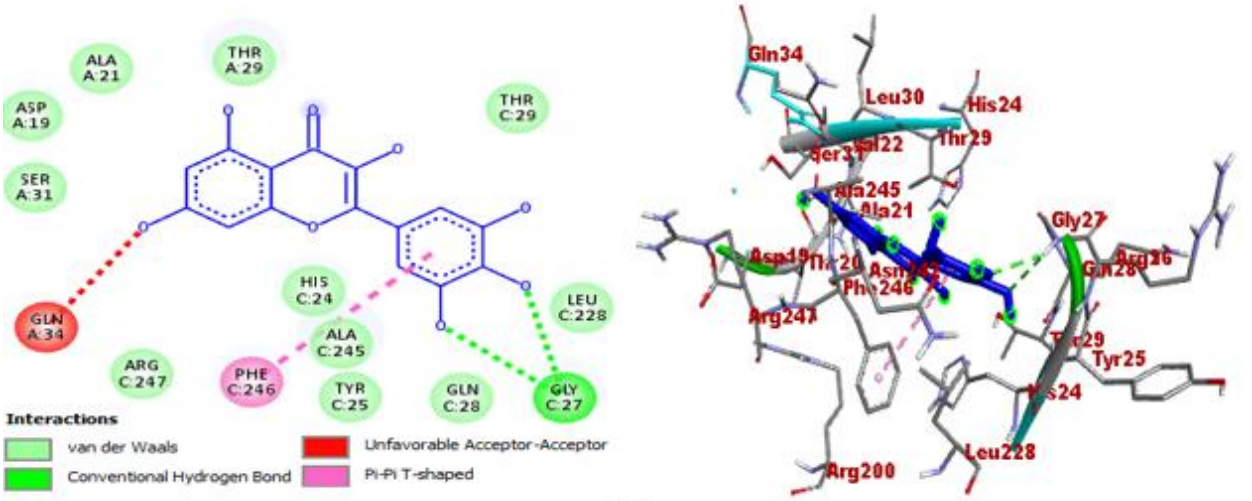
ALA A:21
THR A:29
ASP A:19
THR C:29
SER A:31
HIS C:24
LEU C:228
GLN A:34
ALA C:245
ARG C:247
PHE C:246
TYR C:25
GLN C:28
GLY C:27
Interactions
van der Waals
Conventional Hydrogen Bond
Unfavorable Acceptor-Acceptor
Pi-Pi T-shaped
Gln34
Leu30
His24
Thr29
Ala245
Ala21
Gly27
Asp19
Arg247
Tyr25
Leu228
Arg200

66

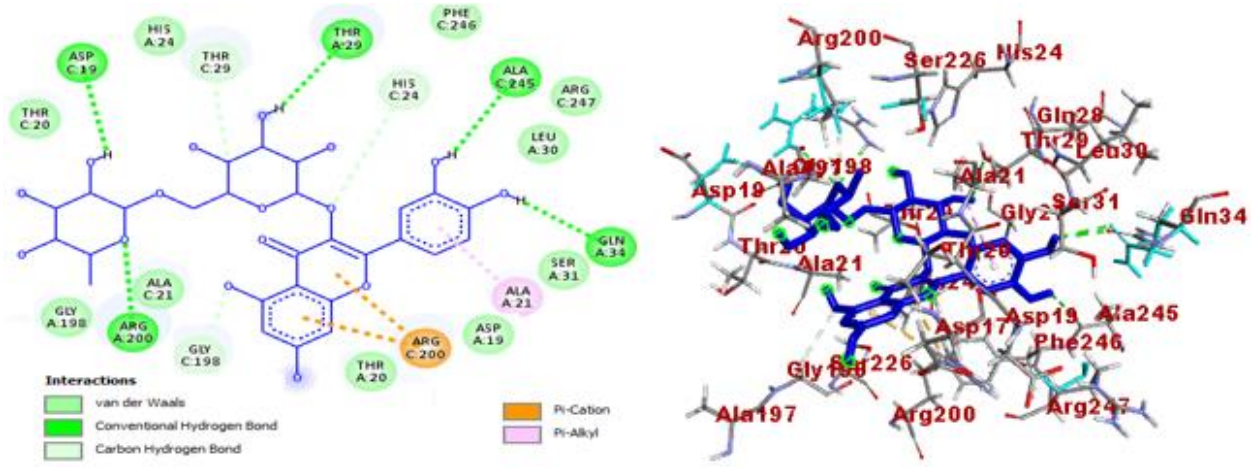
HIS A:24
THR A:29
PHE C:246
ASP C:19
THR C:29
HIS C:24
ALA C:245
ARG C:247
THR C:20
LEU A:30
GLN A:34
SER A:31
ALA C:21
ALA A:21
GLY A:198
ARG A:200
ASP A:19
GLY C:198
ARG C:200
THR A:20
Interactions
van der Waals
Conventional Hydrogen Bond
Carbon Hydrogen Bond
Pi-Cation
Pi-Alkyl
Arg200
Ser226
His24
Gln28
Thr29
Leu30
Asp19
Ala21
Ser31
Gln34
Ala21
Asp19
Ala245
Phe246
Ala197
Arg200
Arg247

37

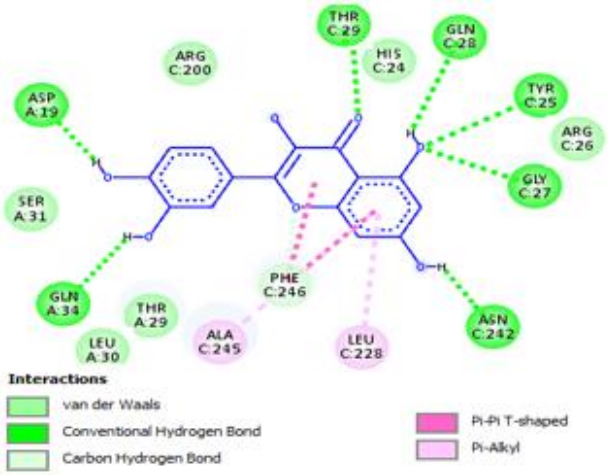
THR C:29
HIS C:24
GLN C:28
ARG C:200
ASP A:19
TYR C:25
ARG C:26
GLY C:27
SER A:31
PHE C:246
GLN A:34
THR A:29
ALA C:245
LEU C:228
ASN C:242
LEU A:30
Interactions
van der Waals
Conventional Hydrogen Bond
Carbon Hydrogen Bond
Pi-Pi T-shaped
Pi-Alkyl

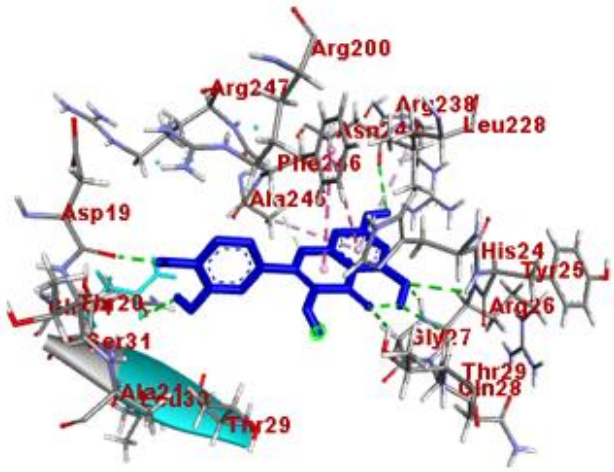
Arg200
Arg247
Arg238
Leu228
Asn244
Phe246
Ala245
Asp19
His24
Tyr25
Arg26
Thr20
Ser31
Gly27
Thr29
Gln28
Tyr29

42

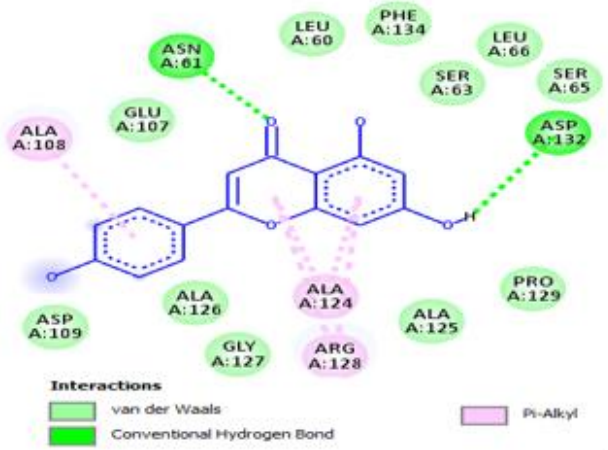
LEU A:60
PHE A:134
ASN A:61
LEU A:66
SER A:63
SER A:65
GLU A:107
ASP A:132
ALA A:108
PRO A:129
ALA A:126
ALA A:124
ALA A:125
ASP A:109
GLY A:127
ARG A:128
Interactions
van der Waals
Conventional Hydrogen Bond
Pi-Alkyl

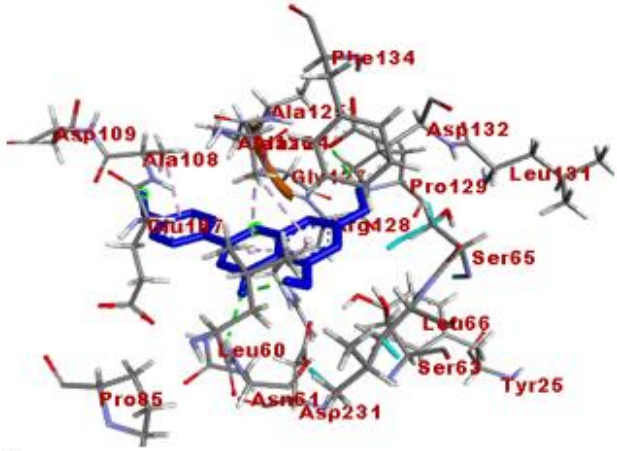
Phe134
Asp109
Asp132
Ala108
Pro129
Leu131
Ser65
Leu66
Leu60
Ser63
Tyr25
Pro85
Asn61
Asp231

87

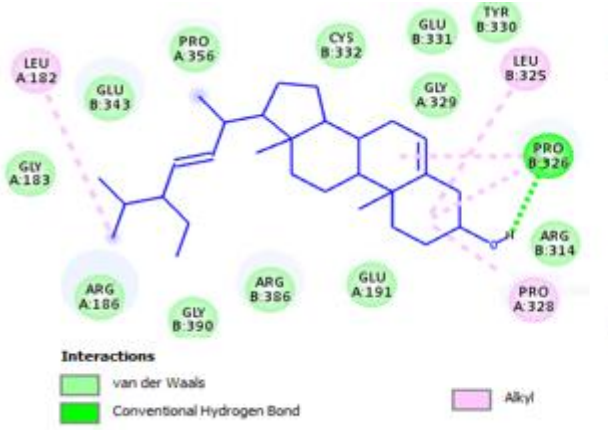
TYR B:330
GLU B:331
CYS B:332
PRO A:356
LEU A:182
LEU B:325
GLU B:343
GLY A:329
PRO B:326
GLY A:183
ARG B:314
ARG A:186
ARG B:386
GLU A:191
PRO A:328
GLY B:390
Interactions
van der Waals
Conventional Hydrogen Bond
Alkyl

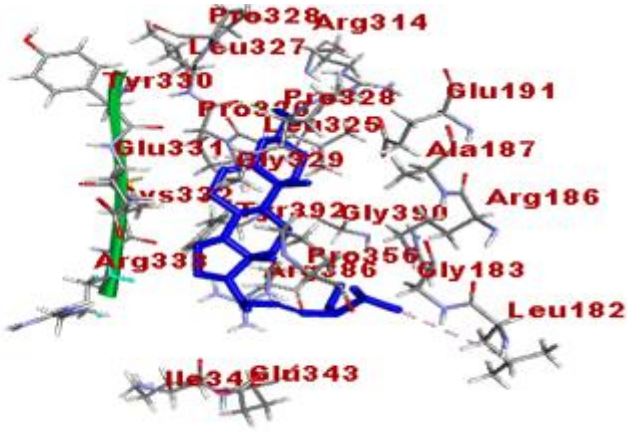
Pro328
Arg314
Leu327
Tyr330
Glu191
Pro328
Leu325
Glu331
Ala187
Gly329
Arg186
Tyr392
Gly390
Pro356
Gly183
Leu182
Glu343

40

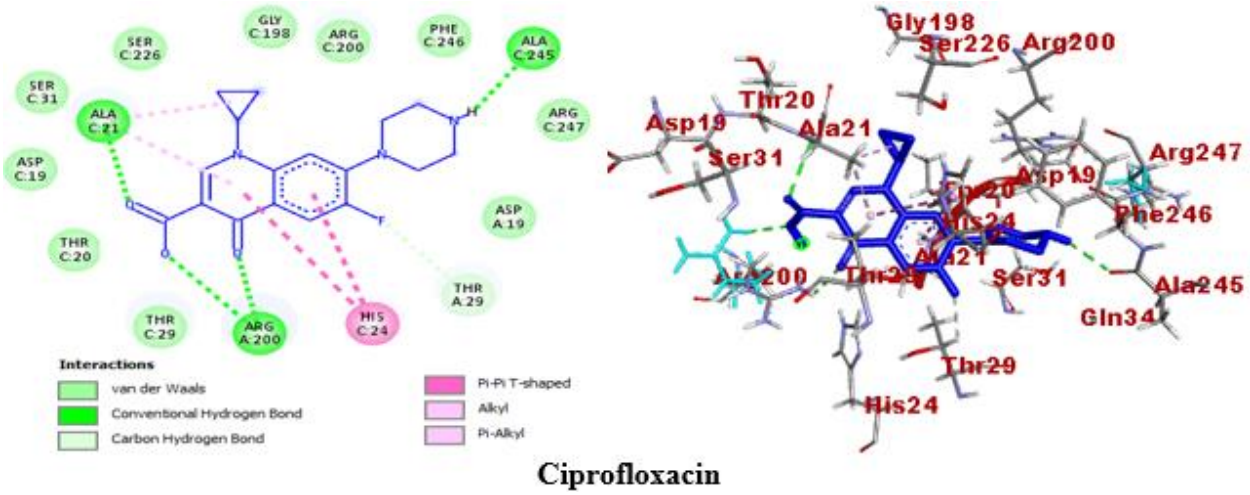

Figure 35: 2D (left) and 3D (right) binding interactions of the compound isolates and ciprofloxacin against *P. aeruginosa* PqsA.

4.4.1.4. Molecular docking study against 10782 streptopain of *S. pyogenes*

Streptopain proteins are cysteine proteases articulated by *S. pyogenes* and are key virulence factors in streptococcal exposures triggering different human diseases, including glomerulonephritis, fever, shock-like syndrome, and pharyngitis (Chen *et al.*, 2003). Thus, it was targeted to molecular docking study as it plays a vital role in the metabolism and survival of the bacterial pathogen. In this study, compound isolates of two plants (*S. siamea* and *Z. spina-christi*) exhibiting auspicious *in vitro* activities against *S. pyogenes* were performed for their molecular docking analyses against 10782 streptopain. The results revealed amino acid interactions against *S. pyogenes* with binding affinities ranging from -7.4 kcal/mol (stigmasterol, **40**) up to -7.0 kcal/mol (lupeol, **39**), and the binding scores were very close to ciprofloxacin (-7.5 kcal/mol). In addition, the computed binding affinities of the compounds were mediated by H-bond interactions. Lupeol (**39**), chrysophanol (**53**), and betulinic acid (**63**) formed two H-bonds each with Gly-163 and Asn-161, Asn-161 and Trp-359, and Asn-167 and Gly-163, respectively. Further residual amino acid interactions (hydrophobic, electrostatic, and Van der Waals) of the docked compounds are depicted in Table 46 and Figure 36.

Table 46: Binding affinity, hydrogen bonds, and residual amino acid interactions of the compound isolates and ciprofloxacin against 10782 streptopain of *S. pyogenes*.

Compound/ ligand	Binding affinity (kcal/mol)	H-bond	Residual amino acid interactions	
			Hydrophobic/Electro static/Halogen	Van der Waals
			S. siamea	
39	-7.0	Gly-163 and Asn-161	__	Gln-162, Ala-189, Trp-359, Ser-279, Cys-192, Gly-339, Gly-338, Val-337, and Leu-377
53	-7.3	Asn-161 and Trp-359	Trp-359, Ala-376, Leu-377, and Ala-189	Gln-162, Gly-163, and Val-362
63	-7.1	Asn-167 and Gly-163	__	Gln-162, Asn-161, Asn-164, His-187, Gln-186, Phe-183, Pro-278, Ala-189, Ser-279, Trp-359, and Leu-377
			Z. spina-christi	
40	-7.4	Val-337	Ala-189 and His-340	Pro-278, Gly-163, Trp-359, Leu-377, Gly-338, Phe-386, Gly-339, Ser-280, Ser-279, Gln-162, Gln-186, and Phe-183
Ciprofloxacin	-7.5	Gln-332, His-340, Ser-279, and Gly-281	Ser-280, Cys-192, Gly-339, and Val-334	Val-193, , Ser-282, Tyr-389, Ala-341, and Gly-333

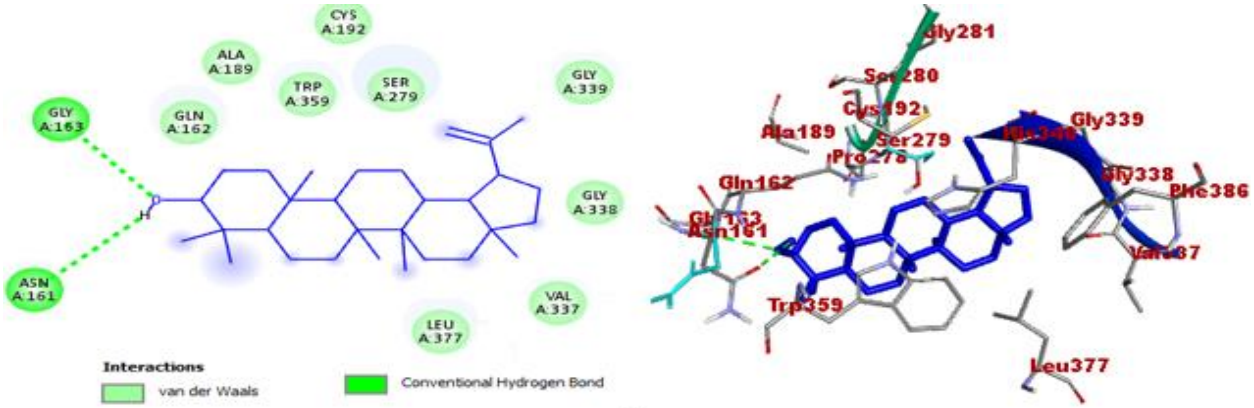

39

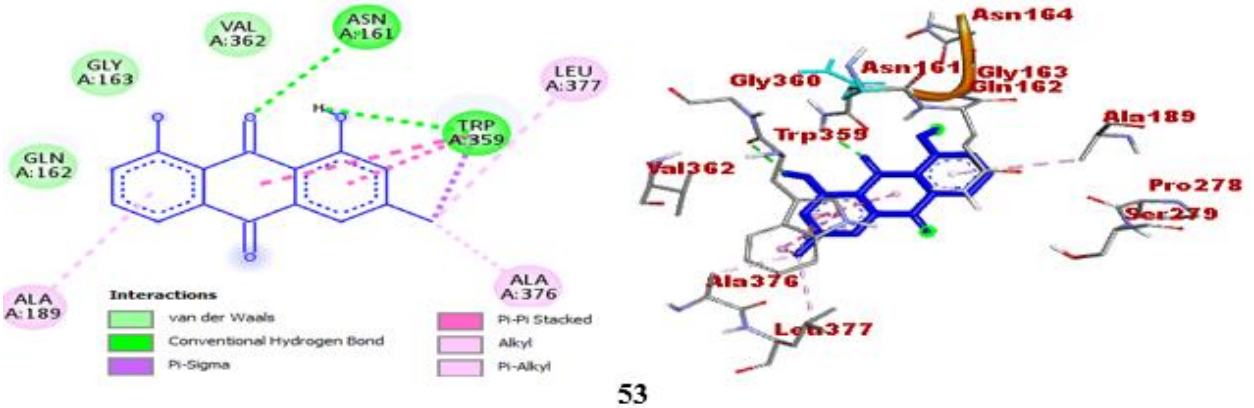

53

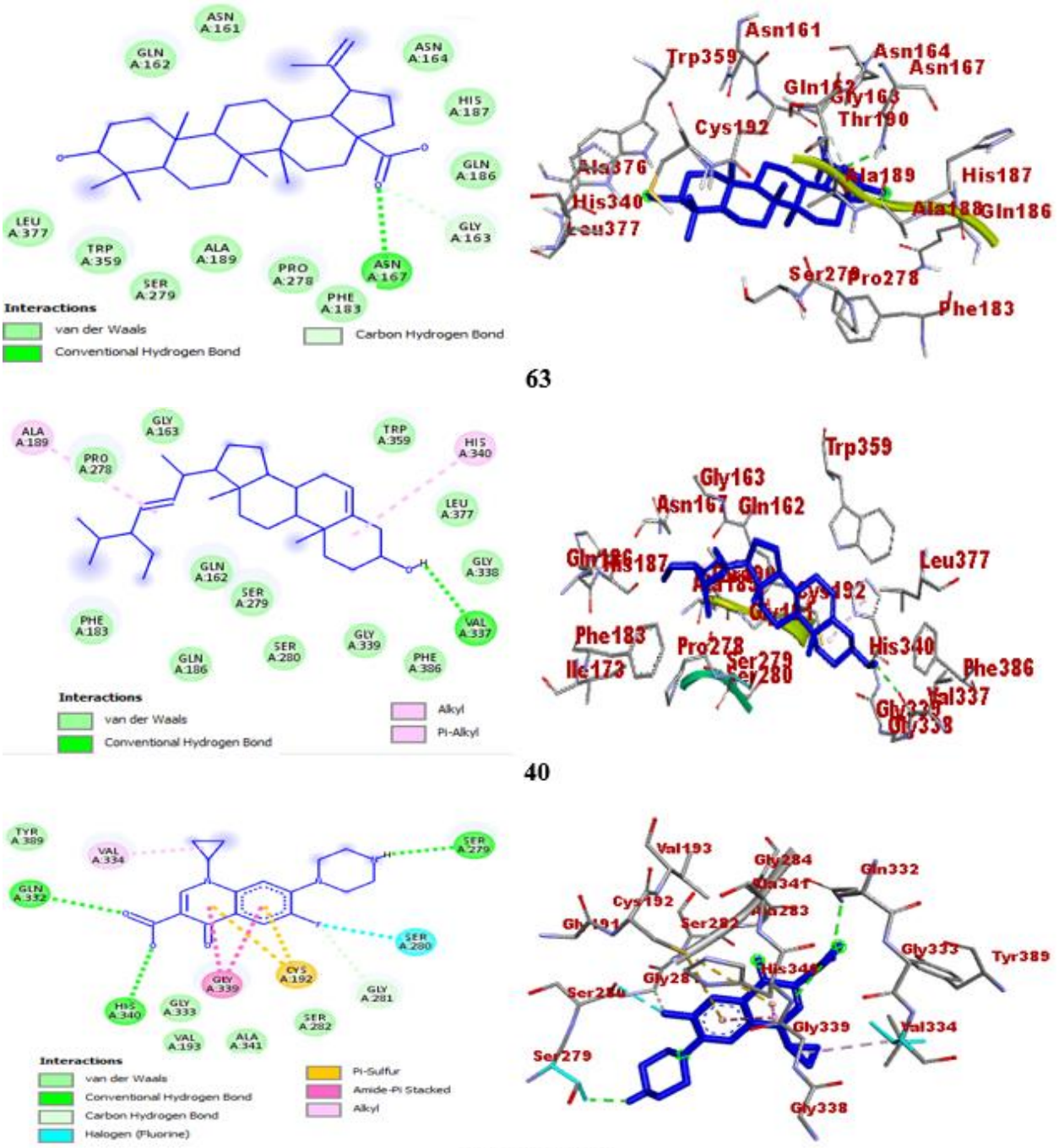

Figure 36: 2D (left) and 3D (right) binding interactions of the compound isolates and ciprofloxacin against 10782 streptopain of *S. pyogenes*.

4.4.1.5. Molecular docking study against human myeloperoxidase

Myeloperoxidase (MPO), a member of the peroxidases subfamily, is amply expressed in immune cells, such as monocytes, neutrophils and lymphocytes, and macrophages. It accumulates in the

cytoplasmic membrane-bound azurophilic granules and these granules are secreted out to the extracellular part by degranulation during stimulation. Literature surveys stated that oxidative stress plays a fundamental role in the secretion of MPO from these cells (Khan *et al.*, 2018). It generates free radicals and reactive oxidants either through halogenation or its peroxidase cycle (Flemmig *et al.*, 2014). After microbe consumption and phagosome formation, MPO reacts with H_2O_2 and produces highly reactive intermediates which can oxidize halide ions and pseudohalide thiocyanates to hypohalous and hypothiocyanous acids, respectively. The formation of these oxidants kill the neutrophils and this belligerent response causes tissue destruction and worsens inflammations. In this regard, MPO leads to various inflammatory problems, including cardiovascular disease (Matos *et al.*, 2020). Neurodegenerative ailments, including rheumatoid arthritis, multiple sclerosis, systemic organ failure, and chronic obstructive pulmonary disease have also been related to MPO. In addition, the inflammation response of COVID-19 during the acute respiratory syndrome stage is associated with elevated levels of MPO (Arazna *et al.*, 2013). Thus, it is important to inhibit the inflated level of MPO in the body using natural antioxidants.

In this work, the compound isolates that showed potential *in vitro* antioxidant activities were subjected to a molecular docking study against MPO to validate their potency. The compounds revealed minimum binding affinities in the range of -8.9 kcal/mol (quercetin-3-*O*-rutinoside, **37**) up to -7.0 kcal/mol (stigmasterol, **40**). The greater binding affinity of quercetin-3-*O*-rutinoside (**37**) can be associated to the presence of many hydroxyl groups in the main skeleton and glucose moiety forming more than one H-bond interactions with the amino acids. The binding scores of the docked compounds were also closely related to ascorbic acid standard (-8.0 kcal/mol) signifying their potential antioxidant activities. Quercetin (**42**) formed the maximum (four) H-bond interactions with Arg-31, Arg-323, Phe-29, and Ile-160 followed by *ε*-viniferin (**25,** Arg-424, Asp-94, and Glu-102), quercetin-3-*O*-rutinoside (**37**, Arg-323, Asp-321, and Ile-160), chrysophanol (**53**, Ile-160, Asn-162, and Arg-323), and betulinic acid (**63**, Arg-31, Asn-162, and Phe-29) that showed three H-bonds each. The H-bonds, hydrophobic/electrostatic, and Van der Waals amino acid interactions of the docked compounds along with ascorbic acid are summarized in Table 47 and their 2D and 3D interactions are portrayed in Figure 37.

Table 47: Binding affinity, hydrogen bonds, and residual amino acid interactions of the compound isolates and ascorbic acid against human myeloperoxidase.

Compound/ ligand	Binding affinity (kcal/mol)	H-bond	Residual amino acid interactions	
			Hydrophobic/Electrostatic	Van der Waals
			C. adenocaule	
23	-7.5	Arg-323	Arg-323, Arg-31, and Val-30	Asp-321, Pro-34, Leu-33, Asn-162, Phe-29, Ala-35, Trp-32, and Lys-505
25	-7.9	Arg-424, Asp-94, and Glu-102	Arg-239, and Arg-333	Phe-147, Phe-366, Thr-238, His-95, Glu-242, Gln-91, Phe-99, Leu-406, Leu-417, Phe-332, Thr-329, Asp-98, Thr-100, Leu-420, and Phe-407
29	-7.7	Glu-102	Arg-333, Asp-94, His-336, Phe-407, and Arg-239	Phe-366, Glu-242, His-95, Gln-91, Ile-339, Phe-332, Thr-329, Asp-98, Leu-417, Phe-99, Thr-100, Leu-420, Asn-421, and Arg-424
66	-7.5	Gln-91, and Arg-333	Met-87, Arg-239, Arg-333, Asp-94, His-95, His-336, and Gly-90	Gln-88, Leu-338, Gly-335, Phe-332, Thr-329, Asp-98, and Ile-339
			D. regia	
37	-8.9	Arg-323, Asp-321, and Ile-160	Arg-323 and Pro-34	Asn-162, Phe-29, Ala-28, Arg-31, Leu-33, Val-30, Trp-32, Pro-34, Lys-505, and Trp-159
42	-7.9	Arg-31, Arg-323, Phe-29, and Ile-160	Arg-323, Ile-160, and Arg-31	Ala-28, Val-30, Asn-162, Leu-33, Pro-34, Ala-35, and Arg-161
87	-7.6	Arg-323 and Arg-161	Arg-323, Arg-31, and Ile-160	Asn-162, Ile-160, Ala-35, Pro-34, Val-30, and Tyr-37
			S. siamea	
53	-7.5	Ile-160, Asn-162, and Arg-323	Cys-153 and Arg-31	Pro-34, Val-30, Ala-28, Thr-159, Ala-152, and Phe-29
63	-7.4	Arg-31, Asn-162, and Phe-29	__	Lys-505, Asp-321, Pro-34, Arg-323, Trp-32, Ile-160, Ala-35, Ala-28, Val-30, and Arg-31
			Z. spina-christi	
40	-7.0	__	Ala-152, Ala-28 Arg-31, Ile-160, and Cys-153	Cys-153, Ala-152, Thr-159, Asn-162, Arg-323, Val-30, Arg-31, and Arg-161
Ascorbic acid	-8.0	Arg-31, Ala-35, Arg-323, Ile-160, and Arg-161	__	Ala-28, Phe-29, Val-30, Thr-159, Asn-162, and Pro-34

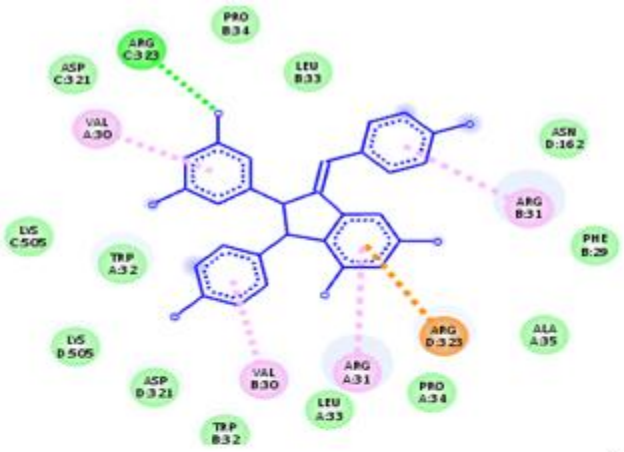
PRO B:34
ARG C:323
ASP C:321
LEU B:33
VAL A:30
ASN D:162
ARG B:31
PHE B:29
LYS C:505
TRP A:32
ARG D:323
ALA A:35
LYS D:505
ASP D:321
VAL B:30
ARG A:31
PRO A:34
LEU A:33
TRP B:32

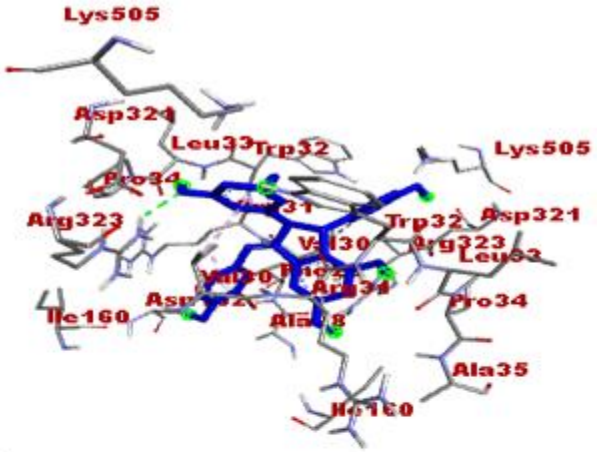
Lys505
Asp324
Leu33
Trp32
Lys505
Pro34
Arg323
Trp32
Asp321
Arg323
Ile160
Pro34
Ala35
Ile160

23

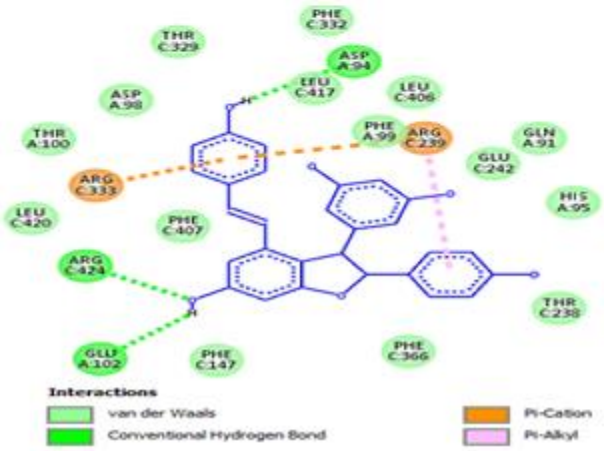
PHE C:332
THR C:329
ASP A:94
LEU C:417
LEU C:406
ASP A:98
THR A:100
PHE A:99
ARG C:239
GLN A:91
GLU C:242
ARG C:333
HIS A:95
LEU C:420
PHE C:407
ARG C:424
THR C:238
GLU A:102
PHE C:147
PHE C:366
Interactions
van der Waals
Conventional Hydrogen Bond
Pi-Cation
Pi-Alkyl

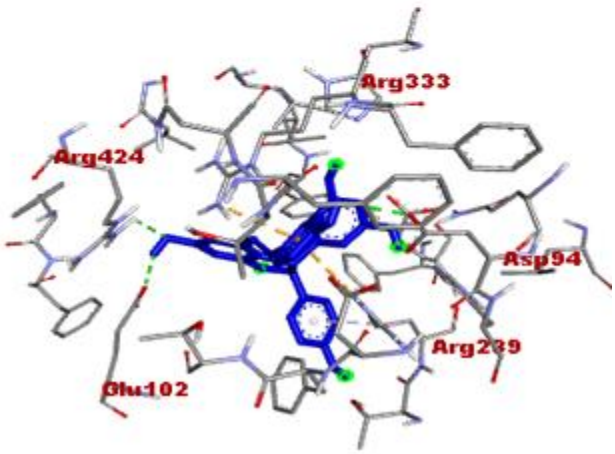
Arg333
Arg424
Asp94
Arg239
Glu102

25

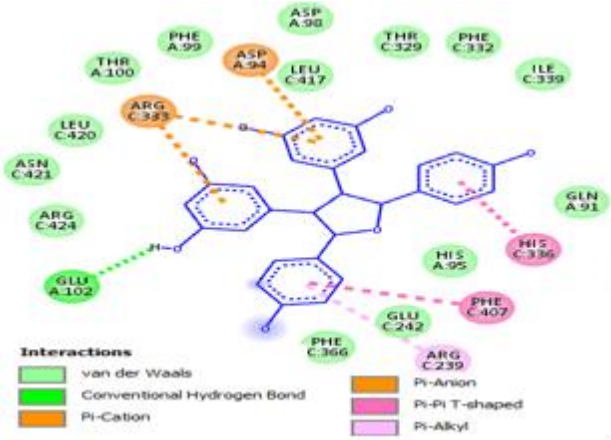
ASP A:90
PHE A:99
THR C:329
PHE C:332
THR A:100
ASP A:94
LEU C:417
ILE C:339
ARG C:333
LEU C:420
ASN C:421
GLN A:91
ARG C:424
HIS C:336
HIS A:95
GLU A:102
PHE C:407
GLU C:242
PHE C:366
ARG C:239
Interactions
van der Waals
Conventional Hydrogen Bond
Pi-Cation
Pi-Anion
Pi-Pi T-shaped
Pi-Alkyl

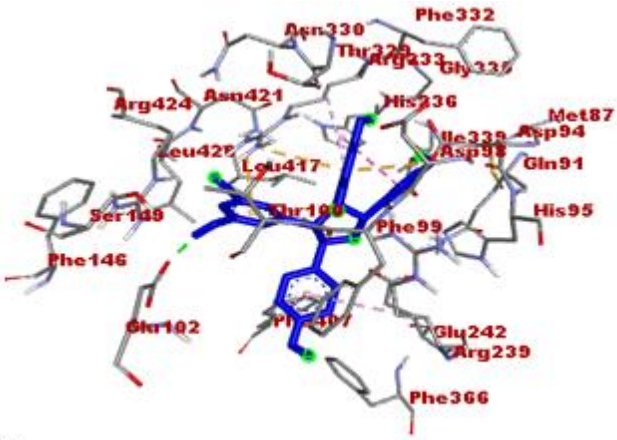
Phe332
Asn330
Arg333
Arg424
Asn421
His336
Met87
Asp94
Leu425
Leu417
Asp93
Gln91
Ser189
Thr190
His95
Phe99
Phe146
Glu102
Glu242
Arg239
Phe366

29

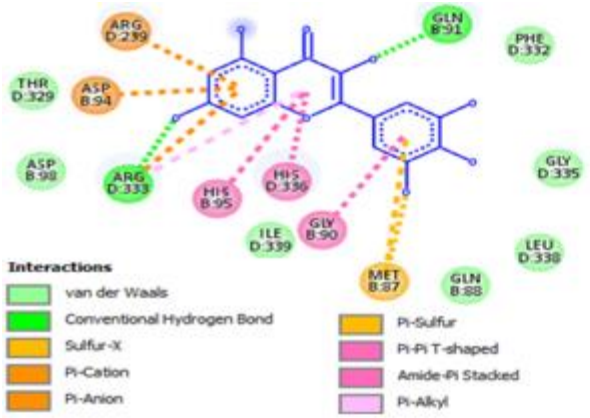
ARG D:239
GLN B:91
PHE D:332
THR D:329
ASP B:94
ASP B:98
ARG D:333
HIS B:95
HIS D:396
GLY D:335
ILE D:339
GLY B:90
LEU D:330
MET B:87
GLN B:88
Interactions
van der Waals
Conventional Hydrogen Bond
Sulfur-X
Pi-Cation
Pi-Anion
Pi-Sulfur
Pi-Pi T-shaped
Amide-Pi Stacked
Pi-Alkyl

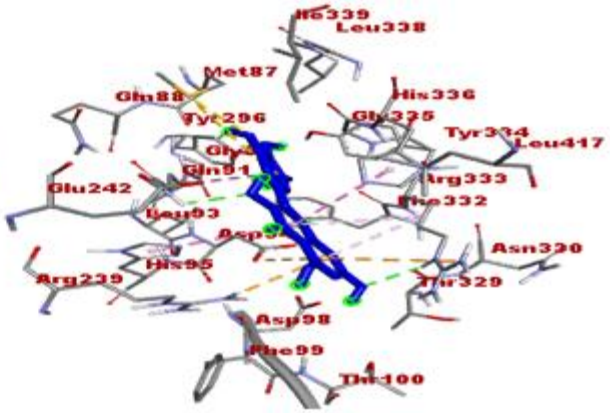
Ile339
Leu338
Met87
Gln88
His336
Tyr296
Glu335
Tyr334
Leu417
Glu242
Arg333
Phe332
Leu93
Asn320
His95
Arg239
Tyr329
Asp98
Phe99
Thr100

66

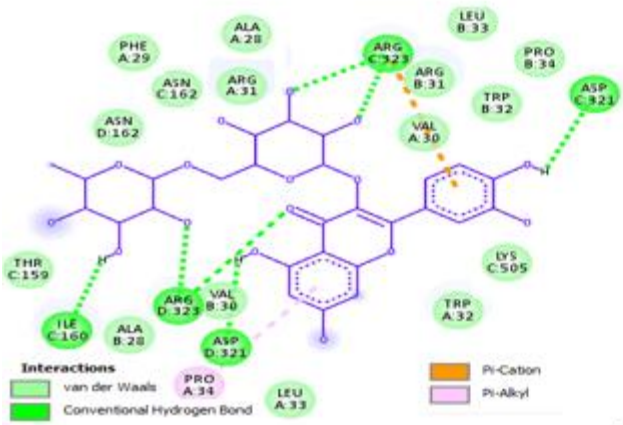
ALA A:28
LEU B:33
PHE A:29
ARG C:323
PRO B:34
ASN C:162
ARG A:31
ARG B:31
TRP B:32
ASP C:321
ASN D:162
VAL A:30
THR C:159
LYS C:505
ARG D:323
VAL B:30
TRP A:32
ILE C:160
ALA B:28
ASP D:321
Interactions
van der Waals
Conventional Hydrogen Bond
PRO A:34
LEU A:33
Pi-Cation
Pi-Alkyl

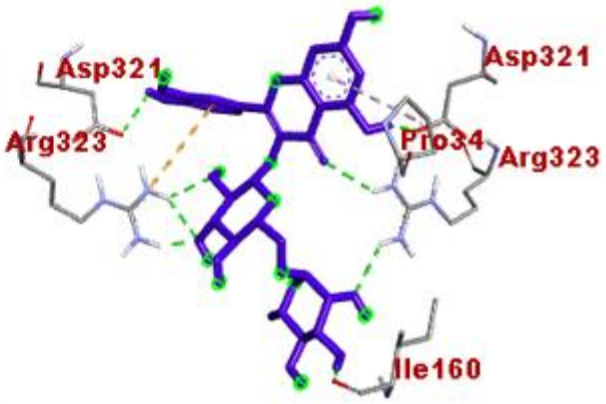
Asp321
Asp321
Arg323
Pro34
Arg323
Ile160

37

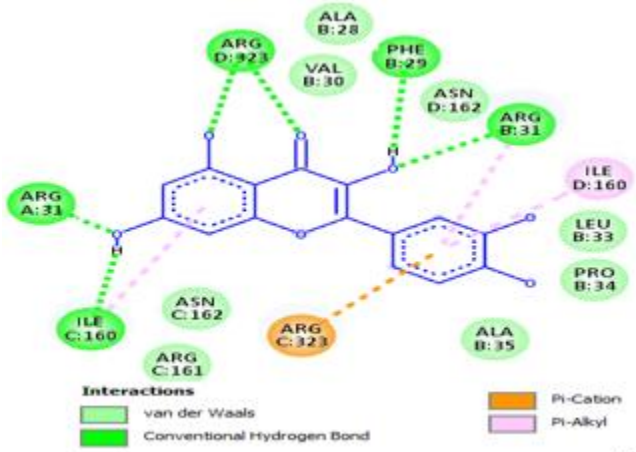
ALA B:28
ARG D:323
PHE B:29
VAL B:30
ASN D:162
ARG B:31
ILE D:160
ARG A:31
LEU B:33
PRO B:34
ASN C:162
ILE C:160
ARG C:323
ALA B:35
ARG C:161
Interactions
van der Waals
Conventional Hydrogen Bond
Pi-Cation
Pi-Alkyl

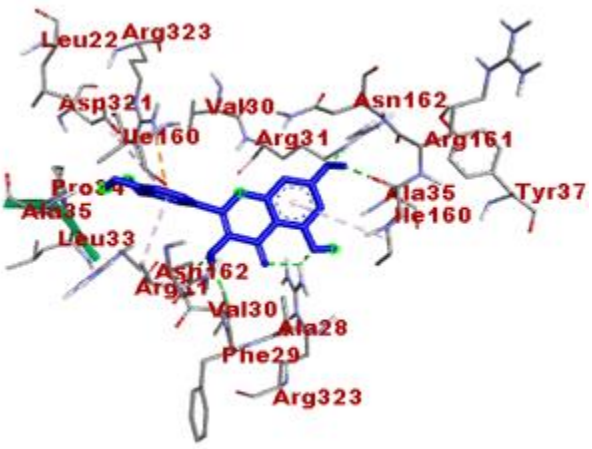
Leu22
Arg323
Asp321
Val30
Asn162
Ile160
Arg31
Arg161
Pro34
Ala35
Tyr37
Ala35
Ile160
Leu33
Asn162
Arg31
Val30
Ala28
Phe29
Arg323

42

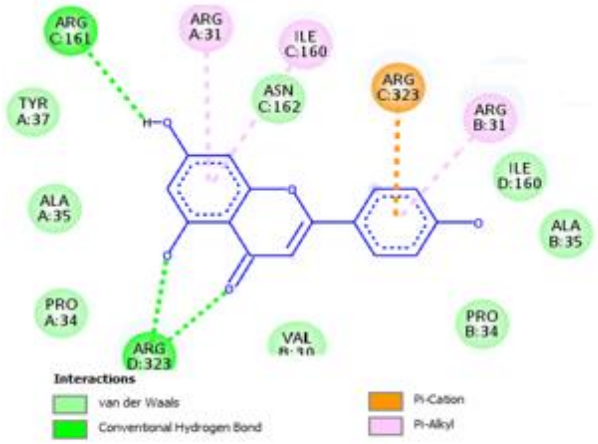
ARG C:161
ARG A:31
ILE C:160
TYR A:37
ASN C:162
ARG C:323
ARG B:31
ILE D:160
ALA A:35
ALA B:35
PRO A:34
PRO B:34
VAL
ARG D:323
Interactions
van der Waals
Conventional Hydrogen Bond
Pi-Cation
Pi-Alkyl

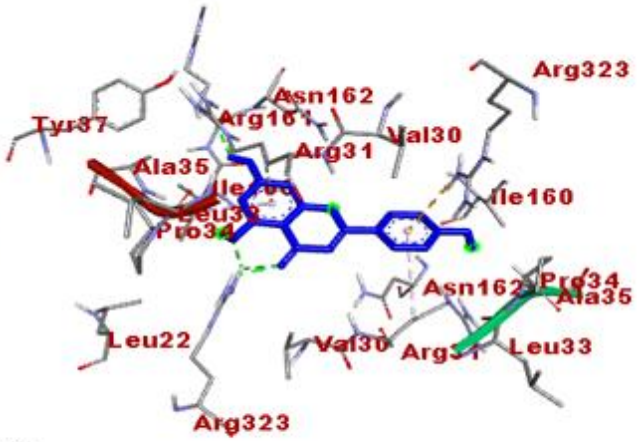
Arg323
Asn162
Tyr37
Arg161
Val30
Arg31
Ala35
Ile160
Leu33
Pro34
Asn162
Pro34
Ala35
Leu22
Val30
Leu33
Arg323

87

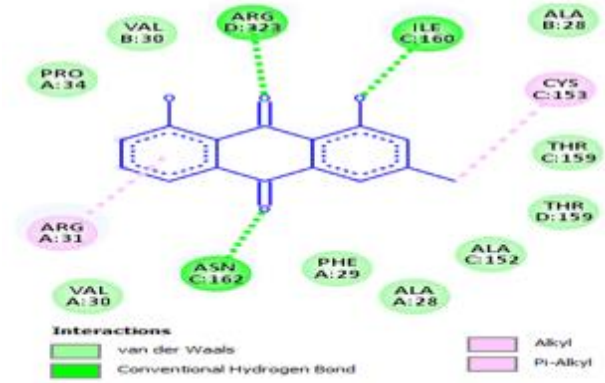
VAL B:30
ARG D:323
ILE C:160
ALA B:28
PRO A:34
CYS C:153
THR C:159
ARG A:31
THR D:159
ASN C:162
PHE A:29
ALA C:152
VAL A:30
ALA A:28
Interactions
van der Waals
Conventional Hydrogen Bond
Alkyl
Pi-Alkyl


Arg323
Phe29
Val30
Arg31
Asn162
Cys153
Cys153
Leu33
Pro34
Ala28
Arg323

53

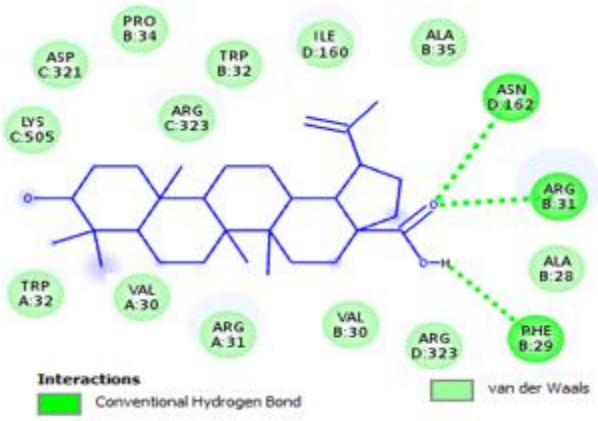
PRO B:34
ASP C:321
TRP B:32
ILE D:160
ALA B:35
ASN D:162
LYS C:505
ARG C:323
ARG B:31
ALA B:28
TRP A:32
VAL A:30
ARG A:31
VAL B:30
ARG D:323
PHE B:29
Interactions
Conventional Hydrogen Bond
van der Waals

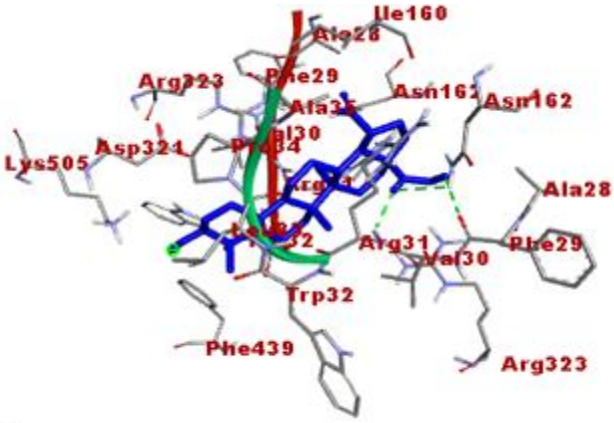
Ile160
Ala28
Arg323
Phe29
Asn162
Asn162
Asp324
Lys505
Ala28
Arg31
Phe29
Val30
Trp32
Phe439
Arg323

63

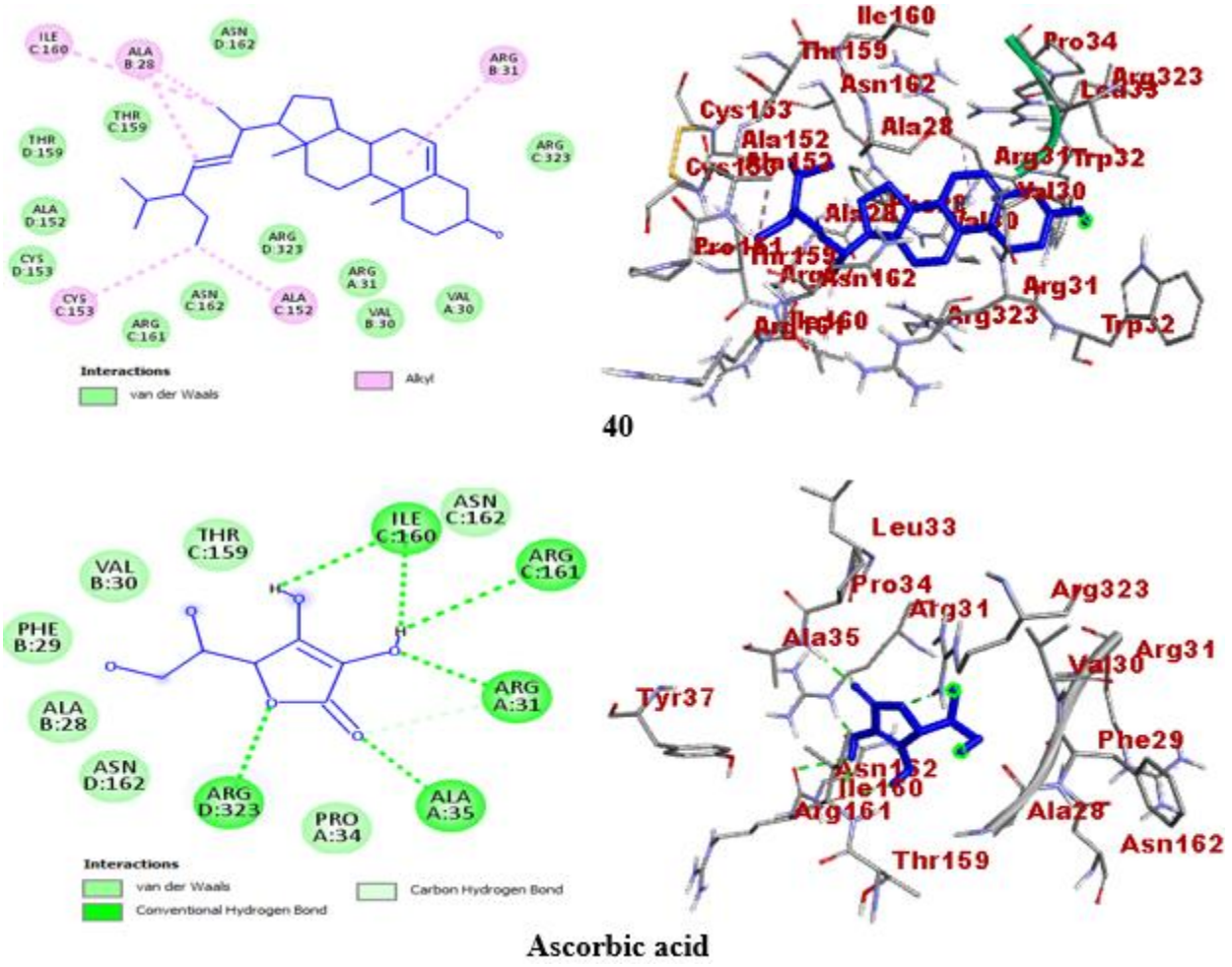

Figure 37: 2D (left) and 3D (right) binding interactions of the compound isolates and ascorbic acid against human myeloperoxidase.

4.4.1.6. Molecular docking study against topoisomerase II*α*

DNA topoisomerase II*α* also encoded by the TOP2A gene is a human enzyme that manages topological DNA stress during transcription. It catalyzes the momentary breaking and recombining of two strands of DNA duplex which permits the strands to pass through each other. Mammalian cells are comprised of two isoforms of the protein named topoisomerase II*α* and topoisomerase II*β,* and most reports suggest that the former is a primary drug target. The alpha gene form is confined in chromosome 17 and the beta form is found in chromosome 3. This enzyme functions as a target in many chemotherapy investigations and a range of mutations in this gene are related to the growth of drug resistance (Deweese and Osheroff, 2009). Emerging investigations have explained that TOP2A is perversely involved in various solid tumors, including lung adenocarcinoma, cervical cancer, and bladder urothelial carcinoma (Kou *et al.*, 2020, Zeng *et al.*,

2019). A high level of TOP2A is associated with unflattering prospects in hepatocellular carcinoma (Cai *et al.*, 2020). The prognostic and clinical values of TOP2A have also been adequately confirmed in nasopharyngeal carcinoma, breast carcinoma, and pancreatic cancer (Lan *et al.*, 2014).

In this investigation, an *in silico* molecular docking study of the compound isolates along with the etoposide standard was performed and the binding affinities, H-bonds, and important residual amino acid interactions of the ligands and the receptor are clearly addressed. The docking results showed that *ε*-viniferin (**25**) exhibited the most stable binding affinity (-9.9 kcal/mol) followed by lupeol (**39**) and parthenocissin A (**23**) (-9.2 kcal/mol each). Remarkably, *ε*-viniferin (**25**) showed a greater binding score than the etoposide standard (-9.4 kcal/mol). Furthermore, all the docked compounds formed at least one H-bond with the amino acids of the target protein showcasing their stability. Quercetin-3-*O*-rutinoside (**37**) formed the maximum (six) number of H-bonds with Ile-715, Glu-839, His-759, Glu-837, Ser-717, and Gly-1007 followed by *ε*-viniferin (**25**) that formed five H-bonds with Asp-831, Glu-839, His-1005, Glu-712, and Ile-715 (Table 48 and Figure 38).

Table 48: Binding affinity, hydrogen bonds, and residual amino acid interactions of the compound isolates and etoposide against topoisomerase IIα.

Compound/ ligand	Binding affinity (kcal/mol)	H-bond	Residual amino acid interactions	
			Hydrophobic/Electro static	Van der Waals
		C. adenocaule		
23	-9.2	Arg-673, Gly-1007, Arg-727, and Glu-837	Leu-829, Pro-724, and Glu-712	Pro-838, Glu-839, Asp-831, Lys-827, Lys-676, Arg-672, Phe-1003, Lys-723, Pro-716, Leu-722, Ile-715, and Ser-717
25	-9.9	Asp-831, Glu-839, His-1005, Glu-712, and Ile-715	Arg-672, Glu-712, Glu-839, Phe-1003 Pro-724, and Leu-829	Met-669, Arg-673, Gly-1007, Asn-708, Lys-676, Trp-840, Lys-728, Glu-837, Arg-727, Lys-723, Pro-716, and Ser-717
29	-8.7	Met-669, Glu-839, and Glu-712	Arg-672, Arg-673, Glu-712, Phe-1003, Met-669, and Pro-724	Trp-840, Leu-829, Glu-837, Arg-727, Ser-717, Leu-722, Pro-716, Lys-723, Ile-715, Gly-1007, Asn-708, Lys-676, Val-1006, and Lys-827
66	-7.5	Gly-1007 and Met-669	Arg-672, Arg-673, Glu-712, and Phe-1003	Pro-724, Arg-727, Ser-717, Lys-676, and Cys-1008
		D. regia		
37	-8.7	Ile-715, Glu-839, His-759, Glu-837, Ser-717, and Gly-1007	Arg-672, Arg-673, Glu-712, and Phe-1003	Lys-728, Leu-829, Pro-838, Arg-727, Trp-840, Pro-716, Met-669, Pro-720, Lys-676, Ser-709, and Arg-713
42	-7.9	Glu-839 and Glu-712	Arg-672, Arg-673, Glu-712, and Phe-1003	Arg-727, Ser-717, Trp-840, Val-1006, His-1005, Gly-1007, Lys-676, Lys-723, Pro-724, Pro-716, and Ile-715
87	-8.4	Arg-672	Arg-673, Glu-712, and Phe-1003	Ser-717, Pro-716, Arg-727, Lys-723, Pro-724, Leu-722, Ile-715, Gly-1007, Lys-676, Lys-827, and Glu-839
		S. siamea		
39	-9.2	Ser-717	Phe-1003	Asp-1004, Gly-1007, Arg-727, Glu-712, Pro-724, Ser-709, Arg-713, Lys-728, Asp-831, Leu-829, Glu-839, and Trp-840
53	-8.3	Gln-544 and Leu-685	Pro-593 and Leu-705	Tyr-684, Asp-683, Glu-682, Arg-672, Leu-592, Gln-542, Tyr-590, Tyr-686, and Ser-591
63	-7.9	Glu-839 and His-758	Leu-829	Lys-728, Asp-831, Pro-838, Trp-840, Arg-727, Glu-837, Pro-724, Glu-712, Tyr-757, and His-759
Etoposide	-9.4	Gln-544, Arg-727, Ser-756, Pro-838, Glu-837, and Glu-712	Lys-728, Lys-614, and His-758	Asp-832, Val-836, Asp-831, Pro-724, Leu-829, Glu-839, Trp-840, Gly-1007, Glu-712, Arg-713, Ser-709, and His-759

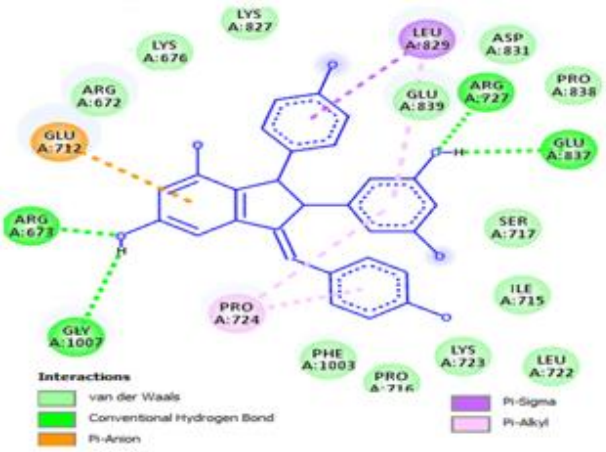
LYS A:827
LYS A:676
ARG A:672
GLU A:712
ARG A:673
GLY A:1007
LEU A:829
ASP A:831
PRO A:838
GLU A:839
ARG A:727
GLU A:837
SER A:717
ILE A:715
PRO A:724
PHE A:1003
LYS A:723
PRO A:716
LEU A:722
Interactions
van der Waals
Conventional Hydrogen Bond
Pi-Anion
Pi-Sigma
Pi-Alkyl

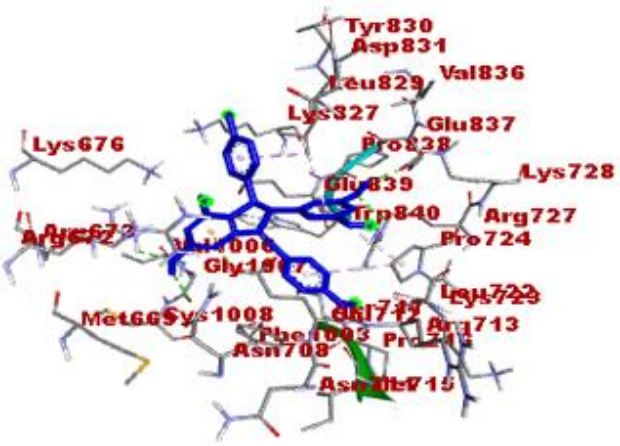
Tyr830
Asp831
Val836
Leu829
Lys827
Glu837
Lys676
Pro838
Lys728
Glu839
Trp840
Arg727
Pro724
Met669
Lys1008
Phe1003
Asn708
Arg713
Lys723
Leu722

23

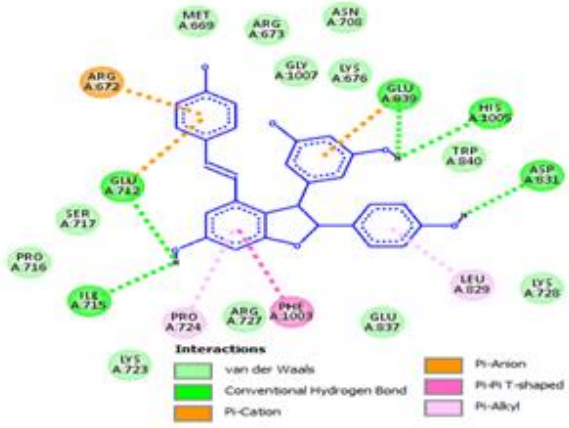
MET A:669
ARG A:673
ASN A:708
GLY A:1007
LYS A:676
ARG A:672
GLU A:839
HIS A:1005
TRP A:840
GLU A:742
ASP A:831
SER A:717
PRO A:716
ILE A:715
LEU A:829
LYS A:726
PRO A:724
ARG A:727
PHE A:1003
GLU A:837
LYS A:723
Interactions
van der Waals
Conventional Hydrogen Bond
Pi-Cation
Pi-Anion
Pi-Pi T-shaped
Pi-Alkyl

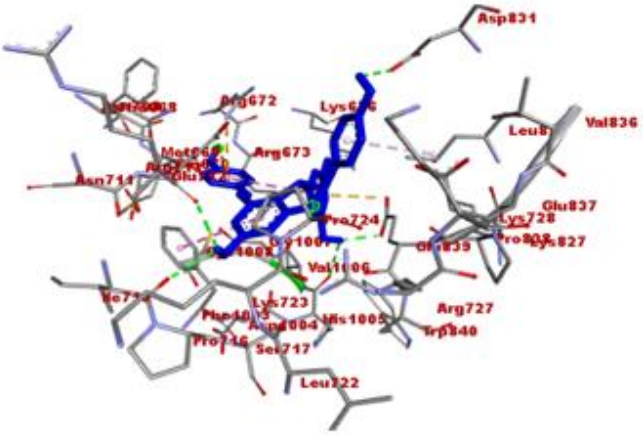
Asp831
Arg672
Lys676
Leu8
Val836
Arg673
Asn714
Glu837
Pro724
Lys728
Lys827
Val1006
Arg727
Lys723
Trp840
Leu722

25

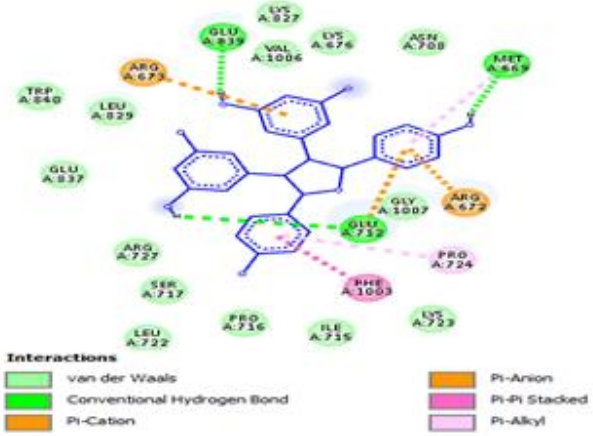
LYS A:827
GLU A:839
VAL A:1006
LYS A:676
ASN A:708
MET A:669
ARG A:673
TRP A:840
LEU A:829
GLU A:837
GLY A:1007
ARG A:672
GLY A:732
ARG A:727
PRO A:724
SER A:717
PHE A:1003
PRO A:716
ILE A:715
LYS A:723
LEU A:722
Interactions
van der Waals
Conventional Hydrogen Bond
Pi-Cation
Pi-Anion
Pi-Pi Stacked
Pi-Alkyl

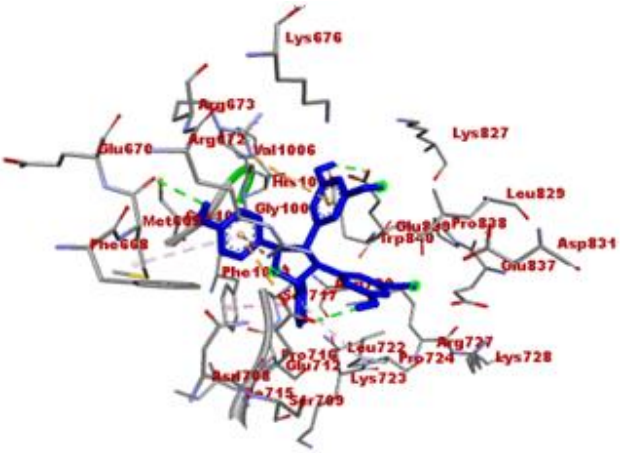
Lys676
Arg673
Glu670
Arg672
Val1006
Lys827
Leu829
Gly1007
Met669
Pro838
Asp831
Phe668
Glu837
Leu722
Arg727
Pro724
Lys728
Glu712
Lys723
Asn708

29

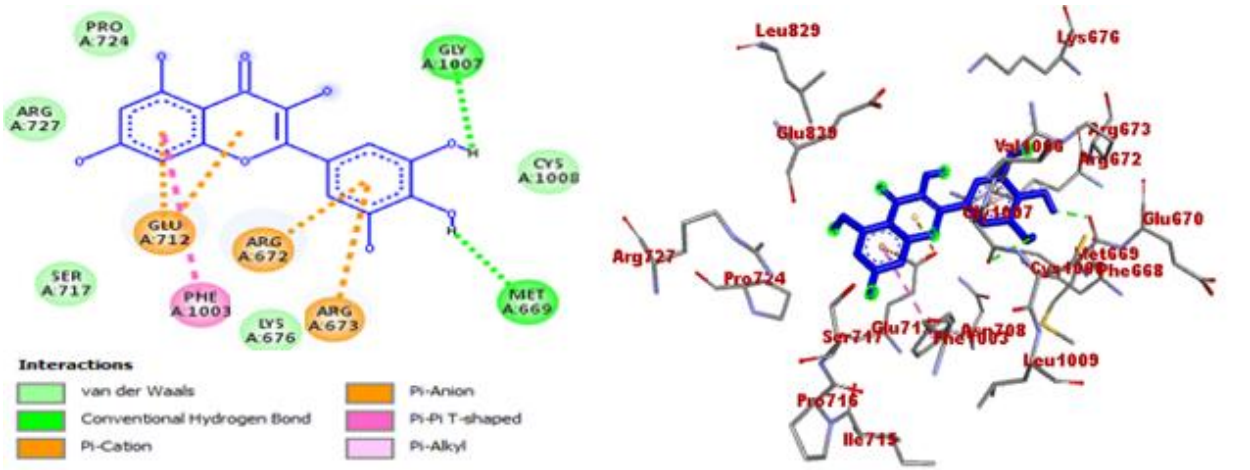
PRO A:724
GLY A:1007
ARG A:727
CYS A:1008
GLU A:712
ARG A:672
SER A:717
PHE A:1003
MET A:669
LYS A:676
ARG A:673
Interactions
van der Waals
Conventional Hydrogen Bond
Pi-Cation
Pi-Anion
Pi-Pi T-shaped
Pi-Alkyl
Leu829
Lys676
Glu839
Arg673
Arg672
Glu670
Arg727
Pro724
Met669
Phe668
Ser717
Leu1009
Pro716
Ile715

66

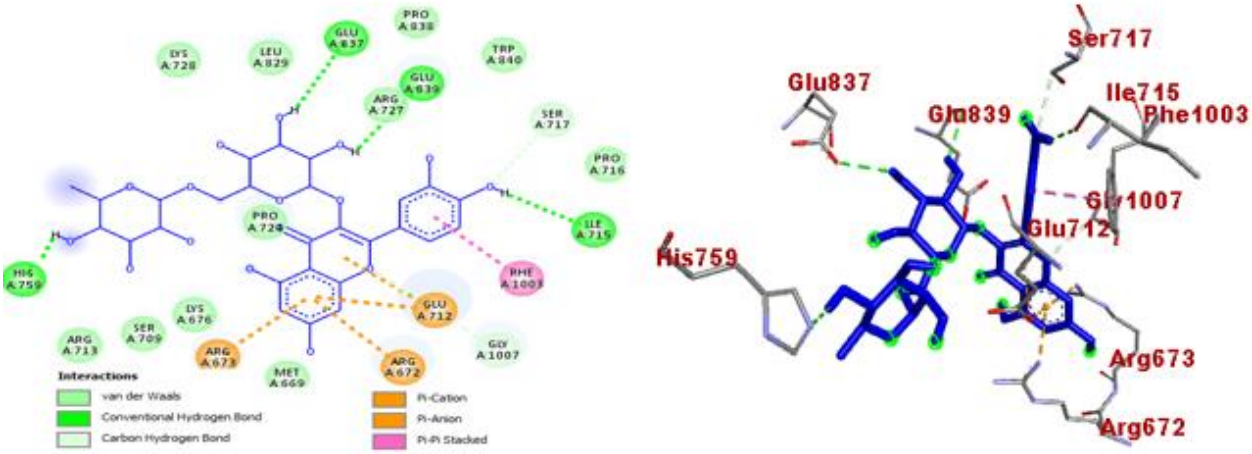
Ser717
Glu837
Ile715
Glu839
Phe1003
Glu712
His759
Arg673
Arg672
Interactions
van der Waals
Conventional Hydrogen Bond
Carbon Hydrogen Bond
Pi-Cation
Pi-Anion
Pi-Pi Stacked

37

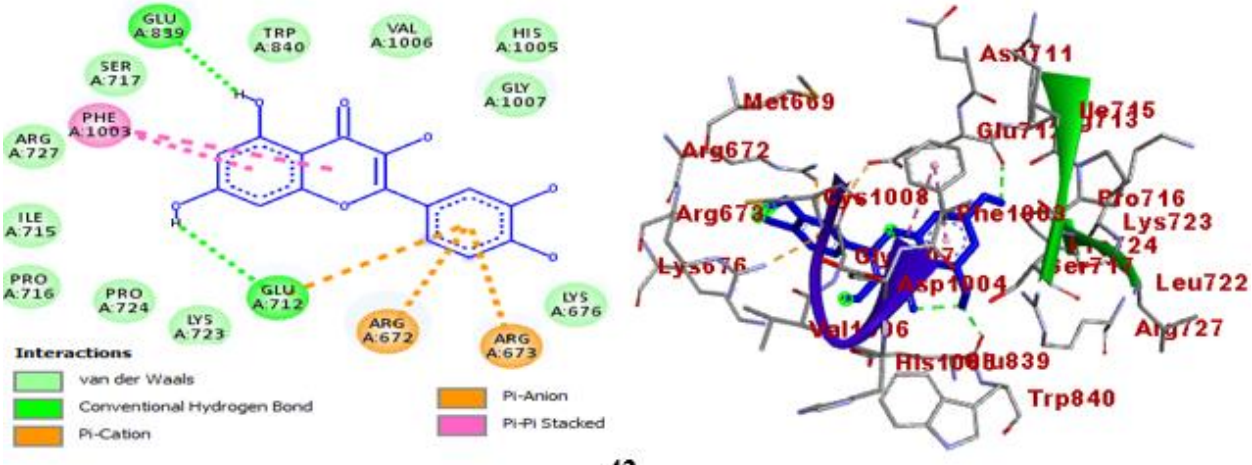
GLU A:839
TRP A:840
VAL A:1006
HIS A:1005
SER A:717
GLY A:1007
PHE A:1003
ARG A:727
ILE A:715
PRO A:716
PRO A:724
LYS A:723
GLU A:712
ARG A:672
ARG A:673
LYS A:676
Interactions
van der Waals
Conventional Hydrogen Bond
Pi-Cation
Pi-Anion
Pi-Pi Stacked
Asp711
Met669
Ile715
Arg672
Arg673
Cys1008
Pro716
Lys723
Lys676
Asp1004
Leu722
Arg727
Trp840

42

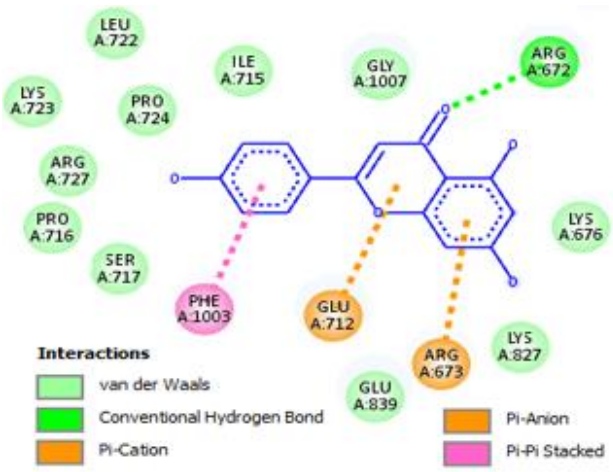
LEU A:722
ILE A:715
GLY A:1007
ARG A:672
LYS A:723
PRO A:724
ARG A:727
PRO A:716
SER A:717
LYS A:676
PHE A:1003
GLU A:712
ARG A:673
LYS A:827
GLU A:839
Interactions
van der Waals
Conventional Hydrogen Bond
Pi-Cation
Pi-Anion
Pi-Pi Stacked

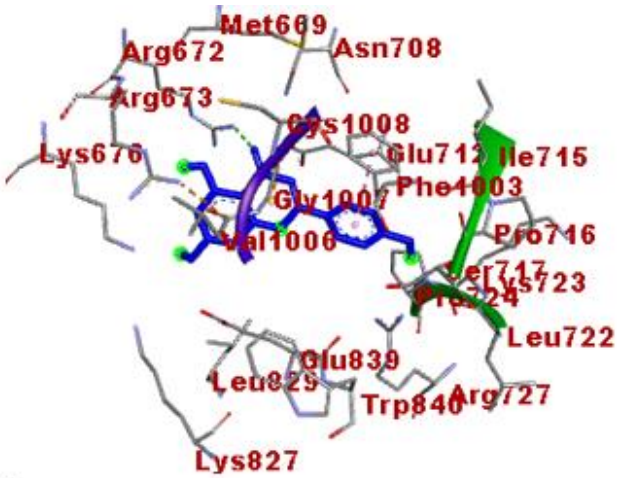
Met669
Arg672
Asn708
Arg673
Lys676
Glu712
Ile715
Phe1003
Pro716
Leu722
Glu839
Leu829
Trp840
Arg727
Lys827

87

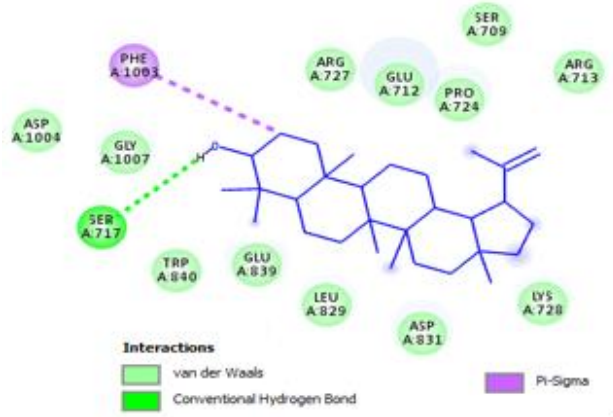
SER A:709
PHE A:1003
ARG A:727
GLU A:712
ARG A:713
PRO A:724
ASP A:1004
GLY A:1007
SER A:717
TRP A:840
GLU A:839
LEU A:829
LYS A:728
ASP A:831
Interactions
van der Waals
Conventional Hydrogen Bond
Pi-Sigma

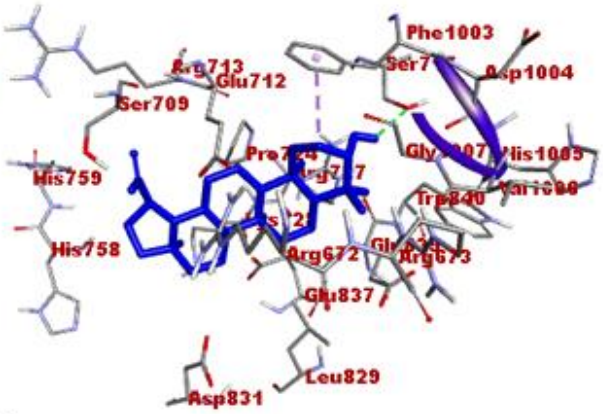
Phe1003
Arg713
Glu712
Ser709
Asp1004
His759
His758
Arg672
Arg673
Glu837
Leu829
Asp831

39

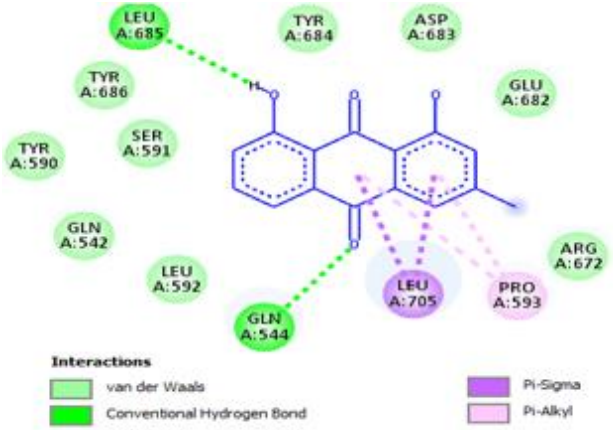
LEU A:685
TYR A:684
ASP A:683
TYR A:686
GLU A:682
SER A:591
TYR A:590
GLN A:542
LEU A:592
ARG A:672
LEU A:705
PRO A:593
GLN A:544
Interactions
van der Waals
Conventional Hydrogen Bond
Pi-Sigma
Pi-Alkyl

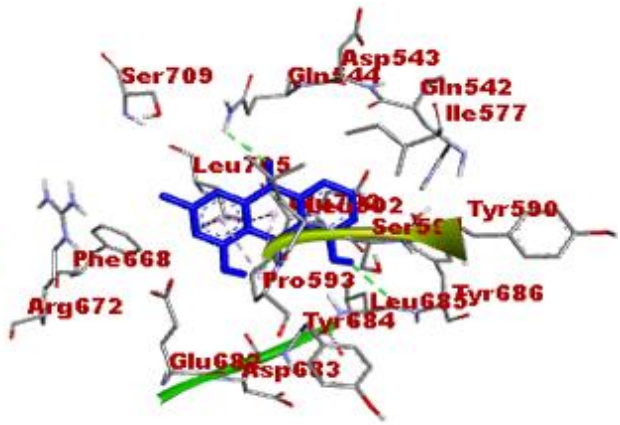
Asp543
Ser709
Gln544
Gln542
Ile577
Tyr590
Phe668
Pro593
Tyr686
Arg672
Tyr684
Asp683

53

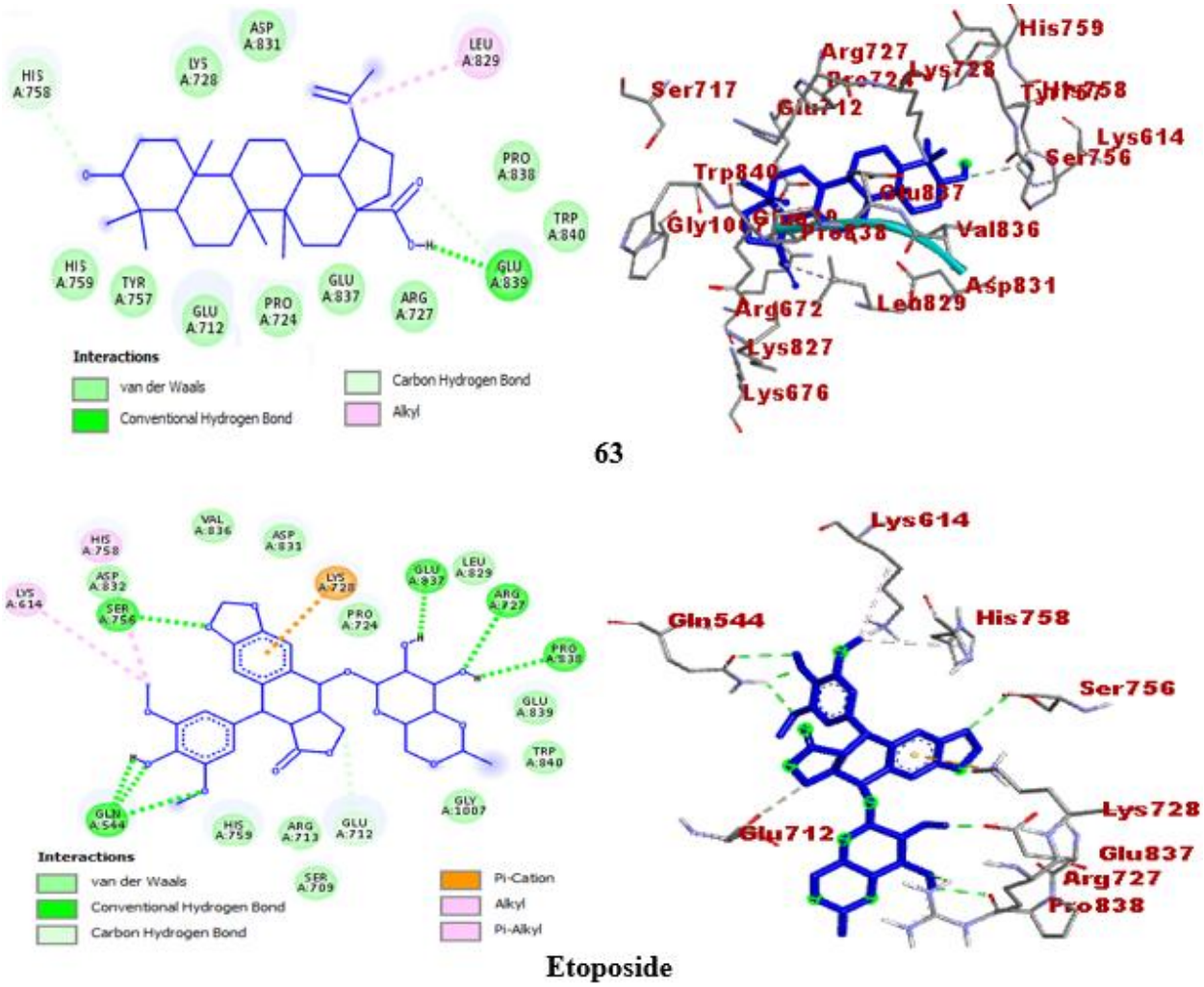

Figure 38: 2D (left) and 3D (right) binding interactions of the compound isolates and etoposide against topoisomerase II*α*.

4.4.2. *In silico* pharmacokinetics (drug-likeness and ADME) and toxicity analysis

Many drugs fail to enter the market due to the fact that they exhibit poor pharmacokinetic profiles. This has demanded the study of pharmacokinetic contemplations at earlier stages of drug development strategies (Hodgson, 2001). This necessitates the quest for lead compounds that are orally absorbed, easily reach the preferred site of action, are unable to produce toxic products before getting to the site of action, and are easily eliminated after hitting the target. An appropriate term for the sum of the above parameters is the ADMET (absorption, distribution, metabolism, elimination, and toxicity) properties (Hodgson, 2001). In modern drug discovery, computer-based approaches have been used to predict the ADMET properties of drug candidates at early stages which have become progressively popular (Paul Gleeson *et al.*, 2011). The basis behind *in silico*

methods are the relative small time and cheap cost needed compared to experimental *in vitro* and *in vivo* approaches for ADMET properties. For example, it takes a minute in a computational model to screen 20,000 molecules than an experimental investigation which can take up to 5 months to do the same task. Thus, an auspicious lead compound is measured by its potency and commendable ADMET properties (also known as a compound's CV). Conversely, compounds with tedious ADMET predictions may be withdrawn from the list of possible drug candidates (Hou and Wang, 2008).

4.4.2.1. Drug-likeness

In this study, the drug-likeness predictions of the compound isolates were anticipated by adopting Lipinski's rule of five (Lipinski *et al.*, 2012) and Veber's rule (Veber *et al.*, 2002). Compounds that afford MW < 500 Daltons, LogP (iLogP) < 5, NHD < 5, and NHA < 10 favor Lipinski's rule of 5, and their drug candidacy is likely. In addition, compounds with TPSA < 140 and NRB < 10 favor Veber's rule and possess good oral bioavailability. Compounds with zero or one Lipinski's violation afford drug candidacy. Thus, all the compound isolates except quercetin-3-*O*-rutinoside (**37**), *β*-sitosteryl palmitate (**84**), and *β*-sitosteryl-3*β*-glucopyranoside-6'-*O*-palmitate (**86**) whom drug-likeness properties are predicted fulfilled Lipinski's rule with zero/one violation each and were in favor of the drug-likeness properties. Furthermore, all the compounds except quercetin-3-*O*-rutinoside (**37**), myricetin (**66**), *β*-sitosteryl palmitate (**84**), *β*-sitosteryl-3*β*-glucopyranoside-6'-*O*-palmitate (**86**), and glyceryl-1-hexacosanoate (**88**) satisfied Veber's rule with TPSA < 140 and NRB < 10. *β*-sitosteryl palmitate (**84**) revealed two Lipinski's (MW>500 and iLogP >5) and one Veber's (NRB>10) violations. Quercetin-3-*O*-rutinoside (**37**) was predicted with three Lipinski's (MW>500, NHD>5, and NHA>10) and one Veber's (TPSA>140 Å) violations. Whereas, *β*-sitosteryl-3*β*-glucopyranoside-6'-*O*-palmitate (**86**) was predicted with two Lipinski's (MW>500 and iLogP >5) and one Veber's (NRB>10) violations (Table 49).

Notably, drug molecules possessing molecular weight <500 Da are easily transported, absorbed, and diffused (Lipinski, 2004). Thereby, all the compounds excluding quercetin-3-*O*-rutinoside (**37**), *β*-sitosteryl palmitate (**84**), and *β*-sitosteryl-3*β*-glucopyranoside-6'-*O*-palmitate (**86**) exhibited MW<500 Da suggested their safe transportation, absorption, and diffusion after administration. The affinity of compounds to lipophilic properties is related to their LogP values

(Daina *et al.*, 2017). Hence, all the compounds except *β*-sitosteryl palmitate (**84**), *β*-sitosteryl-3*β*-glucopyranoside-6'-*O*-palmitate (**86**), and glyceryl-1-hexacosanoate (**88**) showed iLogP<5 values suggesting their optimum lipophilicity. In addition, the number of rotatable bonds (NRB) were computed to be < 10 for most of the compounds signifying their conformation stability (Anza *et al.*, 2021). Pharmacokinetic predictions of drug candidates also showed that the values of the total polar surface area (TPSA) predict the permeability and bioavailability of a molecule. Accordingly, except myricetin (**66**) and quercetin-3-*O*-rutinoside (**37**), all the predicted compounds revealed TPSA< 140 $Å^2$ indicating their safe absorption in the intestine (Table 49).

Table 49: *In silico* drug-likeness predictions of the compound isolates computed by SwissADME.

Compounds	MF	MW (g/mol)	NHD	NHA	NRB	LogP (iLogP)	TPSA ($Å^2$)	LRo5 (violation)	VR (violation)
				C. adenocaule					
19	$C_{29}H_{50}O$	414.71	1	1	6	4.79	20.23	0	0
23	$C_{28}H_{22}O_6$	454.47	6	6	3	2.25	121.38	1	0
25	$C_{28}H_{22}O_6$	454.47	5	6	4	2.41	110.38	0	0
28	$C_{20}H_{30}O_3$	318.45	1	3	0	2.92	46.53	0	0
29	$C_{28}H_{24}O_7$	472.49	6	7	4	2.04	130.61	1	0
66	$C_{15}H_{10}O_8$	318.24	6	8	1	1.08	151.59	1	1
84	$C_{45}H_{80}O_2$	653.12	0	2	22	8.67	26.30	2	1
				D. regia					
37	$C_{27}H_{30}O_{16}$	610.52	10	16	6	1.58	269.43	3	1
40	$C_{29}H_{48}O$	412.69	1	1	5	5.01	20.23	0	0
42	$C_{15}H_{10}O_7$	302.24	5	7	1	1.63	131.36	0	0
86	$C_{51}H_{90}O_7$	815.26	3	7	25	8.45	105.45	2	1
87	$C_{15}H_{10}O_5$	270.24	3	5	1	1.89	90.90	0	0
				S. siamea					
39	$C_{30}H_{50}O$	426.72	1	1	1	4.72	20.23	0	0
53	$C_{15}H_{10}O_4$	254.24	2	4	0	2.22	74.60	0	0
63	$C_{30}H_{48}O_3$	456.70	2	3	2	3.83	57.53	0	0
88	$C_{29}H_{58}O_4$	470.77	2	4	28	6.64	66.76	1	1
89	$C_{22}H_{16}O_6$	376.36	4	6	2	2.27	115.06	0	0
Cipro.	$C_{17}H_{18}FN_3O_3$	331.34	2	5	3	2.24	74.57	0	0

Cipro; ciprofloxacin, MF; molecular formula, MW; molecular weight, LRo5; Lipinski's rule of 5, NHA; number of hydrogen acceptors, NHD; number of hydrogen donors, NRB; number of rotatable bonds, TPSA; total polar surface area, VR; Veber's rule.

4.4.2.2. ADME properties

The ADME properties of most of the compound isolates were predicted and the main ADME parameters including blood-brain barrier (BBB) permeability, gastrointestinal absorption, skin permeation (logKp), transporter P-glycoprotein (P-gp), and drug-mobilizing CYP450 isoforms (CYP1A2, CYP2C9, CYP2C19, CYP2D6, and CYP3A4) inhibitions were computed to study the pharmacokinetic properties of the compounds. The prediction results showed that the LogKp (cm/s) values of the investigated compounds were computed within the range of -10.26 up to 1.96 cm/s. Pharmacokinetic studies affirmed that the skin permeant of drug molecules is inversely correlated with the LogKp values. The more negative the LogKp, the less skin permeant the drug molecule (Daina *et al.*, 2017). Accordingly, parthenocissin A (**23**, -5.60 cm/s), *ε*-viniferin (**25**, -5.24 cm/s), tricuspidatol A (**29**, -6.14 cm/s), myricetin (**66**, -7.40 cm/s), quercetin-3-*O*-rutinoside (**37**, -10.26 cm/s), quercetin (**42**, -7.05 cm/s), apigenin (**87**, -5.80 cm/s), chrysophanol (**53**, -5.34 cm/s), and 4-(2'-hydroxymethyl-4'-hydroxyphenyl)-chrysophanol (**89**, -6.14 cm/s) showed comparable LogKp values with ciprofloxacin (-9.09 cm/s) and hence less skin permeant properties. *ε*-Viniferin (**25**), 3-hydroxy isoagatholactone (**28**), quercetin (**42**), apigenin (**87**), chrysophanol (**53**), and 4-(2'-hydroxymethyl-4'-hydroxyphenyl)-chrysophanol (**89**) were predicted with high gastrointestinal absorption (GIA) in accordance with the prediction values of ciprofloxacin (high). High values of blood-brain barrier (BBB) and gastrointestinal absorption (GIA) suggest favorable absorption and distribution properties of drug molecules (Anza *et al.*, 2021). All the compounds except quercetin-3-*O*-rutinoside (**37**), *β*-sitosteryl palmitate (**84**), and *β*-sitosteryl-3*β*-glucopyranoside-6'-*O*-palmitate (**86**) were predicted non-substrates of permeability glycoprotein (P-gp), and hence non-inhibitors of most of the cytochromes (CYP). Notably, quercetin (**42**) and apigenin (**87**) inhibited three cytochromes (CYP1A2, CYP2D6, and CYP3A4) each, and 4-(2'-hydroxymethyl-4'-hydroxyphenyl)-chrysophanol (**89**) inhibited almost all the predicted cytochromes (CYP1A2, CYP2C9, CYP2D6, and CYP3A4) (Table 50).

Table 50: ADME predictions of the compound isolates computed by SwissADME.

Compounds	LogKp (cm/s)	GIA	BBB	Inhibitor interaction					
				P-gp substrate	CYP1A2	CYP2C19	CYP2C9	CYP2D6	CYP3A4
C. adenocaule									
19	-2.20	Low	No	No	No	No	No	No	No
23	-5.60	Low	No	No	No	No	No	No	No
25	-5.24	High	No	No	No	No	Yes	No	No
28	-5.23	High	Yes	No	No	No	Yes	No	No
29	-6.14	Low	No	No	No	No	No	No	Yes
66	-7.40	Low	No	No	Yes	No	No	No	Yes
84	1.96	Low	No	Yes	No	No	No	No	No
D. regia									
37	-10.26	Low	No	Yes	No	No	No	No	No
40	-2.74	Low	No	No	No	No	Yes	No	No
42	-7.05	High	No	No	Yes	No	No	Yes	Yes
86	-0.56	Low	No	Yes	No	No	No	No	Yes
87	-5.80	High	No	No	Yes	No	No	Yes	Yes
S. siamea									
39	-1.90	Low	No	No	No	No	No	No	No
53	-5.34	High	Yes	No	Yes	No	No	No	Yes
63	-3.26	Low	No	No	No	No	Yes	No	No
88	-0.83	Low	No	No	No	No	No	No	No
89	-6.14	High	No	No	Yes	No	Yes	Yes	Yes
Cipro.	-9.09	High	No	Yes	No	No	No	No	No

BBB; blood-brain barrier, Cipro; ciprofloxacin, CYP; cytochrome-P450, 1A2; family 1 subfamily A member 2, 2C19; family 2 subfamily C member 19, 2C9; family 2 subfamily C member 9, 2D6; family 2 subfamily D member 6, 3A4; family 3 subfamily A member 4, GIA; gastrointestinal absorption, LogKp; skin permeation value, P-gp; p glycoprotein.

The drug-likeness properties of parthenocissin A (**23**), ε-viniferin (**25**), 3-hydroxy isoagatholactone (**28**), tricuspidatol A (**29**), lupeol (**39**), quercetin (**42**), chrysophanol (**53**), betulinic acid (**63**), myricetin (**66**), and apigenin (**87**) were supported by bioavailability radar predictions. The insolubility (INSOLU), lipophilicity (LIPO), polar surface area (POLAR), rotatable bonds (FLEX), molecular weight (SIZE), and optimal area for unsaturation (INSATU) properties were displayed in the bioavailability radar (Figures 39 and 40). Drug-like molecules are suggested to exhibit SIZE (MW) < 500 g/mol, -6 < INSOLU (Log S) < 0, 0 < FLEX (NRB) < 9, -0.7 < LIPO (Log P) < 5, 20 $Å^2$ < POLAR (TPSA) < 140 $Å^2$ and 0.25 < INSATU (fraction Csp3)

< 1 prediction (Islam and Pillay, 2019). Except the INSOLU values of parthenocissin A (**23,** Log S: -6.06), *ε*-viniferin (**25,** Log S: -6.32), lupeol (**39**, Log S: -8.64), and betulinic acid (**63**, Log S: -7.71), POLAR value of myricetin (**66**, TPSA: 151.59 $Å^2$), INSATU values of quercetin (**42**, Csp3: 0.00), myricetin (**66**, Csp3: 0.00), and apigenin (**87**, Csp3: 0.00), the radar plots showed drug-like properties for all the investigated compounds.

In addition, the pharmacokinetic properties of the compounds were established using the BOILED-Egg model to explain the human intestinal absorption (HIA) and blood-brain barrier (BBB) characteristics. Compounds with high BBB penetration and HIA are located in the yolk (yellow) and albumin (white) regions, respectively (Islam and Pillay, 2019). Accordingly, 3-hydroxy isoagatholactone (**28**) and chrysophanol (**53**) were located inside the yolk region explaining their high penetration in the brain and good absorption in the gastrointestinal. Whereas, *ε*-viniferin (**25**), quercetin (**42**), and apigenin (**87**) were located inside the albumin (white) region showcasing their passive absorption by the gastrointestinal tract. Conversely, parthenocissin A (**23**), tricuspidatol A (**29**), lupeol (**39**), betulinic acid (**63**), and myricetin (**66**) located outside the BOILED-Egg explain their poor penetration and absorption. Furthermore, all the compounds in the BOILED-Egg were designated along with a red circle describing their non-substrate (PGP-) properties (Figure 40). Thus, the bioavailability radar and BOILED-Egg model predictions of the investigated compounds suggest their possible drug-like properties.

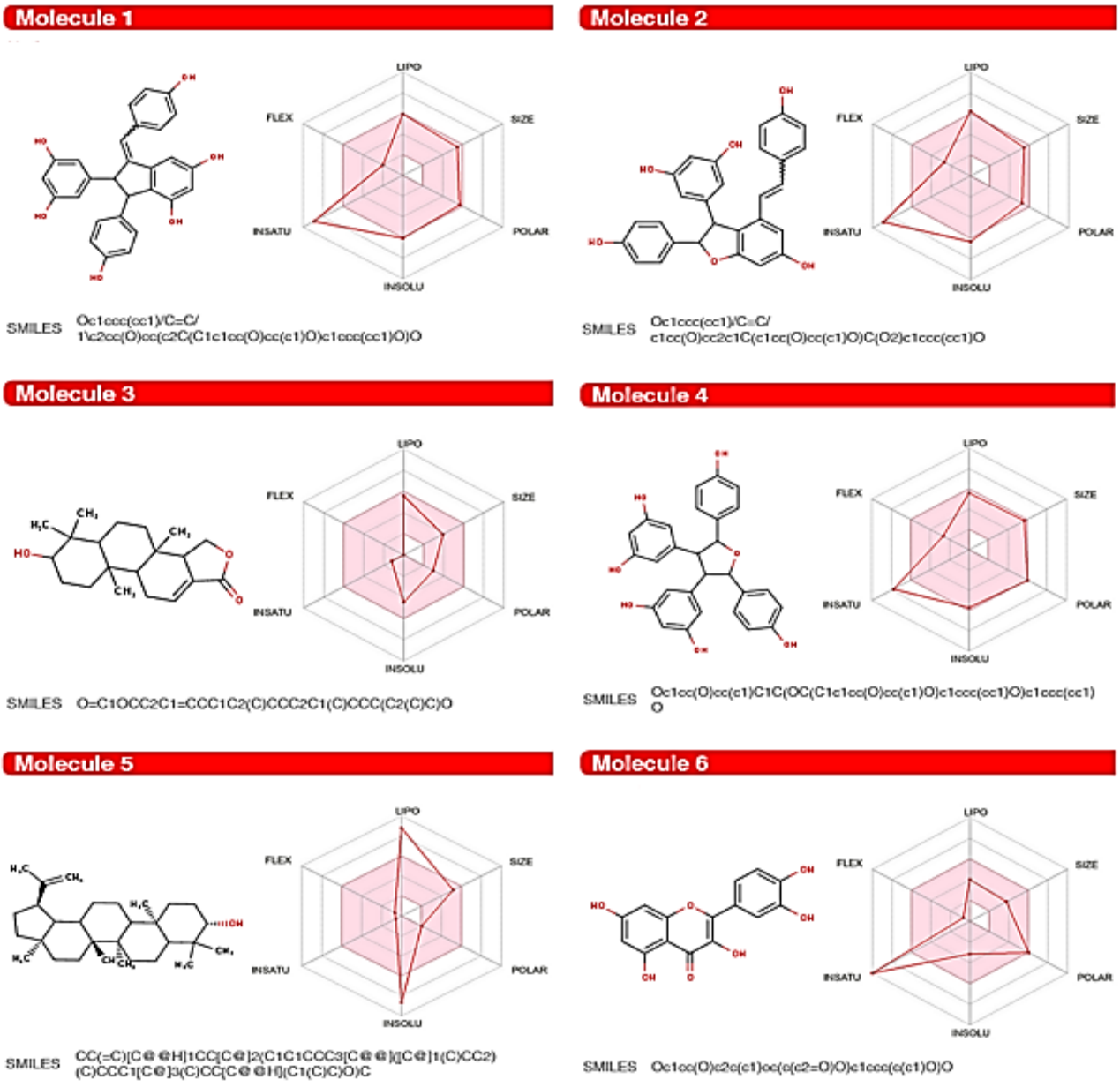

Figure 39: Bioavailability radar of compounds **23**, **25**, **28**, **29**, **39**, and **42**. Molecule 1; parthenocissin A (**23**), Molecule 2; *ε*-viniferin (**25**), Molecule 3; 3-hydroxy isoagatholactone (**28**), Molecule 4; tricuspidatol A (**29**), Molecule 5; lupeol (**39**), Molecule 6; quercetin (**42**).

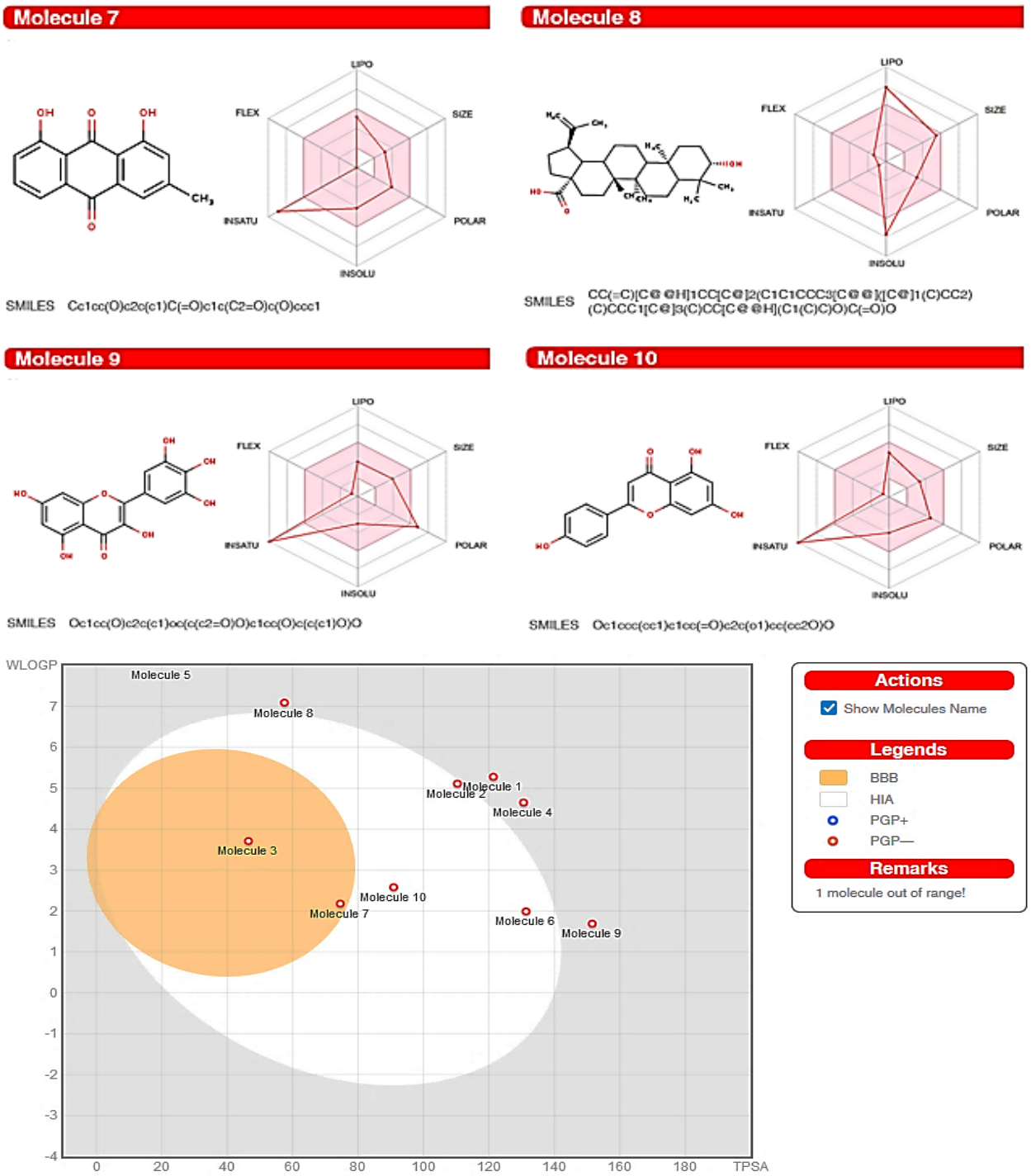

Figure 40: Bioavailability radar of compounds **53**, **63**, **66**, and **87** (top) and BOILED-Egg model of compounds **23**, **25**, **28**, **29**, **39**, **42**, **53**, **63**, **66**, and **87** (bottom). Molecule 1; parthenocissin A (**23**), Molecule 2; ε-viniferin (**25**), Molecule 3; 3-hydroxy isoagatholactone (**28**), Molecule 4; tricuspidatol A (**29**), Molecule 5; lupeol (**39**), Molecule 6; quercetin (**42**), Molecule 7; chrysophanol (**53**), Molecule 8; betulinic acid (**63**), Molecule 9; myricetin (**66**), Molecule 10; apigenin (**87**).

4.4.2.3. Toxicity prediction

The degree to which a drug molecule can harm the organism's organs is determined in terms of toxicity and is one of the major reasons for drug failure in the late step of drug discovery (Durán-Iturbide *et al.*, 2020). Thus, the toxicity study of active principles is crucial to screen their detrimental effects on living organisms and the environment. In this study, the toxicity predictions of most of the compound isolates were computed. The results revealed that the compounds exhibited lethal dose values between $159 \leq LD_{50} \leq 5000$ mg/kg with toxicity classes of 4 and 5 (except quercetin, **42** with toxicity class of 3). According to the EPA's 4 categories of hazard classifications, compounds/chemicals with $LD_{50} \leq 50$ mg/kg are highly toxic, $50 < LD_{50} \leq 500$ mg/kg (moderately toxic), $500 < LD_{50} \leq 5000$ mg/kg (slightly toxic) and $LD_{50} > 5000$ mg/kg (safe chemicals) (Gadaleta *et al.*, 2019). Hence, all the investigated compounds showed no acute toxicity (Table 51).

The prediction tool also showed toxicological (hepatotoxicity, cardiotoxicity, carcinogenicity, immunotoxicity, mutagenicity, and cytotoxicity) endpoints. Accordingly, none of the computed compounds showed hepatotoxicity, thereby no problem with liver functions. In addition, all the compounds exhibited no cytotoxicity which were consistent with the prediction results of ciprofloxacin. Betulinic acid (**63**), *β*-sitosteryl-3*β*-glucopyranoside-6'-*O*-palmitate (**86**), and 4-(2'-hydroxymethyl-4'-hydroxyphenyl)-chrysophanol (**89**) displayed cardiotoxicity and most of the investigated compounds exhibited immunotoxicity properties (Table 51). Thus, the majority of the ADMET properties revealed that most of the investigated compounds possess drug-like properties, and further experimental and computational studies are suggested.

Table 51: Toxicity predictions of the compound isolates computed by ProTox II.

Compounds	LD_{50} (mg/kg)	Toxicity class	Organ toxicity					
			Hepato	**Cardio**	**Carcino**	**Immuno**	**Mutagen**	**Cyto**
			C. adenocaule					
19	890	4	Inactive	Inactive	Inactive	Active	Inactive	Inactive
23	680	4	Inactive	Inactive	Inactive	Active	Inactive	Inactive
25	1050	4	Inactive	Inactive	Active	Active	Inactive	Inactive
28	5000	5	Inactive	Inactive	Inactive	Active	Inactive	Inactive
29	500	4	Inactive	Inactive	Inactive	Inactive	Inactive	Inactive
66	2000	4	Inactive	Inactive	Active	Inactive	Active	Inactive
84	5000	5	Inactive	Inactive	Active	Active	Inactive	Inactive
			D. regia					
37	5000	5	Inactive	Inactive	Inactive	Active	Inactive	Inactive
40	890	4	Inactive	Inactive	Inactive	Active	Inactive	Inactive
42	159	3	Inactive	Inactive	Active	Inactive	Active	Inactive
86	590	4	Inactive	Active	Inactive	Active	Inactive	Inactive
87	2500	5	Inactive	Inactive	Inactive	Inactive	Inactive	Inactive
			S. siamea					
39	2000	4	Inactive	Inactive	Inactive	Active	Inactive	Inactive
53	5000	5	Inactive	Inactive	Inactive	Active	Active	Inactive
63	2610	5	Inactive	Active	Active	Active	Inactive	Inactive
88	5000	5	Inactive	Inactive	Inactive	Inactive	Inactive	Inactive
89	5000	5	Inactive	Active	Inactive	Active	Active	Inactive
Cipro.	2000	4	Inactive	Inactive	Inactive	Inactive	Active	Inactive

Carcino; carcinogenicity, Cardio; cardio-toxicity, Cyto; cytotoxicity, Hepato; hepatotoxicity, Immuno; immunotoxicity, LD; lethal dose, Mutagen; mutagenicity.

5. CONCLUSION AND RECOMMENDATIONS

5.1. Conclusion

In this study, the phytochemistry and biological activities of the root extracts of four plant species namely, *C. adenocaule, D. regia*, *S. siamea*, and *Z. spina-christi* were studied. The silica gel column chromatography of their respective extracts afforded ten, seven, seven, and five compounds including the mixture of *β*-sitosterol (**19**) and stigmasterol (**40**). Stigmasterol (**40**) and *β*-sitosteryl-3*β*-glucopyranoside-6'-*O*-palmitate (**86**) (*D. regia* and *Z. spina-christi)*, diethyl phthalate (**85**) (*C. adenocaule* and *D. regia)*, and the mixture of *β*-sitosterol (**19**) and stigmasterol (**40**) *(D. regia, S. siamea)* were also isolated from two plants. The structural informations of the compound isolates was achieved by comparing the generated IR and NMR data with literature reports. The reported compounds belong to various classes of secondary metabolites including fatty acids and derivatives, stilbene derivatives, flavonoids, terpenoids, quinones, and phthalates. In addition, the volatile components of the leaves and roots of the plant materials were investigated using a GC-MS and revealed plenty of compounds. Thus, the phytochemical findings of this work revealed that the medicinal potential of the investigated plants is strongly related to the presence of diverse classes of compounds that can defend various types of infectious diseases, some of which are also proven in this study.

The *in vitro* antibacterial activities of the extracts of the four plants along with their compound isolates were tested, and the results showed that the CH_2Cl_2: CH_3OH (1:1) extracts of *C. adenocaule* (CAE) and *S. siamea* (SSE) showed the most potent activity (18.00 ± 0.00 mm each) against *E. coli* at the maximum concentration (50 mg/mL). The plausible antibacterial activities of tricuspidatol A (**29**) against *S. aureus* (16.67 ± 0.47 mm) and *E. coli* (16.17 ± 0.24 mm), quercetin (**42**) against *E. coli* (16.50 ± 0.41 mm), chrysophanol (**53**) against *E. coli* (16.33 ± 0.24 mm) and *S. pyogenes* (16.00 ± 0.00 mm) at 2 mg/mL offered proves of their potential uses for therapeutic applications. The antibacterial activity profile of the essential oils of *C. adenocaule* and *Z. spina-christi* was also promising. The results showed that the roots EOs of *C. adenocaule* showed better activities than *Z. spina-christi* and the highest inhibitory activity was observed by the roots EOs of *C. adenocaule* against *S. pyogenes* (13.67 ± 0.34 mm) at 10 mg/mL. The promising IC_{50} values of all the extracts and parthenocissin A (**23**, 0.98 μg/mL), ***ε***-viniferin (**25**, 0.32 μg/mL), tricuspidatol A (**29**, 0.67 μg/mL), quercetin-3-*O*-rutinoside (**37**, 0.81 μg/mL), quercetin (**42**, 1.12

μg/mL), and myricetin (**66**, 1.05 μg/mL) relative to ascorbic acid (0.08 μg/mL) offer evidences for their antioxidant efficacy. Furthermore, the high SI values of the CH_2Cl_2: CH_3OH (1:1) extract of *S. siamea* (SI: 13.32) and methanol extract of *Z. spina-christi* (SI: 28.03) against influenza types A and B viruses validate their possible antiviral effects.

Most of the computed molecular docking results of the compound isolates were in good agreement with the *in vitro* antibacterial and antioxidant activity studies. This suggests that the compounds have the possibility to be used as antibacterial and antioxidant agents which supports the traditional uses of the plants. The drug-likeness predictions showed that all the compound isolates except quercetin-3-*O*-rutinoside (**37**), *β*-sitosteryl palmitate (**84**), and *β*-sitosteryl-3*β*-glucopyranoside-6'-*O*-palmitate (**86**) whom drug-likeness properties are predicted fulfilled Lipinski's rule with zero/one violation. Furthermore, except quercetin-3-*O*-rutinoside (**37**), myricetin (**66**), *β*-sitosteryl palmitate (**84**), *β*-sitosteryl-3*β*-glucopyranoside-6'-*O*-palmitate (**86**), and glyceryl-1-hexacosanoate (**88**), all the compounds satisfy Veber's rule with TPSA < 140 and NRB < 10. Notably, none of the computed compounds showed hepatotoxicity and cytotoxicity properties which were consistent with the prediction results of ciprofloxacin. Thus, the majority of the ADMET properties confirm the drug-like possibilities of most of the investigated compounds and strengthen the traditional medicinal uses of the plants.

5.2. Recommendations

In this study, diversified compounds were isolated and characterized from each plant despite the fact that more compounds can also be isolated using advanced instruments. Overall, the *in vitro* antibacterial and radical scavenging activities along with the phytochemistry and computational analyses of the plants suggest the potential use of most of the compound isolates for further study, and the following recommendations are addressed.

- ✓ Based on the number of compounds isolated in this study, there is a possibility of re-conducting the work to get more compounds along with their extended biological activities. In addition, repeated isolation in large quantities of the compounds isolated in this study should be done to enable structural modification studies and to enhance their biological activity profiles.

- ✓ *In vivo* antibacterial studies against animal models are suggested for parthenociccin A (**23**), *ε*-viniferin (**25**), tricuspidatol A (**29**), quercetin-3-*O*-rutinoside (**37**), quercetin (**42**), chrysophanol (**53**), myricetin (**66**), and apigenin (**87**) that showed promising *in vitro* activities.
- ✓ Further *in vitro* and *in vivo* cytotoxicity tests and their structure-activity relationships are recommended for parthenocissin A (**23**), *ε*-viniferin (**25**), tricuspidatol A (**29**), quercetin-3-*O*-rutinoside (**37**), lupeol (**39**), quercetin (**42**), chrysophanol (**53**), betulinic acid (**63**), myricetin (**66**), and apigenin (**87**) which have showed good *in silico* interactions.
- ✓ The extracts of *C. adenocaule* and *Z. spina-christi* which showed promising anti-acanthamoeba activities can be used as important input for future works and further investigations are yet needed.
- ✓ Further studies are desired on the essential oil profiles of the plants and develop the method for industrial scales and commercial uses such as flavoring, cosmetics, shampoo, and detergents.
- ✓ An extended study is recommended on the compounds exhibiting plausible ADMET properties to transform the findings into advanced scale and further pre-clinical trials.

6. REFERENCES

Abdallah, M., A. Idriss, S. Yahaya and I. Aliyu (2019), ʻAntibacterial activity of ethanolic leaves extracts of *Cassia siamea* against some bacterial isolates from infantile diarrhoeal attending general hospital Damaturu,' *Global Academic Journal of Pharmacy and Drug Research,* 1(1): pp. 5-9.

Abdo, B. M. (2017), ʻSennosides determination of Ethiopian *Senna alexandrina* Mill accessions,' *Natural Products Chemistry and Research,* 5(293): pp. 1-4.

Abdulrahman, M. D., A. M. Zakariya, H. A. Hama, S. W. Hamad, S. S. Al-Rawi, S. W. Bradosty and A. H. Ibrahim (2022), ʻEthnopharmacology, biological evaluation, and chemical composition of *Ziziphus spina-christi* (L.) desf.: A review,' *Advances in Pharmacological and Pharmaceutical Sciences,* Volume 2022, Article ID 4495688, 36 pages.

Abdurrahman, I. and Y. Cai-Xiab (2020), ʻIsolation and characterization of fatty acid derivatives from the stem barks of *Albizia amara* (Fabaceae), Sudanese medicinal plant,' *Chemical Methodologies,* 4(4): pp. 369-377.

Abebe, D., G. Periasamy, A. Karim and H. Bitew (2021), ʻEvaluation of the effect of hydroethanolic root extract and solvent fractions of *Cyphostemma adenocaule* (steud. Ex a. Rich) descoings Ex Wild & Drummond on cell-mediated immune response and blood cell count in mice,' *Evidence-Based Complementary and Alternative Medicine,* Volume 2021, Article ID 1838903, 6 pages.

Abou Auda, M. (2011), ʻAn ethnobotanical use of plants in the middle area, Gaza strip, Palestine,' *Advances in Environmental Biology,* 5(11): pp. 3681-3688.

Abu-Raghif, A. R., G. A. Jasim and M. M. Hanoon (2017), ʻAnti-proliferative activity of *Zizyphus spina-christi* leaves methanol extract against Rhabdomyosarcoma (RD) cell line,' *International Journal of Pharmacy and Pharmaceutical Sciences,* 9(2): pp. 279-282.

Abubakar, A. R. and M. Haque (2020), ʻPreparation of medicinal plants: Basic extraction and fractionation procedures for experimental purposes,' *Journal of Pharmacy and Bioallied Sciences,* 12(1): pp. 1-10.

Adedeji, A. A. and O. O. Babalola (2020), ʻSecondary metabolites as plant defensive strategy: A large role for small molecules in the near root region,' *Planta,* 252(4): pp. 1-61.

Adedoyin, B. A., O. I. Adeniran, A. B. Muhammed, S. M. Dangoggo, L. Nahar, G. P. Sharples and S. D. Sarker (2020), ʻIsolation and characterization of propitious bioactive compounds from *Cassia singueana* L,' *Advancement in Medicinal Plant Research,* 8(4): pp. 89-100.

Adje, F., Y. F. Lozano, E. Meudec, P. Lozano, A. Adima, G. A. N'zi and E. M. Gaydou (2008), ʻAnthocyanin characterization of pilot plant water extracts of *Delonix regia* flowers,' *Molecules,* 13(6): pp. 1238-1245.

Adjé, F. A., Y. F. Lozano, C. Le Gernevé, P. R. Lozano, E. Meudec, A. A. Adima and E. M. Gaydou (2012), ʻPhenolic acid and flavonol water extracts of *Delonix regia* red flowers,' *Industrial Crops and Products,* 37(1): pp. 303-310.

Ads, E. N., S. I. Hassan, S. Rajendrasozhan, M. H. Hetta, S. H. Aly and M. A. Ali (2022), ʻIsolation, structure elucidation and antimicrobial evaluation of natural pentacyclic triterpenoids and

phytochemical investigation of different fractions of *Ziziphus spina-christi* (L.) stem bark using LC-HRMS analysis,' *Molecules*, 27(6): p. 1805.

Ads, E. N., S. Rajendrasozhan, S. I. Hassan, S. M. S. Sharawy and J. R. Humaidi (2017), 'Phytochemical, antimicrobial and cytotoxic evaluation of *Ziziphus spina-christi* (L.) stem bark,' *Biomedical Research*, 28(15): pp. 6646-6653.

Adzu, B., S. Amos, M. Amizan and K. Gamaniel (2003), 'Evaluation of the antidiarrhoeal effects of *Zizyphus spina-christi* stem bark in rats,' *Acta Tropica*, 87(2): pp. 245-250.

Ahmed, J., S. Nirmal, V. Dhasade, A. Patil, S. Kadam, S. Pal, S. Mandal and S. Pattan (2011a), 'Hepatoprotective activity of methanol extract of aerial parts of *Delonix regia*,' *Phytopharmacology*, 1(5): pp. 118-122.

Ahmed, R., K. Nagori, T. Kumar, M. Singh and D. Dewangan (2011b), 'Phytochemical estimation of anthraquinones from *Cassia* species,' *International Journal of Research in Ayurveda & Pharmacy*, 2(4): pp. 1320-1323.

Al-Gubory, K. H., C. Garrel, P. Faure and N. Sugino (2012), 'Roles of antioxidant enzymes in corpus luteum rescue from reactive oxygen species-induced oxidative stress,' *Reproductive Biomedicine Online*, 25(6): pp. 551-560.

Al-Mahweety, J. A. (2016), 'Chemical study on the leaves of *Cyphostemma digitatum*,' *PSM Biological Research*, 1(2): pp. 66-69.

Alalwan, T. A., J. A. Alkhuzai, Z. Jameel and Q. A. Mandeel (2019), 'Quantitative ethnobotanical study of some medicinal plants used by herbalists in Bahrain,' *Journal of Herbal Medicine*, 17: p. 100278.

Alemayehu, I., S. Tadesse, F. Mammo, B. Kibret and M. Endale (2015), 'Phytochemical analysis of the roots of *Senna didymobotrya*,' *Journal of Medicinal Plants Research*, 9(34): pp. 900-907.

Alemu, M. M. (2017), 'Indigenous and medicinal uses of plants in Nech Sar National Park, Ethiopia,' *Open Access Library Journal*, 4(3): p. e3428.

Ali, A. B., A. Z. Almagboul and O. M. Mohammed (2015), 'Antimicrobial activity of fruits, leaves, seeds and stems extracts of *Ziziphus spina-christi*,' *Arabian Journal of Medicinal and Aromatic Plants*, 1(2): pp. 94-107.

Ali, M., I. Azhar, Z. Amtul, V. Ahmad and K. Usmanghani (1999), 'Antimicrobial screening of some Caesalpiniaceae,' *Fitoterapia*, 70(3): pp. 299-304.

Ali, S., S. M. Saudagar Mujahid, S. Aatif and M. Khan (2013), 'Anti-ulcer activity of ethanolic extract of *Caesalpinia pulcherrima* flowers on ethanol-induced gastric ulcers in rats,' *Der Pharmacia Sinica*, 4(2): pp. 119-124.

Allabi, A. C., K. Busia, V. Ekanmian and F. Bakiono (2011), 'The use of medicinal plants in self-care in the Agonlin region of Benin,' *Journal of Ethnopharmacology*, 133(1): pp. 234-243.

Almeer, R. S., S. Alkahtani, S. Alarifi, A. E. A. Moneim, S. Abdi and G. Albasher (2022), 'Ziziphus *spina-christi* leaf extract mitigates mercuric chloride-induced cortical damage in rats,' *Combinatorial Chemistry & High Throughput Screening*, 25(1): pp. 103-113.

Almeer, R. S., M. F. El-Khadragy, S. Abdelhabib and A. E. Abdel Moneim (2018), 'Ziziphus spina-christi leaf extract ameliorates schistosomiasis liver granuloma, fibrosis, and oxidative stress through downregulation of fibrinogenic signaling in mice,' *PloS One,* 13(10): p. e0204923.

Alzahrani, A. M., A. A. Alzahrani and A. A. Alsharm (2020), 'The use of *Ziziphus spina-christi* extract in treating erlotinib (tarceva®) associated rash: A case report,' *Case Reports in Oncology,* 12(3): pp. 909-912.

Amaro-Luis, J. M., A. Duque-Márquez, P. Ramoni-Perazzi and M. Muñoz-Romo (2021), 'Isolation and characterization of stigmasterol from highly consumed leaves by the large fruit-eating bat, Artibeus amplus (chiroptera: Phyllostomidae),' *Interciencia,* 46(9/10): pp. 363-368.

Anza, M., M. Endale, L. Cardona, D. Cortes, R. Eswaramoorthy, N. Cabedo, B. Abarca, J. Zueco, H. Rico and I. Domingo-Ortí (2021), 'Cytotoxicity, antimicrobial activity, molecular docking, drug-likeness and DFT analysis of benzo [c] phenanthridine alkaloids from roots of *Zanthoxylum chalybeum*,' *Biointerface Research in Applied Chemistry,* 12(2): pp. 1569-1586.

Arazna, M., M. P. Pruchniak, K. Zycinska and U. Demkow, (2013). Neutrophil extracellular trap in human diseases. In *Respiratory Regulation-The Molecular Approach*, 756: 1-8.

Arceusz, A., I. Radecka and M. Wesolowski (2010), 'Identification of diversity in elements content in medicinal plants belonging to different plant families,' *Food Chemistry,* 120(1): pp. 52-58.

Assefa, T., H. Tesso, E. Abdisa, L. Guta and Y. Melaku (2023), 'Chemical composition and antibacterial activity of essential oils from selected species of the genus *Cucumis* in Ethiopia,' *Bulletin of the Chemical Society of Ethiopia,* 37(3): pp. 703-715.

Assob, J. C., H. L. Kamga, D. S. Nsagha, A. L. Njunda, P. F. Nde, E. A. Asongalem, A. J. Njouendou, B. Sandjon and V. B. Penlap (2011), 'Antimicrobial and toxicological activities of five medicinal plant species from Cameroon traditional medicine,' *BMC Complementary and Alternative Medicine,* 11(70): pp. 1-11.

Atanasov, A. G., B. Waltenberger, E.-M. Pferschy-Wenzig, T. Linder, C. Wawrosch, P. Uhrin, V. Temml, L. Wang, S. Schwaiger and E. H. Heiss (2015), 'Discovery and resupply of pharmacologically active plant-derived natural products: A review,' *Biotechnology Advances,* 33(8): pp. 1582-1614.

Aung, E. E., A. N. Kristanti, N. S. Aminah, Y. Takaya and R. Ramadhan (2023), 'Phytochemicals constituents in medicinal plant *Syzygium aqueum* (Burm.) Alston (Myrtaceae),' *Egyptian Journal of Chemistry,* 66(3): pp. 301-308.

Azab, S. S., M. Abdel-Daim and O. A. Eldahshan (2013), 'Phytochemical, cytotoxic, hepatoprotective and antioxidant properties of *Delonix regia* leaves extract,' *Medicinal Chemistry Research,* 22: pp. 4269-4277.

Azadi, B. and S. Khaef (2015), 'Volatile constituents of *Haplophyllum buhsei* Boiss. Flowering aerial parts,' *Bulletin of the Chemical Society of Ethiopia,* 29(2): pp. 327-330.

Baby, S. T., S. Sharma, S. Enaganti and P. R. Cherian (2016), 'Molecular docking and pharmacophore studies of heterocyclic compounds as heat shock protein 90 (hsp90) inhibitors,' *Bioinformation,* 12(3): pp. 149-155.

Bahmani, M., A. Jalilian, I. Salimikia, S. Shahsavari and N. Abbasi (2020), 'Phytochemical screening of two Ilam native plants *Ziziphus nummularia* (Burm. F.) Wight & Arn. and *Ziziphus spina-christi* (Mill.) georgi using HS-SPME and GC-MS spectroscopy,' *Plant Science Today,* 7(2): pp. 275-280.

Balogun, O. S., O. S. Ajayi and A. J. Adeleke (2017), 'Hexahydrofarnesyl acetone-rich extractives from *Hildegardia barteri*,' *Journal of Herbs, Spices & Medicinal Plants,* 23(4): pp. 393-400.

Balouiri, M., M. Sadiki and S. K. Ibnsouda (2016), 'Methods for *in vitro* evaluating antimicrobial activity: A review,' *Journal of Pharmaceutical Analysis,* 6(2): pp. 71-79.

Balunas, M. J. and A. D. Kinghorn (2005), 'Drug discovery from medicinal plants,' *Life Sciences,* 78(5): pp. 431-441.

Banerjee, P., A. O. Eckert, A. K. Schrey and R. Preissner (2018), 'Protox-ii: A webserver for the prediction of toxicity of chemicals,' *Nucleic Acids Research,* 46(W1): pp. W257-W263.

Bello, O. M., S. M. Jagaba, O. E. Bello, A. B. Ogbesejana, O. A. Dada, C. O. Adetunji and S. M. Abubakar (2019), 'Phytochemistry, pharmacology and perceived health uses of non-cultivated vegetable *Cyphostemma adenocaule* (Steud. Ex a. Rich.) Desc. Ex Wild and RB drumm: A review,' *Scientific African,* 2: pp. e00053.

Bharath, E., S. Manjula and A. Vijaychand (2011), '*In silico* drug design tool for overcoming the innovation deficit in the drug discovery process,' *International Journal of Pharmacy and Pharmaceutical Sciences,* 3(2): pp. 8-12.

Bhavaniramya, S., S. Vishnupriya, M. S. Al-Aboody, R. Vijayakumar and D. Baskaran (2019), 'Role of essential oils in food safety: Antimicrobial and antioxidant applications,' *Grain and Oil Science and Technology,* 2(2): pp. 49-55.

Bianco, A., A. Venditti, S. Foddai, C. Toniolo and M. Nicoletti (2014), 'A new problem. Contamination of botanicals by phthalates. Rapid detection tests,' *Natural Product Research,* 28(2): pp. 134-137.

Birhanu, Z., A. Endale and Z. Shewamene (2015), 'An ethnomedicinal investigation of plants used by traditional healers of Gondar town, North-Western Ethiopia,' *Journal of Medicinal Plants Studies,* 3(2): pp. 36-43.

Bitew, H., H. Gebregergs, K. B. Tuem and M. Y. Yeshak (2019), 'Ethiopian medicinal plants traditionally used for wound treatment: A systematic review,' *Ethiopian Journal of Health Development,* 33(2): pp. 102-127.

Bouyahya, A., N. El Menyiy, L. Oumeslakht, A. El Allam, A. Balahbib, A. Rauf, N. Muhammad, E. Kuznetsova, M. Derkho and M. Thiruvengadam (2021), 'Pre-clinical and clinical antioxidant effects of natural compounds against oxidative stress-induced epigenetic instability in tumor cells,' *Antioxidants,* 10(10): pp. 1-22.

Boy, H. I. A., A. J. H. Rutilla, K. A. Santos, A. M. T. Ty, I. Y. Alicia, T. Mahboob, J. Tangpoong and V. Nissapatorn (2018), 'Recommended medicinal plants as source of natural products: A review,' *Digital Chinese Medicine,* 1(2): pp. 131-142.

Bozicevic, A., M. De Mieri, A. Di Benedetto, F. Gafner and M. Hamburger (2017), 'Dammarane-type saponins from leaves of *Ziziphus spina-christi*,' *Phytochemistry,* 138: pp. 134-144.

Bui, T. T., K. P. T. Nguyen, P. P. K. Nguyen, D. T. Le and T. L. T. Nguyen (2022), 'Anti-inflammatory and α-glucosidase inhibitory activities of chemical constituents from *Bruguiera parviflora* leaves,' *Journal of Chemistry,* Volume 2022, Article ID 3049994, 9 pages.

Bukar, A., M. Mukhtar and A. Hassan (2009), 'Phytochemical screening and antibacterial activity of leaf extracts of *Senna siamea* (Lam) on *Pseudomonas aeruginosa*,' *Bayero Journal of Pure and Applied Sciences,* 2(1): pp. 139-142.

Bulama, J., S. Dangoggo, M. Halilu, A. Tsafe and S. Hassan (2014), 'Isolation and characterization of palmitic acid from ethyl acetate extract of root bark of *Terminalia glaucescens*,' *Chemistry and Materials Research,* 6(12): pp. 140-144.

Cai, H., B. Shao, Y. Zhou, and Z. Chen (2020), 'High expression of TOP2A in hepatocellular carcinoma is associated with disease progression and poor prognosis,' *Oncology Letters,* 20(5): p. 232.

Cayme, J.-M. C. and C. Y. Ragasa (2004), 'Structure elucidation of β-stigmasterol and β-sitosterol from *Sesbania grandifora* [Linn.] pers. and β-carotene from *Heliotropium indicum* Linn. By NMR spectroscopy,' *Kimika,* 20(1): pp. 5-12.

Chan, K., D. Shaw, M. S. Simmonds, C. J. Leon, Q. Xu, A. Lu, I. Sutherland, S. Ignatova, Y.-P. Zhu and R. Verpoorte (2012), 'Good practice in reviewing and publishing studies on herbal medicine, with special emphasis on traditional Chinese medicine and Chinese materia medica,' *Journal of Ethnopharmacology,* 140(3): pp. 469-475.

Chen, C.-Y., S.-C. Luo, C.-F. Kuo, Y.-S. Lin, J.-J. Wu, M. T. Lin, C.-C. Liu, W.-Y. Jeng and W.-J. Chuang (2003), 'Maturation processing and characterization of streptopain,' *Journal of Biological Chemistry,* 278(19): pp. 17336-17343.

Chen, Y.-C. (2015), 'Beware of docking! ,' *Trends in Pharmacological Sciences,* 36(2): pp. 78-95.

Chimi Fotso, S., A. Tcho Tadjong, W. D. T. Tsopgni, B. N. Lenta, C. N. Nkenfou, J. D. Wansi and F. A. A. Toze (2021), 'Chemical constituents and antimicrobial activities of some isolated compounds from the Cameroonian species of *Senna alata* (*Cassia alata* L. Roxb synonym, the plant list 2013).(Leguminosae),' *Trends in Phytochemical Research,* 5(1): pp. 37-43.

Chouna, J. R., F. Nardella, B. N. Lenta, C. Vonthron-Sénécheau, P. Nkeng-Efouet-Alango and N. Sewald (2016), 'Ceanothane-type triterpenoids from *Cyphostemma adenocaule*,' *Archives of Pharmacal Research*: pp. 1-6.

Clarkson, T. C., A. J. Janich, I. Sanchez-Vargas, E. D. Markle, M. Gray, J. R. Foster, W. C. Black IV, B. D. Foy and K. E. Olson (2021), 'Nootkatone is an effective repellent against *Aedes aegypti* and *Aedes albopictus*,' *Insects,* 12(386): pp. 1-18.

Collin, F., S. Karkare and A. Maxwell (2011), ʻExploiting bacterial DNA gyrase as a drug target: Current state and perspectives,' *Applied Microbiology and Biotechnology*, 92: pp. 479-497.

Cragg, G. M. and D. J. Newman (2013), ʻNatural products: A continuing source of novel drug leads,' *Biochimica et Biophysica Acta (BBA)-General Subjects*, 1830(6): pp. 3670-3695.

d'Almeida Gameiro, M., P. L. Jacob, K. Kortsen, T. Ward, V. Taresco, R. A. Stockman, Y. Chebude and S. M. Howdle (2022), ʻGreener extraction-chemical modification-polymerization pipeline of vernolic acid from Ethiopian Ironweed plant,' *Journal of Polymer Science*: 60(24): pp. 3354-3365.

Daina, A., O. Michielin and V. Zoete (2017), ʻSwissADME: A free web tool to evaluate pharmacokinetics, drug-likeness and medicinal chemistry friendliness of small molecules,' *Scientific Reports*, 7(1): p. 42717.

Dave, H. and L. Ledwani (2012), ʻA review on anthraquinones isolated from *Cassia* species and their applications,' 3(3): pp. 291-319.

De Clercq, E. (2004), ʻAntiviral drugs in current clinical use,' *Journal of Clinical Virology*, 30(2): pp. 115-133.

De Sousa, F., E. Figueiredo and G. F. Smith (2011), ʻThe genus *Cyphostemma* (Planch.) Alston (Vitaceae) in Angola,' *Bradleya*, 2011(29): pp. 79-92.

Degfie, T., J. O. Ombito, T. B. Demissie, R. Eswaramoorthy, A. Dekebo and M. Endale (2022), ʻAntibacterial and antioxidant activities, *in silico* molecular docking, ADMET and DFT analysis of compounds from roots of *Cyphostemma cyphopetalum*,' *Advances and Applications in Bioinformatics and Chemistry*, 15: pp. 79-97.

Delfan, B., M. Bahmani, H. Hassanzadazar, K. Saki, M. Rafieian-Kopaei, M. Rashidipour, F. Bagheri and A. Sharifi (2015), ʻEthnobotany study of effective medicinal plants on gastric problems in Lorestan province, West of Iran,' *Journal of Chemical and Pharmaceutical Research*, 2: pp. 483-492.

Deweese, J. E. and N. Osheroff (2009), ʻThe DNA cleavage reaction of topoisomerase II: Wolf in sheep's clothing,' *Nucleic Acids Research*, 37(3): pp. 738-748.

Dias, D. A., S. Urban and U. Roessner (2012), ʻA historical overview of natural products in drug discovery,' *Metabolites*, 2(2): pp. 303-336.

Donadu, M. G., N. Trong Le, D. Viet Ho, T. Quoc Doan, A. Tuan Le, A. Raal, M. Usai, M. Marchetti, G. Sanna and S. Madeddu (2020), ʻPhytochemical compositions and biological activities of essential oils from the leaves, rhizomes and whole plant of *Hornstedtia bella škorničk*,' *Antibiotics*, 9(6): p. 334.

Dong, J. (2013), ʻThe relationship between traditional Chinese medicine and modern medicine,' *Evidence-Based Complementary and Alternative Medicine*, Volume 2013, Article ID 153148, 10 pages.

Doorandishan, M., M. Gholami, P. Ebrahimi and A. R. Jassbi (2021), ʻSpathulenol as the most abundant component of essential oil of *Moluccella aucheri* (Boiss.) Scheen,' *Natural Volatiles and Essential Oils*, 8(2): pp. 37-41.

Ducrot, P.-H., A. Kollmann, A. E. Bala, A. Majira, L. Kerhoas, R. Delorme and J. Einhorn (1998), ʻCyphostemmins A and B, two new antifungal oligostilbenes from *Cyphostemma crotalarioides* (Vitaceae),' *Tetrahedron Letters*, 39(52): pp. 9655-9658.

Durán-Iturbide, N. A., B. I. Díaz-Eufracio and J. L. Medina-Franco (2020), ʻ*In silico* ADME/Tox profiling of natural products: A focus on BIOFACQUIM,' *ACS Omega*, 5(26): pp. 16076-16084.

Dzul-Beh, A. d. J., K. García-Sosa, A. H. Uc-Cachón, J. Bórquez, L. A. Loyola, H. B. Barrios-García, L. M. Peña-Rodríguez and G. M. Molina-Salinas (2020), ʻ*In vitro* growth inhibition and bactericidal activity of spathulenol against drug-resistant clinical isolates of *Mycobacterium tuberculosis*,' *Revista Brasileira de Farmacognosia*, 29(2019): pp. 798-800.

Egbuna, C., M. Mukherjee, G. N. Rao, L. J. F. J. Gido and H. Tijjani. (2018), ʻIntroduction to phytochemistry', *Phytochemistry*, 2018: pp. 3-36.

Eichberg, J., E. Maiworm, M. Oberpaul, V. Czudai-Matwich, T. Lüddecke, A. Vilcinskas and K. Hardes (2022), ʻAntiviral potential of natural resources against influenza virus infections,' *Viruses*, 14(11): p. 2452.

Ekasari, W., A. Widyawaruyanti, N. C. Zaini, D. Syafruddin, T. Honda and H. Morita (2009), ʻAntimalarial activity of cassiarin A from the leaves of *Cassia siamea*,' *Heterocycles*, 78(7): pp. 1831-1836.

Ekiert, H. M. and A. Szopa, (2023), ʻBiological activities of natural products III', *Molecules*, 28: p. 4854.

El-Kamali, H. H. and S. A. T. Mahjoub (2009), ʻAntibacterial activity of *Francoeuria crispa, Pulicaria undulata, Ziziphus spina-christi* and *Cucurbita pepo* against seven standard pathogenic bacteria,' *Ethnobotanical Leaflets*, 2009(6): p. 6.

El-Sayed, A. M., S. M. Ezzat, M. M. Salama and A. A. Sleem (2011), ʻHepatoprotective and cytotoxic activities of *Delonix regia* flower extracts,' *Pharmacognosy Journal*, 3(19): pp. 49-56.

El Maaiden, E., Y. El Kharrassi, N. A. Qarah, A. K. Essamadi, K. Moustaid and B. Nasser (2020), ʻGenus *Ziziphus*: A comprehensive review on ethnopharmacological, phytochemical and pharmacological properties,' *Journal of Ethnopharmacology*, 259: p. 112950.

El Rabey, H. A., E. S. Attia, M. N. Al-Seeni, A. I. Al-Sieni, I. H. Ibrahim, M. F. Meerasahib, A. M. Shaikh-Omer, A. O. Abuelgassim and O. Abuelgassim (2014), ʻThe hypolipidemic and antioxidant activity of Christ's thorn (*Ziziphus spina-christi*) leaves powder in hypercholesterolemic male rats,' *Life Science Journal*, 11(10): pp. 1010-1021.

Elaloui, M., S. H. Hamdi, H. Ghazghazi, R. B. Nasr, E. Bouslih, Y. Ammari, J. Mediouni and A. Laamouri (2021), ʻCharacterization of epicatechin contents in the *Ziziphus spina-christi* L. root extracts using LC-MS analyses and their insecticidal potential,' *Plant Biosystems-An International Journal Dealing with all Aspects of Plant Biology*, 155(4): pp. 685-690.

Elokely, K. M. and R. J. Doerksen (2013), 'Docking challenge: Protein sampling and molecular docking performance,' *Journal of Chemical Information and Modeling,* 53(8): pp. 1934-1945.

Elsbaey, M., K. F. Ahmad, F. A. Behery, M. M. Amer and M.-F. I. Lahloub (2023), 'Cytotoxic constituents from the rhizomes of *Monstera deliciosa*,' *Records of Natural Products,* 17(2): pp. 372-376.

Elumalai, S., S. Soundararajan, P. Kanagaraj and D. R. Sadhasivam (2022), '*In vitro* antioxidant and antibacterial activity of quercetin isolated from *Indigofera aspalathoides* and quercetin-zinc metal complex,' *International Journal of Health Sciences,* 6(S3): pp. 4314-4326.

Elyemni, M., B. Louaste, I. Nechad, T. Elkamli, A. Bouia, M. Taleb, M. Chaouch and N. Eloutassi (2019), 'Extraction of essential oils of *Rosmarinus officinalis* L. by two different methods: hydrodistillation and microwave-assisted hydrodistillation,' *The Scientific World Journal,* Volume 2019, Article ID 3659432, 6 pages.

Fajriah, S., M. Megawati and A. Darmawan (2016), 'Apigenin, an anticancer active compound isolated from *Macaranga gigantifolia* leaves,' *Journal of Tropical Life Science,* 6(1): pp. 7-9.

Faridi, P., M. M. Zarshenas, Z. Abolhassanzadeh and A. Mohagheghzadeh (2010), 'Collection and storage of medicinal plants in the canon of medicine,' *Pharmacognosy Journal,* 2(8): pp. 216-218.

Fenetahun, Y. and G. Eshetu (2017), 'A review on ethnobotanical studies of medicinal plants used by agro-pastoral communities in Ethiopia,' *Journal of Medicinal Plants,* 5(1): pp. 33-44.

Ferrari, G., S. Matuska and P. Rama (2011), 'Double-biguanide therapy for resistant *Acanthamoeba keratitis*,' *Case Reports in Ophthalmology,* 2(3): pp. 338-342.

Feyisayo, A., A. V. Oluwafemi and O. O. Oluokun (2015), 'Evaluation of antioxidant capacity and membrane stabilizing potential of stem and root of *Cyphospenna adenocaulis* (Steud),' *African Journal of Biotechnology,* 14(21): pp. 1820-1827.

Feyisayo, A. K. and O. O. Oluokun (2013), 'Isolation, fractionation, chemical constituents and activities of polysaccharides of stem and root of *Cissus adenocaulis* (Steud),' *Journal of Medicinal Plants Research,* 7(43): pp. 3211-3219.

Fikadu, G. and G. Mulugeta (2022), 'Phytochemical investigation on the root of *Cyphostemma adenocaule* (Steud. Ex A. Rich),' *Algerian Journal of Natural Products,* 10(1): pp. 904-917.

File, T., H. Dinka and L. Golassa (2019), 'A retrospective analysis on the transmission of *Plasmodium falciparum* and *Plasmodium vivax*: The case of Adama city, East Shoa zone, Oromia, Ethiopia,' *Malaria Journal,* 18(1): pp. 1-5.

Flemming, J., J. Remmler, F. Röhring and J. Arnhold (2014), '(−)-epicatechin regenerates the chlorinating activity of myeloperoxidase *in vitro* and neutrophil granulocytes,' *Journal of Inorganic Biochemistry,* 130: pp. 84-91.

Fotie, J., A. Nkengfack, M. G. Peter, M. Heydenreich and Z. Fomum (2004), 'Chemical constituents of the ethyl acetate extracts of the stem bark and fruits of *Dichrostachys cinerea* and the roots of *Parkia bicolor*,' *Bulletin of the Chemical Society of Ethiopia,* 18(1): pp. 111-115.

Fowler, D. (2006), 'Traditional fever remedies: A list of Zambian plants,' *Kirkia,* 18(19): pp. 35-48.

Fridlender, M., Y. Kapulnik and H. Koltai (2015), 'Plant derived substances with anti-cancer activity: from folklore to practice,' *Frontiers in Plant Science,* 6: p. 799.

Gaba, M., P. Gaba, S. Singh and G. Gupta (2010), 'An overview on molecular docking,' *International Journal of Drug Development & Research,* 2(2): pp. 219-231.

Gadaleta, D., K. Vuković, C. Toma, G. J. Lavado, A. L. Karmaus, K. Mansouri, N. C. Kleinstreuer, E. Benfenati and A. Roncaglioni (2019), 'SAR and QSAR modeling of a large collection of LD_{50} rat acute oral toxicity data,' *Journal of Cheminformatics,* 11: pp. 1-16.

Garg, B., T. Bisht and Y.-C. Ling (2014), 'Sulfonated graphene as highly efficient and reusable acid carbon catalyst for the synthesis of ester plasticizers,' *RSC advances,* 4(100): pp. 57297-57307.

Godini, A., M. Kazem, G. Naseri and M. Badavi (2009), 'The effect of *Zizyphus spina-christi* leaf extract on the isolated rat aorta,' *The Journal of the Pakistan Medical Association,* 59(8): p. 537.

Gonçalves, S., D. Gomes, P. Costa and A. Romano (2013), 'The phenolic content and antioxidant activity of infusions from Mediterranean medicinal plants,' *Industrial Crops and Products,* 43: pp. 465-471.

Greub, G. and D. Raoult (2004), 'Microorganisms resistant to free-living amoebae,' *Clinical Microbiology Reviews,* 17(2): pp. 413-433.

Guan, L., H. Yang, Y. Cai, L. Sun, P. Di, W. Li, G. Liu and Y. Tang (2019), 'ADMET-score–a comprehensive scoring function for evaluation of chemical drug-likeness,' *Medchemcomm,* 10(1): pp. 148-157.

Haba, F., A. Kamelina, J. Laberche and B. VASSILIEV (2000), 'Structure de la feuille et sa variabilité intraspécifique chez les plantes ligneuses tropicales: *Cassia siamea* Lam.(sempervirente) et *Cassia sieberiana* dc (caducifoliee),' *Revue de Cytologie et de Biologie Végétales, Le Botaniste,* 23(3-4): pp. 35-40.

Hafiz, T. A. and M. A. Mubaraki (2016), 'The potential role of *Ziziphus spina-christi* leaf extracts against *Plasmodium berghei*-induced liver and spleen injury,' *Biomedical Research India,* 27(4): pp. 1027-1032.

Halim, M. A., M. Chowdhury, A. Wadud, M. Uddin, S. Sarker and M. Uddin (2007), 'The use of plants in traditional health care practice of the" Shaiji" community in Southwestern Bangladesh,' *Journal of Tropical Forest Science,* 19(3): pp. 168-175.

Hamill, F., S. Apio, N. Mubiru, R. Bukenya-Ziraba, M. Mosango, O. Maganyi and D. Soejarto (2003), 'Traditional herbal drugs of Southern Uganda, Literature analysis and antimicrobial assays,' *Journal of Ethnopharmacology,* 84(1): pp. 57-78.

Hayden, F. G. and A. T. Pavia (2006), 'Antiviral management of seasonal and pandemic influenza,' *The Journal of Infectious Diseases,* 194(2): pp. S119-S126.

Hema, R., S. Kumaravel, S. Gomathi and C. Sivasubramaniam (2010), 'Gas chromatography-mass spectroscopic analysis of *Lawsonia inermis* leaves,' *Life Science Journal,* 7(4): pp. 48-50.

Hodgson, J. (2001), 'ADMET turning chemicals into drugs,' *Nature Biotechnology,* 19(8): pp. 722-726.

Holmes, E. C., A. C. Hurt, Z. Dobbie, B. Clinch, J. S. Oxford and P. A. Piedra (2021), 'Understanding the impact of resistance to influenza antivirals,' *Clinical Microbiology Reviews,* 34(2): pp. 00224-00220.

Hong, J. (2011), 'Role of natural product diversity in chemical biology,' *Current Opinion in Chemical Biology,* 15(3): pp. 350-354.

Hosen, S., R. Dash, M. Khatun, R. Akter, M. H. R. Bhuiyan, M. Rezaul, N. J. M. Karim, F. Ahamed, K. S. Islam and S. Afrin (2017), '*In silico* ADME/T and 3D QSAR analysis of KDR inhibitors,' *Journal of Applied Pharmaceutical Sciences,* 7(1): pp. 120-128.

Hosny, M. (2012), 'Phytoconstituents from *Delonix regia* Raf roots and their biological activities,' *Al-Azhar Journal of Pharmaceutical Sciences,* 46(2): pp. 149-160.

Hou, T. and J. Wang (2008), 'Structure–ADME relationship: Still a long way to go? ,' *Expert Opinion on Drug Metabolism & Toxicology,* 4(6): pp. 759-770.

Hussain, M., S. M. Raza, K. H. Janbaz, M. R. U. Khan, A. Aziz and A. Majeed (2014), '*In vitro* comparative study of antimicrobial activity of whole plant and root's bark of *Delonix regia* (Bojer Ex. Hook),' *International Journal of Pharma Sciences,* 4(5): pp. 736-741.

Innis, S. M. (2016), 'Palmitic acid in early human development,' *Critical Reviews in Food Science and Nutrition,* 56(12): pp. 1952-1959.

Islam, M. A., S. K. Mondal, S. Islam, A. Shorna, M. Nourin, S. Biswas, M. S. Uddin, S. Zaman and M. A. Saleh (2023), 'Antioxidant, cytotoxicity, antimicrobial activity, and *in silico* analysis of the methanolic leaf and flower extracts of *Clitoria ternatea*,' *Biochemistry Research International*, Volume 2023, Article ID 8847876, 12 pages.

Islam, M. A. and T. S. Pillay (2019), 'Identification of promising anti-DNA gyrase antibacterial compounds using de novo design, molecular docking and molecular dynamics studies,' *Journal of Biomolecular Structure and Dynamics*, 38 (6): pp. 1798-1809.

Jacob, L. and M. Latha (2013), '*In vitro* antioxidant activity of *Clitoria ternatea* Linn,' *International Journal of Research in Phytochemistry and Pharmacology*, 3(1): pp. 35-39.

Jahan, I., M. S. Rahman, M. Z. Rahman, M. A. Kaisar, M. S. Islam, A. Wahab and M. A. Rashid (2010), 'Chemical and biological investigations of *Delonix regia* (Bojer Ex Hook.) Raf,' *Acta Pharmaceutica,* 60(2): pp. 207-215.

Jangiti, R. K., G. R. Battu, L. N. Majji and M. R. Talluri (2013), 'Evaluation of antidiabetic activity of *Cassia siamea* leaves in alloxan induced diabetic rats,' *International Journal of Phytopharmacology,* 4(4): pp. 237-240.

Javanian, M., M. Barary, S. Ghebrehewet, V. Koppolu, V. Vasigala and S. Ebrahimpour (2021), ʻA brief review of influenza virus infection,' *Journal of Medical Virology,* 93(8): pp. 4638-4646.

Jiang, H., J. Wang, J. SU, M. Fang, N. Yang, J. Yang, F. Wan, H. Xiao and J. Tang (2015), ʻEffect of tetrahydropalmatine on expression of Cav1. 2 in dorsal root ganglion neurons in mice with sciatic nerve chronic constriction injury,' *Chinese Pharmacological Bulletin,* 12: pp. 1598-1602.

Jima, T. T. and M. Megersa (2018), ʻEthnobotanical study of medicinal plants used to treat human diseases in Berbere district, Bale zone of Oromia regional state, South East Ethiopia,' *Evidence-Based Complementary and Alternative Medicine,* Volume 2018, Article ID 8602945, 16 pages.

Joo, Y. E. (2014), ʻNatural product-derived drugs for the treatment of inflammatory bowel diseases,' *Intestinal Research,* 12(2): pp. 103-109.

Jun, D., H. Tomoe, H. Yusuke, E. Wiwied, W. Aty, S. Osamu, S. Motoo and M. Hiroshi (2012), ʻNew tricyclic alkaloids, cassiarins G, H, J, and K from leaves of *Cassia siamea*,' *Chemical & Pharmaceutical Bulletin,* 60(2): pp. 219-222.

Kaisoon, O., S. Siriamornpun, N. Weerapreeyakul and N. Meeso (2011), ʻPhenolic compounds and antioxidant activities of edible flowers from Thailand,' *Journal of Functional Foods,* 3(2): pp. 88-99.

Kamagaté, M., C. Koffi, N. M. Kouamé, A. Akoubet, N. Alain, R. Yao and H. Die (2014), ʻEthnobotany, phytochemistry, pharmacology and toxicology profiles of *Cassia siamea* Lam,' *The Journal of Phytopharmacology,* 3(1): pp. 57-76.

Kamatenesi, M. M., A. Acipa and H. Oryem-Origa (2011), ʻMedicinal plants of Otwal and Ngai sub counties in Oyam district, Northern Uganda,' *Journal of Ethnobiology and Ethnomedicine,* 7: pp. 1-14.

Karthika, P. and N. Jayshree (2013), ʻFormulation and evaluation of sunscreen cream containing flower extract of *Delonix regia*,' *International Journal of Pharmacy and Life Sciences,* 1(16): pp. 111-129.

Kaur, G., M. S. Alam, Z. Jabbar, K. Javed and M. Athar (2006), ʻEvaluation of antioxidant activity of *Cassia siamea* flowers,' *Journal of Ethnopharmacology,* 108(3): pp. 340-348.

Kaur, J., M. Gulati, N. K. Jha, J. Disouza, V. Patravale, K. Dua and S. K. Singh (2022), ʻRecent advances in developing polymeric micelles for treating cancer: breakthroughs and bottlenecks in their clinical translation,' *Drug Discovery Today,* 27(5): pp. 1495-1512.

Kaur, P. and S. Arora (2010), ʻPolyphenols of Caselpiniaceae,' *Journal of Chinese Clinical Medicine,* 5(5): p282.

Kefalew, A., Z. Asfaw and E. Kelbessa (2015), ʻEthnobotany of medicinal plants in Ada'a district, East Shewa zone of Oromia regional state, Ethiopia,' *Journal of Ethnobiology and Ethnomedicine,* 11(1): pp. 1-28.

Khaleel, S. (2018), ʻAnti-oz-glucosidase, anti-o-amylase and anti-inflammatory effects of leaf extracts of *Ziziphus spina-christi* (Sedr) grown in Jordan,' *Research Journal of Biological Sciences,* 13(1): pp. 1-7.

Khaleel, S., A. Jaran and M. Haddadin (2016), ʻEvaluation of total phenolic content and antioxidant activity of three leaf extracts of *Ziziphus spina-christi* (Sedr) grown in Jordan,' *British Journal of Medicine and Medical Research,* 14(6): pp. 1-8.

Khan, A. A., M. A. Alsahli and A. H. Rahmani (2018), ʻMyeloperoxidase as an active disease biomarker: Recent biochemical and pathological perspectives,' *Medical Sciences,* 6(2): p 33.

Khan, M., A. Odokpe and T. Tor-Anyiin (2020), ʻIsolation and characterization of stigmasterol and *β*-sitosterol from *Cassia sieberiana* (Fabaceae) leaf extract,' *Journal of Chemical Society of Nigeria,* 45(1): pp. 135-142.

Khare, C. P. (2008). *Indian medicinal plants: An illustrated dictionary*. Springer Science & Business Media.

Khorasani Esmaeili, A., R. Mat Taha, S. Mohajer and B. Banisalam (2015), ʻAntioxidant activity and total phenolic and flavonoid content of various solvent extracts from *in vivo* and *in vitro* grown *Trifolium pratense* L. (Red clover),' *BioMed Research International,* Volume 2015, Article ID: 643285, 11 pages.

Kibuuka, M. S. and G. Anywar (2015), ʻMedicinal plant species used in the management of hernia by traditional medicine practitioners in Central Uganda,' *Ethnobotany Research and Applications,* 14: pp. 289-298.

Kim, S. B., S. H. Hwang, H.-W. Suh and S. S. Lim (2017), ʻPhytochemical analysis of *Agrimonia pilosa* Ledeb, its antioxidant activity and aldose reductase inhibitory potential,' *International Journal of Molecular Sciences,* 18(2): p379.

Koné, W. and K. K. Atindehou (2008), ʻEthnobotanical inventory of medicinal plants used in traditional veterinary medicine in Northern Côte d'Ivoire (West Africa),' *South African Journal of Botany,* 74(1): pp. 76-84.

Korji, S. H. (2012), ʻInhibition of nitrate reductase production from gram-negative bacteria using *Ziziphus spina-christi* extract and comparing with some antibiotics,' *Iraqi Journal of Agricultural Sciences,* 43(2): pp. 144-150.

Kou, F., H. Sun, L. Wu, B. Li, B. Zhang, X. Wang and L. Yang (2020), ʻTOP2A promotes lung adenocarcinoma cells' malignant progression and predicts poor prognosis in lung adenocarcinoma,' *Journal of Cancer,* 11(9): p2496.

Koudouvo, K., D. S. Karou, K. Kokou, K. Essien, K. Aklikokou, I. Glitho, J. Simpore, R. Sanogo, C. De Souza and M. Gbeassor (2011), ʻAn ethnobotanical study of antimalarial plants in Togo Maritime region,' *Journal of Ethnopharmacology,* 134(1): pp. 183-190.

Koyama, J., I. Morita, K. Tagahara, Y. Nobukuni, T. Mukainaka, M. Kuchide, H. Tokuda and H. Nishino (2002), ʻChemopreventive effects of emodin and cassiamin B in mouse skin carcinogenesis,' *Cancer Letters,* 182(2): pp. 135-139.

Kumar, P., V. Lomash, P. Jatav, A. Kumar and S. Pant (2016), ʻPrenatal developmental toxicity study of *n*-heneicosane in wistar rats,' *Toxicology and Industrial Health,* 32(1): pp. 118-125.

Kumar, S., V. Kumar and O. Prakash (2010), ʻAntidiabetic and anti-lipemic effects of *Cassia siamea* leaves extract in streptozotocin-induced diabetic rats,' *Asian Pacific Journal of Tropical Medicine,* 3(11): pp. 871-873.

Kunle, O. F., H. O. Egharevba and P. O. Ahmadu (2012), ʻStandardization of herbal medicines-a review,' *International Journal of Biodiversity and Conservation,* 4(3): pp. 101-112.

Kuwabara, N., Y. Matsuo, T. Ueki, Y. Nakamura, N. Kase, T. Okayasu, Y. Mimaki, E. Tachikawa, S. Sato and H. Yamada (2022), ʻInhibitory effect of *Rhei rhizoma* constituents on the cortisol production in acth-stimulated bovine adrenal fasciculata cells,' *Traditional Medicine,* 3(2): pp. 1-7.

Lan, J., H.-Y. Huang, S.-W. Lee, T.-J. Chen, H.-C. Tai, H.-P. Hsu, K.-Y. Chang and C.-F. Li (2014), ʻTOP2A overexpression as a poor prognostic factor in patients with nasopharyngeal carcinoma,' *Tumor Biology,* 35: pp. 179-187.

Ledwani, L. and M. Singh (2004), ʻIsolation and characterization of anthraquinones from the stem bark of *Cassia siamea*,' 43B: pp. 2257-2258.

Levine, C., H. Hiasa and K. J. Marians (1998), ʻDNA gyrase and topoisomerase IV: Biochemical activities, physiological roles during chromosome replication, and drug sensitivities,' *Biochimica et Biophysica Acta (BBA)-Gene Structure and Expression,* 1400(1-3): pp. 29-43.

Li, Y., P. S. Kumar, S. Tan, C. Huang, Z. Xiang, J. Qiu, X. Tan, J. Luo and M. He (2022), ʻAnticancer and antibacterial flavonoids from the callus of *Ampelopsis grossedentata*; a new weapon to mitigate the proliferation of cancer cells and bacteria,' *RSC advances,* 12(37): pp. 24130-24138.

Lin, W., P. Shen, Y. Song, Y. Huang and S. Tu (2021), ʻReactive oxygen species in autoimmune cells: function, differentiation, and metabolism,' *Frontiers in Immunology,* 12: Article ID 635021, 16 pages.

Lins, A. P., J. D. a. Felicio, M. M. Braggio and L. C. Roque (1991), ʻA resveratrol dimer from *Parthenocissus tricuspidata*,' *Phytochemistry,* 30(9): pp. 3144-3146.

Lipinski, C. A. (2004), ʻLead-and drug-like compounds: The rule-of-five revolution,' *Drug Discovery Today: Technologies,* 1(4): pp. 337-341.

Lipinski, C. A., F. Lombardo, B. W. Dominy and P. J. Feeney (2012), ʻExperimental and computational approaches to estimate solubility and permeability in drug discovery and development settings,' *Advanced Drug Delivery Reviews,* 64: pp. 4-17.

Luangpirom, A. and N. Saenbuaphan (2006), ʻHypoglycemic effect of *Senna siamea* (Lam.) leaf extract in rats,' 11(1): pp. 77-83.

M Calderon-Montano, J., E. Burgos-Morón, C. Pérez-Guerrero and M. López-Lázaro (2011), ʻA review on the dietary flavonoid kaempferol,' *Mini Reviews in Medicinal Chemistry,* 11(4): pp. 298-344.

Madani, I., D. A. A. Ibrahim and H. M. Hamdeen (2021), 'Abundance and ethnomedicinal use of tree and shrub species in Azaza and Mokla forests in the Blue Nile state, Sudan,' *EPRA International Journal of Multidisciplinary Research (IJMR),* 7(7): pp. 167-173.

Madu, C., B. Inyang, K. Nwachukwu, M. Nwegbu, L. Alli and M. Okoh (2021), 'Protective effects of *Delonix regia* leave extract on sodium arsenite-induced hepatotoxicity in rats,' *American Journal of Phytomedicine and Clinical Therapeutics,* 9(8): pp. 1-6.

Maitera, O., M. Khan and T. James (2011), 'Phytochemical analysis and the chemotherapeutics of leaves and stem-bark of *Nauclea latifolia* grown in Hong, Adamawa State Nigeria,' *Asian Journal of Plant Science and Research,* 1(3): pp. 16-22.

Majji, L. N., G. R. Battu, R. K. Jangiti and M. R. Talluri (2013), 'Evaluation of *in-vitro* antibacterial activity of *Cassia siamea* leaves,' *International Journal of Pharmacy and Pharmaceutical Sciences,* 5(3): pp. 263-265.

Masondo, N. and N. Makunga (2019), 'Advancement of analytical techniques in some South African commercialized medicinal plants: Current and future perspectives,' *South African Journal of Botany,* 126: pp. 40-57.

Matata, D. Z., F. Machumi, O. D. Ngassapa, M. J. Moshi, F. M. Mafumiko, K. Oosthuizen, B. Swanepoel, L. Venables, T. C. Koekemoer and P. E. Kazyoba (2021), 'Evaluation of root extract of *Cyphostemma adenocaule* (Vitaceae) for antioxidant activity, brine shrimp toxicity, and antiproliferative activity against HeLa cervical cancer cells,' 7(1): pp. 19-27.

Matos, I. d. A., N. B. da Costa Junior and F. C. Meotti (2020), 'Integration of an inhibitor-like rule and structure-based virtual screening for the discovery of novel myeloperoxidase inhibitors,' *Journal of Chemical Information and Modeling,* 60(12): pp. 6408-6418.

Mbatchi, S., B. Mbatchi, J. Banzouzi, T. Bansimba, G. N. Ntandou, J.-M. Ouamba, A. Berry and F. Benoit-Vical (2006), '*In vitro* antiplasmodial activity of 18 plants used in Congo Brazzaville traditional medicine,' *Journal of Ethnopharmacology,* 104(1-2): pp. 168-174.

Mbouangouere, R., P. Tane, D. Ngamga, P. Djemgou, M. Choudhary and B. Ngadjui (2007), 'Piptaderol from *Piptadenia africana,*' *African Journal of Traditional, Complementary and Alternative Medicines,* 4(3): pp. 294-298.

McGinty, D., C. Letizia and A. Api (2010), 'Fragrance material review on isophytol,' *Food and Chemical Toxicology,* 48 (3): pp. S76-S81.

Melaku, Y., T. Getahun, M. Addisu, H. Tesso, R. Eswaramoorthy and G. Ankita (2022), 'Molecular docking, antibacterial and antioxidant activities of compounds isolated from Ethiopian plants,' *International Journal of Secondary Metabolite,* 9(2): pp. 208-328.

Mining, J., Z. Lagat, T. Akenga, P. Tarus, M. Imbuga and M. Tsanuo (2014), 'Bioactive metabolites of *Senna didymobotrya* used as a biopesticide against *Acanthoscelides obtectus* in Bungoma, Kenya,' *Journal of Applied Pharmaceutical Science,* 4(9): pp. 56-60.

Miranda, J. J., S. Kinra, J. P. Casas, G. Davey Smith and S. Ebrahim (2008), 'Non-communicable diseases in low-and middle-income countries: Context, determinants, and health policy,' *Tropical Medicine & International Health,* 13(10): pp. 1225-1234.

Mohammed, A., M. Liman and M. Atiku (2013), 'Chemical composition of the methanolic leaf and stem bark extracts of *Senna siamea* Lam,' *Journal of Pharmacognosy and Phytotherapy*, 5(5): pp. 98-100.

Mohammed Rahmatullah, M. R., M. Haque, S. Islam, F. J. Farhana Jamal, A. Bashar, R. A. Rasheda Ahmed, I. A. Ishtiaq Ahmed, R. J. Rownak Jahan, S. A. Shamima Ahsan and M. Chowdhury (2010), 'A survey on the use of medicinal plants by folk medicinal practitioners in three areas of Pirojpur district, Bangladesh,' 4(2): pp. 247-259.

Mojab, F., M. Kamalnezhad, N. Ghaderi and P. H. Vahidi (2003), 'Phytochemical screening of some species of Iranian plants,' 2: pp. 77-82.

Morita, H., S. Oshimi, Y. Hirasawa, K. Koyama, T. Honda, W. Ekasari, G. Indrayanto and N. C. Zaini (2007), 'Cassiarins A and B, novel antiplasmodial alkaloids from *Cassia siamea*,' *Organic Letters*, 9(18): pp. 3691-3693.

Moroy, G., V. Y. Martiny, P. Vayer, B. O. Villoutreix and M. A. Miteva (2012), 'Toward *in silico* structure-based ADMET prediction in drug discovery,' *Drug Discovery Today*, 17(1-2): pp. 44-55.

Musa, N. M., M. S. Sallau, A. O. Oyewale and T. Ali (2024), 'Antimicrobial activity of lupeol and *β*-amyrin (triterpenoids) isolated from the rhizome of *Dolichos pachyrhizus* Harm,' *Advanced Journal of Chemistry*, 7(1): pp. 1-14.

Muschietti, L., R. Vila and W. Setzer, (2013). 'Tropical protozoan diseases: Natural product drug discovery and development,' *Evidence-Based Complementary and Alternative Medicine*, Volume 2013, Article ID 404250, 2 pages.

Nadembega, P., J. I. Boussim, J. B. Nikiema, F. Poli and F. Antognoni (2011), 'Medicinal plants in Baskoure, Kourittenga Province, Burkina faso: An ethnobotanical study,' *Journal of Ethnopharmacology*, 133(2): pp. 378-395.

Namukobe, J., J. M. Kasenene, B. T. Kiremire, R. Byamukama, M. Kamatenesi-Mugisha, S. Krief, V. Dumontet and J. D. Kabasa (2011), 'Traditional plants used for medicinal purposes by local communities around the Northern sector of Kibale national park, Uganda,' *Journal of Ethnopharmacology*, 136(1): pp. 236-245.

Nanasombat, S. and N. Teckchuen (2009), 'Antimicrobial, antioxidant and anticancer activities of Thai local vegetables,' *Journal of Medicinal Plants Research*, 3(5): pp. 443-449.

Narramore, S., C. E. Stevenson, A. Maxwell, D. M. Lawson and C. W. Fishwick (2019), 'New insights into the binding mode of pyridine-3-carboxamide inhibitors of *E. coli* DNA gyrase,' *Bioorganic and Medicinal Chemistry*, 27(16): pp. 3546-3550.

Nerio, L. S., J. Olivero-Verbel and E. Stashenko (2010), 'Repellent activity of essential oils: A review,' *Bioresource Technology*, 101(1): pp. 372-378.

Ngamrojanavanich, N., S. Manakit, S. Pornpakakul and A. Petsom (2006), 'Inhibitory effects of selected Thai medicinal plants on Na+, K+-ATPase,' *Fitoterapia*, 77(6): pp. 481-483.

Ngo, L. T., J. I. Okogun and W. R. Folk (2013), '21st century natural product research and drug development and traditional medicines,' *Natural Product Reports*, 30(4): pp. 584-592.

Nguyen, A. T., H. Malonne, P. Duez, R. Vanhaelen-Fastre, M. Vanhaelen and J. Fontaine (2004), ʻCytotoxic constituents from *Plumbago zeylanica*,' *Fitoterapia*, 75(5): pp. 500-504.

Njoku, I. S., N.-U. Rahman, A. M. Khan, I. Otunomo, O. T. Asekun, O. B. Familoni and C. Ngozi (2022), ʻComparison of three different extraction methods for the determination of the quality of the leaf volatile oils of *Delonix regia* (Bojer Ex Hook. Raf),' *Tropical Journal of Natural Product Research,* 6(1): pp. 71-75.

Nna, P., T. Tor-Anyiin, J. Igoli, M. Khan and J. Anyam (2017), ʻPhytochemical and antimicrobial screening of root extracts of *Dacryodes edulis*,' *Biotechnology Journal International,* 19(3): pp. 1-9.

Nsonde-Ntandoua, G., L. Lucantoni, J. Banzouzi, M. Ndounga, S. Yerbanga, J. Ouambaf, A. Habluetzel, F. Esposito and A. Abena, (2010). Mosquitocidal and antifecundity effects of coumarin and betulinic acid isolated from *Cassia siamea* (Fabaceae) stem bark chloroform extract on female anopheles stephens (dipteria cilicidae). Abstract, actes du Symposium International, Bénin.

Ntandou, G. N., J. Banzouzi, B. Mbatchi, R. Elion-Itou, A. Etou-Ossibi, S. Ramos, F. Benoit-Vical, A. Abena and J. Ouamba (2010), ʻAnalgesic and anti-inflammatory effects of *Cassia siamea* Lam. stem bark extracts,' *Journal of Ethnopharmacology,* 127(1): pp. 108-111.

Ochwang'i, D. O., C. N. Kimwele, J. A. Oduma, P. K. Gathumbi, J. M. Mbaria and S. G. Kiama (2014), ʻMedicinal plants used in treatment and management of cancer in Kakamega County, Kenya,' *Journal of Ethnopharmacology,* 151(3): pp. 1040-1055.

Odason, E. and J. Kolawole (2007), ʻOf the aqueous extract of the root of *Cassia siamea* Lam.(Ceasalpiniaceae),' *Nigerian Journal of Pharmaceutical Research,* 6(1): pp. 66-69.

Ode, O., S. Saka and G. M. Oladele (2011), ʻThe global relevance of traditional medicine and herbal plants, the Nigerian perspective,' *International Journal of Applied Biology and Pharmaceutical Technology,* 2(4): pp. 280-289.

Ododo, M. M., M. K. Choudhury and A. H. Dekebo (2016), ʻStructure elucidation of *β*-sitosterol with antibacterial activity from the root bark of *Malva parviflora*,' *SpringerPlus,* 5: pp. 1-11.

Ogbiko, C., Z. Adiya, S. Adamu, A. Isah and I. Ibrahim (2021), ʻPhytochemical, nutritional and antimicrobial properties of the leaves of Nigerian *Ziziphus spina–christi* (L.) Willd,' *Journal of Pharmaceutical and Allied Sciences,* 18(1): pp. 3445-3452.

Ogbole, O., J. Adeniji, E. Ajaiyeoba, R. Kamdem and C. Mohammed (2014), ʻAnthraquinones and triterpenoids from *Senna siamea* (Fabaceae) Lam inhibit poliovirus activity,' *African Journal of Microbiology Research,* 8(31): pp. 2955-2963.

Ogunkunle, A. and T. A. Ladejobi (2006), ʻEthnobotanical and phytochemical studies on some species of *Senna* in Nigeria,' *African Journal of Biotechnology,* 5(21): pp. 2020-2023.

Ogunwande, I. A., N. O. Avoseh, G. Flamini, A. S. O. Hassan, A. O. Ogunmoye, A. O. Ogunsanwo, K. O. Yusuf, A. O. Kelechi, Z. A. Tiamiyu and G. O. Tabowei (2013), ʻEssential oils from the leaves of six medicinal plants of Nigeria,' *Natural Product Communications,* 8(2): pp. 243-248.

Olonisakin, A., 2014, ʻ1-Hexadecene from aerial parts of *Ageratina adenophora*,' *Science Research Anals*, 6(1): pp. 10-18.

Orwa, C., A. Mutua, R. Kindt, R. Jamnadass and A. Simons, (2013). *Delonix regia*. Agroforestry.

Oshimi, S., Y. Tomizawa, Y. Hirasawa, T. Honda, W. Ekasari, A. Widyawaruyanti, M. Rudyanto, G. Indrayanto, N. C. Zaini and H. Morita (2008), ʻChrobisiamone A, a new bischromone from *Cassia siamea* and a biomimetic transformation of 5-acetonyl-7-hydroxy-2-methylchromone into cassiarin A,' *Bioorganic and Medicinal Chemistry Letters*, 18(13): pp. 3761-3763.

Otimenyin, S., J. Kolawole and M. Nwosu (2010), ʻPharmacological basis for the continual use of the root of *Senna siamea* in traditional medicine,' *International Journal of Pharma and Bio Sciences,* 1(3): pPS67.

Owuor, B. O. and D. P. Kisangau (2006), ʻKenyan medicinal plants used as antivenin: A comparison of plant usage,' *Journal of Ethnobiology and Ethnomedicine,* 2: pp. 1-8.

Oyebade, K., A. Daspan, Y. Denkok, T. Alemika and O. Ojerinde (2021), ʻAntimicrobial, antioxidant, and antiproliferative properties of the leaves of *Senna siamea*,' *Journal of Complementary and Alternative Medical Research,* 14(1): pp. 22-29.

Padumanonda, T., L. Suntornsuk and W. Gritsanapan (2006), ʻQuantitative analysis of barakol content in *Senna siamea* leaves and flowers by TLC-densitometry,' *Medical Principles and Practice,* 16(1): pp. 47-52.

Page, M. G. and J. Heim (2009), ʻProspects for the next anti-*pseudomonas* drug,' *Current Opinion in Pharmacology,* 9(5): pp. 558-565.

Palermo, G. and M. De Vivo (2015), ʻComputational Chemistry for drug discovery,' *Encyclopedia of Nanotechnology*: pp. 1-15.

Pandey, A. K. and Y. Tripathi (2017), ʻEthnobotany and its relevance in contemporary research,' *Journal of Medicinal Plants Studies,* 5(3): pp. 123-129.

Papari Moghadam Fard, M., S. Ketabchi and M. H. Farjam (2020), ʻChemical composition, antimicrobial and antioxidant potential of essential oil of *Ziziphus spina-christi* Var. Aucheri grown wild in Iran,' *Journal of Medicinal Plants and By-product*, 9: pp. 69-73.

Parasuraman, S., G. S. Thing and S. A. Dhanaraj (2014), ʻPolyherbal formulation: Concept of Ayurveda,' *Pharmacognosy Reviews,* 8(16): pp. 73-80.

Parekh, A., D. Smeeth, Y. Milner and S. Thuret, (2017). The role of lipid biomarkers in major depression. In *Healthcare*, 5(5): PP. 1.17.

Parul, R., M. J. Alam and M. S. Rana (2014), ʻAntinociceptive and cytotoxic potential of ethanolic extract of *Delonix regia* (leaves),' *Indian Journal of Pharmaceutical and Biological Research,* 2(1): p55.

Patel, D. K., R. Kumar, D. Laloo and S. Hemalatha (2012), ʻNatural medicines from plant source used for therapy of diabetes mellitus: An overview of its pharmacological aspects,' *Asian Pacific Journal of Tropical Disease,* 2(3): pp. 239-250.

Paul Gleeson, M., A. Hersey and S. Hannongbua (2011), '*In-silico* ADME models: A general assessment of their utility in drug discovery applications,' *Current Topics in Medicinal Chemistry,* 11(4): pp. 358-381.

Perkin, A. G. (1902), 'Xxi, myricetin. Part II,' *Journal of the Chemical Society, Transactions,* 81: pp. 203-210.

Pieczenik, S. R. and J. Neustadt (2007), 'Mitochondrial dysfunction and molecular pathways of disease,' *Experimental and Molecular Pathology,* 83(1): pp. 84-92.

Pimm, S. L., C. N. Jenkins, R. Abell, T. M. Brooks, J. L. Gittleman, L. N. Joppa, P. H. Raven, C. M. Roberts and J. O. Sexton (2014), 'The biodiversity of species and their rates of extinction, distribution, and protection,' *Science,* 344(6187): p1246752.

Pizzino, G., N. Irrera, M. Cucinotta, G. Pallio, F. Mannino, V. Arcoraci, F. Squadrito, D. Altavilla and A. Bitto (2017), 'Oxidative stress: Harms and benefits for human health,' *Oxidative Medicine and Cellular Longevity,* 2017: Article ID 8416763, 13 pages.

Prado, R., S. O. Francis, M. N. Mason, G. Wing, R. G. Gamble and R. Dellavalle (2011), 'Nonmelanoma skin cancer chemoprevention,' *Dermatologic Surgery,* 37(11): pp. 1566-1578.

Prasad, M., K. Rao, D. Santhosha, R. Chaitanya and B. David (2010), 'Medicinal pants used by the ethnic practitioners in Nalgonda district, Andhra Pradesh, India,' *International Journal of Research in Ayurveda and Pharmacy (IJRAP),* 1(2): pp. 493-496.

Priya, N. and P. S. Kumari (2017), 'Antiviral activities and cytotoxicity assay of seed extracts of *Piper longum* and *Piper nigrum* on human cell lines,' *International Journal of Pharmaceutical Sciences Review and Research,* 44(1): pp. 197-202.

Qian, W., X. Xiong, Z. Fang, H. Lu and Z. Wang (2014), 'Protective effect of tetramethylpyrazine on myocardial ischemia-reperfusion injury,' *Evidence-Based Complementary and Alternative Medicine,* Volume 2014, Article ID 107501, 9 pages.

Ramsewak, R. S., M. G. Nair, S. Murugesan, W. J. Mattson and J. Zasada (2001), 'Insecticidal fatty acids and triglycerides from *Dirca palustris*,' *Journal of Agricultural and Food Chemistry,* 49(12): pp. 5852-5856.

Rekha, D. (2013), 'Study of medicinal plants used from Koothanoallur and Marakkadai, Thiruvarur district of Tamil Nadu, India,' *Hygeia Journal for Drugs and Medicines,* 5(1): pp. 164-170.

Remi-Esan, I., O. O. Bankole, A. Shittu and O. Ogunfeitimi (2020), '*In vitro* antioxidant activities of aqueous leaf extract of *Delonix regia*,' *International Journal of Creative and Innovative Research in All Studies,* 2(12): pp. 146-154.

Rivers, M. C., N. A. Brummitt, E. N. Lughadha and T. R. Meagher (2011), 'Genetic variation in *Delonix s.l* (Leguminosae) in Madagascar revealed by AFLPS: Fragmentation, conservation status and taxonomy,' *Conservation Genetics,* 12: pp. 1333-1344.

Rohaiza, S., W. Yaacob, L. Din and I. Nazlina (2012), 'Chemical constituents of stem bark of *Shorea faguetiana*,' 41(12): pp. 1571-1577.

Rusciano, G., P. Capriglione, G. Pesce, S. Del Prete, G. Cennamo, D. Di Cave, L. Cerulli and A. Sasso (2013), ʻRaman microspectroscopy analysis in the treatment of *Acanthamoeba keratitis*,' *PLoS One,* 8(8): p. e72127.

Sachidananda Swamy, H., M. Asha, M. Chaithra, M. Vivek and P. K. T. Yoshoda Kambar (2014), ʻAntibacterial activity of flower extract of *Caesalpinia pulcherrima*, *Delonix regia* and *Peltaphorum ferrugineum* against urinary tract pathogens,' *International Research Journal of Biological Sciences,* 3(4): pp. 80-83.

Said, A., G. Fawzy, E.-S. A. A. tabl and O. Tzakou (2010), ʻVolatile constituents of *Zizyphus jujuba* aerial parts and *Zizyphus spina-christi* fruits from Egypt,' *Journal of Essential Oil Bearing Plants,* 13(2): pp. 170-174.

Sakna, S. T., A. Mocan, H. N. Sultani, N. M. El-Fiky, L. A. Wessjohann and M. A. Farag (2019), ʻMetabolites profiling of *Ziziphus* leaf taxa via UHPLC/PDA/ESI-MS in relation to their biological activities,' *Food Chemistry,* 293: pp. 233-246.

Salmerón-Manzano, E., J. A. Garrido-Cardenas and F. Manzano-Agugliaro (2020), ʻWorldwide research trends on medicinal plants,' *International Journal of Environmental Research and Public Health,* 17(10): p. 3376.

Salmerón-Manzano, E. and F. Manzano-Agugliaro (2020), ʻWorldwide research on low-cost technologies through bibliometric analysis,' *Inventions,* 5(1): pp. 1-22.

Sama, K., V. Xavier and A. Raja (2011), ʻPreliminary phytochemical screening of root bark of *Delonix regia*,' *International Research Journal of Pharmacy,* 2(10): pp. 42-43.

Sanon, S., E. Ollivier, N. Azas, V. Mahiou, M. Gasquet, C. Ouattara, I. Nebie, A. Traore, F. Esposito and G. Balansard (2003), ʻEthnobotanical survey and *in vitro* antiplasmodial activity of plants used in traditional medicine in Burkina faso,' *Journal of Ethnopharmacology,* 86(2-3): pp. 143-147.

Santos, R., A. Conceição, I. Lula, F. Oliveira and R. Oliveira (2018), ʻTriterpenes esterified with fatty acid isolated from *Pouteria macahensis* T.D Penn (Sapotaceae) leaves,' 10(5): pp. 1-8.

Sati, S. C., S. Nitin, U. Rawat and O. Sati (2010), ʻMedicinal plants as a source of antioxidants,' *Research Journal of Phytochemistry,* 4(4): pp. 213-224.

Satiraphan, M. S., (2012). Phytochemical screening of two Thai tropical rainforest Dipterocarps: Hopea odorata Roxb. and Dipterocarpus costatus Gaertn. F. Université René Descartes-Paris V; Silpakorn University. Faculty of Pharmacy.

Schripsema, J. and D. Dagnino (1996), ʻElucidation of the substitution pattern of 9, 10-anthraquinones through the chemical shifts of peri-hydroxyl protons,' *Phytochemistry,* 42(1): pp. 177-184.

Seble, W., Z. Asfaw and E. Kelbessa (2015), ʻEthnobotanical study of medicinal plants used by local communities of Minjar-shenkora district, North Shewa zone of Amhara region, Ethiopia,' *Journal of Medicinal Plants Research,* 3(6): pp. 1-11.

Sengera, G. O., E. O. Kenanda and J. M. Onyancha (2023), ʻAntibacterial, antioxidant potency, and chemical composition of essential oils from dried powdered leaves and flowers of

Hypericum revolutum subsp. *Keniense* (Schweinf.),' *Evidence-Based Complementary and Alternative Medicine,* Volume 2023, Article ID 4125885, 15 pages.

Shabir, G., F. Anwar, B. Sultana, Z. M. Khalid, M. Afzal, Q. M. Khan and M. Ashrafuzzaman (2011), 'Antioxidant and antimicrobial attributes and phenolics of different solvent extracts from leaves, flowers and bark of gold mohar [*Delonix regia* (Bojer Ex Hook.) Raf.],' *Molecules,* 16(9): pp. 7302-7319.

Shanmukha, I., H. P. Harshil Patel, J. P. Jignesh Patel and R. Riyazunnisa (2011), 'Quantification of total phenol and flavonoid content of delonix regia flowers,' 3(1): pp. 280-283.

Sharifi-Rad, J., C. Quispe, A. Turgumbayeva, Z. Mertdinç, S. Tütüncü, E. F. Aydar, B. Özçelik, S.-W. Anna, S. Mariola and A. Koziróg (2023), '*Santalum* genus: Phytochemical constituents, biological activities, and health promoting-effects,' *Zeitschrift für Naturforschung C,* 78(1-2): pp. 9-25.

Sharma, S. and S. Arora (2015), 'Phytochemicals and pharmaceutical potential of *Delonix regia* (Bojer Ex Hook) Raf a review,' *International Journal of Pharmacy and Pharmaceutical Sciences,* 7(8): pp. 17-29.

Shewale, V. D., T. A. Deshmukh, L. S. Patil and V. R. Patil (2012), 'Anti-inflammatory activity of *Delonix regia* (Boj. Ex. Hook),' *Advances in Pharmacological and Pharmaceutical Sciences,* Volume 2012, Article ID 789713, 4 pages.

Shiramane, R. S., K. V. Biradar, B. V. Chivde, H. Shambhulingayya and V. Goud (2011), '*In vivo* antidiarrhoeal activity of ethanolic extract of *Delonix regia* flowers in experimentally induced diarrhea in wistar albino rats,' *International Journal of Research in Pharmacy and Chemistry,* 1(3): pp. 2231-2781.

Shrivastava, S. R., P. S. Shrivastava and J. Ramasamy (2018), 'World health organization releases global priority list of antibiotic-resistant bacteria to guide research, discovery, and development of new antibiotics,' *Journal of Medical Society,* 32(1): pp. 76-77.

Shwe, H. H., K. K. Win, T. T. Moe, A. A. Myint and T. Win (2019), 'Isolation and structural characterization of lupeol from the stem bark of *Diospyros ehretioides* wall,' *IEEE-SEM,* 7(8): pp. 140-144.

Siddiqui, R. and N. A. Khan (2012), 'Biology and pathogenesis of acanthamoeba,' *Parasites and Vectors,* 5(6): pp. 1-13.

Singh, S., S. K. Singh and A. Yadav (2013), 'A review on *Cassia* species: Pharmacological, traditional and medicinal aspects in various countries,' *American Journal of Phytomedicine and Clinical Therapeutics,* 1(3): pp. 291-312.

Singh, V., N. Guizani, M. M. Essa, M. S. Rahman and S. Selvaraju (2012), '*In vitro* antioxidant activities of *Ziziphus spina-christi* fruits (red date) grown in Oman,' *Biotechnology,* 11(4): pp. 209-216.

Singleton, W., T. Ward and F. Dollear (1950), 'Physical properties of fatty acids. Some dilatometric and thermal properties of stearic acid in two polymorphic forms,' *Journal of the American Oil Chemists' Society,* 27(4): pp. 143-146.

Smith, Y. A. (2009), ʻDetermination of the chemical composition of *Senna-siamea* (*Cassia* leaves),' *Pakistan Journal of Nutrition,* 8(2): pp. 119-121.

Soliman, H. and Y. Shattory (2017), ʻSeparation of palmitic acid from overused oil for production of heterogeneous organic derivatives of potential biological activities,' *Egyptian Journal of Chemistry,* 60(4): pp. 591-600.

Subramanian, D. and S. Venugopal (2011), ʻComparative study of antioxidant activities of *Cassia auriculata* and *Cassia siamea* flowers,' *International Research Journal of Pharmacy,* 2(12): pp. 208-212.

Sudarikov, D. V., Y. V. Gyrdymova, A. V. Borisov, J. M. Lukiyanova, R. V. Rumyantcev, O. G. Shevchenko, D. R. Baidamshina, N. D. Zakarova, A. R. Kayumov and E. O. Sinegubova (2022), ʻSynthesis and biological activity of unsymmetrical monoterpenylhetaryl disulfides,' *Molecules,* 27(16): p5101.

Suleiman, R. K., S. A. Umoren, W. Iali and B. El Ali (2022), ʻIsolation of new constituents from whole plant of *Salsola imbricata* Forssk. of Saudi origin,' *ACS omega,* 7(23): pp. 20332-20338.

Suliman, M. B. and A. A. Mohammed (2018), ʻPreliminary phytochemical screening and antibacterial activity of ethanolic and aqueous extracts of Sudanese medicinal plant *Ziziphus spina-christi* L. leaves,' *Arabian Journal of Medicinal and Aromatic Plants,* 4(1): pp. 36-44.

Sulimov, A., D. Kutov, I. Ilin, D. Zheltkov, E. Tyrtyshnikov and V. Sulimov (2019), ʻSupercomputer docking with a large number of degrees of freedom,' *SAR and QSAR in Environmental Research,* 30(10): pp. 733-749.

Sultana, S., S. Nafees and A. Khan (2013), ʻPerillyl alcohol as a protective modulator against rat hepatocarcinogenesis via amelioration of oxidative damage and cell proliferation,' *Human & Experimental Toxicology,* 32(11): pp. 1179-1192.

Swier, J. (2012), ʻSustainability of medicinal plant trade in southern Benin,' *Plant use of the Motherland: linking West African and Afro-Caribbean Ethnobotany Student Projects Ethnobotany*.

Szentmáry, N., L. Daas, L. Shi, K. L. Laurik, S. Lepper, G. Milioti and B. Seitz (2019), ʻAcanthamoeba keratitis–clinical signs, differential diagnosis and treatment,' *Journal of Current Ophthalmology,* 31(1): pp. 16-23.

Tanaka, T., M. Iinuma and H. Murata (1998), ʻStilbene derivatives in the stem of *Parthenocissus quinquefolia*,' *Phytochemistry,* 48(6): pp. 1045-1049.

Teangpook, C., U. Paosangtong, Y. Titatarn, S. Onhem and W. Puminat (2011), ʻProduction and nutrition of Khi lek (*Siamese cassia*) curry from central Thailand,' *Agriculture and Natural Resources,* 45(3): pp. 510-520.

Teklay, A., B. Abera and M. Giday (2013), ʻAn ethnobotanical study of medicinal plants used in Kilte Awulaelo district, Tigray region of Ethiopia,' *Journal of Ethnobiology and Ethnomedicine,* 9: pp. 1-23.

Temerk, H., W. Salem, W. Sayed and F. Hassan (2017), ʻAntibacterial effect of phytochemical extracts from *Ziziphus-spina christi* against some pathogenic bacteria,' *Egyptian Journal of Botany,* 57(3): pp. 595-604.

Tetik, F., S. Civelek and U. Cakilcioglu (2013), ʻTraditional uses of some medicinal plants in Malatya (Turkey),' *Journal of Ethnopharmacology,* 146(1): pp. 331-346.

Thongsaard, W., S. Chainakul, G. Bennett and C. Marsden (2001), ʻDetermination of barakol extracted from *Cassia siamea* by HPLC with electrochemical detection,' *Journal of Pharmaceutical and Biomedical Analysis,* 25(5-6): pp. 853-859.

Tuenter, E., K. Foubert, D. Staerk, S. Apers and L. Pieters (2017), ʻIsolation and structure elucidation of cyclopeptide alkaloids from *Ziziphus nummularia* and *Ziziphus spina-christi* by HPLC-DAD-MS and HPLC-PDA-(HRMS)-SPE-NMR,' *Phytochemistry,* 138: pp. 163-169.

Udegbunam, R., S. Udegbunam and G. Anosa (2013), ʻAnalgesic and anti-inflammatory effects of *Cyphostemma vogelii* (Hook. F.) Desc. Root extract in mice,' *African Journal of Biotechnology,* 12(17): pp. 2288-2292.

Ugwah, M. O., E. U. Etuk, S. O. Bello, A. A. Aliero and C. J. Ugwah-Oguejiofor (2013), ʻComparative studies of anti-ulcerogenic activities of three Nigerian medicinal plants: A preliminary evaluation,' *Journal of Medicinal Plants Research,* 7(9): pp. 490-495.

Valentini, G., L. Chiarelli, R. Fortin, M. L. Speranza, A. Galizzi and A. Mattevi (2000), ʻThe allosteric regulation of pyruvate kinase: A site-directed mutagenesis study,' *Journal of Biological Chemistry,* 275(24): pp. 18145-18152.

Vasait, R. D. (2016), ʻScreening of antibacterial properties of crude leaves extracts of plant *Cassia siamea* collected from Baglan region,' *Screening,* 6(11): pp. 42-43.

Veber, D. F., S. R. Johnson, H.-Y. Cheng, B. R. Smith, K. W. Ward and K. D. Kopple (2002), ʻMolecular properties that influence the oral bioavailability of drug candidates,' *Journal of Medicinal Chemistry,* 45(12): pp. 2615-2623.

Veerachari, U. and A. Bopaiah (2011), ʻPreliminary phytochemical evaluation of the leaf extract of five *Cassia* species,' *Journal of Chemical and Pharmaceutical Research,* 3(5): pp. 574-583.

Veigas, J. M., P. Divya and B. Neelwarne (2012), ʻIdentification of previously unreported pigments among carotenoids and anthocyanins in floral petals of *Delonix regia* (Hook.) Raf,' *Food Research International,* 47(1): pp. 116-123.

Venza, I., M. Venza, M. Visalli, G. Lentini, D. Teti and F. S. d′ Alcontres (2021), ʻRos as regulators of cellular processes in melanoma,' *Oxidative Medicine and Cellular Longevity,* 2021: Article ID 1208690, 19 pages.

Vivek, M., S. S. HC, M. Manasa, S. Pallavi, Y. Kambar, M. Asha, M. Chaithra, P. K. TR, N. Mallikarjun and R. Onkarappa (2013), ʻAntimicrobial and antioxidant activity of leaf and flower extract of *Caesalpinia pulcherrima, Delonix regia* and *Peltaphorum ferrugineum,*' *Journal of Applied Pharmaceutical Science,* 3(8): pp. 064-071.

Wang, L.-S., C.-T. Lee, W.-L. Su, S.-C. Huang and S.-C. Wang (2016), 'Delonix regia leaf extract (Drle): A potential therapeutic agent for cardioprotection,' *PLoS One*, 11(12): p. e0167768.

Warren, G. L., C. W. Andrews, A.-M. Capelli, B. Clarke, J. LaLonde, M. H. Lambert, M. Lindvall, N. Nevins, S. F. Semus and S. Senger (2006), 'A critical assessment of docking programs and scoring functions,' *Journal of Medicinal Chemistry*, 49(20): pp. 5912-5931.

Wei, H., Y. Peng, G. Ma, L. Xu and P. Xiao (2012), 'Advances in studies on active components of *Saussurea lappa* and their pharmacological actions,' *Chinese Traditional and Herbal Drugs*, 43(3): pp. 613-620.

WHO. (2019). *WHO global report on traditional and complementary medicine 2019*. World Health Organization.

Wijayasiriwardena, C., P. Sharma, M. Chauhan and A. Pillai (2009), 'Pharmacognostical investigation of unexplored leaf drug *Delonix elata* (L.) gamble from folklore practice,' *International Journal of Research in Ayurveda*, 30(1): pp. 68-72.

Xu, R., X.-Q. Liu, D.-X. Tie, Y.-H. Zhao and D.-R. Wan (2008), 'Study on pharmacognostic identification of *Cassia siamea*,' *Zhong yao cai= Zhongyaocai= Journal of Chinese Medicinal Materials*, 31(7): pp. 974-977.

Yadav, M. K., K. Mailar, J. Nagarajappa Masagalli, J.-J. Song and W. J. Choi (2019), 'Ruthenium chloride-induced oxidative cyclization of *trans*-resveratrol to (±)-*ε*-viniferin and antimicrobial and antibiofilm activity against *Streptococcus pneumoniae*,' *Frontiers in Pharmacology*, 10: p.890.

Yakubu, A. H., M. M. Mohammed, A. B. Bababe and H. Y. Braimah (2021), 'Phytochemical screening, antioxidant and antibacterial activities of the root extract of *Cyphostemma adenocaule* (Steud. Ex A. Rich.) wild & Rb Drumm,' *Biology, Medicine, and Natural Product Chemistry*, 10(2): pp. 105-110.

Yang, L., K. S. Wen, X. Ruan, Y.-X. Zhao, F. Wei and Q. Wang (2018), 'Response of plant secondary metabolites to environmental factors,' *Molecules*, 23(4): pp. 1-26.

Yarnell, E. and K. Abascal (2004), 'Botanical treatment and prevention of malaria: Part 2 selected botanicals,' *Alternative and Complementary Therapies*, 10(5): pp. 277-284.

Yirga, G., M. Teferi and M. Kasaye (2011), 'Survey of medicinal plants used to treat human ailments in Hawzen district, Northern Ethiopia,' *International Journal of Biodiversity and Conservation*, 3(13): pp. 709-714.

Yuan, H., Q. Ma, L. Ye and G. Piao (2016), 'The traditional medicine and modern medicine from natural products,' *Molecules*, 21(5): p.559.

Yun, X.-j., H.-m. Shu, G.-y. Chen, M.-h. Ji and J.-y. Ding (2014), 'Chemical constituents from barks of *Lannea coromandelica*,' *Chinese Herbal Medicines*, 6(1): pp. 65-69.

Yusuf, A., M. A. Shaikat, M. A. Bhuiya, M. Dutta, A. K. Nath and P. R. Dash (2023), 'Utilizing the medicinal properties of *Delonix regia* for diseases and beyond: A review of its phytochemistry and pharmacology,' *Tropical Journal of Natural Product Research*, 7(12): p.5355.

Zavascki, A. P., C. G. Carvalhaes, R. C. Picao and A. C. Gales (2010), 'Multidrug-resistant *Pseudomonas aeruginosa* and *Acinetobacter baumannii*: resistance mechanisms and implications for therapy,' *Expert Review of Anti-infective Therapy,* 8(1): pp. 71-93.

Zeng, S., A. Liu, L. Dai, X. Yu, Z. Zhang, Q. Xiong, J. Yang, F. Liu, J. Xu and Y. Xue (2019), 'Prognostic value of TOP2A in bladder urothelial carcinoma and potential molecular mechanisms,' *BMC Cancer*, 19: pp. 1-12.

Zhai, Z., H. An, G. Wang, Y. Luo and Y. Hao (2015), 'Functional role of pyruvate kinase from *Lactobacillus bulgaricus* in acid tolerance and identification of its transcription factor by bacterial one-hybrid,' *Scientific reports,* 5(1): p.17024.

Zhang, L., J. Yan, X. Liu, Z. Ye, X. Yang, R. Meyboom, K. Chan, D. Shaw and P. Duez (2012), 'Pharmacovigilance practice and risk control of traditional Chinese medicine drugs in China: current status and future perspective,' *Journal of Ethnopharmacology,* 140(3): pp. 519-525.

Zhang, Y., D. Wang, L. Yang, D. Zhou and J. Zhang (2014), 'Purification and characterization of flavonoids from the leaves of *Zanthoxylum bungeanum* and correlation between their structure and antioxidant activity,' *PLoS One,* 9(8): p. e105725.

Zhao, S., W. Ye, J. Gu, J. Liu, X. Zhang, Z. Yin, H. Wang, L. Zhang, Y. Guo and J. Feng (2012), 'Medicinal plant resources in Lingnan area and emergency medicine in Ge Hong Zhou Hou Bei Ji Fang,' *Asia Pacific Traditional Medicine* 8: pp. 11-12.

Zhong, Y., X. Zhang, X. Cai, K. Wang, Y. Chen and Y. Deng (2014), 'Puerarin attenuated early diabetic kidney injury through down-regulation of matrix metalloproteinase 9 in streptozotocin-induced diabetic rats,' *PLoS One,* 9(1): p. e85690.

Zhu, F., X. H. Ma, C. Qin, L. Tao, X. Liu, Z. Shi, C. L. Zhang, C. Y. Tan, Y. Z. Chen and Y. Y. Jiang (2012), 'Drug discovery prospect from untapped species: Indications from approved natural product drugs,' *PLoS One,* 7(7): p. e39782.

Zito, P., M. Labbozzetta, M. Notarbartolo, M. Sajeva and P. Poma (2019), 'Essential oil of *Cyphostemma juttae* (Vitaceae): Chemical composition and antitumor mechanism in triple negative breast cancer cells,' *PLoS One,* 14(3): p. e0214594.

APPENDICES

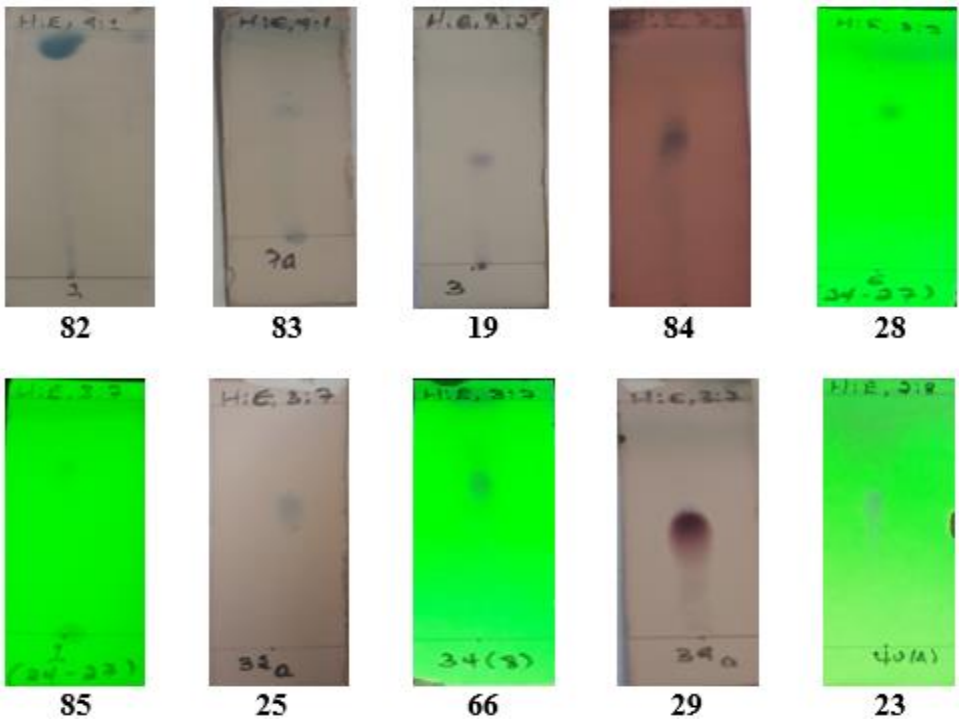

Appendix 1: TLC profile of the isolated compounds from roots of *C. adenocaule*.

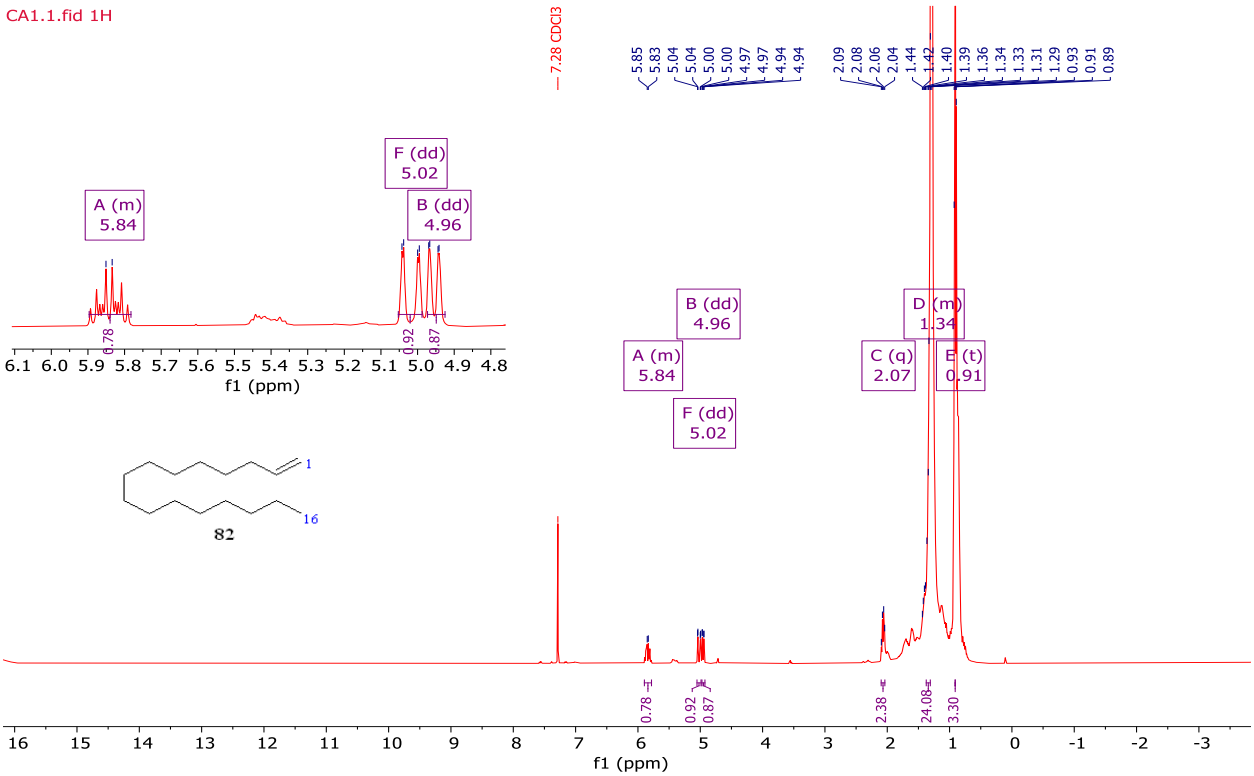

A: ^{1}H NMR (400 MHz, $CDCl_3$) spectrum of compound **82**.

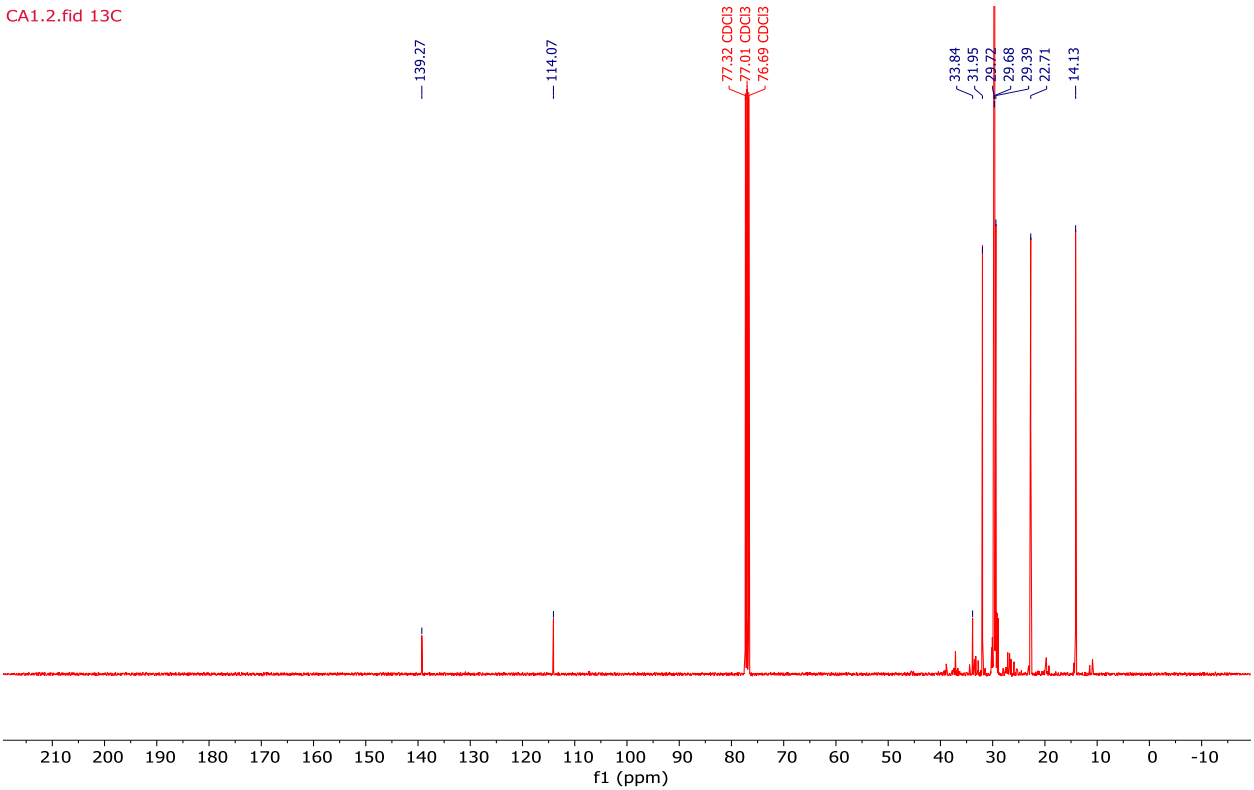

B: ^{13}C NMR (100 MHz, $CDCl_3$) spectrum of compound **82**.

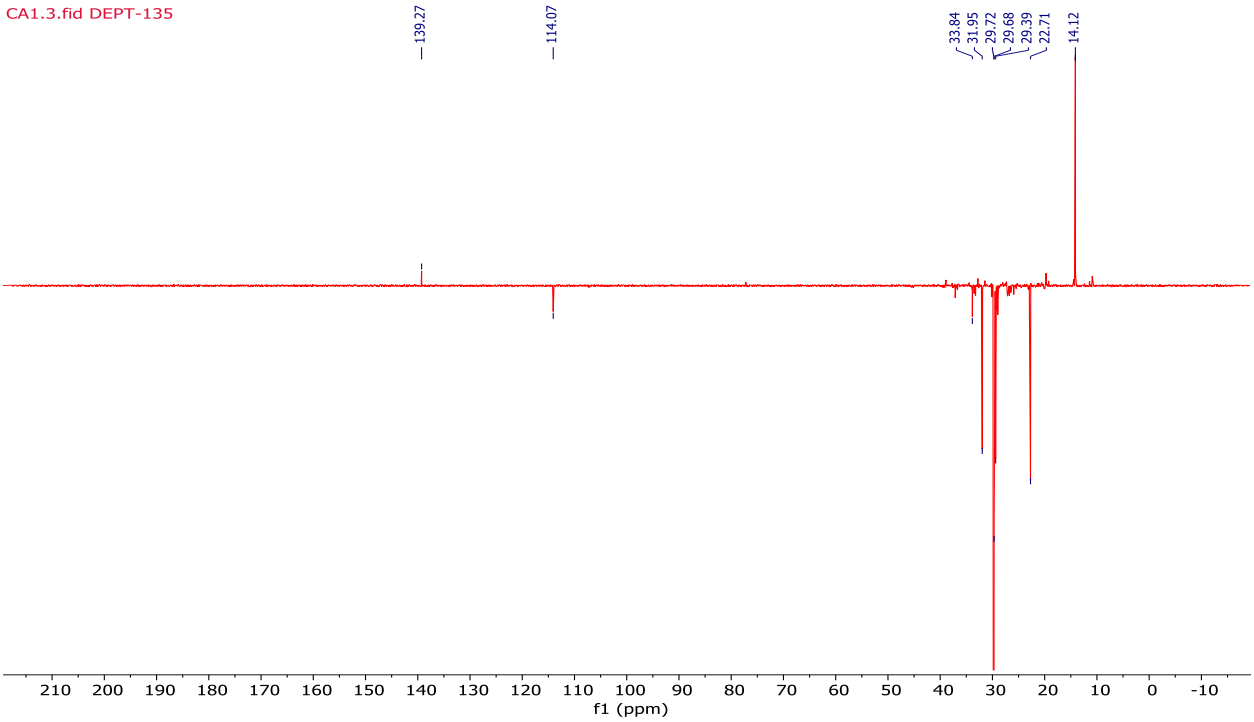

C: DEPT-135 spectrum of compound **82**.

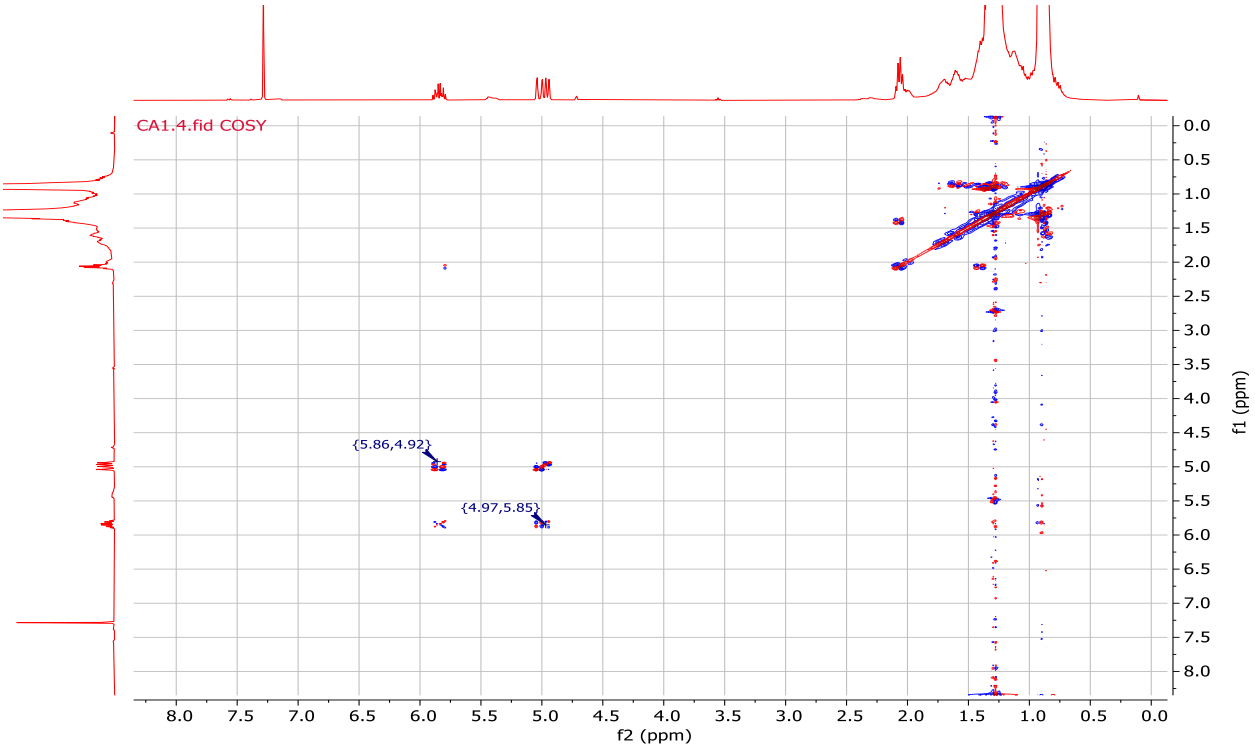

D: COSY spectrum of compound **82**.

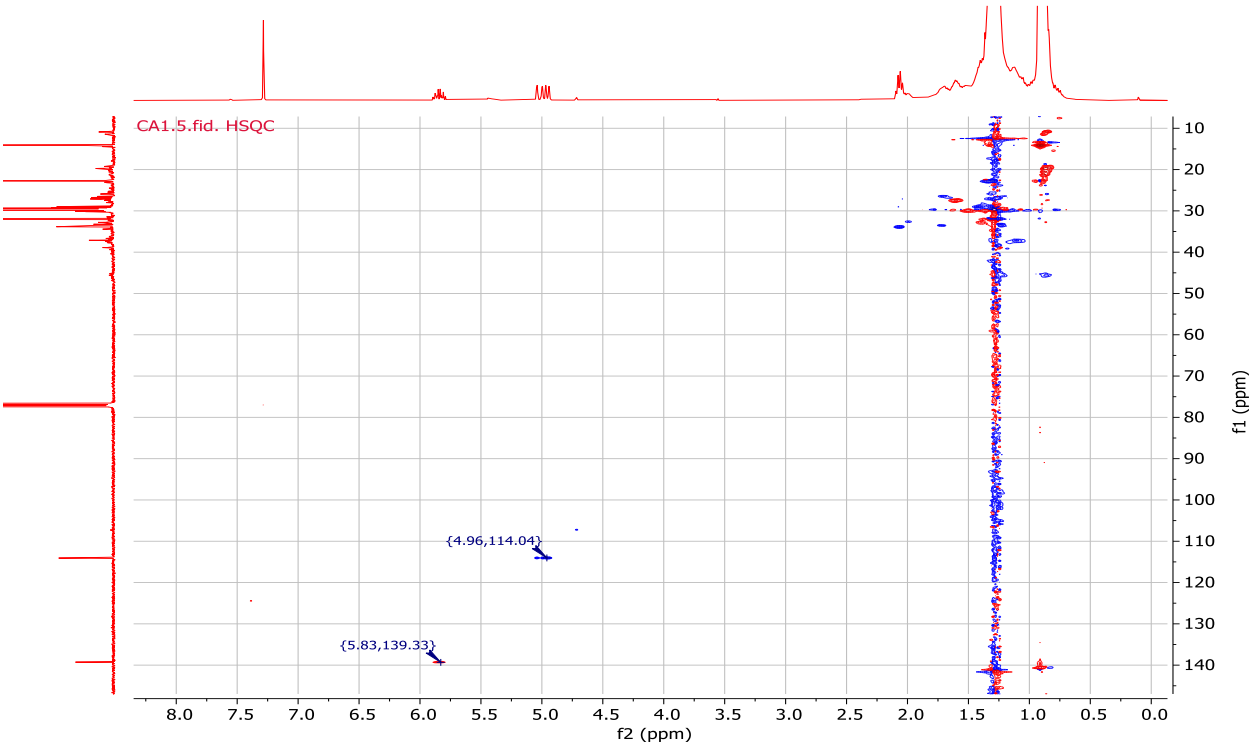

E: HSQC spectrum of compound **82**.

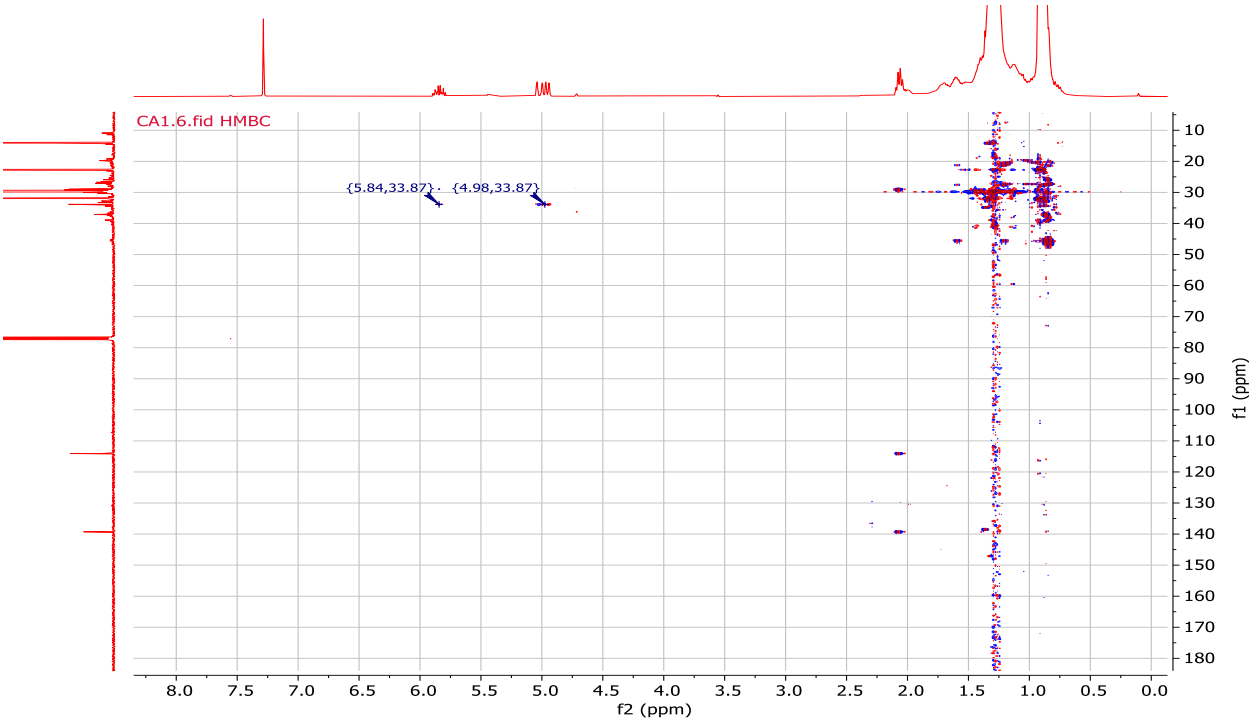

F: HMBC spectrum of compound **82**.

Appendix 2: ^{1}H, ^{13}C, DEPT-135, COSY, HSQC, and HMBC NMR spectra of compound **82.**

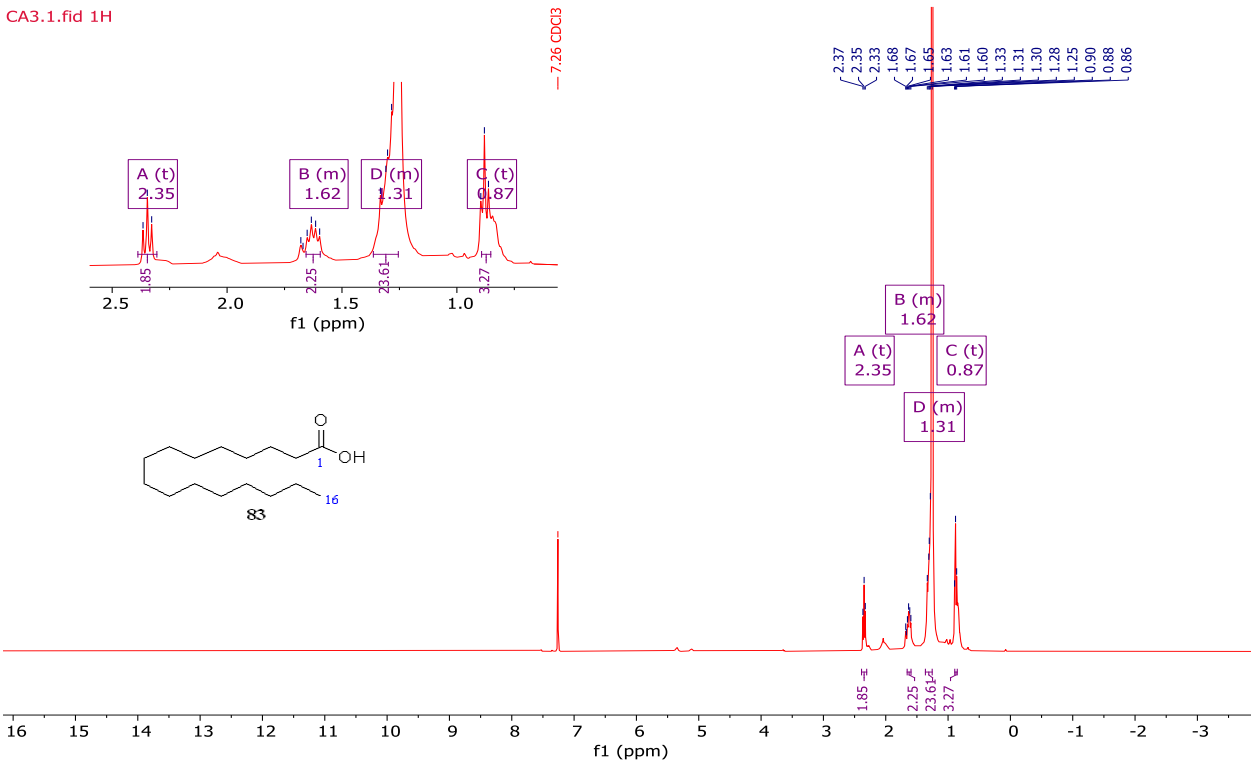

A: ^{1}H NMR (400 MHz, $CDCl_3$) spectrum of compound **83**.

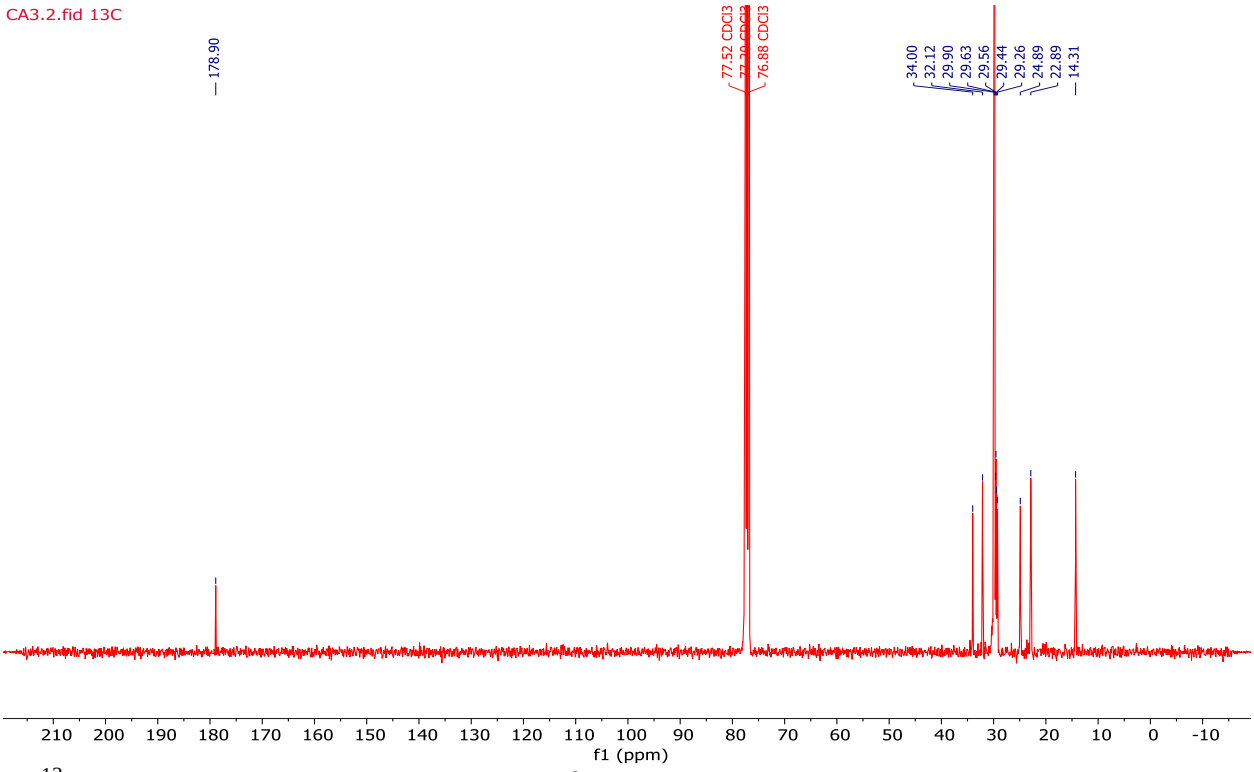

B: ^{13}C NMR (100 MHz, $CDCl_3$) spectrum of compound **83**.

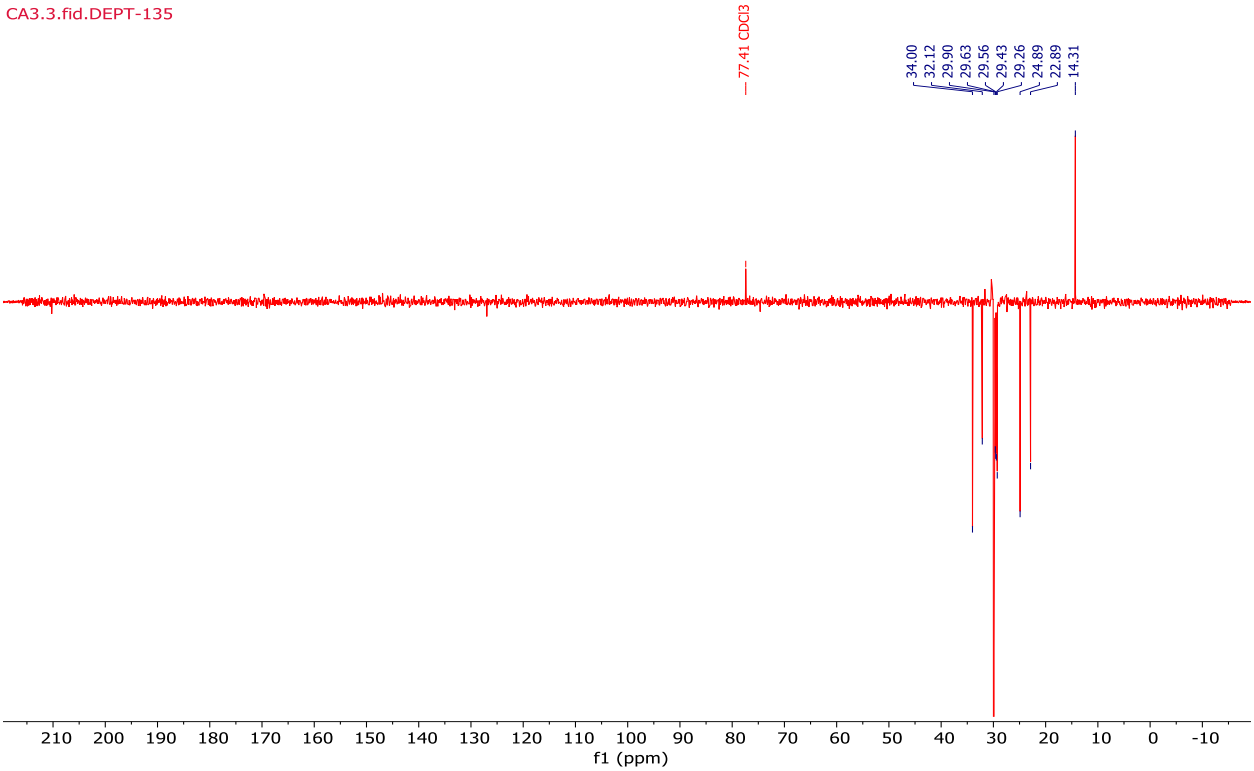

C: DEPT-135 spectrum of compound **83**.

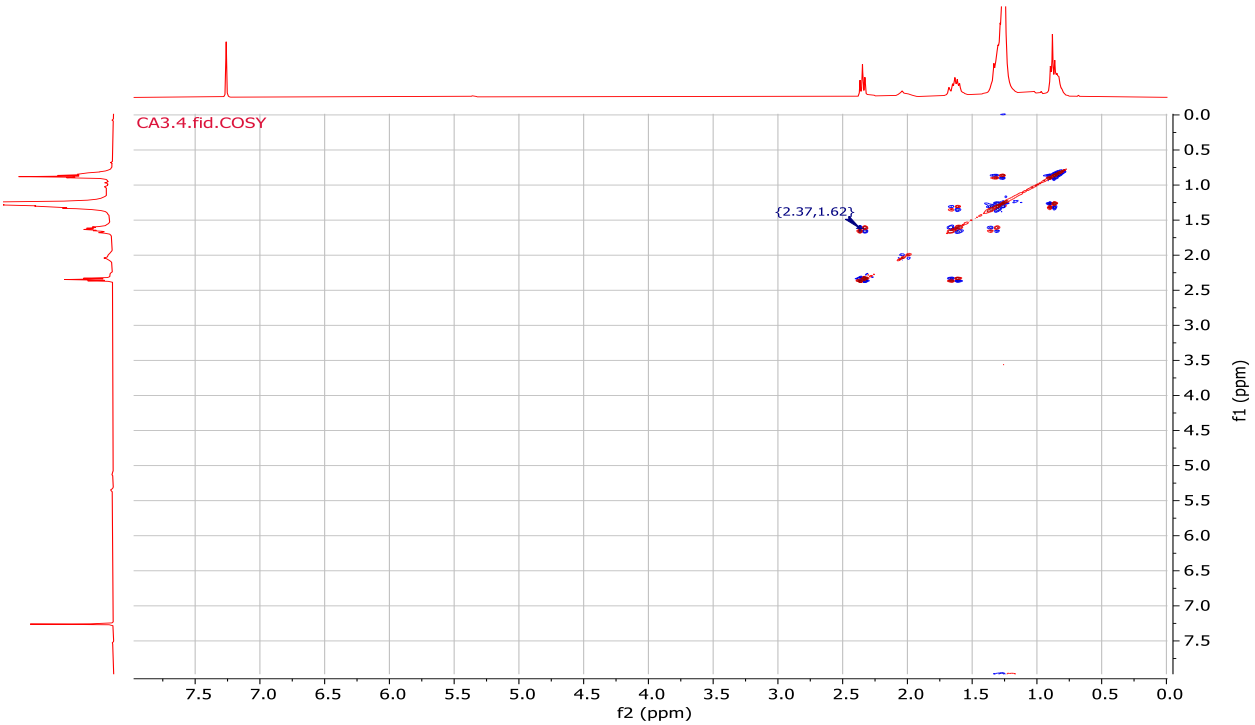

D: COSY spectrum of compound **83**.

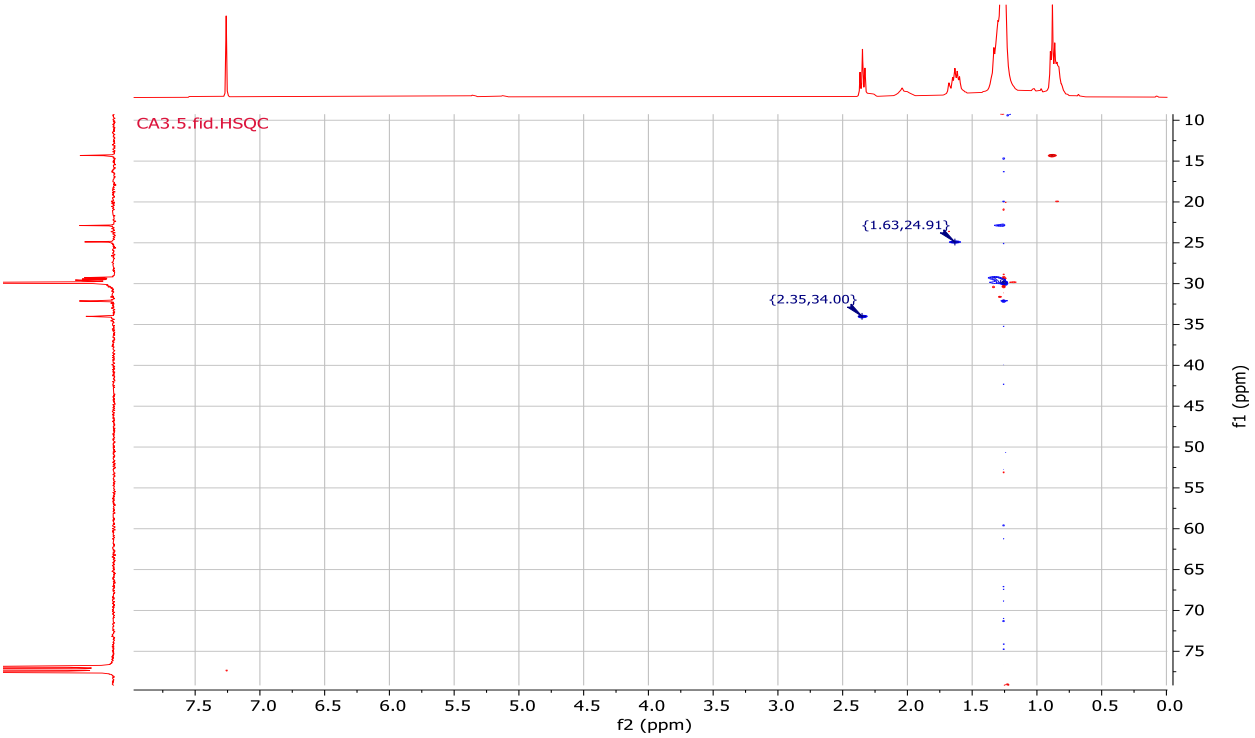

E: HSQC spectrum of compound **83**.

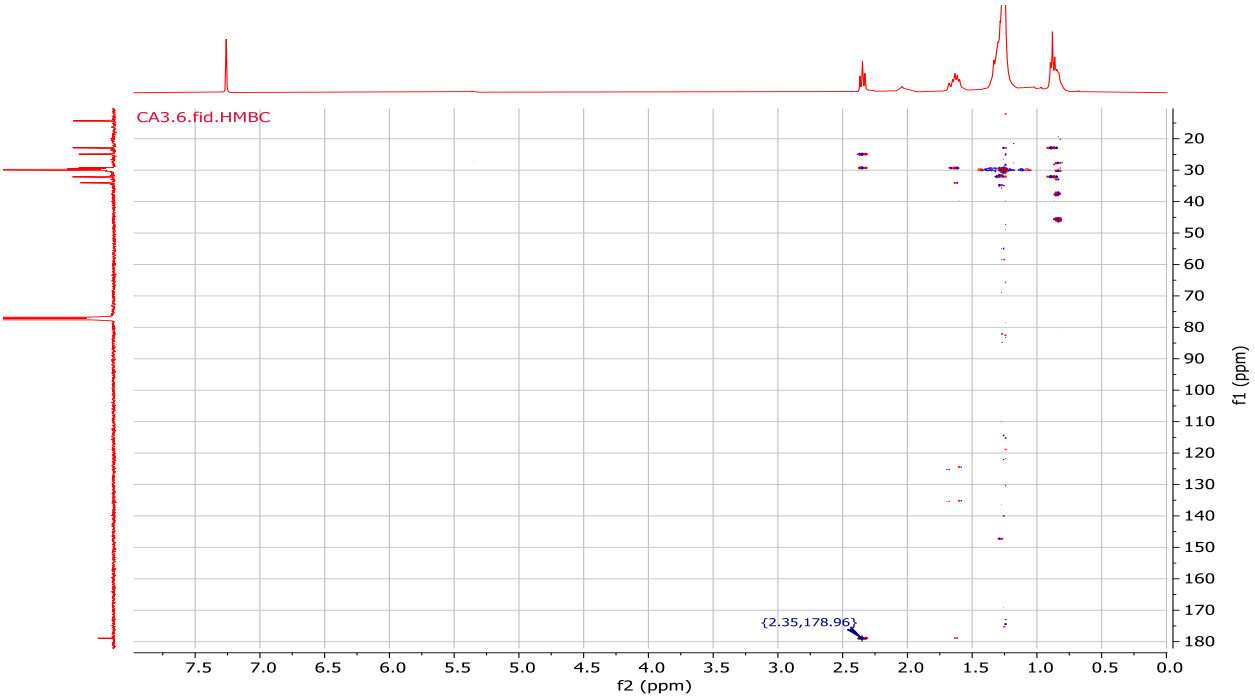

F: HMBC spectrum of compound **83**

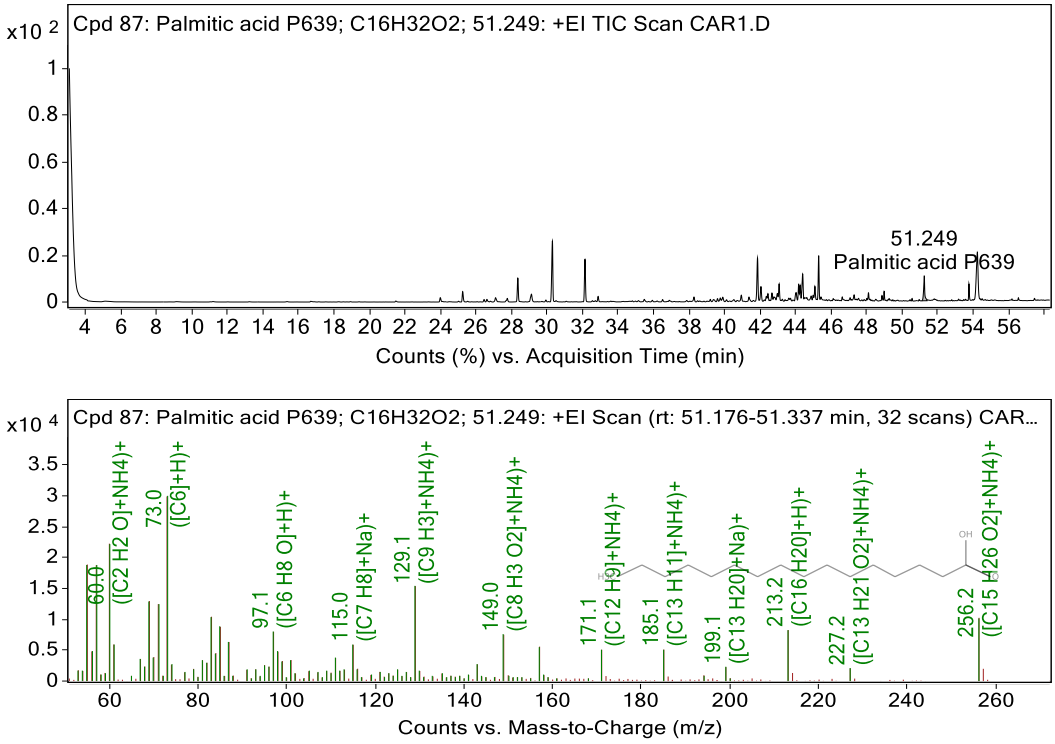

G: GC (top) and mass fragmentation pattern (bottom) of compound **83**.

Appendix 3: ^{1}H, ^{13}C, DEPT-135, COSY, HSQC, and HMBC NMR spectra, and GC and mass fragmentation pattern of compound **83**.

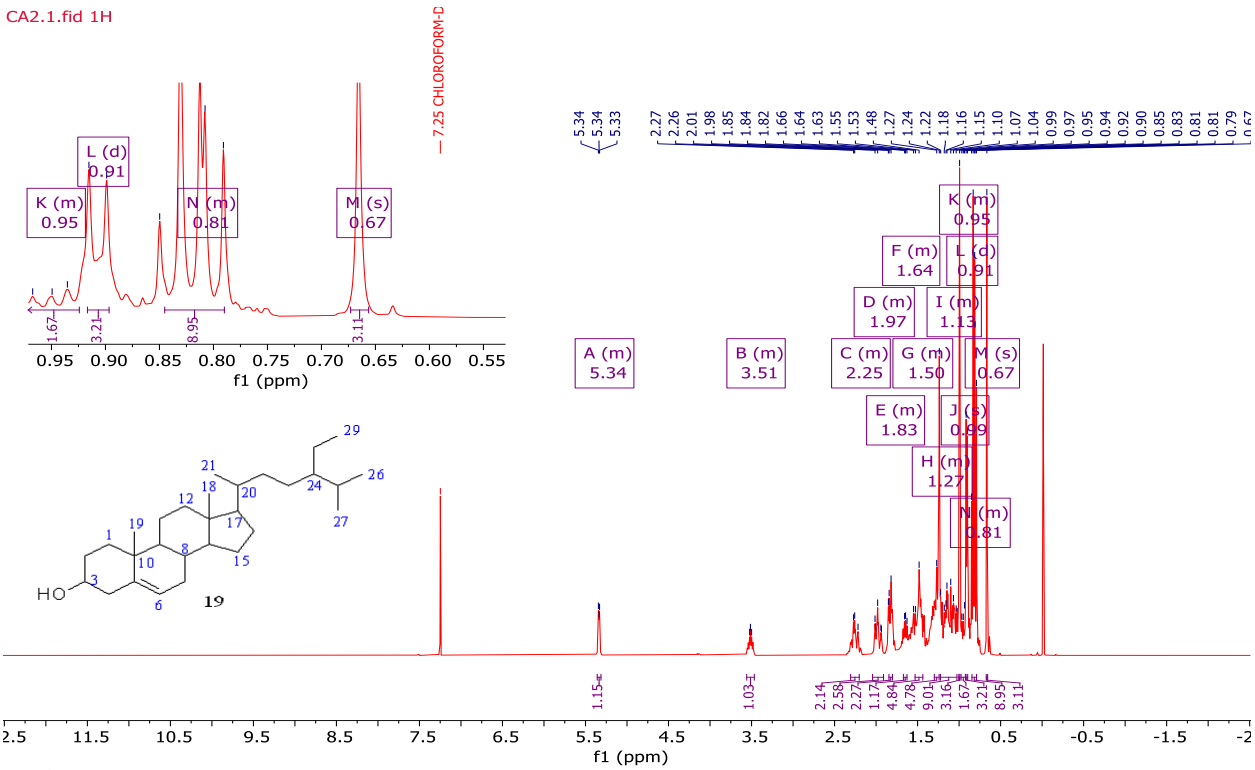

A: ^{1}H NMR (400 MHz, $CDCl_3$) spectrum of compound **19**.

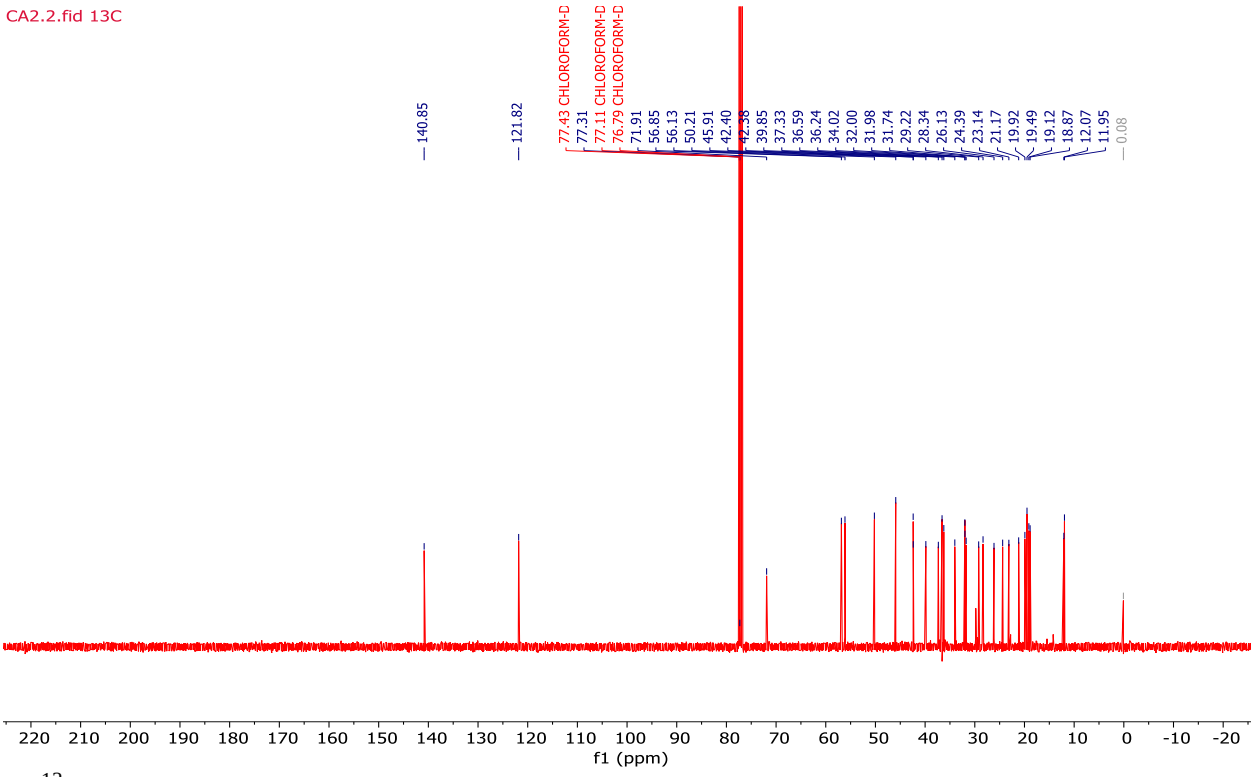

B: ^{13}C NMR (100 MHz, $CDCl_3$) spectrum of compound **19**.

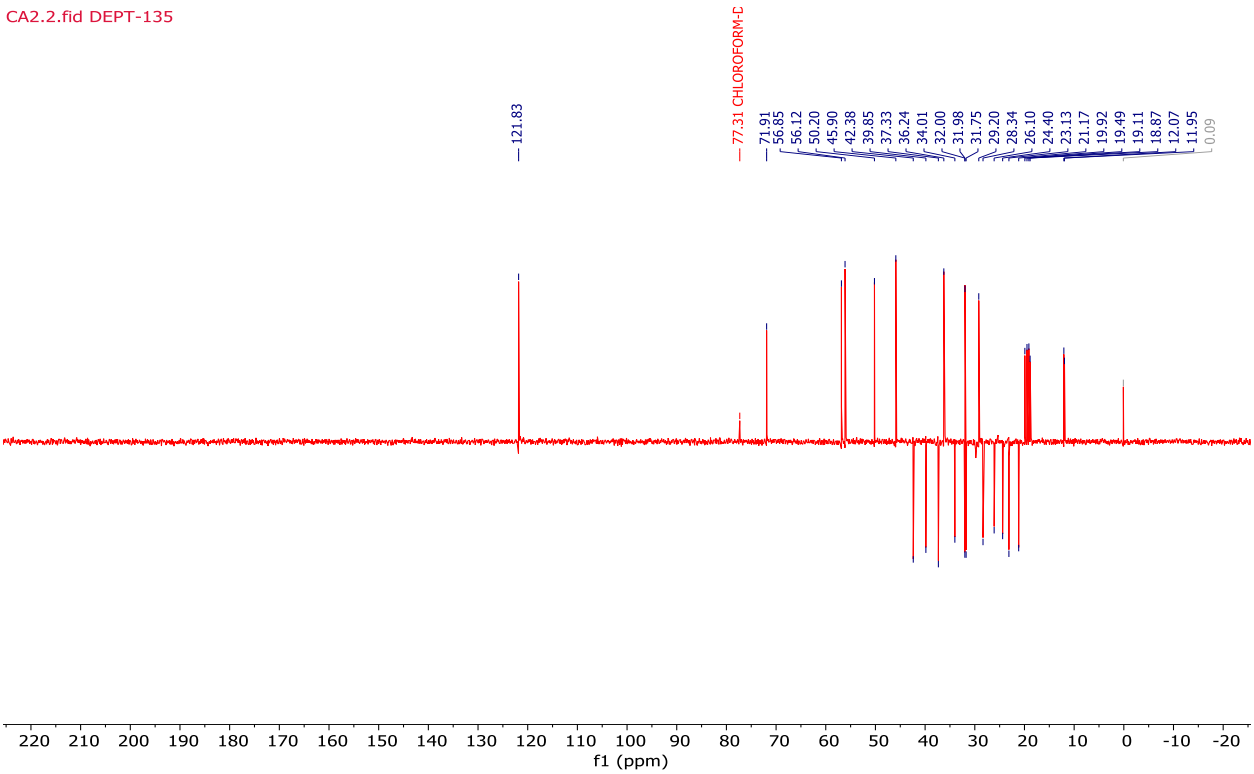

C: DEPT-135 spectrum of compound **19**.

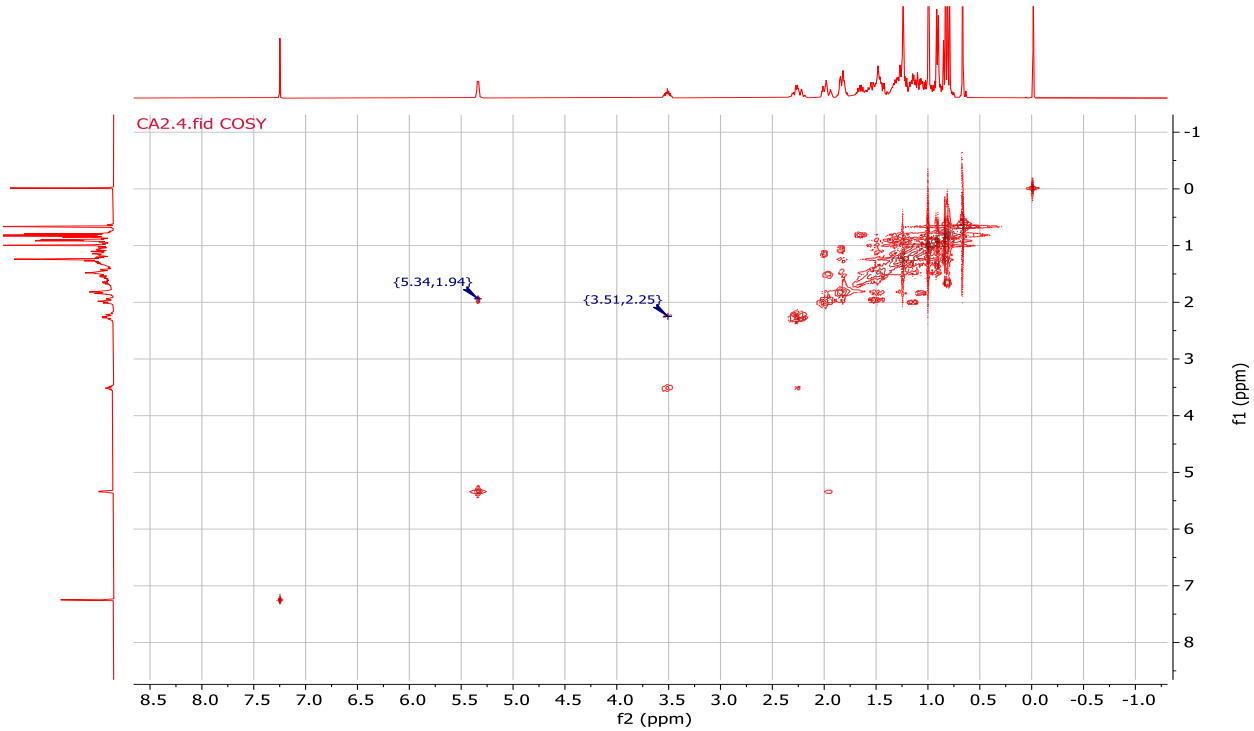

D: COSY spectrum of compound **19**.

Appendix 4: ^{1}H, ^{13}C, DEPT-135, and COSY NMR spectra of compound **19**.

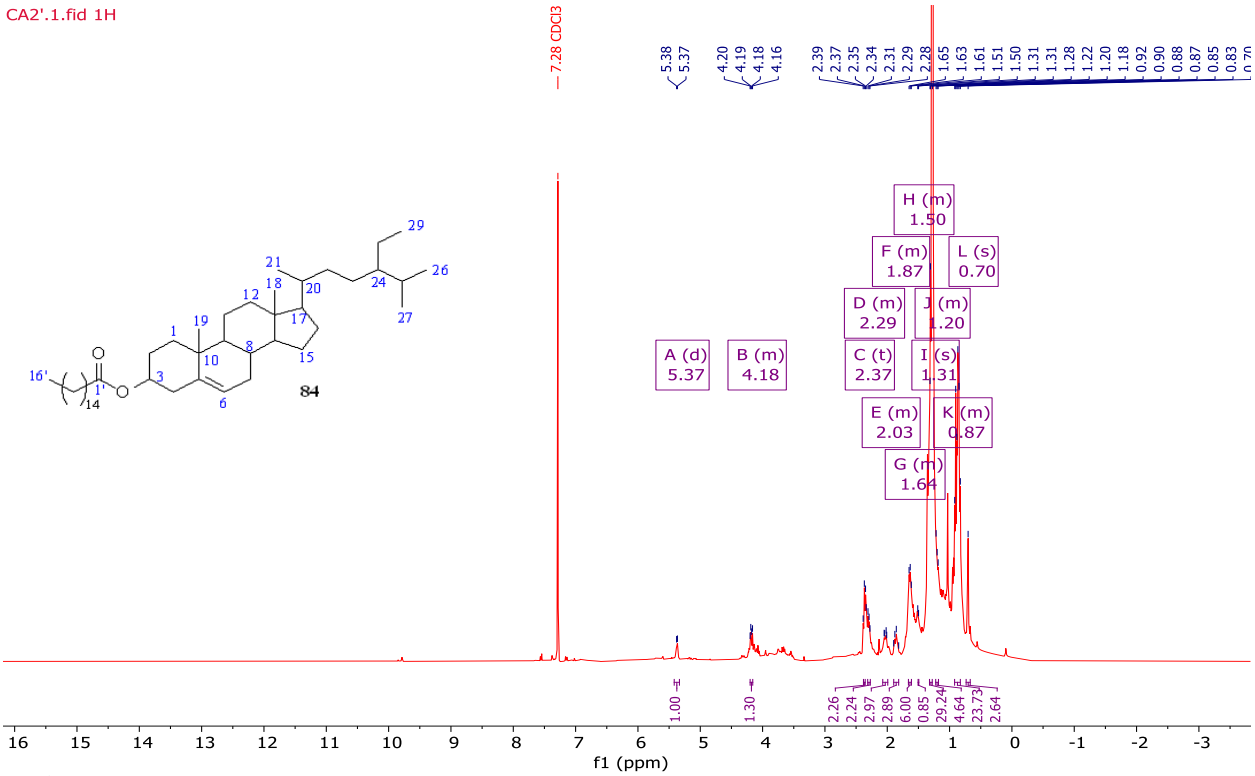

A: ^{1}H NMR (400 MHz, $CDCl_3$) spectrum of compound **84**.

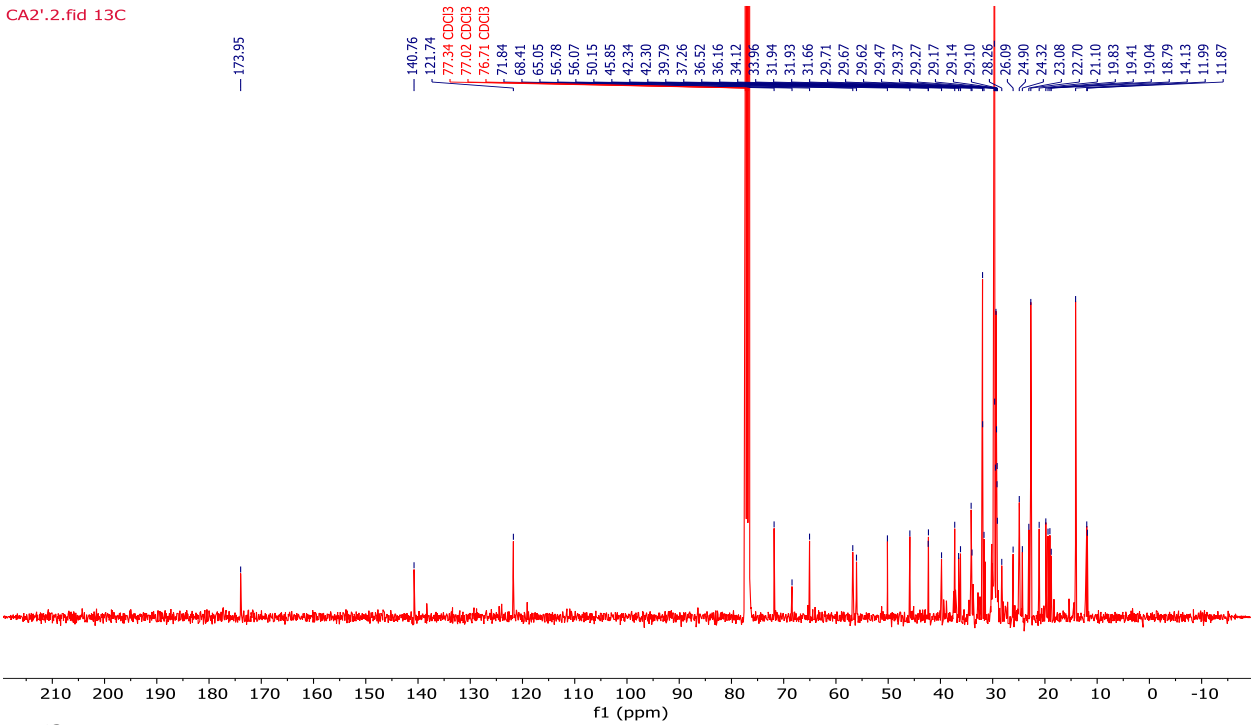

B: ^{13}C NMR (100 MHz, $CDCl_3$) spectrum of compound **84**.

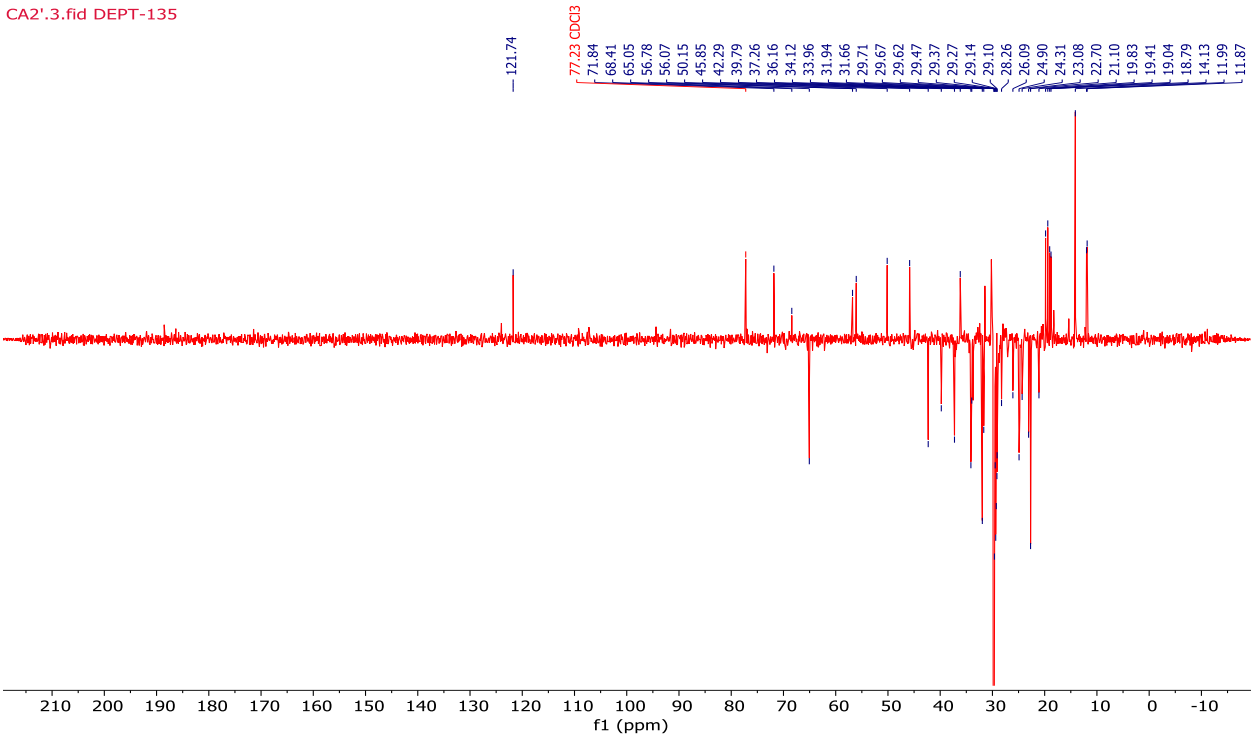

C: DEPT-135 spectrum of compound **84**.

- ✓ The spectrum also showed signals of a glycerol impurity at δ_H 3.75-3.50, and δ_C 68.4, and 65.0 ppm.

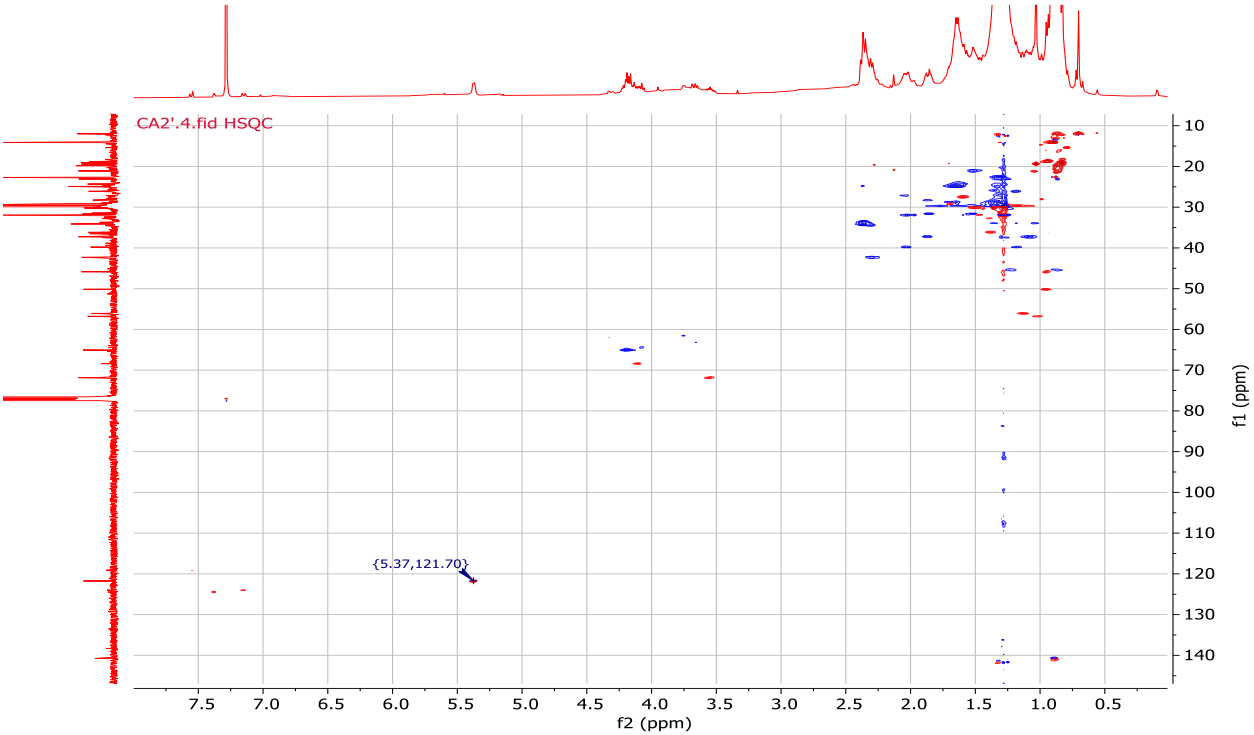

D: HSQC spectrum of compound **84**.

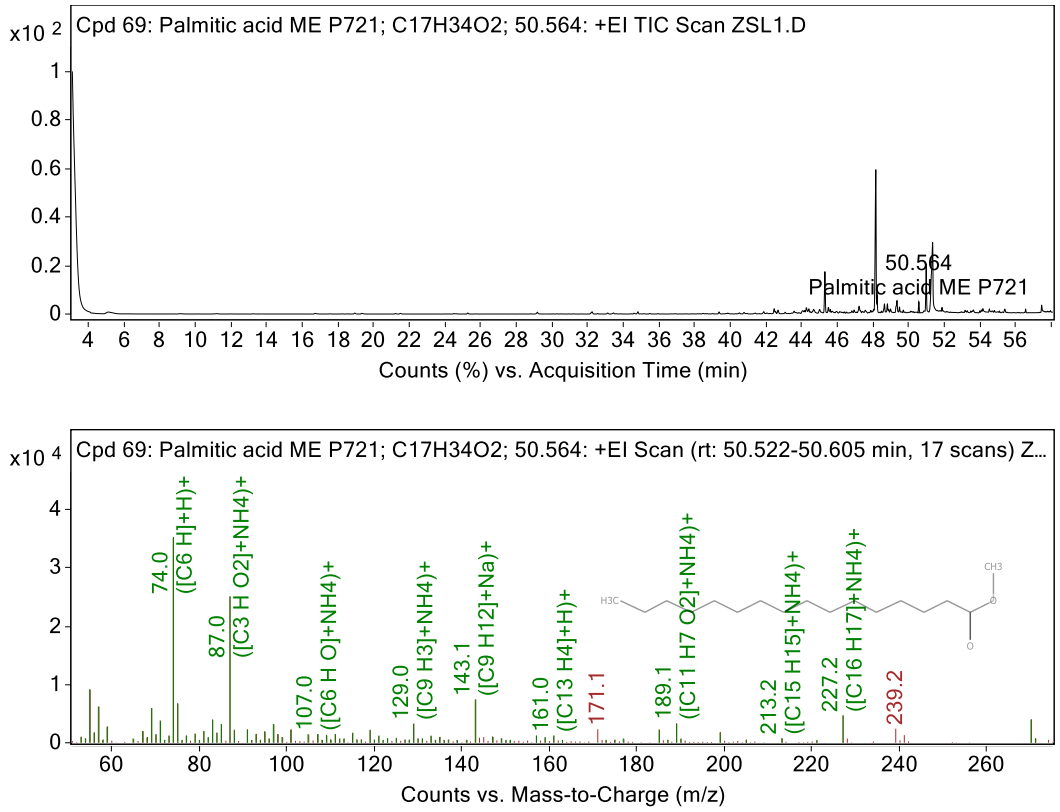

E: GC (top) and mass fragmentation pattern (bottom) of palmitic acid methyl ester generated from the transesterification process of compounds **84** and **86**.

Appendix 5: ^{1}H, ^{13}C, DEPT-135, and HSQC NMR spectra of compound **84**, and GC and mass fragmentation pattern of palmitic acid methyl ester.

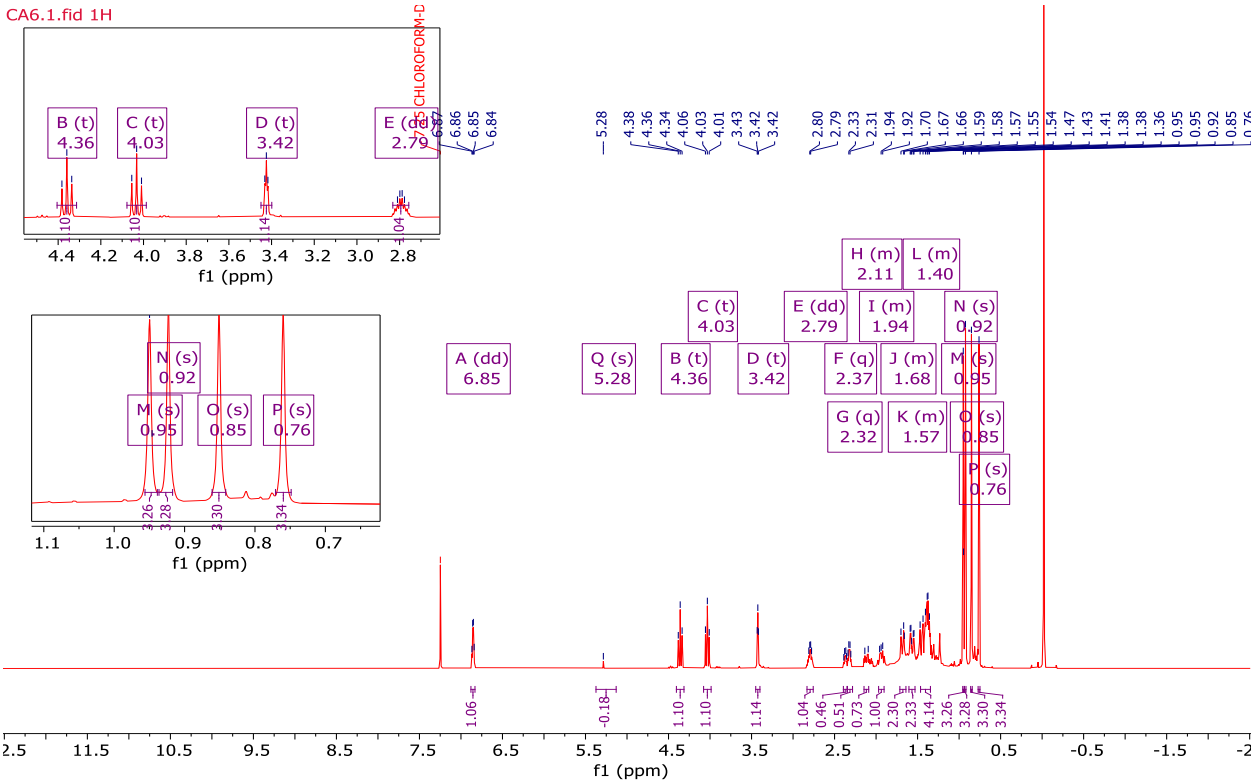

A: ^{1}H NMR (400 MHz, $CDCl_3$) spectrum of compound **28**.

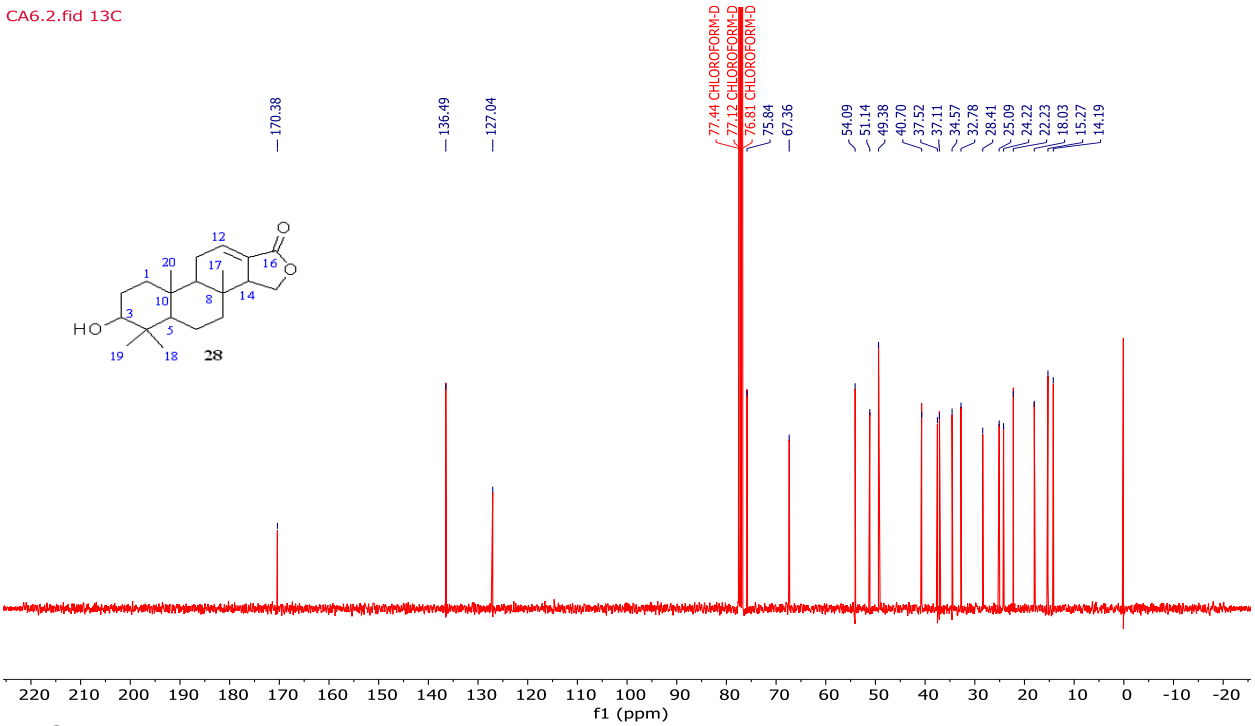

B: ^{13}C NMR (100 MHz, $CDCl_3$) spectrum of compound **28**.

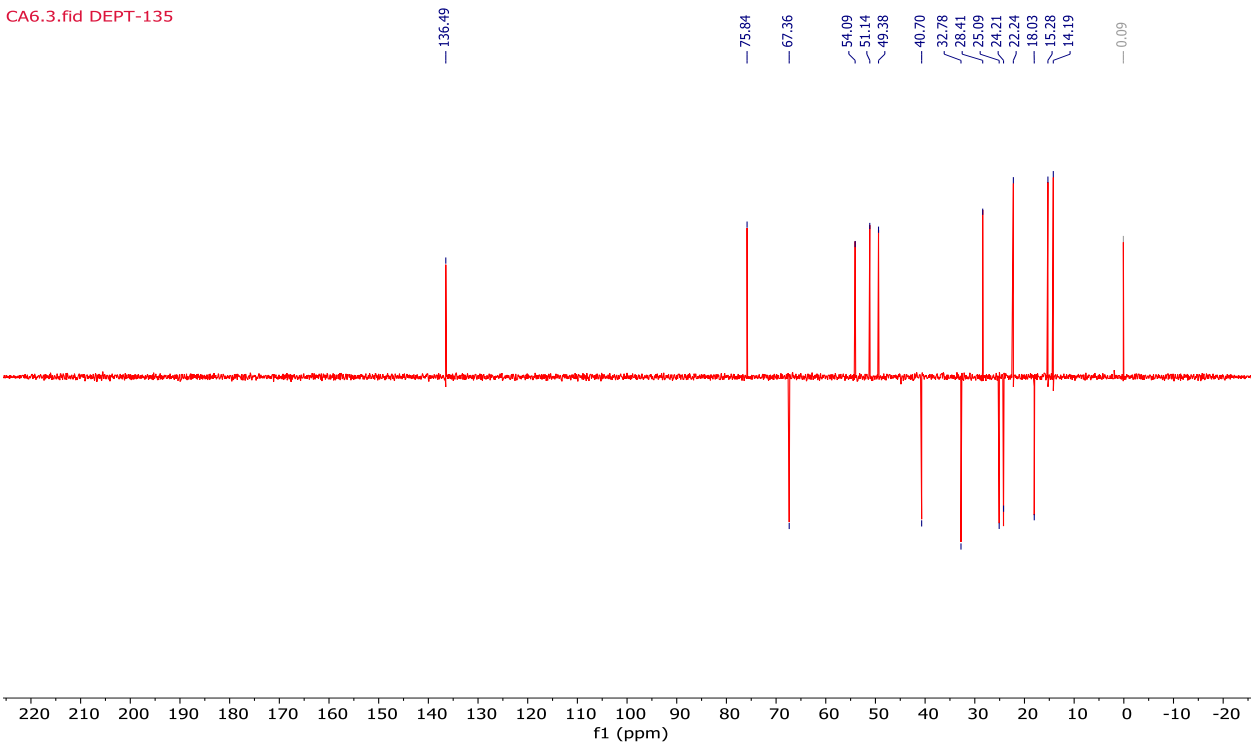

C: DEPT-135 spectrum of compound **28**.

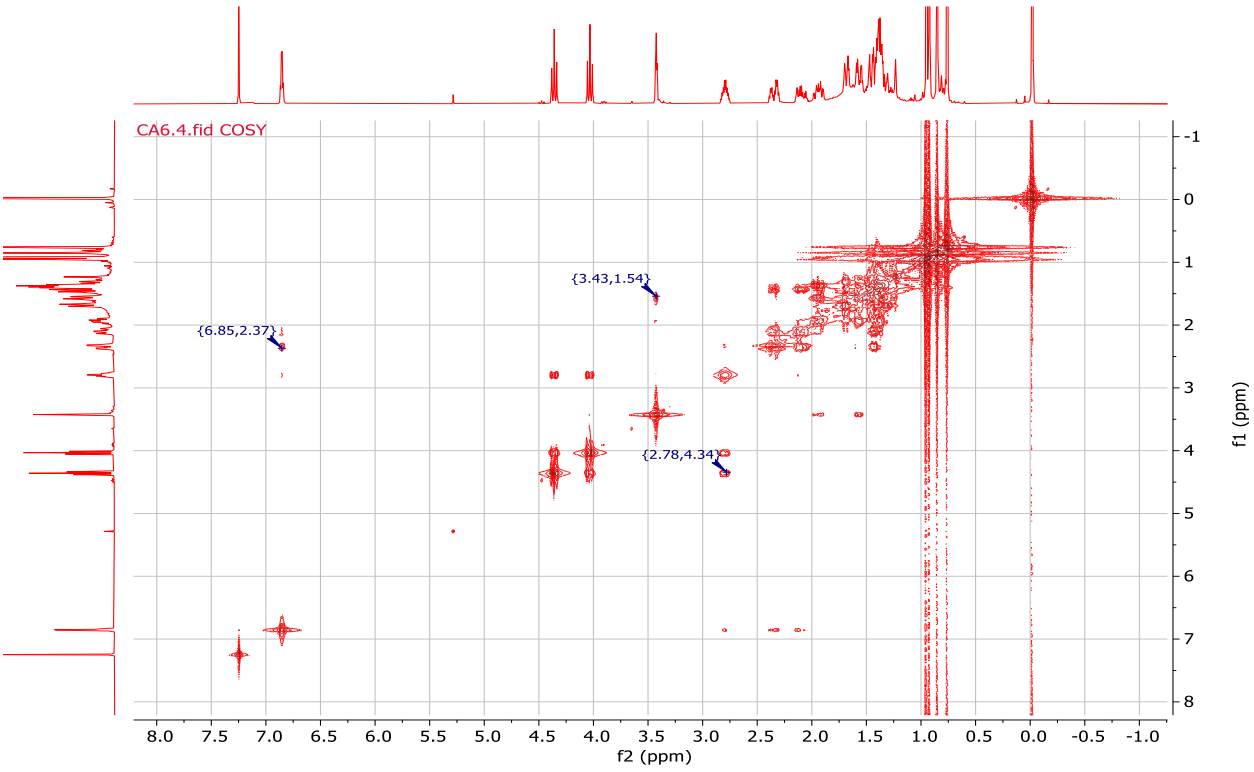

D: COSY spectrum of compound **28**.

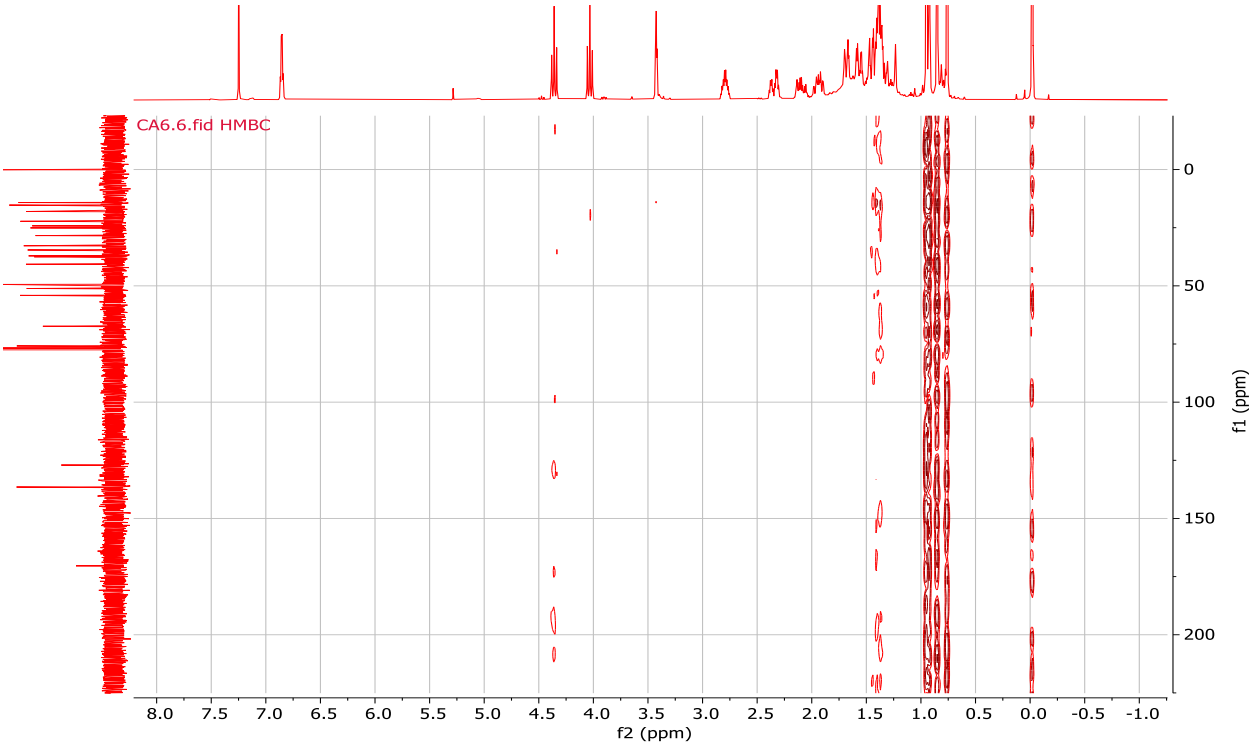

E: HMBC spectrum of compound **28**.

Appendix 6: ^{1}H, ^{13}C, DEPT-135, COSY, and HMBC NMR spectra of compound **28**.

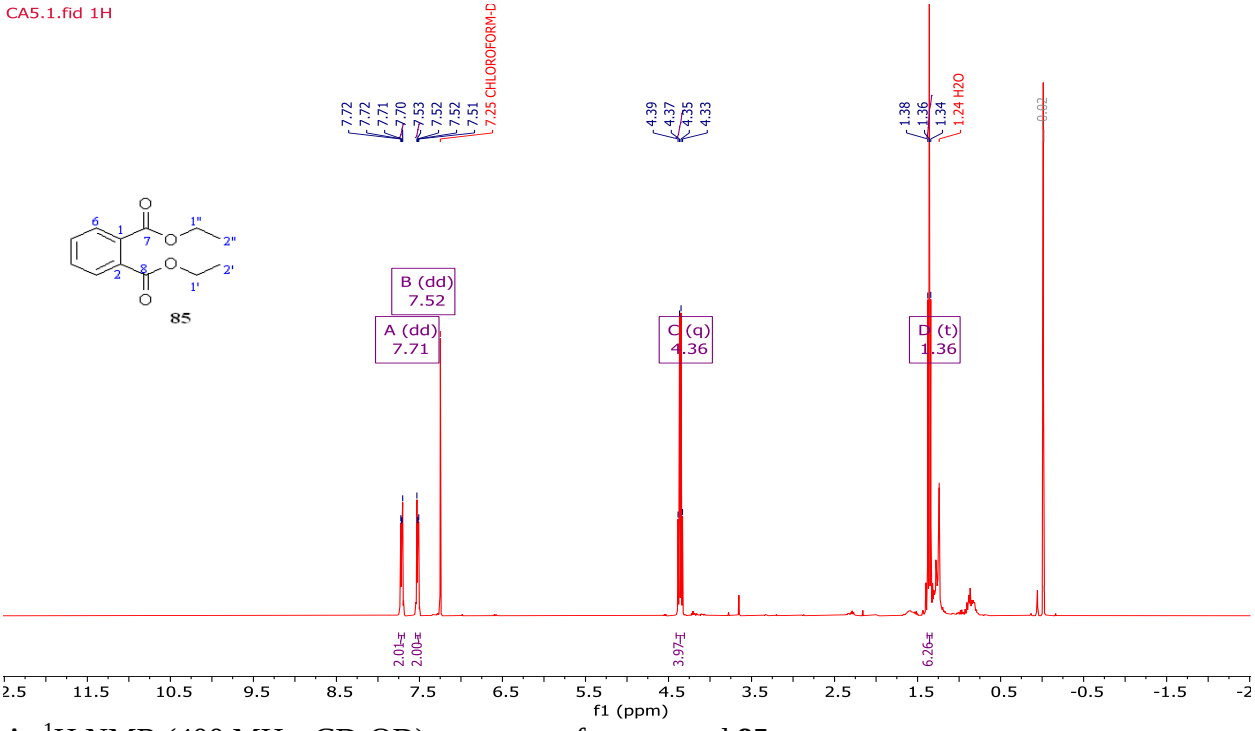

A: ^{1}H NMR (400 MHz, CD_3OD) spectrum of compound **85**.

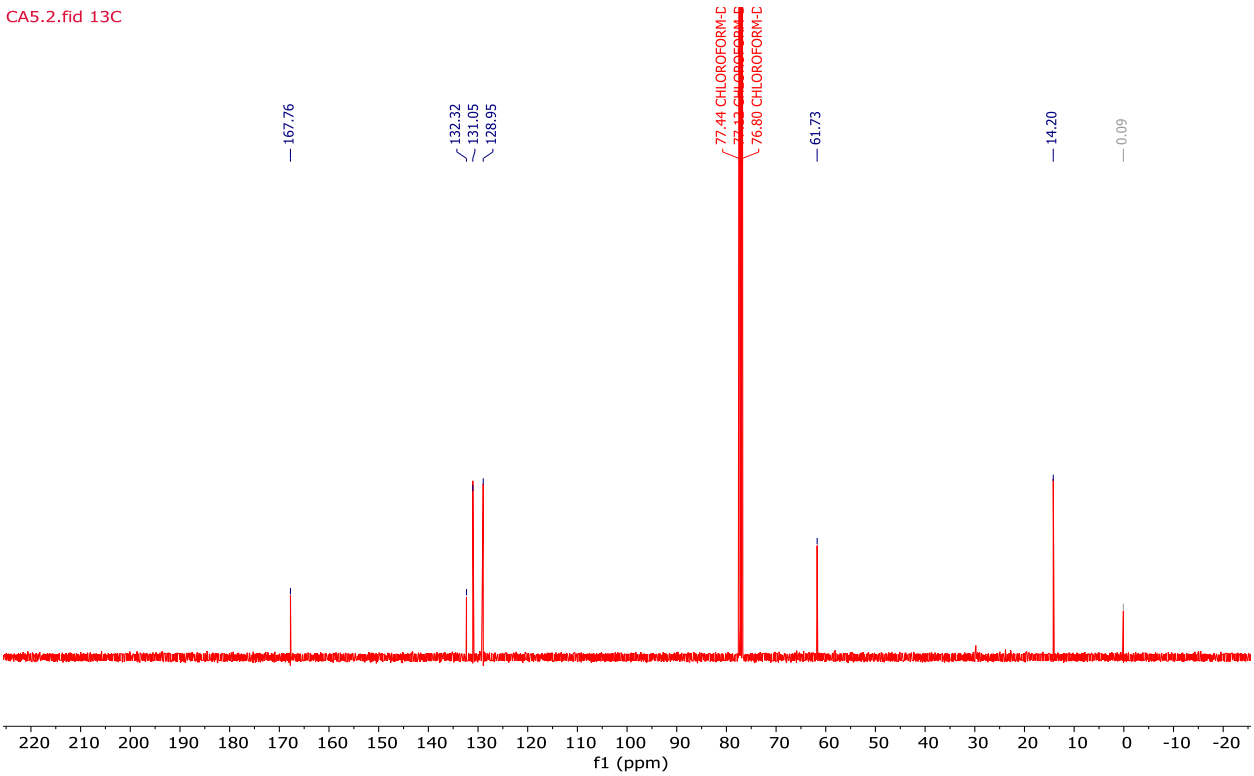

B: ^{13}C NMR (100 MHz, CD_3OD) spectrum of compound **85**.

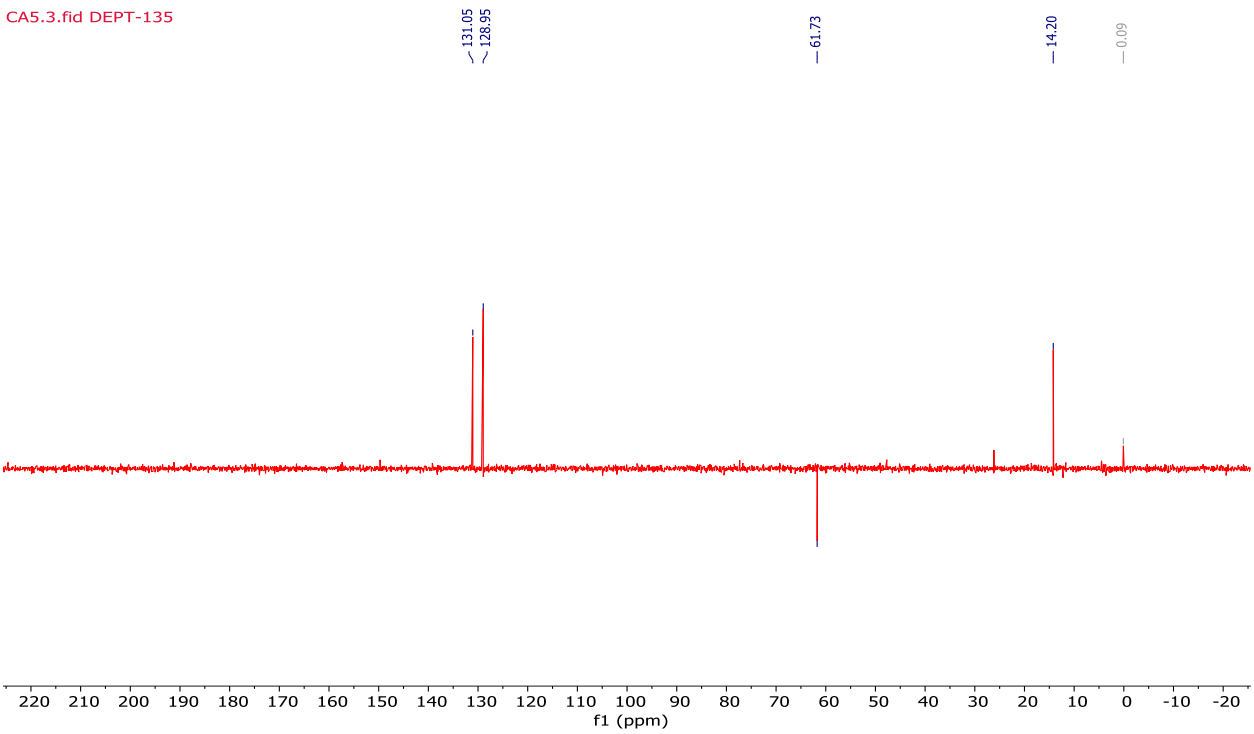

C: DEPT-135 spectrum of compound **85**.

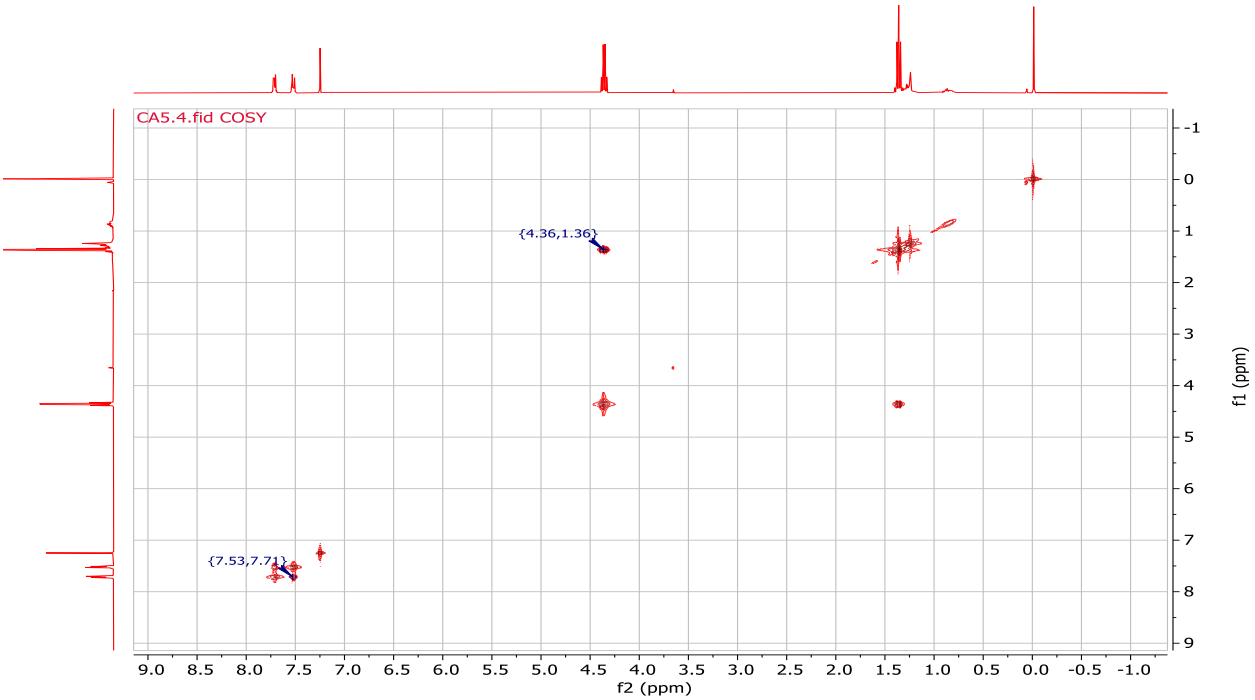

D: COSY spectrum of compound **85**.

Appendix 7: ^{1}H, ^{13}C, DEPT-135, and COSY NMR spectra of compound **85**.

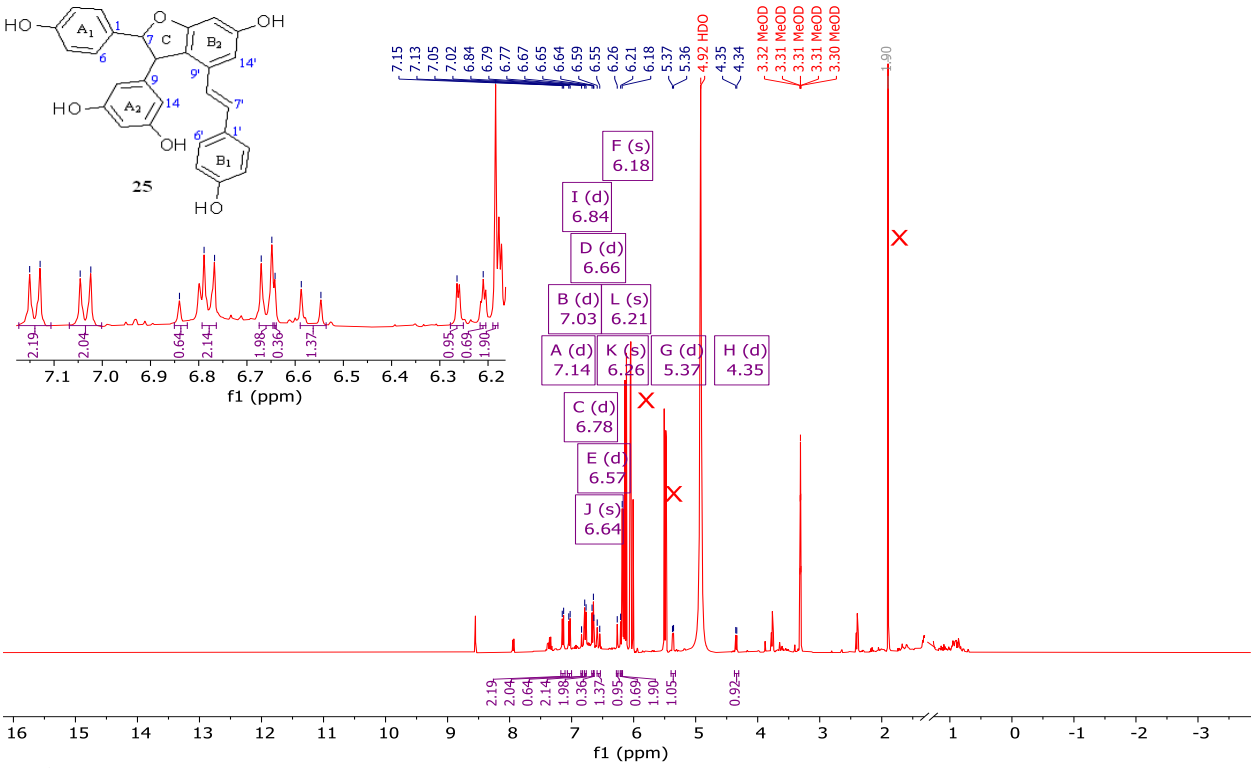

A: ^{1}H NMR (400 MHz, CD_3OD) spectrum of compound **25**.

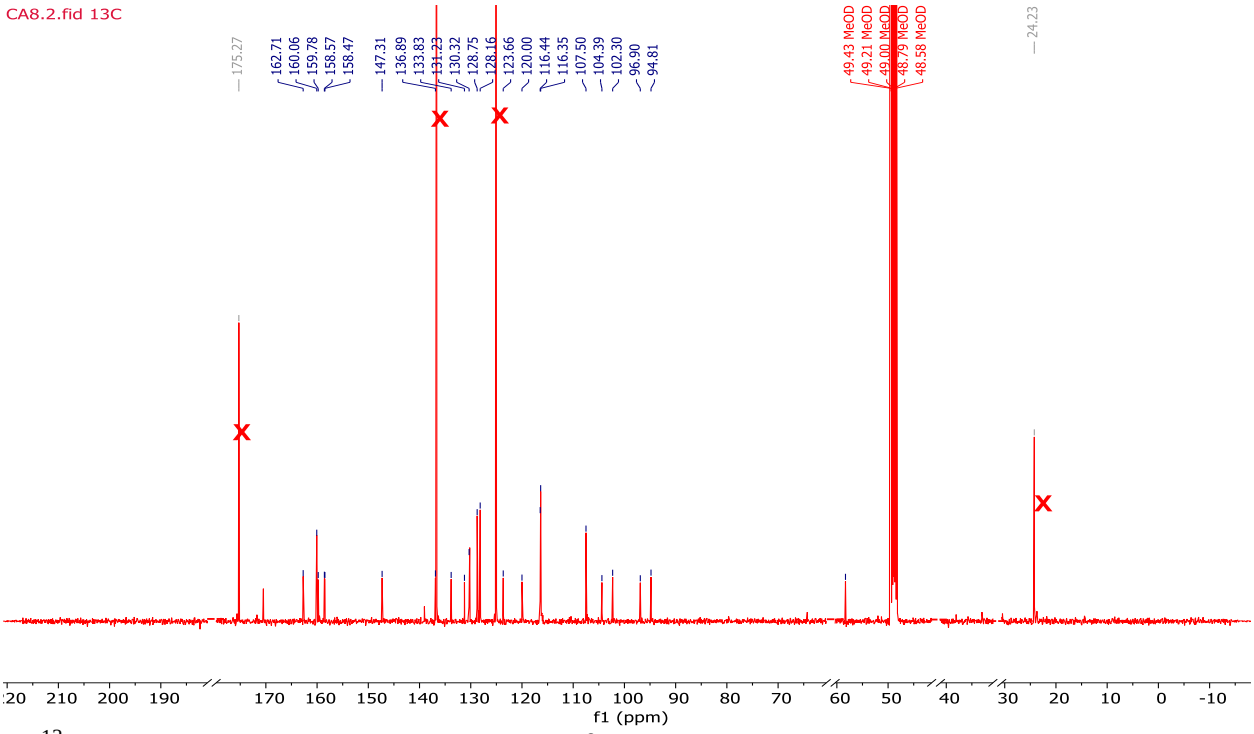

B: ^{13}C NMR (100 MHz, CD_3OD) spectrum of compound **25**.

- ✓ The spectra also displayed an acrylate contaminant at δ_H 8.55, 6.12, 6.03, 5.49, 1.90, and δ_C 175.2, 136.6, 125.0, and 24.2.

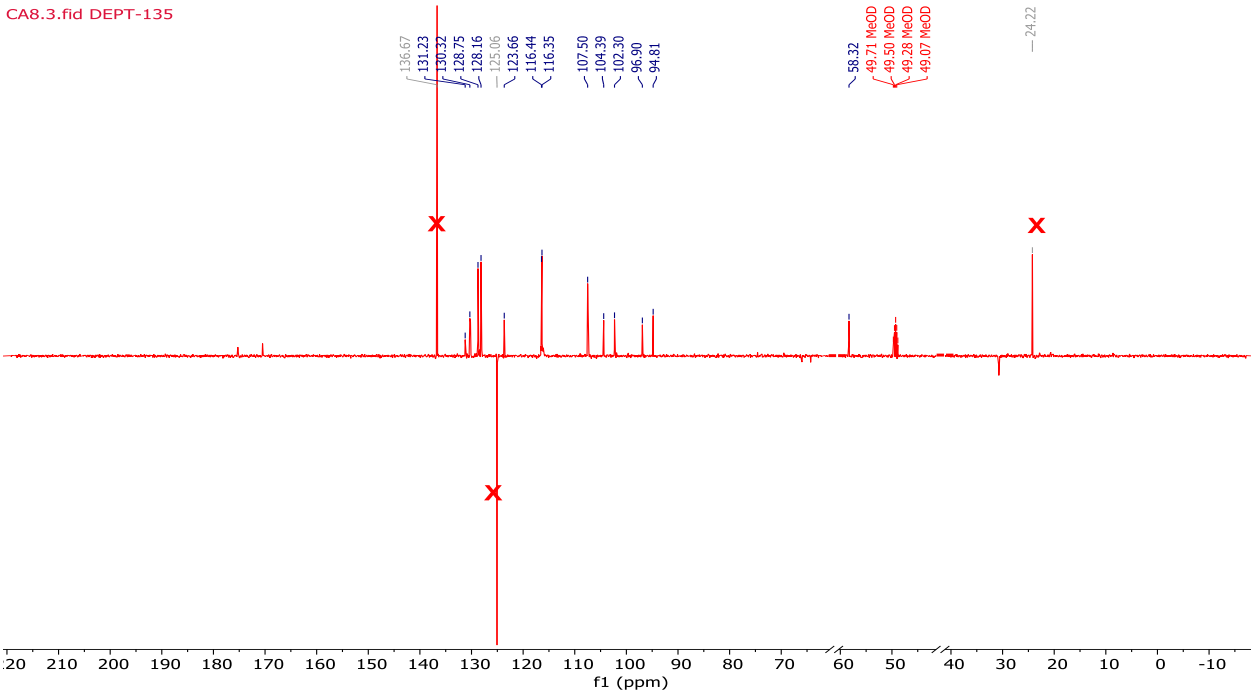

C: DEPT-135 spectrum of compound **25**.

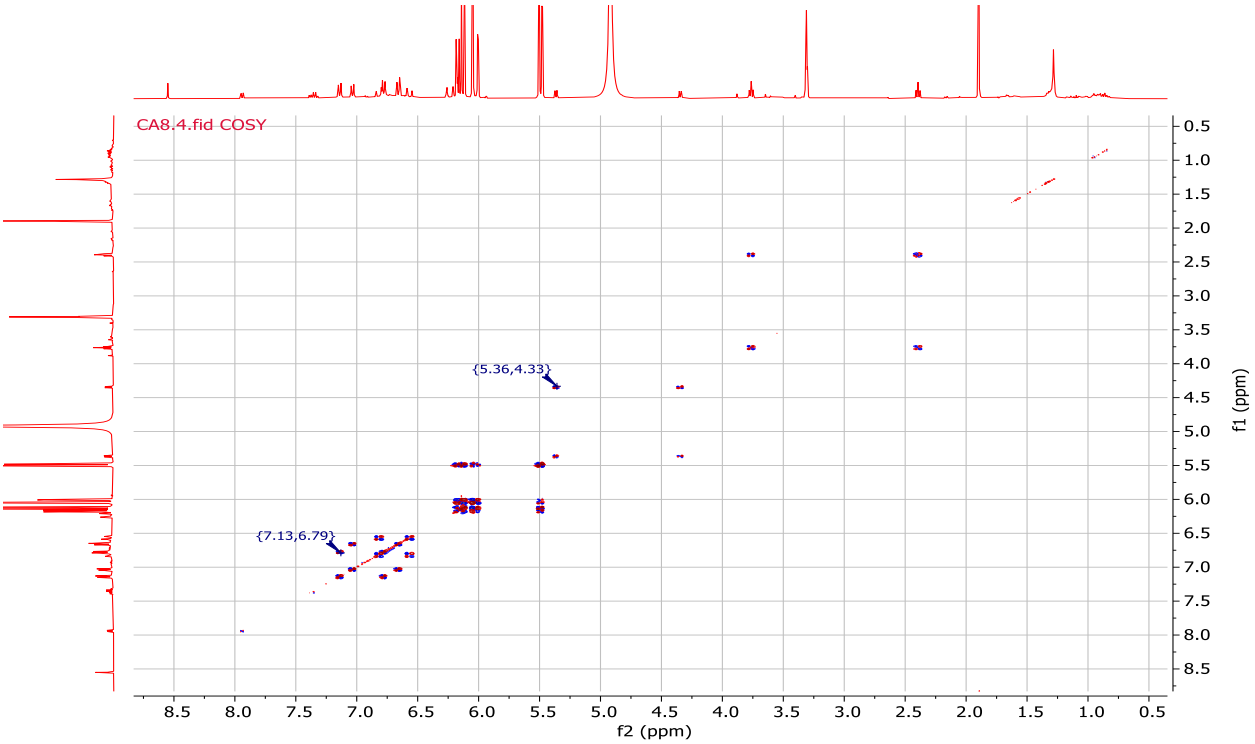

D: COSY spectrum of compound **25**.

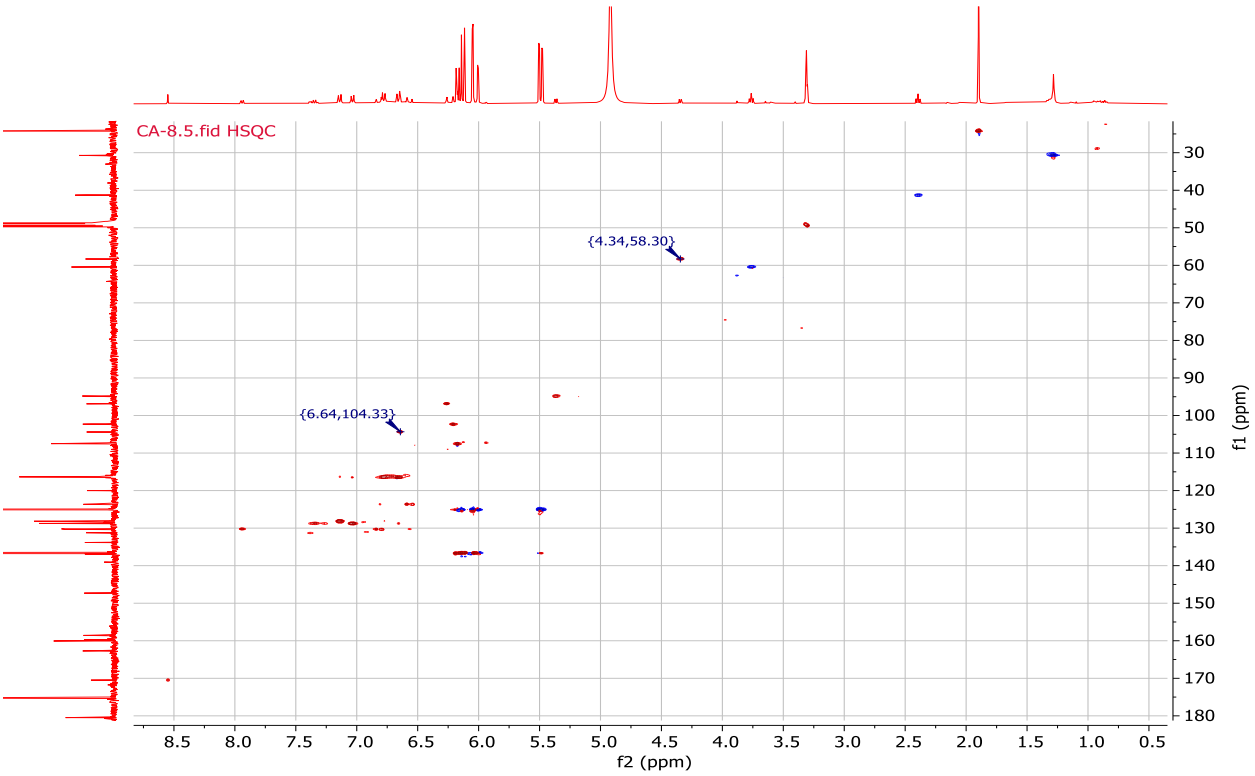

E: HSQC spectrum of compound **25**.

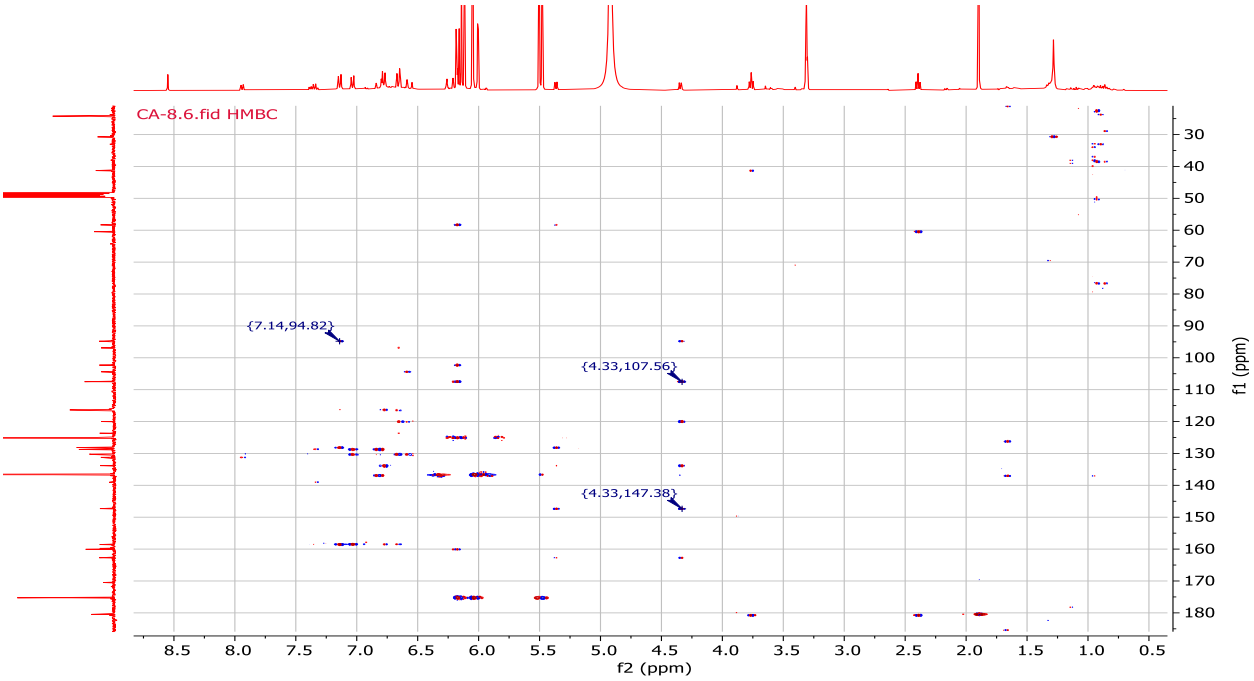

F: HMBC spectrum of compound **25**.

Appendix 8: ^{1}H, ^{13}C, DEPT-135, COSY, HSQC, and HMBC NMR spectra of compound **25**.

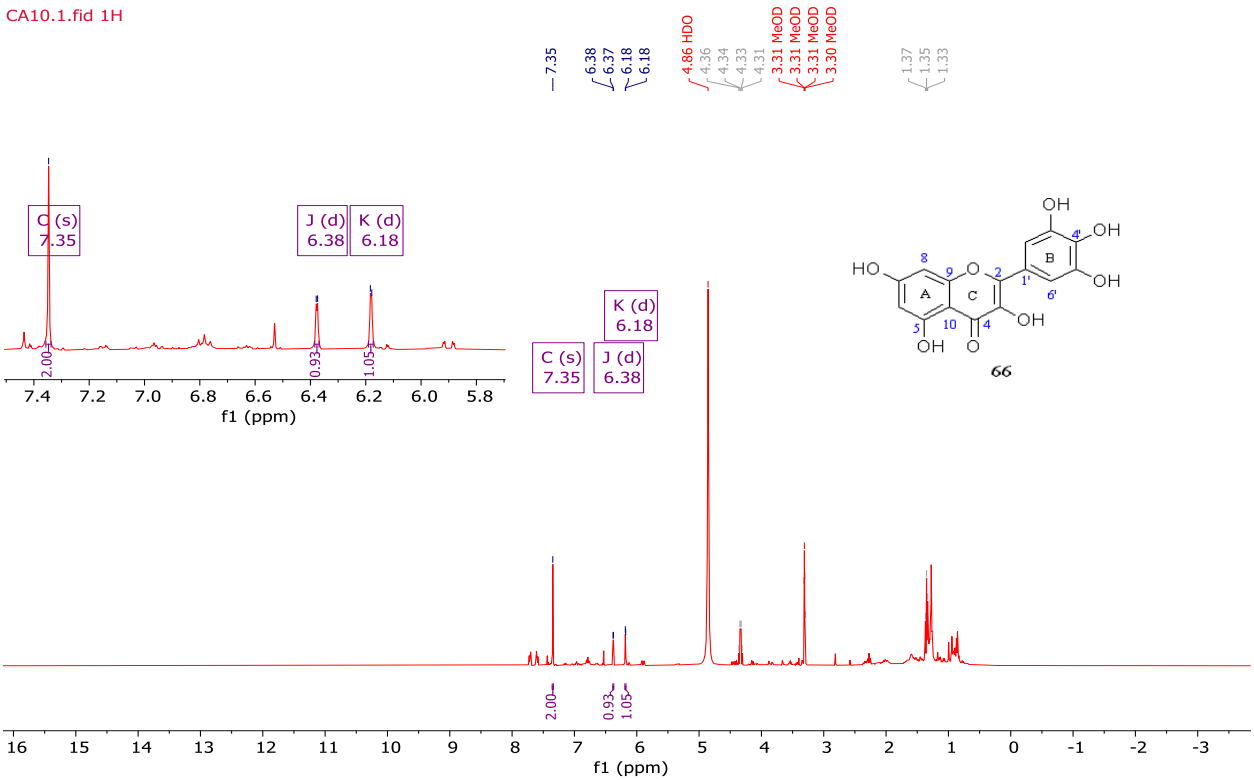

A: ^{1}H NMR (400 MHz, CD_3OD) spectrum of compound **66**.

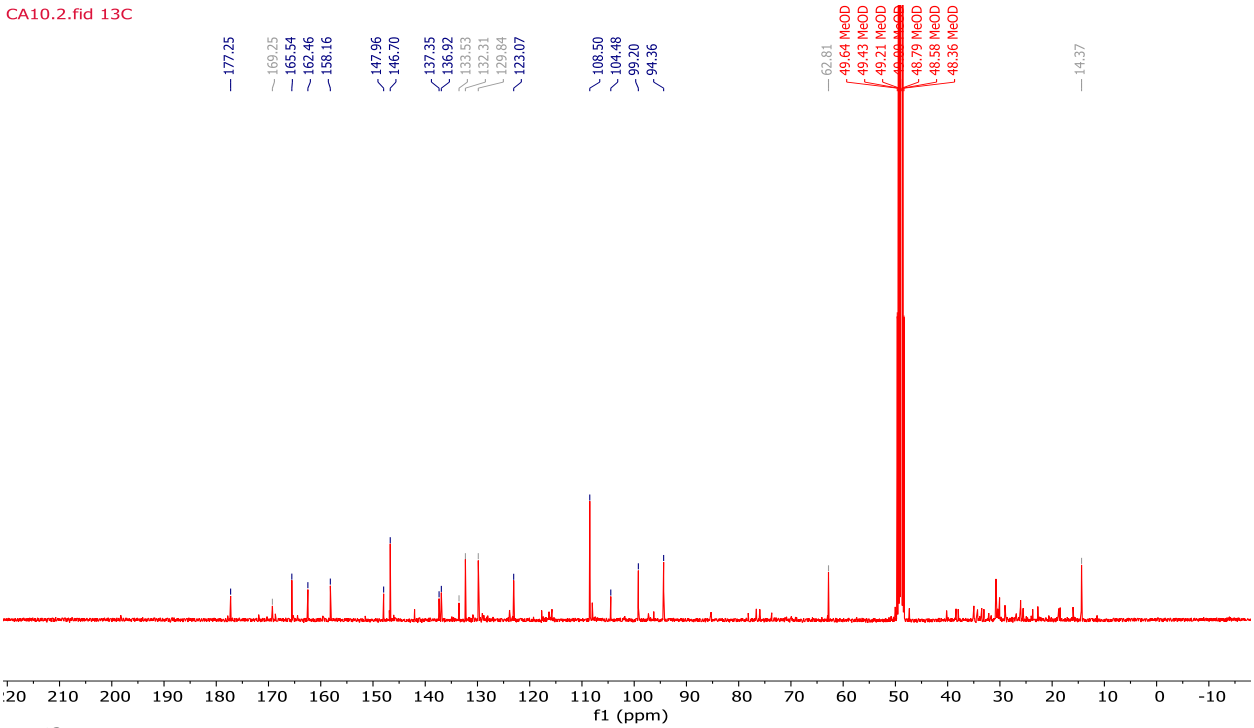

B: ^{13}C NMR (100 MHz, CD_3OD) spectrum of compound **66**.

- ✓ The spectra have some diethyl phthalate contaminant at δ_H 7.71, 7.60, 4.33 and 1.34, and δ_C 169.2, 133.5, 132.3, 129.8, 62.8 and 14.3.

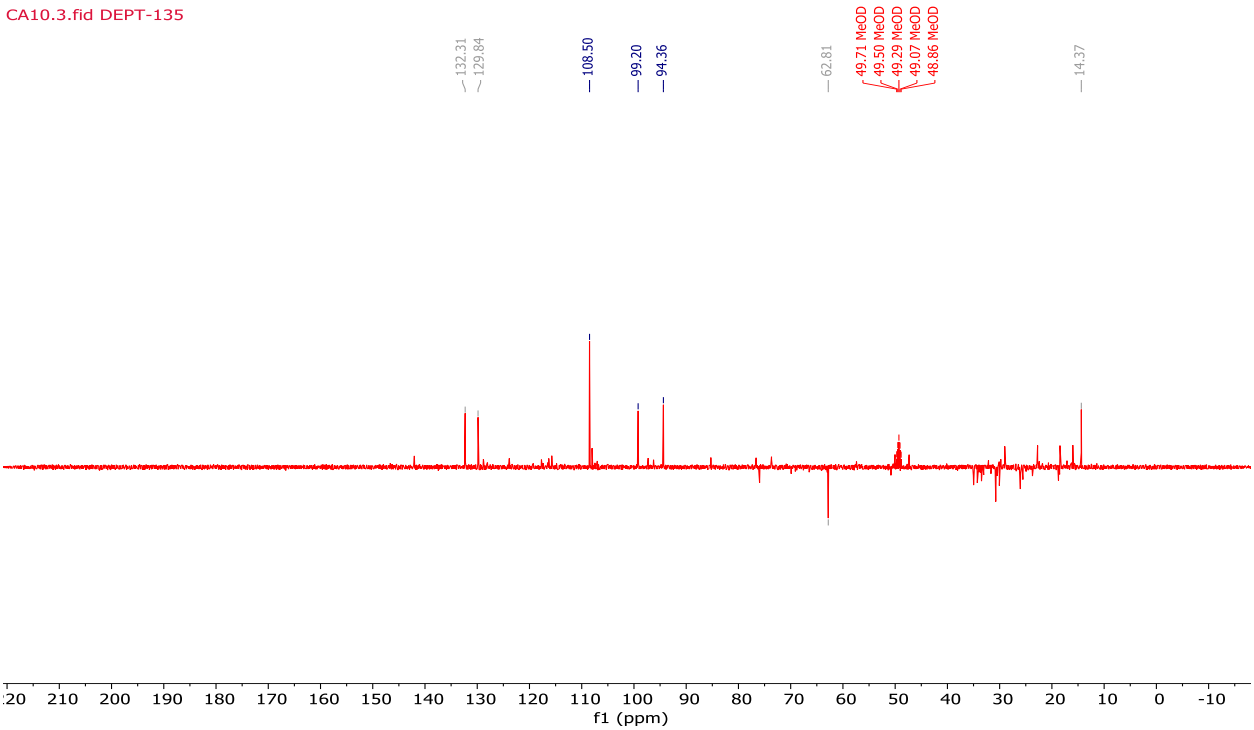

C: DEPT-135 spectrum of compound **66**.

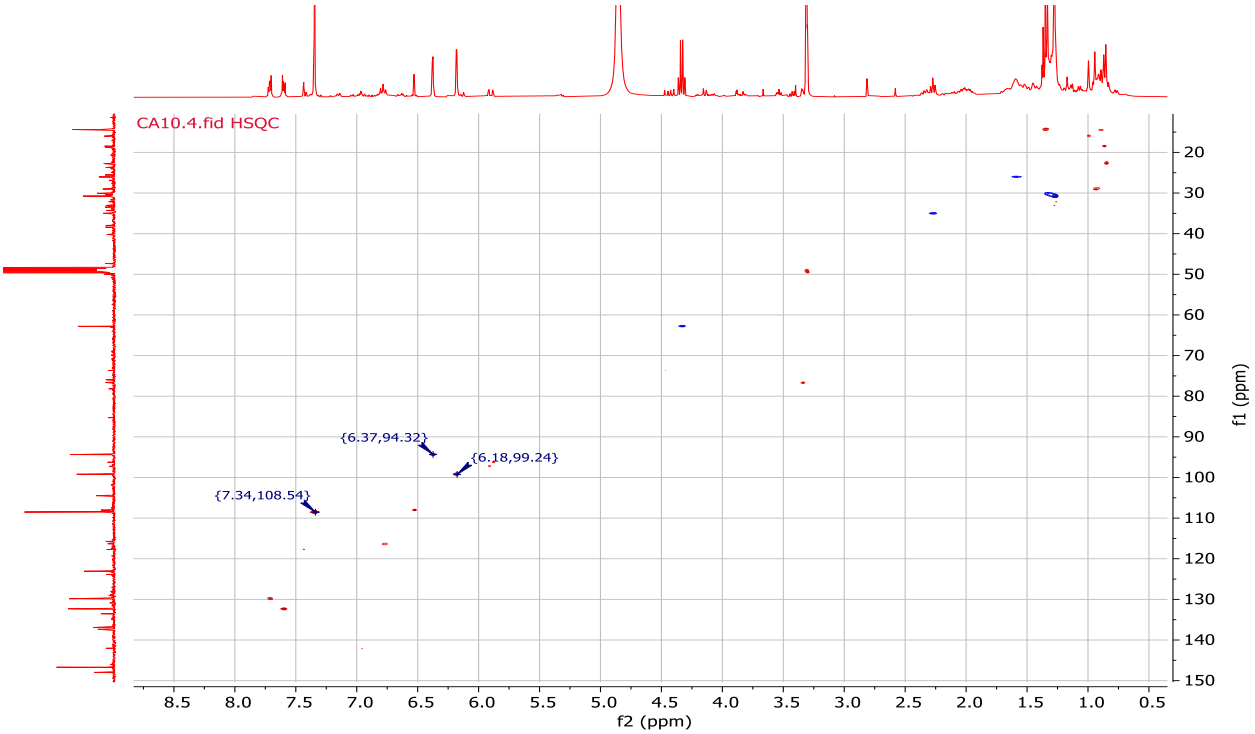

D: HSQC spectrum of compound **66**.

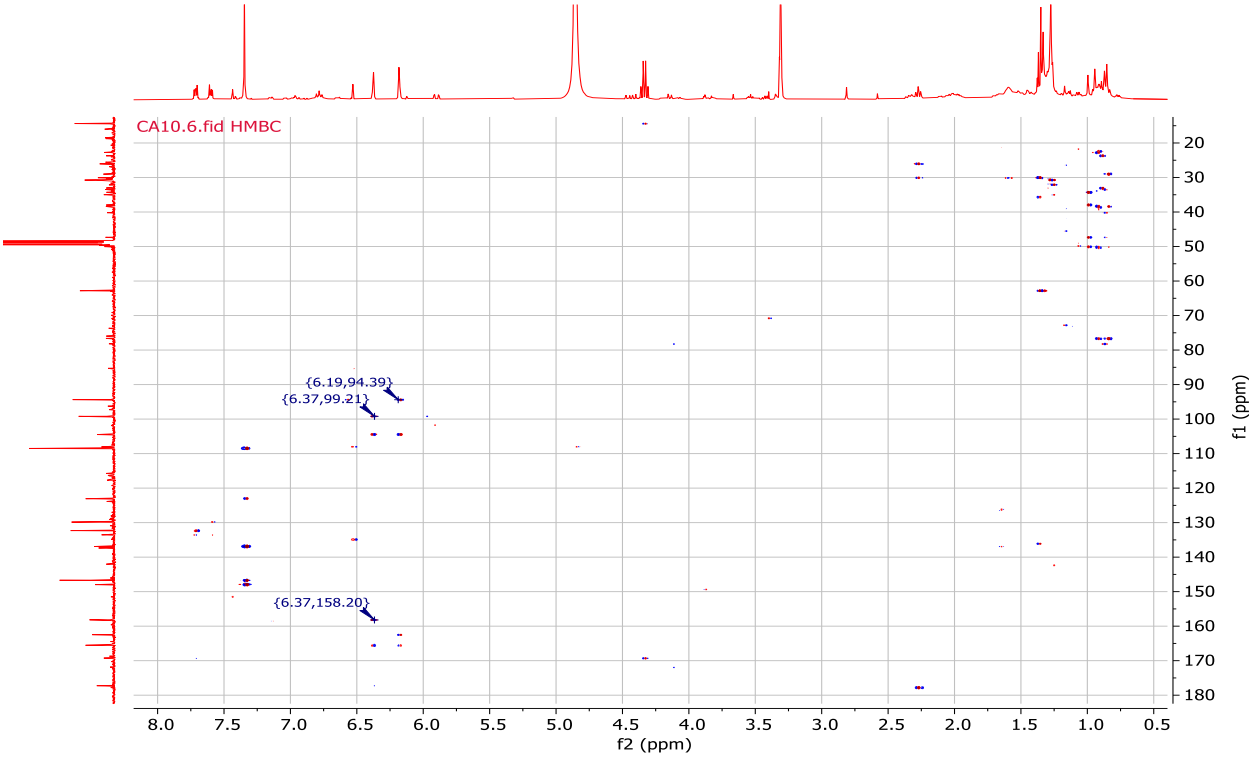

E: HMBC spectrum of compound **66**.

Appendix 9: ^{1}H, ^{13}C, DEPT-135, HSQC, and HMBC NMR spectra of compound **66**.

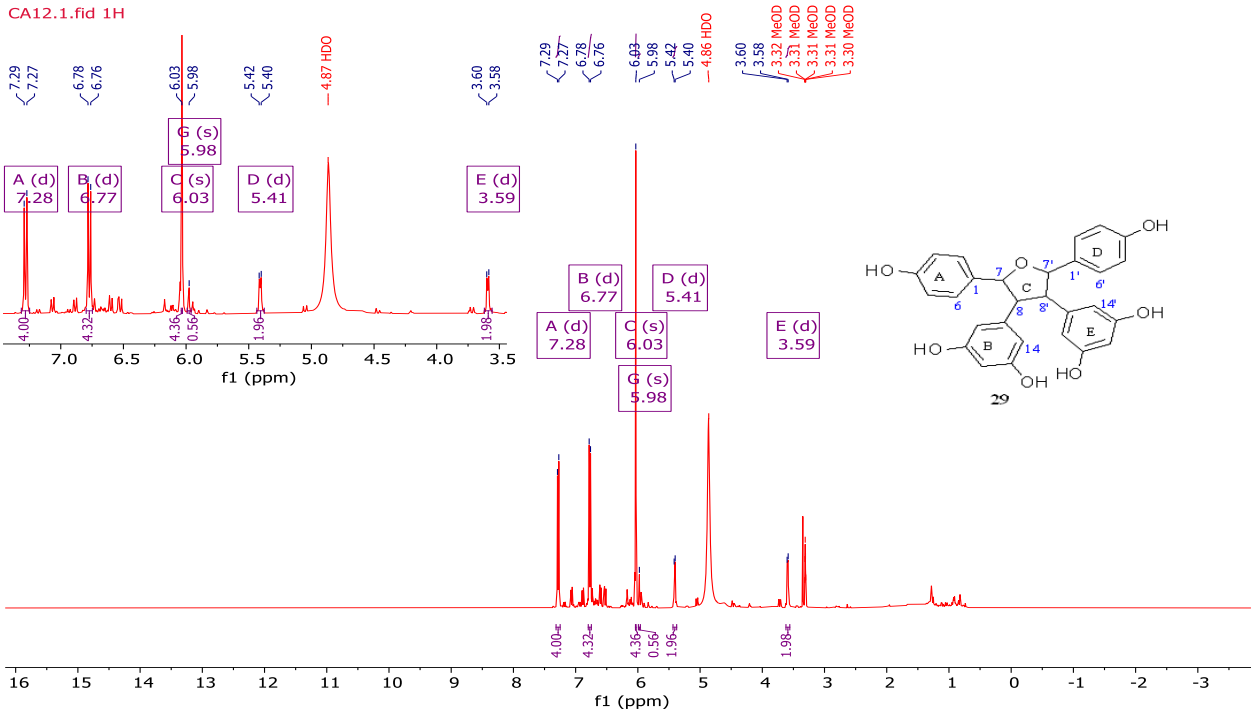

A: ^{1}H NMR (400 MHz, CD_3OD) spectrum of compound **29**.

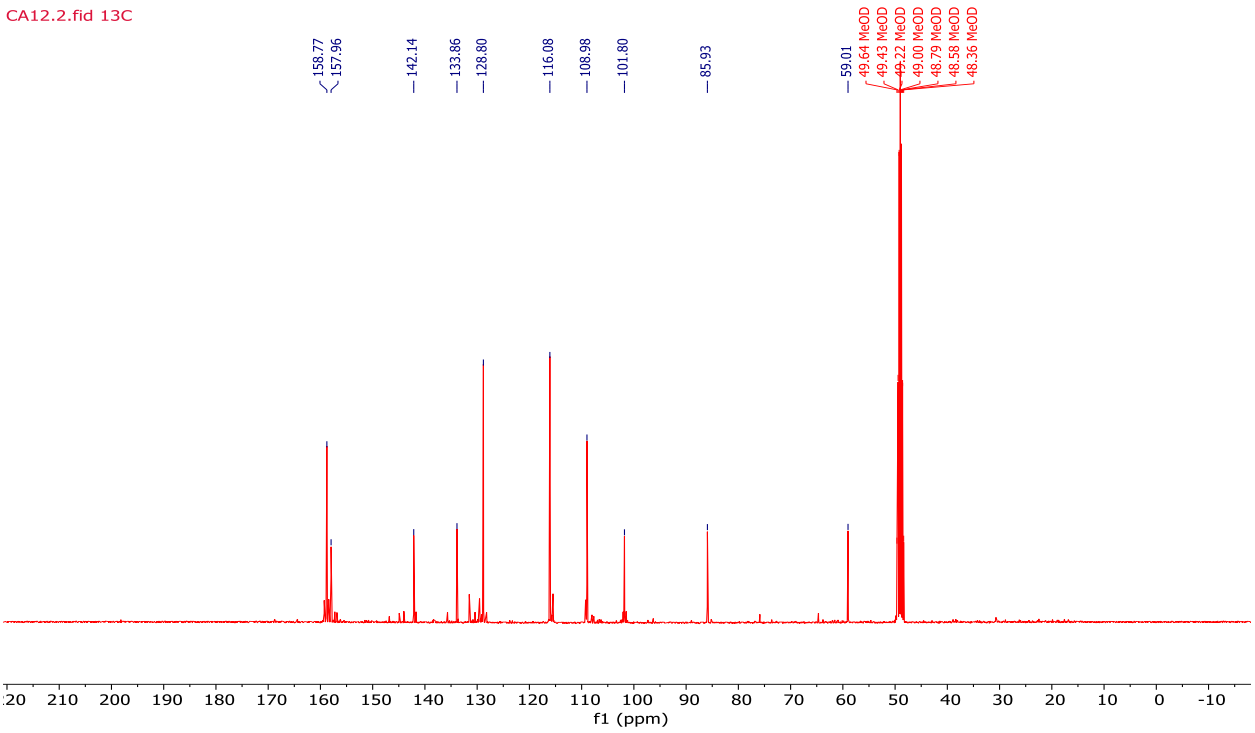

B: ^{13}C NMR (100 MHz, CD_3OD) spectrum of compound **29**.

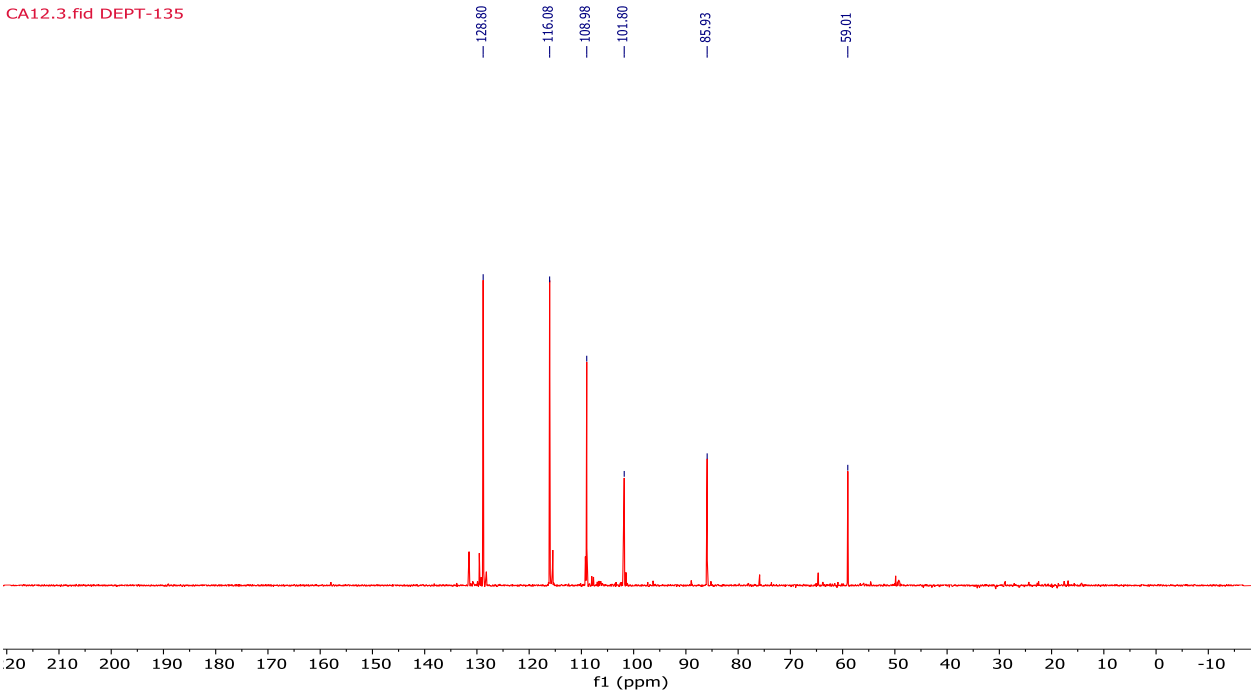

C: DEPT-135 spectrum of compound **29**.

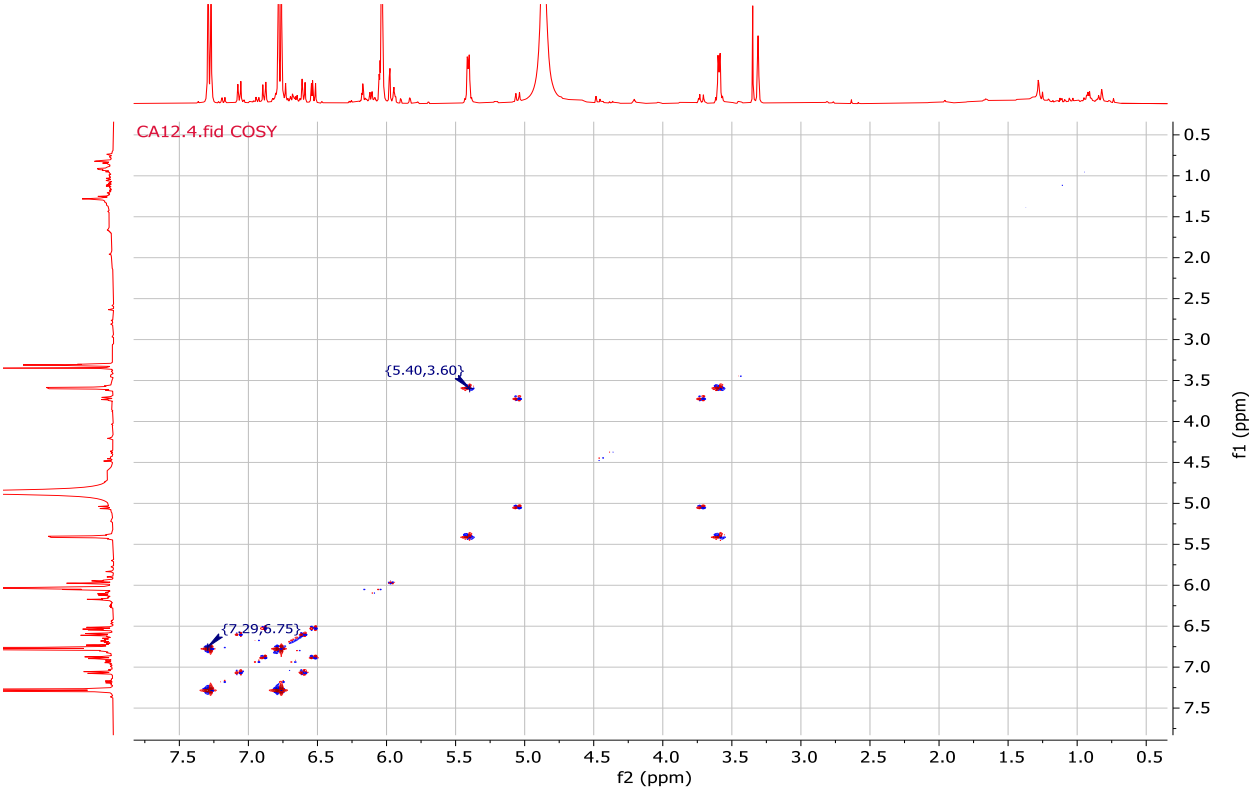

D: COSY spectrum of compound **29**.

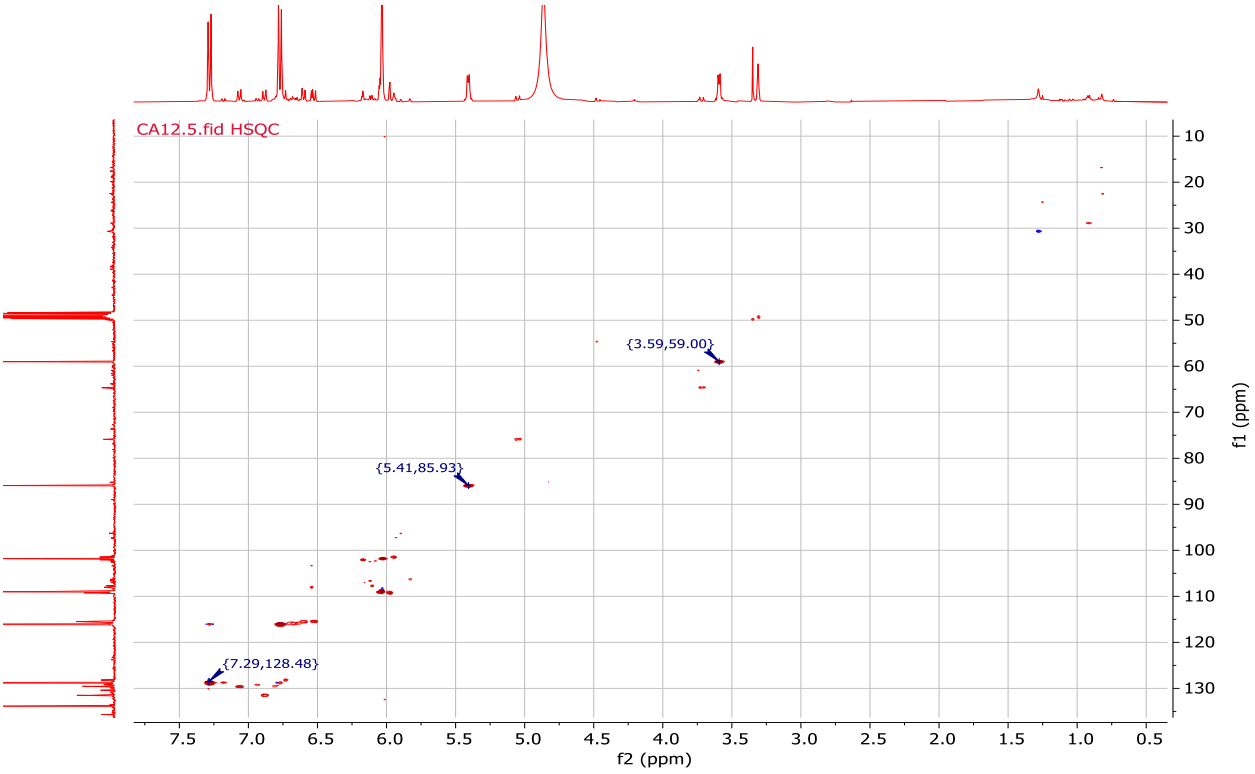

E: HSQC spectrum of compound **29**.

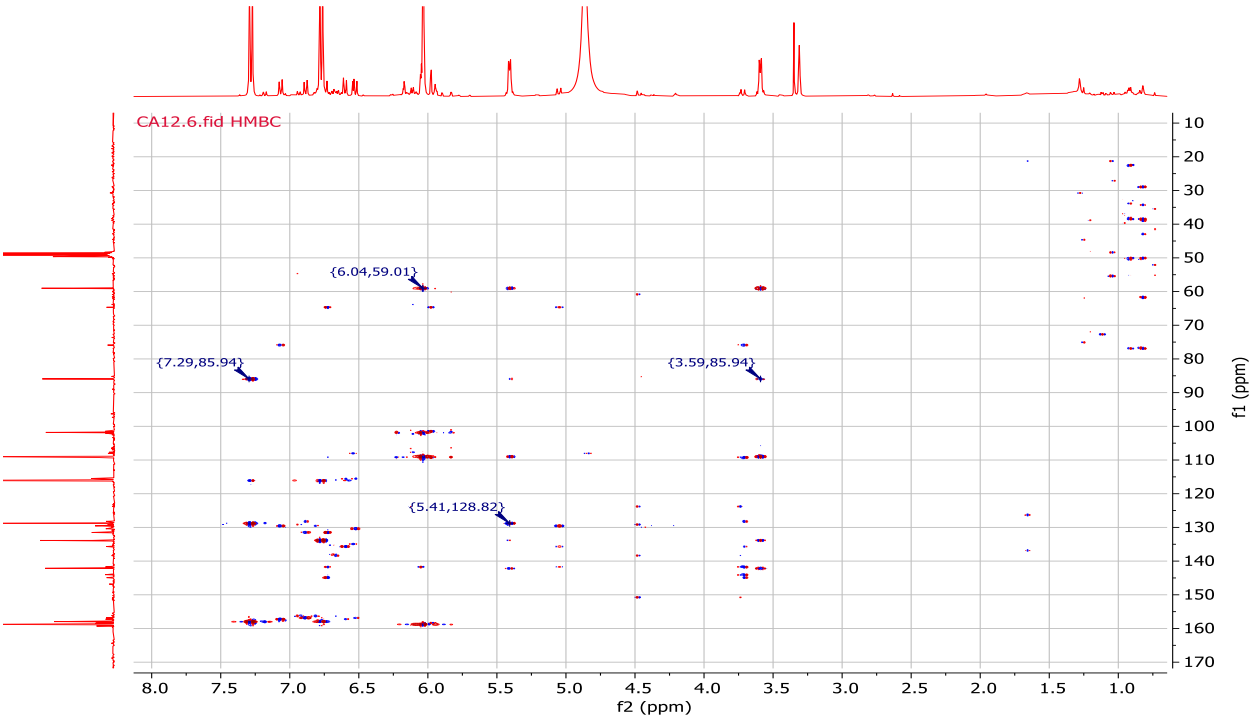

F: HMBC spectrum of compound **29**.

Appendix 10: ^{1}H, ^{13}C, DEPT-135, COSY, HSQC, and HMBC NMR spectra of compound **29**.

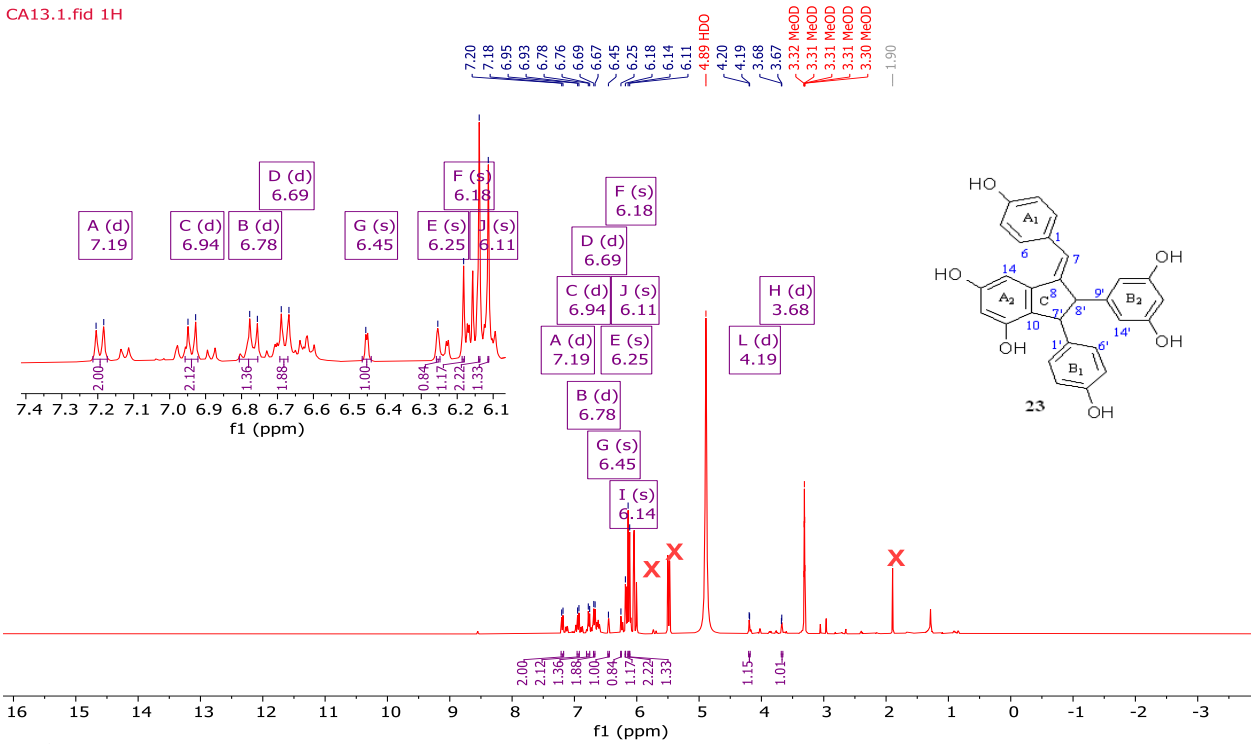

A: ^{1}H NMR (400 MHz, CD_3OD) spectrum of compound **23**.

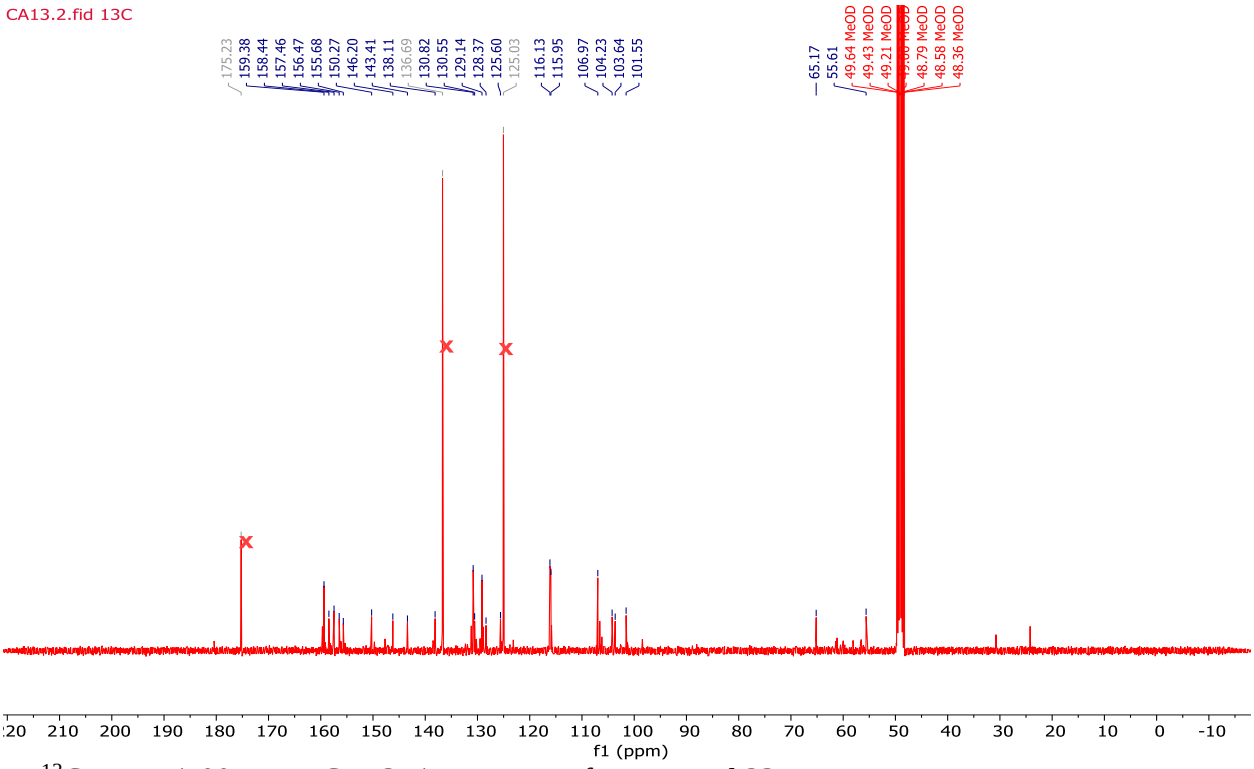

B: ^{13}C NMR (100 MHz, CD_3OD) spectrum of compound **23**.

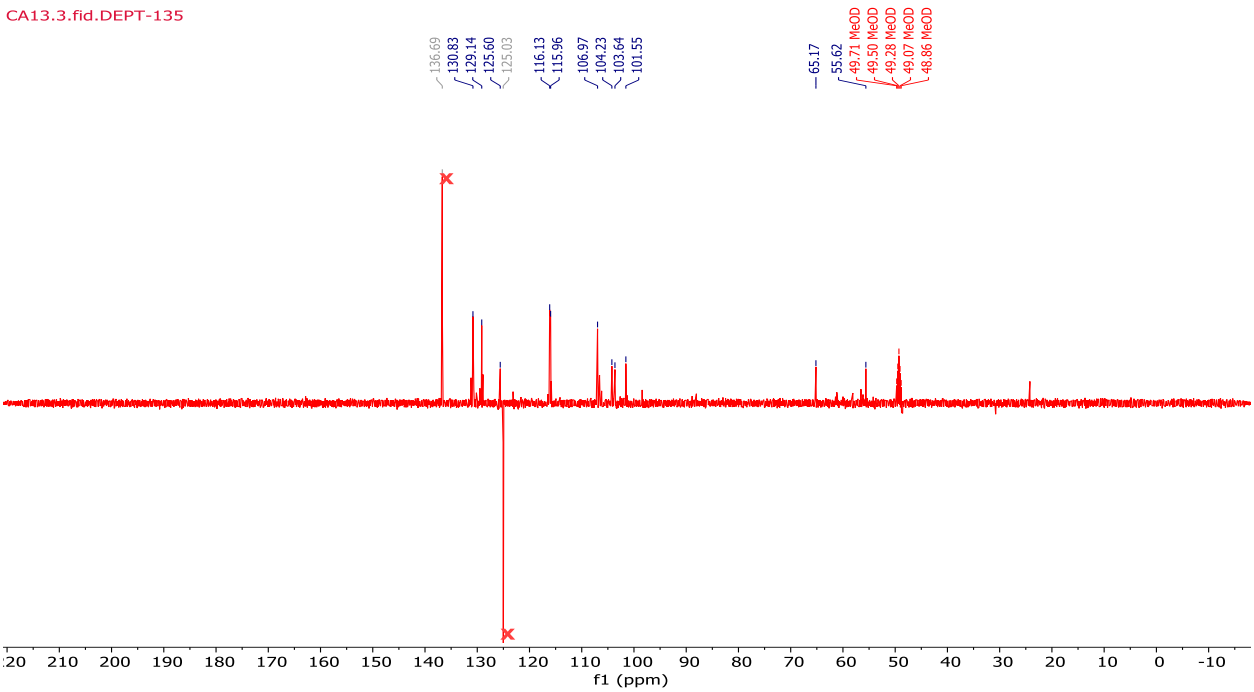

C: DEPT-135 spectrum of compound **23**.

- ✓ The spectra also showed an acrylate contaminant at δ_H 6.04, 6.00, 5.49, and 1.90, and at δ_C 175.2, 136.7, 125.0 and 24.2. Preparative TLCs are made up of silica gel, and to adhere it to the glass, some manufacturers use acrylates as an adhering agent. There is a likely probability that these adhering agents were detected by NMR considering the fact that the final purification in our case was done by PTLC. During filtration acetone and methanol solvents were used, and acetone likely broke down the acrylic polymer used as a binding agent and possibly the acrylates mixed with the filtrate.

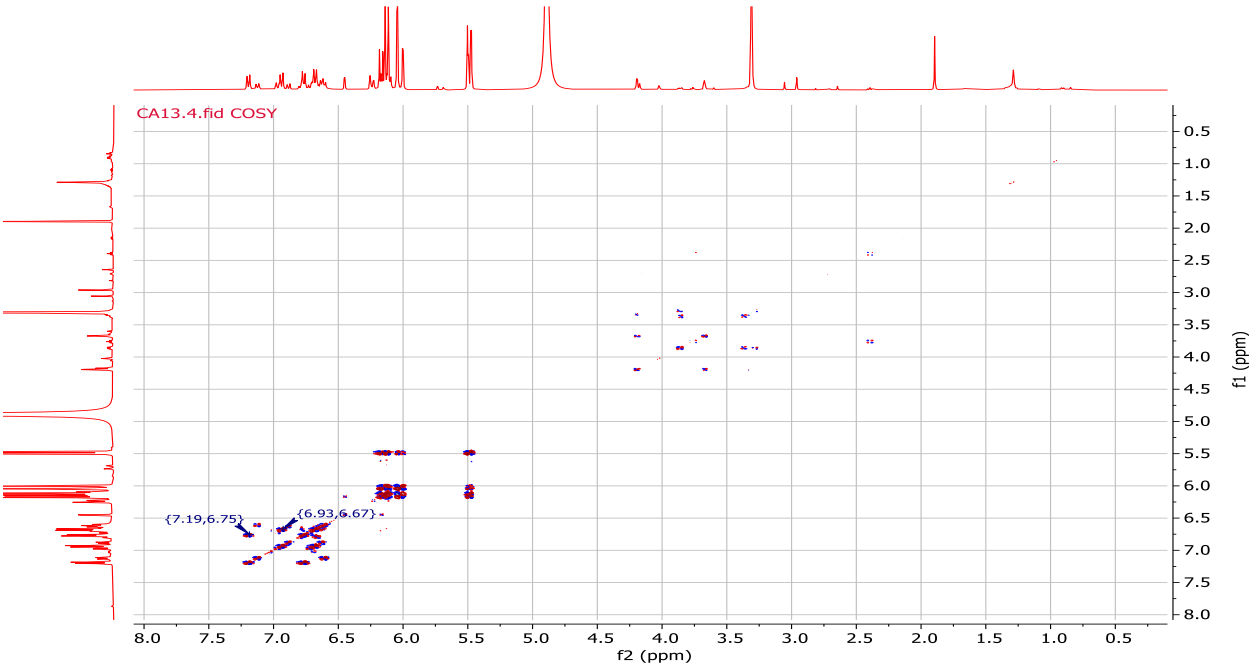

D: COSY spectrum of compound **23**.

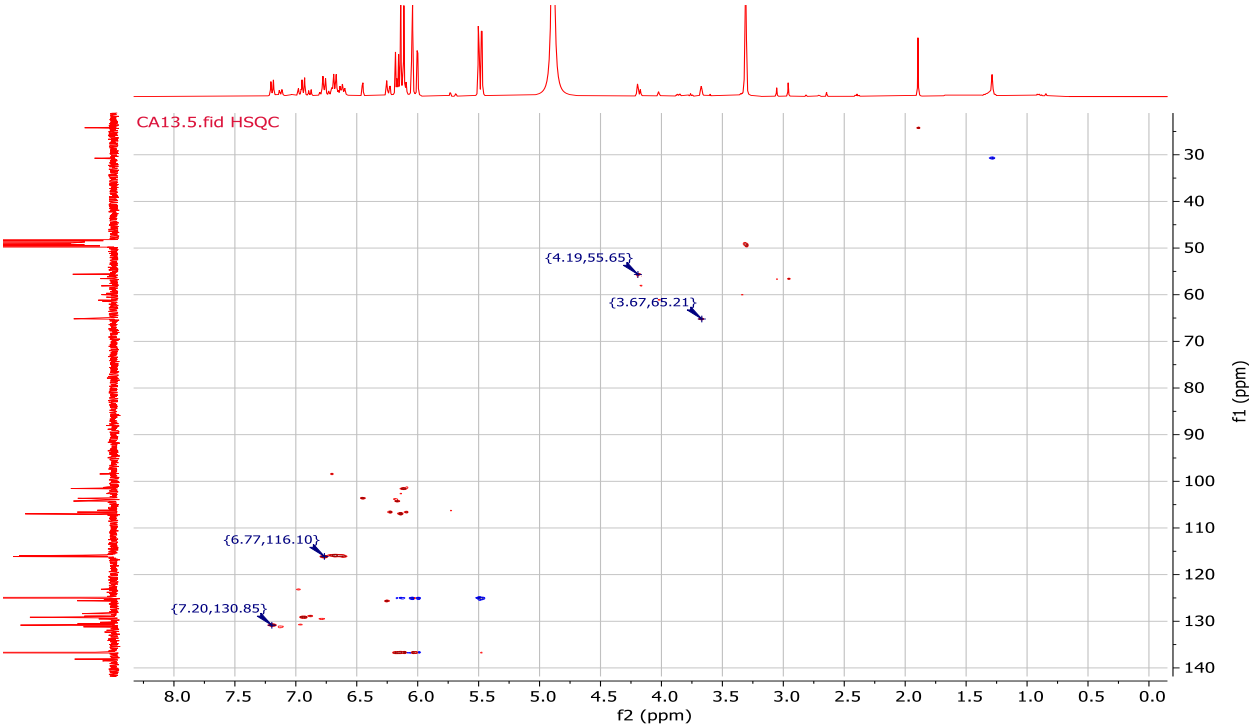

E: HSQC spectrum of compound **23**.

F: HMBC spectrum of compound **23**.

Appendix 11: ^{1}H, ^{13}C, DEPT-135, COSY, HSQC, and HMBC NMR spectra of compound **23**.

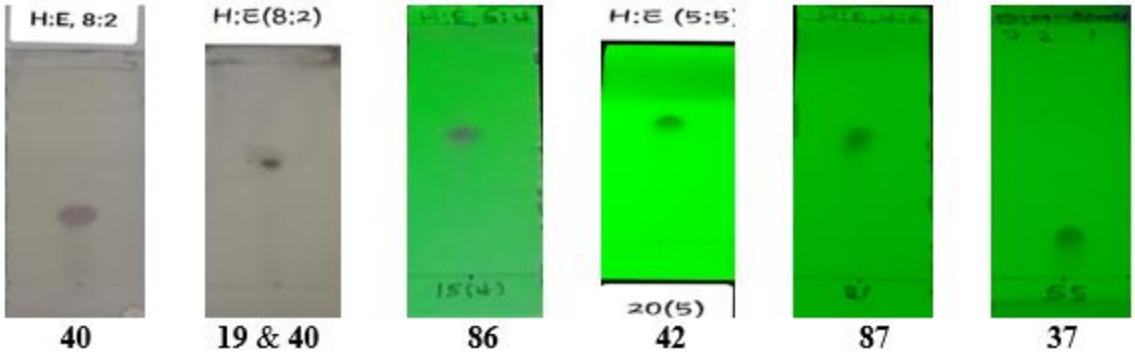

Appendix 12: TLC profile of the compound isolates from roots of *D. regia*.

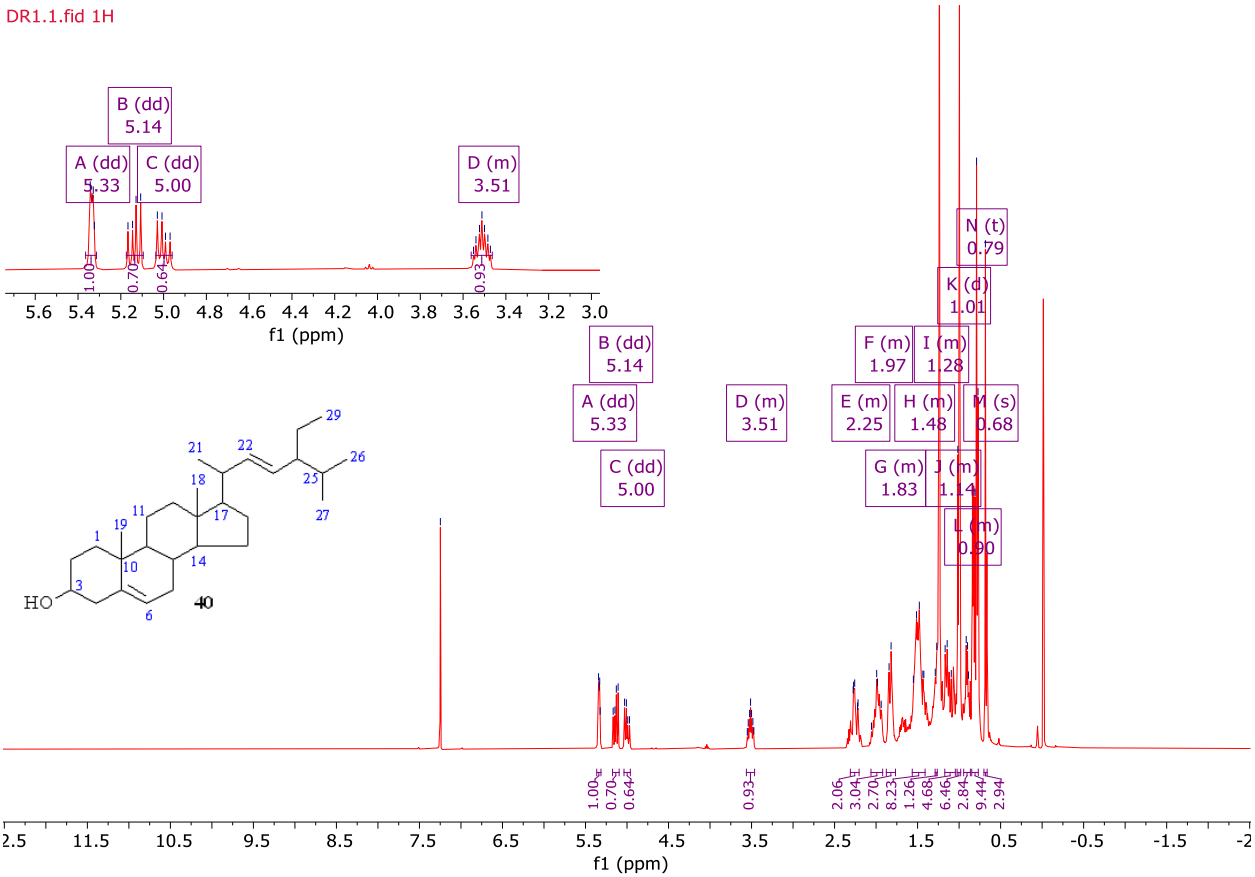

A: ^{1}H NMR (400 MHz, $CDCl_3$) spectrum of compound **40**.

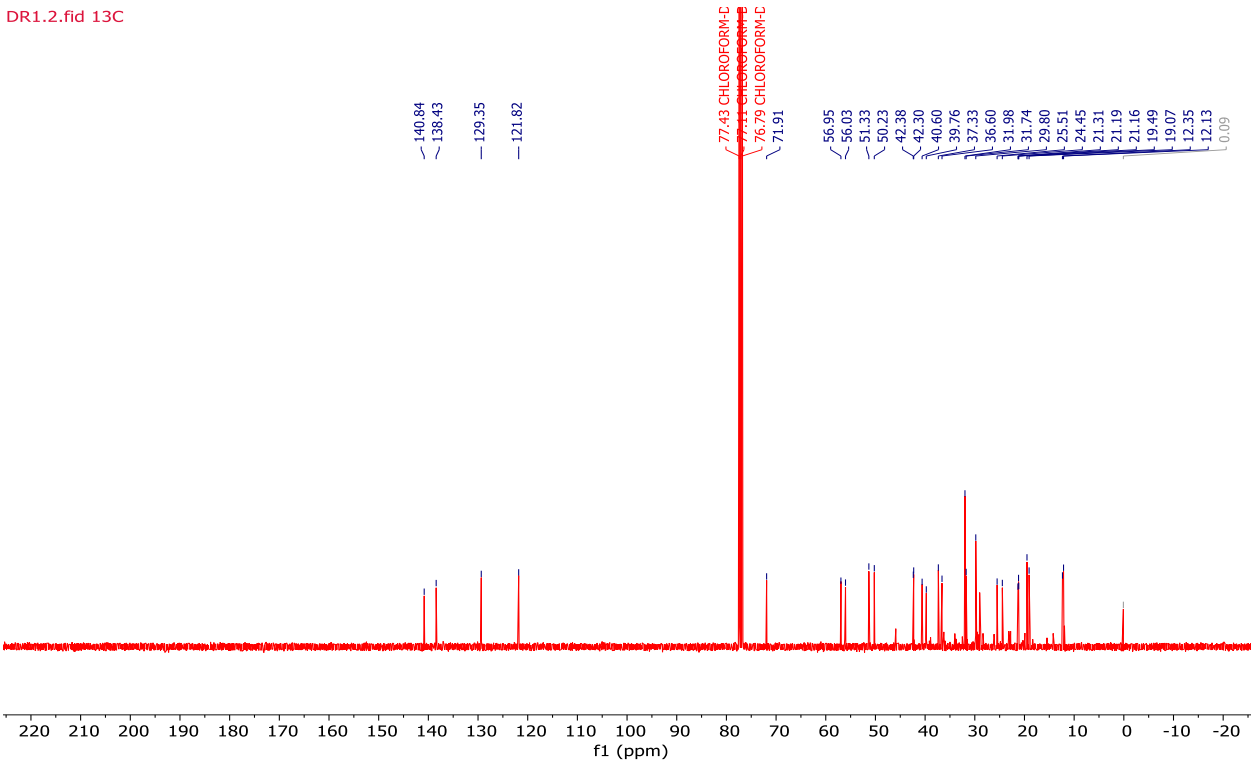

B: ^{13}C NMR (100 MHz, $CDCl_3$) spectrum of compound **40**.

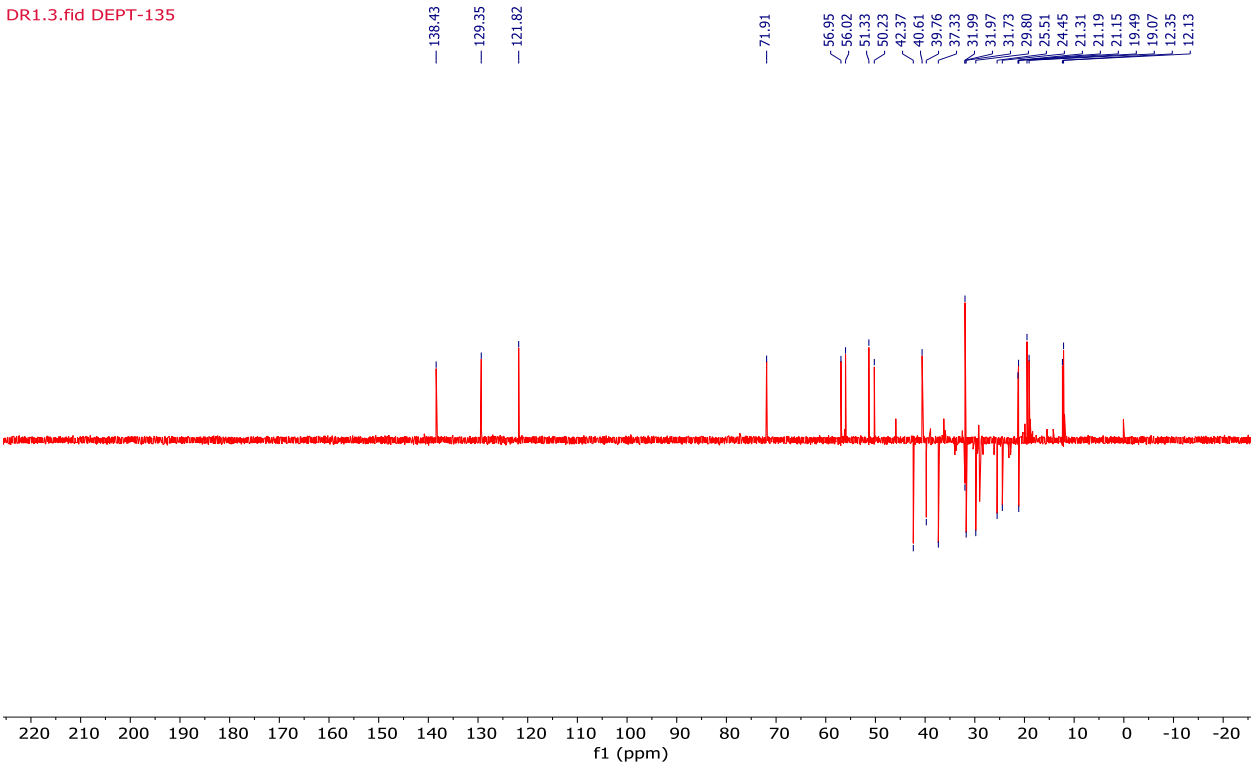

C: DEPT-135 spectrum of compound **40**.

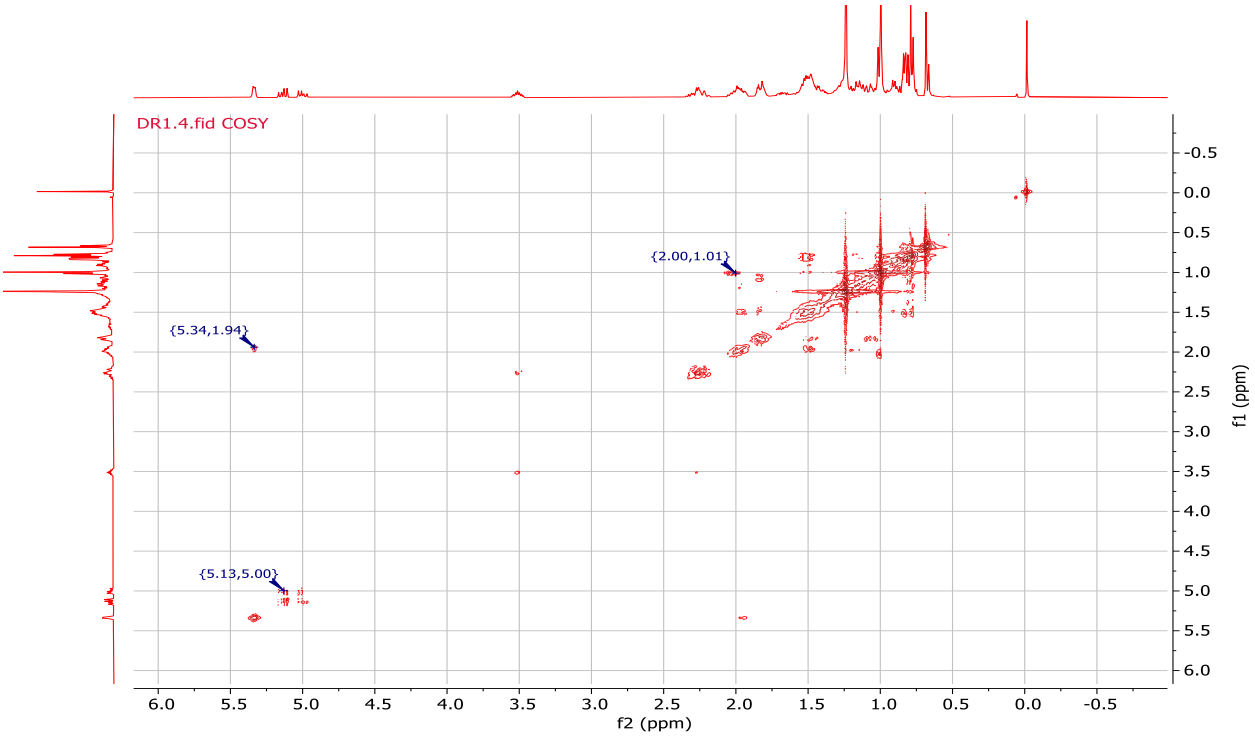

D: COSY spectrum of compound **40**.

Appendix 13: ^{1}H, ^{13}C, DEPT-135, and COSY NMR spectra of compound **40**.

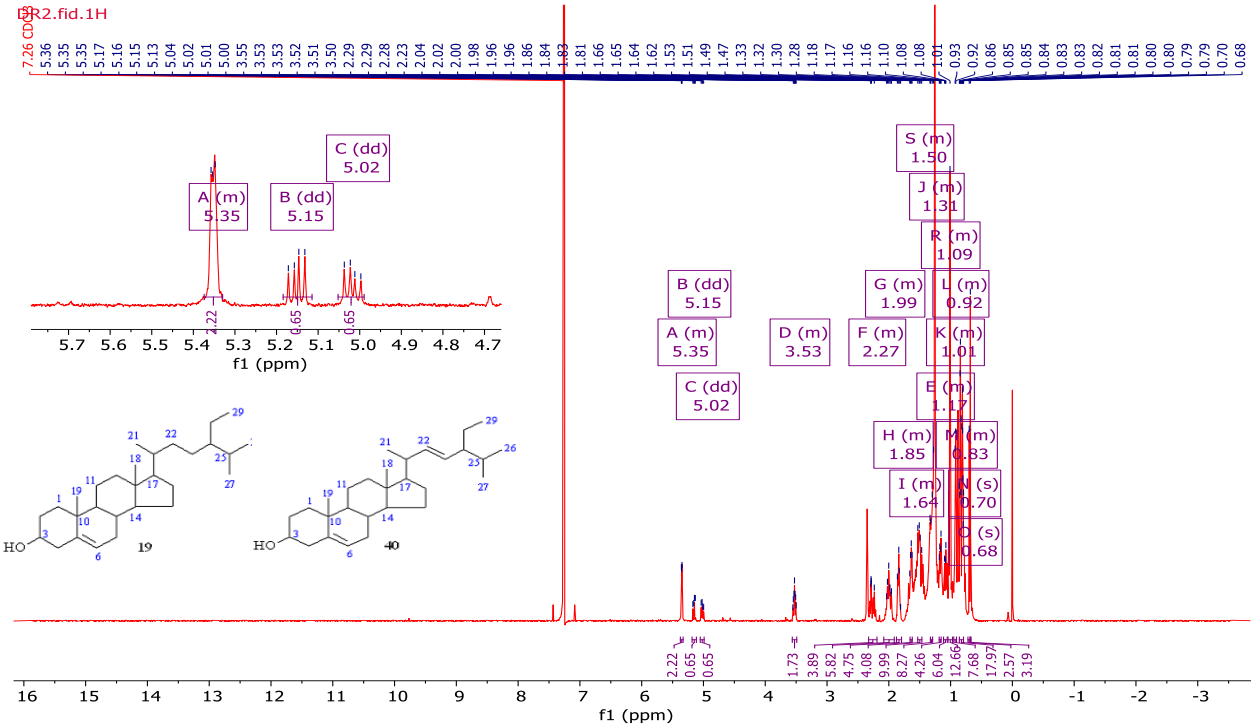

A: ^{1}H NMR (400 MHz, $CDCl_3$) spectrum of the mixture of compounds **19** and **40**.

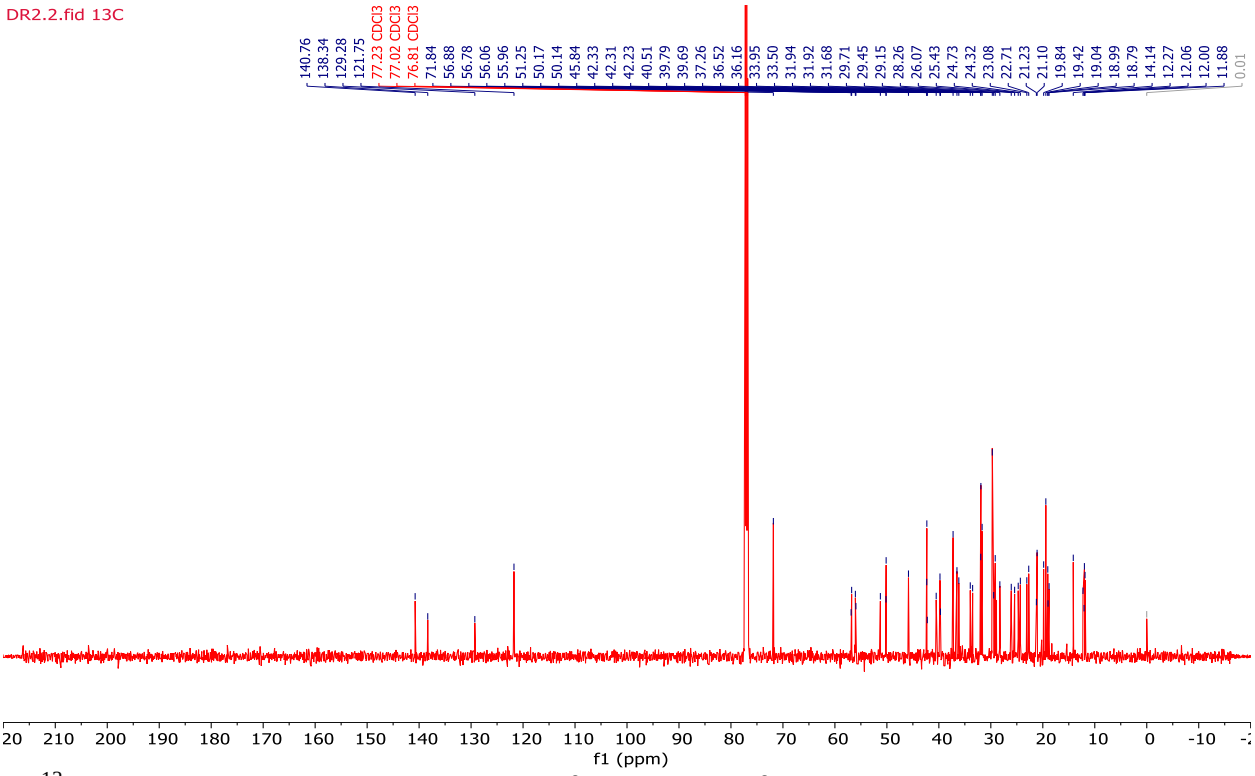

B: ^{13}C NMR (100 MHz, $CDCl_3$) spectrum of the mixture of compounds **19** and **40**.

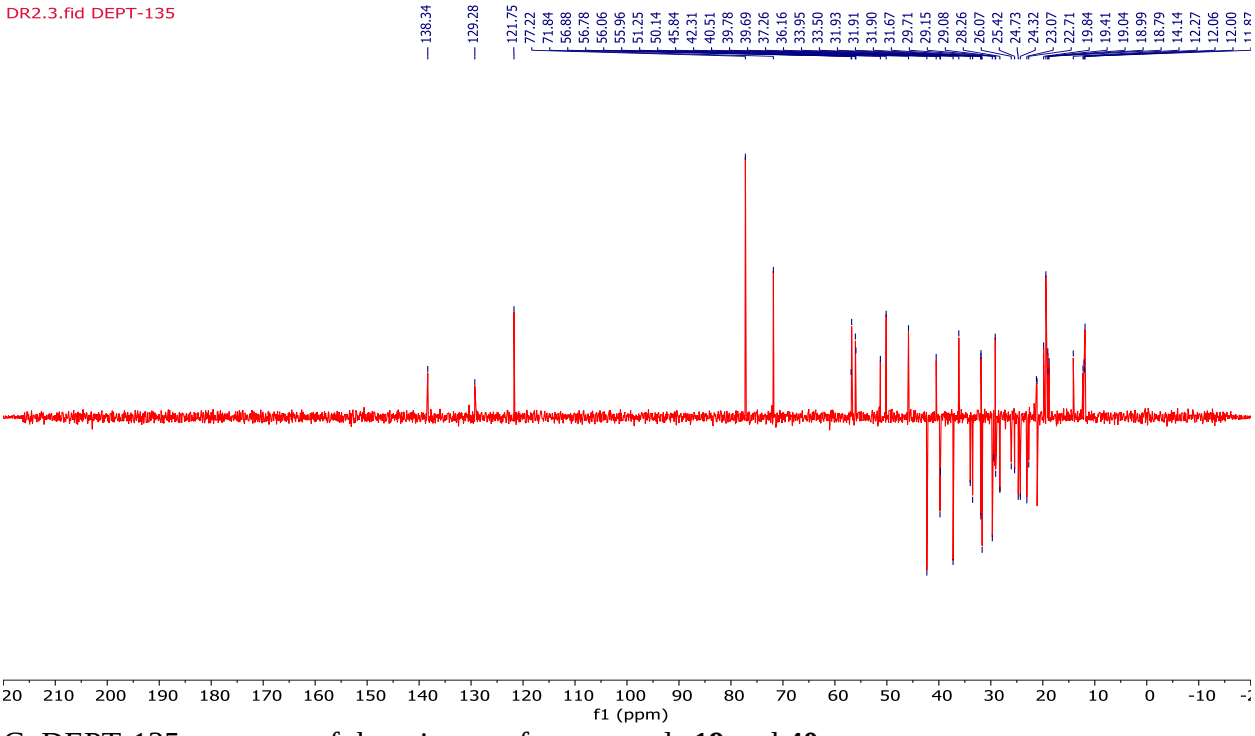

C: DEPT-135 spectrum of the mixture of compounds **19** and **40**.

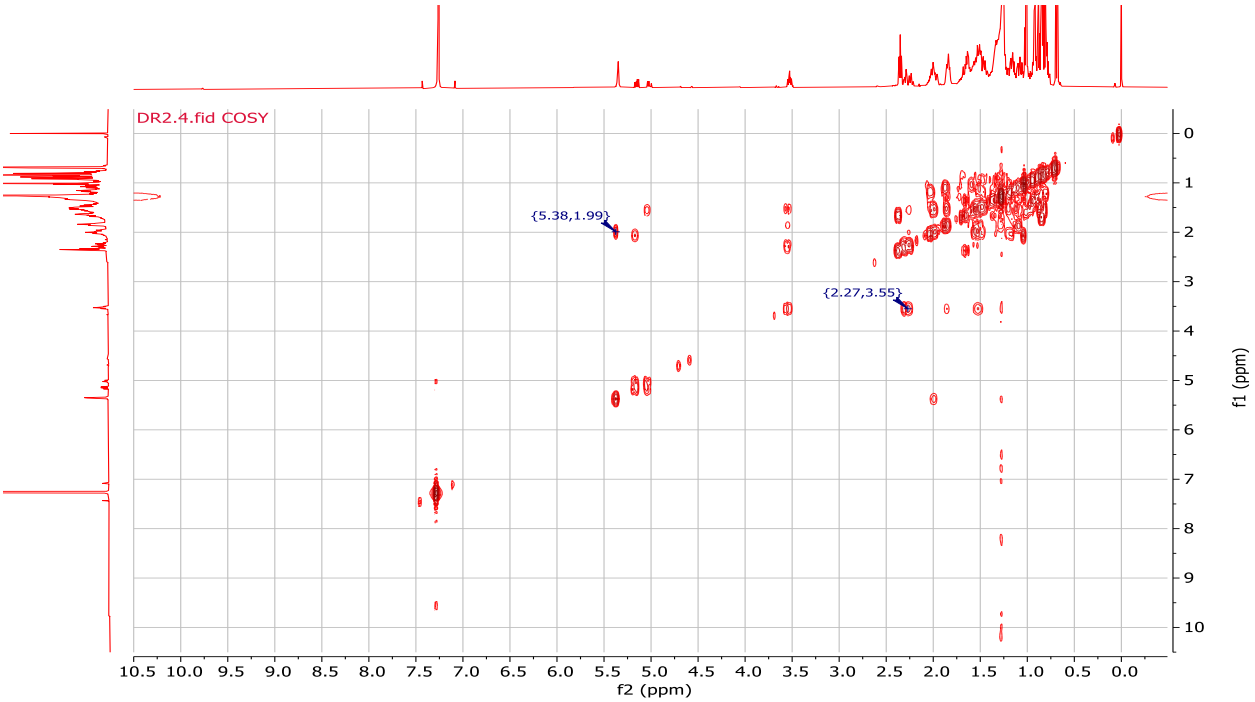

D: COSY spectrum of the mixture of compounds **19** and **40**.

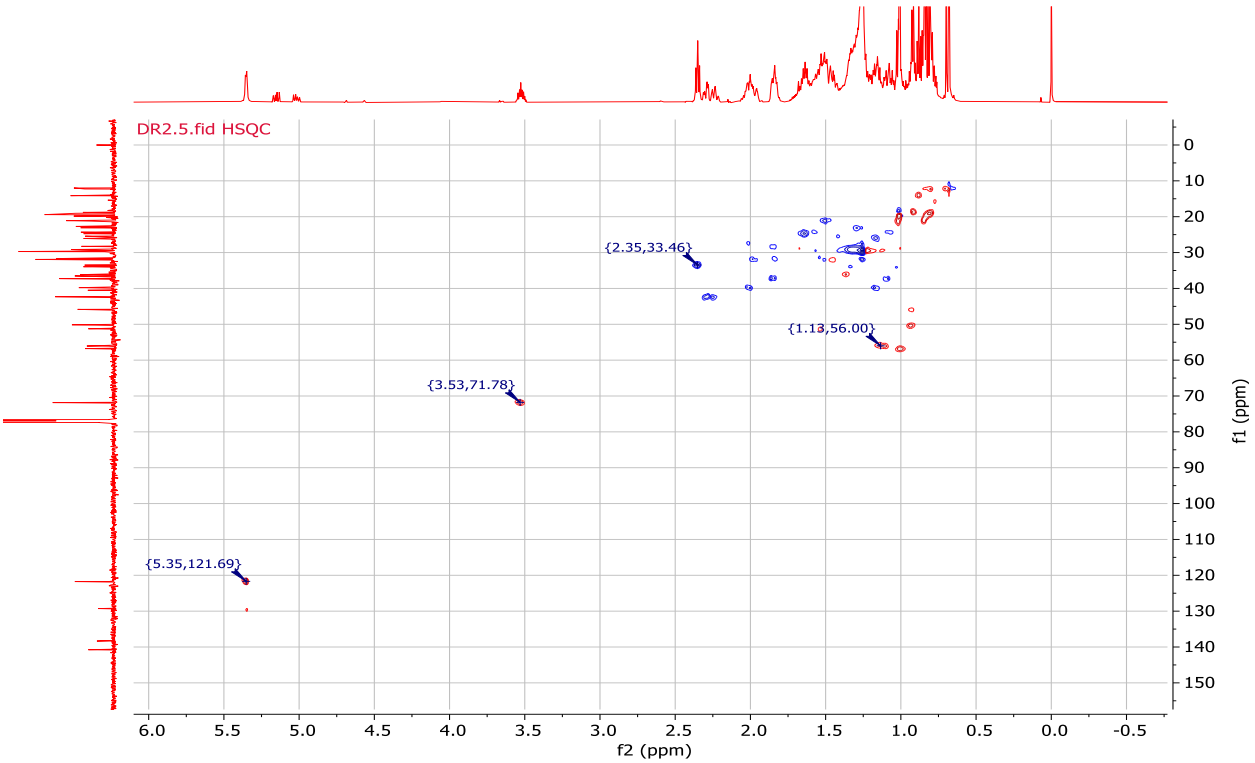

E: HSQC spectrum of the mixture of compounds **19** and **40**.

Appendix 14: ^{1}H, ^{13}C, DEPT-135, COSY, and HSQC NMR spectra of the mixture of compounds **19** and **40**.

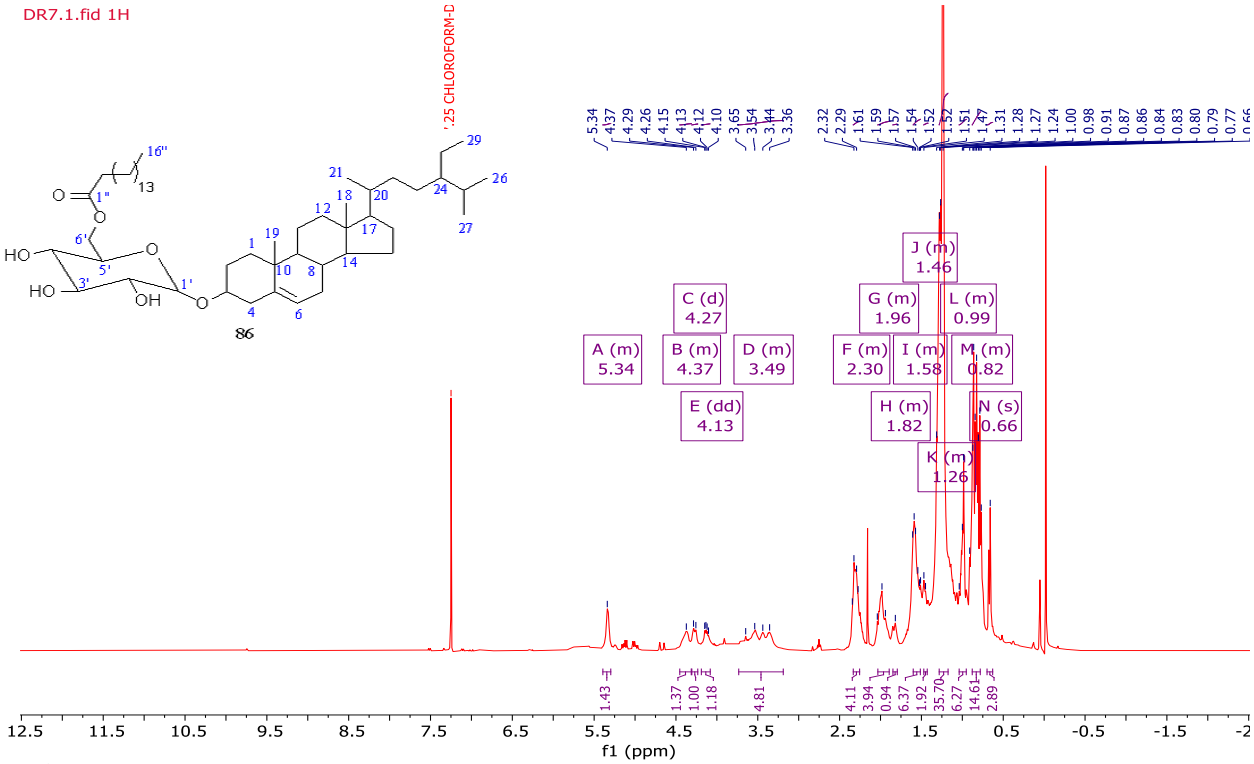

A: ^{1}H NMR (400 MHz, $CDCl_3$) spectrum of compound **86**.

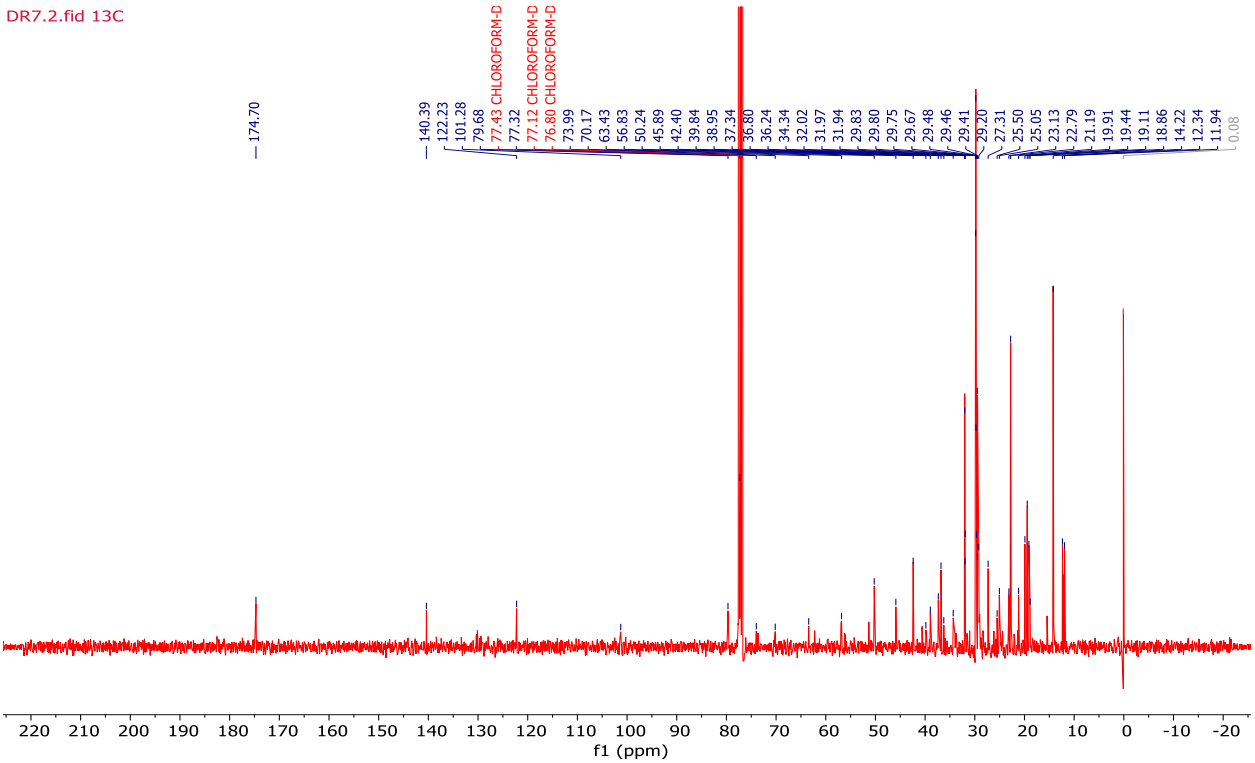

B: ^{13}C NMR (100 MHz, $CDCl_3$) spectrum of compound **86**.

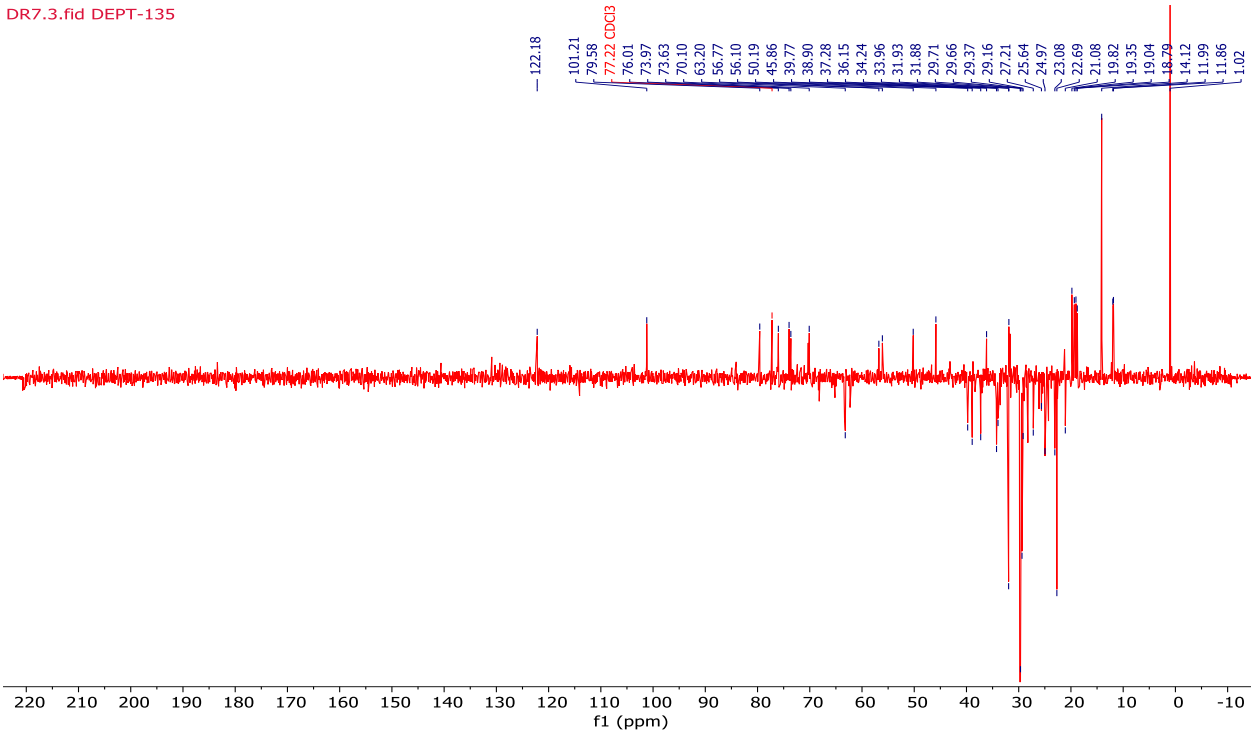

C: DEPT-135 spectrum of compound **86**.

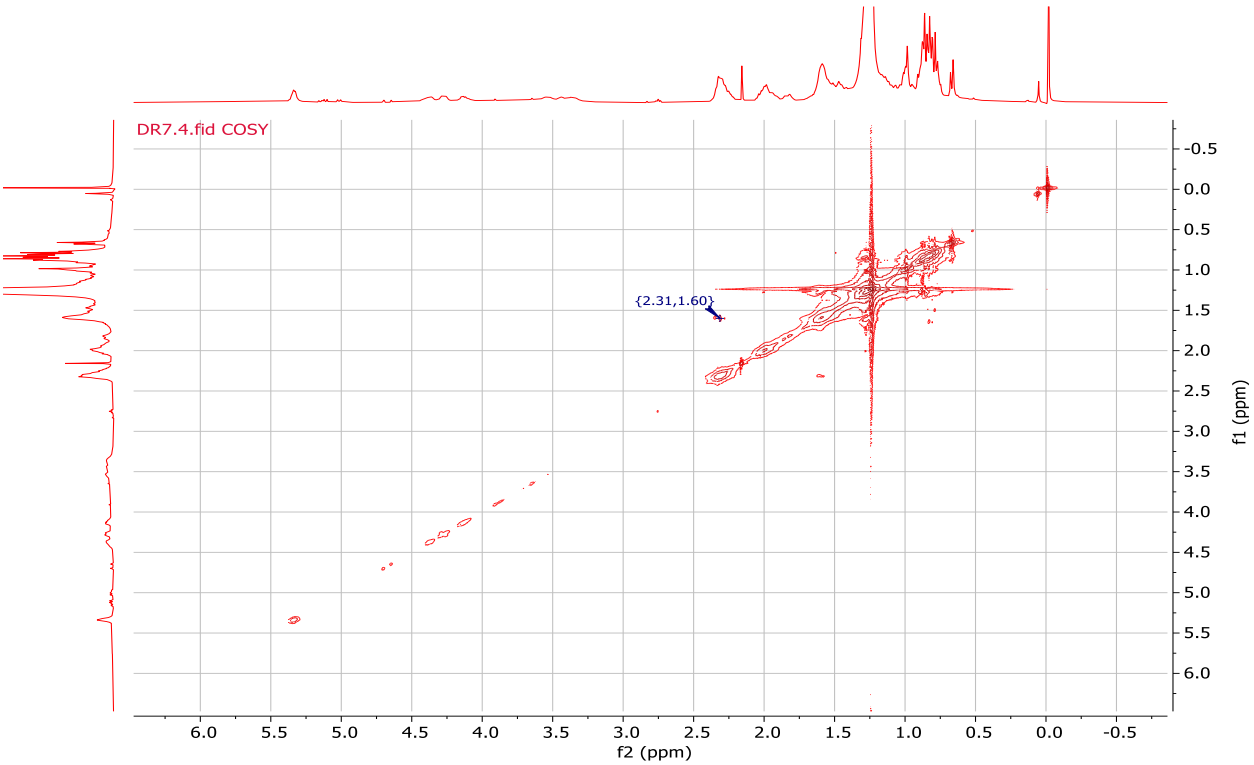

D: COSY spectrum of compound **86**.

Appendix 15: ^{1}H, ^{13}C, DEPT-135, and COSY NMR spectra of compound **86**.

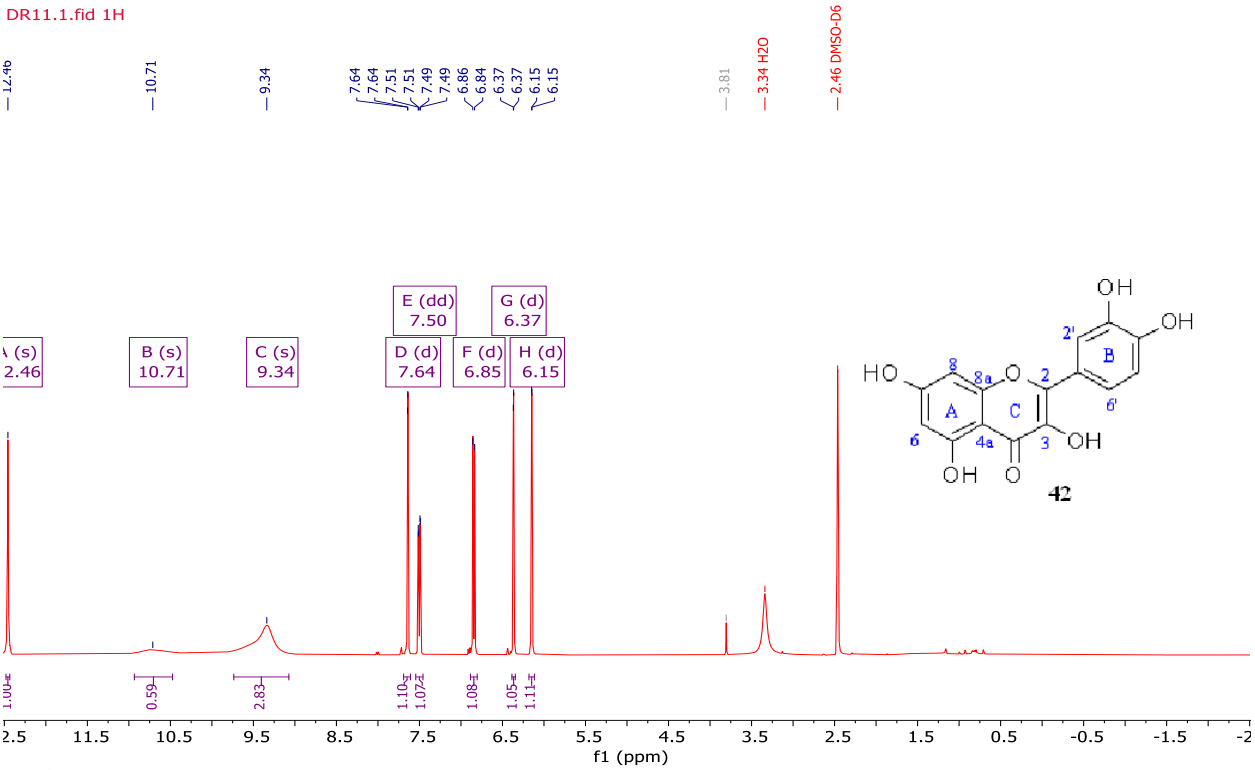

A: ^{1}H NMR (400 MHz, DMSO-d_6) spectrum of compound **42**.

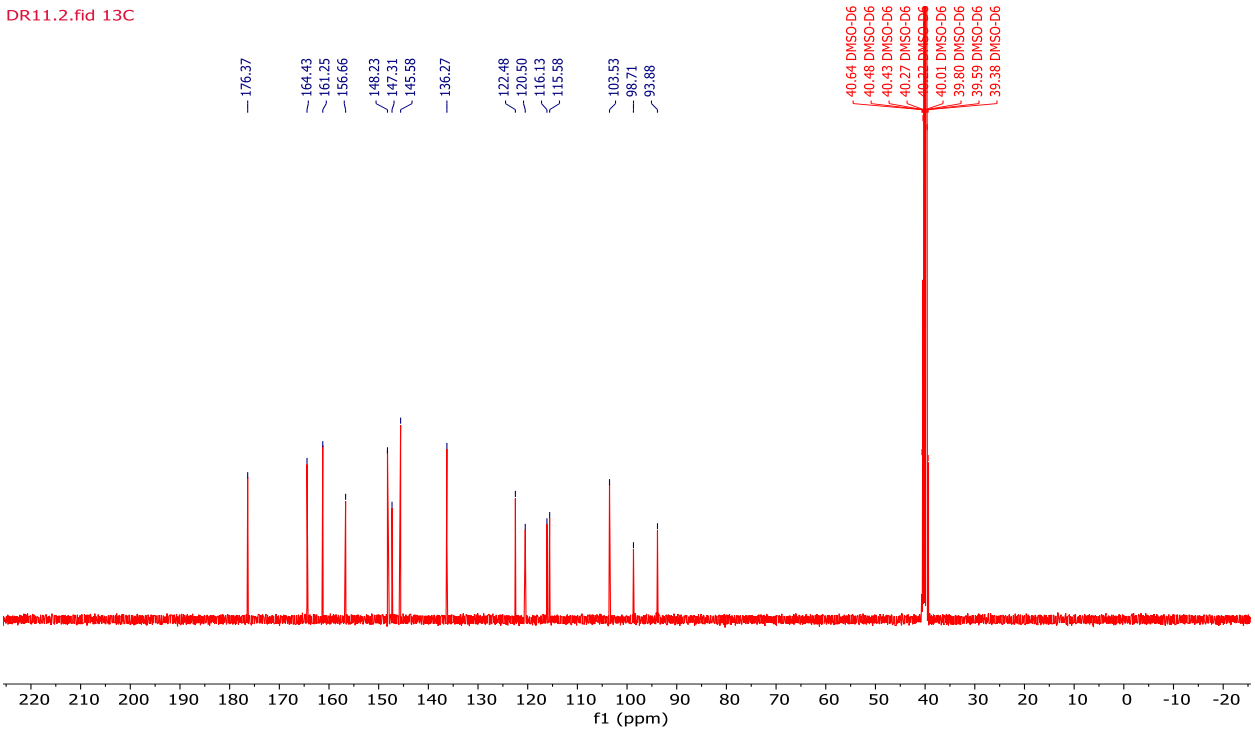

B: ^{13}C NMR (100 MHz, DMSO-d_6) spectrum of compound **42**.

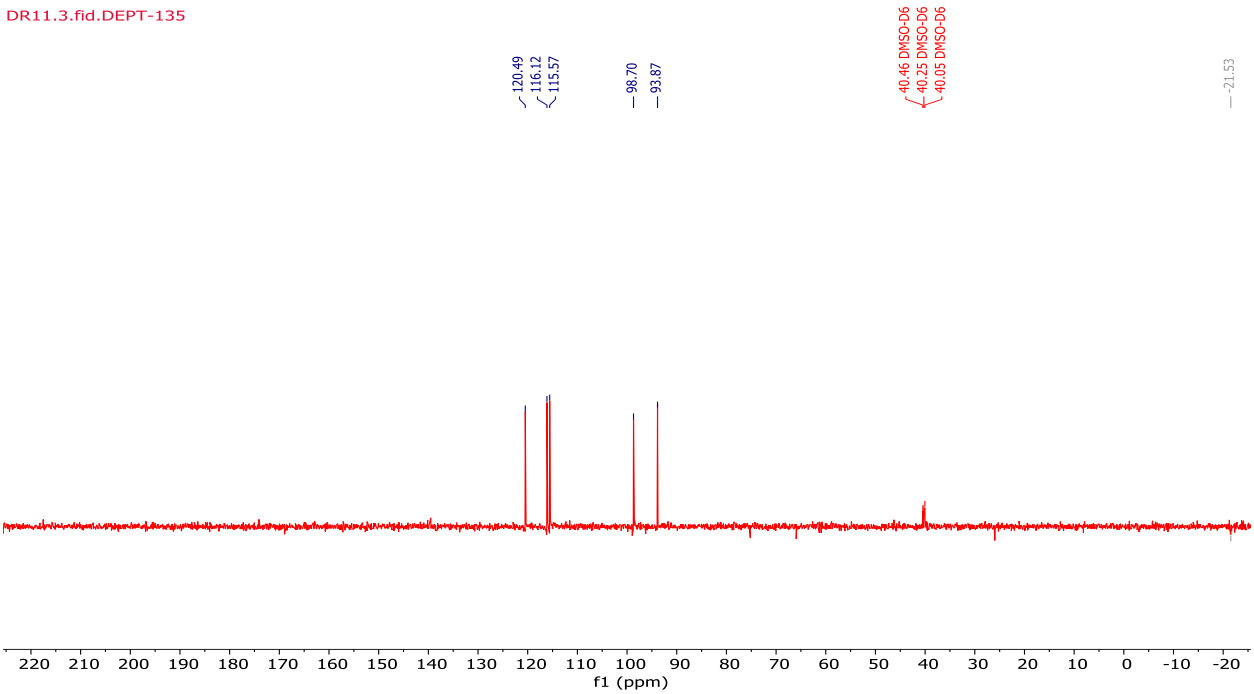

C: DEPT-135 spectrum of compound **42**.

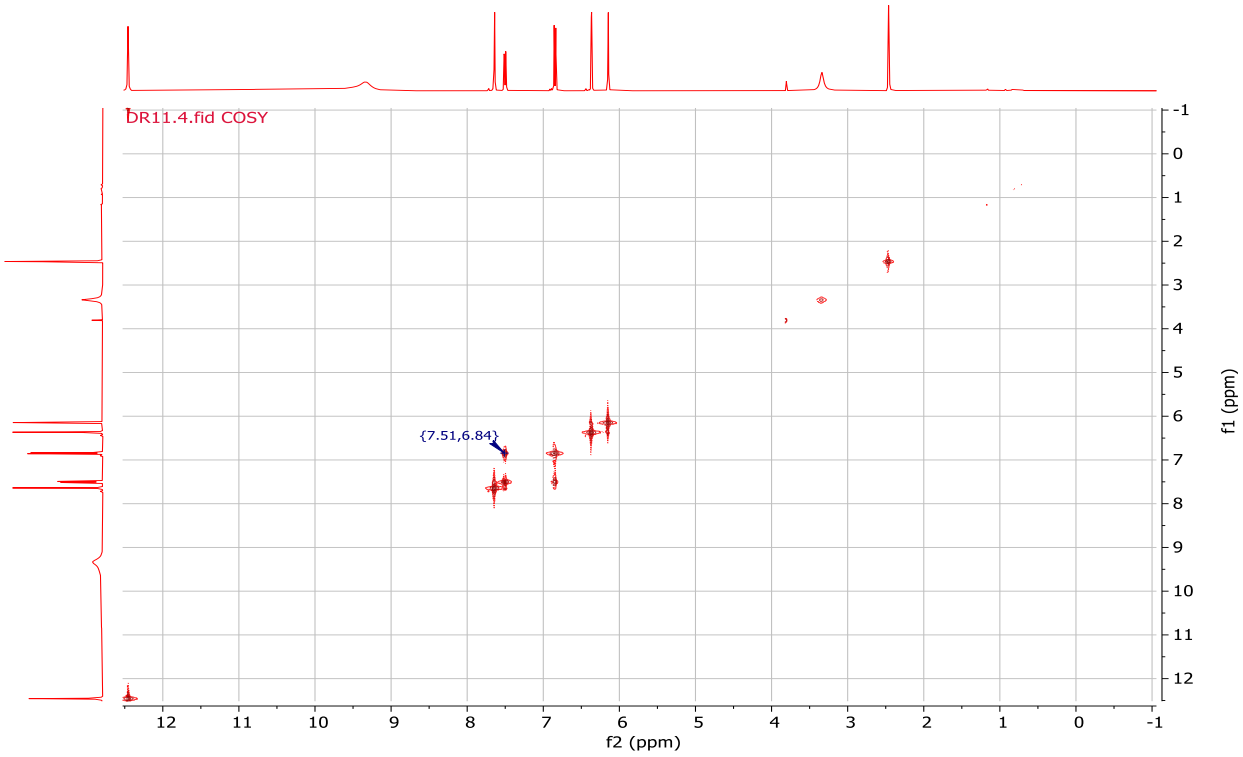

D: COSY spectrum of compound **42**.

Appendix 16: ^{1}H, ^{13}C, DEPT-135, and COSY NMR spectra of compound **42**.

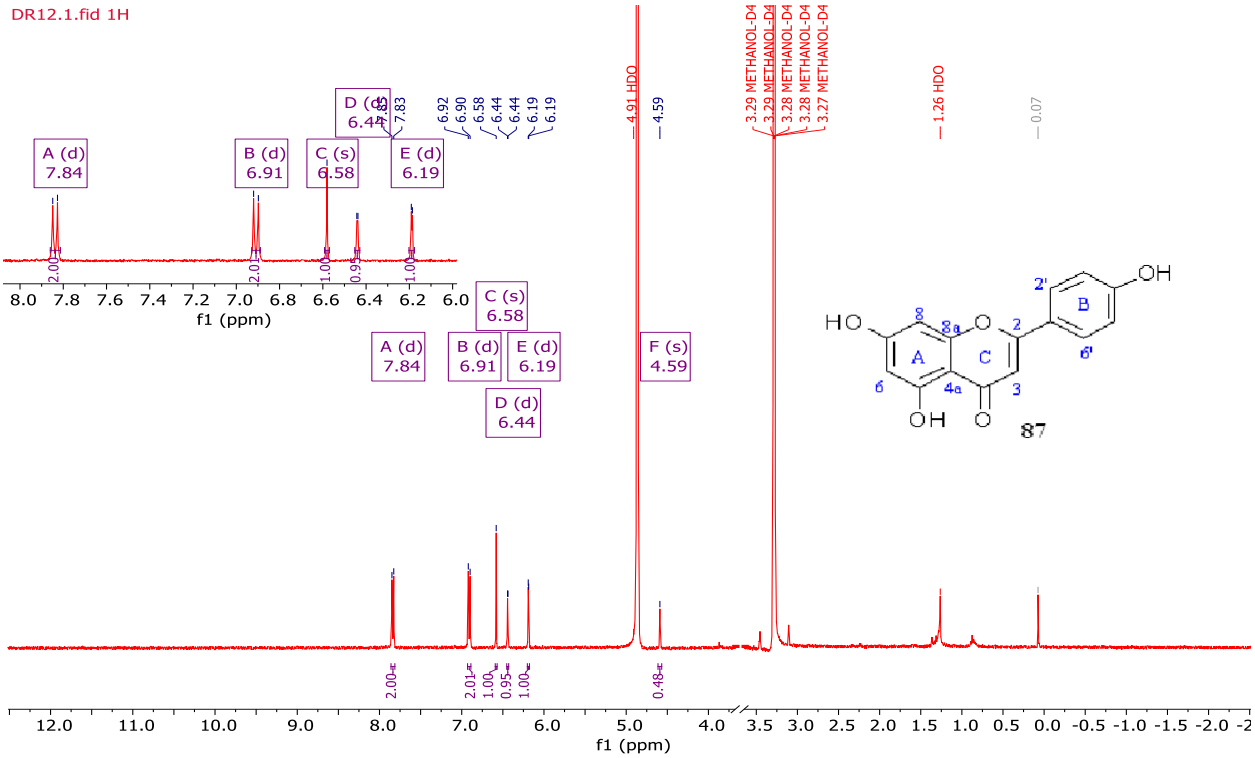

Appendix 17: ^{1}H NMR (400 MHz, CD_3OD) spectrum of compound **87**.

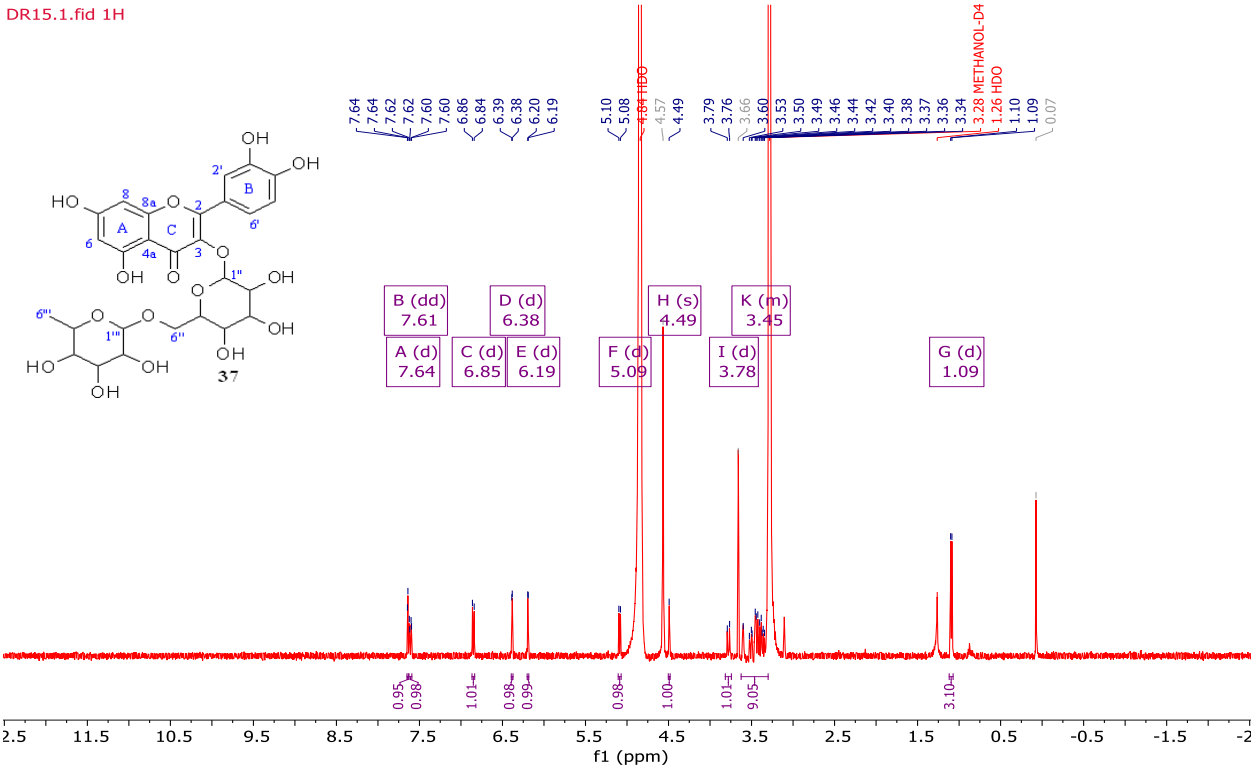

A: ^{1}H NMR (400 MHz, CD_3OD) spectrum of compound **37**.

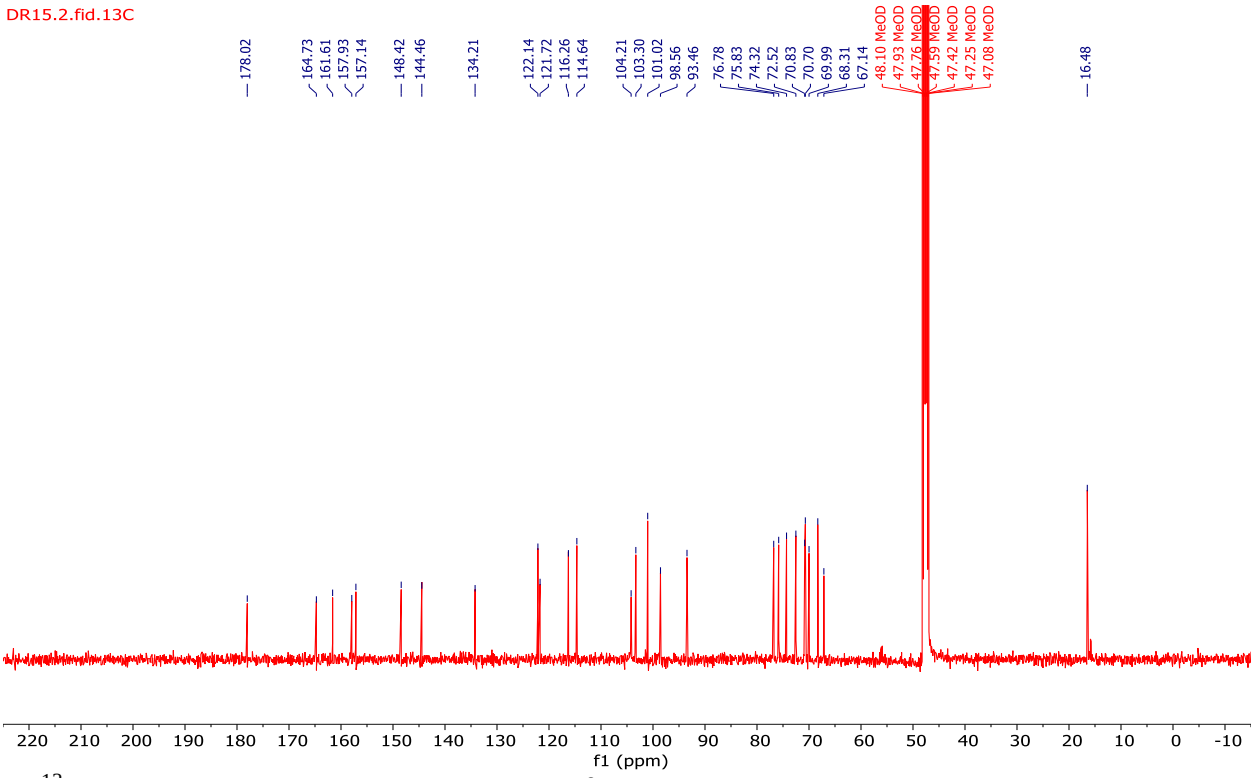

B: ^{13}C NMR (100 MHz, CD_3OD) spectrum of compound **37**.

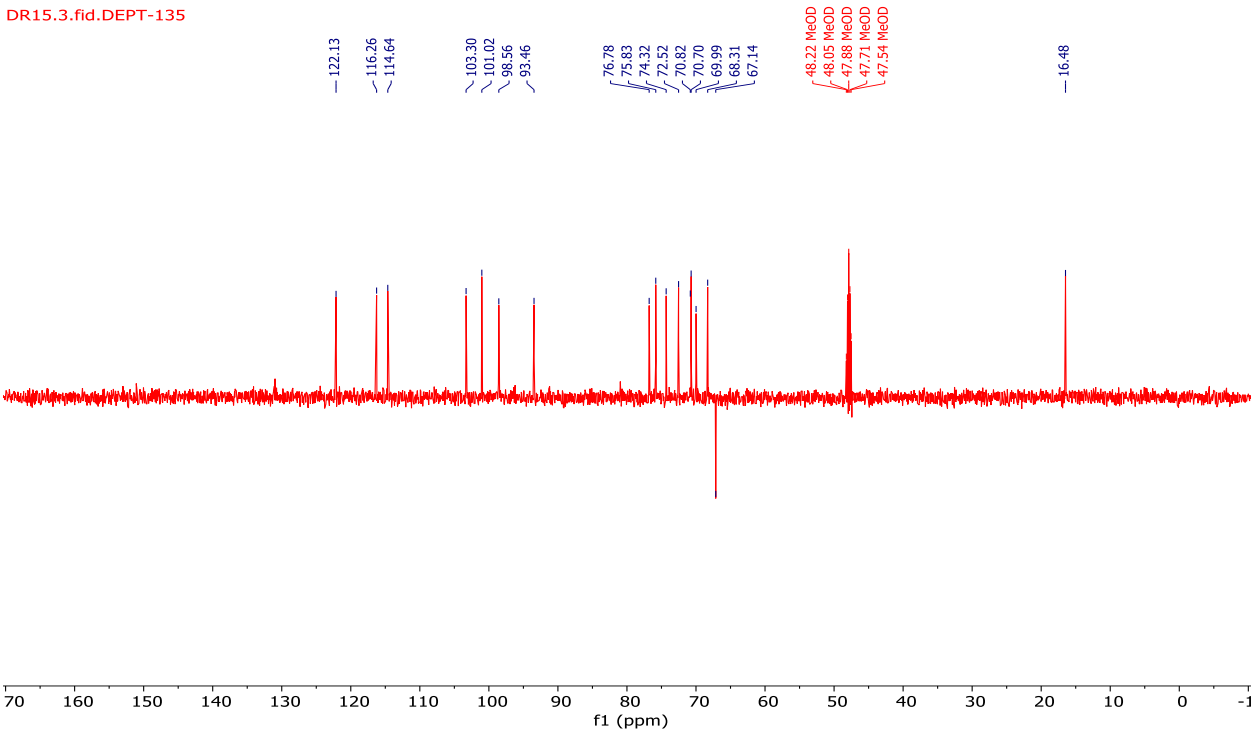

C: DEPT-135 spectrum of compound **37**.

Appendix 18: ^{1}H, ^{13}C, and DEPT-135 NMR spectra of compound **37**.

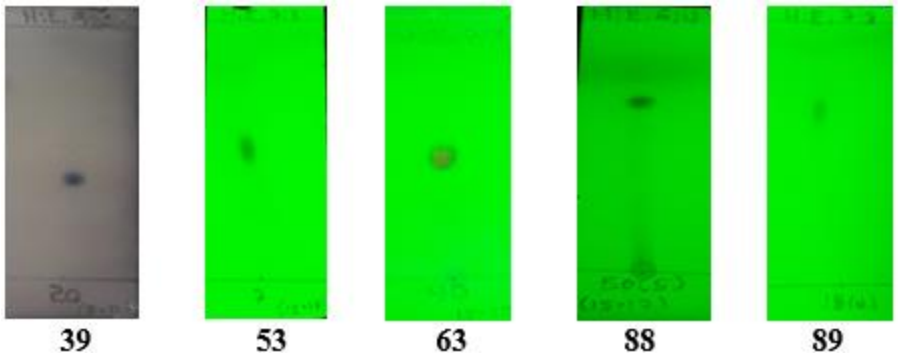

Appendix 19: TLC profile of the isolated compounds from roots of *S. siamea*.

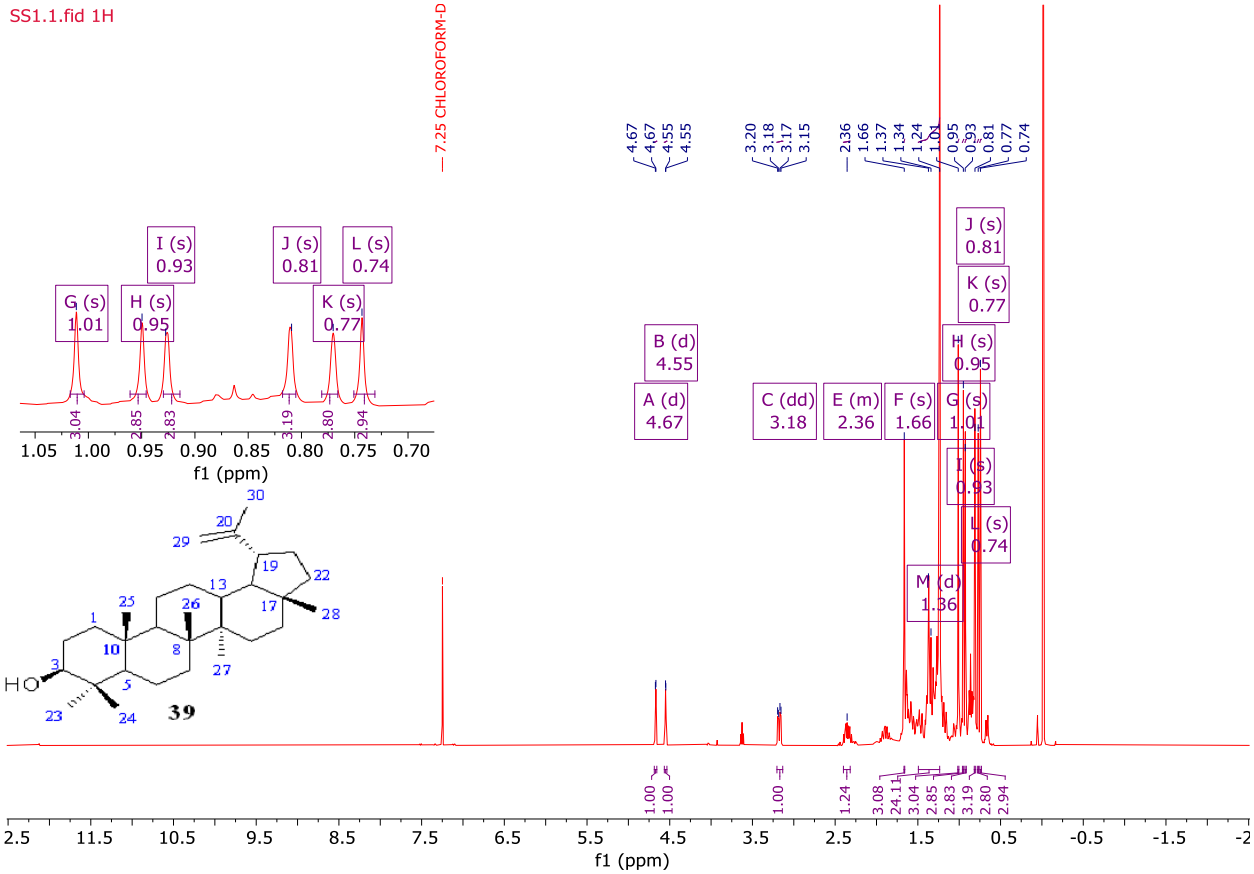

A: ^{1}H NMR (400 MHz, $CDCl_3$) spectrum of compound **39**.

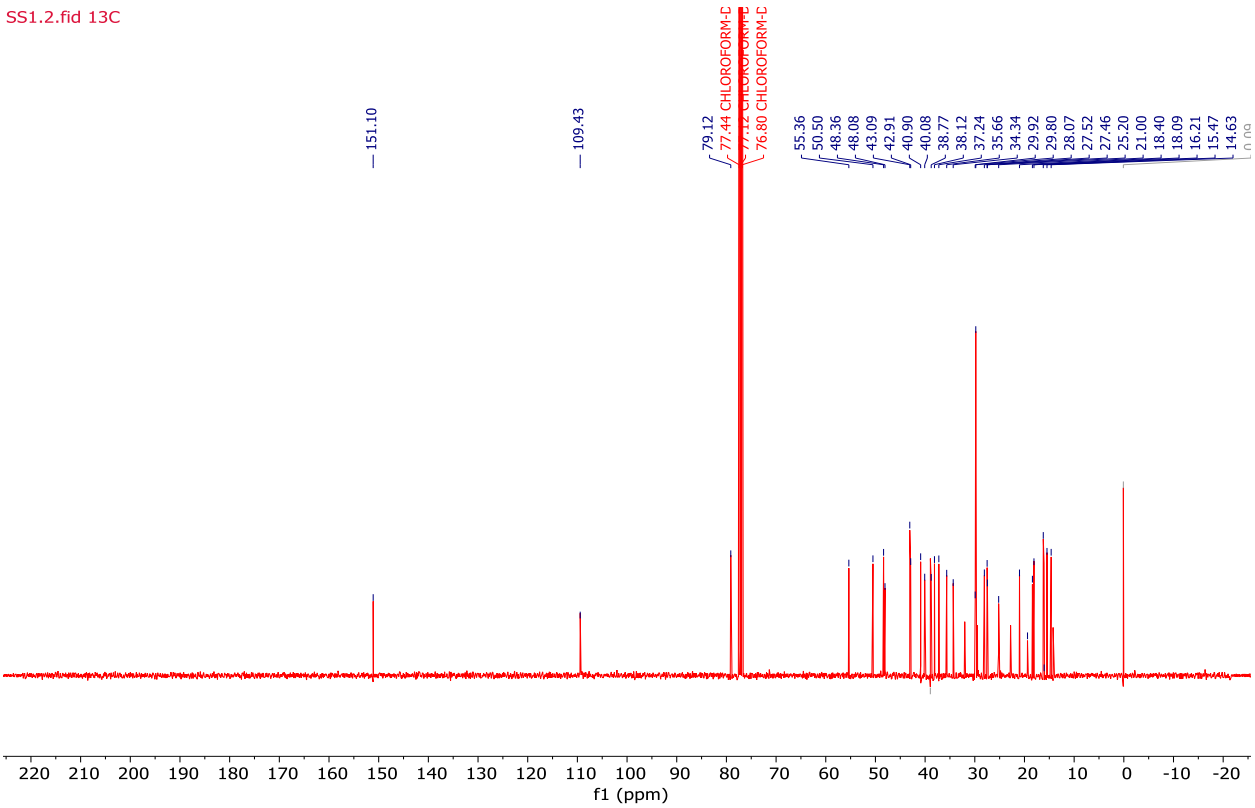

B: ^{13}C NMR (100 MHz, $CDCl_3$) spectrum of compound **39**.

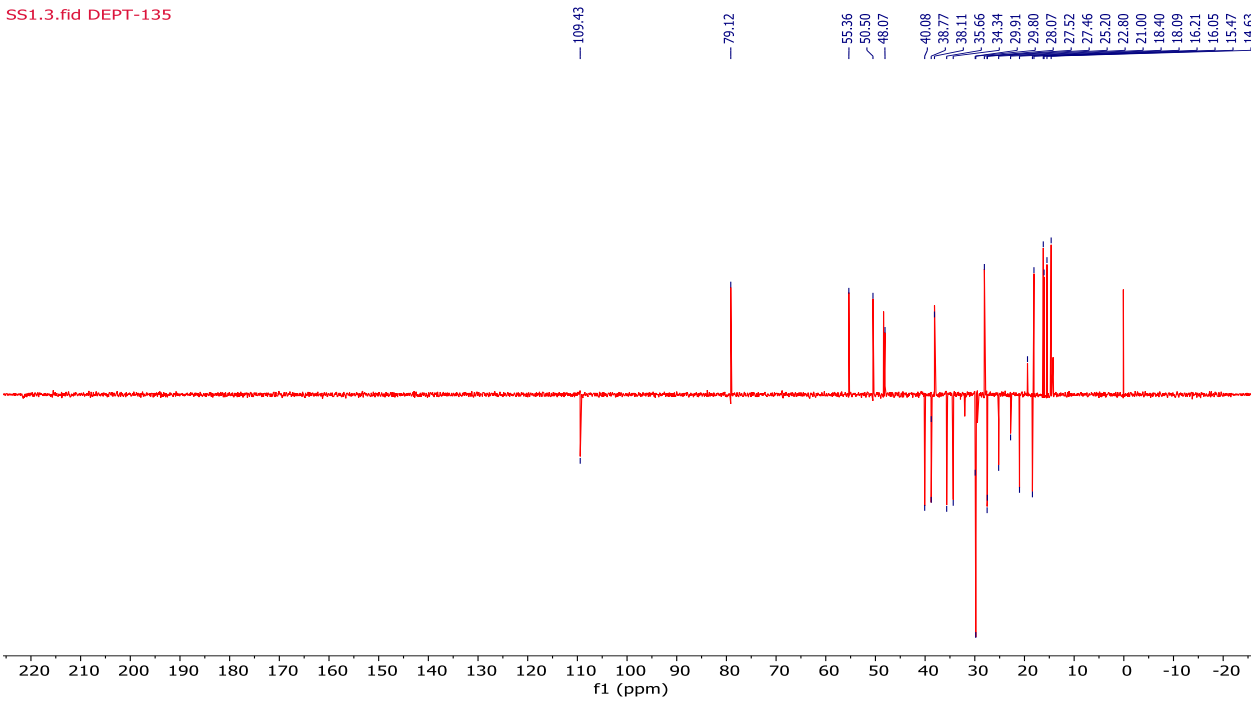

C: DEPT-135 spectrum of compound **39**.

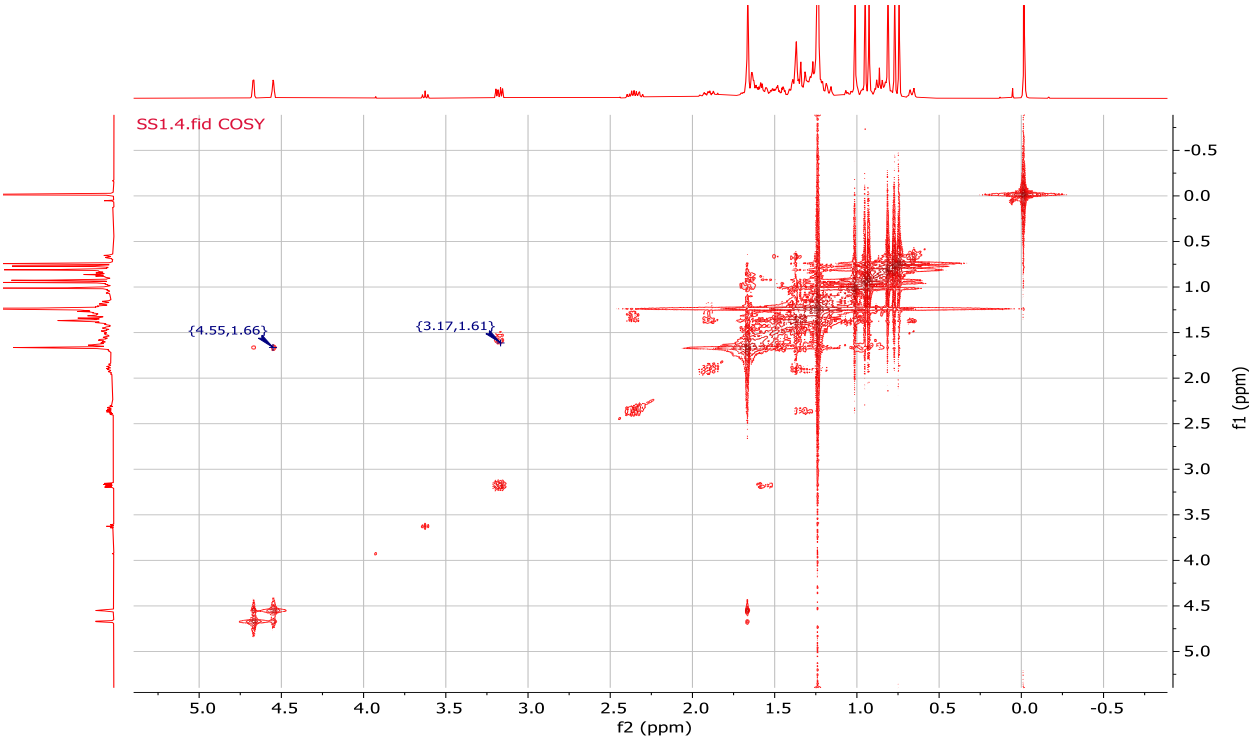

D: COSY spectrum of compound **39**.

Appendix 20: ^{1}H, ^{13}C, DEPT-135, and COSY NMR spectra of compound **39**.

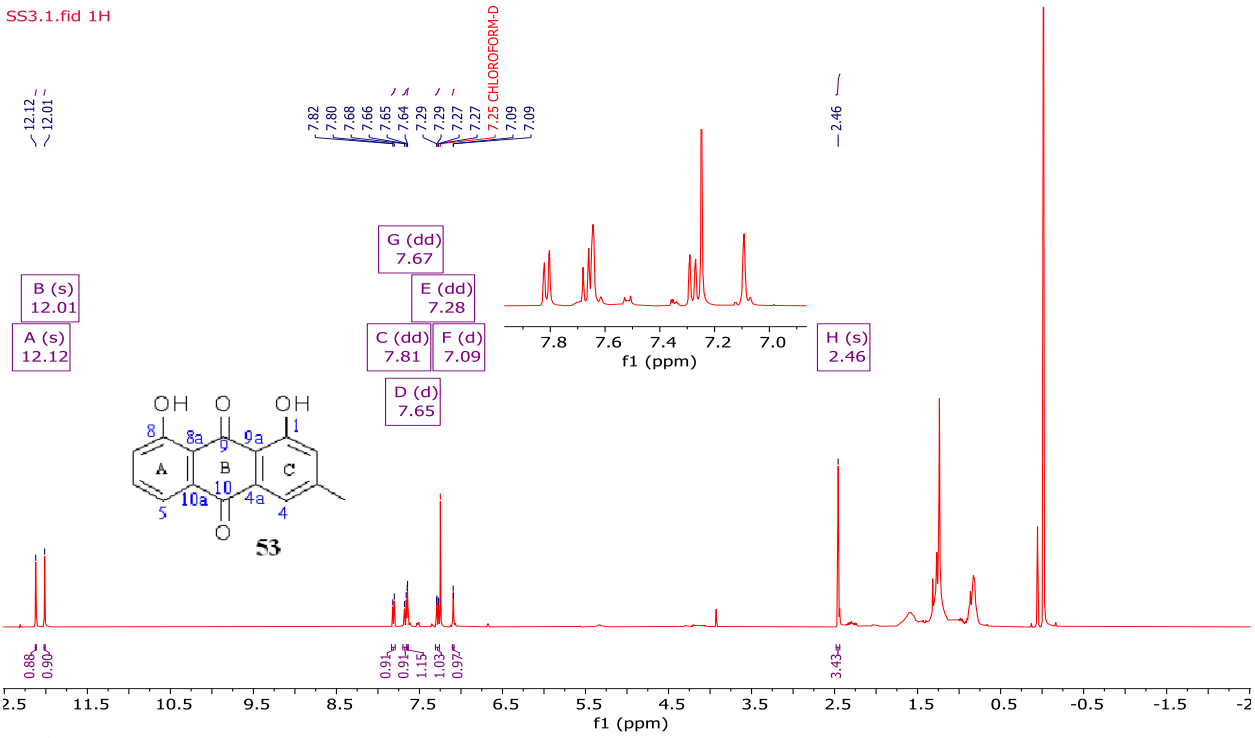

A: ^{1}H NMR (400 MHz, $CDCl_3$) spectrum of compound **53**.

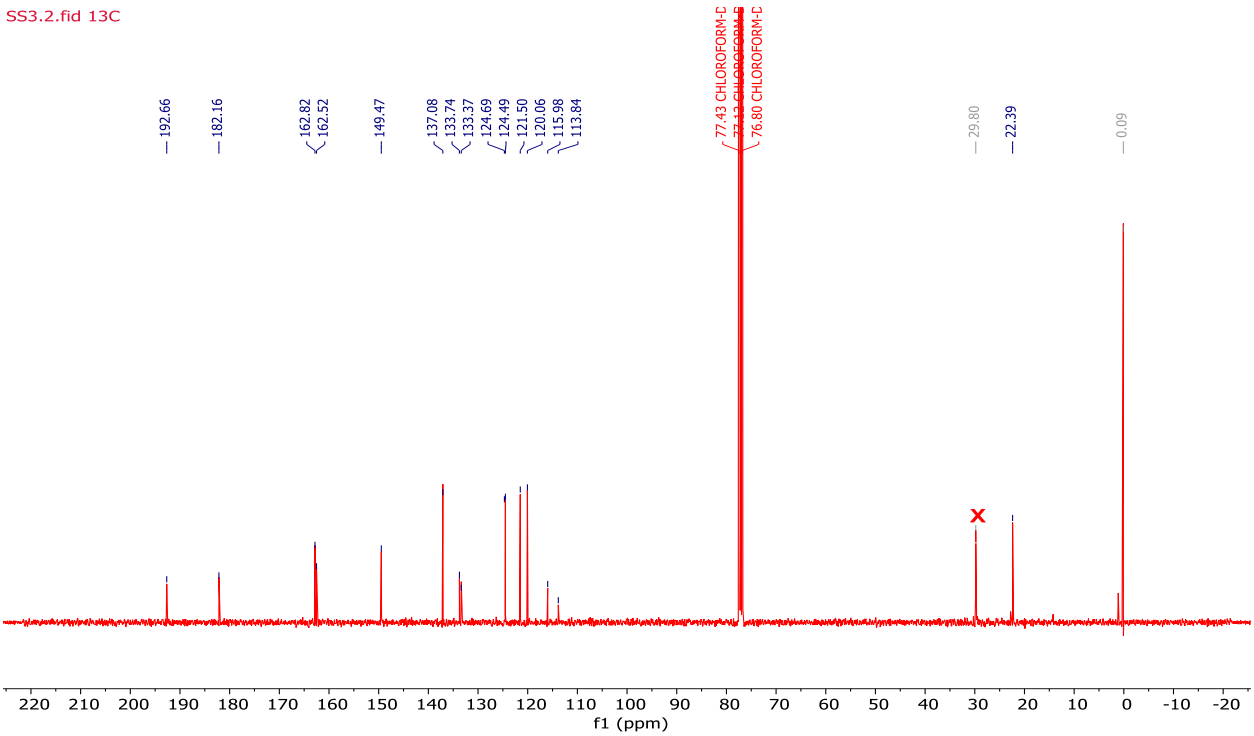

B: ^{13}C NMR (100 MHz, $CDCl_3$) spectrum of compound **53**.

- ✓ The spectra showed signals of hexane impurity at δ_H 1.31, 1.29, and 0.83 and δ_C 29.8, 22.8, and 14.2.

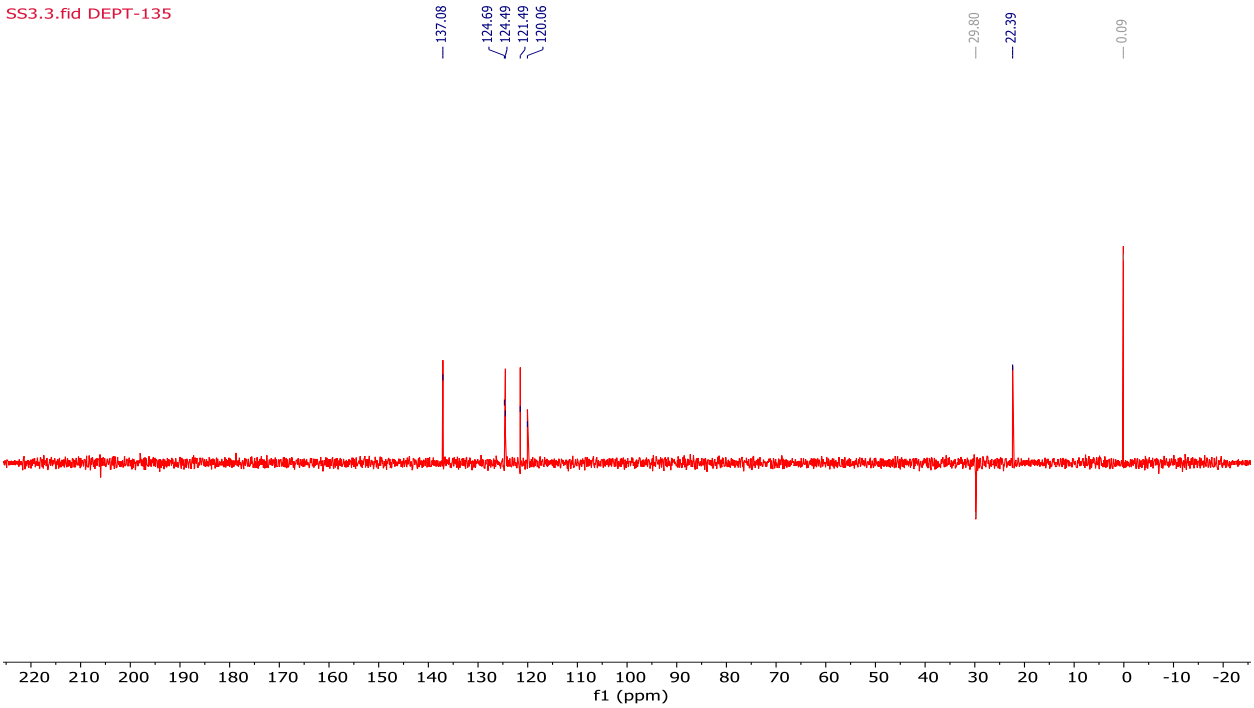

C: DEPT-135 spectrum of compound **53**.

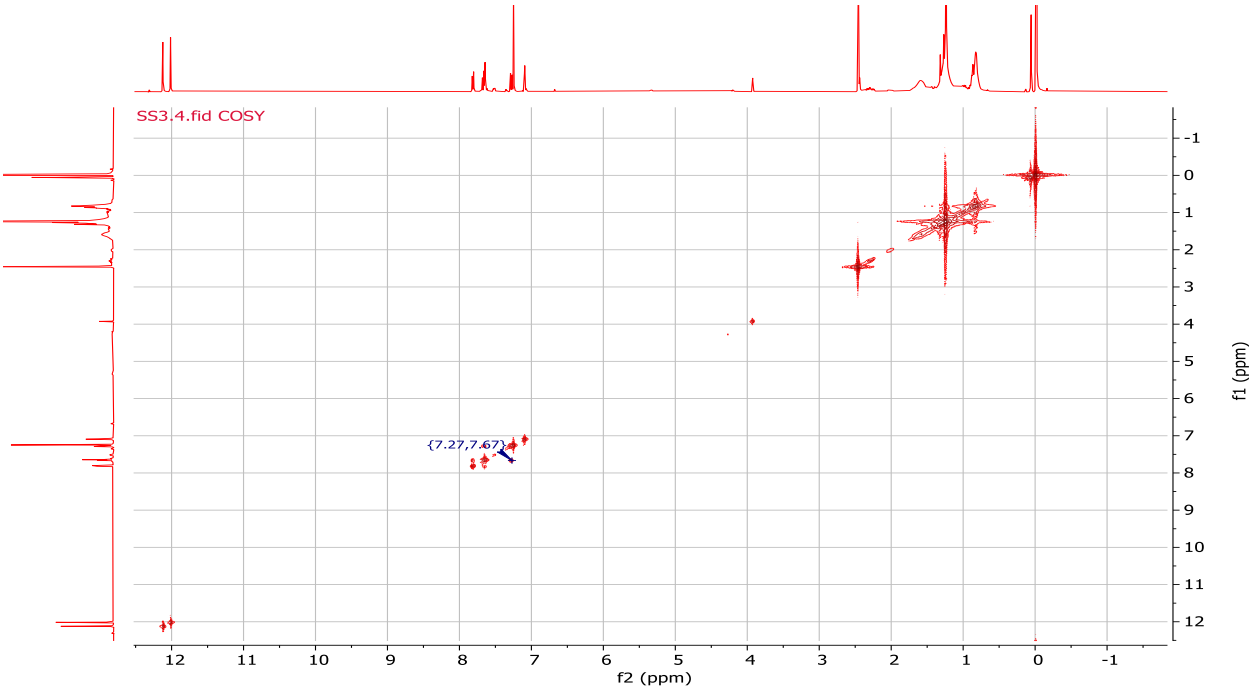

D: COSY spectrum of compound **53**.

Appendix 21: ^{1}H, ^{13}C, DEPT-135, and COSY NMR spectra of compound **53**.

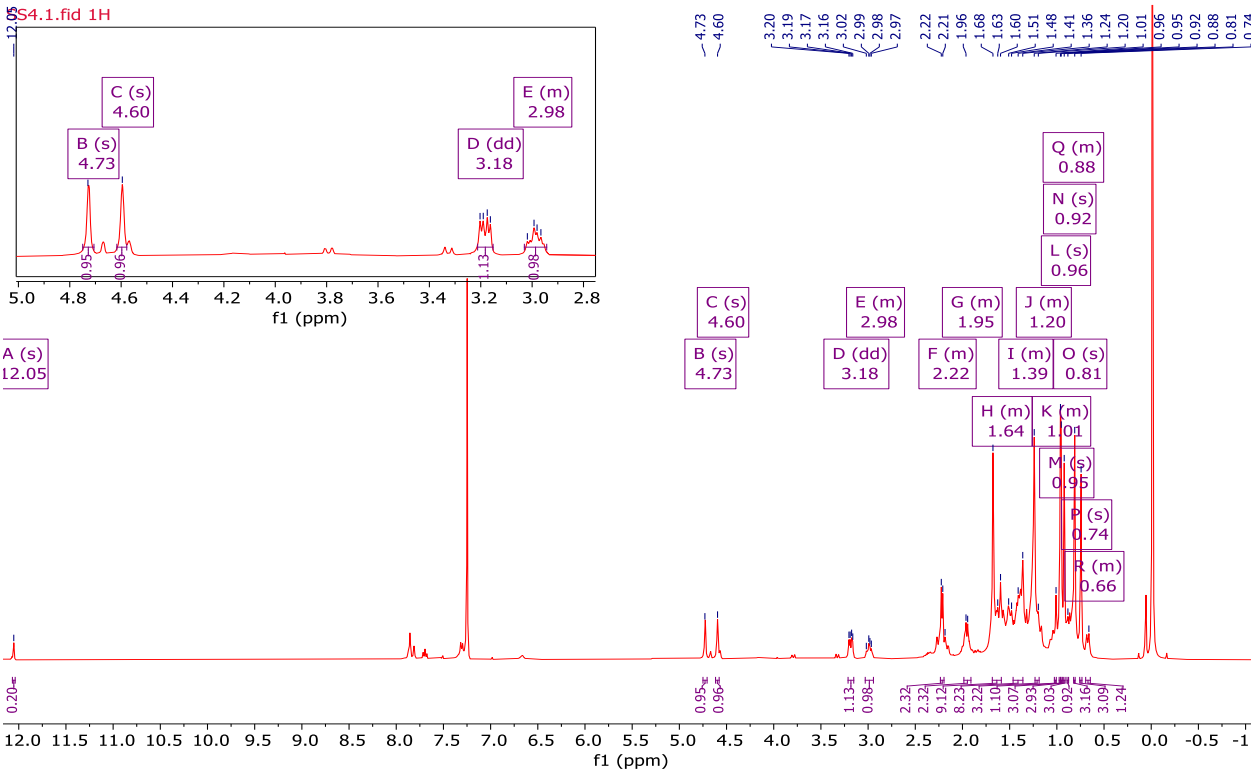

A: ^{1}H NMR (400 MHz, $CDCl_3$) spectrum of compound **63**.

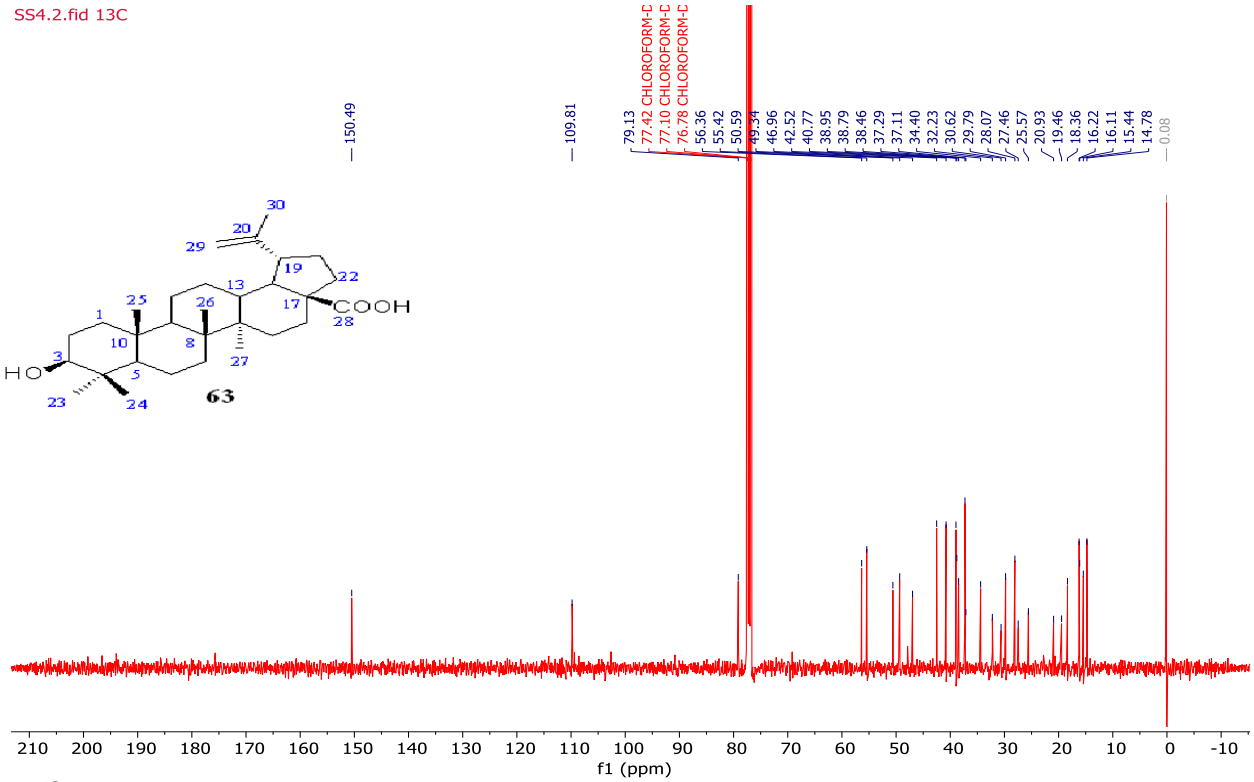

B: ^{13}C NMR (100 MHz, $CDCl_3$) spectrum of compound **63**.

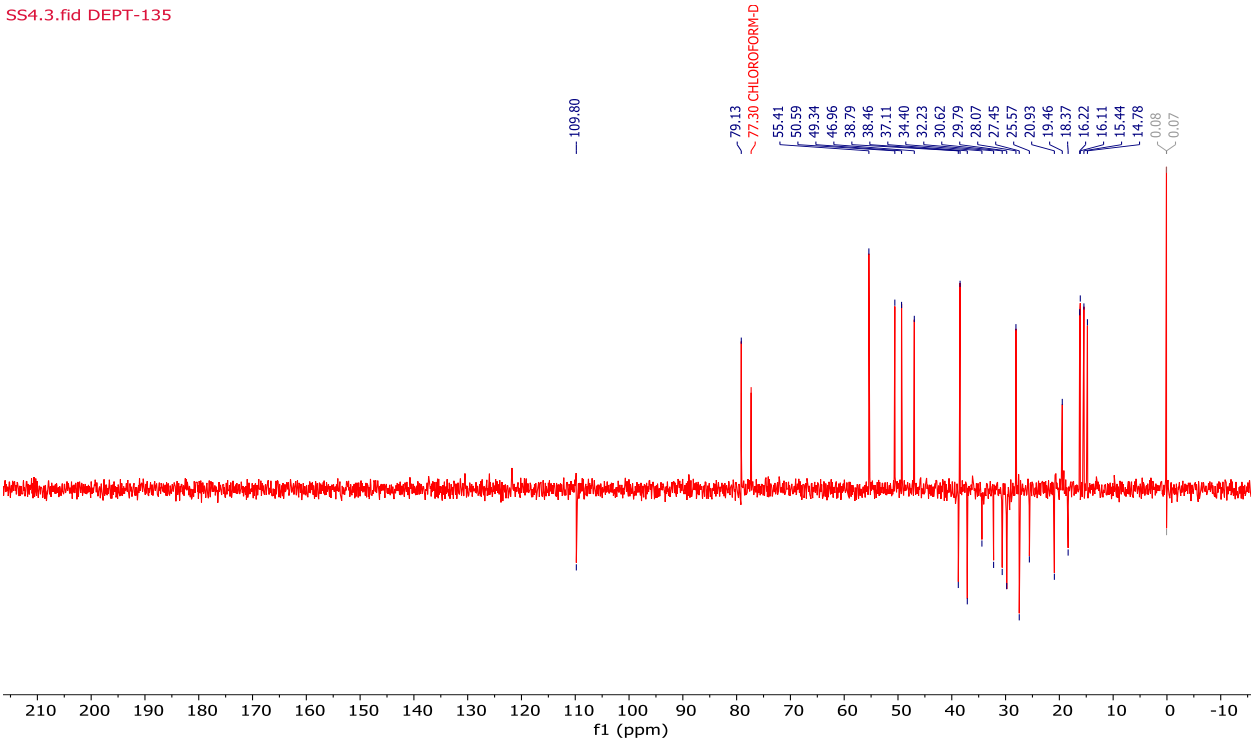

C: DEPT-135 spectrum of compound **63**.

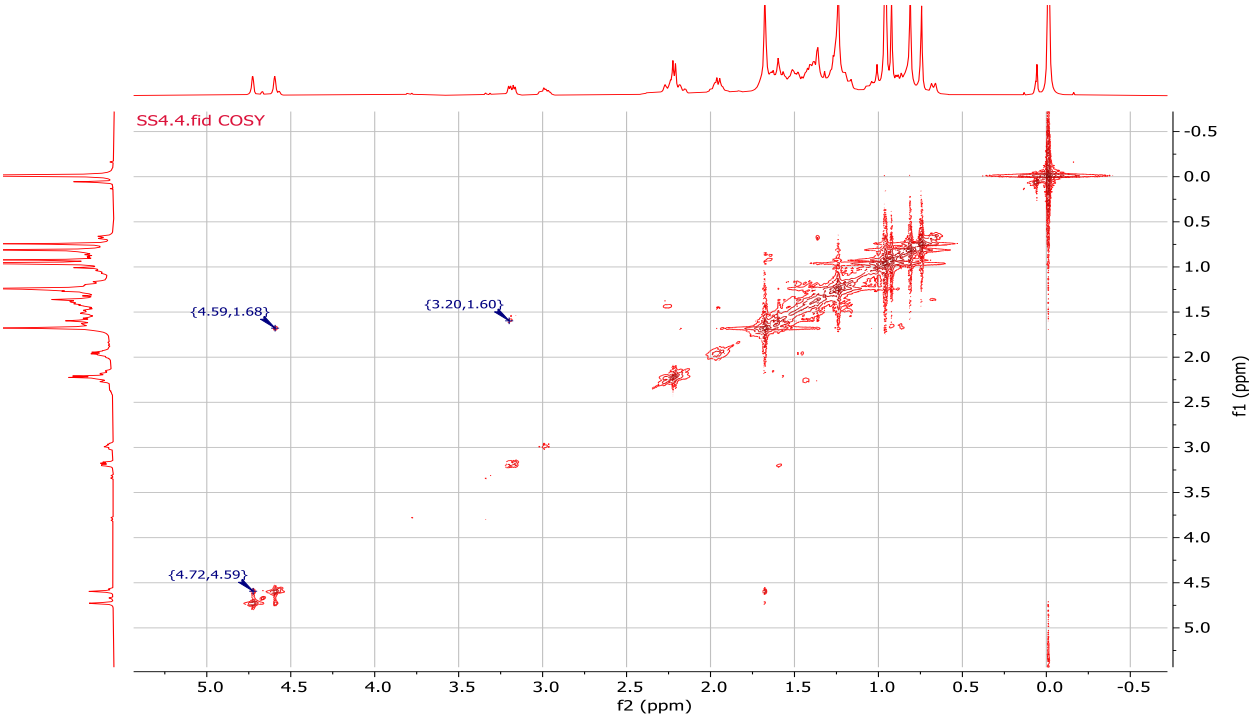

D: COSY spectrum of compound **63**.

Appendix 22: ^{1}H, ^{13}C, DEPT-135, and COSY NMR spectra of compound **63**.

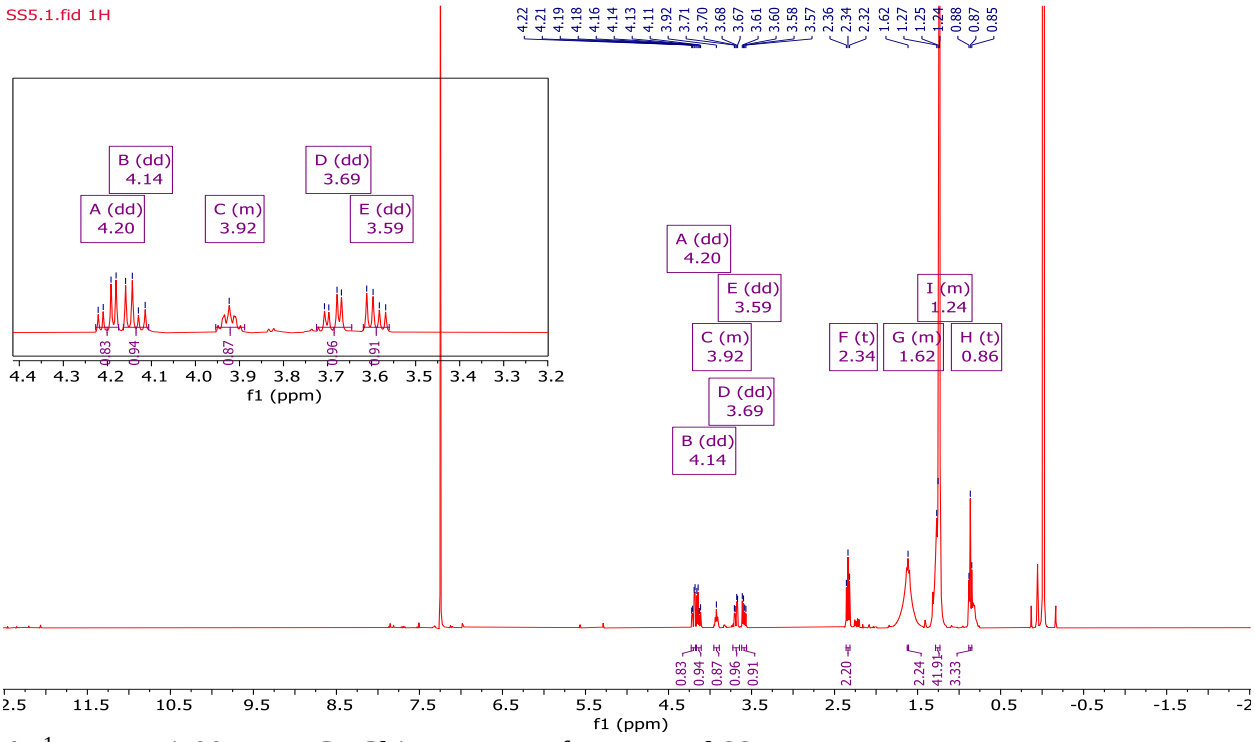

A: ^{1}H NMR (400 MHz, $CDCl_3$) spectrum of compound **88**.

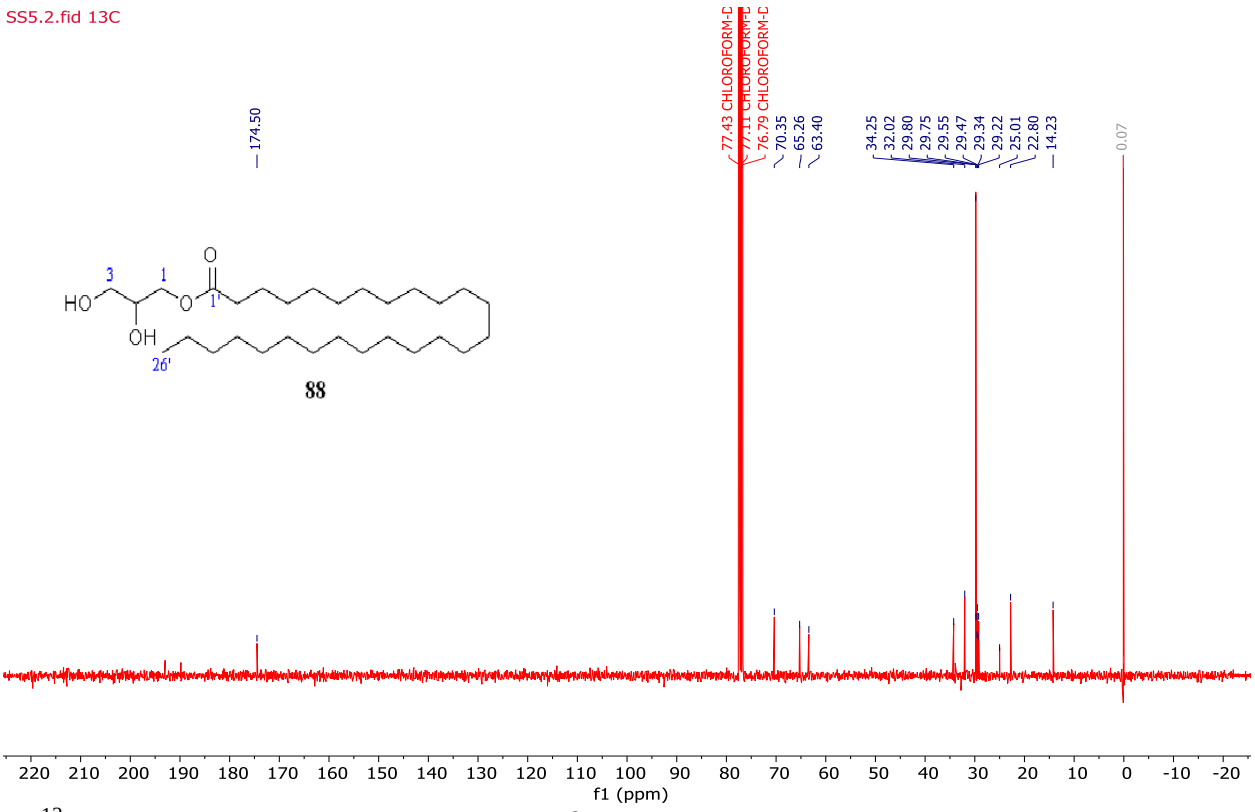

B: ^{13}C NMR (100 MHz, $CDCl_3$) spectrum of compound **88**.

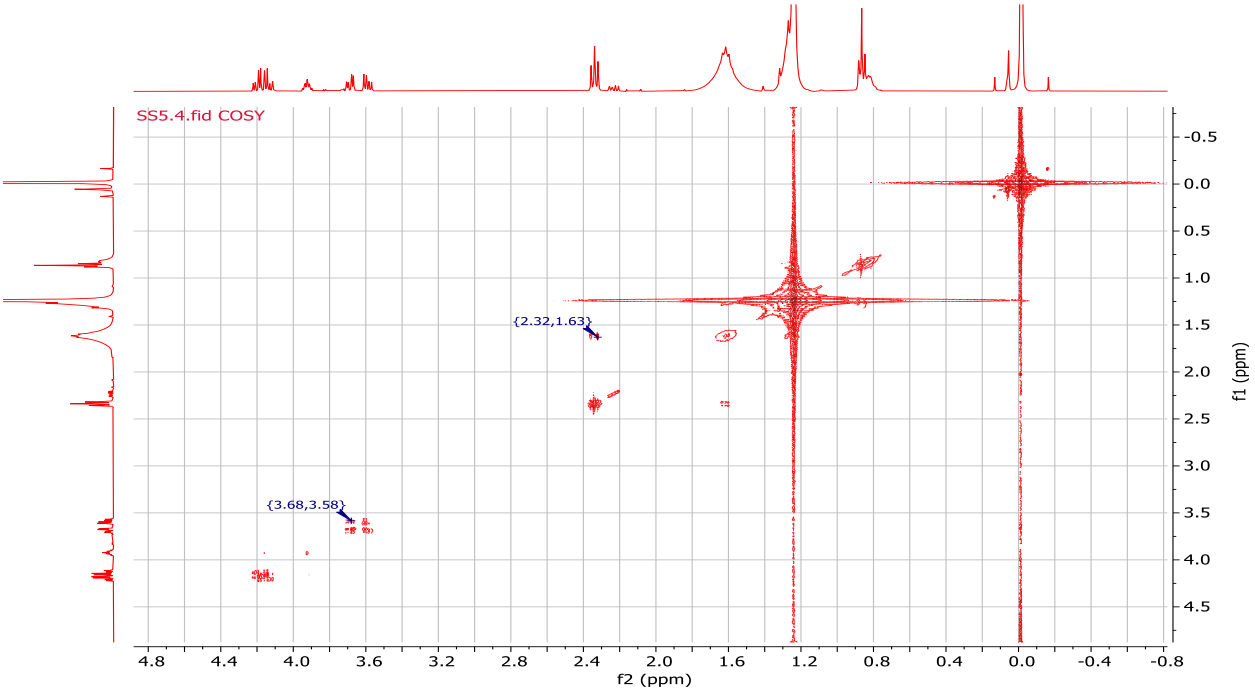

C: COSY spectrum of compound **88**.

Appendix 23: ^{1}H, ^{13}C, and COSY NMR spectra of compound **88**.

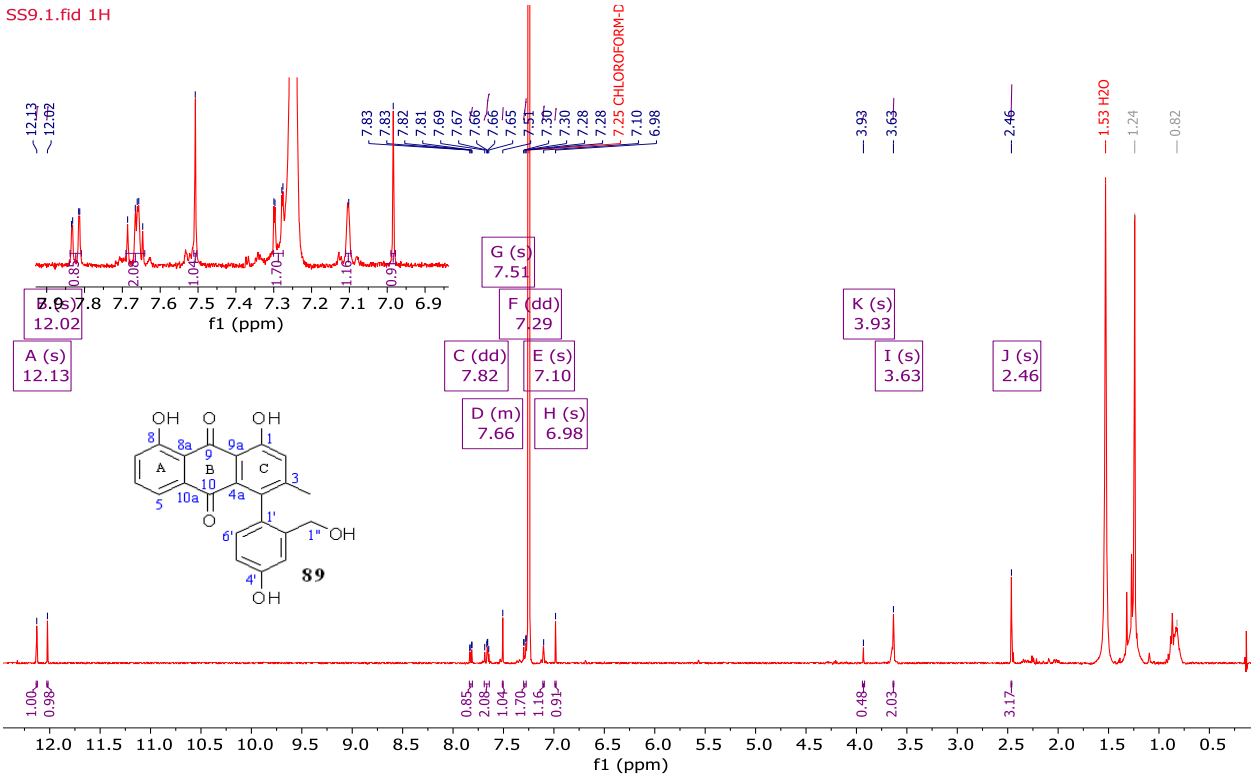

Appendix 24: ^{1}H NMR (400 MHz, $CDCl_3$) spectrum of compound **89**.

- ✓ The spectrum also has some hexane impurity in the range δ_H 1.31-1.23 and 0.80 ppm.

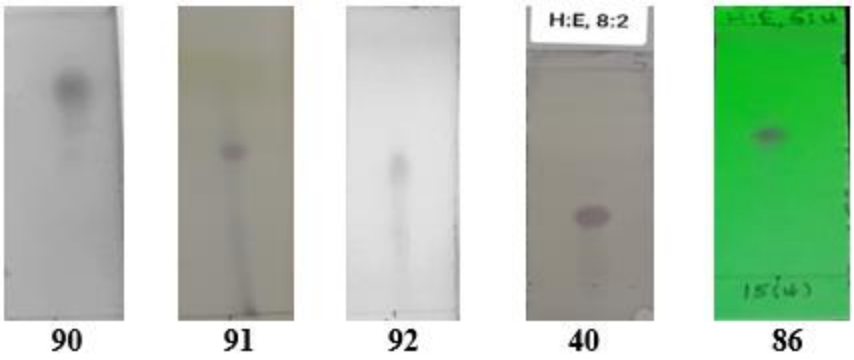

Appendix 25: TLC profile of the isolated compounds from roots of *Z. spina-christi*.

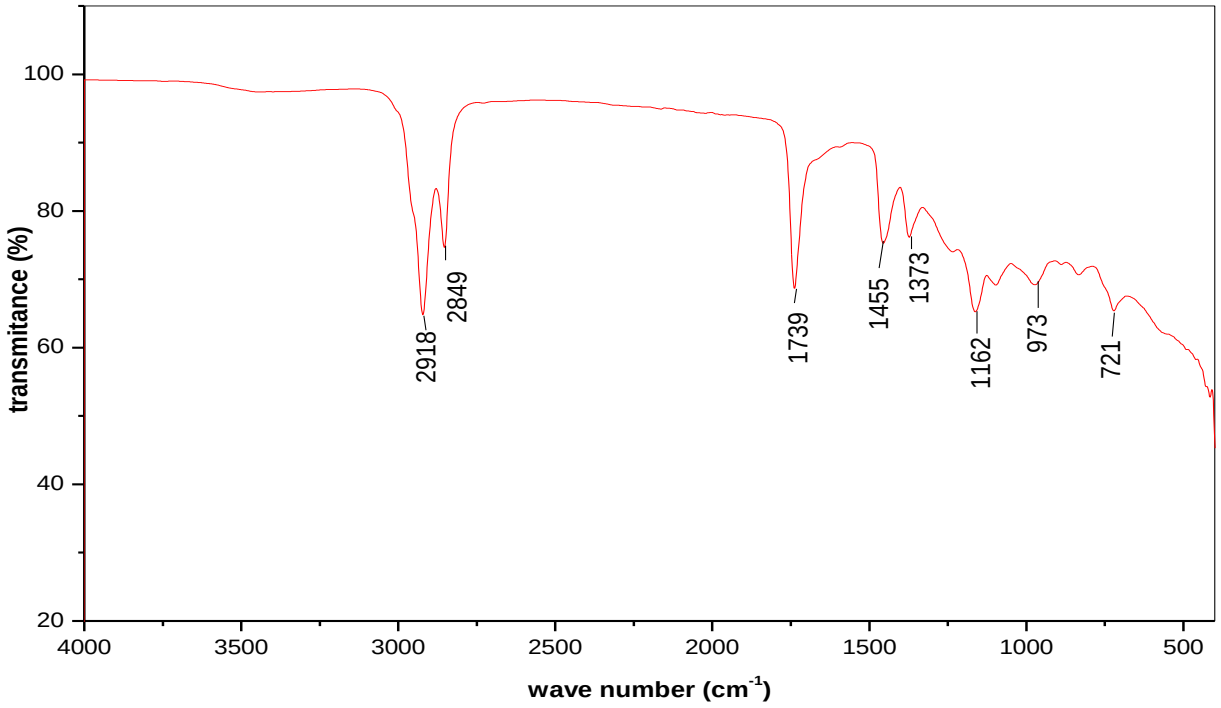

A: FTIR spectrum of compound **90**.

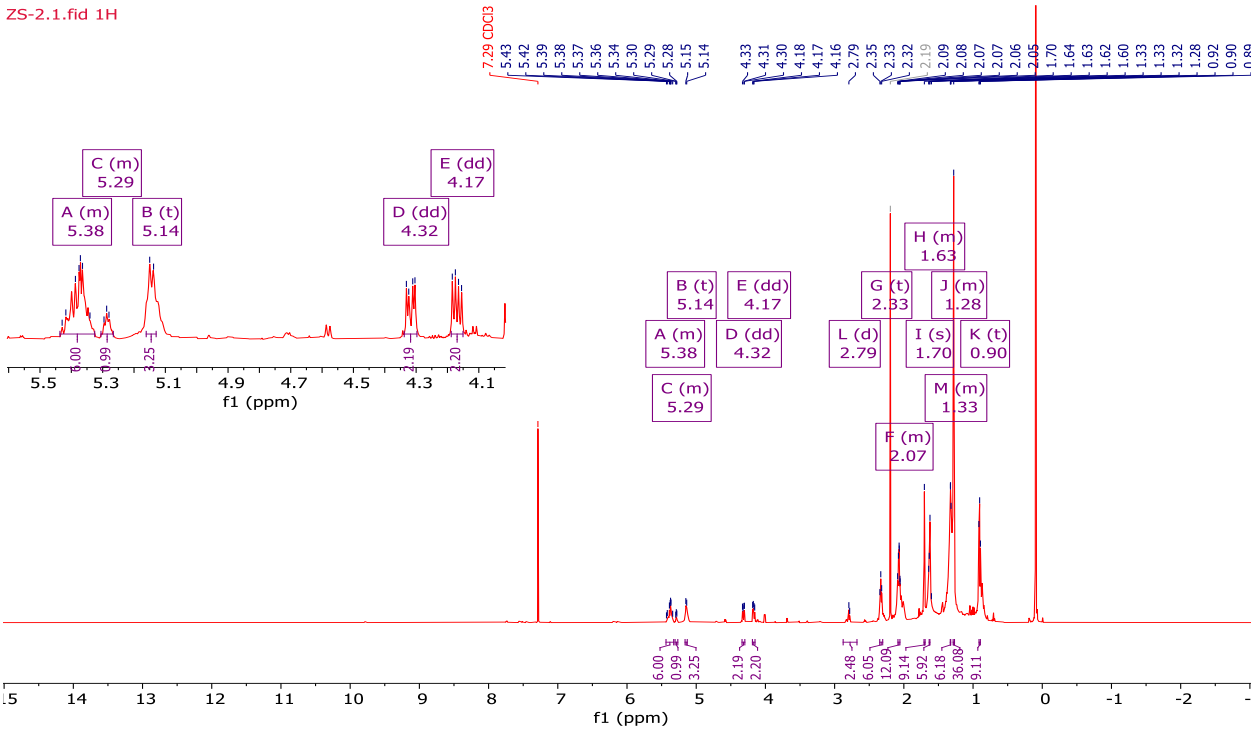

B: ^{1}H NMR (600 MHz, $CDCl_3$) spectrum of compound **90**.

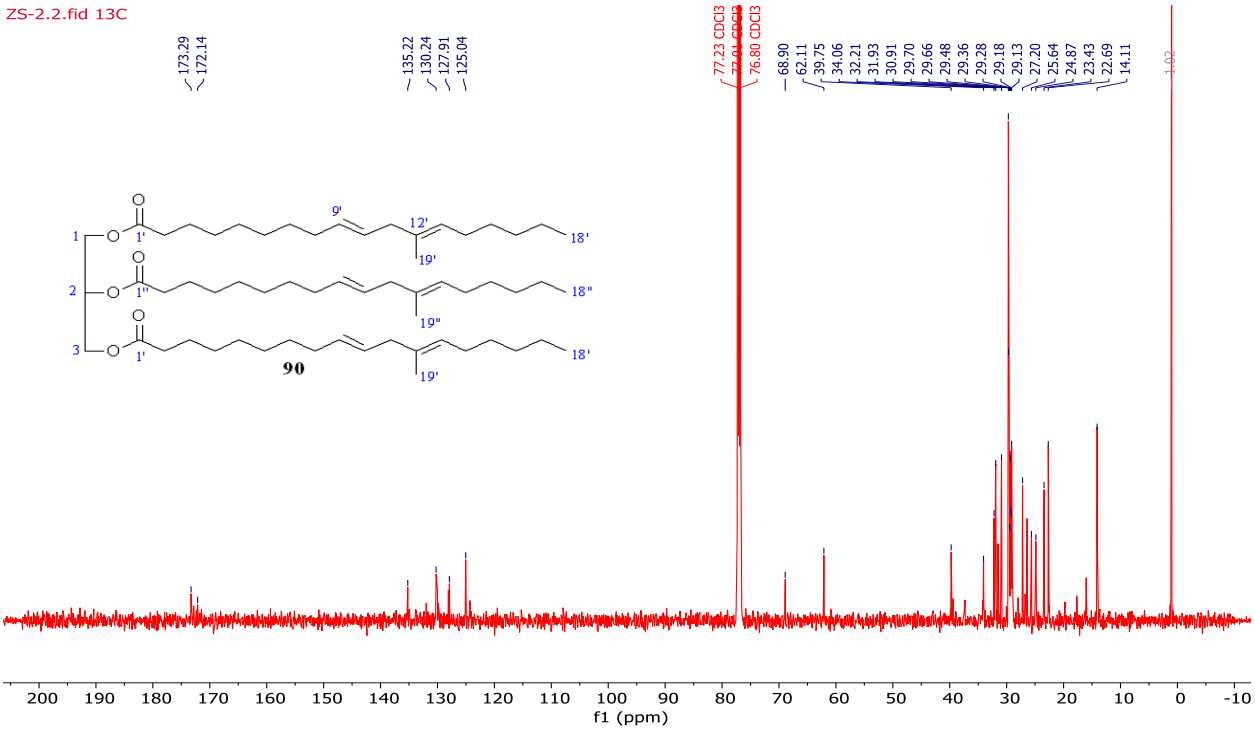

C: ^{13}C NMR (150 MHz, $CDCl_3$) spectrum of compound **90**.

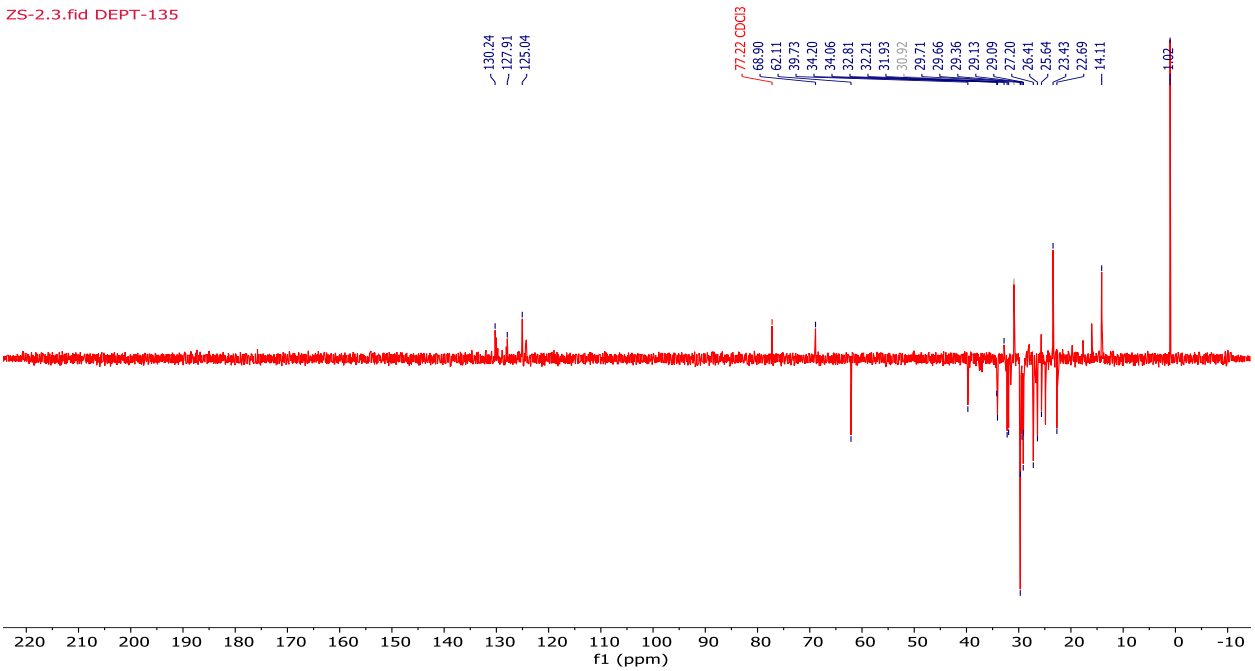

D: DEPT-135 spectrum of compound **90**.

- ✓ The spectrum also displayed signals of acetone impurity at δ_H 2.19 (6H, *s*) and δ_C 206.9, and 30.9 and were out of the spectral analyses.

Appendix 26: FTIR and ^{1}H, ^{13}C, and DEPT-135 NMR spectra of compound **90**.

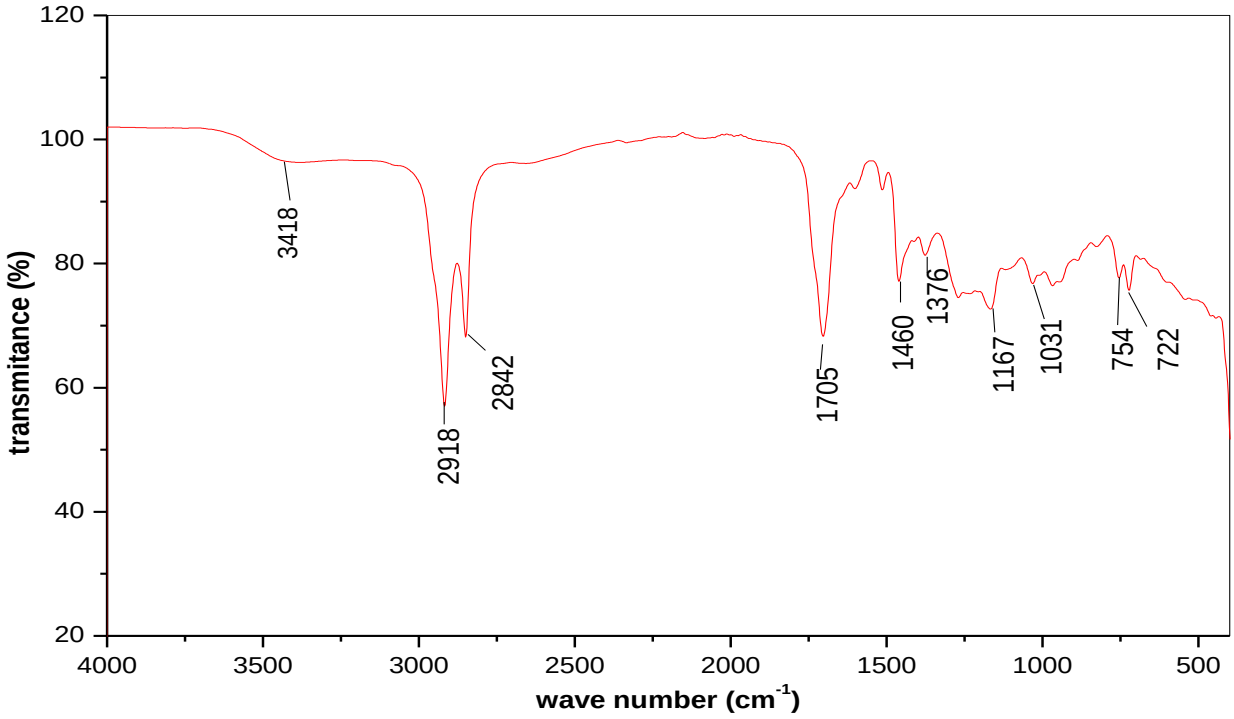

A: FTIR spectrum of compound **91**.

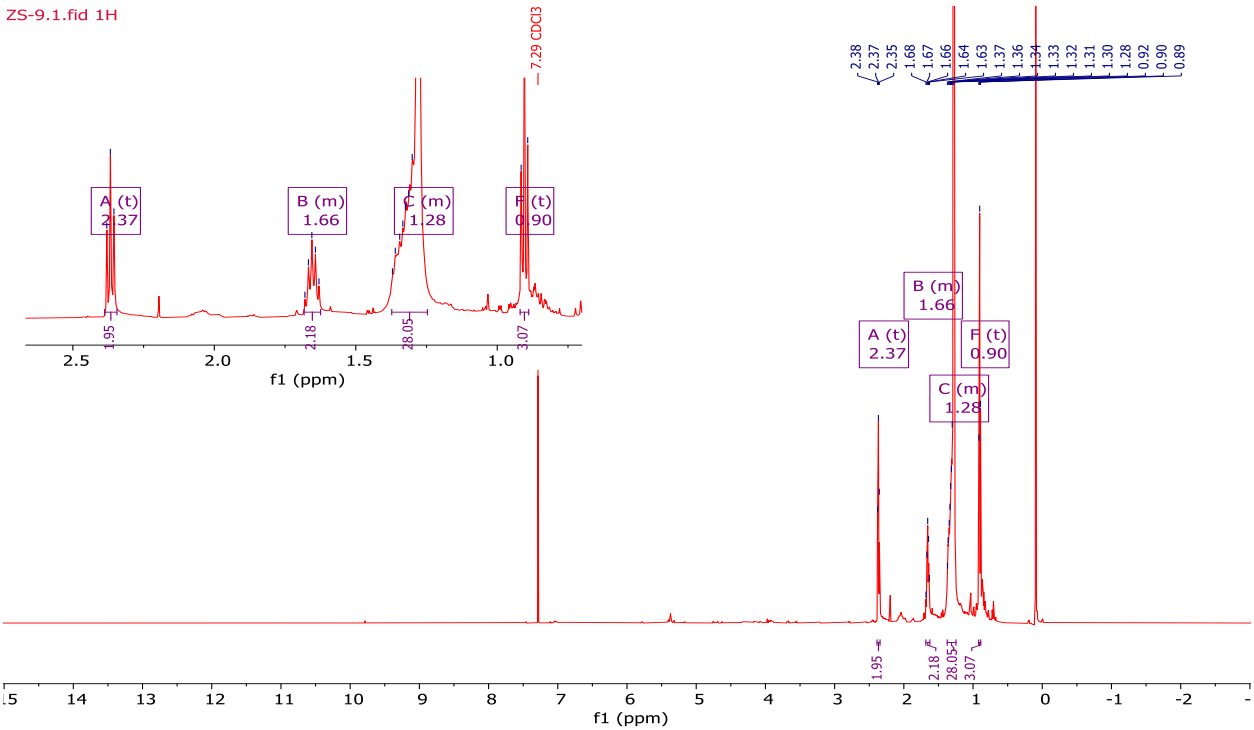

B: ^{1}H NMR (600 MHz, $CDCl_3$) spectrum of compound **91**.

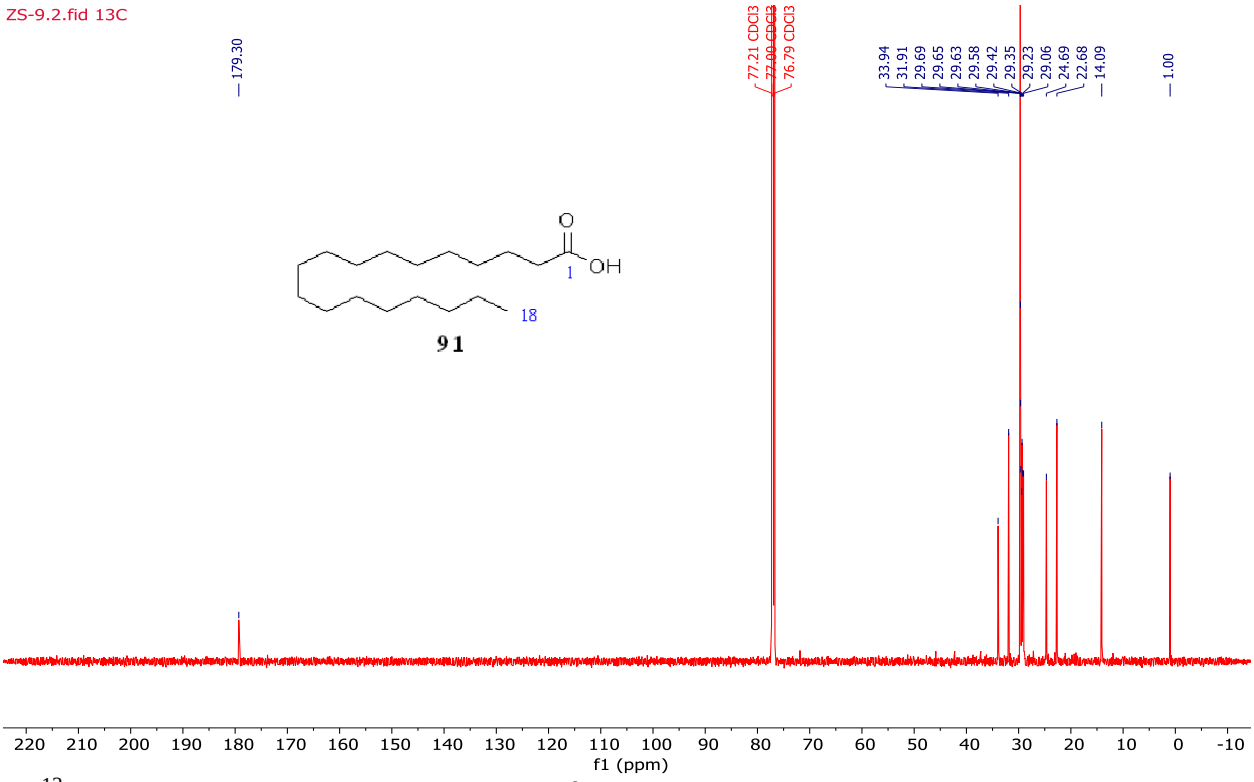

C: ^{13}C NMR (150 MHz, $CDCl_3$) spectrum of compound **91**.

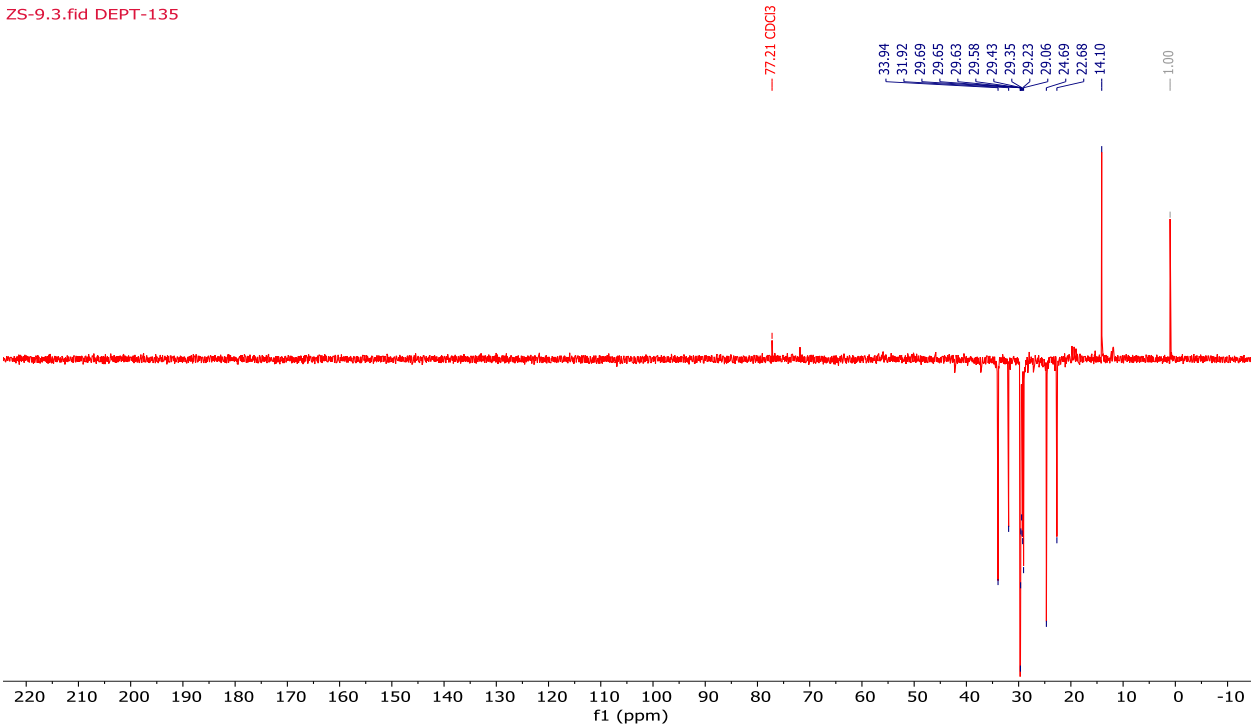

D: DEPT-135 spectrum of compound **91**.

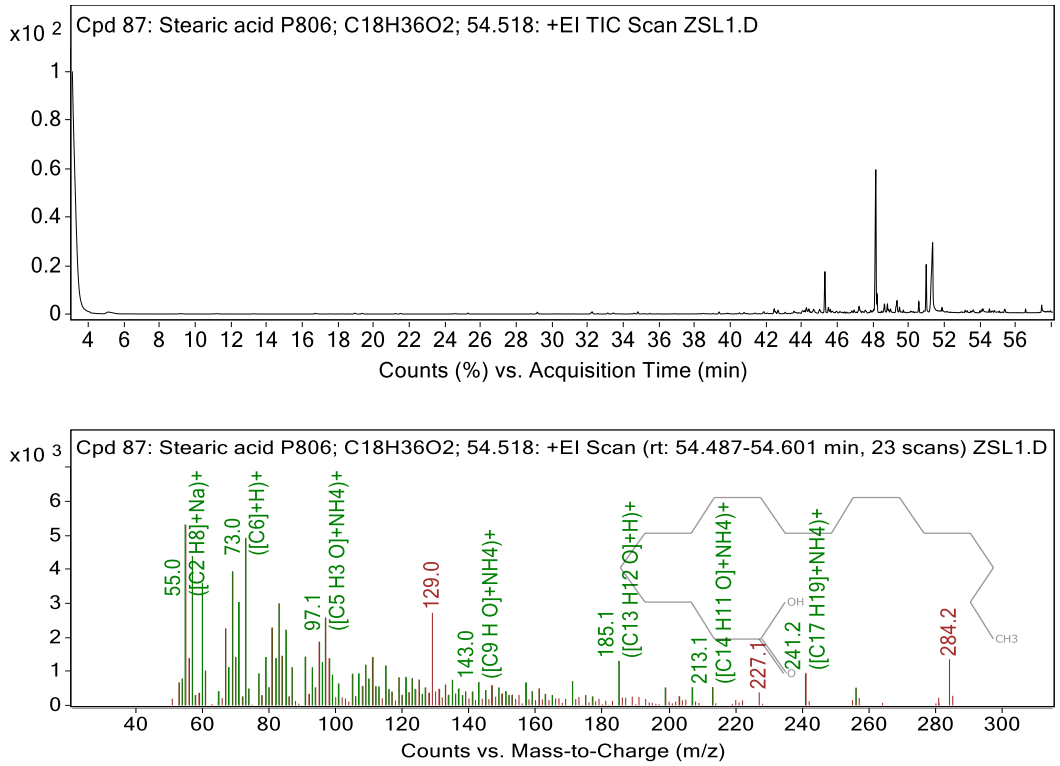

E: GC (top) and mass fragmentation pattern (bottom) of compound **91**.

Appendix 27: FTIR, ^{1}H, ^{13}C, and DEPT-135 NMR, and GC spectra of compound **91**.

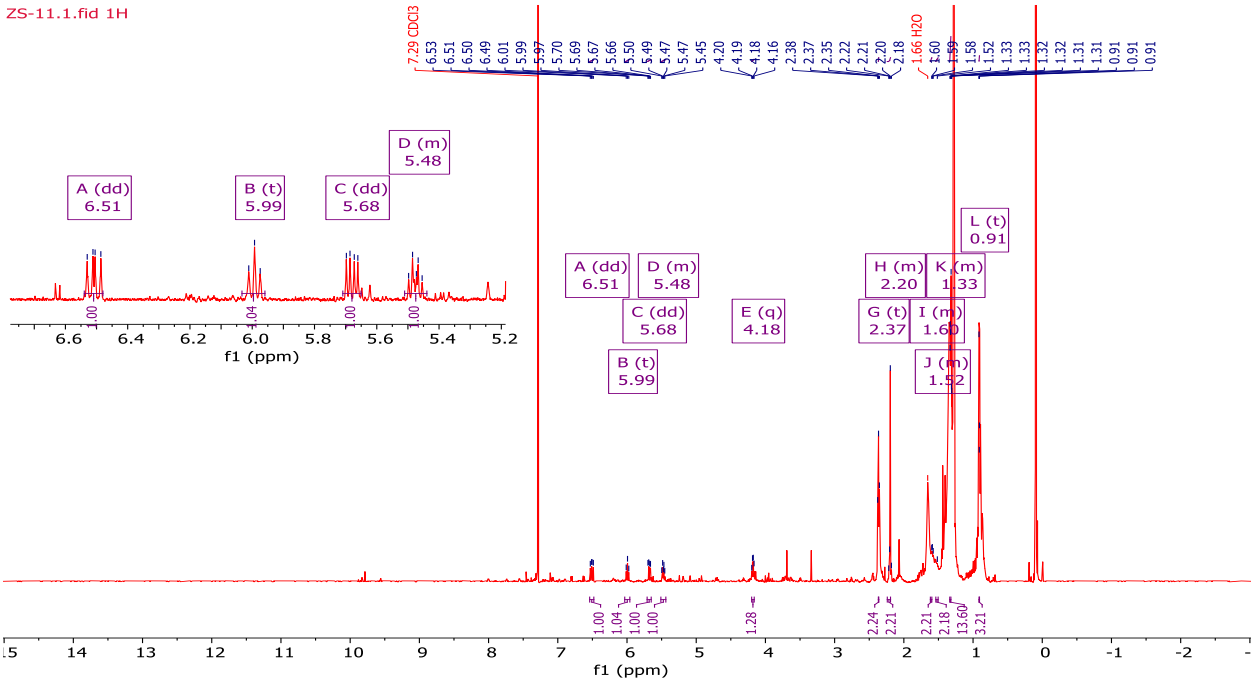

A: ^{1}H NMR (600 MHz, $CDCl_3$) spectrum of compound **92**.

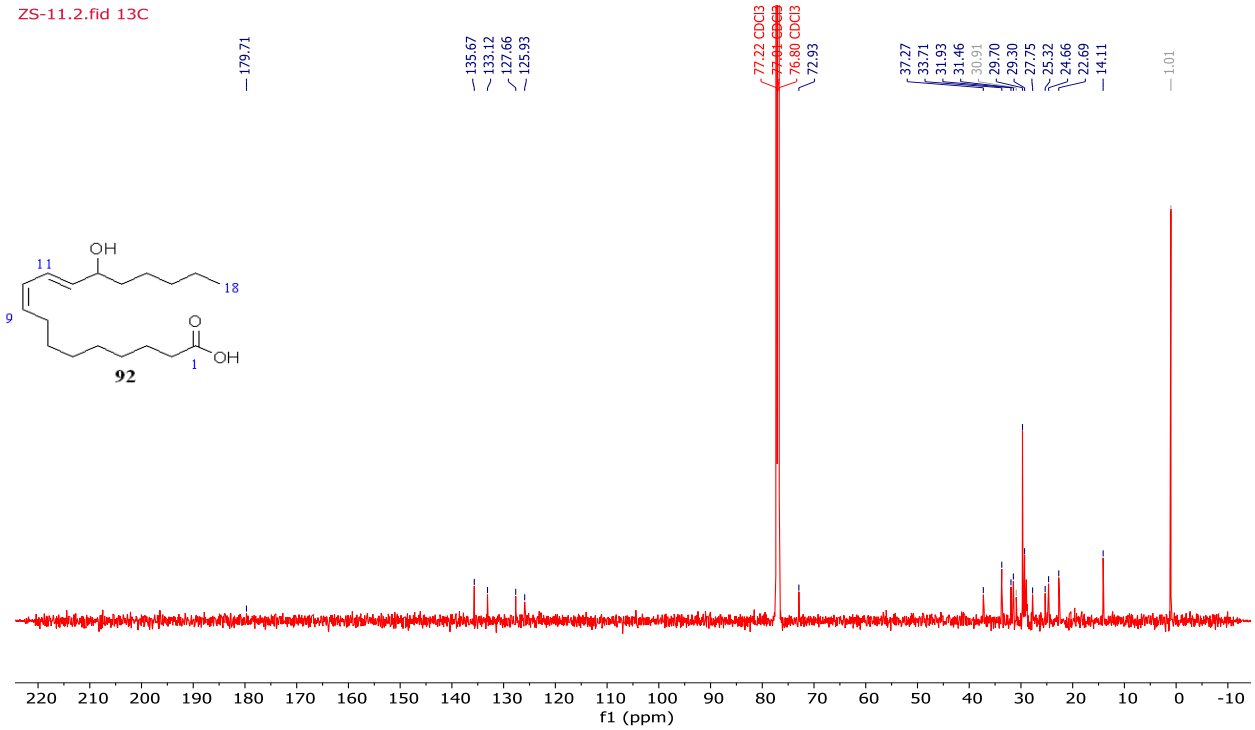

B: ^{13}C NMR (150 MHz, $CDCl_3$) spectrum of compound **92**.

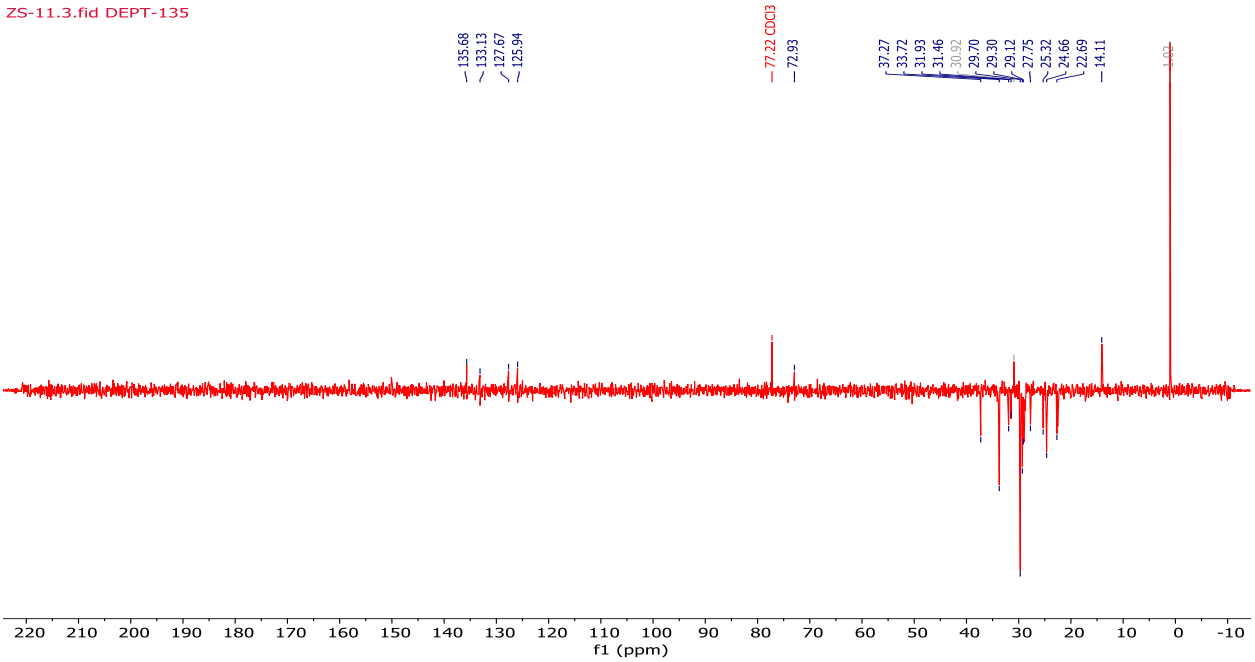

C: DEPT-135 spectrum of compound **92**.

- ✓ Signals at δ_H 2.19 (6H, s), and δ_C 30.9 attributed to some undried acetone impurity in the sample.

Appendix 28: ^{1}H, ^{13}C, and DEPT-135 NMR spectra of compound **92**.

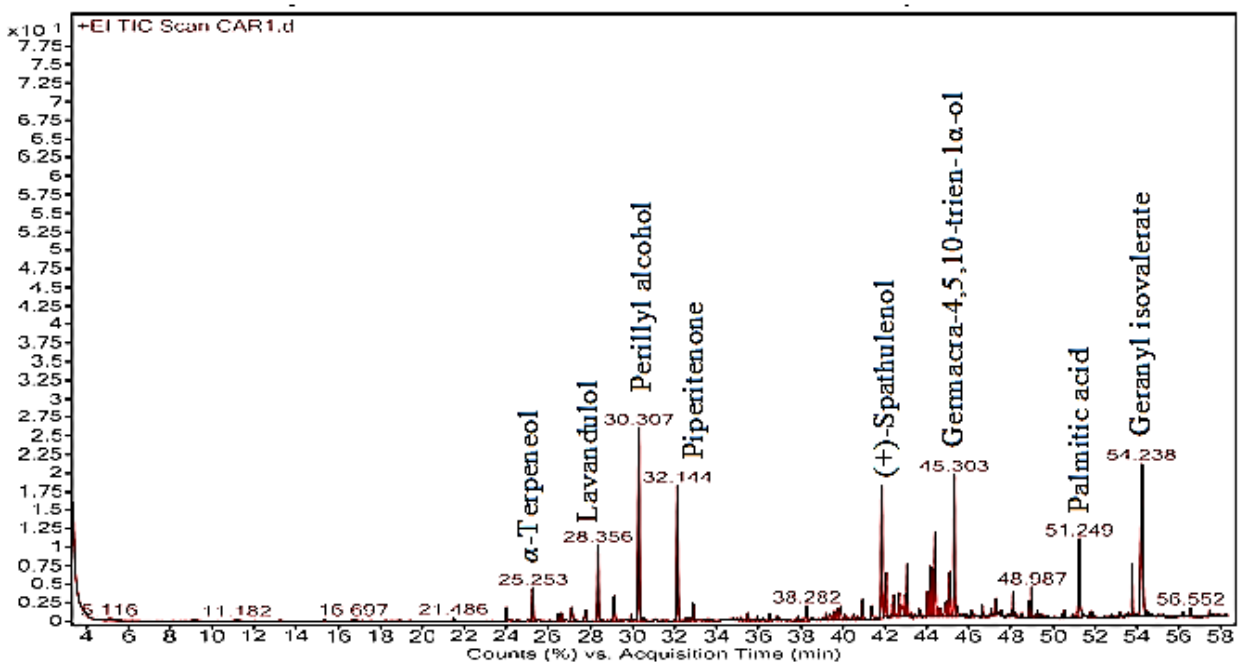

A)

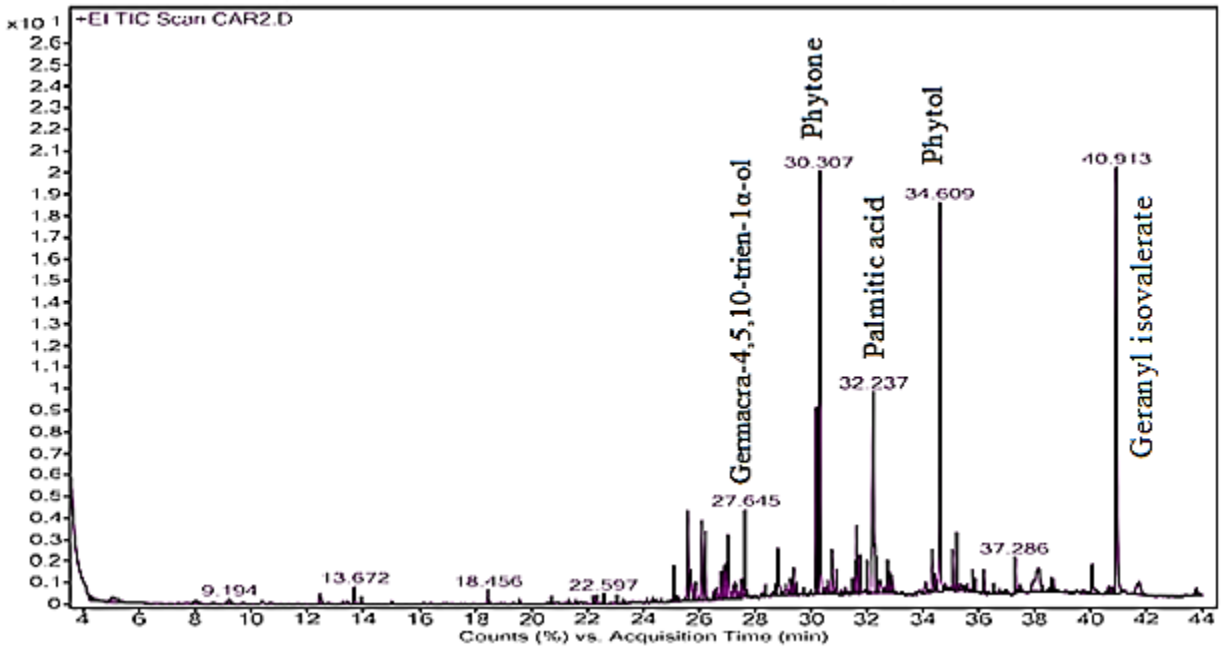

B)

Appendix 29: Gas chromatogram of the leaves (A) and roots (B) EOs of *C. adenocaule*.

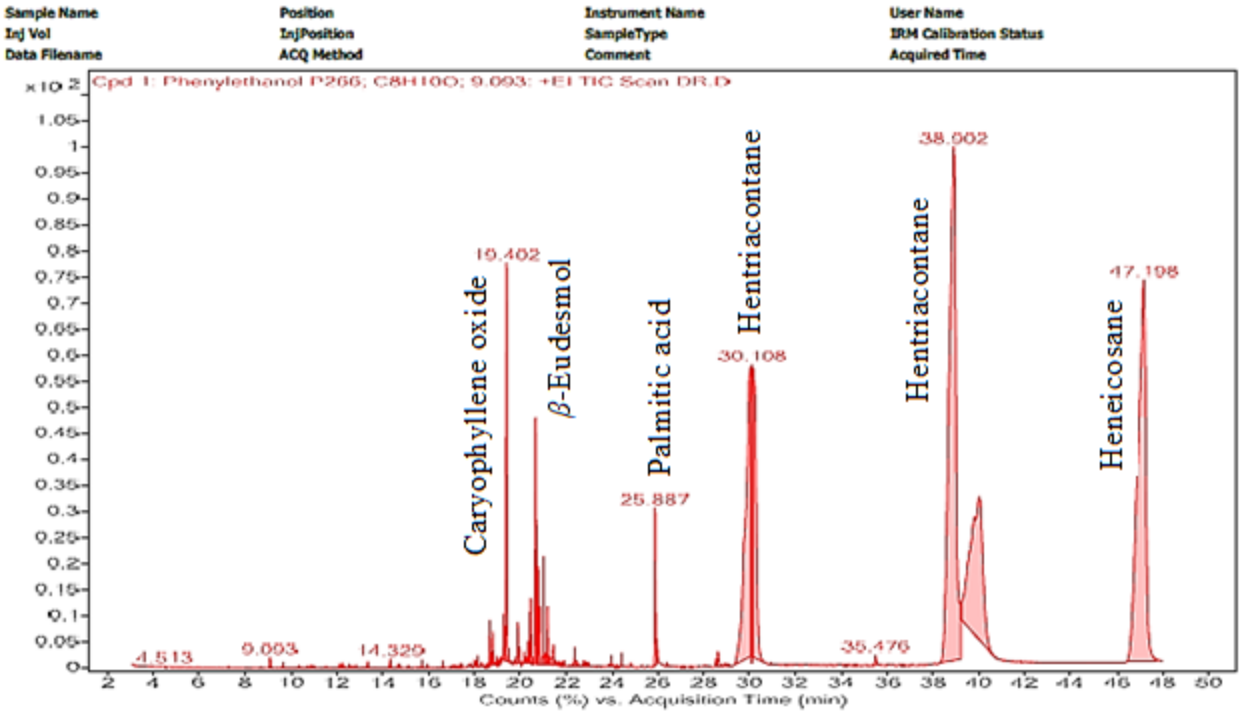

Appendix 30: Gas chromatogram of the roots EOs of *D. regia*.

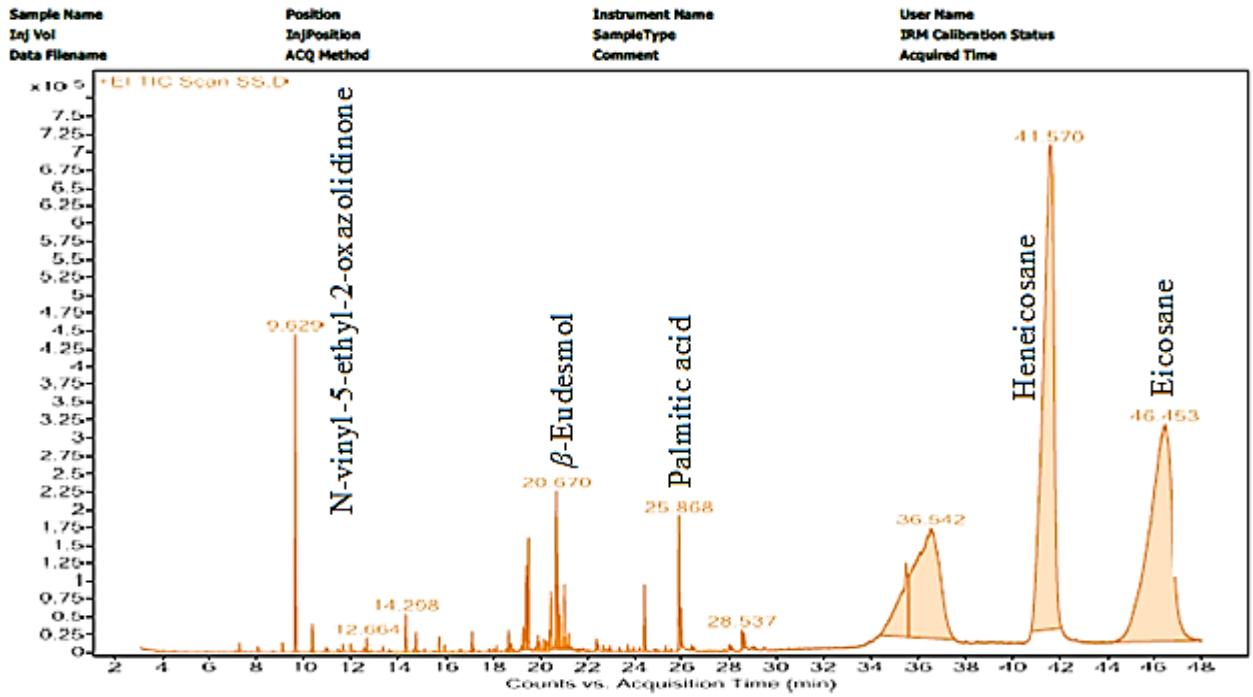

Appendix 31: Gas chromatogram of the roots EOs of *S. siamea*.

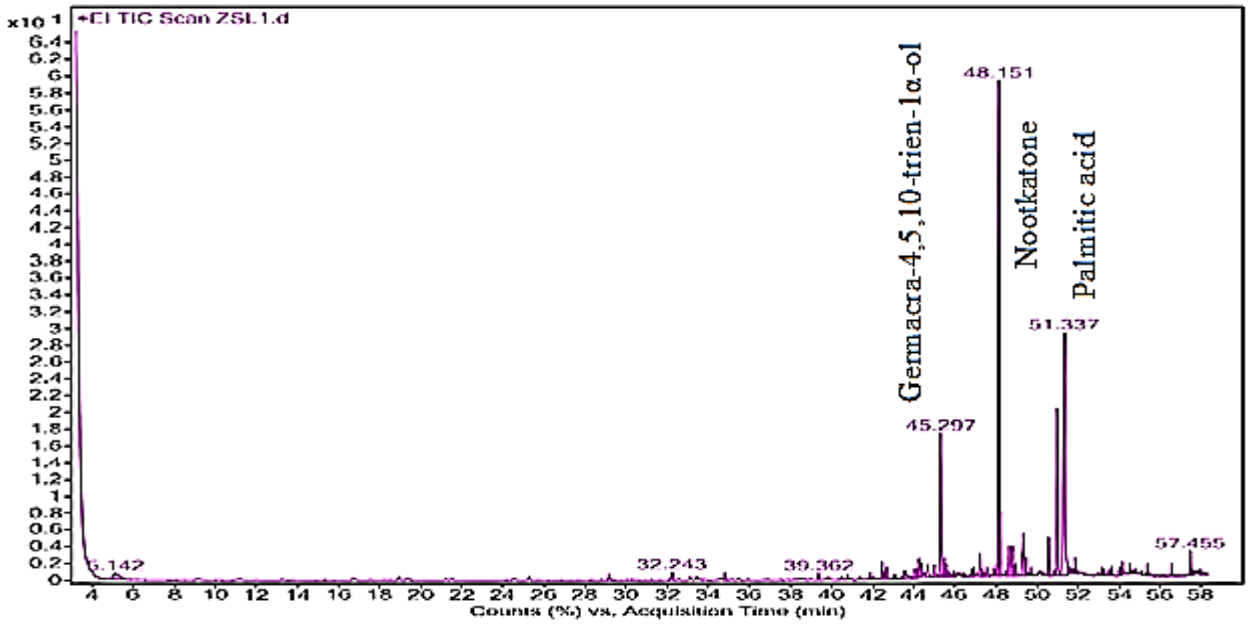

A)

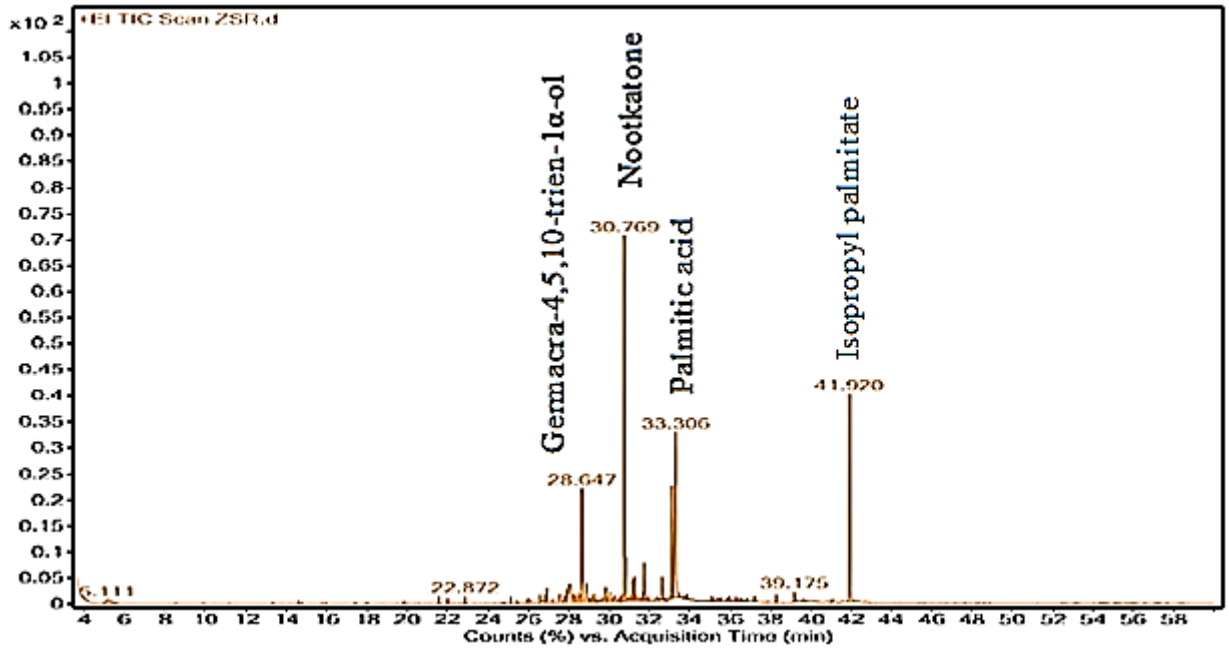

B)

Appendix 32: Gas chromatogram of the leaves (A) and roots (B) EOs of *Z. spina-christi*.

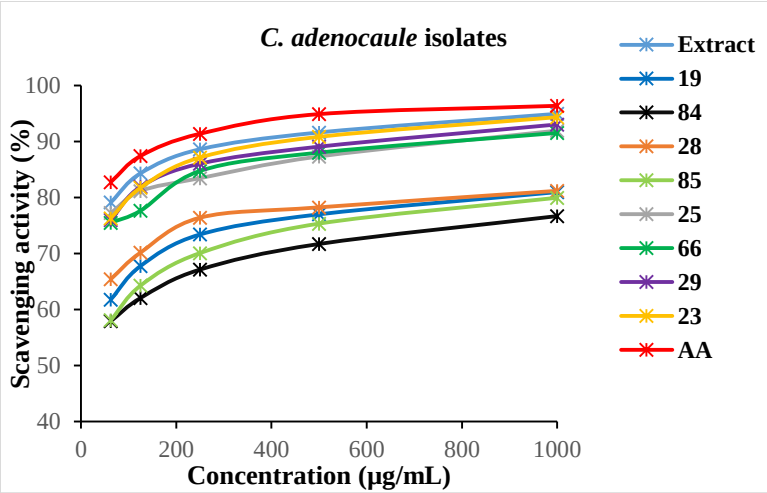

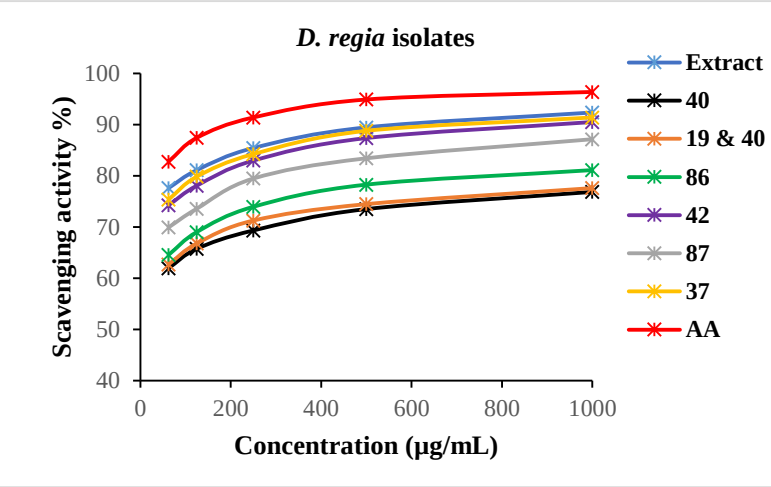

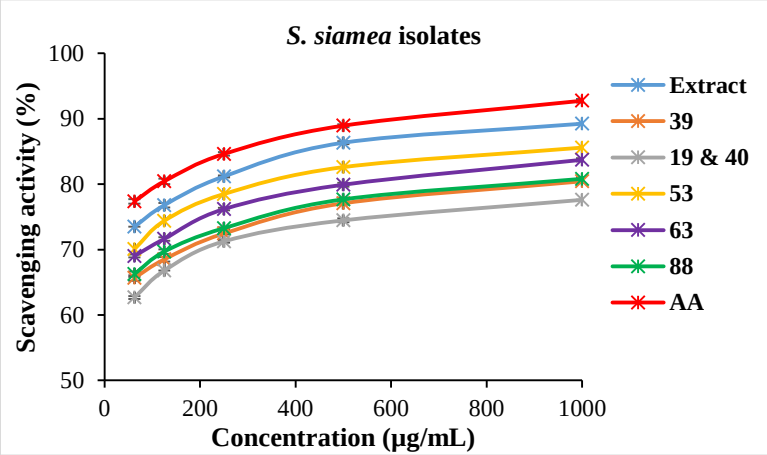

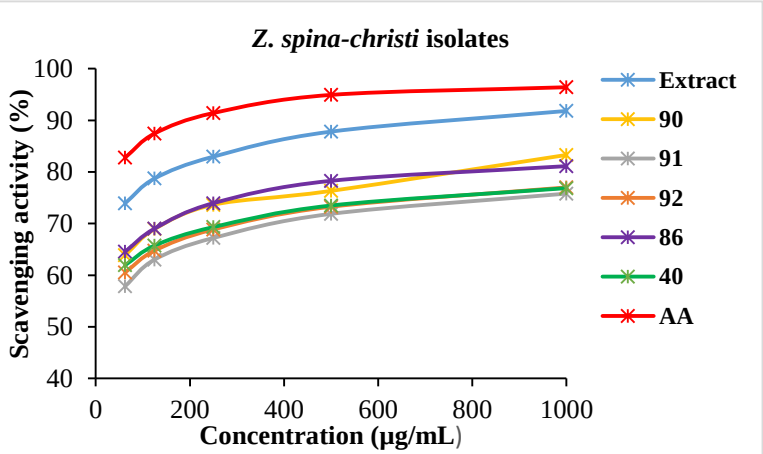

Appendix 33: DPPH radical scavenging activity (%) of the extracts, compound isolates, and ascorbic acid against different concentrations (graphical portrayal). AA: Ascorbic acid.

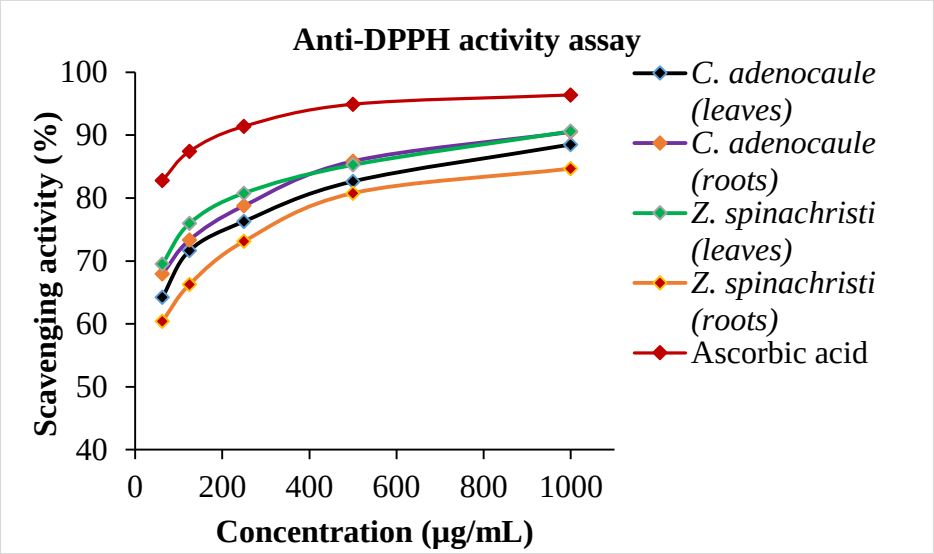

Appendix 34: DPPH radical scavenging activity (%) of the essential oils of *C. adenocaule* and *Z. spina-christi* against different concentrations (graphical portrayal).

PUBLICATIONS

Published articles

1. Gebrehiwot, H., Dekebo, A., & Annisa, M. E. (2022). Chemical composition, pharmacological activities and biofuel production of *Eichhornia crassipes* (Water hyacinth): a review. *Journal of the Turkish Chemical Society Section A: Chemistry*, 9(3), 849-866. https://doi.org/10.18596/jotcsa.1033493

2. Gebrehiwot, H., Dekebo, A., Shenkute, K., Ensermu, U., & Endale, M. (2024). Chemical composition, antibacterial and antioxidant activities of essential oils from *Cyphostemma adenocaule* and *Ziziphus spinachristi*. *Bulletin of the Chemical Society of Ethiopia*, 38(1), 167-186. https://doi.org/10.4314/bcse.v38i1.13

3. Gebrehiwot, H., Melaku, Y., Aliye, M., Ensermu, U., Dekebo, A., Endale, M., ... & Hunsen, M. (2024). Antibacterial and Antioxidant Efficacies of Secondary Metabolites from the Roots of *Cyphostemma adenocaule*: A Combined *In Vitro* and *In Silico* Study. *Journal of Tropical Medicine*, 2024(1), Article ID: 1679695, 30 pages. https://doi.org/10.1155/2024/1679695

4. Gebrehiwot, H., Ensermu, U., Dekebo, A., Endale, M., & Hunsen, M. (2024). Exploring the medicinal potential of *Senna siamea* roots: an integrated study of antibacterial and antioxidant activities, phytochemical analysis, ADMET profiling, and molecular docking insights. *Applied Biological Chemistry*, *67*(48), 1-22. https://doi.org/10.1186/s13765-024-00899-2

5. Gebrehiwot, H., Ensermu, U., Dekebo, A., Endale, M., & Nefo Duke, T. (2024). *In Vitro* Antibacterial and Antioxidant Activities, Pharmacokinetics, and *In Silico* Molecular Docking Study of Phytochemicals from the Roots of *Ziziphus spina-christi*. *Biochemistry Research International*, *2024*(1), Article ID: 7551813, 22 pages. https://doi.org/10.1155/2024/7551813

Under review

6. Gebrehiwot, H., Melaku, Y., Getaneh, E., Shenkute, K., Dekebo, A., Ahmed, M., Endale, M., and Hunsen, M. *Delonix regia* Roots: Insights of its Phytochemistry and Medicinal Potential, Molecular Modeling, and Pharmacokinetics of its Compound Isolates. *BMC Complementary Medicine and Therapies*, Year_####_ Volume_####_Issue_####_:pp_####_.